1450

NOVEMBER 1978 PPPL-1450

UC-20d

A SYSTEMS STUDY OF TOKAMAK FUSION-FISSION REACTORS

PLASMA PHYSICS LABORATORY

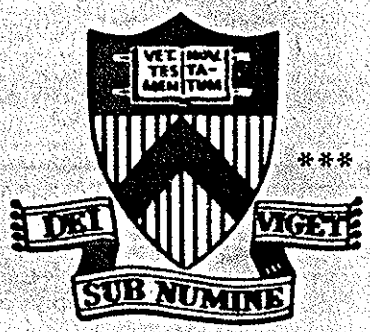

PRINCETON UNIVERSITY
PRINCETON, NEW JERSEY

This work was supported by the U. S. Department of Energy Contract No. EY-76-C-02-3073.

NOTICE

Printed in the United States of America.

Available from
National Technical Information Service
U. S. Department of Commerce
5285 Port Royal Road
Springfield, Virginia 22151
Price: Printed Copy $__*__; Microfiche $3.00

*Pages	NTIS Selling Price
1-50	$ 4.00
51-150	5.45
151-325	7.60
326-500	10.60
501-1000	13.60

A Systems Study of Tokamak Fusion-Fission Reactors

F. H. Tenney, C. G. Bathke,[a] W. G. Price, Jr.,[b]
W. H. Bohlke,[c] R. G. Mills, E. F. Johnson,[d]
A. M. M. Todd, C. H. Buchanan,[e] S. L. Gralnick[f]
Plasma Physics Laboratory, Princeton University
Princeton, New Jersey 08540

Present Addresses

[a]Los Alamos Scientific Laboratory, Los Alamos, N.M.

[b]Mathtech, Inc., Princeton, N.J.

[c]Stone and Webster Engineering Corporation, Boston, Mass.

[d]Department of Chemical Engineering, Princeton University

[e]General Electric Company, Schenectady, New York

[f]Grumman Aerospace Corporation, Princeton, N.J.

Table of Contents

References are located at the end of each section identified by capital letters. To facilitate finding references (and figures) the appropriate letter has been placed under the page number in long sections.

I. Introduction and Executive Summary

A. Features of the Study

This publication reports the results of a two to three year effort at a systematic analysis of a wide variety of tokamak-driven fissioning blanket reactors, i.e., fusion-fission hybrids. It addresses the quantitative problems of determining the economically most desirable mix of the two products: electric power and fissionable fuel and shows how the price of electric power can be minimized when subject to a variety of constraints. An attempt has been made to avoid restricting assumptions, and the result is an optimizing algorithm that operates in a six-dimensional parameter space. Comparisons are made on sets of as many as 100,000 distinct machine models, and the principal results of the study have been derived from the examination of several hundred thousand possible reactor configurations.

B. Advantages of Hybrid Systems

1. Neutronic Abundance

The fundamental advantage of fusion-driven fissioning machines is neutronic abundance. In fission reactors and in hypothetical fusion reactors there is a scarcity of neutrons. In the case of chain-reacting fission systems this results from the relatively small number of neutrons released in a reactor core per fission event. In the case of pure fusion systems

it results from the absence of tritium in nature. The most easily exploited tritium breeding reaction is

$$Li^6 + n \rightarrow T + He^4 \qquad (1)$$

which requires one neutron, whereas the fusion reaction,

$$D + T \rightarrow He^4 + n, \qquad (2)$$

yields only one neutron. To make a pure fusion system work one or more neutron-multiplying isotopes must be added to the system. This is readily accomplished, but, as with pure fission, the neutron excess is but slight.

The neutron of reaction (2) is born at 14 MeV, an energy not even approachable in a fission system. The potential advantage of hybrids can be readily appreciated from Figure 1, taken from Perry and Weinberg.[1] This curve plots the number of fission neutrons released per neutron absorbed in four fissionable isotopes. Curves for fertile isotopes are similar at the upper energy end. It is the large value of η (4.5 or more) at 14 MeV that leads to neutronic abundance unique to hybrid systems.

2. Subsidiary Advantages

a. Subcriticality

For a fission chain reaction to be maintained, the neutron multiplication, k, must be maintained at the critical value of one. The system must be capable of $k > 1$ to allow for compensation of the effect of buildup of neutron absorption "poisons" in time. A driven system need not have $k = 1$. Indeed k will always be less than one, and the designer, freed of the criticality constraint, has broader design opportunities. Further-

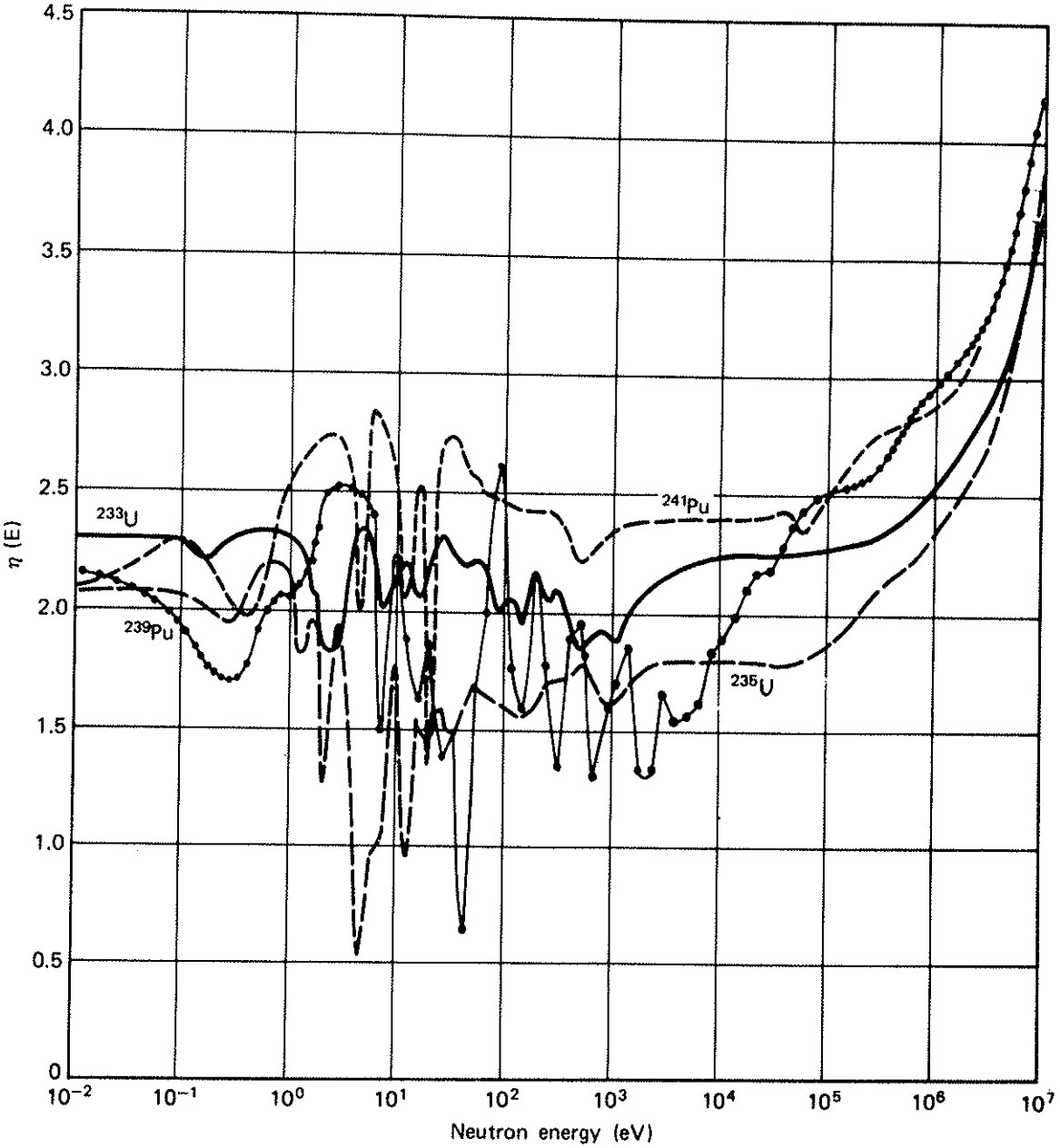

Fig. 1. Number of Fission Neutrons Released, η, as a Function of Absorbed Neutron Energy.

more when k_∞ (the multiplication of a conceptual infinite, leakage-free lattice) is less than one, there is no possible criticality accident.

b. Doubling Time Irrelevant

The value of the doubling time is a critical parameter for a fission breeder. In order to breed fissionable fuel the lattice must have a substantial inventory of fissionable fuel to begin operations, and the number of years required to reproduce this inventory (the doubling time) has important economic implications. It is not necessary for a hybrid to have a substantial inventory. In fact some variations need have none at all; so there are no doubling time limitations on the rate at which a new style hybrid reactor could be adopted by industry should it prove economically attractive.

c. Reduced Wall Irradiation

An important concern to students of hypothetical fusion reactors has been the high rate of radiation damage to the vacuum or first wall. In most hybrid reactors, the bulk of the energy will be generated in the blanket rather than in the fusion component. The wall irradiation levels required drop substantially, and the wall may become a permanent rather than renewable feature of the machine.

d. Easier Plasma Requirements

Again because the fusion or plasma power is much reduced compared to that required in pure fusion designs, the plasma requirements for some machines are reduced substantially, and practical applications of hybrids may be possible considerably earlier than practical applications of pure fusion.

3. Potential Applications

The hybrid could prove to be inherently superior to the fast breeder reactor for making use of our vast U^{238} fuel reserves.

C. Suggestions for Exploitation of These Advantages

There is a great variety of machines conceivable of the hybrid type. Many different styles of application are imaginable. It has been suggested that the hybrid advantage be used to provide stand-alone fuel factories generating little power or even being power consumers. It has been suggested that the hybrid be used to exploit marginal plasma devices. It has been suggested that they be power producing only, burning the fissionable fuel produced in situ. It has also been suggested that the neutron excess be used to burn actinides to convert the long-lived radioactive wastes of fission plants to relatively short-lived and to stable isotopes. Several groups have studied rather detailed conceptual designs for such devices. The economic value of these proposed designs varies widely among them.

We have concluded that a hybrid machine should be a substantial power producer with a by-product of fissionable fuel, the optimum ratio of fuel production to power production being determined by current market economics.

D. Approach of this Study

We believe that detailed design or study of a single hypothetical model, useful as it may be to identify problems and demonstrate the value of some feature or another, is of

limited value in helping decide upon the most desirable form of machine. We also believe that it is very difficult to try to draw significant conclusions from intercomparison of individual design studies done by different groups at different times for different purposes. We have adopted the strategy of applying the same cost algorithm to a very wide class of possible machines and then methodically examining a very large number of machines subject to appropriate constraints. We have, however, restricted the search to tokamaks and to one class of blankets. Detailed discussion of this technique follows in the text of this report and in a companion report by C. G. Bathke.[2]

E. Major Conclusions

1. Power Production Is Important

Many of our results can be effectively presented in the form of the graph shown in Figure 2. These curves represent the cost of electric power produced by various machines as a function of the market price of fissionable fuel. The straight line marked LWR is the characteristic for one (and only one) machine. The characteristic of any consumer of fuel will be a straight line of positive slope. The characteristic for a substantial producer of fuel (in addition to electricity) would be a straight line of negative slope.

All possible hybrid machines of a given net power output would be represented by a dense set of straight lines. A hybrid machine curve is the lower envelope of all these straight line characteristics. Thus each point on the curve represents a different machine, the one delivering the lowest cost power for a given price of fuel.

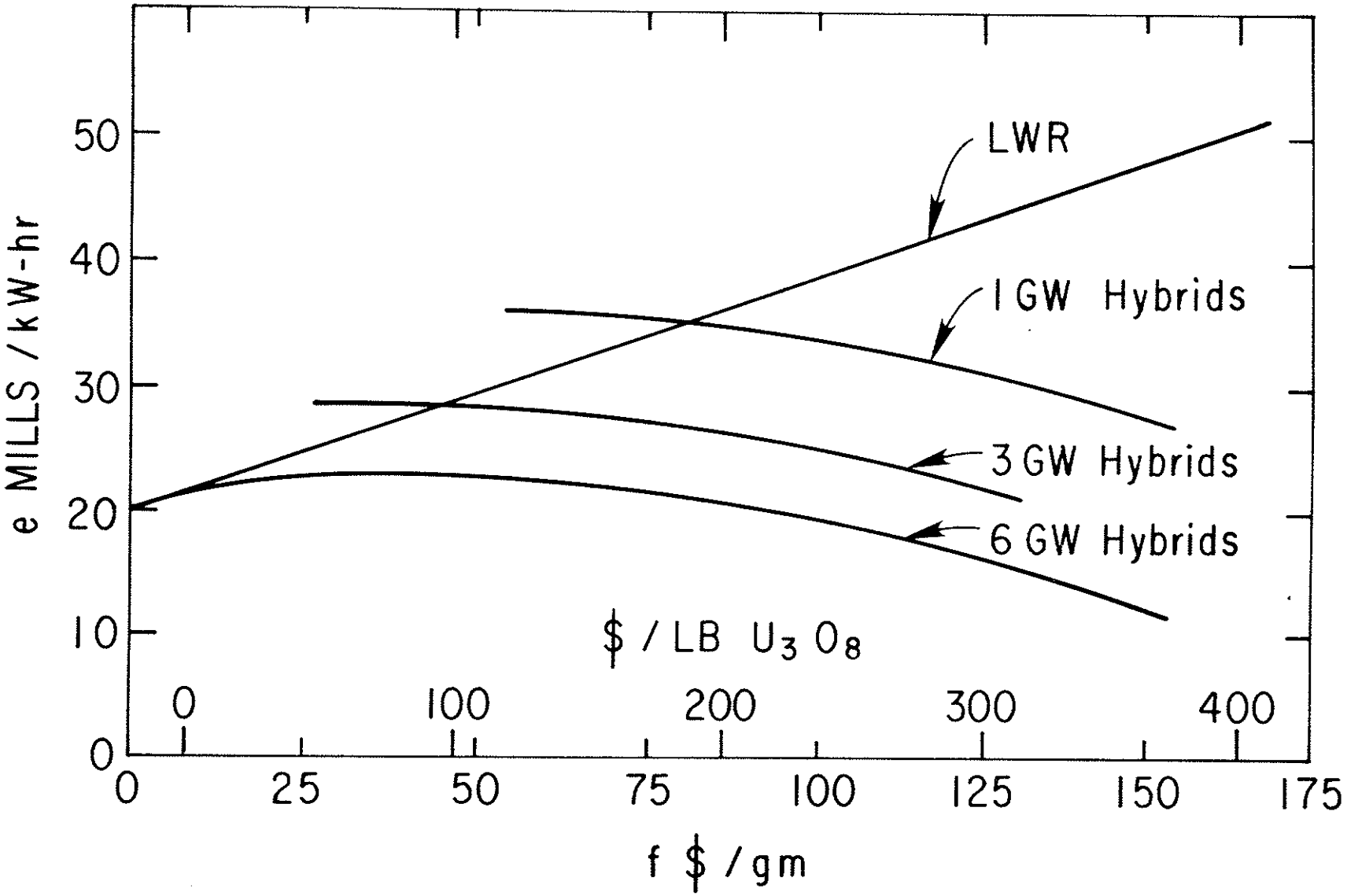

Fig. 2. Optimum Hybrid Reactors and the LWR Reactor.

As one would expect, as the price of fuel rises, the optimum machine produces a proportionally greater amount of fuel. Unless the price of fuel is quite high, however, power production should be emphasized.

2. Fission-Fusion "Parks"

The intersection of the LWR and hybrid characteristics occurs at the stable market price of fissionable fuel and indicates the price at which power will be sold. Note that successful hybrids would place an upper bound on the market price for fissionable fuels, both those artificially bred (Pu^{239} or U^{233}) and their natural competitor U^{235}. The data in Figure 2 imply that if hybrids can be deployed, there will be no need to mine the Chattanooga shales or other high cost uranium ores.

3. Evolutionary Prognosis

An early proof of the possibility of hybrids would allow a very reassuring program for future development of the utility industry. A guarantee of future reasonable fuel costs would allow the accelerated production of current design LWR reactors to fill our immediate power needs. Subsequent commercial development of the low net power hybrid (say twenty years hence) would supplement the LWR's, provide them with fuel and take up the load of retired power stations. As the capacity of networks grew, making larger unit stations acceptable, the larger hybrids (which consume, in situ, all the bred fuel) would slowly replace the LWR's in an orderly manner as the LWR's aged, with

no progressive increase in the real cost of power. Finally the scene would be prepared for the eventual dominance of the pure fusion reactor sometime in the coming century. This attractive natural evolution would fit well existing and planned utility practice and could avoid the need for fission breeding reactors.

4. Sensitivities

An important part of the work reported here was to seek parameters to which the cost of power was sensitive. In many cases we found a remarkable insensitivity. Effects produced by varying, for example, physical size, magnetic field, plasma pressure, certain profile characteristics, etc., would be compensated by other changes. There were two exceptions. The expected economies of scale are present, namely the larger power stations produce lower cost power. The other sensitive parameter was the confinement characteristics of the plasma as characterized, for example, by the $n_i\tau$, or Lawson parameter. The cost of power is very sensitive to this basic quantity. As a consequence, no definitive statement can be made today concerning the cost of hybrid or fusion power pending further results from the research program.

F. The Nation's Fuel Reserves

It is not widely realized that the United States Federal Government owns and has in storage an incredibly large amount of potential fuel. As a result of uranium enrichment operations for nuclear power stations and especially for military and naval defense purposes, the tailings of depleted uranium-238

(depleted from a 0.7% natural uranium-235 content to about 0.2%) amount to close to 250,000 tons. We do not today have a developed technology to burn this fuel. But when we do, this fuel reserve will be equivalent in energy content to six times that of the unpumped Arabian oil pool or to about half of the entire unmined central U.S. coal reserves.[3] In recent years it appeared that a fast breeder reactor technology would be necessary to exploit this reserve; it appears to us that the hybrid is probably a better way to burn our uranium-238. Some versions of the hybrid can avoid commerce in plutonium and both ends of the uranium fuel cycle (i.e., enrichment in the beginning and plutonium separation later).

References

[1]A. M. Perry and A. M. Weinberg, Thermal Breeder Reactors, Annual Review of Nuclear Science (Annual Reviews, Inc., Palo Alto, California, 1972) Vol. 22, pp. 317-354.

[2]C. G. Bathke, An Algorithm for Locating the Extremum of a Multi-Dimensional Constrained Function and its Application to the PPPL Hybrid Study, Princeton Plasma Physics Laboratory Report PPPL-1424 (1978).

[3]M. K. Hubbard, The Energy Resources of the Earth, Energy and Power (W. H. Freeman and Company, San Francisco, 1971) pp. 31-40.

II. The Rationale for Hybrids

A. Use of 14 MeV Neutrons

The fusion reactions of primary interest are:

$$D + T \rightarrow He^4 + n + 17.6\ MeV \quad (1)$$

$$\left.\begin{aligned} D + D &\rightarrow He^3 + n + 3.3\ MeV \\ D + D &\rightarrow T + p + 4.0\ MeV \end{aligned}\right\} \text{equal probability} \quad (2)$$

$$D + He^3 \rightarrow He^4 + p + 18.3\ MeV \quad (3)$$

There are several dozen others, a very few of which are of possible interest, but it is likely that if fusion is ever of significant commercial impact, it will be through the use of one or more of the above three reactions.

Since neither tritium nor helium-three occurs to any great extent in nature, only deuterium should be viewed as a primary fuel reserve. If the first reaction, which has at least a two order of magnitude advantage in cross section over the others at low collision energies, is to be exploited, some way must be found to breed the tritium, and there are only two suitable materials from which to breed tritium: deuterium and lithium.

To first approximation, a successful D-T fusion reactor has

$$D + T \rightarrow He^4 + n \quad (4)$$

proceeding in the plasma and

$$n + Li^6 \rightarrow T + He^4 \quad (5)$$

proceeding at the same rate in the blanket. Thus the system is catalyzing the reaction

$$D + Li^6 \rightarrow 2\ He^4.$$

This is to first approximation only as it is not possible to induce every neutron from (4) to produce (5). Because of inevitable losses of some of the neutrons, it is necessary to incorporate neutron multipliers. The two most useful are

$$n + Li^7 \rightarrow T + He^4 + n \tag{7}$$

and

$$n + Be^9 \rightarrow 2\ He^4 + 2n, \tag{8}$$

but lead or uranium could also be used. Thus in a "pure" fusion D-T reactor the primary fuels are deuterium and lithium-six, but lithium-seven, beryllium, and possibly other isotopes are secondary fuels.

To breed tritium from deuterium, the 50-50 D-T plasma suitable for the above must be "leaned out" to less than one percent tritium to force reaction (1) and the second branch of (2) to proceed at the same rate to catalyze

$$3\ D \rightarrow He^4 + p + n. \tag{9}$$

The power density is very much reduced compared to operation with (4) due to the much smaller cross section for the D-D reaction and the low tritium density.

The power density can be increased, while still catalyzing (9), by adding sufficient He^3 to cause the upper branch of reaction (2) and reaction (3) to proceed at the same rate.

This has been called the catalyzed-D fuel mixture, and appears to be the second highest fusion power density system available. See Figure 1. The factor of seventy power density reduction is sufficiently great to convince most fusion power planners to adopt reaction (4) as the basis for the fusion reactor. Even with its large relative advantage over the others, it may still be desirable to attempt to increase the power density even more as can be achieved by variants of the TCT (two component torus) concept where energetic beams are used to increase $\langle \sigma v \rangle$ over what can be achieved in a thermal plasma.

Choice of the D-T reaction automatically introduces the neutron budget problem. Although it is not difficult to design blankets that have adequate breeding excesses, there is little neutron surplus in a "pure" fusion system.

A fission reactor also has a tight neutron budget. It must be controllable, yet maintain criticality. The problem is associated with the low yield of neutrons (~ 2.3) from a fission induced by slow neutrons. Even in a fast breeder, there are few neutrons above 8 MeV; so a pure fission system cannot exploit the large neutron yield available from the fertile isotopes (U^{238}, Th^{232}) at high neutron energy.

In a hybrid system the neutron shortage common to "pure" fusion and "pure" fission is removed by allowing 14 MeV neutrons to produce fissioning of fertile isotopes. A 14 MeV neutron-induced fissioning of U^{238} produces on the average about four and a half neutrons. The hybridization of these two forms

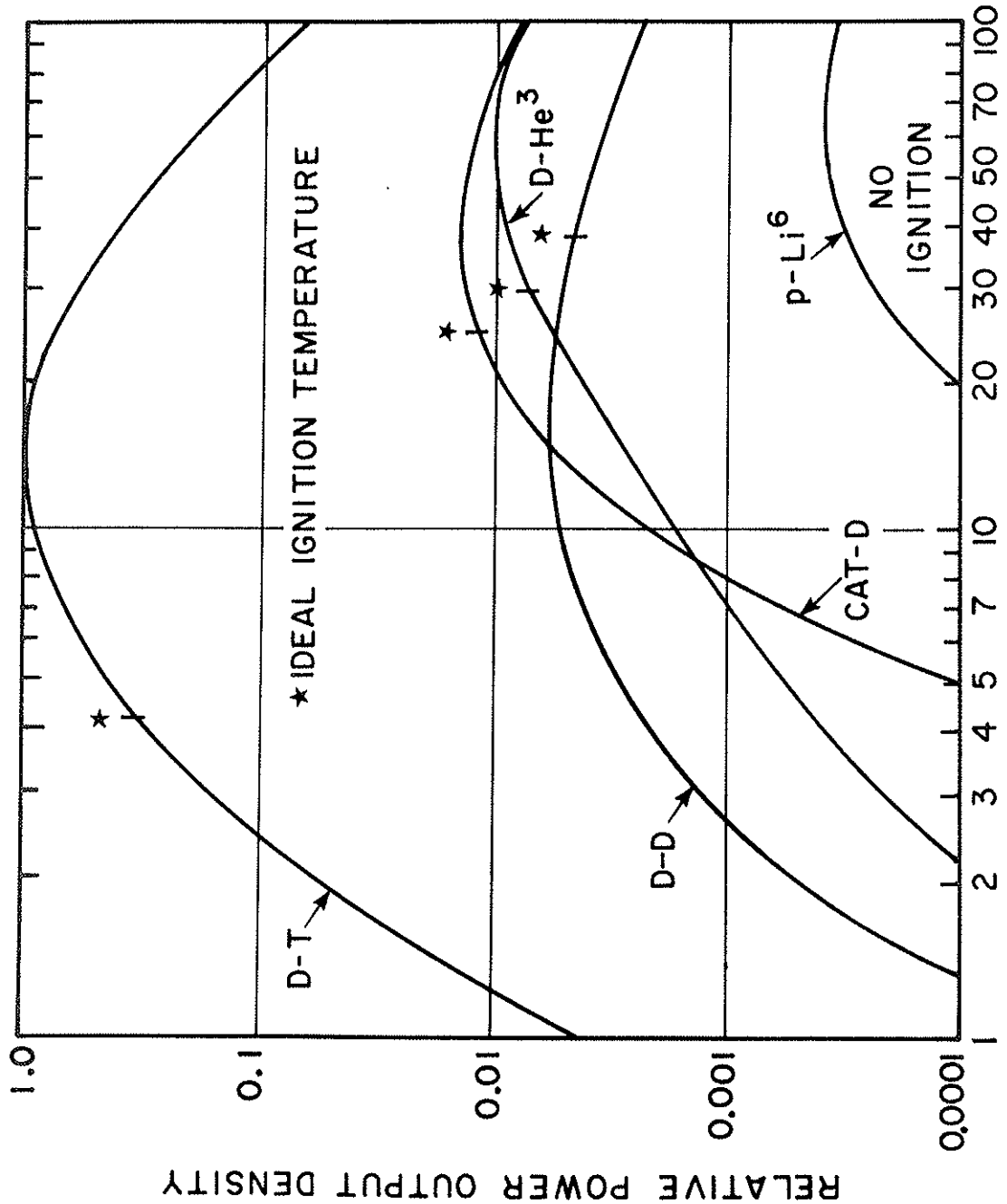

Fig. 1. The Relative Output Power Densities for Various Reactions.

of nuclear power produces an effect that is impossible for either alone to achieve, the generation of a very neutron-rich medium. Such a medium can breed more tritium than is consumed in the plasma, can breed more fertile material into fissile material than fissile material is burned, can drive a sub-critical lattice into large scale power generation and have spare neutrons left over.

The selection of the most beneficial manner to exploit this potential advantage is a complex problem. A person concerned over the relatively low power densities predicted for fusion reactors (resulting in large power plants) might regard it as the key to more power from a certain sized plant. A mirror machine designer might see it as an adequate answer to the low Q mirror problem. A utility executive might view it as a potential alternate source of fissile fuel for his light water reactors. Someone concerned over radioactive waste disposal might regard it as the answer to the suggestion of burning the long-lived actinides in situ to shorter half-lived or stable materials. A person dismayed by the delays being experienced by the LMFBR development program might embrace it as a better way to burn our vast U^{238} reserves.

A hybrid reactor is not a producer of a single product, electricity. It may be able to sell in addition (or instead) Pu^{239}, tritium, other isotopes (He^3, U^{233} as examples) or an actinide disposal service. One should not be hasty in assuming the best product for which to design. A controversy has developed

between factions favoring "optimize for fuel production" vs. those advocating "optimize for power production." The supporting logic is frequently weak or invalid.

Some favoring optimization for fuel production have justified their approach by asserting that since fusion reactors will be more expensive in investment cost per kilowatt than the fully developed light water reactors (LWR's), that it is bound to be more economic to burn plutonium in LWR's than in fusion reactors, hence one should optimize for fuel production. In the opposite camp it has been pointed out that increasing the burnup of plutonium in situ greatly increases the power out of a given machine and that clearly this should be done. Both arguments are faulty.

The former argument would be valid if we had a special source of plutonium and contemplated whether to build a hybrid reactor in which to burn it or to build an LWR in which to burn it. Actually the hybrid is the source of plutonium, and the choice is between burning it in situ or separating the plutonium, building an LWR, and burning the plutonium in the LWR.

The second argument is faulty because the easiest way to increase the in situ burning of plutonium is by increasing the fuel enrichment, i.e., the plutonium inventory. In cases where the plutonium has a high value, this can increase the investment cost sufficiently to reduce the economy rather than enhance it.

Actually, as should be no surprise, the optimal mix of a two-product system depends on the prices for the two products. As long as plutonium remains cheap, a plant should be designed for in situ burning of the bred plutonium. If the price of plutonium rises to high levels, it is better to sell it.

A careful system optimization is needed to give definitive answers to the question of the best hybrid system. This report presents the results of such a study.

From the point of view of researchers in the field of controlled thermonuclear reactors, the most promising aspect of the various suggestions for hybrid systems is the opportunity for a much earlier application of fusion technology for public benefit than seems possible if they are restricted to "pure" fusion. The large advantage of hybrids can be used to offset certain problems of proposed fusion systems. As has been mentioned above, it could be used to compensate for the low Q's of mirror systems (or of inertial pellet systems). The Lawson criterion can be dropped as much as two orders of magnitude for a hybrid, thus the conventional target of 10^{14} seconds per cubic centimeter confinement index ($n_i\tau$) may be avoided should such performance prove elusive. In the work represented here, however, the advantage has essentially been used to make low β toroids practical as fusion reactors. Previous studies of pure fusion have shown that average betas should be about four percent or more for practical "pure fusion" reactors. In this report, the effective betas are near one percent.

Should nature be so uncooperative as to restrict toroids to only one percent, it would be difficult indeed to design a practical pure fusion reactor. Since the power density scales as β^2, power density would be reduced by about a factor of sixteen, and the machine forced to at least twice the size (in linear dimensions) of those treated in the earlier studies. With a hybrid system, low betas suffice.

B. Utilization of Fertile Material

The type of hybrid that has generated the greatest interest in the past is the fissile fuel factory: the hybrid that is optimized to produce fissile fuel for sale. It is felt by the electric utility industry that some such "artificial" source of fissile material must be found because of the limited proven reserves of natural uranium.

In a modern LWR, burnup of about 3.3% can be achieved from fuel that is initially enriched to about 2.6%, because of the internal conversion of fertile uranium to fissile plutonium (the LWR has a conversion ratio, CR, of about 0.5). However, making allowance for the tails discharged from the enrichment facility and discounting the possibility of recycle of plutonium from spent fuel, only about 0.7% of the natural uranium mined is ultimately burned. At this rate, the projected demand for uranium ore will exceed known resources (at moderate prices) near the end of this century, i.e., in about 25 years. Although fission reactors have been operated that produced more fissile fuel than they consumed, these breeders have either been experiments or weapons production facilities. Commercially practical

breeders have not yet been built, and if they ever are, it is not clear that they will be socially acceptable. Therefore the utility industry has a keen interest in schemes, such as the fusion-fission hybrid, which offer a way to convert fertile material (uranium-238 or thorium-232) into fissile fule (plutonium-239 or uranium-233).

A simple analysis will indicate the potential value of the hybrid. If the inner layer of the blanket consists mostly of uranium, a fraction, f, of the fusion neutrons will induce fast fission. Given N, the average number of neutrons per fission, there will be a total of $(1 - f) + fN$ neutrons in the blanket. Deducting one neutron to regenerate the tritium, and allowing a fractional parasitic loss, p, there will be $(1 - p)\,[(1 - f) + fN] - 1$ excess neutrons, each of which could produce a fissile atom.

Taking $f = 0.6$ (perhaps optimistic), $N = 4.5$ at 14 MeV (since N is an increasing linear function of energy), and $p = 0.2$, there could be 1.5 fissile atoms bred per fusion. Assuming recoverable energies of 22 MeV per fusion and 198 MeV per fission, this is equivalent to 5.6 kg of plutonium per megawatt year of fusion energy, or (including the fast fission energy) 1 kilogram per megawatt year of hybrid thermal energy. Operating at 70% capacity factor and 30% net efficiency, a 1 GW(e) hybrid with this performance would breed 2290 kg of plutonium a year, enough to fuel 6.5 LWR's at the same power. It must be

noted, however, that detailed studies of particular hybrids have found that such breeding is not always physically achievable, nor economically desirable.

C. The Thorium Cycle vs. the Uranium Cycle

As exemplified above, it is generally assumed that the fissile fuel produced in a hybrid will be plutonium. However, it is technically possible for a hybrid to use the thorium-uranium fuel cycle instead. Basic nuclear data (the value of η, secondary neutrons per absorption) can be used to compare the intrinsic value of the three fissile nuclides as reactor fuels. For fast reactors Pu-239 is the best; for thermal reactors U-233 is the best. In both cases U-235 ranks third, but since the others are not available in nature, it is the most important. To obtain quantitative estimates of the relative values of these fuels in the early 1990's (when hybrids might become a market factor) an economic study[1] was commissioned from Combustion Engineering, Inc., Nuclear Power Systems.

The purpose of this study was to determine the parity value, relative to 90% enriched U-235, of Pu-239 and U-233 in "typical" LWR's, LMFBR's, and HTGR's. Standard economic parameters were used, e.g., 16% carrying charge; 8% discount rate; 6% inflation, \$85 per Separative Work Unit; ore at 53\$/lb U_3O_8, 0.3% tails; fabrication, reprocessing, and shipping costs and times estimated case-by-case. However, since this was a fuel cycle cost study, no allowance was made for capital cost differences between reactor types. Table I, from Ref. 1, summarizes the results.

Table I. Estimated fissile fuel values in the early 1990's. (from Ref. 1)

Isotope	Reactor	Parity	$/g (1975 $)
Fissile Pu	LWR	0.67	35
	HTGR	0.75	40
	LMFBR	0.90	47
U-233	LWR	0.85	45
	HTGR	0.76	40

Since these are indifference values, supply and demand in an active fuel market might lead to somewhat different real prices. The surprisingly low values for U-233 are due to a conservatively high estimate of fabrication and reprocessing charges, based on the few operating thorium cycle reactors. The high value of plutonium in the LMFBR is irrelevant, since that reactor type would be an independent competitor.

The principal conclusion from this study is that U-233 is distinctly a more valuable fuel than Pu-239, particularly for light water reactors, but that the advantage is not large. This is most important for the evaluation of the economics of the hybrid, since it appears that more Pu-239 than U-233 can be made in a given plant. Typically the lesser value of the plutonium is compensated by the greater quantity which can be sold.

The difference in the rate of production of fissile material from thorium and from uranium is ultimately due to their energy-dependent cross sections. Previous studies of hybrid blankets have attributed the poorer breeding with thorium to its lower fission cross section at 14 MeV, 0.35b compared to 1.1b for U-238. Since the total cross section is about 6b for both, this means that a DT neutron will only produce about one-third as many fissions in a thorium blanket as in a uranium blanket of equal (atom) thickness, and thus there will be fewer excess neutrons.

However, when allowance is made for n-2n and n-3n reactions, there are nearly as many secondary neutrons per

collision from Th-232 as from U-238. Few of these secondaries will have energies above 6 MeV but many will be above 1 MeV, i.e., there will be a large population of secondary neutrons above the fission threshold but below that for n-2n reactions. In this energy range the U-238 fission cross section is about 0.55b, but it is only about 0.13b for Th-232. This explains the better performance of the uranium blankets; in these there is a considerably greater probability of fast fission induced by secondary neutrons, with a correspondingly greater neutron multiplication and excess neutron production.

D. Power Producing Hybrids

A hybrid that produces fissile material will sell it as a fuel for fission power plants. Since fission reactors are expensive, the question naturally arises - Why not just burn up the fissile material in the hybrid itself? Such a hybrid reactor would have to be provided with a blanket with better cooling, but the incremental cost might not be large since the fast fissions used for producing the fissile fuel also release large amounts of energy. Offsetting this expense would be the considerable savings of not building the fission reactor. The energy conversion equipment and balance of plant would, of course, be required in either case.

Another factor is of great importance to the economics of power-producing hybrids: fissile material is currently underpriced relative to its true value as an energy source. This is due to the fact that uranium ore is sold at a price to cover the mining cost, and is enriched for a fee to cover the expenses of that process. Reactor fuel produced from enriched ore is not sold at a market-set price which makes nuclear power just break-even with its nearest competitor. Competition with ore may set a ceiling on the price which a hybrid can charge for the fissile fuel it produces that is less than the value of the energy it represents; however, by burning the fuel in-house and selling the energy directly, the full revenue can be obtained.

On the other hand, a pure fission reactor is optimized to produce energy as cheaply as possible. Typically the power density is large to minimize the capital investment. Also, if the fissile fuel is expensive, the reactor can be operated at high conversion ratio, thereby burning cheap fertile material as part of its fuel. The optimization of a hybrid is limited by constraints imposed by the fusion neutron source. Because of the plasma region, the overall power density cannot be made very large. Because the plasma provides a surface source of neutrons, power tends to decrease through the blanket. The large surface (and attendant leakage) of the blanket makes it harder to achieve a high multiplication factor, while the requirements that a multiplier face the plasma and that tritium be bred limit the options for blanket layout.

There are also intangible factors which should be considered in choosing a mode of hybrid operation. For example, transportation of fissile materials might be reduced if it were burned in the hybrid; on the other hand, this would increase the accident hazard in the hybrid due to fission products and actinides. Assuming that the intangibles balance out, the choice between hybrids can be made on an economic basis, i.e., the balance of costs and revenues. The degree of power production simply becomes an additional parameter in a hybrid optimization study. Typically this is expressed by the blanket energy multiplication factor, with feedback into the cost for a more expensive blanket, a bigger balance of plant, reduced fissile sales,

and greater output of power. Thus an ad hoc choice of hybrid mode need not be made.

E. Historical Background

1. Early Thoughts

The idea of a device in which both fusion events and fission events would occur is nearly as old as the controlled thermonuclear research program itself. In the early 1950's hybrid concepts were developed in response to two problems: the breeding of tritium for sustaining the DT reaction in a fusion device and the breeding of fissile material for the development of nuclear weapons.[2,3,4] In particular the concepts developed in the Materials Testing Accelerator Program by 1953 contain the essential physics and much of the techniques envisioned in the so-called "mainline" hybrid concepts today. According to Powell,[5]

> "The underlying principle of this proposal is the concept of bombarding a preionized tritium or deuterium target with a beam of accelerated deuterons or tritons. By this means incident beam energy losses through ionization could be minimized, leaving a substantial fraction of the incident beam energy available for nuclear interaction.
>
> "A secondary but critical principle is the concept of a depleted uranium blanket surrounding the target chamber. By means of this blanket the energetic 14 MeV neutrons from the (DT) reaction would cause fast fission and would thus be multiplied. Subsequently the neutrons could be captured in U-238 to form plutonium or in Li-6 to breed tritium. This concept of breeding in conjunction with a thermonuclear reaction is believed to be novel and capable of realizing breeding gains many times greater than the 0.3-0.5 gain from the breeder reaction systems currently under consideration by the Commission."

Powell goes on to propose a 200 keV beam of deuterons incident on a tritium plasma at a temperature of 1 keV and a density of 10^{14} - 10^{15} ions/cm^3. The beam would not only produce the desired fusion reactions but would also provide "considerable assistance in maintaining a high plasma temperature." Each 14 MeV neutron was expected to produce about one fast fission in U-238, thereby releasing about 200 MeV of additional energy.

In a follow-up report Imhoff[6] evaluated the idea of simultaneous injection of 50 keV deuterons and tritons into a magnetic mirror configuration, thus anticipating the physics underlying the current suggestion by Jassby[7] of a colliding beam torus. Imhoff also appreciated the difference between driven and thermonuclear plasmas when he wrote:

> "The primary difference between the controlled and driven thermonuclear reaction lies in the conditions imposed upon the energy balance. The controlled thermonuclear reaction system depends primarily upon the energy released by the thermonuclear reaction to maintain the system temperature once it has been initially created... The driven thermonuclear system relaxes this requirement by allowing additional amounts of energy to be added to the system continuously or intermittently by the injection of the particles at reaction energies."

Thus over twenty years ago most of the advantages claimed for hybrid systems were pointed out: The enhanced breeding of fissile material and tritium, net power production at relaxed plasma conditions relative to a pure fusion device, and the conservation of uranium ore. However, these ideas

were not actively pursued. The discovery of abundant domestic uranium ores, the adequate production of plutonium by fission reactions, and the discovery of the fast (n, 2n) tritium producing reaction in Li-7 all acted to remove the incentive to develop the hybrid ideas. Perhaps of equal significance was the inability of anyone to produce a plasma of high enough temperature that would last long enough to be of interest.

2. More Recent Work

Most of the work on hybrid ideas in the 1960's centered around calculation of the neutronics of the blanket that was to surround the source of fusion neutrons. The development of cross-section data and of more sophisticated computer codes provided better estimates of blanket performance. Some attempt was made to include the effects of blanket structure and coolants, but the impact of engineering constraints was generally ignored. This neglect probably reflected the lack of any detailed design of a fusion reactor. This situation had been remedied by the 1970's, and a few hybrid blanket studies have been made with reference to specific fusion reactors[8,9,10] in which considerable mechanical detail has been developed. These detailed studies reflect the rising interest in evaluating the economic value of a hybrid system. The essential economic issue is: How will the cost of electricity be affected by the use of hybrid devices? The sense of urgency in this issue rests on the perceived growth in demand for electrical power and the perceived difficulty in obtaining the fuel to meet that demand whether the fuel be fossil

or nuclear.[11] In addition, because the hybrid reduces the performance requirements on the fusion part of the system, there has been an attempt to find a near term application of fusion techniques as a step on the way to the development of pure fusion reactors. The result of these interests has been an increased funding of hybrid conceptual design studies.[12,13] The fusion devices considered in these studies include: mirrors, tokamaks, electron-beam-driven plasmas, theta pinches, and laser-pellet-driven systems.

There has been great interest in hybrid reactors in the Soviet Union.[14,15,16]

Excellent reviews of the hybrid work prior to the early 1970's can be found in Refs. 17 and 18.

F. Commercialization of Fusion

1. Reduced Constraints on Plasma Performance

The final rationale for developing hybrid reactors is the possibility they afford of earlier commercialization of fusion processes than would be possible via pure fusion reactors. The chief argument for this possibility lies in the reduced demands placed on plasma performance in a hybrid reactor as compared to the plasma performance required in a pure fusion reactor.

The plasma in the hybrid reactor is imagined to be a driven plasma, that is, energy is to be injected into the plasma from sources external to the plasma such as by beams of energetic atoms. This injection of energy permits the plasma to operate at a lower value of τ_E - the time required for the thermal energy content of a typical unit volume of plasma to be removed

from the plasma- than otherwise. Furthermore, the effective multiplication by the hybrid blanket of the fusion power developed in the plasma may provide more energy than is required for injection into the plasma, thereby enabling the hybrid reactor to produce net power even though the fusion power produced by the plasma is comparable, or even less than, the power injected into the plasma. Thus the plasma of a hybrid reactor need not be a net producer of energy whereas in a pure fusion reactor the plasma is the chief source of energy production. Therefore the plasma in a hybrid reactor could operate at lower densities, lower pressures, and have a reduced capability for energy containment than could the plasma of a pure fusion reactor.

It is the sense that it will be easier to produce a plasma satisfying the requirements for a hybrid reactor than for a pure fusion reactor that underlies the judgment that the earliest commercialization of fusion plasmas will come via hybrid reactors. However, it is not clear that the economics associated with the relaxed demands on the hybrid plasma will be attractive. In fact, one of the principal conclusions of this study is that the economics of tokamak hybrids drives the demands on the plasma toward those for a pure fusion reactor. Thus while the technical requirements on the hybrid plasma may be relaxed, the economic requirements of the hybrid reactor will prevent the full realization of the relaxed technical requirements.

2. Reduced Constraints on Blanket Design

The concept of hybrid operation can affect the commercialization of fusion through relaxation of some of the

constraints on blanket design as well as through its implications for plasma performance requirements. For example, in a pure fusion reactor it is important that the first wall be able to operate at a temperature comparable to that of the blanket. This allows the energy deposited in the wall, 15 to 25% of the total, to be recovered for conversion at high efficiency. In a hybrid the energy multiplication due to fission is so large that the wall heating becomes only a small fraction of the total, so that efficient recovery is not required. This allows operation of the first wall at reduced temperatures (e.g., with water cooling), which greatly alleviates the radiation damage problem.

Another consequence of the fission heating is that the power density profile can be flattened or tailored in other ways. In a pure fusion reactor the power and tritium production densities fall off rapidly through the blanket, making inefficient use of material. In a hybrid the power density can be brought closer to the state-of-the-art in cooling capability throughout the blanket, thereby decreasing the capital investment per unit of power.

Another degree of flexibility in hybrid operation is introduced by the possibility of operating with a tritium breeding ratio less than one. It has been shown[19] that the cost of tritium bred in a fission reactor may (in certain circumstances) be less than the added revenue obtained by diverting an equivalent neutron from tritium production to fissile fuel

production. This would allow the operation of hybrids without lithium-loaded blankets in a true symbiosis with hybrid-fueled fission reactors.

References

[1]Economic Study of Potential Fissile Fuels Bred in Fusion/Fission Hybrids, Combustion Engineering Power Systems Report CEND-373 (1976).

[2]F. H. Tenney, A Brief Review of the Fusion-Fission Hybrid Reactor, Proceedings of the Second Topical Meeting on the Technology of Controlled Nuclear Fusion (National Technical Information Service, Springfield, Virginia, 1976) Conf-760935, Vol. II, pp. 641-656; also Princeton Plasma Physics Laboratory Report PPPL-1318 (1976).

[3]B. R. Leonard, Jr., A Review of Fusion-Fission (Hybrid) Concepts, Nuclear Technology 20, 161 (1973).

[4]L. M. Lidsky, Fission-Fusion Systems: Hybrid, Symbiotic, and Augean, Nuclear Fusion 15, 151 (1975).

[5]F. Powell, Proposal for a Driven Thermonuclear Reactor, California Research and Development Company Report LWS-24920 (Rev.) (1953).

[6]D. H. Imhoff, A Driven Thermonuclear Power Breeder, California Research Corporation Report CR-1 (1954).

[7]D. L. Jassby, Reactor Aspects of Counterstreaming-Ion Tokamak Plasmas, Nuclear Fusion 16, 15 (1976).

[8]R. A. Krakowski, D. J. Dudziak, T. A. Oliphant, K. I. Thomassen, G. E. Bosler, F. L. Ribe, Prospects for Converting Th-232 to U-233 in a Linear Theta-Pinch Hybrid Reactor (LTPHR),

Conceptual Fusion-Fission Energy Systems, S. L. Bogart, ed., U.S. Energy Research and Development Administration Report ERDA-4 (1974) pp. 249-323; also Los Alamos Scientific Laboratory Report LA-UR-74-1861-Rev. (1974).

[9]W. C. Wolkenhauer, B. R. Leonard, Jr., A. M. Sutey, R. W. Moir, Conceptual Design of a Fusion-Fission Hybrid Reactor Based on a Mirror Fusion Reactor with a Subcritical Gas-Cooled Fission Blanket, Proceeding of the First Topical Meeting on the Technology of Controlled Nuclear Fusion, G. R. Hopkins, ed. (National Technical Information Service, Springfield, Virginia, 1974) Conf-740402, Vol. I, pp. 238-255.

[10]Conceptual Design of the Blanket and Power Conversion System for a Mirror Hybrid Fusion-Fission Reactor, General Atomic Company Report GA-A14021 (1976).

[11]E. L. Draper, Jr., and S. J. Gage, The Fusion-Fission Breeder: Its Potential in a Fuel-Starved Thermal Reactor Economy, Technology of Controlled Thermonuclear Fusion Experiments and the Engineering Aspects of Fusion Reactors, E. L. Draper, Jr., ed. (National Technical Information Service, Springfield, Virginia, 1974) Conf-721111, pp. 132-143.

[12]Conceptual Fusion-Fission Energy Systems, S. L. Bogart, ed., U.S. Energy Research and Development Administration Report ERDA-4 (1974).

[13]Proceedings of the Joint US-USSR Symposium on Fusion Fission Reactors (National Technical Information Service, Springfield, Virginia, 1976) Conf-760733.

[14]I. N. Golovin, The Place of Hybrid Reactors in the World Energy System, U.S. Energy Research and Development Administration Report ERDA-TR-17 (1974).

[15]S. V. Marin, D. V. Markovskiy, L. P. Smirnov, G. Ye. Shatalov, Certain Parameters of the Blanket of a Thermonuclear Reactor with a Fissionable Substance, ibid.

[16]I. N. Golovin, G. E. Shatalov, B. N. Kolbasov, Some Aspects of Hybrid Thermonuclear Reactors, Izvestiya Akad. Nauk SSSR: Enginetika I Transport, No. 6, 23-34 (1975); also Lawrence Livermore Laboratory Report UCRL-Trans-11166 (1976).

[17]B. R. Leonard, Jr., A Review of Fusion-Fission (Hybrid) Concepts, op. cit.

[18]L. M. Lidsky, Fission-Fusion Systems: Hybrid, Symbiosis, and Augean, op. cit.

[19]W. G. Price, Jr., The Cost of Tritium Bred in a Critical Fission Reactor, Princeton Plasma Physics Laboratory Report PPPL-1344 (1977).

III. Tokamak Hybrids

A. Basis of the Hybrid Study

This study addresses the question: Is there a commercially interesting tokamak hybrid reactor that can be built in the 1990's? A subsidiary question is: Can such a device be viewed as a practical spin-off from an eminently successful Toroidal Fusion Test Reactor (TFTR) experiment at the Princeton Plasma Physics Laboratory? The answers to the questions are sought through a systems study of a conceptual design of a hybrid reactor.

There are five premises upon which this study rests. The first premise is that the fusion core of the hybrid will be a neutral beam-driven plasma in a tokamak. The choice of a beam-driven plasma not only reflects the design of the TFTR, but also reflects the hoped-for usefulness of such plasmas.

Interest in neutral beam-driven tokamak plasmas has been high because of three possibilities: first, that beam-driven target plasmas of deuterium and tritium could release quantities of fusion energy comparable to the energy delivered to the plasma by the beams;[1] second, that such beam-driven plasmas could sustain much greater energy loss rates than could an ignited plasma of the same temperature;[1,2] and third, that for a pressure-limited plasma the fusion power developed via neutral beams could exceed that developed via ignition.[3,4] Thus the hope was raised that through the use of beam-driven plasmas an interesting amount of fusion power could be developed before

well confined plasmas, capable of attaining the conventional Lawson criterion, could be achieved.

The second premise is that the tokamak will be run in a quasi steady state with a burn time of 1000 seconds.

The tokamak is viewed as an inherently pulsed device by virtue of the limited time the discharge current can be maintained. The discharge current is commonly induced and maintained by transformer action in which a primary winding produces a changing magnetic flux through the core of the tokamak, and the plasma forms the single turn secondary circuit. Since the flux change is limited by the current carrying capability of the primary winding, the time of the discharge, the "burn time," has some limit after which the discharge current is reduced to zero, and the tokamak reset for the next discharge. There have been calculations[5,6] to show that neutral beams could be used to support the tokamak discharge current in steady state, but this possibility has not been considered in this study.

The output product of the reactor will be proportional to the duty factor, i.e., the ratio of the burn time to the sum of the burn time and the time for resetting the tokamak. Therefore it seems that the larger the duty factor, the more profitable will be the economics of the reactor. Assuming the interesting hybrid reactors will be comparable to the 2000 MW(e) pure fusion reactor studied previously at PPPL,[7] the time to reset the tokamak is estimated, somewhat optimistically perhaps, to be about 100 seconds. This estimate, coupled with the desire to have a

duty factor of at least 0.9, results in the specification of a 1000-second burn time. Accounting for some production of useful product during the startup and shutdown portion of the reset time, the duty factor is taken, again optimistically, to be 0.95.

The third premise is that a magnetic poloidal field divertor will be used in either a single or a double null configuration. (See Figures 1 and 2.) The divertor serves as a pump,[8] a magnetic limiter, and as a means of reducing impurities in the discharge plasma.[9,10]

The divertor acts as a pump by providing a magnetic guide path for plasma to flow out of the discharge volume into a remote place for deionization and the eventual pumping of the resulting neutral gas. The necessity of this technique follows from the following considerations. If plasma were converted to neutral particles before leaving the discharge chamber and if, as deemed necessary for neutral beam transport through the blanket, the neutral density around the plasma were kept below 10^{12} cm^{-3} (corresponding to a pressure $< 3 \times 10^{-5}$ torr at 300 K), then to pump 1000 amperes equivalent of DT neutral molecules per second would require a black hole area, that is, a perfectly absorbing area, in excess of 20 m^2. Since the fastest pumps, cryopumps, appear at the very best to be equivalent to 1/3 of a black hole and since a particle throughput of several thousand amperes equivalent is expected, excellent pumping areas of a few hundred m^2 would be required in the wall bounding the discharge volume. This optimistic figure constitutes an

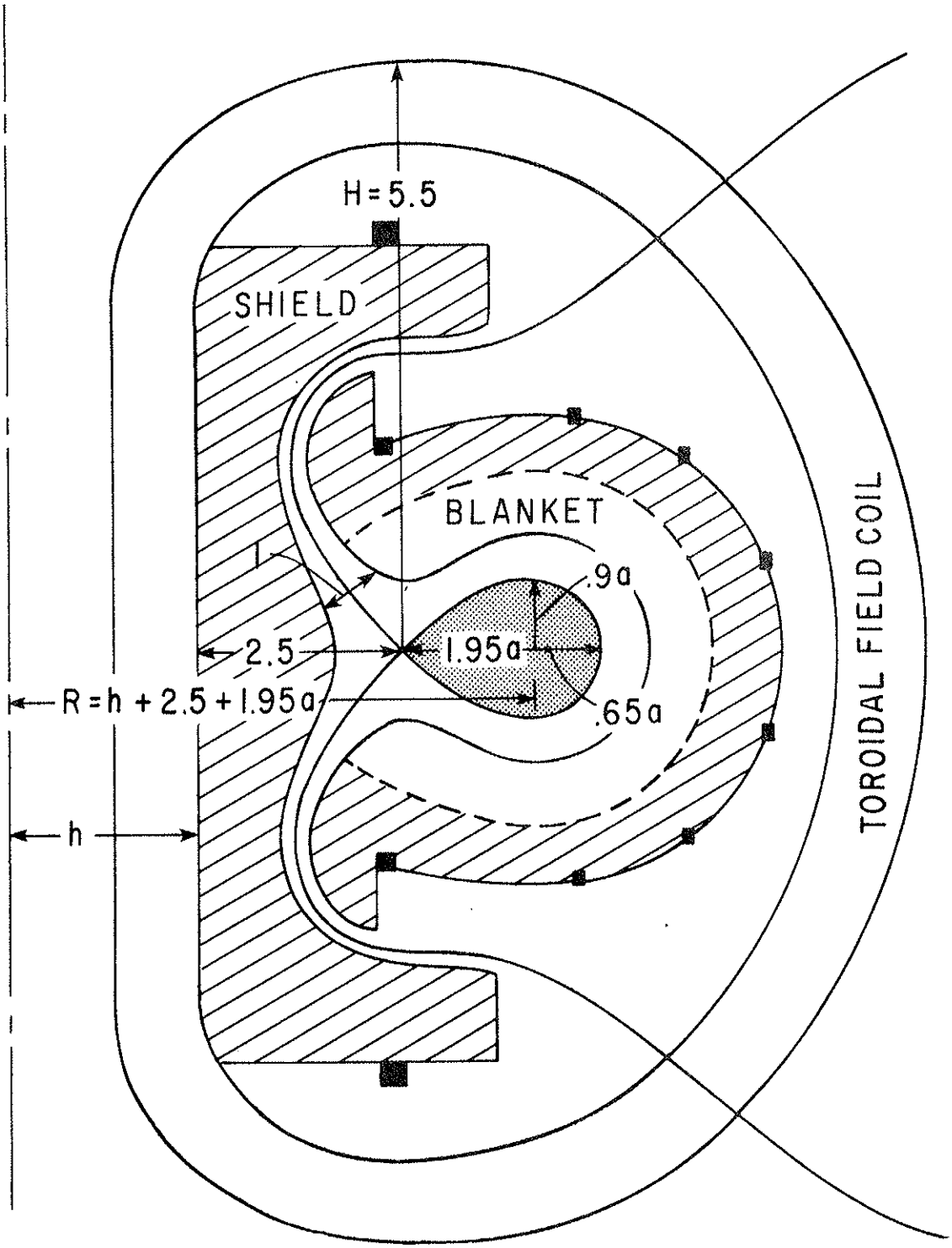

Fig. 1. Cross Section of a Single Null Configuration.

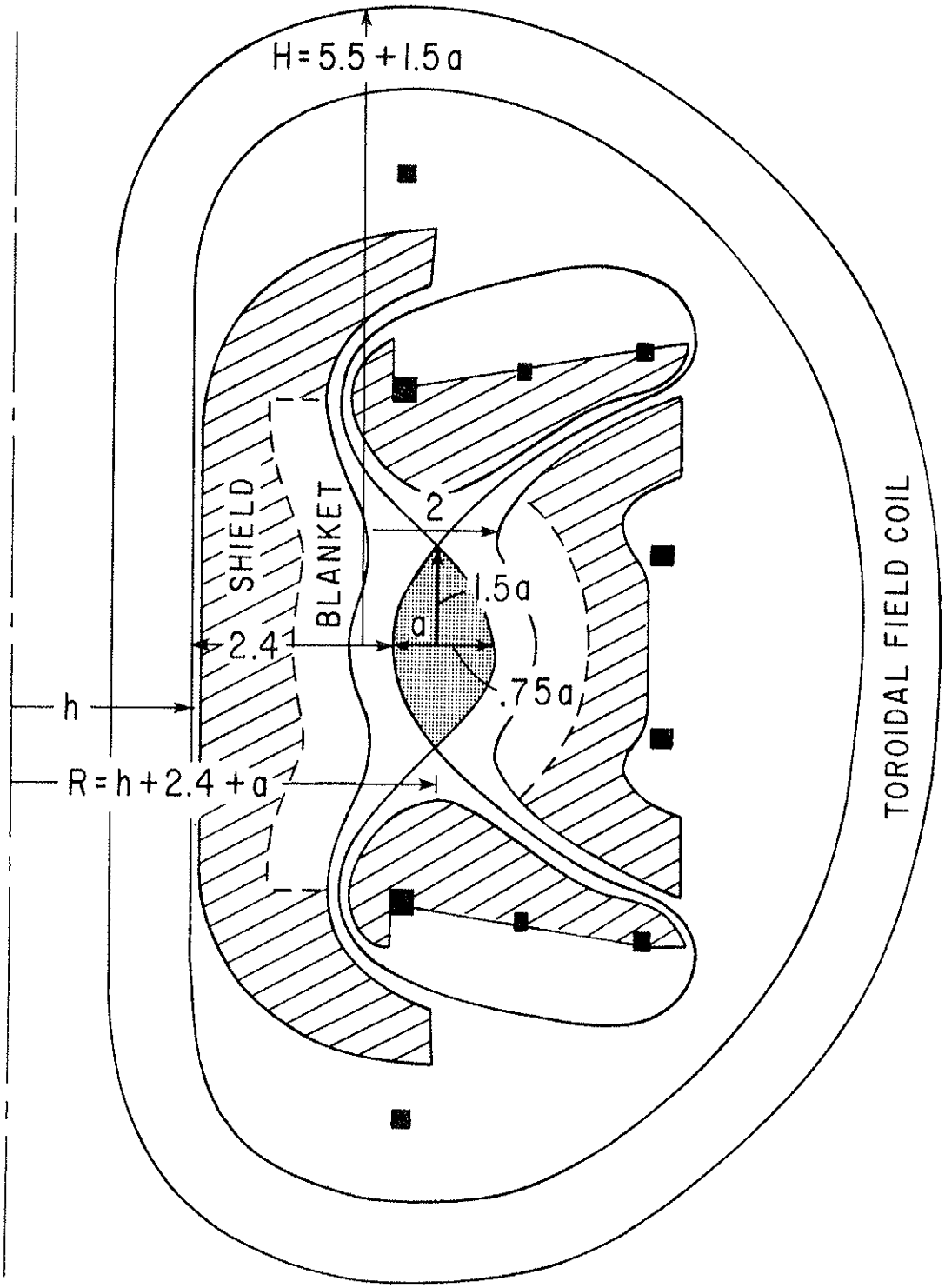

Fig. 2. Cross Section of a Double Null Configuration.

unrealistic fraction of the reactor's wall area to be devoted to pumping. Consequently the throughput of particles must be effectively removed from the discharge volume prior to neutralization while they are so energetic as to be ionized. This is the function to be accomplished by the magnetic divertor.

It has been conjectured that a magnetic divertor can be used to modify the plasma density at the edge of the discharge region and thereby modify both the radial density profile and the rate of plasma flow out of the discharge region. In turn such effects would modify the fueling requirements of the plasma. However such possibilities have not been incorporated into the analysis. It has been assumed the divertor will keep the plasma "clean", and for sake of simplicity the analysis takes $Z_{eff} = 1$.

The use of a poloidal divertor affects the geometry of the plasma, as indicated in Figures 1 and 2, and also affects the size and hence the cost of the toroidal field coils.

The fourth premise of this study is that the economics of the operation of the hybrid reactor will determine the desirability of one design over another design. Since the product of the hybrid reactor is both fissile fuel and electrical power, the most desirable design is taken to be that design which produces the lowest cost of electric power for a given price of fissile fuel. The price of fissile fuel can be viewed as a free parameter or can be related to the economics of a consumer of fissile fuel such as a light water fission reactor. In the latter

case it is imagined the hybrid reactor sells its fissile fuel to one or more fission reactors which, in turn, must adjust their price of electrical power to accommodate the expense of the fuel. The price of fissile fuel is then determined by assuming there is a common price of electricity for both the hybrid reactor and the fission reactors and that each reactor must be independently profitable. This model is referred to as the "park model." The only product of the "park" is electric power at a single price.

The overall economic attractiveness of the park will be measured not only by the cost of its electric power but by the price of fissile fuel internal to the park economics as well. For if the park price of fissile fuel is higher than the market price for fissile fuel produced outside the park, then there would presumably be no incentive for the fission reactors to purchase the more expensive fissile fuel from the hybrid reactor. The price of fissile fuel produced outside the park presumably reflects not only any enrichment costs, but the cost of ore as well. Therefore as ore becomes of lower grade and the cost of fissile fuel produced outside the hybrid rises, there will come a time when the park price of fissile fuel will become competitive. At this time the hybrid reactor will become economically attractive.

The fifth and final premise of this study relates to the design of the hybrid blanket. This subject is discussed in the next section.

Uranium has been chosen as the neutron multiplier and fertile material and hence the bred fissile material is plutonium. The primary reason for the choice of the U-Pu system instead of the alternative Th-U system is its greater productivity. This point is discussed briefly in Section II.C. The secondary reason for this choice of materials is that the neutronic cross sections available to us were better known for the U-Pu system than for the Th-U system.

References

[1]J. M. Dawson, H. P. Furth, and F. H. Tenney, Production of Thermonuclear Power by Non-Maxwellian Ions in a Closed Magnetic Field Configuration, Phys. Rev. Letters 26, 1156 (1971).

[2]H. P. Furth and D. L. Jassby, Power Amplification Conditions for Fusion-Reactor Plasmas Heated by Reacting Ion Beams, Phys. Rev. Letters 32, 1176 (1974).

[3]D. L. Jassby, Optimization of Fusion Power Density in the Two Energy-Component Tokamak, Nuclear Fusion 15, 453 (1975).

[4]F. H. Tenney, Reactor Applications of Two-Component Plasmas, IEEE Transactions on Plasma Science PS-4, 157 (1976).

[5]T. Ohkawa, New Methods of Driving Plasma Current in Fusion Devices, Nuclear Fusion 10, 185 (1970).

[6]V. V. Fomenko, Excitation of a Current in a Maxwellian Plasma by Means of an Ion Beam, Nuclear Fusion 15, 1091 (1975).

[7]A Fusion Power Plant, R. G. Mills, ed., Princeton Plasma Physics Laboratory Report MATT-1050 (1974); F. H. Tenney, A 2100 MW(e) Fusion Power Plant, Fusion Reactor Design Problems (International Atomic Energy Agency, Vienna, 1974) pp. 17-25.

[8]A. V. Georgievsky, S. L. Gralnick, D. L. Jassby, D. M. Meade, L. G. Saksogavsky, A. M. Stephanovsky, F. H. Tenney, Conceptual Design of a Divertor for a Tokamak Experimental Power Reactor, Proceedings of the Sixth Symposium on Engineering

Problems of Fusion Research (Institute of Electrical and Electronics Engineers, New York, 1976) IEEE Pub. No. 75CH1097-5-NPS, pp. 583-585.

[9]L. Spitzer, Jr., The Stellarator Concept, Phys. Fluids 1 (1958); see pp. 262-263.

[10]C. R. Burnett, D. J. Grove, R. W. Palladino, T. H. Stix, K. E. Wakefield, The Divertor, a Device for Reducing the Impurity Level in a Stellarator, Phys. Fluids 1, 438 (1958).

B. Conceptual Blanket

1. Basic Regions of the Blanket

The blanket of a pure fusion reactor is a "passive" system, transforming the fast fusion neutrons into heat and tritium. In contrast, the blanket of a hybrid is an active system, where most of the reactor energy is produced. For this reason the blanket performance model is a major element of any hybrid systems analysis code. In order to ensure that the model used in the current study is realistic, a conceptual blanket design was developed, analyzed, and parameterized. The elements of this conceptual design are described below. These are specific physical choices from among several alternatives; the Blanket Nucleonics Appendices, A, B, and C, discuss the blanket options in more detail. Insofar as the blanket model used in the systems analysis deals with abstract performance indices, alternative blanket concepts capable of the same performance are fully substitutable.

The chosen conceptual blanket consists of five functional regions: the wall, the multiplier, the burner, the scavenger, and the shield. The first and last elements provide the physical interface to other systems. The shield protects the coils from radiation that leaks through the inner regions; while the wall is the vacuum barrier between the plasma and the rest of the reactor.

The multiplier zone is the region where the fusion neutrons interact with a fast-fissionable material. Neutron multiplication by fission and stimulated emission in this region

is a key requirement for satisfactory hybrid operation. Since uncollided source neutrons are the most effective in neutron multipliers, this zone is placed directly adjacent to the wall. Since the flux of source neutrons is rapidly attenuated through this region, the law of diminishing returns restricts its thickness.

The known cheap fast-fissionable materials are, as it happens, also fertile. Thus the multiplier region will unavoidably also be a great breeder of fissile material. Although many hybrid reactor studies have taken this production of fissile fuel as the design goal, it has not been demonstrated that this is, in general, the best application of the hybrid concept. In fact, given the low price of fissile fuel and the high cost of energy, there is strong reason to suspect that a hybrid which converts its own bred fissile material into energy may be economically attractive.

To allow the exploration of this point the conceptual blanket includes a burner region, where energy may be produced from a deliberate loading with fissile fuel. This region also produces most of the tritium required to sustain the fusion cycle. The burner region lies behind the multiplier. Neutrons leaking from the multiplier (i.e., not captured by the fertile material) are thermalized in a moderator sub-region and then captured either by lithium or the fissile fuel.

Between the burner region and the shield is a scavenger zone. The purpose is to intercept the potentially large leakage of neutrons from the burner and produce tritium while reducing

the load on the shield. It is, therefore, both the first stage of the shielding system and the last stage of the blanket proper.

2. Selection of Fuel Materials

In the context of a hybrid reactor the term fuel is ambiguous, being applicable to the tritium, the lithium from which it is bred, the fissile material, the fertile material from which it is bred, and the fast fissionable material. The choice of fuels to be placed in each of the regions of the blanket determines the limits on the range of performance; operating points within this range are selected by adjusting the thickness and density of each constituent.

In this conceptual blanket the multiplier region is loaded with metallic depleted uranium fuel rods. Adequate performance of the rest of the hybrid requires a high reaction rate of the fusion neutrons with the uranium; this dictates a fuel material containing a maximum of uranium and a minimum of other nuclides. Obviously uranium is also the fertile material, and plutonium will be the fissile fuel bred for sale or for self-consumption in the burner region.

Although metallic fuel is subject to changes in shape and volume after irradiation, preliminary studies indicated that burnup greater than 1% (fissions per U atom) would not be of significant benefit to the hybrid economics. The financial advantages of frequent sales of bred plutonium and of low blanket inventories offset the increased costs of fabrication

and reprocessing. For such low burnup swelling should not become a problem, and dimensional stabilization can be achieved by alloying the uranium with, for example, 7% (by weight) of molybdenum.

The molten salt flibe - lithium beryllium fluoride - has been chosen for use in the burner and scavenger regions. Pure fusion reactor design studies have shown its suitability for breeding tritium; the molten salt (fission) reactor program has demonstrated its applicability to fission reactor technology. Therefore it seems an ideal choice for a power producing hybrid.

In both the burner region and the scavenger region the salt is nearly the eutectic, 52 m/o BeF_2 and 48 m/o LiF. However, in the burner region a small portion of the lithium is replaced by PuF_3, less than 0.25 m/o. One of the attractive features of the use of flibe is that the plutonium fraction is continuously adjustable, which allows the blanket power production to be held constant despite the continual increase in the power production by the multiplier. (Without such a control mechanism, the balance-of-plant, which dominates the plant cost, would have to be scaled to the peak power, while revenue would only scale to the average.)

The burner contains a large amount of graphite for neutron moderation; consequently the plutonium competes with the lithium for thermal neutrons. In order to minimize the expensive inventory of plutonium, the lithium in the burner is depleted to 0.1 atom % in lithium-6. On the other hand the lithium in

the scavenger region is enriched to 15% in lithium-6 to maximize the absorption of leaking neutrons. Taking the two regions together, the average lithium composition approximates the natural isotopic ratio. Thus the hybrid would consume the total output, heads and tails, of a lithium isotopic enrichment plant.

The eutectic composition of the flibe was chosen to allow the maximum temperature swing in the primary coolant. For high multiplication blankets it may be necessary to use the flibe itself as a coolant, particularly to remove the heat generated in the graphite region. Based on molten salt reactor experience this should not be difficult, since the low electrical conductivity of the salt should mitigate the problems of flow across the magnetic fields.

3. Structural and Coolant Materials

The basic structural material assumed in all parts of the conceptual blanket is stainless steel. Since the "best" steel for fusion application is not yet known, SS-316 has been used as the nominal design basis. The choice of a steel structure was dictated by a desire to be conservative where that is possible, to concentrate uncertainty in unavoidable aspects of the design.

Since most of the power in the hybrid is produced in the multiplier and burner regions, the first wall is cooled with water. This is distinctly advantageous from the mechanical standpoint, since the wall can be maintained at a comparatively low temperature, relatively free of thermal cycling. Radiation

damage limits the usefulness of steel to temperatures below about 600^{o}C, and for operation at only a few hundred degrees the first wall lifetime should easily exceed that of the plant.

The primary coolant for the rest of the blanket is helium. This is essential for the multiplier region, where the presence of materials other than uranium strongly degrades the performance. In the burner region helium is used because of its compatibility with the flibe and tritium system requirements and so that a combined cooling cycle with the multiplier is possible.

4. Blanket Configuration

A schematic illustration of the blanket configuration is shown in Figure 1. The water-cooled first wall surrounds the plasma. As the primary vacuum vessel it must conform to the shape of the plasma and divertor channel. On the inside of the torus (for the single-null separatrix design) there is only shield material between the first wall and the toroidal field coil; fortunately only a small fraction of the neutrons strike this region.

The blanket proper surrounds the plasma on the outer side of the torus. To withstand the vacuum load, the first wall is assumed to be a shell of high stiffness, for example a double-wall structure with an internal spacer web and water coolant in this space. The multiplier zone immediately outboard consists of several staggered layers of pressure tubes, each containing the metallic uranium fuel as rods or slugs cooled by helium. The

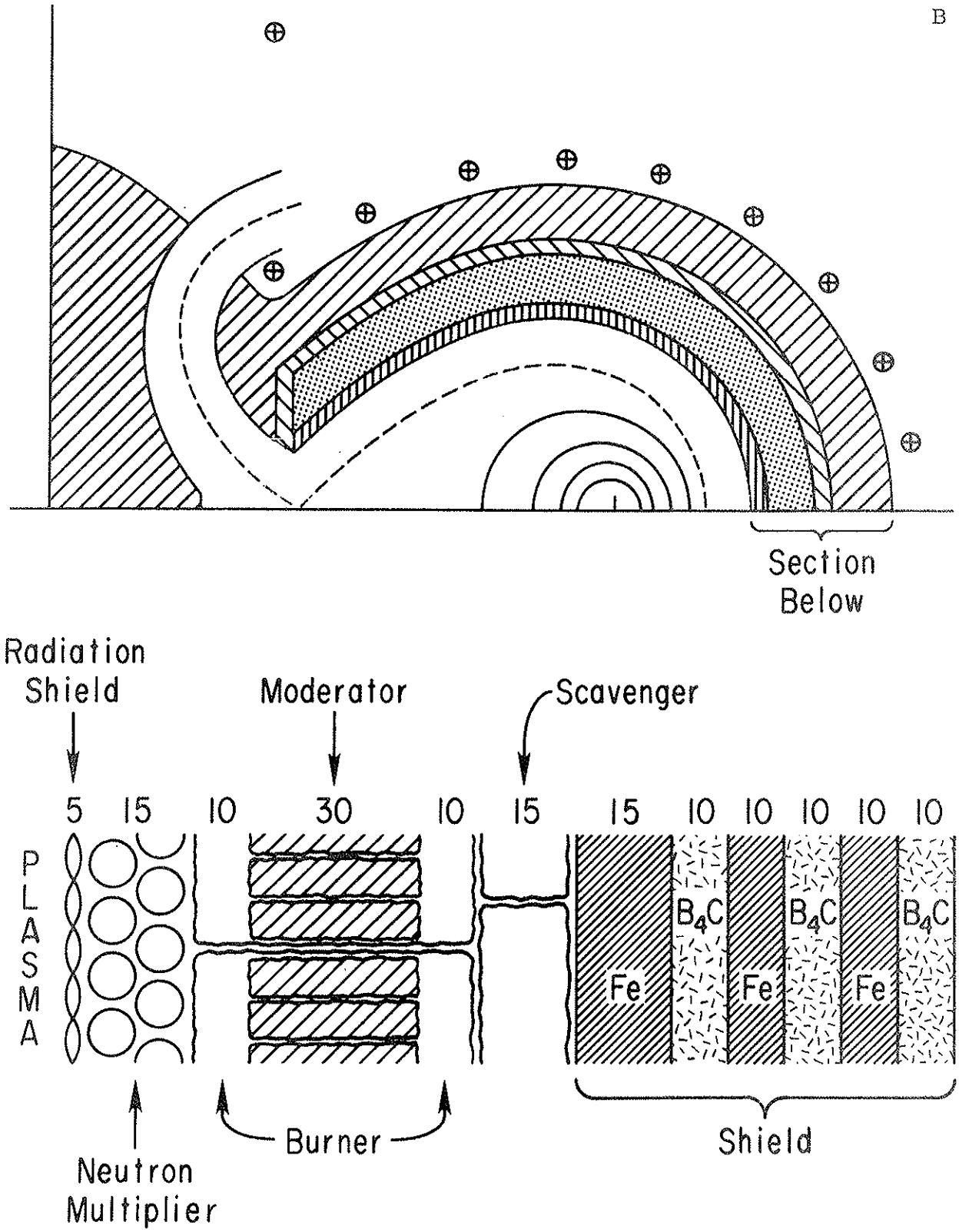

Fig. 1. Schematic Illustration of Blanket Configuration.

space between the tubes could be air or mild vacuum, vented to exhaust any helium leakage from leaking pressure tubes.

The burner region is a large steel tank, penetrated by tubing through which the primary helium coolant flows. The tank contains the flibe and an appropriate volume fraction of graphite for neutron moderation (graphite being cheaper than Pu-flibe for this purpose). Behind the burner is the scavenger zone, the separate region containing lithium-6 enriched flibe and somewhat less helium cooling.

The space between the rear of the blanket and the vertical field coils is filled with a neutron shield. In addition, the shield will extend along the sides of the divertor channel and around the neutral beam injection penetrations.

IV. Systems Analysis

A. Introduction

The methodology of this study is a systems analysis of Tokamak Hybrid Reactors. Many such systems are compared and evaluated, and the effects of the variation of parameters and constraints are determined. To do this we must first define the system, i.e., Hybrid Reactor, that is being analyzed. Our basis for this definition is the specification of a minimum set of parameters that define a unique hybrid machine. It turns out that for the modeling used it is necessary to specify six parameters (a, h, W_o, H/T, T_e, M) to do this. Each such set of parameters may be viewed as a vector in a six dimensional space. We shall refer to a particular choice of these parameters as a "six vector." An economic norm is introduced in this vector space via a costing algorithm described in Section IV.G, and using this norm we can seek solutions (i.e., six vectors) that minimize the cost of electricity produced by the tokamak hybrid reactor under various conditions. Alternatively the economic norm can be used as a basis of comparison of any selected set of six vectors. These two types of calculations, optimization and survey, have both been performed.

The construction of the parameter space in which these calculations are performed involves the reduction of the complex models describing the physical behavior of the system to a set of algebraic relationships amongst the several parameters. Thus,

for example, rather than solve an MHD equilibrium equation for each potential model machine and then test the stability of the resulting solution, the results of equilibrium code analyses were used to formulate a scaling law relating the plasma pressure and the geometric parameters of the device (see Section IV.C), and stability was assured by invoking constraints (see Section IV.F) that caused six vectors that were deemed to represent unphysical or otherwise undesirable solutions to be rejected.

The selection of the components of the six space will be described in the subsequent sections. Elements of the economic modeling are then presented followed by a description of certain constraints that are placed on the six-space. The economic norm used in the study is then described followed by a discussion of calculational techniques, and finally the results of the calculations are presented.

B. Plasma

In the quest for a set of parameters sufficient to delineate a hybrid, the formulation of the power flow (see Figure 1) determines the quantities that must necessarily be calculated, e.g., the beam power P_i, the fusion power, $P_F = Q\nu P_i$, where ν is the fraction of the incident beam power actually absorbed by the plasma, and the blanket energy multiplication, M.

Computational considerations provide the motivation for simplifying the model employed in the calculation of these quantities. The modeling process will ultimately yield a list of irreducibles, i.e., the parameters of the hybrid.

A steady state zero dimensional model has been used to describe the plasma. We consider a background plasma consisting of both deuterium and tritium at some bulk temperature common to both the ions and electrons. The composition and the temperature of this plasma are sustained by the injection of energetic neutral beams of tritons and deuterons into the plasma. The injection energy of the tritons is taken to be 1.5 times the injection energy of the deuterons to ensure equal penetration of the plasma by both beams. The velocity distribution functions for the deuterons and tritons is taken to be isotropic in direction and to be approximated by the sum of a Maxwellian velocity distribution, characterized by the bulk plasma temperature, plus a "hot" distribution of slowing down beam ions. The total reactivity of the plasma is then the sum of four reactivities: that due to the bulk plasma alone, that due to the slowing down deuterons with the background tritons, that due to the slowing down tritons with

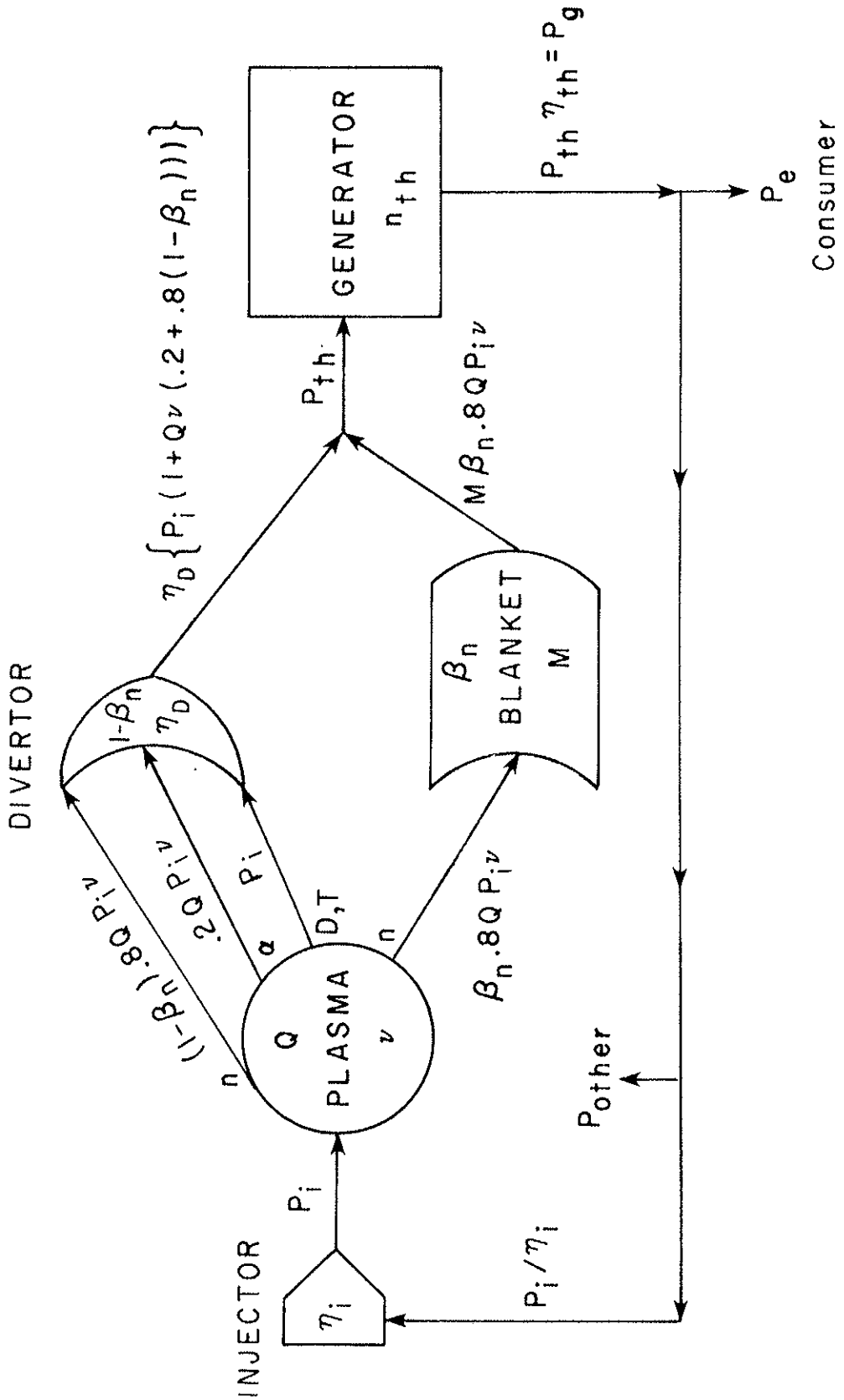

Fig. 1. Power Flow In Hybrid Reactor.

the background deuterons, and that due to the slowing down deuterons and tritons interacting with each other. Four parameters characterize the reactivity of the plasma. They are: the deuteron beam injection energy, W_o; the background plasma temperature, T_e; the ratio of the densities of the superthermal or "hot" ions to electrons, n_h/n_e; and the ratio of D to T in the background plasma. The reactivity is also proportional to n_e^2. However, the electron density is constrained by considerations of both beam penetration and the maximum plasma pressure that the tokamak discharge can sustain. To illustrate the manner in which the model works some preliminary calculated results of this plasma model are presented in Figures 2-5 which are taken from Ref. 1.

Figure 2 presents Q, the ratio of total fusion power produced to total beam power deposited in the plasma versus n_h/n_e. Q is insensitive to the absolute value of n_e. Here a 50:50 mixture of D and T in the background plasma has been assumed as well as complete retention of the fusion alpha particles during their slowing down. For plasmas rich in superthermal ions the value of Q tends to be limited to that achievable by the beam-plasma and beam-beam interactions alone. The values of the plasma energy confinement time parameter $n_e\tau_E$, shown in dotted curves, are relatively low in order to accommodate the high beam power. The reverse is true for plasmas that are lean in superthermal ions. The higher values of Q reflect the larger fraction of the plasma reactivity being produced by the thermal background plasma rather than by the beams. Also, with the reduction of plasma heating by the beams it is necessary to reduce the

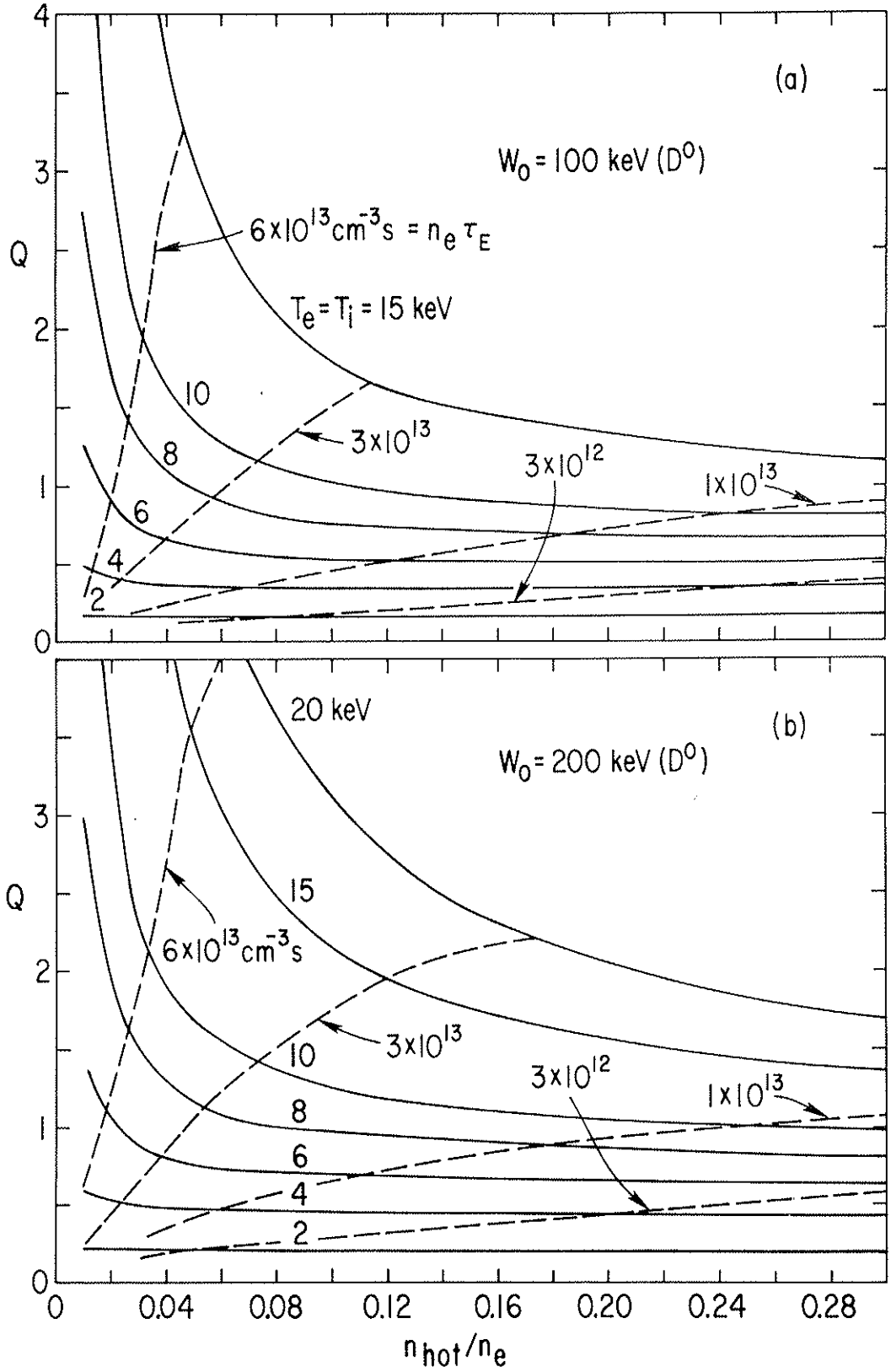

Fig. 2. Q, the ratio of total fusion power produced to total beam power deposited in the plamsa versus n_h/n_e.

energy loss rate from the plasma, and hence relatively high values of $n_e\tau_E$ are necessary. The value of $n_e\tau_E$ is thus to be viewed as a requirement on the plasma behavior that is determined by the choice of other parameters in the plasma model.

Total fusion power and wall loading of an entire reactor can be approximated with the plasma model provided additional assumptions are made regarding the plasma geometry and the strength of the toroidal and poloidal magnetic fields. The results shown in Figures 3 to 5 apply to circular plasmas with: the aspect ratio equal to four; the "safety factor," q, equal to 2.5 at the edge of the plasma; and the plasma pressure being limited by either "beta-poloidal" (the ratio of plasma pressure to the pressure of the poloidal magnetic field) equalling two-thirds the plasma aspect ratio or the e-folding length of beam penetration equalling half the plasma minor radius.

Figure 3 relates Q to the total fusion power developed in different sizes of plasma. For a choice of W_o and n_h/n_e there is a unique relationship among Q, T_e, and $n_e\tau_E$ as indicated in Figure 2. (The "uniqueness" is a consequence of the insensitivity of the product $n_e\tau_s$ to changes in density. Here τ_s is the "slowing down" time for the injected particles.) For reactors with plasma minor radii greater than 1 meter it is apparent that a blanket multiplication of 10 can lead to thermal power levels of a few gigawatts and for values of $n_e\tau_E$ in the vicinity of 10^{13} sec cm^{-3}. Furthermore there is a maximum fusion power for a fixed plasma size. Conceptually one arrives at this maximum by somehow adjusting the value of $n_e\tau_E$.

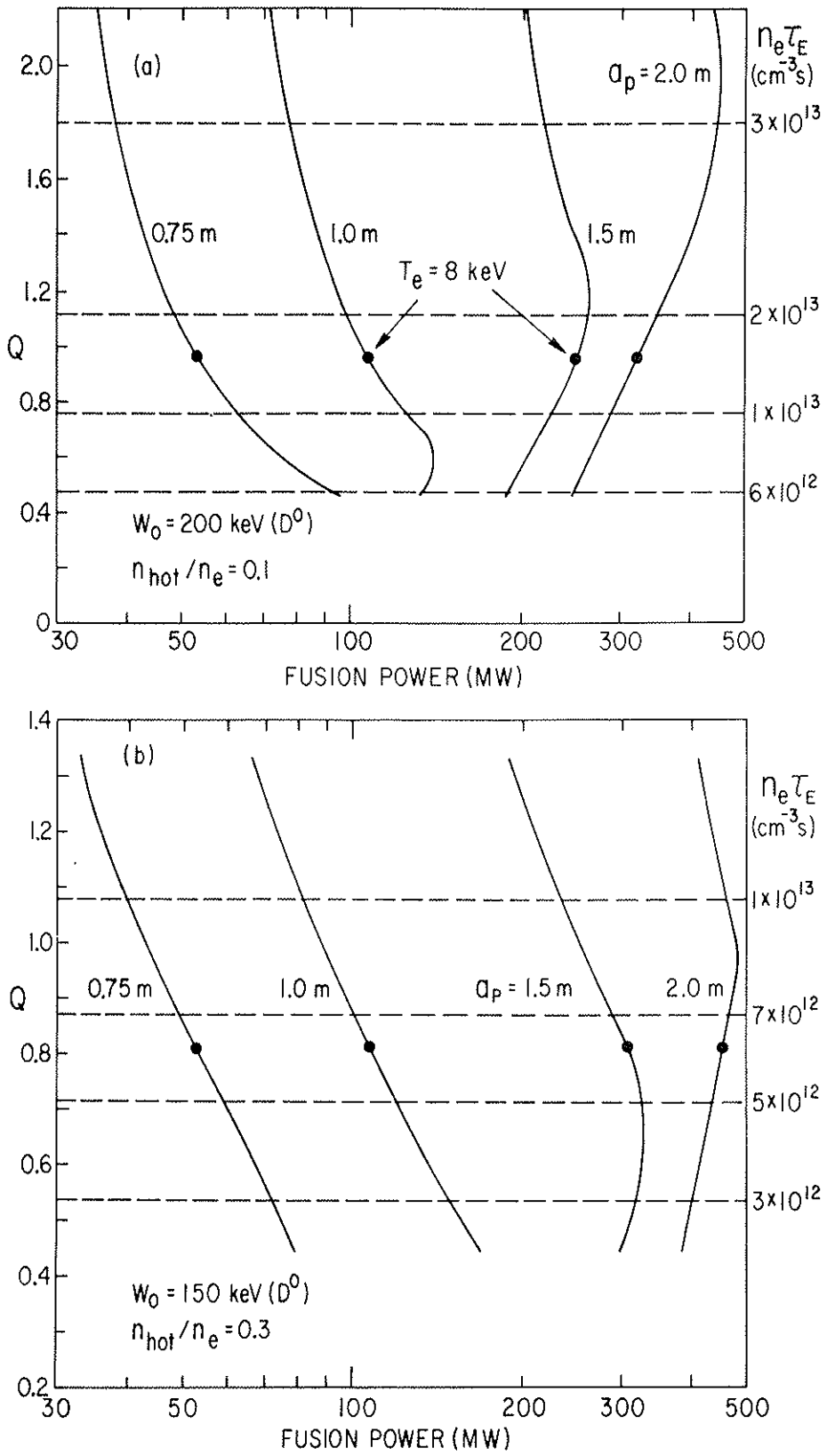

Fig. 3. Relation of Q to total fusion power developed in different sizes of plasma.

Figure 4 displays the neutron wall loading versus W_o for various plasma sizes. (The wall is taken to lie 20 cm beyond the plasma in these calculations.) The maximum in wall loading is created by the limitations placed on the plasma density. For low values of injection energy, the plasma density is being limited by the requirement that the beams penetrate sufficiently deep into the plasma. At high values of injection energy the density is limited by the limit placed on beta-poloidal. The main effect of increasing n_h/n_e seems to be to shift the maxima in wall loading to lower values of injection energy. This shift is caused by the beta-poloidal limit of the plasma being reached at lower injection energies when the relative population of energetic ions is increased. Generally the wall loadings are less than 1 MW/m^2.

Figure 5 displays another consequence of the limitations on plasma density. Here the wall loading is given versus the toroidal magnetic field. The "knee" in the curves occurs when the plasma pressure is limited simultaneously by the beta-poloidal and beam penetration constraints. For magnetic fields below the knee, the plasma pressure is being limited by the value of beta-poloidal. Hence increasing the toroidal magnetic field allows the discharge current to be increased - in order to preserve the assumed value of $q = 2.5$ at the plasma surface - and hence the poloidal field strength and hence the plasma pressure. In this part of the curve the wall loading reflects the plasma pressure and displays a B^4 dependence. However, for magnetic fields above the knee the pressure is limited by the requirement of beam

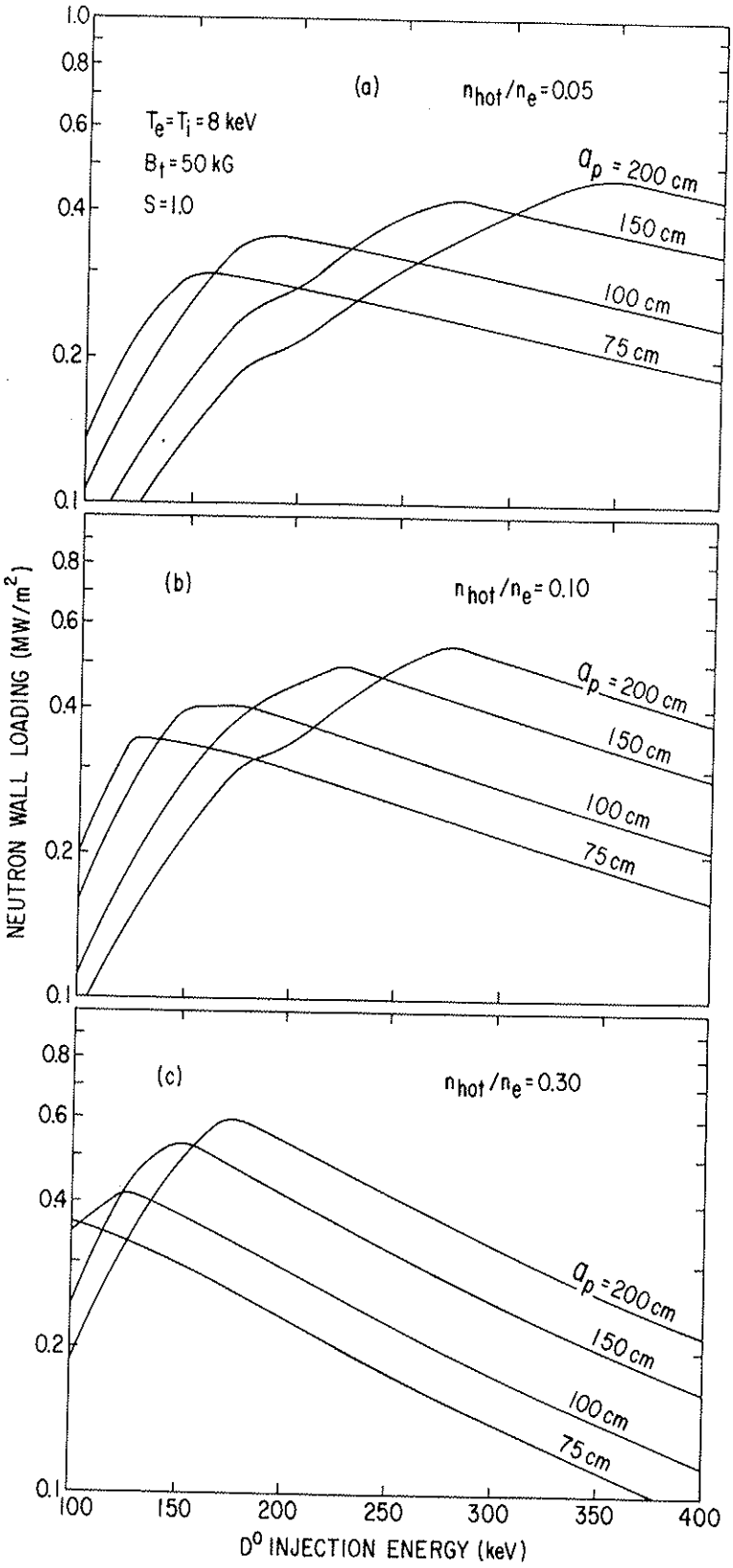

Fig. 4. Neutron wall loading versus W_o for various plasma sizes.

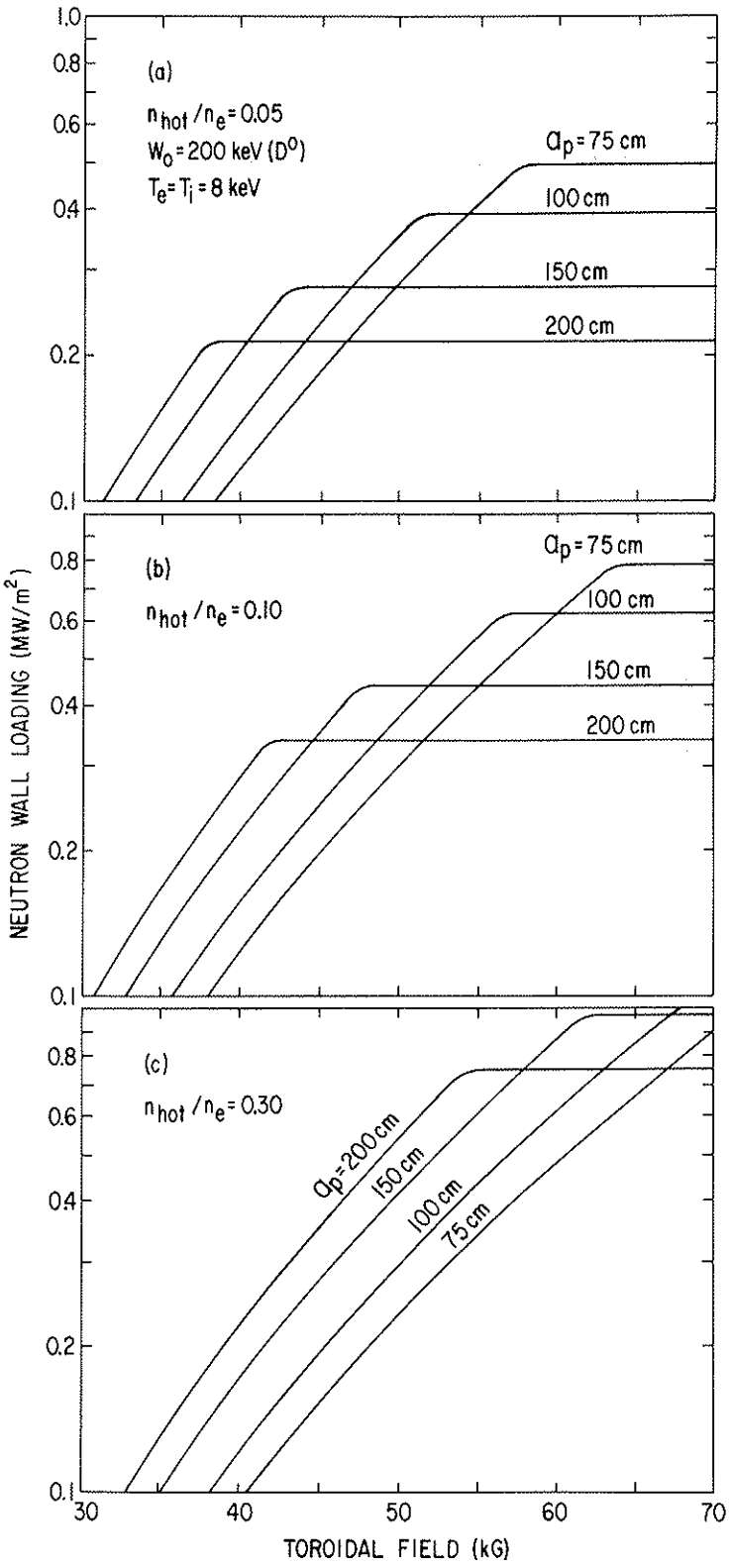

Fig. 5. Wall loading versus the toroidal magnetic field.

penetration and therefore cannot increase with higher magnetic fields. Thus smaller plasma sizes can capitalize on higher magnetic fields and hence higher densities before becoming beam penetration limited. Another feature of the curves in Figure 5 is the increase in maximum wall loading at the knee with an increase in the relative population of hot ions. This effect is a consequence of the interplay between the beta-poloidal limitations and the requirement for beam penetration. To see this effect consider that for a beta-poloidal limited plasma, an increase in hot ion density requires a proportionally larger decrease in the cooler background ion density and hence a decrease in the electron density. Now at T_e = 8 keV the reactivity is dominated by the sum of the beam-plasma and beam-beam interactions and is rather weakly affected by an increase in (n_h/n_e). However the beam penetration depth varies almost inversely with the electron or background ion density and will therefore increase with (n_h/n_e). Thus an increase in $n_{h/}n_e$ will allow an increase in pressure without violating the beam penetration limit. To reach the beam penetration limit the magnetic field must be increased to allow the increase in pressure, which in turn will increase the wall loading at the knee.

We now turn to a more detailed account of the plasma modeling and the power flow within the hybrid.

The first quantity to be considered is the beam power, νP_i, absorbed by the target plasma. Here P_i is the beam power incident upon the plasma and ν is the fraction of P_i actually absorbed by the plasma. Since one function of the beams is to

contribute to the refueling of the plasma both deuterium and tritium beams are used. Since the plasma is comprised of deuterium and tritium in a ratio of densities n_D/n_T, the beams are injected at rates, S, consistent with the assumption that both D and T are lost from the plasma at an equal rate, i.e.,

$$\frac{S_D}{S_T} = \frac{n_D}{n_T} \quad . \tag{1}$$

Furthermore, to obtain equal penetration of the plasma by the beams the velocities of the injected D and T atoms are assumed equal in magnitude. Since all of the collisional processes involving the beams are a function of relative speed only, the D and T beams are extracted from the injectors, transported through beam lines, and absorbed by the plasma with identical efficiencies for each process. Consequently, the beam energy, W_o, of only the deuterium need be specified.

The presence of the beams will give rise to a suprathermal population of ions. Charge neutrality requires that the electron density equal the ion density, i.e.,

$$n_e = n_D + n_T + n_{hot} \quad . \tag{2}$$

The alpha particle density is assumed negligible in Eq. (2) but not for the pressure calculation treated below. If the small alpha particle contribution to n_e had been retained in Eq. (2), the calculational procedure would have been burdened with an additional iterative procedure because the density of alpha particles depends both on n_e (through the slowing down process) and on the reaction rate that, in turn, scales with n_e. The hot population, n_{hot}, of Eq. (2) is comprised of hot D and hot T, i.e.,

$$n_{hot} = n_{hotD} + n_{hotT} \quad . \tag{3}$$

The hot ion densities of Eq. (3) may be related to their respective injection rates appearing in Eq. (1) through the ion distribution function.

The ion distribution function follows from the plasma model which is taken to be a thermal background plasma into which suprathermal ions of D and T are isotropically injected. The background plasma ions are represented by a Maxwellian distribution function,

$$f_i(v) = n_i \left(\frac{b^2}{\pi}\right)^{3/2} \exp\left(-b^2 v^2\right), \tag{4}$$

where $b^2 \equiv m_i/2T_i$. The suprathermal ion velocity distribution results from the energetic injected ions slowing down in the background plasma and is taken to be the sum of two functions, $f_{1i}(v)$ and $f_{2i}(v)$, respectively describing the ions with speeds below and above the injection speed, v_o. Assuming that the losses from the slowing down ion population are negligible while the ions are slowing down, we take $f_{1i}(v)$ to simply reflect the conservation of ions in velocity space, namely:

$$4\pi v^2 \left(\frac{dv}{dt}\right)_i f_{1i}(v) = \text{Const.} = -S_i \quad . \tag{5}$$

Here S_i is the injection rate of the ith species of ion, and $\left(\frac{dv}{dt}\right)_i$ is the rate of slowing down calculated according to the prescription of Sivukhin,[2] namely:

$$\left(\frac{dv}{dt}\right)_i = \frac{-4\pi e^2}{mv^2} \sum{}^{*} L\, n^* e^{*2} \left[\frac{\Phi(b^* v)}{m^*} - \frac{2b^* v(m+m^*)}{mm^*\sqrt{\pi}} e^{-b^{*2} v^2} \right] \quad . \tag{6}$$

Here $\Phi(b^* v)$ denotes the error integral, the symbol Σ^* means the sum over all the species of background particles labelled by the symbol *, $b^{*2} \equiv m^*/2T^*$, and L is the coulomb integral. We further take all species of background particles to have the same temperature T.

Eq. (6) describes a "convective flow" in velocity space. The principal effect of accounting for the diffusion of the injected ions in velocity space is the existence of an energetic "tail" of ions above the injection speed, v_o, given by the function.[3]

$$f_{2i}(v) = f_{1i}(v_o) \exp \left[- b^2 (v^2 - v_o^2)\right] \quad . \tag{7}$$

This distribution falls off rapidly above v_o, but because the fusion cross sections are high for this speed range, the diffusive effects probably account for a 5% to 10% increase in the calculated reaction rates of the plasma. Examples of plasma reactivity using this modeling, and applied to plasmas of circular cross section and simple pressure constraints, can be found in Refs. 1 and 4.

The hot ion densities used in Eq. (3) are then found by the formula,

$$n_{\text{hot } i} = 4\pi \int_{v_1}^{v_o} f_{1i}(v)\, v^2 dv + 4\pi \int_{v_o}^{\infty} f_{2i}(v) v^2 dv \quad . \tag{8}$$

Here the lower limit of integration, v_1, is chosen to approximate where the hot ion distribution function equals the background Maxwellian function. The reactivity of the plasma is relatively

insensitive to v_1, which, in turn, is a relatively insensitive function of the ratio, n_{hot}/n_e. We have chosen $v_1 = \sqrt{8T/m_i}$.

The incident beam power, P_i, is thus a function of injection energy, W_o; relative D and T concentrations, $n_D/(n_D+n_T)$; the fraction of suprathermals, n_{hot}/n_e; the temperature, T; and the electron density, n_e.

The hybrid is operated at the value of $n_D/(n_D+n_T)$ that maximizes the fusion power, P_F. The optimal value of this fraction ranges from 0.5 for ignited plasmas to 0.55 for heavily beam driven plasmas.

The electron density, n_e, is determined through a limitation on the total plasma pressure that is discussed below in Section IV.C. The plasma pressure, P, is the sum of the partial pressures associated with the background plasma, the beams, and the energetic alpha particles from the fusion reactions. We take

$$P = n_e \left[T\,(2 - n_{hot}/n_e) + \frac{1}{3} W_o\, n_{hot}/n_e \left[\frac{1 + \frac{3}{2}\gamma}{1+\gamma}\right] + 6.64 \times 10^{-16}\, P_\alpha\, \tau_{sd}^{\alpha} \right] \ (\mathrm{keV/cm^3}) \quad . \tag{9}$$

Here

$$\gamma \equiv \frac{n_{hotT}}{n_{hotD}} \quad . \tag{10}$$

The numerical approximation to Eq. (10) (that is accurate to better than 10%) used in our calculations is

$$\gamma = 5(.45 - \frac{n_D}{n_D+n_T}) + 2 \quad . \tag{11}$$

The beam and alpha partial pressures of Eq. (9) are taken to be two-thirds of the average particle energy. The average particle energy is taken to be half the initial particle energy. The origin of the alpha particle pressure is predominately those alpha particles of high energy. The time, τ_{sd}^{α}, an alpha particle spends in slowing down in the background plasma

$$\tau_{sd}^{\alpha} \equiv \int_{E_o}^{2T} \frac{dE}{\frac{dE}{dt}} \quad . \tag{12}$$

The energy loss rate, dE/dt, in Eq. (12) is calculated via Eq. (6) and the relation dE/dt = mv dv/dt.

The alpha power, P_{α}, absorbed by the plasma is

$$P_{\alpha} = r f_{\alpha} P_F \tag{13}$$

where r is a measure of the alpha particle confinement. It has been assumed that r will exceed 0.8 and has been taken, somewhat arbitrarily, to be 0.832. The fraction, f_{α}, of the total fusion power density, P_F, in alpha particles is taken as 3.5/17.6. The calculation of P_F includes the thermal reactions, the beam-background reactions, and the beam-beam reactions of all plasma species, i.e., D-T, D-D, and T-T. However, the D-T reactions dominate all other reactions so that there is little loss of accuracy in this selection of f_{α}.

The fusion power density, P_F, is just the product of the general reaction rate, R_{α}, and the energy released per reaction of species 1 and 2, E_{12}. Thus

$$P_F = E_{12} R_{\alpha} \quad . \tag{14}$$

The reactivity of the plasma is calculated as follows. The reacting ions are characterized according to their distribution function as either thermal ions or suprathermal ions. All the possible types of interactions among these species yield the following decomposition of R_α:

$$R_\alpha = R_{TT} + R_{ST} + R_{SS} \quad . \tag{15}$$

The subscripts T and S of Eq. (15) denote the reacting species, i.e., thermals and suprathermals, respectively. The terms R_{TT}, R_{ST}, and R_{SS} are calculated via the equation,

$$R = \int\int f_1 \, f_2 \sigma(|\bar{v}_1 - \bar{v}_2|) \, |\bar{v}_1 - \bar{v}_2| \, d\bar{v}_1 \, d\bar{v}_2 \quad , \tag{16}$$

where the distribution functions, f_1 and f_2, are the appropriate distributions appearing in Eqs. (4) - (7) as determined by the type of interaction, e.g., beam-beam, etc., and σ is the fusion cross section.[5] The terms R_{TT}, R_{ST}, and R_{SS} of Eq. (15) are

$$R_{TT} = n_1 \, n_2 \left(\frac{1}{2\pi m_1}\right)^{\frac{1}{2}} \left[\frac{m_2}{(m_1 + m_2)kT}\right]^{\frac{3}{2}} \int_0^\infty dE \; E\sigma(E) \exp\left(\frac{-m_2 E}{(m_1 + m_2)kT}\right), \tag{17}$$

$$R_{ST} = 8n_2 \, \frac{\pi m_2}{RT} \int_{\sqrt{\frac{8RT}{m_1}}}^\infty dv_1 \; v_1^2 \, f_1(v_1) \int_0^\infty dv_2 v_2^2 \sigma(\tfrac{1}{2} m_1 v_R^2) \exp \frac{-m_2(v_2^2 + v_1^2)}{2kT} \cdot |v_R| \sinh \frac{(m_2 v_1 v_2)}{kT} \quad , \tag{18}$$

$$R_{SS} = 8\pi^2 \int_{\sqrt{\frac{8RT}{m_1}}}^\infty dv_1 v_1^2 \int_{\sqrt{\frac{8RT}{m_2}}}^\infty dv_2 v_2^2 \int_{-1}^1 d\mu \; f_1(v_1) \, f_2(v_2) \, |v_R| \sigma(\tfrac{1}{2} m_1 v_R^2) \quad , \tag{19}$$

where $$v_R^2 = v_1^2 + v_2^2 - 2 \, \underline{v}_1 \cdot \underline{v}_2 \quad .$$

T is the plasma temperature, and m_i, v_i and n_i are the mass, velocity, and density, respectively, of ion, i, which is either an incident or background ion denoted by i = 1 or i = 2, respectively. The above equations, 17 through 19, are valid for a point model. For a discussion of the effects of introducing density and temperature profiles upon the reaction rate calculations see Appendix II.

The density dependence of P_α and τ_{sd}^{α} of Eq. (9) can be demonstrated to be:

$$P_\alpha \propto n_e^2 \quad , \tag{20a}$$

and

$$\tau_{sd}^{\alpha} \propto n_e^{-1} \quad . \tag{20b}$$

The above formulae permit the tabulation of the quantities P_α and τ_{sd}^{α} at a particular density, e.g., 10^{14} cm^{-3}, with extrapolation to other densities according to the proportionalities (20a,b). The extrapolation process is found to have an inaccuracy of $\leq$ 5% within the density range of interest, i.e., 10^{13} - 10^{15} cm^{-3}. Furthermore, the calculation of P_α at $n_e = 10^{14}$ cm^{-3} for arbitrary values of the variables, W_o, T, n_{hot}/n_e, and $n_D/(n_D + n_T)$, is performed by an interpolation in a lattice of the aforementioned variables. A quadratic polynominal, fitted to the precalculated values of P_α in the lattice, is the basis of the interpolation algorithm, thereby introducing another inaccuracy of $\leq$ 5% in the calculation of P_α. The interpolation format required that the range of the variables be fixed a priori:

$$150 \leq W_o \leq 300 \text{ keV} \tag{21}$$

$$0.45 \leq n_D/(n_D + n_T) \leq 0.65 \tag{22}$$

with either

$$6 \leq T \leq 16 \text{ keV} \tag{23}$$

and

$$0.04 \leq n_{hot}/n_e \leq 0.3 \tag{24}$$

or

$$6 \leq T \leq 18 \text{ keV} \tag{25}$$

and

$$0 \leq n_{hot}/n_e \leq 0.04 \quad . \tag{26}$$

The ranges of Eqs. (21-24) represent the authors' initial estimate of interesting TCT operating parameters. As the study proceeded, the parameter range was extended with Eqs. (25) and (26) to permit ignition of the plasma.

The list of plasma characteristics is completed with the specification of the operating pressure, P. The criterion adopted for determining P is that it be maximized under certain constraints and is discussed in the following section, IV.C. Specification of P resulted in the introduction of three new parameters: the minor radius of the plasma, a; the toroidal field coil location, h; and the pressure profile parameter, α.

The final quantity to be determined for the power balance of Figure 1 is the blanket multiplication, M. By specifying the gross electric power, P_g, the conservation of energy principle dictates what M must be. Constraints are then imposed upon M to yield only achievable values of M. The blanket properties associated with each value of M are described in Section IV.D.

The major quantities necessary to calculate P_i, Q, and M in the power flow are now complete. Several other quantities remain to be calculated or specified, e.g., n_T and n_i and are described in other sections. However, the major calculations described above have specified the hybrid parameters. To recapitulate, they are: the deuterium injection energy, W_o; the fraction of the density that is suprathermal, n_{hot}/n_e; the plasma temperature T; the minor plasma radius, a; the location of the inside edge of the TF coil, h; and the gross electric power, P_g. These six parameters and subsets thereof are those parameters that are permitted to vary in both the survey calculations and the optimization process.

References

[1]D. L. Jassby and H. H. Towner, Fusion Reactivities and Neutron Source Characteristics of a Beam-Driven Toroidal Reactor with Both D and T Injection, Princeton Plasma Physics Laboratory Report MATT-1180 (1976).

[2]D. V. Sivukhin, Coulomb Collisions in a Fully Ionized Plasma, Reviews of Plasma Physics, M. A. Leontovich, ed. (Consultants Bureau, New York, 1966) Vol. 4, pp. 93-128.

[3]E. A. Frieman, private communication.

[4]F. H. Tenney, A Tokamak Hybrid Study, Proceedings of the US-USSR Symposium on Fusion-Fission Hybrid Reactors (National Technical Information Service, Springfield, Virginia, 1976) Conf-760733, pp. 71-80.

[5]B. H. Duane, Fusion Cross-Section Theory, Battelle Northwest Laboratories Report BNWL-1685 (1972).

C. Scaling of Beta and Size

To incorporate poloidal field divertors into the hybrid design requires both special coil designs and judgments as to maximum allowable pressures sustainable in the non-circular plasmas bounded by a separatrix. The coil locations must allow ample space for both the blanket and shielding and a gap between the plasma edge and the first material wall.

To explore these considerations rather extensive numerical explorations were made of several axisymmetric toroidal equilibria for separatrix-bounded plasmas of both the single null and double null variety. These explorations extended over major radii from 5.5 m to 15 m.

The axisymmetric plasma equilibria are described by the Grad-Shafranov equation for the poloidal magnetic flux, $\Psi(X,Z)$:

$$X\frac{\partial}{\partial X}\left(\frac{1}{X}\frac{\partial \Psi}{\partial X}\right)+\frac{\partial^2 \Psi}{\partial Z^2} = -4\pi^2\left(X^2\mu_o\frac{\partial p}{\partial \Psi} + R^2\frac{B_o^2}{2}\frac{\partial g^2}{\partial \Psi}\right) \qquad (1)$$

$$= 2\pi X J_\phi$$

Here X, Z, ϕ are cylindrical coordinates, $p(\Psi)$ is the plasma pressure, and $g(\Psi) = XB_\phi/(RB_o)$ where B_ϕ is the toroidal magnetic field. At the magnetic axis $X = R$ and $B_\phi = B_o$. (Eq. (1)) follows from the equations,

$$\nabla \times \underline{B} = \mu_o \underline{J}$$

and

$$\nabla p = \underline{J} \times \underline{B} ,$$

plus the assumption of axisymmetry.) Eq. (1) was solved numerically under the assumptions of

$$p(\psi) = p_o\left(\frac{\psi_\ell - \psi}{\psi_\ell - \psi_o}\right)^\alpha \tag{2}$$

and

$$g(\psi) = 1 + g_o\left(\frac{\psi_\ell - \psi}{\psi_\ell - \psi_o}\right)^\alpha \tag{3}$$

where the subscript, ℓ, refers to values at the bounding surface of the plasma and the subscript, o, to values at the magnetic axis and where we assume $g_o << 1$. Most of the calculations were done with the profile parameter, α, set equal to 2.

The equilibria were characterized by two constraints, namely: the plasma q ("safety factor") > 1.0 at the magnetic axis, and $J_\phi > 0$ everywhere in the plasma. The first constraint prevents the onset of the Kruskal-Shafranov magnetohydrodynamic instability. The second constraint is an intuitive statement that current distributions in which J_ϕ can take on both positive and negative values will be unstable, the positive and negative current channels tending to rotate about each other. Since J_ϕ tends to become negative as the ratio, $\beta \sim p/B^2$, is increased, the second constraint serves to limit β.

Sample configurations are shown in Figures 1 and 2. These figures illustrate the view that the separatrix surface must extend far from the plasma to provide a well-shielded area for pumping. In addition, these designs incorporate a minimum of 1 m of shielding for coils and structure in direct line with the plasma, upwards to 0.5 m of shielding for regions subject

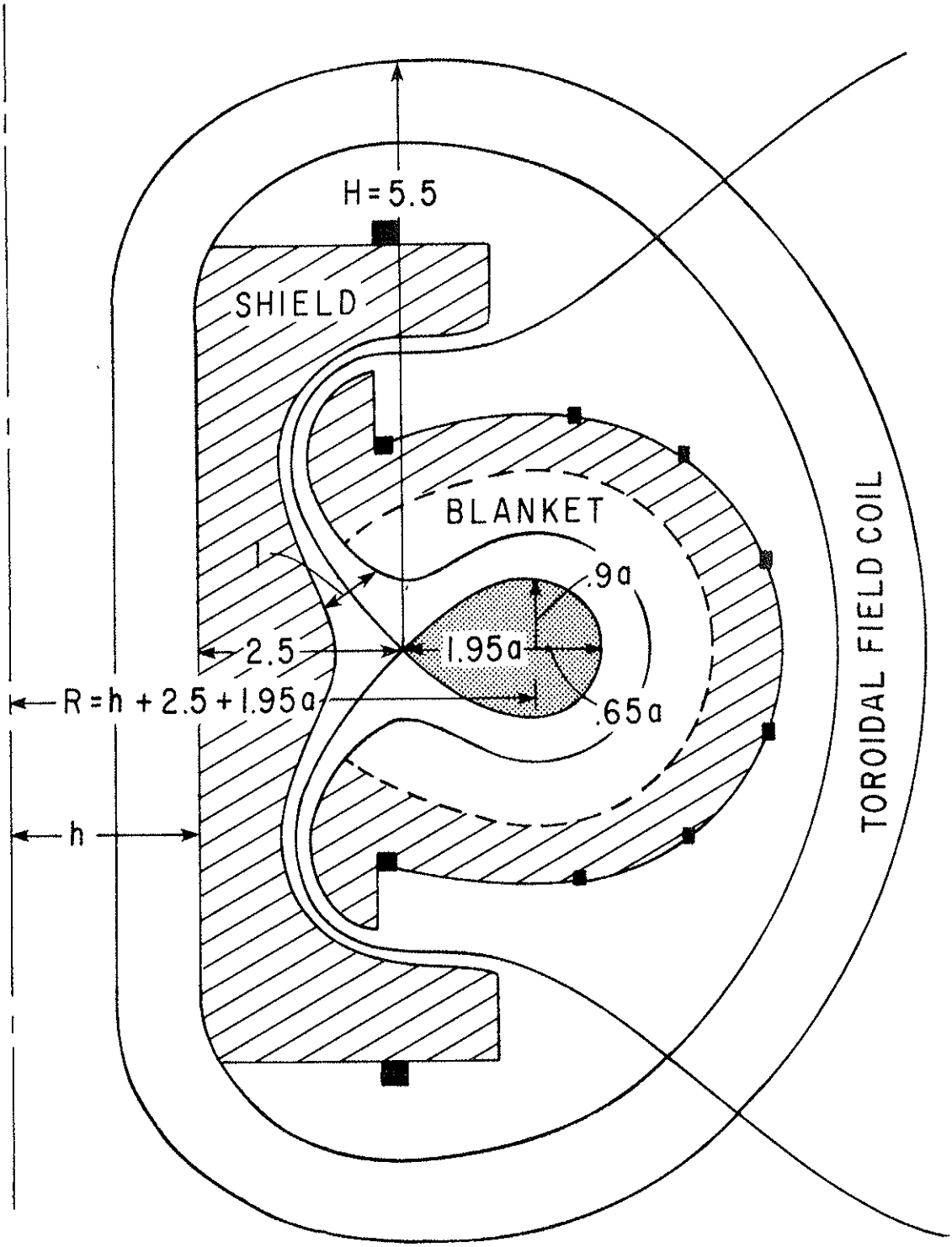

Fig. 1. Cross Section of Single Null Configuration.

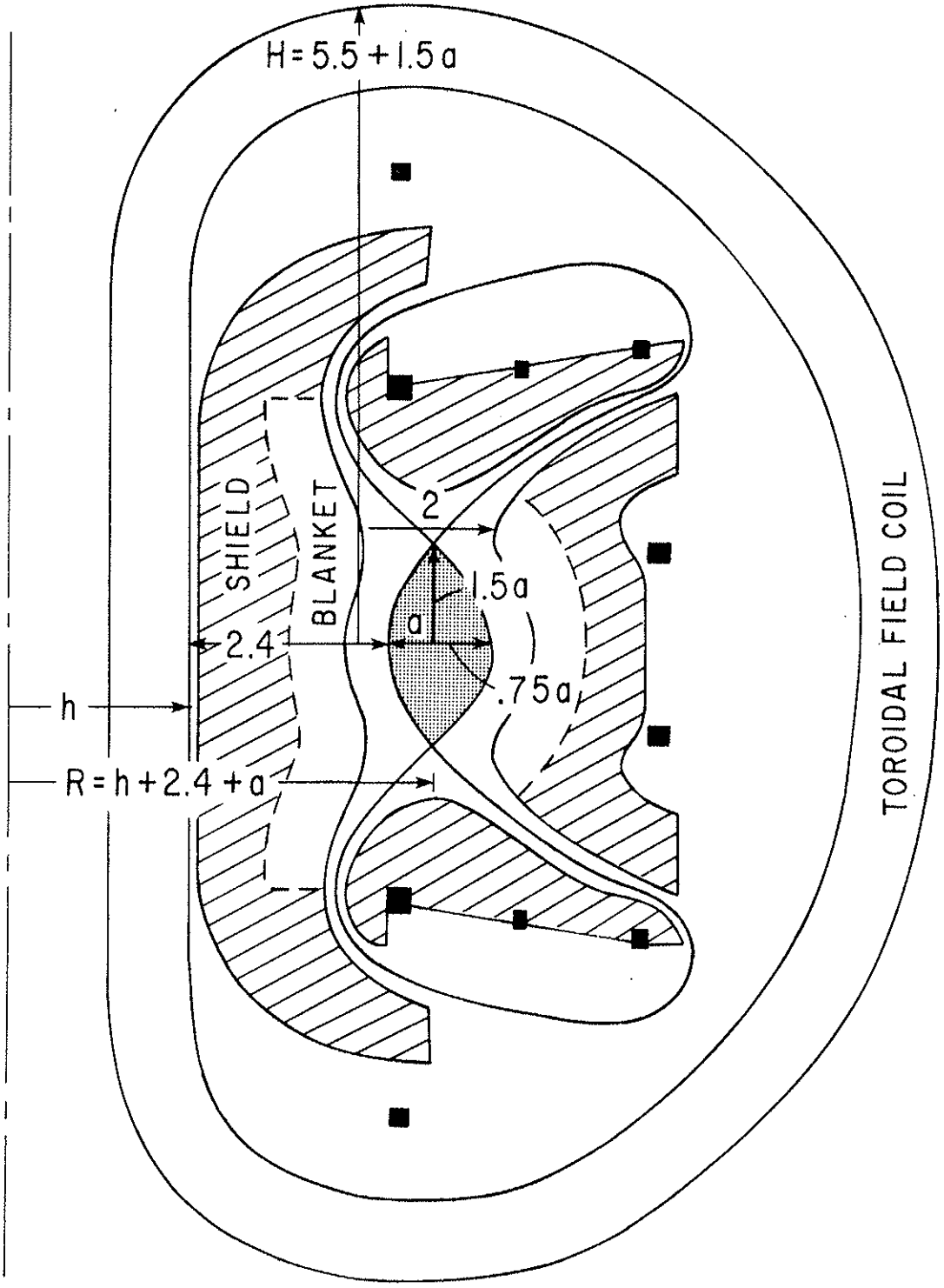

Fig. 2. Cross Section of Double Null Configuration.

to neutron streaming, and a 0.5 m clearance between the separatrix and the first wall of the blanket.

In the case of the single null configuration, the above criteria impose no constraints on the design regardless of plasma size. It is easy to create the necessary vacuum poloidal field with coils placed far from the plasma thus allowing ample space for the blanket to provide structural shielding. The path of the separatrix passes conveniently into a pumping region without approaching any of the field coils too closely.

In contrast the double null configuration requires coils (assumed to be superconducting) carrying relatively large currents to be located comparatively close to the plasma. This circumstance creates difficulties in shielding these coils. The physical size of the coils was based on an effective current density of 1275 A/cm^2. This figure allows sufficient room for dynamic stabilization of the superconductor, support structure, and liquid helium Dewars. It is also difficult to guide the separatrix away from the plasma to a pumping area and maintain adequate width of the divertor channels while still providing adequate shielding of the coils that perform this function. These problems are particularly acute in the smaller machines.

The style of the vacuum poloidal field for the single null configurations is shown in Figure 3. The separatrix surface is also indicated. There are several points of interest here. First is the "good curvature" of the magnetic field in the region of the plasma. This curvature is expected to produce equilibria stable against rigid body displacements.

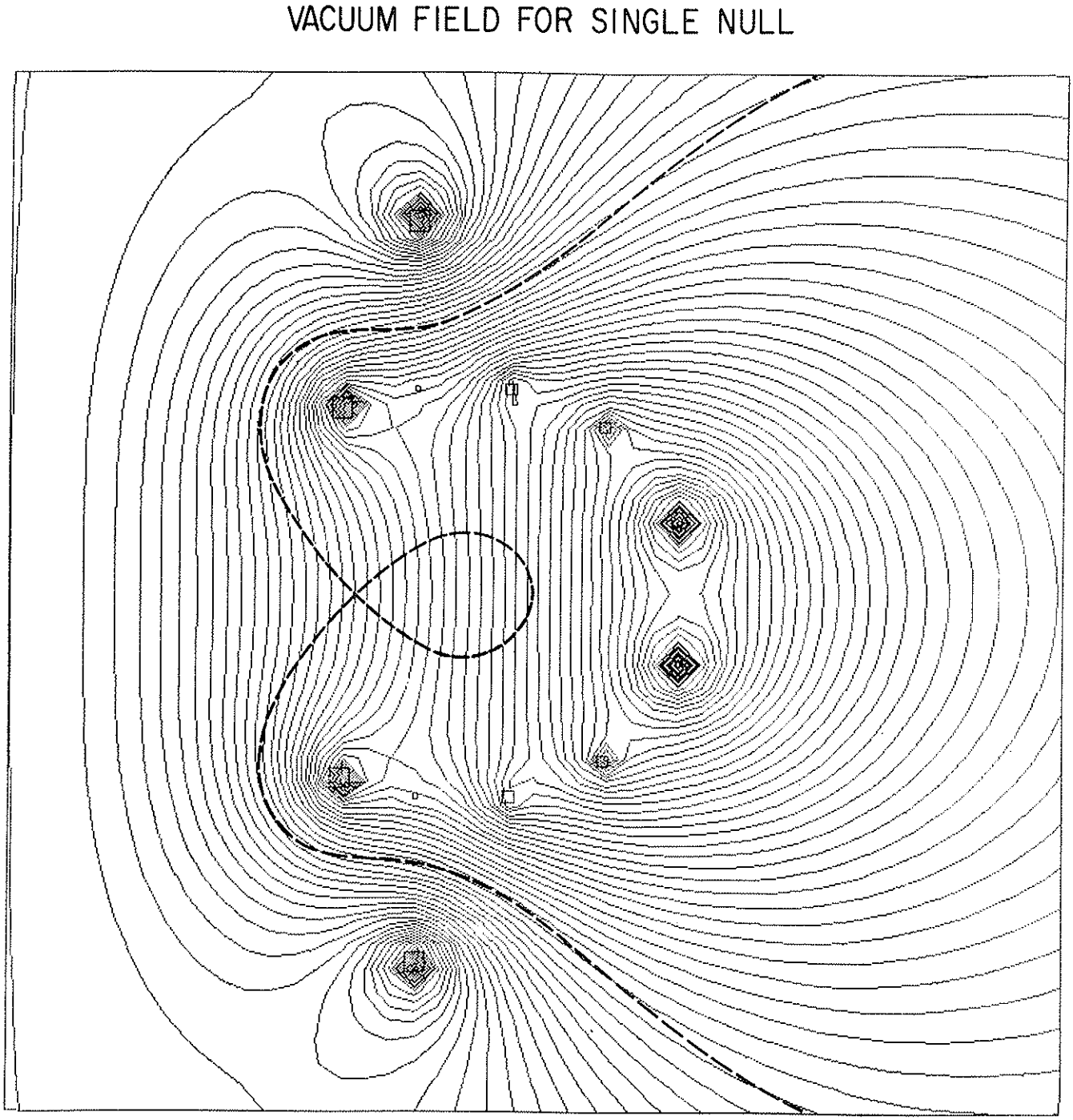

Fig. 3. Vacuum Magnetic Field for Single Null Configuration.

Second is the rather abrupt increase in field strength in the neighborhood of the null point. This design feature enables an expansion (or contraction) of that part of the separatrix surface enclosing the discharge while keeping the null point and the remainder of the separatrix surface nearly fixed in space. The separatrix surface can therefore function as an expanding magnetic limiter during start-up.

Third is the coupling of the entire poloidal flux that links the discharge in a sense to help induce the discharge current. The demand in the ohmic heating core is thereby reduced.

Figure 4 shows representative equilibrium flux surfaces for the single null configuration. The crowding of the flux surfaces toward larger major radii is a result of plasma pressure. The crowding facilitates neutral beam penetration.

The style of the vacuum poloidal field for the double null configuration, together with the separatrix surface, is shown in Figure 5. A striking feature of this magnetic field is the "bad curvature" in the region of the plasma. This curvature produces equilibria that are unstable against rigid body displacements. Plasmas at larger major radii have vacuum fields with both "good" and "bad" curvature, but the persistence of "bad" curvature over a large portion of the plasma is characteristic of the double null designs. The double null configurations require stabilization against vertical displacements. How to achieve such stabilization via auxilary coils, etc., was not considered in this study, the assumption being that stabilization would not have a large economic impact.

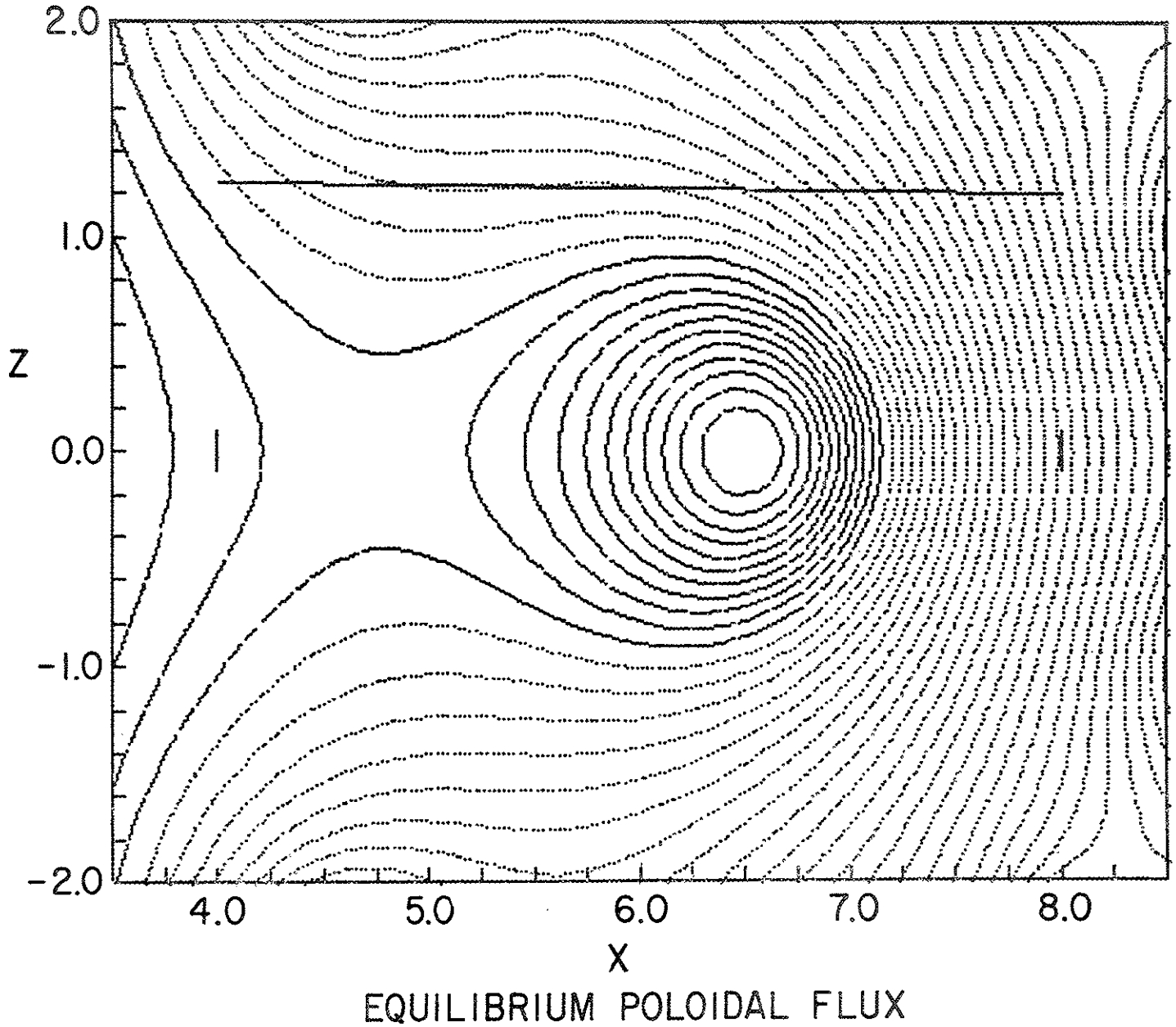

Fig. 4. Equilibrium Poloidal Magnetic Flux for Single Null Configuration.

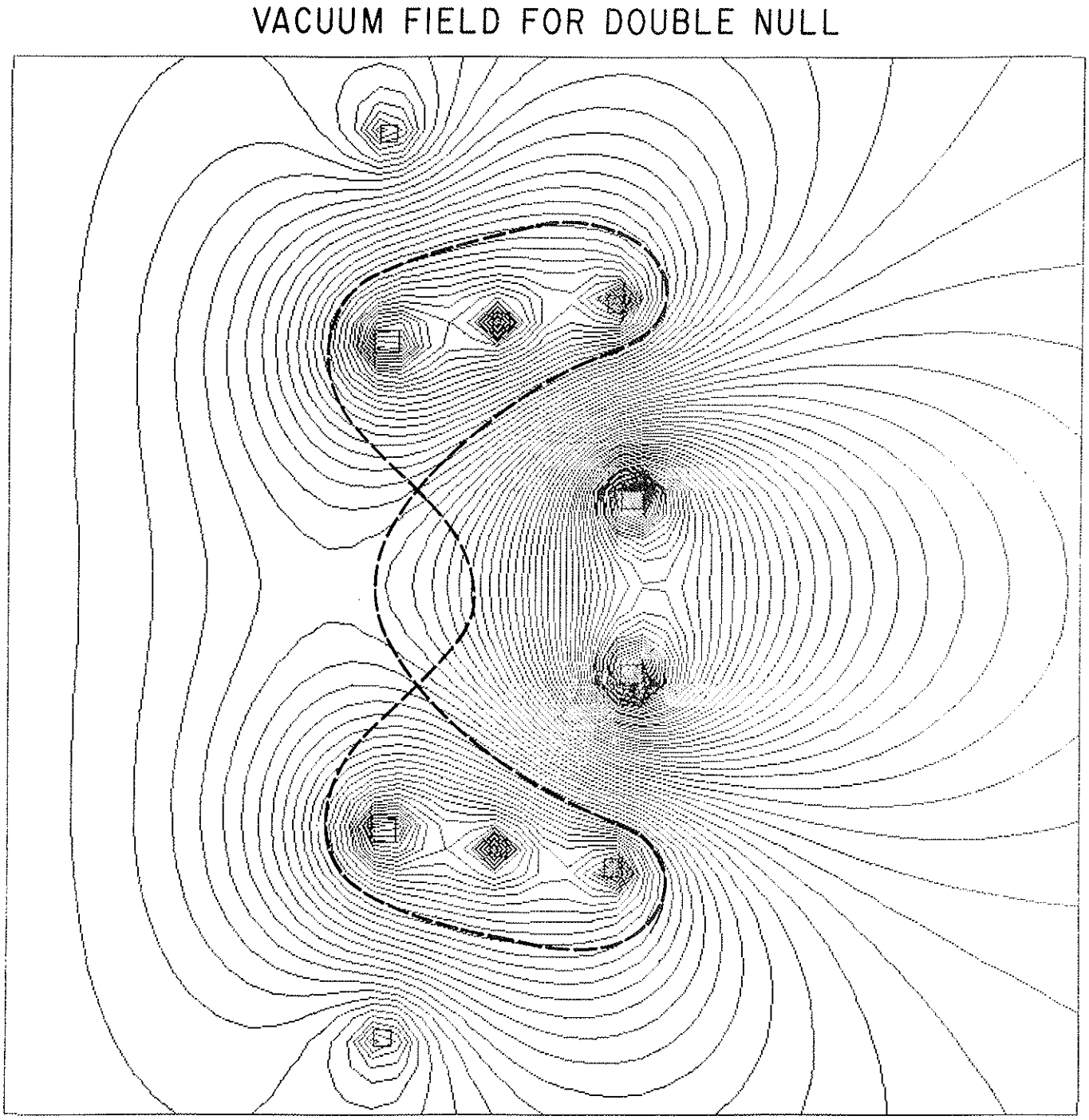

Fig. 5. Vacuum Magnetic Field for Double Null Configuration.

Another feature of the vacuum field of the double null configuration is the large fraction of the poloidal flux that links the discharge in a sense that opposes the induction of the discharge current. This feature increases the demand on the ohmic heating core.

Figure 6 shows representative equilibrium flux surfaces for the double null configuration. In comparison with the single null configuration of Figure 4, the double null shape is more non-circular and vertically elongated. These differences are thought to account for the fact that the double null configurations could generally support larger values of β than the single null configurations.

The purpose of the numerical exploration of various plasma equilibria over a variety of physical sizes was to develop simple, analytic scaling relations that could specify a family of tokamak plasmas operating at the maximum pressure allowed by the adopted constraints on the equilibrium. The adopted scaling of the geometry is shown in Figures 1 and 2 where the major radius of the plasma, R, is related to the location of the toroidal field coil, h, and the quantity "a" is defined in terms of the plasma volume, V, namely $a^2 = V/2\pi^2R$. The size of the toroidal field coils must be large enough to clear the blanket and poloidal coil structure. The designated height of the coils, H, is a minimum requirement.

The formulae developed for scaling the discharge current, I, and the maximum pressure, p_o, consistent with the numerical

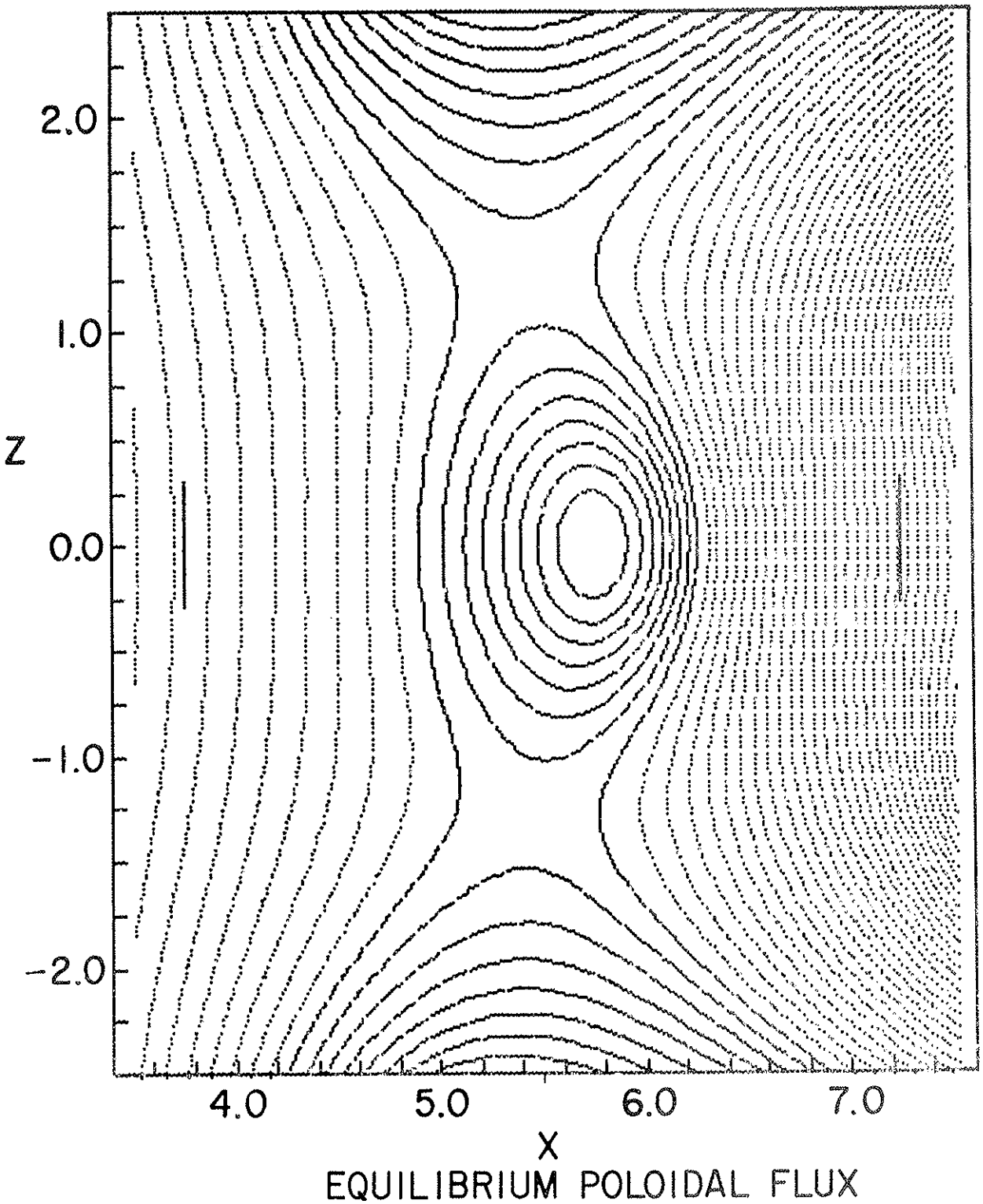

Fig. 6. Equilibrium Poloidal Magnetic Field for Double Null Configuration.

studies were arrived at via a quasi theoretical modeling using the above mentioned constraints of $J_\phi > 0$ and $q = q_o > 1.0$ at the magnetic axis. We begin the modeling by calculating

$$q_o = \frac{2B_o}{R\mu_o J_o} \tag{4}$$

$$(\mu_o = 4\pi \times 10^{-7})$$

We assume a maximum toroidal magnetic field of 16 tesla at the inner radius of the toroidal field coil, h, so that $B_o = 16\ h/R$. Then from Eqs. (1-3) we have

$$J_o = \left(\frac{2\pi R\alpha}{\psi_\ell - \psi_o}\right)\left(p_o + \frac{g_o B_o^2}{\mu_o}\right) \tag{5}$$

Following the analysis of tokamak equilibrium by Greene et al.,[1] we assume the following formula for g_o:

$$g_o = f_a^{(1)} C_1(\alpha)\left(1 - C_2(\alpha)\langle\beta_\theta\rangle\right) \tag{6}$$

where $f_a^{(1)} = B_p/B_o$, and where B_p is the average magnitude of the poloidal magnetic field at the nominal minor radius, a. We therefore express the poloidal flux within the plasma as:

$$\psi_\ell - \psi_o = C_3(\alpha) B_o R a f_a^{(1)} \quad . \tag{7}$$

In addition we define

$$\langle\beta\rangle \equiv \frac{2\mu_o\langle p\rangle}{B_o^2} = \frac{2\mu_o C_4(\alpha) p_o}{B_o^2} \tag{8}$$

and

$$\langle \beta_p \rangle \equiv \frac{2\mu_o \langle p \rangle}{B_p^2} \tag{9}$$

where the "$\langle\ \rangle$" indicate an average over the plasma cross section.

In the above formulae, (6, 7, and 8), the various $C_i(\alpha)$ are to be chosen to fit the numerical experience with the various equilibria selected. In particular we find a good choice for the single null configurations to be $C_4 = 1.9/(\alpha + 1)^2$. We also have from Eqs. (1-3)

$$J_\phi \sim \left(X^2 \mu_o p_o + R^2 B_o^2 g_o\right) .$$

Requiring $J_\phi > 0$ implies, using the above relationships,

$$\left(\langle \beta_p \rangle / 3.8C_1\right) \left((\alpha + 1)^2 - 3.8C_1C_2R^2/X^2\right) + 1 \geq 0. \tag{10}$$

The following choices appear to be reasonable:

$$3.8C_1 = (2\alpha - 1)^2/0.6 ,$$

and

$$3.8C_1C_2 = 4\alpha .$$

Then Eq. (10) yields a condition on $\langle \beta_p \rangle$ for $J_\phi > 0$ at $X = R_o - a$. (J_ϕ is smallest at the minimum major radius), namely

$$\langle \beta_p \rangle < \frac{(2\alpha - 1)^2}{0.6\left(4\alpha - (\alpha + 1)^2 \left(1 - \frac{a}{R}\right)^2\right)} . \tag{11}$$

Finally, the single null numerical experience leads to the choice of $2C_3/ (3.9\ C_1\mu_o) = 6.1 \times 10^7$ which in turn produces from Eq. (5) the expression,

$$q_o = \frac{6.1 \times 10^7 ha^2}{R^2 I\alpha} \left[1 + 0.6 \langle \beta_\phi \rangle \left(\frac{\alpha - 1}{2\alpha - 1}\right)^2\right]^{-1} \qquad (12)$$

Setting $q_o = 1.1$ in the above equation produces, in conjunction with Eq. (11), the following scaling formula for the single null discharge current

$$I = \frac{5.55 \times 10^7 ha^2}{R^2\alpha} \left[1 + \frac{(\alpha - 1)^2}{\gamma}\right]^{-1} \qquad (13)$$

where $\gamma \equiv 4\alpha - (\alpha + 1)^2(1 - a/R)^2$. Note that in view of the single null geometry shown in Figure 1,

$$R = h + 2.5 + 1.95a \ ,$$

and hence I is a function only of h, a, and α. The scaling expression for p_o is found via Eqs. (9 and 11) together with the relations for

$$p_o = \langle p \rangle / C_4(\alpha) = \langle p \rangle (\alpha + 1)^2/1.9 \qquad (14)$$

and

$$B_P = \mu_o I/2\pi a \ .$$

We find

$$p_o = 1.27 \times 10^{-8} \frac{I^2(\alpha + 1)^2 (2\alpha - 1)^2}{a^2\gamma} \qquad (15)$$

We note p_o is a function only of h, a, and α.

For the double null configurations the scaling formulae are somewhat different, namely

$$I = \frac{6.1 \times 10^7 h a^2}{R^2 \alpha} \left(1 + \frac{(\alpha - 1)^2}{\gamma}\right)^{-1} \qquad (16)$$

$$p_o = 1.11 \times 10^{-8} \frac{I^2 (\alpha + 1)^2 (2\alpha - 1)^2}{a^2 \gamma} \qquad (17)$$

and

$$C_4(\alpha) = 2.3/(\alpha + 1)^2 \quad .$$

The constraint on $\langle \beta_p \rangle$ given by the expression (11) holds for both the single and double null configurations.

Eqs. (15 and 17) are shown in Figure 7 for the choice of $\alpha = 2$.

The above pressure scalings led to values of $\langle \beta \rangle$ of only 1 or 2 percent. Late in the hybrid study a "new pressure" scaling was used, but only for double null configurations. The scaling relations were adapted from a study of PDX configurations and are

$$\langle p \rangle = \frac{B_o^2}{2\mu_o} \cdot \frac{0.2}{A} \qquad (18)$$

where $A \equiv R/a$, and

$$I = \frac{2\pi a^2 h B_{max}}{R^2 \mu_o q_o} \qquad (19)$$

with $B_{max} = 16$ tesla, and $q_o = 1.12$.

This scaling leads to values of $\langle \beta \rangle \sim 4\%$ which is appreciably higher than the values of $\langle \beta \rangle$ obtainable from the previous equilibria. The reason the PDX configuration led to

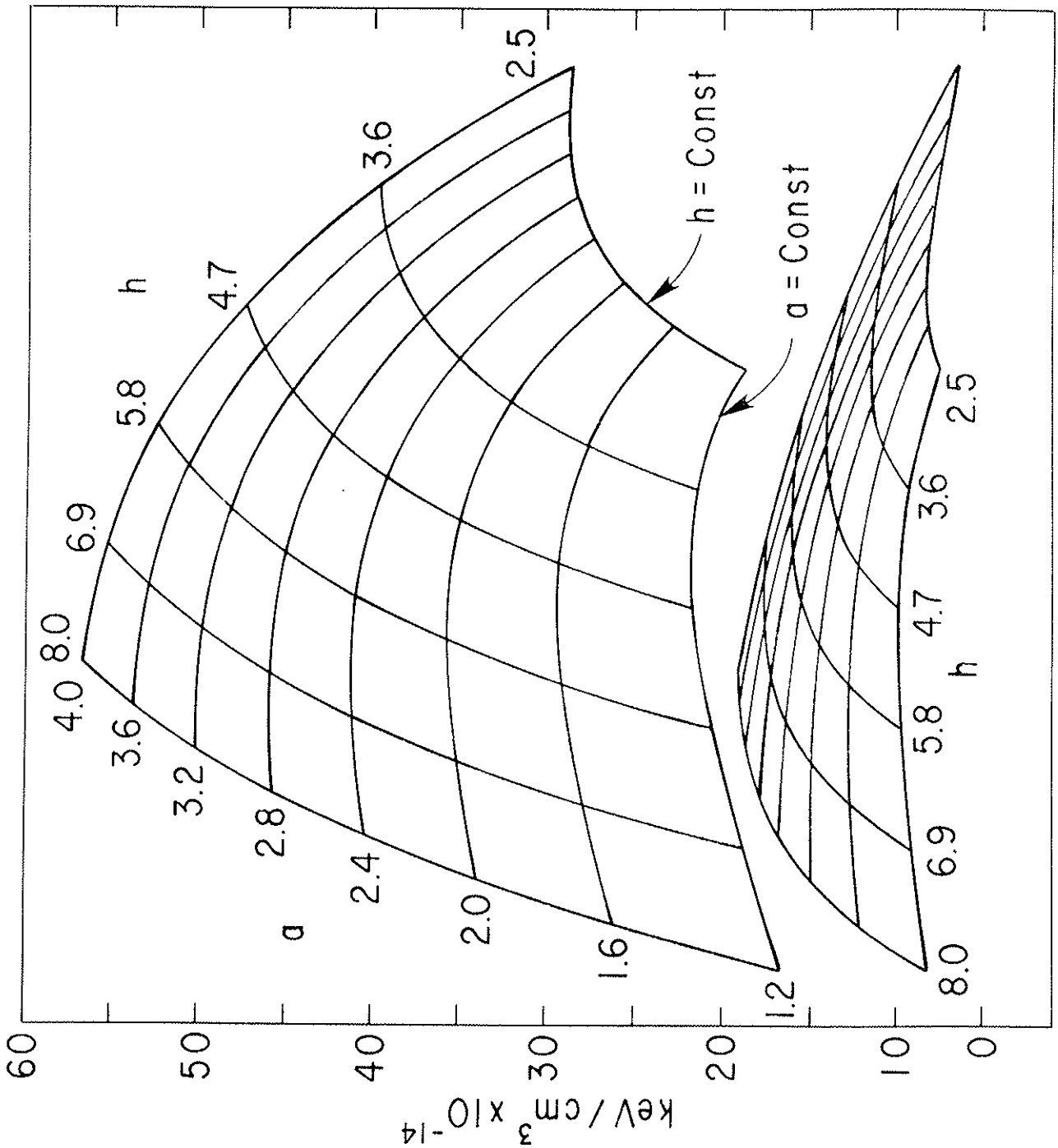

Fig. 7. Pressure Carpets for the Double Null (upper) and Single Null (lower) Configurations.

higher value of $\langle\beta\rangle$ lies in the assumptions made for $p(\Psi)$ and $g(\Psi)$, namely:

$$p(\Psi) = k\delta\Psi\left(C_4 + C_1\chi + \frac{C_2}{2}\chi^2 + \frac{C_{3\chi}}{\alpha + 1}^{\alpha + 1}\right)$$

where

$$\delta\Psi = \psi_\ell - \psi_o$$

$$\psi_o \equiv \Psi - \psi_o \,/\delta\Psi$$

and

$$g(\psi) = \left(1 - \left(1 - \frac{1}{R}\right) 2C_5 p\right)^{1/2}$$

where the C's are suitably chosen.

The "old" and "new" pressure "carpets" for the double null configuration are shown in Figure 8.

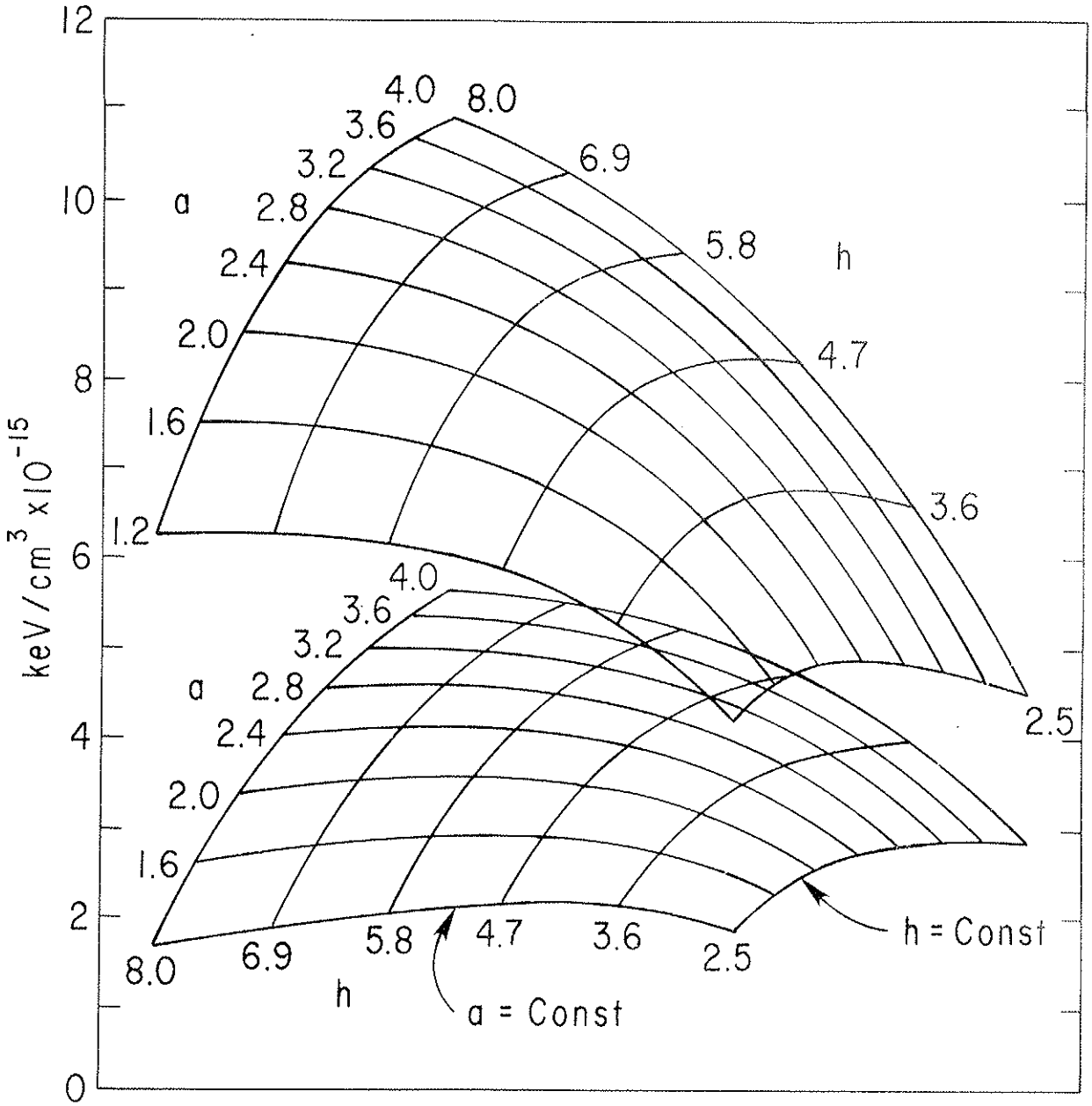

Fig. 8. "Old" Pressure (lower) and "New" Pressure (upper) Carpets for the Double Null Configuration.

Reference

[1]J. M. Greene, J. L. Johnson, K. E. Weimer, Tokamak Equilibrium, Phys. Fluids 14, 671 (1971).

D. Blanket Performance

1. Parameters for the Blanket

The systems analysis of the hybrid requires only a very abstract description of the blanket in terms of major performance parameters. Functional relationships among these parameters are determined from auxiliary studies of the "real" blanket and then supplied as the elements of a black box to the systems code.

The three fundamental parameters of a hybrid blanket are: T, the tritium breeding ratio, tritons produced per fusion neutron hitting the blanket; F, the fissile breeding ratio, net fissile atoms produced per fusion neutron hitting the blanket; and M, the blanket multiplication, the energy released by each fusion neutron hitting the blanket divided by 14.06 MeV, the initial neutron energy.

For a hybrid that deliberately loads fissile fuel in order to increase the blanket multiplication there are two additional important parameters: S, the density (or other index) of the fissile loading; and P, the gross fissile breeding ratio, equal to F plus the allowance for self-consumption.

A complicating factor must now be considered: all five basic blanket parameters are functions of time. This dependence is conveniently expressed in terms of the integrated wall load. (The wall load, W, is the energy flow of fusion neutrons through the first wall, 14 MeV times the neutron current.) A useful auxiliary time parameter is the burnup sustained by the uranium fuel in the multiplier after exposure to a given integrated wall load.

To discuss the time dependence, the subscript "i" will indicate initial values, when burnup and integrated wall load are zero. The subscript "f" will indicate final values, when the burnup reaches its discharge value, B, and the integrated wall load is J. Non-subscripted parameters will usually refer to average values.

A further complication arises from the fact that not all the fusion neutrons hit the blanket, only a fraction, Z. Therefore, some of the reactor performance parameter targets must be divided by Z to obtain values on the "per fusion neutron hitting the blanket" basis used above; correspondingly the calculated blanket performance parameters must be reduced by the factor Z before being used to analyze reactor performance.

Other factors may also have to be applied to extract reactor performance parameters from blanket performance figures. For example, the blanket multiplication, M, keyed to the fusion neutron energy, is just one component of the overall reactor energy multiplication factor: this global figure of merit must incorporate other terms to account for the recovery of neutrons which miss the blanket, and of the whole fusion alpha-particle energy.

2. Method of Solution

Given the specific design of a particular blanket, all the performance parameters can be calculated using standard nucleonic analysis methods. However, for a parametric systems analysis at least one of the parameters must be left (by definition)

as an independent variable; the nucleonic analysis then provides values of the other parameters as functions of the free variable(s).

For this hybrid reactor analysis it has been found most convenient to use M, the average blanket multiplication, as the principal independent parameter. Although this is normally the output, rather than the input, of a neutronic calculation, there is no reason in principle why the blanket problem could not be solved in this reverse manner. In practice, however, it is most convenient to evaluate a series of blankets in the regular way, parameterize the results, and then invert the resulting black box.

In the hybrid systems analysis code the multiplier burnup target, B, is pre-specified, along with the required overall tritium breeding ratio. When a given reactor is to be evaluated, the dimensions determine Z, the fraction of neutrons hitting the blanket, and the required blanket, T, is found by multiplying 1/Z times the reactor, T. In addition, the reactor power balance is solved for M, the required blanket multiplication.

This completes the specification of a sufficient set of independent variables to solve for the remaining parameters of the required blanket. The solution is iterative (using the parametric equations described below) and seeks a self-consistent set of parameters where the initial conditions and the lifetime imply the desired average multiplication.

Unfortunately, the solution extracted from this model does not always represent an acceptable blanket. Two modes of

failure can occur. In one, the net fissile breeding ratio (F) is negative, i.e., the blanket is a consumer of fissile fuel. This is not impossible, but it does violate one of the basic guidelines of the study, that the hybrids considered should all be self-sufficient in fissile fuel. Since F decreases as M increases, the effect is to exclude from the hybrid survey all reactors which require blanket multiplications above a certain limit.

The other mode of failure is indicated by too low a calculated value of M_i. This initial multiplication corresponds to the fresh blanket with no buildup of fissile fuel. For any given type of blanket, there is some physically irreducible value of M_i, corresponding to no deliberate initial loading of fissile fuel. Therefore when the model requires that M_i be less than this value, it is a signal that the requested average M is impossibly low. This leads to the exclusion from the hybrid survey of reactors which require blanket multiplications below a certain limit.

The assumed value of T affects the upper limiting value of M strongly and the lower limit weakly, but the requirement that T be (marginally) greater than one is, of course, one of the basic guidelines of the study. In addition, both the upper and lower limits of M will depend in principle on the assumed value of B, the multiplier burnup. This, however, is not a fundamental parameter, and so there is some latitude to extend the range of M by varying B.

As B is increased, fuel cycle costs associated with processing the multiplier fall, but radiation damage to the fuel elements increases. A nominal value can be used for B that is low enough to have confidence in the integrity of the multiplier, and fortunately this value is high enough that the reactor cost analysis is insensitive to B. As B is decreased, the fuel cycle costs increase very rapidly, as the expense of fabricating and reprocessing large masses of fuel must be covered by smaller amounts of recovered fissile material per cycle.

However, it is as B is decreased that the allowable range of M is expanded. The source of this behavior can be demonstrated at the lower limit with the following argument: A freshly loaded blanket will offer some absolutely irreducible value of blanket multiplication; as the exposure increases, fissile fuel is bred, and some of it fissions; this produces energy, thus increasing the cycle-average of M. The effect of B on the upper limit of M is more obscure, since it derives from the balance among a number of factors affecting the utilization of fissile material in the multiplier and the burner, e.g., the degree of thermalization, the capture-to-fission ratio, the amount of fast fission, etc. Clouding the picture is the coarseness of the parametric equation being used to model this hybrid. Within the context of that model, however, decreasing B does raise the maximum allowable M.

To exploit this possibility of using B as an active parameter, when the blanket model finds that the required M is outside the allowable range it will attempt to decrease B so

as to extend the limit just to M. This allows further consideration by the systems code of some reactors which otherwise would have been rejected. Unfortunately little benefit is realized from this; the steeply increasing fuel cycle cost function makes most such reactors uneconomic.

3. Parametric Formulation

Within the hybrid systems code the blanket performance is evaluated using a small set of polynomial parametric equations. The form and constants in these equations were fitted to more detailed nucleonic blanket calculations as described in Appendix I.

Actually within the code there are six models available: for nominal and "super" performance of time-independent, ramping, or constant-power blankets. Most of the results of this study were obtained using the nominal, constant-power model.

In each of the models the target burnup, B, is specified as B_o. The target tritium breeding ratio, T, is calculated as $T = T_o/Z$, where T_o is also specified, and Z is the fraction of fusion neutrons that hit the blanket. The latter value is calculated as $Z = (1+Z_o)/2$, where Z_o is the fractional coverage of the blanket over the whole plasma chamber wall.

Two conditions are used to screen out unacceptable blankets. First, the net recoverable production of fissile material (H) must not be less than zero, i.e., the reactor must not be a consumer of fissile fuel. Note that H is equal to F-eP, where e is the fractional loss in the fissile recovery process. The second condition is that S, the fissile inventory of the

burner region (here given in mole percent of PuF_3 in the flibe), must not be less than zero at any time. This is another way of expressing the condition that the required multiplication cannot be less than that intrinsically provided by the multiplier alone.

The time-independent model is operationally unrealistic, but contains most of the features of the others in simplified form. The blanket multiplication M is, of course, constant. The integrated wall load, J, of fusion neutrons is derived from the burnup using the equation $B = (b_1 + b_2 M) J$. The fissile inventory is related to M by the equation $S = (s_1 M - s_2)/(s_3 M + s_4)$. The gross fissile production in the multipler (P) and the net fissile production for both multiplier and burner (F) are given by $P = p_1 + p_2 M - T$ and $F = f_1 - f_2 M - T$.

The second model makes allowances for time-dependent behavior of the multiplier performance, but with no provision for leveling the whole blanket performance. Thus as the exposure of the fertile material increases and fissile fuel builds up in the multiplier, with the fissile concentration in the burner held constant, the blanket multiplication will ramp up.

The target, M, requested of the model is assumed to be the cycle average value, and the ramp is assumed to be linear in J. Unfortunately the burnup is no longer linear in J because of the extra fissioning of the bred fuel. Consequently a pair of equations must be solved simultaneously for J and M_i, the initial multiplication:

$$M = M_i + (a_1 + a_2 M_i + a_3 M_i^2) J;$$

$$B = (b_1 + b_2 M_i) J(1 + (b_3 + b_4 M_i + b_5 M_i^2) J) .$$

The numerical solution proceeds by substituting J from the first equation into the second, and using Newton's method to find M_i.

The initial (and constant) value of the fissile concentration is obtained from the formula $S = (s_1 M_i - s_2)/(s_3 M_i + s_4)$. The gross production of fissile fuel is parameterized only by the initial multiplication, $P = p_1 + p_2 M_i - T$. However, the net fissile formula incorporates terms which reduce the cycle-averaged value due to the in-situ burnout of bred material:

$$F = (f_1 - f_2 M_i - T) - J(f_3 + f_4 M_i + f_5 M_i^2) .$$

Thus for a given M_i, F is a decreasing function of J while M (average) is an increasing function.

For this model the final multiplication is also calculated from $(M_i + M_f) = 2 M$. Since the power handling equipment in the reactor must have a capacity of M_f, but the average plant output (and thus revenue) is proportional only to M, the power peaking factor, M_f/M, is an important parameter in the economic evaluation portion of the hybrid code.

The third blanket model avoids the severe penalties imposed by the power peaking effect by holding the blanket multiplication constant. This is accomplished by reducing the fissile content of the burner to compensate for the buildup in the multiplier region. Essentially the same parametric formulas developed for the second model are used again, but with a reinterpretation of some of the terms. A fictitious blanket which ramps up to the requested M is found, and then a declining ramp of S is superimposed.

Using the same variation with J, two equations must be solved simultaneously for M_i and J:

$$M = M_i + 2(a_1 + a_2 M_i + a_3 M_i^2)J \ ;$$

$$B = (b_1 + b_2 M_i)J \ (1 + (b_3 + b_4 M_i + b_5 M_i^2)J) \ .$$

Newton's method is used as for the second model, starting again with an initial guess of $M_i = 0$.

The initial and final values of the burner fissile concentration are calculated using M_i and $M_f = M$:

$$S_i = (s_1 M_f - s_2)/(s_3 M_f + s_4) \ ;$$

$$S_f = (s_1 M_i - s_2)/(s_3 M_i + s_4) \ .$$

Here S_f corresponds to a fixed concentration blanket which would start at M_i and ramp up to a final blanket multiplication of M; thus it is the concentration that will exist at the end-of-cycle. On the other hand S_i corresponds to a fixed concentration blanket which would ramp up from an initial multiplication of M, thus it is the concentration at the start-of-cycle. Clearly S_f will be less than S_i, and so S_f is used as the limiting value to screen out unrealistic blankets. For the economic evaluation, the average concentration in the burner is assumed to be $S = (S_i + S_f)/2$, consistent with the linearized treatment of the multiplier region.

The fissile production formulas in the previous model were keyed to the initial multiplication, although M was allowed to ramp. To use them for the constant M model, they are evaluated

at the value of multiplication that would give an average M in the ramp model equal to the constant (average) M. The presumption is that the buildup of fissile material depends principally on the total blanket average power (i.e., surplus neutrons from burner fission are available for fertile capture). Thus

$$M_a = M - (M_f - M_i)/2 \ ;$$

$$P = p_1 + p_2 M_a - T \ ;$$

$$F = (f_1 - f_2 M_a - T) - J(f_3 + f_4 M_a + f_5 M_a^2) \ .$$

As mentioned at the beginning of this section, the three models described above can be applied with both "normal" (nominal) and "super" performance parameters. The normal blanket uses functional fits to blanket performance figures actually calculated for the reference design. The super blanket presumes the same functional dependence but with one key element extrapolated to superior performance. In the reference blanket each fusion neutron induces (on the average) about 0.43 fast fissions in the uranium multiplier. For the super blanket this has been boosted to 0.6, arbitrarily.

In support of the super blanket, it should be noted that this higher level of primary fissions is approximately that claimed for the blankets of the series of Mirror Hybrids studied at LLL.[1] However, such performance has not been observed in comparable calculations performed at PPPL. (The differences are discussed in Ref. 2). Therefore, the nominal blanket has been used as the basis for most of these hybrid studies, with the super blanket for occasional comparison.

Table I presents the numerical constants needed in the blanket performance parametric equations for both the nominal and super blankets. Figures 1 and 2 show corresponding plots of some of the important blanket parameters. Approximate values of M, F and the concentration of PuF_3, p, are shown in Figure 3 for both the nominal and super blankets.

Table I. Numerical constants for the blanket performance parametric equations.

	Normal (Nominal)	Super-Blanket
B_o	0.005	0.005
T_o	1/0.975	1/0.975
e	0.9801	0.9801
a_1	0.7409	1.0871
a_2	0.08289	0.10754
a_3	0.002146	0.002146
b_1	0.00214	0.002958
b_2	6.93×10^{-6}	6.93×10^{-6}
b_3	0.0343	0.0598
b_4	0.00758	0.00849
b_5	0.000351	0.000301*
s_1	1.468	1.468
s_2	10.276	14.68
s_3	1.429	1.429
s_4	77.17	116.77
p_1	1.457	2.137
p_2	0.0593	0.0593
f_1	2.131	3.1
f_2	0.037	0.037
f_3	0.0219	0.0566
f_4	0.00479	0.00726
f_5	0.00023	0.00023

(*inadvertently changed to 0.00301 in the code as run, with little effect on the results)

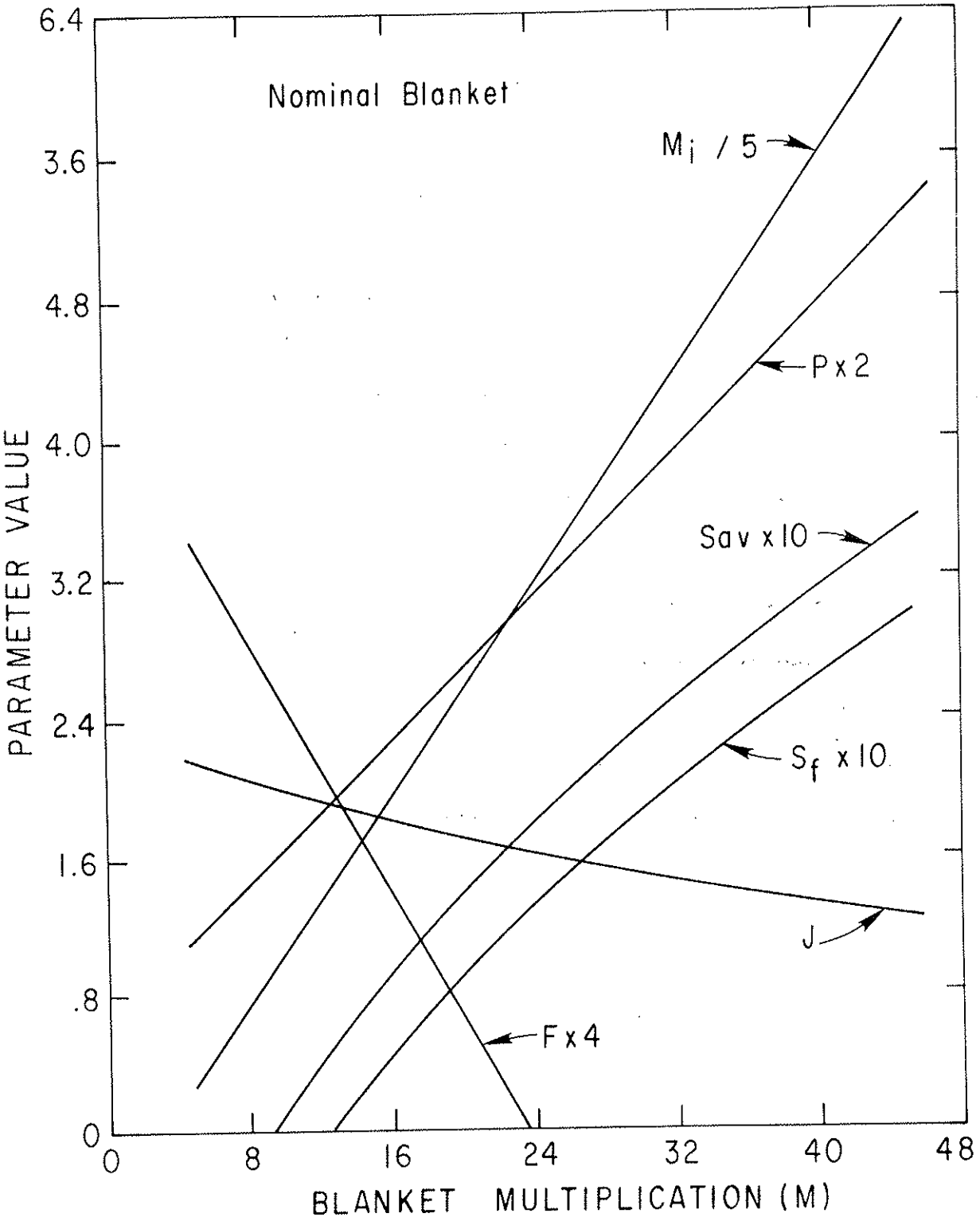

Fig. 1. Performance Parameters (Defined in the Text) Derived by Varying the (Constant) Blanket Multiplication in the Nominal Blanket Mode.

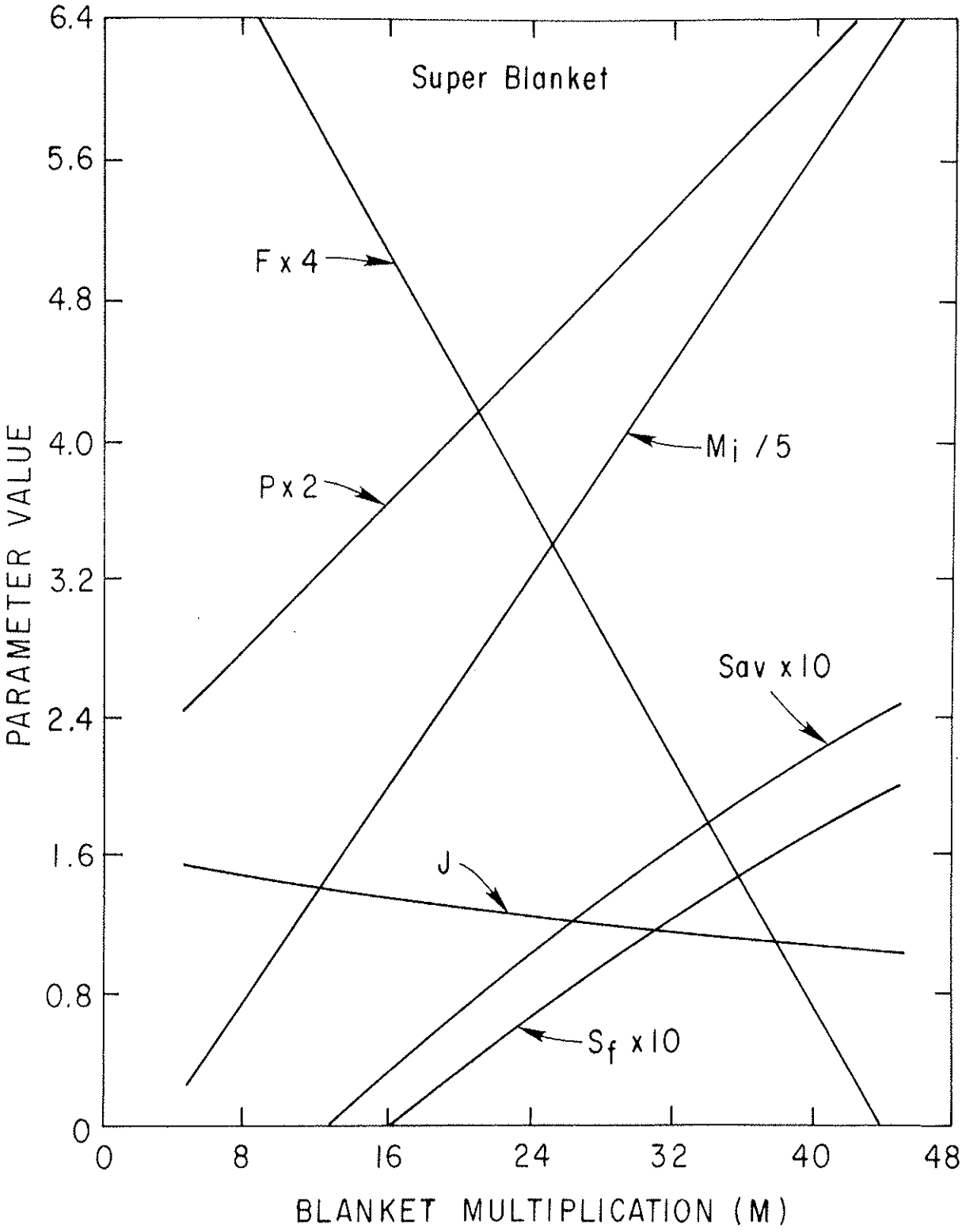

Fig. 2. Performance Parameters (Defined in the Text) Derived by Varying the (Constant) Blanket Multiplication in the "Super" Blanket Model.

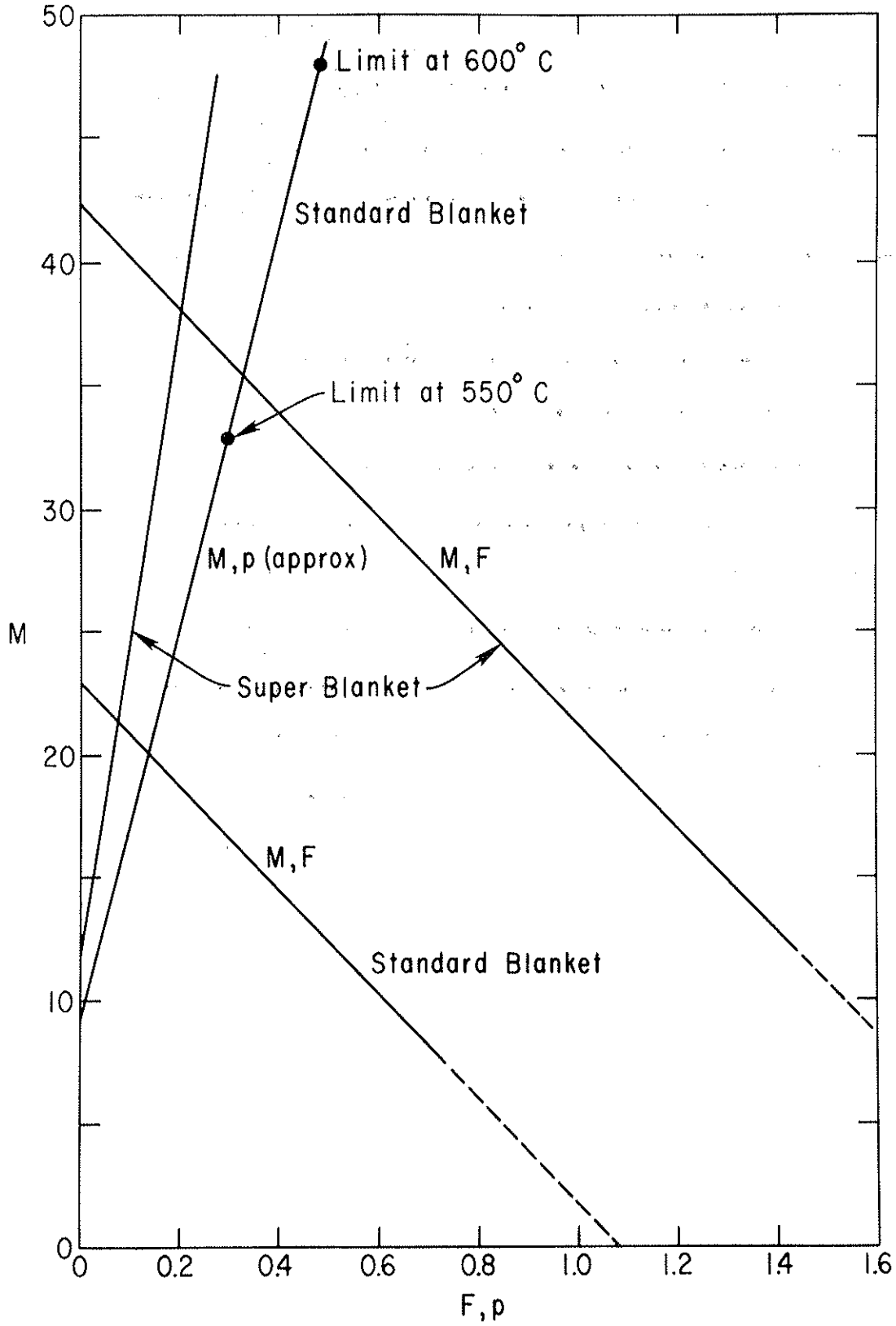

Fig. 3. Approximate Averaged Blanket Properties:
M = blanket energy multiplication = blanket energy production/14 MeV
F = net fissile fuel atoms bred/fission neutron
p = mole % of PuF_3 in molten salt.

References

[1]J. D. Lee, D. J. Bender, R. W. Moir, K. R. Schultz, Mirror Hybrids - A Status Report, Proceedings of the Second Topical Meeting on the Technology of Controlled Nuclear Fusion, G. L. Kulcinski, ed. (National Technical Information Service, Springfield, Virginia, 1976) Conf-760935, Vol. II, pp. 689-710; also Lawrence Livermore Laboratory Report UCRL-78079 (1976).

[2]L. Ku and W. G. Price, Jr., Neutronic Calculation and Cross Section Sensitivity Analysis of the Livermore Mirror Fusion/Fission Hybrid Reactor Blanket, Princeton Plasma Physics Laboratory Report PPPL-1370 (1977).

E. Economic Scaling of System

1. Hybrid Power Output

The hybrid model was originally conceived to determine gross and net electric power output based on fusion core size and blanket performance. The ultimate survey was performed holding gross electric power fixed (see Section V.A), but the original version is more instructive for showing the model.

The thermal power developed by the reactor is a combination of fission power from the blanket and high energy particle attenuation in the divertor. Neutron attenuation in the first wall, converter, and salt region plus heating from converter and blanket fissions constitute the blanket power output. This is given by the relation,

$$P_{BL} = M_B \times W_L \times Z_w, \qquad (1)$$

where

P_{BL} = blanket power, MW

M_B = average blanket multiplication

W_L = average neutron wall load, MW/m^2

Z_W = effective wall area backed by blanket, m^2.

Z_W is less than the theoretical wall area (assuming the wall completely surrounds the plasma) since divertor channels and beam ports occupy several tens of square meters. For each device surveyed, the wall area reduction is computed.

The power developed in the divertor includes attenuation of equivalent beam power, attenuation of equivalent alpha power, and attenuation of neutrons that do not enter the blanket region. The first two factors are based on an energy balance around the plasma. The third factor derives from a fusion neutron balance. Power deposited in the divertor, P_D, is assumed to be sufficiently high grade that it can be collected and transported with 80 percent efficiency. The remaining 20 percent is collected and dissipated by a low temperature wall and divertor collection plate cooling system.

$$P_D = \left[P_B + A_W * W_L \, (3.5/14.06 + (1 - Z_W/A_W))\right] \eta_D \qquad (2)$$

where

A_W = theoretical wall area

η_D = divertor thermal collection efficiency.

The thermal energy transported from the blanket and divertor is converted to electricity at a net efficiency (η_{th}) of 38 percent. Of this gross output, a substantial fraction is recirculated within the hybrid station. Neutral beam injectors consume power at a rate

$$P_I = P_B/\eta_I$$

where

P_I = power to injectors, MW

P_B = beam power to plasma, MW

η_I = injector efficiency = $0.89 - 0.0018W_o$

W_o = injection energy, keV.

The injector efficiency relationship is based on Ref. 1 for positive (D^+, T^+) ions including direct conversion of un-neutralized ions. This correlation is assumed valid in the range 100-300 keV. The injection energy is optimized by the plasma model. For ignited reactors the beams are "turned off" after heating is completed. In this case, P_I is equal to the cycle average of the beam power necessary to start up (assumed to be 3 MW = 100 MW*3% for these calculations).

The remainder of the recirculating power is consumed by plant auxiliaries. This includes pumps, compressors, chillers, the liquid helium refrigeration system, and helium circulators. For survey purposes this recirculating power fraction (α) was assumed to be 10 percent of gross power output. The total net electric power output is then

$$P_N = \left[P_{BL} + P_D \ \eta_{th}\right] \ (1 - \alpha) - P_I. \qquad (3)$$

2. Plant Capacity Factor

Plant capacity factor, g, is the product of three factors: 1) availability, 2) duty factor, and 3) load factor. Availability, A, is defined as the ratio of hours per year that the plant is available to produce power to the total number of hours per year (8760). Duty factor, δ, is a function of possible cyclic operation. For a steady state operation, $\delta = 1$. For pulsed operation of 950 seconds and 50 seconds recovery, $\delta = 0.95$.

Load factor, L, depends on the utility's use of the plant. Base load units run at or near rated capacity, i.e., L = 1. Peaking units may vary considerably, i.e., $0.1 \leq 1.0$.

Availability will depend on two factors - refueling outages and maintenance outage.

$$A = \frac{T_p}{T_p + T_R + T_M} \tag{4}$$

where

T_p = time at power (hour/year)

T_R = refueling time (hour/year)

T_M = maintenance time (hour/year).

Typically for light water reactors, the refueling time may vary from six to eight weeks per year, with all maintenance performed during refueling. If T_R equals six weeks,

$$A = \frac{46}{46 + 6} = 0.88 \ .$$

In addition to refueling outages, the replacement of the first wall for fusion-fission hybrids is expected to be a time consuming operation. First wall replacement frequency depends on wall lifetime and, hence, wall loading.

The wall life in full power years is

$$\tau = \frac{\tau_o}{W_L} = \frac{\tau_o \ A_W}{P_f \ V_p} * \frac{17.6}{14.1} \tag{5}$$

where

τ_o = wall capability ($MWyr/m^2$)

W_L = wall load MW/m^2

A_W = theoretical wall area, m^2

P_f = fusion power density

V_p = plasma volume.

The annual time consumed per full power year for first wall replacement is T_W/τ where T_W is the required time for a total wall replacement operation. To find the time consumed for wall replacement on an annual basis, T_W is scaled by the factor, T_F, which is the equivalent annual time at full power. This factor, T_F, also scales the refueling time, which can be expressed as $T_R = K\ T_F$. Then,

$$A = \frac{T_p}{T_p + K\ T_F + \frac{T_W T_F}{\tau}}$$

Since we assume that the reactor is base loaded, essentially all operation is at full power ($L = 1$), and $T_p = T_F$. Then,

$$A = \frac{1}{1 + K + \frac{T_W}{\tau}}$$

or

$$A = \frac{1}{1 + K + \frac{W_L\ T_W}{\tau_o}} .$$

The plant capacity factor is then expressed as

$$g = L\delta A = \frac{L\delta}{1 + K + \frac{W_L T_W}{\tau_o}} . \qquad (6)$$

For this study we have assumed

$$\delta = 0.95$$

$$K = 1/3$$

$$T_W = 0.5 \text{ year}$$

$$\tau_o = 5 \text{ MW-yr/m}^2$$

$$L = 1.$$

Then,

$$g = \frac{0.95}{\frac{4}{3} + \frac{W_L}{10}} = \frac{0.7125}{1 + 0.075\ W_L} \quad .$$

3. Cost Scaling Factors

a. Introduction

The selection of fusion-fission hybrid reactor physical parameters is justified by a prediction of the costs of electricity and fissile fuel produced by a plant having those parameters as design bases. For the hybrid, the component of the cost of electricity exerting the most leverage is the capital cost. A set of scaling factors was developed to predict the variation in cost with changes in reactor parameters.

Because no comparable design exists from which to extrapolate costs, other fusion reactor design reports and cost estimates were examined as well as traditional references from the fission industry.[2] The costs, by PPC system of accounts classification, are presented in Table I. Although costs for the Lawrence Livermore Laboratory (LLL) mirror hybrid are not generally applicable to a tokamak design, that design does use high power neutral beam injectors vital to the start-up and operation of the tokamak hybrid.

Table I. Cost Comparison of Thermal and Hybrid Fusion Plant Designs.

Acct. No.	Account Description	Cost ($\times 10^{-3}$) PRD[3]	UWMAK II[6]	LLL-Hybrid[1]
20	Land and Land Rights			
201	Land and Privilege Acquisition	1,000	1,200	1,000
	Total Account 20	1,000	1,200	1,000
21	Structures and Site Facilities			
211	Site Improvements	1,500	8,000	2,600
212	Reactor Building	76,000	45,250	16,360
213	Turbine Building	4,310	26,650	1,190
214	Intake and Discharge Structures	4,290	1,300	-
215	Reactor Auxiliary Building	4,710	23,375	7,170
216	Radioactive Waste Building	-	-	1,660
217	Fuel Storage Building	1,840	-	-
218	Miscellaneous Buildings	7,610	56,215	-
219	Stacks	-	800	-
	Total Account 21	100,260	161,590	28,980

Table I. (continued)

Acct. No.	Account Description	Cost ($\times 10^{-3}$)		
		PRD	UWMAK II	LLL-Hybrid
22	Reactor Plant Equipment			
221	Reactor Equipment			
.1	Magnets, Reactor Foundation & Supports	145,270	184,850	301,200
.2	Shield	19,380	70,820	77,130
.3	Blankep	28,100	193,850	34,780
.4	Neutral Beam Injectors	-	80,000	45,170
.5	-	-	-	-
.6	Vacuum Vessel	13,440	1,320	-
221	Total 221	206,190	530,840	458,280
222	Main Heat Transfer & Transport System	177,690	194,562	64,320
223	Auxiliary Cooling Systems	63,000	21,172	-
224	Radioactive Waste Treatment & Disposal	-	330	-
225	Nuclear Fuel Handling & Storage Systems (Deuterium, Tritium)	7,900	2,220	82,890
226	Other Reactor Plant Equipment	6,600	14,355	27,290
227	Instrumentation and Control	10,600	11,700	2,950
	Contingency	-	-	112,870
	Total Account 22	471,980	775,179	748,600

Table I. (continued)

Acct. No.	Account Description	PRD	UWMAK II	LLL-Hybrid
23	Turbine Plant Equipment			
231	Turbine-Generators	59.590	69,000	49,000
232	Heat Rejection System	10,500	37,000	11,200
233	Condensing System	15,700	23,000	-
234	Feed-Heating System	17,700	23,000	20,000
235	Other Turbine Plant Equipment	16,300	5,000	800
236	Instrumentation and Control	5,000	3,000	2,800
	Direct Energy Convertor	-	-	23,500
	Contingency	-	-	9,660
	Total Account 23	124,790	160,000	116,960
24	Electric Plant Equipment			
241	Switchgear	2,800	4,292	22,300
242	Station Service Equipment	10,100	8,527	-
243	Switchboards	1,220	2,786	-
244	Protective Equipment	570	95	-
245	Electrical Structures & Wiring Containers	3,500	1,150	-
246	Power and Control Wiring	13,700	8,618	-
247	Magnet Power Supplies	33,600	32,500	1,130
248	Magnet Rectifiers	-	210	-
	Total Account 24	65,490	58,178	23,430

Acct. No.	Account Description	Cost ($\times 10^{-3}$)		
		PRD	UWMAK II	LLL-Hybrid
25	Miscellaneous Plant Equipment			
251	Transportation & Lifting Equipment	5,800	12,750	850
252	Air and Water Systems	5,800	5,660	-
253	Communications Equipment	300	220	-
254	Furnishings and Fixtures	4,300	480	400
	Total Account 25	16,200	19,110	1,250
26	Special Materials			
261	Moderator	-	-	-
262	Reflector	-	-	-
263	Reactor Coolant	430	2,760	-
264	Intermediate Coolant	-	2,850	-
265	Turbine Cycle Working Fluids	-	-	-
266	Other Materials	1,900	210	-
	Total Account 26	2,330	5,820	-
91	Construction Facilities, Equipment & Services	61,300	24,300	5,110
92	Engineering Services	33,000	48,500	28,230
93	Other Costs	30,040	90,800	28,520
94	Interest during Construction	210,910	253,400	234,360
	Total Plant Capital Investments	1,117,300	1,598,077	1,251,440

Table I. (concluded)

Account No.	Account Description	Cost ($\times 10^{-3}$)		
		PRD	UWMAK II	LLL-Hybrid
	Plant Output	2030 MWe	1716 MWe	610 MWe/690 kg Pu/yr
	Mills/kWh	15.17	24.74	39.7 with fuel @ $20/g
	$/kWe	599	940	1985

b. Vacuum Vessel, Blanket, and Structure Costs

From consideration of the arrangement of tokamak fusion reactors it seemed that the most important consideration in the costing of the vacuum vessel and structure cost was the first wall area. Thus, this serves as the major cost index. However for equal wall area, a large minor radius (a), small major radius (R) machine more efficiently utilizes structure than the small a, large R device. Therefore, a volumetric correction term was added, essentially penalizing the large aspect ratio machine. (This correction term is not considered to be valid for an aspect ratio less than 4 since the interior configuration would be extremely intricate. However survey machines rarely favored small aspect ratios.) The cost formula is CWALL = 10^4 (20. - 3.1a) $4\pi 2R\ (a + \Delta)$ where Δ is the scrapeoff layer thickness. The formula is shown as a function of wall area and plasma radius in Figure 1.

Also shown in Figure 1 are the actual costs for the Princeton Reference Design [3] and costs which would result from using the model's predictions. The 25% difference between actual and predicted reflects the independent derivation of the costing models used.

c. Superconducting Magnet Costs

The superconducting magnet system costs are assumed to scale with stored energy following a relationship prepared by Lubell.[4] This relationship was developed for NbTi superconductors, however, while the high field of the tokamak hybrid requires Nb_3Sn. Figure 2 shows a plot of the costs predicted

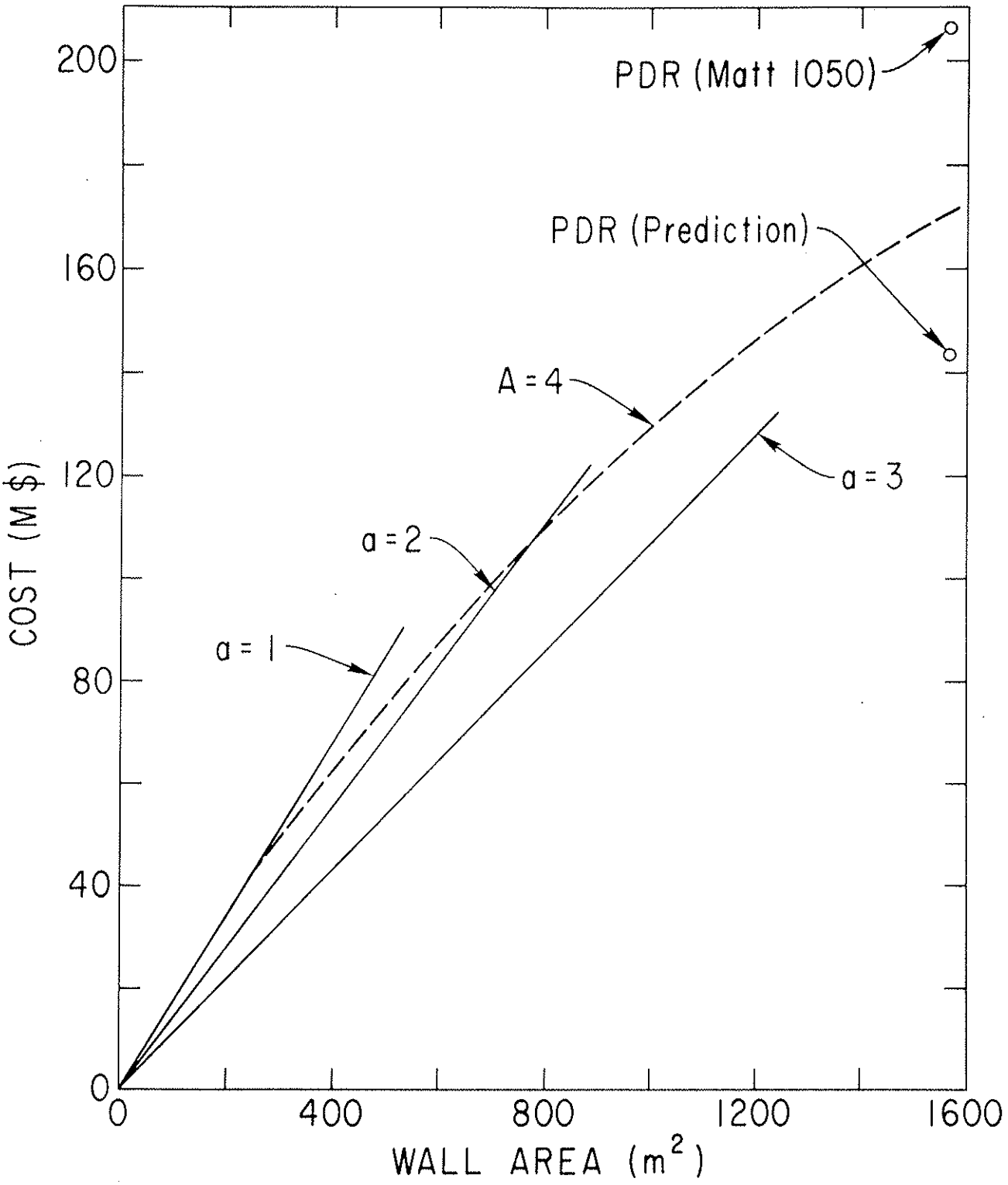

Fig. 1. Vacuum Vessel and Structure Costs.
The parameter a is the plasma minor radius in meters and A is the ratio of major to minor plasma radii.

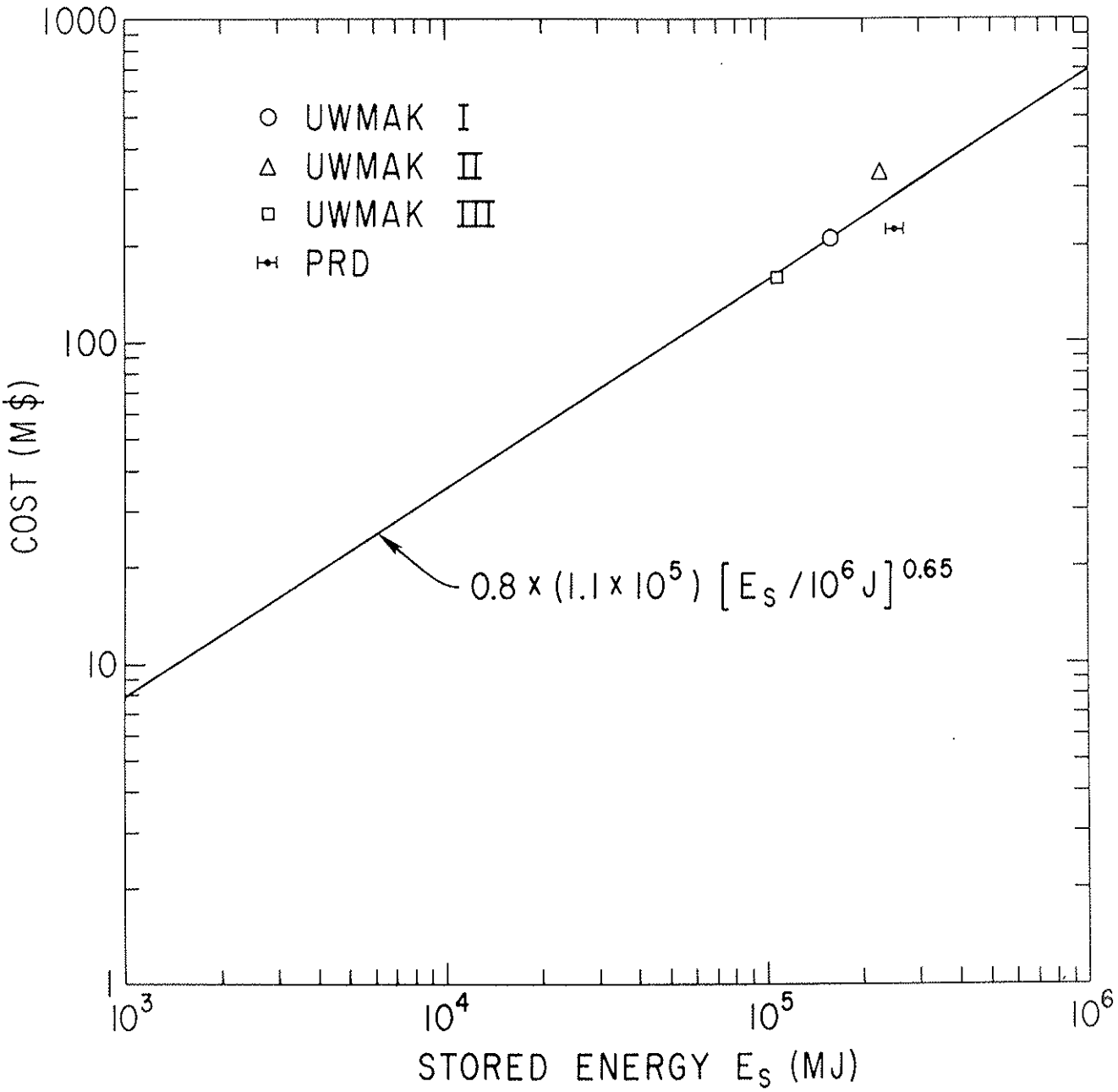

Fig. 2. Cost of Superconducting Magnet System.

by Lubell and design cost estimates by PRD and UWMAK's I, II, and III.[5,6,7] To account for inflation and differences in cost of superconducting material projected by Powell,[8] Lubell's predicted relationship is modified by a factor of 0.8.

The stored energy is calculated for a "D-coil" system fitted to the plasma and divertor by a coil sizing subroutine. This stored energy (in MJ) is used as the value of E_s in Lubell's formula which is based on circular superconducting coils.

$$CMAG = 0.88 \times 10^5 (E_s)^{0.65} . \quad (7)$$

Also included in this cost are power supplies and poloidal field coil costs. Both costs can vary substantially for different devices, depending upon final optimization of plasma shape, burn time, and divertor configuration. These considerations require a far greater level of design than was possible in the survey approach utilized in this study. Thus there is no explicit dependence of the magnet costs on the magnitude of the discharge current.

The magnet costs are sensitive to the exponent of stored energy. A change from 0.65 to 0.72 yields 37 percent increase in the cost of electricity for the nominal hybrid by multiplying the magnet costs by a factor of 2.37.

d. Neutral Beam Injector Costs

Neutral beam injector costs should scale as the delivered beam power and as the particle velocity, i.e., the square root of injection energy. These relationships are used by LLL in the mirror hybrid study cost parameterization.[1] Some uncertainty

exists over the dollars/kW cost normalization. Estimates offered in the literature range from approximately $100 to $500/kW. The LLL value is $208/kW for 100 keV injection. For this study the multiplier is taken as $300/kW at 100 keV. Costs for various beam powers and injection energies are presented in Figure 3.

Costs for the injection system were based on the total peak input power requirements for the plasma irrespective of whether the injectors are used only for heating to ignition or for continuous subignition operation. However a minimum of 100 MW of installed capacity was assigned to all machines.

The change in the cost of electricity with the $/kW cost multiplier is small. A 50 percent increase (300 to 450 $/kW) yields only a 1.7 percent increase in electricity cost for the nominal hybrid.

e. Balance-of-Plant Costs

Balance-of-plant (BOP) costs are by far the largest cost category in the cost scaling. Included in this category are all costs related to heat transport and power conversion, land, buildings, auxiliary systems, and plant control systems. The BOP costs are determined by a formula which combines costs linear with power, costs nonlinear with power, and costs that are essentially invariant.

In the first category fall costs associated with the turbine generator set and auxiliary systems. Invariant costs include land, administration building and warehouse, site preparation, radwaste systems, and miscellaneous handling equipment.

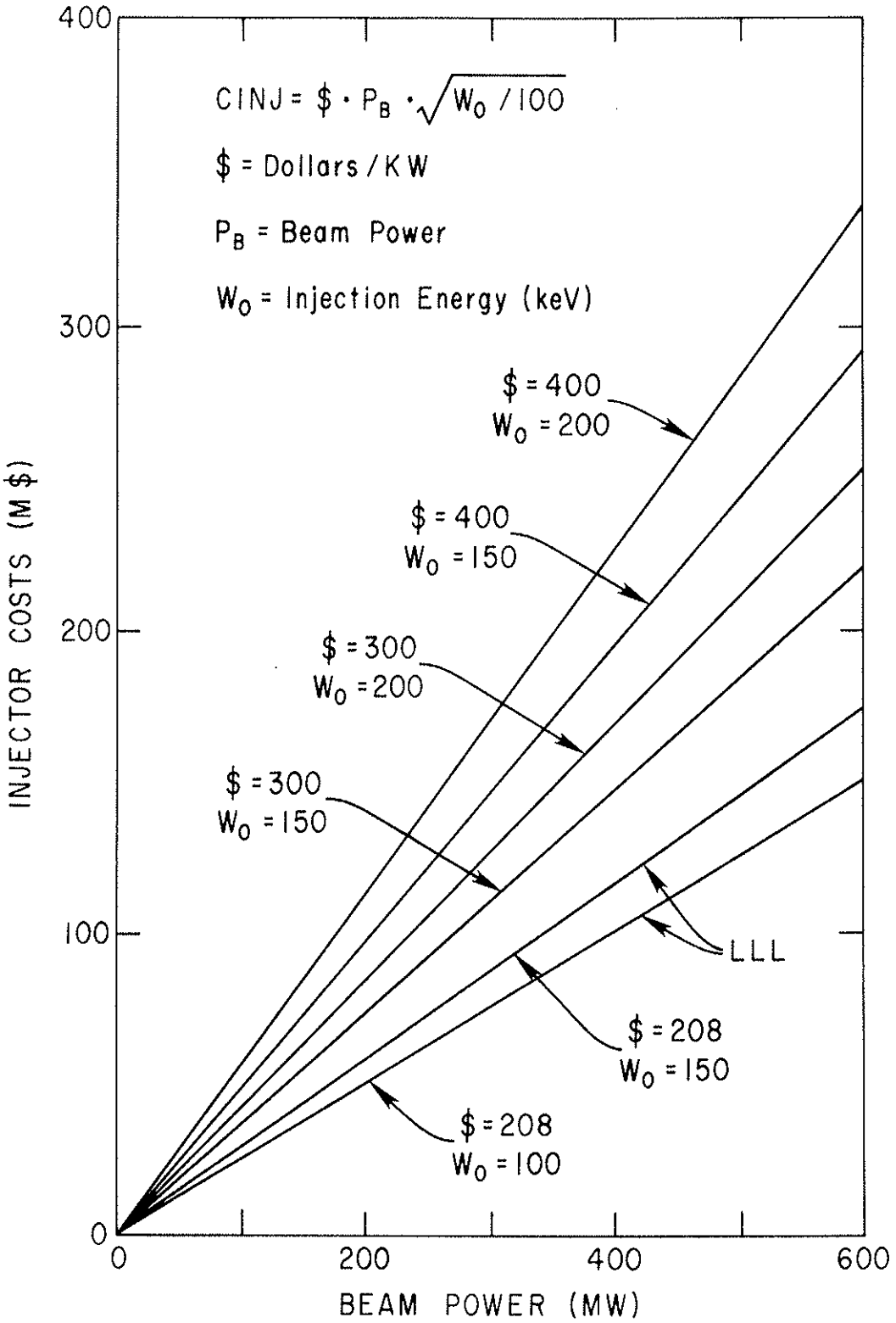

Fig. 3. Cost of Neutral Beam Injection System.

Nonlinear costs are the major BOP item. These costs are assumed to vary with gross electric power (P_g) to the 0.6 power.[9] Included in these costs are plant structures (except those listed above), heat transport systems, feedwater heating systems, thermal heat rejection systems, and plant control and electrical systems. The effect of combining these costs into the equation, $CBOP = [50 + 0.033\ P_g + 585\ (P_g/1807)^{0.6}] \times 10^6$ is shown in Figure 4.

To accommodate "electric breeders," i.e., plants which produce no net power but much fissile fuel, a lower limit on BOP costs of $\$200 \times 10^6$ is imposed. This limit is achieved for $P_g = 175$ MW.

Surprisingly the sensitivity of costs of electricity to the exponent or power is small. A 10 percent change (0.6 to 0.66) gives only a 1.3 percent increase in electricity costs for the nominal hybrid. Increasing the exponent from 0.6 to 0.9 yields a 7 percent increase.

f. Indirect Costs

Indirect costs are added to direct costs. These costs represent construction facilities, services, equipment, and office costs; cost of engineering services and other owner's costs. As a percentage of direct costs, they are 23, 14, and 8 percent,[7] respectively, for a total of 45 percent.

g. Interest during Construction

Interest During Construction (IDC) costs represent funds borrowed during construction. Project life is assumed to be 10 years, interest rate, 8 percent, and a "S-shaped"

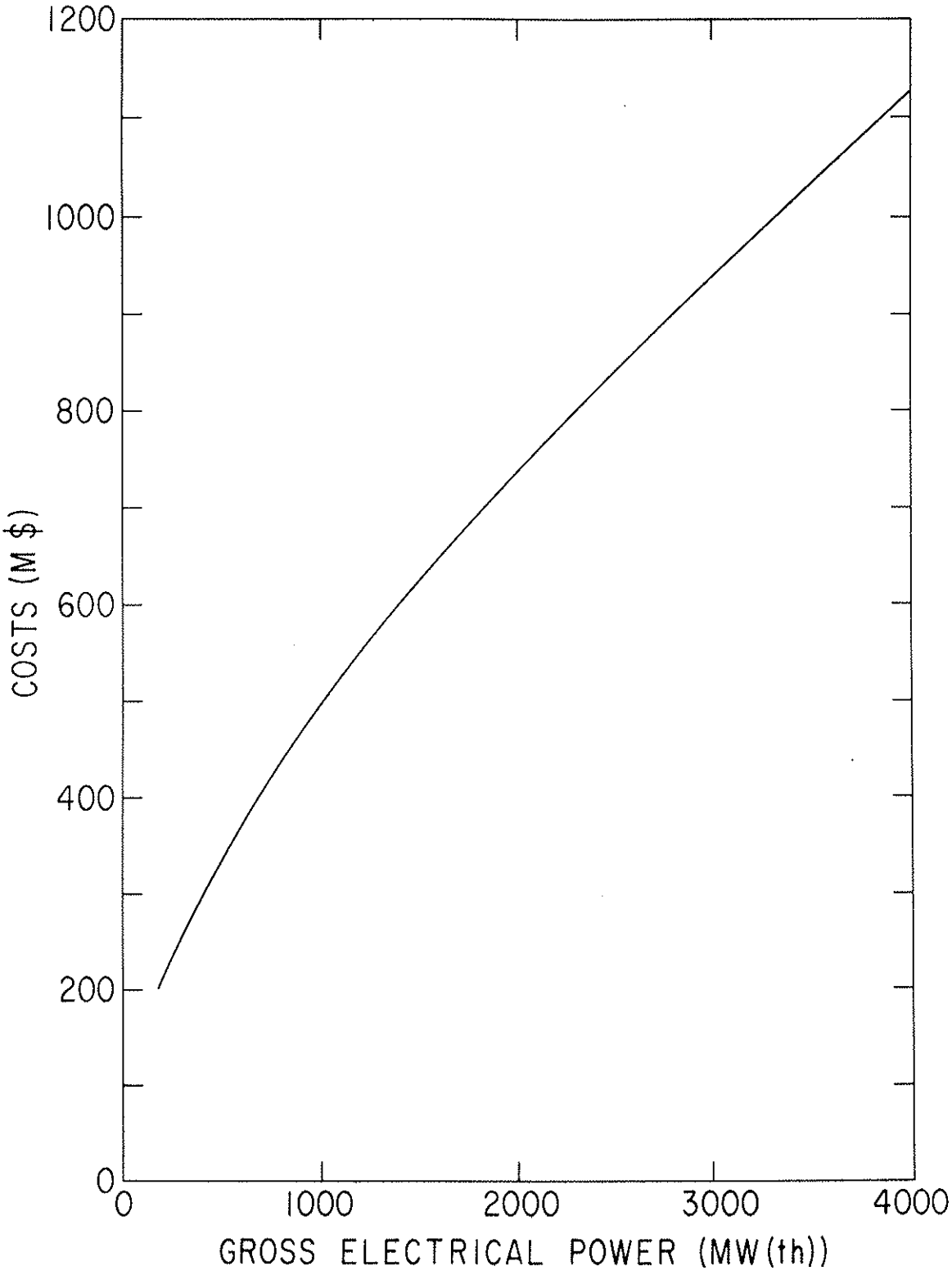

Fig. 4. Balance of Plant Costs.

curve of expenditures vs. time. For these assumptions, IDC costs represent 33.12 percent of total direct plus indirect costs.

h. Contingency

Contingency funds are not assigned in the cost scaling. Contingency is normally allocated on the basis of items unspecified by the engineering detail. Obviously, engineering detail is not present in this survey formulation, and cost scaling techniques themselves can produce errors on the order of the assigned contingency percentage.

4. Fuel Cycle Costs

a. Introduction

The fusion-fission hybrid produces two saleable commodities. The first, electric energy, is distributed and sold in the conventional sense. The second, fissile fuel, has a limited market, namely, fission reactors. While the desirability of hybrid-produced electric energy is easily judged by its cost, a measure readily understood by almost everyone, scientific or lay, the desirability of fissile fuel is not so easily assessed.

The dramatic increases in the cost of U_3O_8 since 1974 have focused attention on the limited extent of known uranium ore resources. Concurrently, concerns over nuclear proliferation and long-term radioactive waste storage have served effectively to suspend commercialization of spent fuel reprocessing.

The front end effect, namely ore costs, is the stimulus for the study of a fusion-fission hybrid device. The back end effect casts a pall of uncertainty over all nuclear efforts.

For this study the cost assumptions are apolitical in the sense that the cost bases are predicated upon the assumption that spent fuel reprocessing facilities would operate as designated in the early 1970's with nominal safeguards required. Dollar figures cited are 1976 dollars.

If it were not for the time value of money, fuel cycle cost calculations would be trivial. One would calculate the mass of material handled in a given operation, determine (or estimate) a unit price for that operation, sum the products of mass and unit price, and report the cost as that sum divided by the energy ultimately produced by the material. These direct costs, in fact, are not all of the actual fuel cycle costs. The principles of accounting, involving the time flow of disbursements and revenues, requires that the time value of money be considered. The resulting costs, called indirect costs, combined with the direct costs, determine the total fuel cycle costs reportable for a nuclear power plant.

For a fossil plant, and possibly for a pure fusion plant, this bookkeeping is much simplified. Fuel on hand is either consumed in a few months or, in pure fusion, kept in small inventory so that the time value of money is irrelevant.

Because of the nature of the parametric study, elegant fuel cycle cost codes developed over the last decade were not used. These codes require a high degree of detail for both neutronics and timing of operations and cash flow over the plant design life.

Instead, an equilibrium batch model[10] was adapted for both hybrid reload batches and an LWR for comparison. For the hybrid blanket inventory portion a breeder type batch analysis technique[11] was used. A qualitative description of these models follows.

Models for both the hybrid and the LWR have been derived on a consistent basis, since the value of hybrid-produced fissile fuel is determined by the allowable cost of fuel consumed by fissile burners (see Section IV.G).

b. Converter

i. Blanket Inventory

The cost of providing the uranium converter region and the plutonium in the molten salt (the dominant cost relative to the flibe) is incurred prior to initial operation. This investment is maintained for each batch so that the annual cost equals the carrying charge on the investment.

Following the formulation of Ref. 11, the salt cost component equals the cost of the molten salt plutonium plus storage charges from day of purchase to start of commercial operation, both multiplied by the carrying charge rate.

The converter cost component is the final (salvage) value times the carrying charge, plus the difference between initial and final value amortized by a sinking fund factor[12] over 30 years.

ii. Direct Costs

Direct cost items for the converter region include the following:

1. Purchase of tails (UF_6)
2. Fabrication of fuel elements
3. Shipping spent fuel
4. Reprocessing spent fuel and long-term storage of wastes
5. Credit for reclaimed uranium in spent fuel
6. Credit for reclaimed plutonium in spent fuel.

These costs are calculated based on mass inputs to the various operations multiplied by their respective unit costs.

iii. Indirect Costs

Indirect costs for the converter region include the following:

1. Preirradiation carrying charges on material purchase, conversion, and fabrication
2. Carrying charges on average value of fuel during irradiation
3. Carrying charges on average fabrication investment during irradiation
4. Carrying charges on fuel during decay and shipping
5. Pre- and post-irradiation carrying charges on recycled plutonium (salt region)
6. Carrying charges displaced by accumulation, i.e., credit for expenses incurred after receipt or revenue, namely shipping and reprocessing.

These indirect costs are assessed on the basis of incurred expense (or credit) multiplied by the approximate carrying charge rate; then this product multiplied by the time interval from the date of the operation to the irradiation period. Irradiation carrying charges are based on the duration of the irradiation period.

Carrying charge rates used are those for depreciating capital, nondepreciating capital, and working capital.

c. LWR Fuel Costs

i. Direct Costs

Direct cost items for the Pu LWR fuel cycle include the following:

1. Purchase of makeup U_3O_8
2. Conversion to UF_6
3. Purchase of makeup plutonium
4. Fabrication of mixed oxide fuel elements
5. Shipping of spent fuel
6. Reprocessing spent fuel
7. Credit for reclaimed uranium
8. Credit for reclaimed plutonium.

As before, these costs are calculated on the basis of mass multiplied by unit cost.

ii. Indirect Costs

Indirect costs for the LWR fuel cycle include the following:

1. Preirradiation carrying charges on material purchase, conversion, and fabrication

2. Irradiation carrying charges on the average value of the fuel while in core
3. Carrying charges in the average fabrication investment during irradiation
4. Carrying charges on fuel during decay and shipping
5. Carrying charges displaced by accumulation, i.e., credit for the deferred expenses of shipping and reprocessing.

These indirect costs are assessed on the basis of incurred expense (or credit) multiplied by the appropriate carrying charge rate; then this product multiplied by the time interval from the date of the operation to the irradiation period start or finish. Irradiation carrying charges are based on the duration of the irradiation period. Initial core costs are included with the plant capital costs.

d. Unit Costs

As described above, operation costs are taken as the product of mass per operation and cost per unit mass. Unit costs were developed based on fission industry experience or estimates for similar operations.

The fabrication cost of the hybrid converter should be in the same range as the fabrication cost of enriched uranium LWR fuel. Tolerances are expected to be less stringent than for LWR pellet and cladding, but the coextrusion of slug and cladding may be more difficult. Since LWR fuel costs are approximately \$70/kg,[13] this value was selected as the lower limit of costs. Low throughput or difficulty in clad fuel

bonding could conceivably increase this cost. An upper limit of $150/kg is considered suitable to allow for these uncertainties. While the lower limit is used in the survey analysis, the upper limit is used to test the sensitivity of the hybrid fabrication cost. A change from 70 to 150 $/kg adds 3 mills/kWh to the cost of electricity, a change of 8 percent.

The fabrication cost of mixed (U and Pu) oxide fuel for the LWR has been estimated to be $70/kg more than the fabrication cost of UO_2 elements.[14] This gives a nominal cost of $140/kg. The range of values used was 100-270 $/kg with the lower limit used for survey calculations. However sensitivity checks indicate than an increase from $100 to $270 will result in less than 5 percent increase in the cost of electricity.

The cost of reprocessing spent fuel was judged to be the same for both hybrid and LWR. The range of costs considered was 100-200 $/kg.[15] Values used in the survey were $100/kg of heavy metal for reprocessing plus $25/kg of waste for long-term storage. Great uncertainty exists in the probable costs of reprocessing, even in the absence of political pressures. No commercial reprocessing has been performed in the United States since 1972. It is interesting to note, however, that costs of electricity are particularly insensitive to the reprocessing costs chosen. $200/kg unit costs result in only a 1 percent increase in the cost of electricity over $100/kg costs.

Approximately 200,000 tons of enrichment process tails (uranium depleted of U-235) are currently being stored at the

various diffusion plants. While ore of this "enrichment" may be considered to have a negative value in some fuel cycle economics,[15] it is considered to be available at some nominal price from the U.S. government (DOE). A value of $5/kg of UF_6 has been assigned. Doubling the price effects only a 0.2 mill/kWh increase in the price of electricity.

Blankets composed of natural uranium have also been studied. In these cases the cost of natural uranium ore has been derived from the value of the fissile fuel produced. The relationship used was the one giving the parity price (cost of 1 gm of 93 percent enriched uranium fluoride) in terms of the cost of natural uranium fluoride.[16] The value of bred plutonium has been assumed to be 60 percent of parity. Thus, when the cost of bred fissile and separative work is known, the corresponding cost of natural uranium can be determined as a function of tails assay (weight percent of U-235 in tails). The basis for this assumption is that, in a competitive market in which two fissile species (Pu-239 and U-235) are available, the cost of the new product (Pu-239), in order to gain market penetration, must be equal to or less than that of the traditional product. If the costs are equated, the market cost of makeup natural uranium can than be determined.

e. Salt Processing and Makeup

A small flow of molten salt is removed from the blanket for conditioning and fission product removal. The process used is essentially similar to that proposed for the molten salt breeder reactor. The operating costs for this process are assumed to

be \$1 x 10^6/yr. Equipment costs for salt handling are included in the invariant part of the balance of plant capital cost estimates. For comparison, the Molten Salt Breeder Reactor project estimated capital and operating expenses of 0.3 mill/kWh(e)[17] or about \$2 x 10^6/yr. Calculations show that the cost of electricity is essentially insensitive to this factor.

Depletion of lithium and beryllium by neutron capture is calculated, and the cost of makeup is added to the salt reprocessing costs. Costs of lithium and beryllium are assumed to be 20 and 33 \$/kg, respectively. This cost also makes a negligible contribution to the cost of electricity.

f. Operating and Maintenance Costs

Replacement of portions of the first wall and blanket supporting structure that suffer excessive radiation damage is expected to be an expensive and time consuming process. Because it will be performed on an infrequent basis, its costs are treated separately.

The costs are proportional to first wall area and the annual integrated wall load with replacement cost assumed to be \$$10^4$/$m^2$. In determining the replacement interval the first wall capability is assumed to be 5 MW-yr/m^2. The frequency is then equal to the product of wall load (MW/m^2) and capacity factor, divided by the first wall capability. As an example, a wall load of 0.5 MW/m^2, and capacity factor of 0.75 yields a replacement frequency of 9.075 yr^{-1} or total replacement every 13 years.

Normal operating and maintenance costs are assigned at the rate of 1.5 mills/kWh of net power output. This figure

represents approximately \$20 x 10^6/yr in normal operating and maintenance costs (for a hybrid of 3000 MW gross electric power). At this same rate, LWR operating and maintenance costs approach \$10 x 10^6/yr. Current estimates are in the range of \$4-7 x 10^6/yr for 1,000 MWe LWR units.[18]

References

[1]R. W. Moir et al., Progress on the Conceptual Design of a Mirror Hybrid Fusion-Fission Reactor, Lawrence Livermore Laboratory Report UCRL-51797 (1975).

[2]United Engineers and Constructors, 1000 MWe Central Station Power Plant Investment Cost Study, U.S. Atomic Energy Commission Report WASH-1230 (1973).

[3]A Fusion Power Plant, R. G. Mills, ed., Princeton Plasma Physics Laboratory Report MATT-1050 (1974).

[4]M. S. Lubell, Superconducting Toroidal Magnets for Fusion Feasibility Experiments and Power Reactors, Proceedings of the Fifth International Cryogenic Engineering Conference, K. Mendelssohn, ed. (IPC Science and Technology Press, Guildford, England, 1974) pp. 164-173.

[5]B. Badger et al., UWMAK I: A Wisconsin Toroidal Fusion Reactor Design, University of Wisconsin Report UWFDM-68, rev. (1974).

[6]B. Badger et al., UWMAK II: A Conceptual Tokamak Power Reactor Design, University of Wisconsin Report UWFDM-112 (1975).

[7]B. Badger et al., UWMAK III: A High Performance, Non circular Tokamak Power Reactor Design, University of Wisconsin Report UWFDM-150 (1975).

[8]J. R. Powell, Design and Economics of Large DC Fusion Magnets, Proceedings of the 1972 Applied Superconducting Conference (Institute of Electrical and Electronics Engineers, New York, 1972) IEEE Pub. No. 72CHO682-5-TABSC, pp. 346-353.

[9]M. M. El-Wakil, Nuclear Energy Conversion (Intext Educational Publishers, New York, 1971).

[10]J. F. Bader et al., Estimating Average Nuclear Fuel Costs, Power Engineering, November 1969, pp. 50-53.

[11]P. Dragoumis et al., Estimating Nuclear Fuel Cycle Costs, Nucleonics 21, 40 (1966).

[12]E. L. Grant and W. G. Ireson, Principles of Engineering Economy, 5th ed. (Ronald Press Co., New York, 1970).

[13]The Nuclear Industry 1974, U.S. Atomic Energy Commission Report WASH-1174-74 (1975).

[14]D. E. Deonigi, The Value of Plutonium Recycle in Thermal Reactors, Nuclear Technology 18, 80 (1973).

[15]The Nuclear Fuel Cycle, U.S. Energy Research and Development Administration Report ERDA-33 (1975).

[16]NUS Corporation, Guide for Economic Evaluation of Nuclear Reactor Plant Designs, U. S. Atomic Energy Report NUS-531 (1969).

[17]A. M. Perry and H. F. Bauman, Reactor Physics and Fuel-Cycle Analyses, Nuclear Technology 8, 208 (1970).

[18]W. W. Brandfon, An Analysis of Power Generation Costs: 1985-2000, Electric Light and Power 54, 12 (1976).

F. The Constraints

The only constraint imposed upon the construction of the domain of parameter space to be used was that the domain should embrace a broad spectrum of possibly interesting machines. Under such sweeping generalities, the inclusion of elements, i.e., "6 vectors," that correspond to undesirable machines (a machine is termed undesirable if it violates a design criterion, a basic physics law, etc.) is inevitable. Consequently, more stringent criteria that reflect the degree of acceptability of each element of the domain must be invoked.

A constraint may be categorized as either a barrier type or a penalty type. The barrier type of constraint requires the absolute compliance with a specified criterion. A failure to conform with the criterion results in the rejection of that element from the domain of possible machines. Six such constraints are present in the analysis. They pertain to: the core size, the plasma confinement, the plasma current, the blanket performance, the beam power, and the net electrical power output.

The penalty type of constraint does not result in the rejection of a particular element (6-vector) from the domain of parameter space, but does result in the adjustment of some quantity derived from the chosen 6-vector. Two such constraints are present in the analysis. They pertain to the penetration of the neutral beams into the plasma and the value of β_θ.

We first discuss the barrier type constraint.

1. The Core Constraint

The core constraint requires the current density in the OH windings (see Figure 1) not to exceed a materials limit of 1,250 amps/cm^2.[1] The current in the OH coils must generate a sufficiently large flux swing in order to induce and sustain the plasma for the duration of the plasma burn. However, the total flux swing linking the plasma is the sum of the core flux swing, ϕ_{CORE}, induced by the OH coils and the flux swing, ϕ_{VERT}, originating from the rise in the vertical field, B_v, as it follows the growth of the plasma current to its steady state. This condition may be written as

$$\phi_{CORE} + \phi_{VERT} = \phi_{PLASMA} + \phi_{BURN}. \qquad (1)$$

ϕ_{PLASMA} is the increment of flux necessary to induce the plasma current, and ϕ_{BURN} is the flux change necessary to maintain the plasma current during the burn time.

An expression for ϕ_{CORE} may be obtained by equating it with the flux through the core under steady conditions. Modeling the magnetic field in the core after that of an infinite solenoid as shown in Figure 1, we find

$$\phi_{CORE} = \pi B_c R_{OH}^2 \left\{ 1/3\left(\frac{W_1}{R_{OH}}\right)^2 - \frac{W_1}{R_{OH}} + 1 \right\} 10^{-8}. \qquad (2)$$

Assuming a uniform current density, J, in the OH coil yields

$$B_c = 4\pi \frac{J}{10} W_1 \quad , \qquad (3)$$

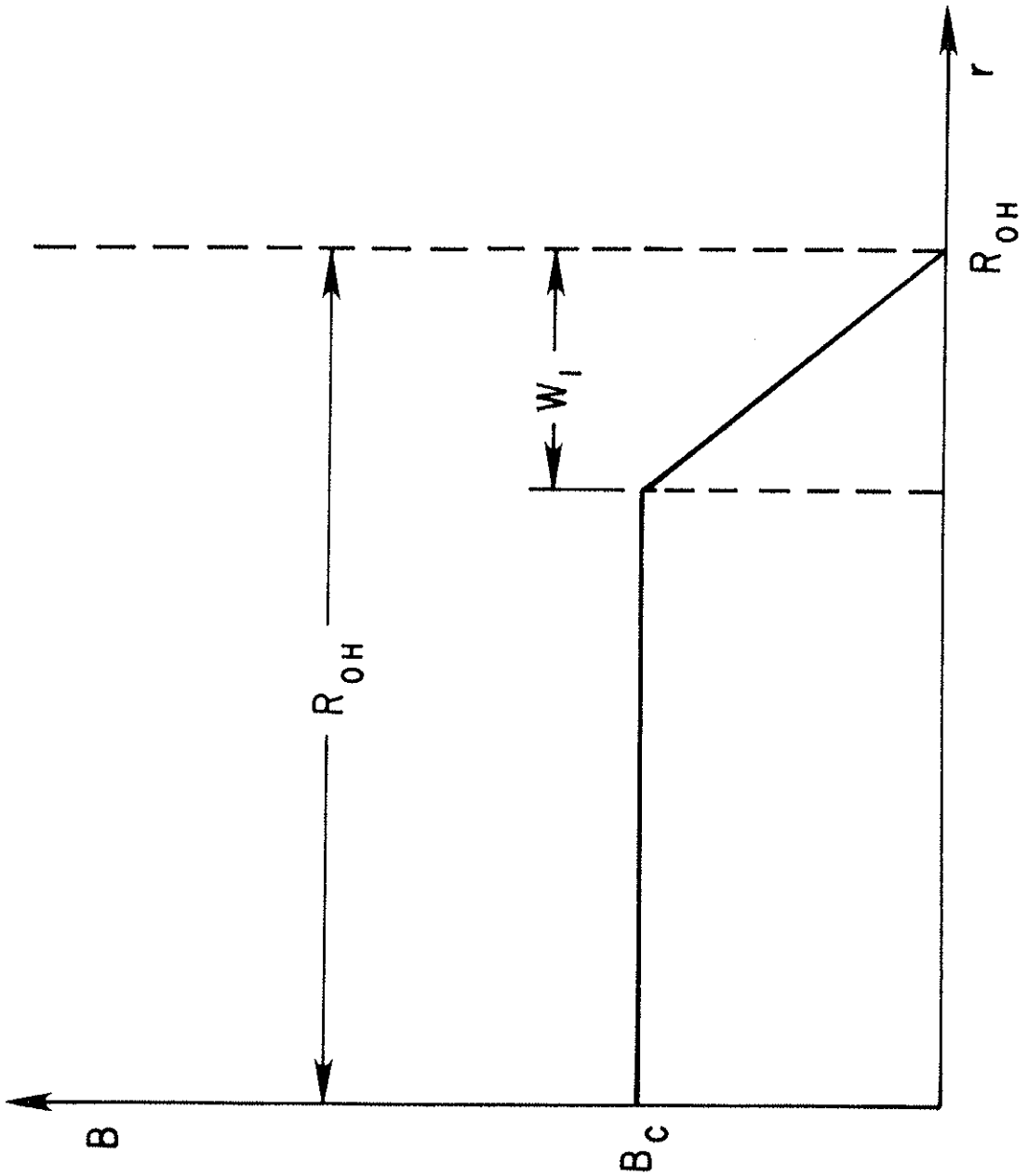

Fig. 1. The assumed spatial dependence of B_c. The ohmic coils are of width W_1, and their outside edge is located at R_{OH}.

and upon substituting this expression into Eq. (2) we have

$$\phi_{CORE} = \pi R_{OH}^3 \frac{2\pi}{5} J \left(\frac{W_1}{R_{OH}}\right) \left\{1 - \frac{W_1}{R_{OH}} + \frac{1}{3}\left(\frac{W_1}{R_{OH}}\right)^2\right\} 10^{-8}. \quad (4)$$

Here R_{OH} and W_1 are expressed in cm, J is in amp/cm^2, and ϕ is in volt-seconds. Specifically we take $W_1 \leq 90$ cm (because then B_c = 14T at maximum J) and R_{OH} = h - 150 cm. We have assumed the TF coil to be 100 cm thick and to be supported by a 50 cm thick cylinder.

The vertical field flux, ϕ_{VERT}, is estimated by employing the spatial dependence for B_v as displayed in Figure 2.

The vertical field flux is therefore

$$\phi_{VERT} = \pi R^2 B_v \left\{1 + \left(\frac{k-1}{4}\right)\left(1 + \frac{h}{R}\right)\right\} . \quad (5)$$

The magnitude of the vertical field necessary to support tokamak MHD equilibrium is taken to be

$$B_v = - \frac{I}{10R} \left\{\ln \frac{8R}{a} - 1.25 + \beta_\theta\right\} \quad (6)$$

where I is the plasma current in amps, R and a are in cm, and B_v is in gauss. Eq. (6) is derived from Eq. (97) of Ref. 2, and assumes a uniform current distribution and a spatially parabolic pressure distribution in the plasma. Upon substitution of Eq. (6) into Eq. (5), the ϕ_{VERT} in volt-seconds is found to be

$$\phi_{VERT} = - \pi R I 10^{-9} \left\{\ln \frac{8R}{a} - 1.25 + \beta_\theta\right\} \left\{1 + \left(\frac{k-1}{4}\right)\left(1 + \frac{h}{R}\right)\right\} . \quad (7)$$

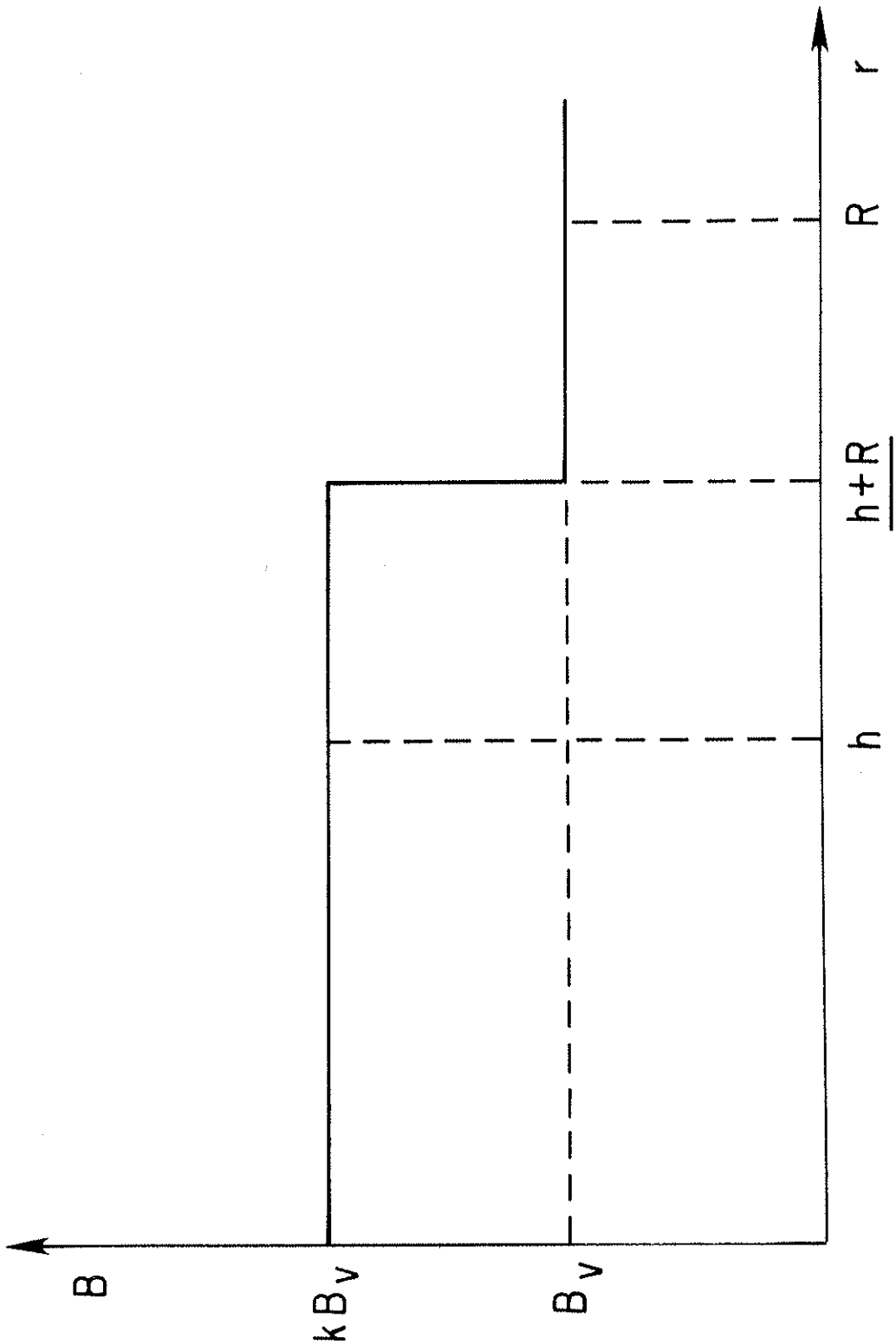

Fig. 2. The assumed spatial dependence of B_v. The plasma center is at R. The inside edge of the TF coils is at h.

Now k is taken as 1.85 for the single null magnetic field configuration, and -0.8 for the double null configuration. These choices for k reflect the numerical study of plasma equilibria described above in Section IV.C. The reversal of the vertical field in the central region for the double null configuration is illustrated in Figure 3.

The flux change ϕ_{PLASMA} necessary to induce the plasma current to its full steady state level is taken as

$$\phi_{PLASMA} = - 3/2 \; LI \quad . \tag{8}$$

The factor of 3/2 appearing in Eq. (8) has been introduced to allow for resistive losses during startup. To estimate the plasma inductance[3] we model the plasma as a thin circular wire. This model is consistent with the assumption inherent in the calculation of the vertical magnetic field, B_V. We take the plasma inductance to be

$$L = 4\pi \; R(\ln 8 \; R/a - 1.75) \times 10^{-9} \text{ henries} \quad . \tag{9}$$

Substituting Eq. (9) into Eq. (8) yields

$$\phi_{PLASMA} = - 6 \times 10^{-9} \; \pi \; R(\ln 8 \; R/a - 1.75) \; I \text{ voltseconds} \tag{10}$$

The flux change, ϕ_{BURN}, is

$$\phi_{BURN} = - I \; r \; t \tag{11}$$

where I is the steady state plasma current, r is the plasma resistance, and t is the length of time associated with the

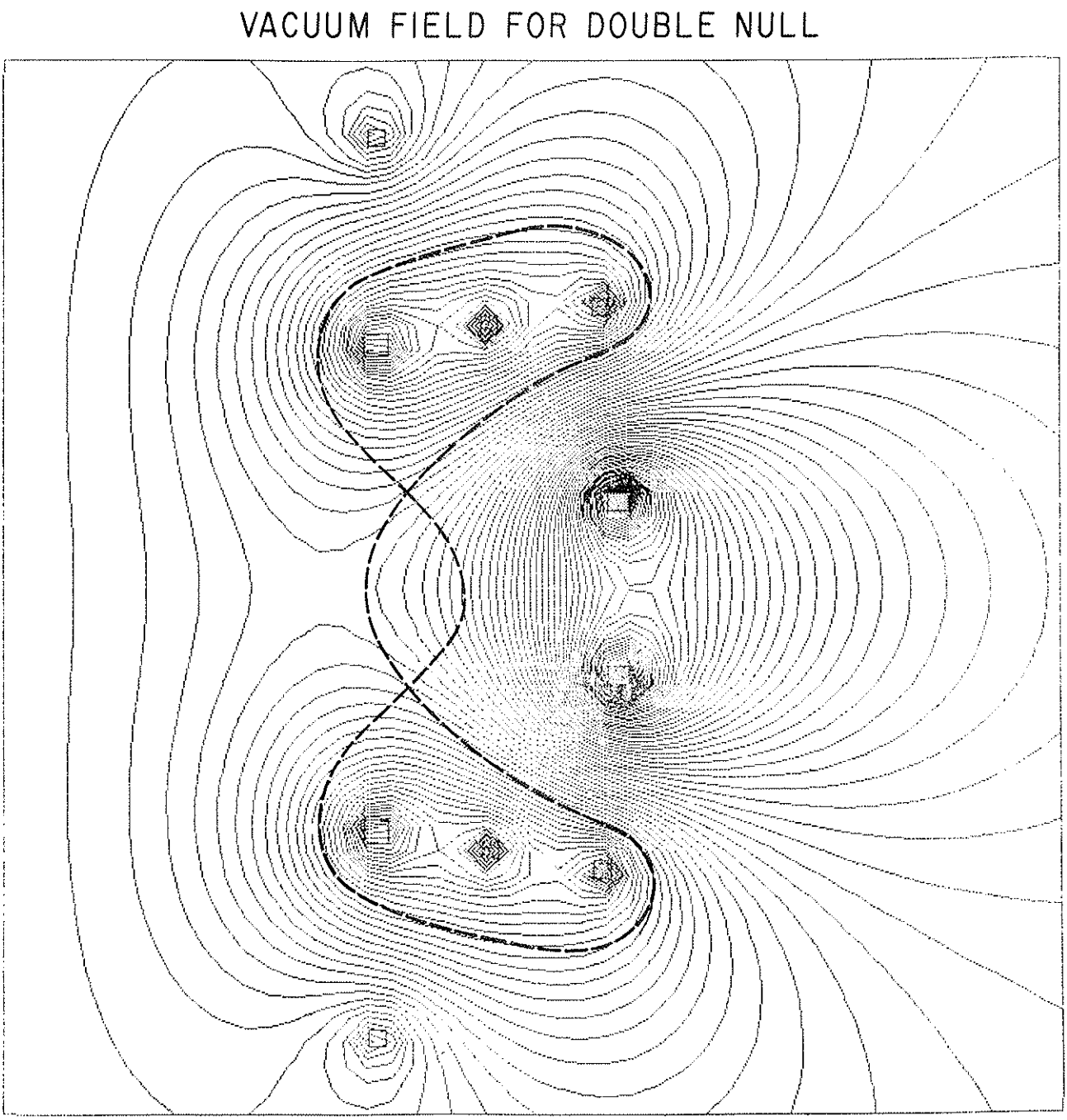

Fig. 3. Vacuum Magnetic Field for Double Null Configuration.

burn. The burn time has been assumed to be 1000 seconds. The resistance, r, for a toroidal conductor is

$$r = \eta \, 2\frac{R}{a^2} \tag{12}$$

where the plasma resistivity, η, is taken to be the Spitzer electrical resistivity, for a hydrogenic (Z = 1) plasma

$$\eta = 6.53 \times 10^3 \; \frac{\ln \Lambda}{(T\ ^{o}K)^{3/2}} \quad \text{ohm-cm} \; . \tag{13}$$

The coulomb logarithm, $\ln \Lambda$, is given a value of 18 corresponding to a plasma temperature of about 10 keV and an electron density of 10^{20} m^{-3}. Then, the final expression for ϕ_{BURN} is

$$\phi_{BURN} = - 5.95 \times 10^{-3} \frac{R}{a^2} T^{-3/2} I \quad \text{volt-seconds} \tag{14}$$

where T is the plasma temperature in keV, I is the plasma current in amperes, and R and a are in cm.

Equation (1) may be solved for the current density, J, in the OH coils in a straightforward manner employing the expressions for ϕ_{CORE}, ϕ_{VERT}, ϕ_{PLASMA}, and ϕ_{BURN} found in Eqs. (4), (7), (10), and (14), respectively. The value of J obtained is construed as the magnitude of the current change that must occur in the OH coil. By a prudent choice of initial current, the peak current density in the OH coil need only reach half of the required current swing. Therefore, the current density, J, is to be compared with twice the critical value of 1,250 amp/cm^2. Should J exceed this value of 2,500 amp/cm^2, the associated point in parameter space is deemed unacceptable.

2. The Plasma Confinement Constraint

A second barrier constraint deals with the confinement of the plasma. Plasma confinement can be measured either by an energy or a particle confinement time. Both characteristic times are derived from an energy balance imposed upon a representative cubic centimeter of plasma. The first is obtained by considering only the energy input to the plasma. The only energy sources considered are the beam power, P_B, deposited in the plasma and the alpha particle power, P_α, heating the plasma. (The ohmic heating is considered to be inconsequential.) Then, the power sources are the sum, i.e.,

$$P_{so} = P_B + P_\alpha \quad . \tag{15}$$

Under steady state operating conditions, the sources of power are just balanced by the rate at which power flows from the plasma. The equation,

$$P_B + P_\alpha = \sum_i n_i(3/2\ kT_i)/\tau_E \quad , \tag{16}$$

serves to define the energy confinement time, τ_E, of the plasma where n_i and T_i are the density and temperature of the i^{th} species, respectively, and the summation is over the plasma ions and electrons.

An expression for the particle confinement time, τ_p, may be obtained by considering a more detailed expression for the power sinks, P_{si}, e.g.,

$$P_{si} = P_{rad} + P_{dif} + P_{cond} + P_{ion} + P_{cx} \quad . \tag{17}$$

The term P_{rad} accounts for the bremsstrahlung radiation losses in a hydrogenic plasma and is

$$P_{rad} = 1.334 \times 10^{-19} \; n_e^2 \; (kT)^{1/2} \; \frac{ergs}{cm^3 \; sec} \qquad (18)$$

where n_e is the electron density in cm^{-3}, and kT is the temperature in ergs. The terms P_{dif} and P_{cond} represent losses due to particle diffusion and thermal conduction. In this study, these two losses are assumed to be equal in magnitude. Then,

$$P_{dif} = P_{cond} = \sum_i n_i \; (3/2 \; kT)/\tau_p \quad . \qquad (19)$$

The terms P_{ion} and P_{cx} represent, respectively, the losses accompanying the ionization of neutrals and the charge exchange of fast ions with slow neutrals. In a steady state these losses will be proportional to the sources of neutrals which are the injected neutral beams and the current of recycled atoms. Particle conservation requires the ion loss rate to be balanced by the ion sources. Neglecting the loss rate of ions by fusion reactions we have (since Z = 1):

$$\frac{n_e}{\tau_p} = J_{rec} + J_{beam} \quad . \qquad (20)$$

The J_{rec} is the sum of reionized atoms recycling from the plasma via material walls plus any deliberate low energy fueling of the plasma such as by pellet injection. Exactly how J_{rec} is divided between these two processes is beyond the scope of

this study.

We take

$$P_{ion} = \frac{n_e}{\tau_p} \times U_I \quad , \tag{21}$$

where U_I is chosen to be 25 eV per ionizing event, and

$$P_{cx} = \frac{1}{10} J_B(\frac{3}{2} kT) + \frac{1}{8} \left\{\frac{n_e}{\tau_p} - J_B\right\} \frac{3}{2} kT \ . \tag{22}$$

The first term in P_{cx} estimates the loss of energy arising as a consequence of charge exchange between plasma ions and the injected neutral beam. The estimate assumes that some ionization of the charge exchange neutrals takes place before they can leave the plasma.[5] The second term in P_{cx} estimates the loss of energetic neutrals arising from the recycle current. At plasma temperatures of 5 to 20 keV charge exchange is the most likely interaction between a slow neutral and an ion.[6] Hence, of the current of low energy neutrals entering the plasma, approximately half will penetrate deep into the plasma for eventual ionization, and half will leave the plasma having undergone charge exchange in the cooler outer regions of the plasma. These charge exchange neutrals will carry with them a fraction of the average energy of the plasma ions.

We note that P_{ion} and P_{cx} are small compared to P_{diff}.

Having defined all of the terms of Eq. (17) and by equating Eqs. (17) and (15), the particle confinement

time is found to be:

$$\tau_p = \frac{\sum n_i \left| 3.09375\ kT + 0.0125 \right|}{P_\alpha + P_B - 3.333 \times 10^{13} \sqrt{kT} + 0.0375\ J_B\ kT} \qquad (23)$$

where kT is expressed in keV, P_α and P_B in keV/cm^3-sec, J_B in cm^{-3}-sec^{-1}, n_i in cm^{-3}, and τ_p in sec.

These calculations of τ_E and τ_p are interpreted as the confinement times that must be met in order to preserve steady state conditions of constant density, temperature, etc. In addition to these, other confinement times, which are assumed to be based upon the physics of the transport mechanisms involved, may be calculated. In this study, three such confinement times have been employed, namely, one based upon the trapped electron mode of plasma transport, another based upon Alcator scaling, and a third, utilizing a machine independent value for the confinement parameter, $n_e\tau_p$, of 5×10^{13} cm^{-3} sec.

The relation between τ_p and a theoretical diffusion coefficient, D, is taken to be

$$\tau_p = a^2/4D\ . \qquad (24)$$

The trapped electron τ_p is based upon our rendition of the trapped electron transport appearing in the "Rutherford-Düchs code".[7] We use the trapped electron diffusion coefficient D_{TE} appearing in Eq. (14) of Ref. 7. In this formulation we take $Z_{eff} = 1$, the parameters $r_n = r_T = 4\ a/3\alpha$ (where a is the minor radius and α is the pressure profile factor used in the

pressure scaling calculations), and the parameter $\theta = 1/2\ \sqrt{\beta/\beta_\theta}$. Eq. (24) then yields the confinement time, τ_p, to be:

$$\tau_p \equiv 0.25\ a^2 \times 10^4 \left[\frac{h\ B_s^{1/2}}{RT(3.9 \times 10^{14})} + \frac{A + B}{C\ \exp D} \right]$$

where

$$A \equiv 1.16 \times 10^5\ \frac{\alpha T^{1/2}}{R} \left(\frac{\beta}{\beta_\theta}\right)^{1/4} \left(\frac{n_D + n_T}{n_D + 1.22\ n_T}\right)^{1/2}$$

$$B \equiv 1.84 \times 10^{-10}\ n_e T^{-3/2}\ \ln\left(1.09 \times 10^{14}\ T\ n_e^{-1/2}\right)$$

$$C = 6.6 \times 10^7\ \left(R/a\right)^{1/2}\ \frac{1}{B_s}\ \left(\frac{T\alpha}{h}\right)^2$$

$$D = -\ \frac{Rn_e}{T^2} \left(\frac{\beta_\theta}{\beta} \cdot \frac{R}{a}\right)^{1/2} \ln\left(1.09 \times 10^{14}\ T\ n_e^{-1/2}\right) \qquad (25)$$

The distances a, h, R appearing in Eq. (25) are all in meters whereas the density, n_e, is in cm^{-3}, the temperature, T, in keV, and B_s, the field at the coil, is usually taken to be 160 kilogauss.

By simplifying Eq. (25), a more manageable expression for $n\tau$ is obtained in Eq. (25a) which will prove valuable in the discussions of the results.

$$n_e\tau \approx n_e a^{5/2} ((R/a) I)^{1/2} \left(\frac{B}{T_e}\right)^{3/2} \left[\frac{8R\ n_e}{T_e^{\ 2}\ 10^{14}}\ (aB/I)^{1/2} + 10 \right] \qquad (25a)$$

The Alcator formula[8] for the energy confinement time τ_E is taken as

$$\tau_E = 2.12 \times 10^{-6} \, n_e \, a^3 \, (B/RI)^{1/2} \qquad (26)$$

where $B = \frac{h}{R} B_s$ is the magnetic field at R; n_e is expressed in cm^{-3}; a and R in cm; the magnetic field, B, in kilogauss and the plasma current, I, in megamperes.

The $n\tau$ constraint requires that, for a particular choice of physics-derived confinement time, τ_{PHY}, the corresponding energy balance or particle balance-derived confinement time, τ_{EB}, be less than the former, i.e.,

$$n_e \tau_{EB} < n_e \tau_{PHY} \, . \qquad (27)$$

The above prescription is based upon the postulate that τ_{PHY} functions as an upper bound on the achievable confinement time for a particular device. In order to enhance confinement, it would require choosing parameters that characterize a distinctly separate machine. However, confinement may be "spoiled" by some unspecified means without affecting the parameters characterizing a particular machine, or the machine cost of performance. Then

the existence of a set of possible machines is assured, under the proviso of (27) whose operating values of τ_{EB} will be necessarily equal but less than the τ_{PHY} of (27). We will refer to τ_{EB} as the "required" and to τ_{PHY} as the "allowed" confinement times.

3. The Plasma Current Constraint

This constraint requires the plasma current, I, to exceed 1 megampere. Such a strong current is assumed necessary to confine the alpha particles. Although machines satisfying this requirement served as the basis of the pressure scaling employed in this study, utilization of this scaling does not guarantee it. Consequently, the seemingly redundant imposition of this constraint is necessary.

4. Blanket Performance Constraint

This constraint requires the blanket energy multiplication, M, to fall between the appropriate limits of 8 and 27. For the details of the blanket design and their implications for the range of the blanket multiplication, M, the reader is referred to Section IV.D, Blanket Performance.

5. Neutral Beam Power Constraint

A fifth constraint is applied to the beam power, requiring that it be lower than a critical value P_{BMAX}. The calculation of P_{BMAX} is based upon the assumption that the combined area of all beam port openings may consume no more than 50% of a band in the first wall, running toroidally around the tokamak on the outward side, i.e., at r = R + a + 0.5.

The height of this band is equal to the distance between the plasma edge and its magnetic center, e.g., 0.65a for the single null. The beam ducts are envisioned as intersecting the first wall at 45°. Furthermore, the ducts may transport no more than 0.025 Amps/cm^2 for beam energies on the order of 200 keV which is assumed to be the equivalent of a power limit of 50 MW/m^2. Then

$$P_{BMAX} = 72.2 \quad a(R + a + 0.5) \quad , \tag{27.5}$$

where P_{BMAX} is the beam power in megawatts, and the distances a and R are both in meters. The factor of 0.5 appearing in Eq. (27.5) represents the thickness of the scrapeoff layer. The requirement that the beam power be less than P_{BMAX} is a very liberal constraint, being seldom invoked.

6. Net Power Constraint

This constraint requires positive net electrical power output for the hybrid. Intuition suggested that electrical power consuming hybrids would be unattractive economically. In order to reduce the computational time spent upon machines which would ultimately be judged uninteresting, a constraint was constructed which prevented the selection of power-consuming hybrids. Subsequent examination of this constraint as related to the survey results indicates the machines which were overlooked are indeed economically unattractive and remain so unless the fissle fuel price, FFP, becomes large (> 300 $/g). Therefore, the imposition of this constraint has not introduced any bias

into the study.

7. The Penalty Constraints

The second set of constraints imposed in this study is of the penalty type. Under this type of constraint, those machines that violate a particular criterion may regain acceptability by incurring a prescribed penalty which may reflect the degree of violation of the initial criterion. Thus, unlike the situation under the barrier type constraint, a sharp distinction between acceptable and unacceptable machines does not exist. Only two penalty type constraints are employed in this study, one pertaining to beam penetration of the plasma and the other, to MHD stability.

a. The Penetration Constraint

This constraint requires that the beams penetrate the plasma. The penetration criterion employed is a function of the fraction, x, of beam drive necessary to sustain the plasma, i.e.,

$$x = \frac{P_B}{P_B + P_\alpha} \tag{28}$$

where P_B and P_α are the beam and alpha power absorbed by the plasma. Such a parameterization reflects the authors' opinion that a very nearly ignited plasma need not require full penetration of the beams into the plasma center. However, even

an ignited plasma must be subject to the penetration criteria because the beams are viewed as an essential part of the start-up process. Under the supposition that in the heavily beam-driven cases the criterion must reduce to that of Rome et al.,[9] the penetration criterion is then taken as:

$$\frac{A}{\bar{N}} \leq \lambda \quad \text{where } N = \begin{cases} 2 & \text{for } x \geq 0.8, \text{ i.e., } Q < 1.25 \\ 10(1-x) & \text{for } 0.2 < x < 0.8 \\ 8 & \text{for } x \leq 0.2 \text{ i.e., } Q \geq 20. \end{cases} \quad . \quad (29)$$

The symbols A and λ appearing in Eq. (29) are , respectively, the distance from the plasma outer edge to the magnetic axis (A = 0.65a for single null and 0.75a. for double null) measured in centimeters and the mean free path for ionizing the neutral beam. The ionizing processes considered in the calculation of λ[10] are represented by the third and first terms of Eq. (30), respectively, and charge exchange is represented by the second term of Eq. (30). Thus,

$$1/\lambda = n_i \left\{ \frac{3.6 \times 10^{-12}}{E} \log_{10}\left(\frac{E}{6}\right) + \frac{0.6937 \times 10^{-14} \left(1 - 0.155 \log_{10} E\right)^2}{1 + 0.1112 \times 10^{-14} E^{3.3}} \right\} + \frac{n_e 10^{\left(-0.5151 \log_{10} T - \frac{2.563}{\log_{10} T} - 5.231\right)}}{(1.92 \times 10^{12} E)^{1/2}} \quad (30)$$

where E is the proton energy measured in eV corresponding to a deuteron of the same speed, T is the plasma temperature in eV, and n_e and n_i are the electron and cold ion densities, respectively, measured in cm^{-3}.

In the event that the criterion of Eq. (29) is not satisfied, the density is not permitted to realize the maximum value afforded by the pressure scaling (see Section IV.C on Pressure), but rather, a lower value of density is determined by imposing the equality branch of Eq. (29). The magnetic field, B, and the plasma current, I, are both reduced by the square root of the factor by which the density was reduced. The simultaneous adjustment of B and I preserves both the β and β_θ of the pressure scaling while reducing B reduces the cost of the TF magnets.

b. The β_θ Constraint

This constraint modifies the value of β_θ as calculated by the pressure scaling prescription given by Eq. (IV.C.11). Early numerical observations of MHD stability using the PEST code[11] resulted in the following stability requirement:

$$\beta_\theta \leq c \; R/a \; . \tag{31}$$

The constant c was taken as 0.82 for the single null configuration and 0.77 for the double null. If a tentative design point has a value of β_θ larger than allowed by Eq. (31), the β_θ is taken as c R/a for further calculations in the pressure

algorithm. Thus the immediate consequence of violating Eq. (31) is a reduction in plasma pressure. This reduction in pressure is shown in Figure 4. This figure shows the pressure as a function of a and h. The full lines show the pressures that satisfy Eq. (31). The dotted lines show the pressure given by Eqs. (IV.C 15 and 17) before the β_θ constraint described here is applied. It is apparent from this figure that the β_θ constraint has reduced the allowed plasma pressure over the entire prescribed range of the parameters a and h.

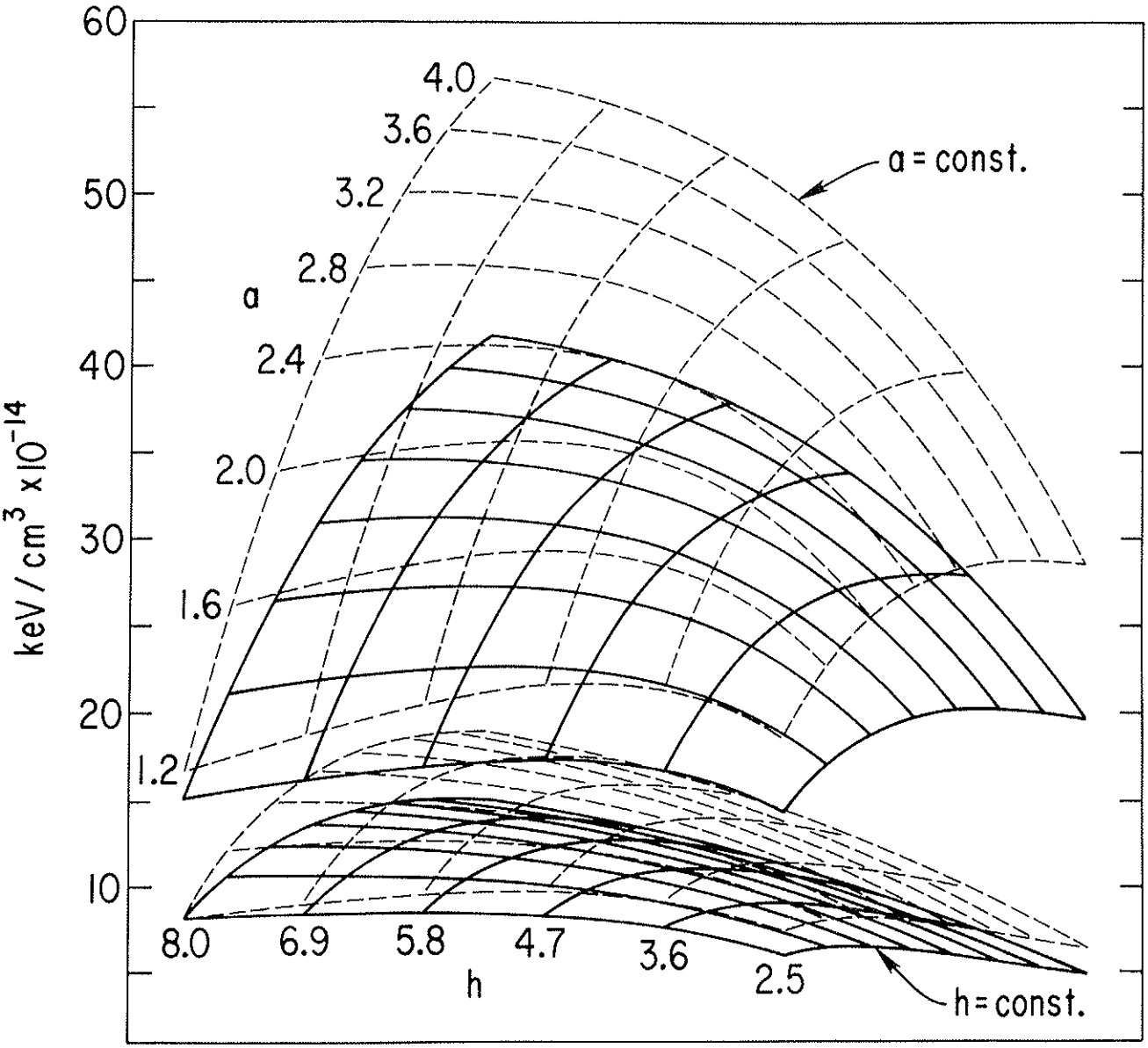

Fig. 4. Pressure carpets constrained (solid line) by β_θ and unconstrained (dashed line) for the double null (upper pair) and single null (lower pair) configuration.

References

[1]Private Communication, J. File to F. H. Tenney.

[2]J. M. Greene, J. L. Johnson, and K. E. Weimer, Tokamak Equilibrium, Phys. Fluids 14, 671 (1971).

[3]W. R. Smythe, Static and Dynamic Electricity (McGraw-Hill Book Company, Inc., New York, 1939) 1st ed., p. 315.

[4]L. Spitzer, Jr., Physics of Fully Ionized Gases (Interscience Publishers, New York, 1961) 2nd ed., p. 139.

[5]J. G. Cordey, W. G. F. Core, J. Sheffield, Calculation of the Gain Factor Q in Two-Component Plasma Systems, Nuclear Fusion 15, 755 (1975). (See Fig. 4 and discussion.)

[6]D. R. Sweetman, Ignition Conditions in Tokamak Experiments and Role of Neutral Injection Heating, Nuclear Fusion 13, 157 (1973). (See Fig. 10.)

[7]P. H. Rutherford and D. F. Düchs, A Computer Model of Radial Transport in Tokamaks, Nuclear Fusion 17, 565 (1977). (See Eq. 14.)

[8]D. R. Cohn, R. R. Parker, D. L. Jassby, Characteristics of High-Density Tokamak Ignition Reactors, Nuclear Fusion 16, 31 (1976); D. L. Jassby, D. R. Cohn, R. R. Parker, Reply to "Comments on the Paper, 'Characteristics of High-Density Tokamak Ignition Reactors'", Nuclear Fusion 16, 1045 (1976).

[9]J. A. Rome, J. D. Callen, J. F. Clarke, Neutral-Beam Injection into a Tokamak: Part I: Fast Ion Spatial Distribution for Tangential Injection, Nuclear Fusion 14, 141 (1974).

[10]A. C. Riviere, Penetration of Fast Hydogen Atoms into a Fusion Reactor Plasma, Nuclear Fusion 11, 363 (1971); P. H. Rutherford and D. F. Düchs, A Computer Model of Radial Transport in Tokamaks, Princeton Plasma Physics Laboratory Report MATT-1272 (1976); J. A. Rome et al., op. cit.

[11]R. C. Grimm, J. M. Greene, and J. L. Johnson, Computation of the Magnetohydrodynamic Spectrum in Axisymmetric Toroidal Confinement Systems, Methods in Computational Physics, J. Killeen, ed. (Academic Press, New York, 1976) Vol. 16, pp. 253-280.

G. Model for Computing Cost of Electricity

1. Introduction

The cost of electricity for a given power plant is determined by balancing revenues with expenses on an annual basis.

$$\phi C + O + F = eE \qquad (1)$$

where ϕ = annual fixed charge rate, yr^{-1}

C = plant capital cost, \$

O = annual operating and maintenance costs, \$/yr

F = fuel cycle costs, \$/yr

e = cost of electricity generated, \$/MW(e)hr = mills/kW(e)hr

E = annual energy production, MW(e)hr

Rearranging, $e = (\phi C+O+F)/E \qquad (2)$

This equation is the basis for various approaches to finding the hybrid plant that produces electricity at attractive rates.

ϕ has been defined as 0.15 for this study. Current projections of power costs available in the literature use ϕ in a range from 0.14 to 0.19. The sensitivity of costs of electricity to ϕ are large.

Plant capital costs sum the individual cost components described in Section IV.E.3. Operating costs include wall replacement and normal operating and maintenance charges. Fuel

cycle costs may be positive or negative depending on the amount and value of fissile fuel produced or consumed.

The annual energy produced is the product of plant capacity factor and plant rated net output. For LWR's, this is defined to be 6.57×10^6 MWhr per year. This figure models an LWR of 1000 MW(e) rated net output operating with a plant capacity factor of 0.75.

2. Nuclear Park

The calculation of the cost of hybrid generated electricity is complicated by the fact that the cost depends on the selling price of the bred fissile fuel. This dependency occurs in the calculation of carrying charges for the hybrid fuel cycle as well as the credit for the sale of fissile fuel produced.

In this study the hybrid electricity costs are generally calculated as functions of an assumed price of bred fissile fuel. This allows great flexibility in comparing the hybrid to other fission and non-fission sources of energy. However, the fissle fuel value must be chosen at some point in order to allow discussion of a particular hybrid embedded in a given energy system.

One solution to this problem is to formulate a nuclear "park" (or closed system) in which fissile fuel is produced and consumed. Raw material enters in the form of tails or natural uranium ore. Electricity is the only saleable

product; its price is dependent upon the price of operating the various units in the park.

The model consists of one hybrid power plant and N fissile fuel consumers that in this study are assumed to be light water reactors. (N is greater than zero and can have fractional values). Each LWR is assumed to have an output of 1000 MW(e) at a capacity factor of 0.75. The value of N is determined by the amount of fissile fuel produced: $G_B = N * 350$ kg where G_B is the net fissile fuel (after reprocessing) bred in the hybrid, and 350 kg represents the kilograms of fissile species required as annual makeup by each LWR.

Other units of the model represent fabrication and reprocessing units. Charges for these operations are incorporated via unit costs as described in Section IV.E.4.d.

By definition, in the nuclear park the price of electricity is identical for both the hybrid and the LWR's. Since fissile fuel is exchanged within the park, it also must have identical values for both types of power plants. These identities allow the writing of revenue balances for the park as a whole as well as for the hybrid and LWR's individually.

In effect Eq. (1) is applied to the hybrid and to the LWR, and the resulting pair of equations is used to solve for the two unknowns, e, and the price of fissile fuel, f. The following procedure is used to solve for e and f.

For a given hybrid, capital costs are calculated as described above. Capital costs for the LWR are specified to

be $750/kWe. Hybrid annual fuel production and capacity factor are calculated based on blanket and plasma performance. Annual energy outputs for both hybrid and LWR's are calculated using the fact of a linear relationship between e and f, as described in the next section. Two arbitrary prices of fissile fuel are assumed and the corresponding costs of electricity calculated using fuel cycle costs for both the hybrid and the LWR's as described above. From these calculated pairs of numbers, the straight lines describing the economics of the hybrid and the LWR are determined. The sought for values of e and f are defined by the intersection of these two straight lines.

Changing the character of the hybrid plasma, blanket, or both, necessarily changes the costs of electricity and fissile fuel. Thus, a wide range of hybrid parameters can be examined to determine the optimum product costs as well as the mix of fuel and power produced.

Since the model LWR's are essentially identical to those fueled with enriched U-235, the park calculations can also be used to determine the point of hybrid market penetration. Assuming that the bred plutonium carries a value of 60 percent of parity, one can readily calculate (for a given cost of separative work and tails assay) the "shadow" price of natural uranium feedstock to the enrichment process which would lead to electricity at the same price.

3. "Best Hybrid" Model

The cost of hybrid-generated electricity, e, is a function of the selling price of the bred fissile fuel, f. According to the above economic model e turns out to be a linear function of f.

The value of f enters into Eq. (1) of Section IV.G.1 through the fuel cycle costs, F, in two ways: the annual charge associated with the investment in the initial blanket inventory (Section IV.E.4.b.i) and the annual charge associated with the direct and indirect costs described in Sections IV.E.4.b.ii and 4.b.iii. The direct and indirect costs can be written as $(a_1 + a_2 f - G_B f)$ where a_1 and a_2 are independent of f and where G_B is the net fissile fuel (after reprocessing) bred in the hybrid. The quantity $G_B f$ is the revenue from the sale of fissile fuel and appears as a "credit" in the fuel cycle "costs". Thus we can write for F,

$$F = a_1 + f(a_2 - G_B + \phi\, a_3) \tag{3}$$

where $a_3 f$ is the initial investment in fissile fuel in the blanket. Substituting Eq. (3) into Eq. (1) we have:

$$eE = (\phi C + O + a_1) + (a_2 + \phi a_3 - G_B)f, \tag{4}$$

$$= b + s f. \tag{5}$$

These equations display the linear relationship between e and f for a given choice of hybrid plant design. The plant design affects both the quantity, b, and the "slope", s, in Eq. (5). In particular if G_B is large enough, s will be negative, a situation we expect for designs with "low" values

of blanket M and hence "high" values of blanket F. Such designs are "fuel producers" as compared to designs of "power producers" which have high values of blanket M and hence low values of blanket F. (It should be remembered that none of the hybrid designs considered in this study has a net consumption of either energy or fissile fuel.) The "power producers" will have positive values of s.

Equation 5 is displayed in Figure 1 for several hybrid designs taken from this study, each of which generates 3 GW of gross electric power. For each value of f there is a "best" hybrid in the sense that there is some hybrid design that produces electricity for the smallest cost, e. The nature of this "best hybrid" design changes as one considers different values of f. (See Table I.) The set of "best hybrids" defines a "best hybrid" envelope.

Also shown in Figure 1 is a straight line representing Eq. (4) applied to a 1000 MW(e) light-water reactor (LWR). The intersection of the LWR line with the line for a particular hybrid design defines the values of e and f that would characterize the economics of a nuclear park, in the sense of the preceeding section, using this pair of reactor designs. The "best park solution" for the hybrid designs shown in Figure 1 would be determined by the intersection of the LWR line with the "best hybrid" envelope. This particular choice of hybrid design will be simply referred to as "the park solution" (for 3 GW(e) gross) or "the park hybrid".

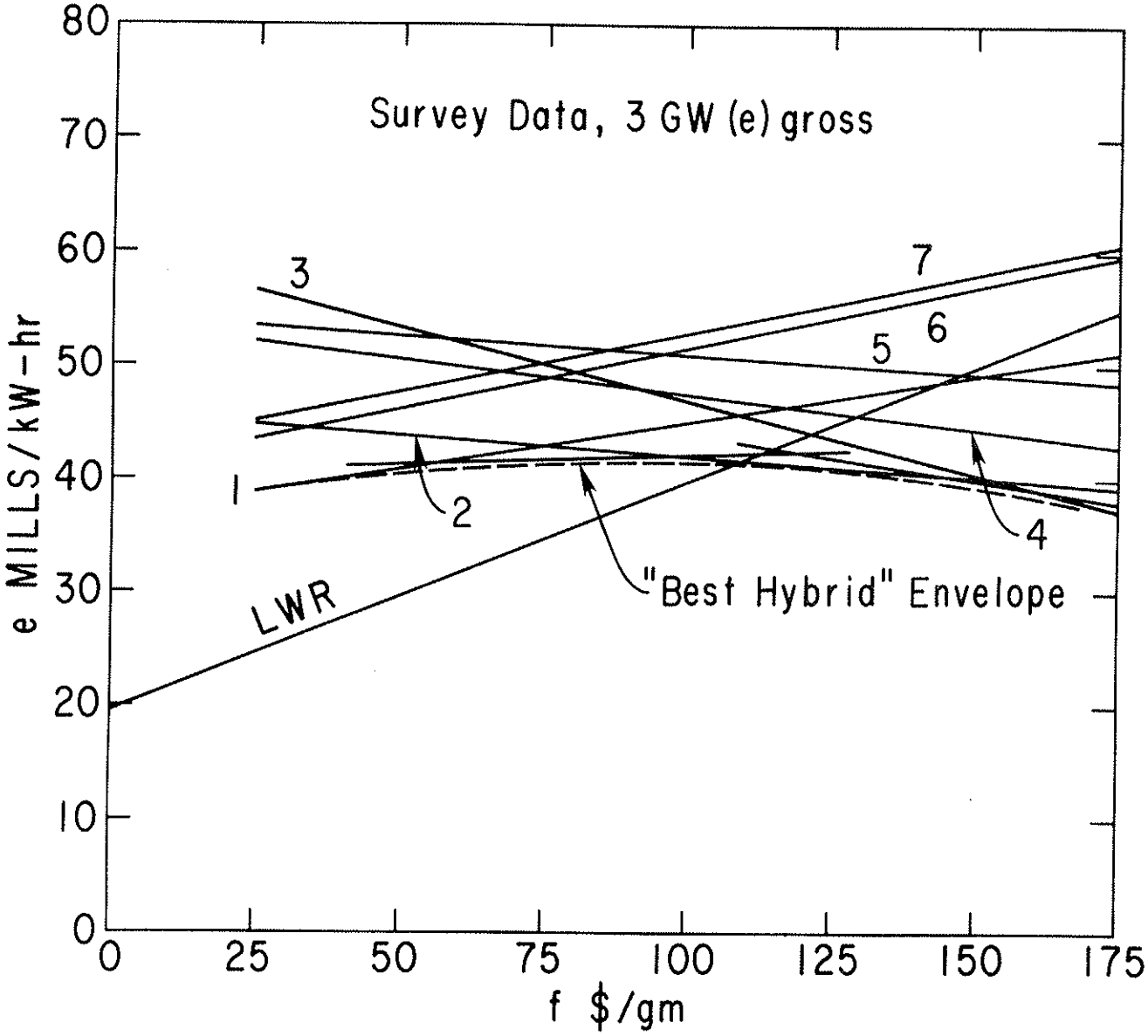

Fig. 1. Power cost vs. fissile fuel price for various hybrid reactors and a light water reactor (LWR).

Table I. Parameters for hybrid lines in Figure 1.

Line	R (m)	a (m)	M	T_e (keV)	H/T	W_L (MW/m^2)	W_o (kV)	I (MA)	NLWR	P_{net} (GWe))
1	11.1	2.0	23.1	8	0.075	0.34	200	3.2	0.042	2.12
2	13.7	2.8	11.1	7	0.010	0.43	200	5.2	4.46	2.04
3	13.7	2.8	9.1	9	0.030	0.51	166	5.2	6.24	1.81
4	18.3	4.0	9.6	7	0.010	0.27	183	6.2	5.90	1.98
5	13.9	4.0	10.6	9	0.05	0.31	166	6.9	4.87	1.74
6	10.0	2.0	25.8	6	0.100	0.34	150	3.1	0.0	2.00
7	13.6	1.6	25.1	7	0.100	0.48	150	2.1	0.0	2.06

4. Significance of the Park Model

The park model described in the preceding Section 2 assumes that the hybrid reactor and the fissile fuel consumers, exemplified by LWR's, are economically independent of each other. The "park solution" corresponds to the intersection of the best hybrid envelope and the LWR line as shown by the solid lines in Figure 2. The "park value" of fissile fuel, f_p, is just that value of f at which the hybrid reactor can sell its produced fissile fuel to the LWR's such that both enterprises can survive economically and at a common cost of producing electricity, namely, the "park cost" of electricity, e_p.

If the LWR's can purchase fissile fuel, say U-235, in a market at a cost corresponding to a plutonium price of $f < f_p$, then their cost of producing electricity will be less than e_p, and there will be no incentive to build the plutonium producing hybrids. However, once the market value of fissle fuel rises to where the corresponding price of plutonium exceeds f_p, there will be an incentive to build the hybrids and convert the fissile fuel consumers to burn the hybrid product.

The costs of the hybrids in this study assume the fertile material, U-238, to come from the tails of the uranium enrichment industry and hence to have only a nominal cost. Hence the park hybrid could keep the cost of electricity at e_p until the cheap supply of tails ran out and further mining of natural uranium ore was needed. At such time the cost of the

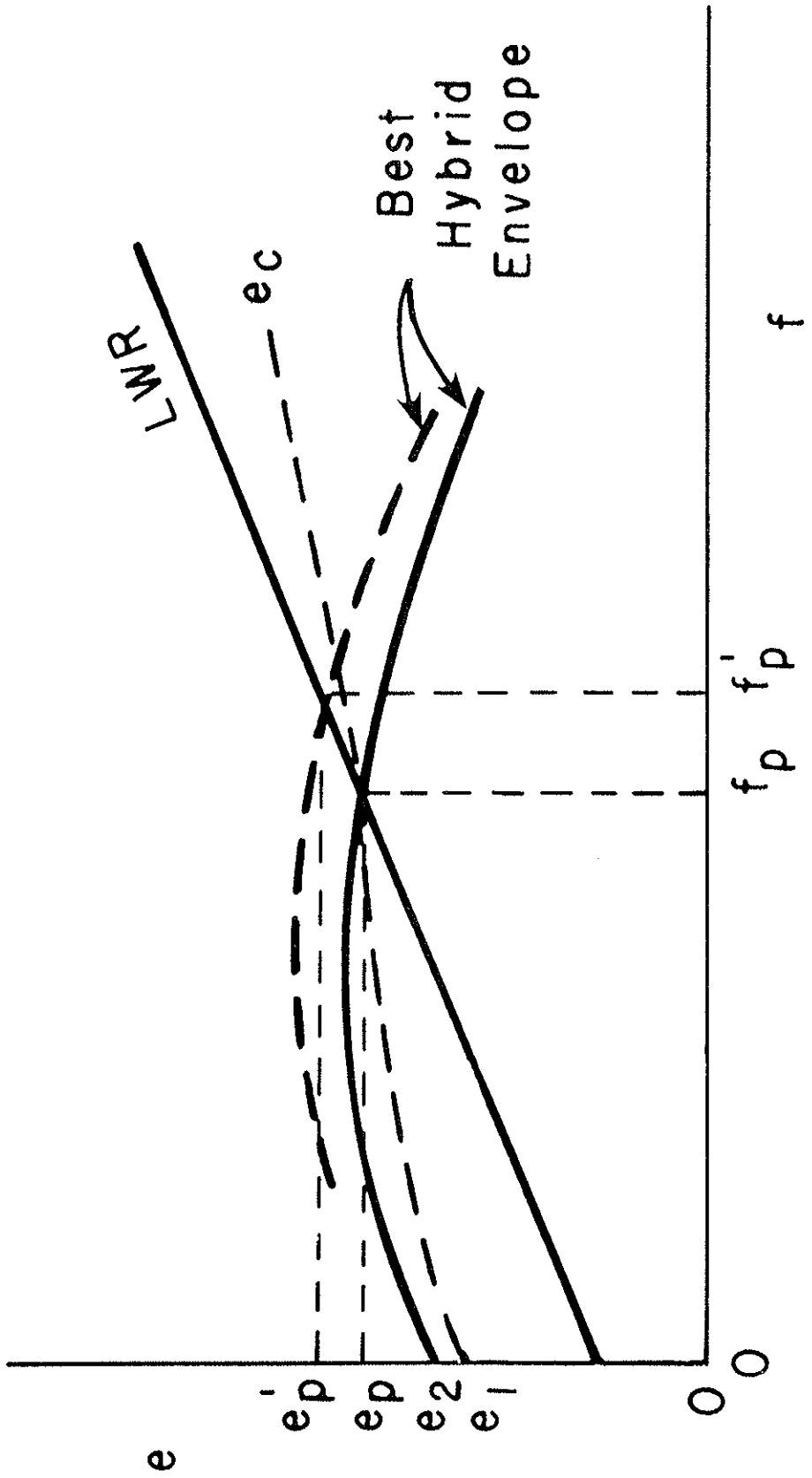

Fig. 2. Power Cost vs. Fissile Fuel Price Schematic.

hybrid would increase, and the best hybrid envelope would rise to higher values of e as indicated by the dotted best hybrid envelope curve in Figure 2. The cost of producing electricity would rise to e_p', and the value of fissile fuel would rise to f_p'.

The question arises of what happens to the cost of electricity, e, if the economics of the hybrid reactor and the fissile fuel consumers in the nuclear park are combined so that the price of fissile fuel, f, can be treated as a free parameter, simply a "bookkeeping quantity"? Consider an arbitrary value assigned to f and let the cost of producing electricity be e for the hybrid reactor and e' for the LWR where $e \neq e'$ unless $f = f_p$. If the annual quantity of electricity produced is E units for best hybrid and E' units for each of the N LWR's in the nuclear park, then the combined cost, e_c, of producing the total annual production of electricity is

$$e_c = \frac{eE + e' NE'}{E + NE'} \quad . \tag{6}$$

Thus e_c will lie between the best hybrid envelope and the LWR line as shown in Figure 2.

Now the slope of the e_c curve is everywhere positive. To show this we write Eq. (5) twice, once for the hybrid reactor and once, using primes, for the LWR reactor. Thus

$$eE = b + S f \ ,$$

and

$$e' E' = b' + S' f .$$

Therefore

$$e_c (E + NE') = (b + Nb') + (S + NS') f.$$

Hence, using Eq. (4) we have

$$\frac{de_c}{df} = S + NS'$$
$$= (a_2 + Na'_2) + \phi (a_3 + NA'_3) - (G_B + NG'_B).$$

But G'_B is the annual makeup of fissile fuel required by an LWR and hence as an algebraic quantity must be a negative number. In fact, $(G_B + NG'_B) = 0$. Since the a's are intrinsically positive (they represent inventories of fissile fuel), we have the desired result, $de_c/df > 0$. It follows, therefore, that raising f above f_p will result in e_c being greater than e_p. However, if f is lowered below f_p, the cost of electricity can fall. In the limit of $f = 0$ we have $e_c = e_1$ as shown in Figure 2. (Since the best hybrids for $f = 0$ will probably produce very little if any net fissile fuel, e_1 will probably approach e_2, the cost of electricity of the best hybrid for $f = 0$.) If the selling price of electricity reflected the cost $e_1 < e_2$, then the operation of the LWR's would in effect be subsidizing the operation of the hybrid.

Beyond the scope of this study lie numerous considerations implied by the use of the three curves: LWR, best hybrids, and composite e_c. These include, as examples, the effects of subsidies, tax policies, or collusion (causing artificial price floors) on the possible accelerated development of hybrids. Among these considerations is the minimum electricity price to be expected (e_1)

under the force of competition from pure fusion or a machine hybrid/LWR symbiosis lacking any significant external plutonium (or U^{233}) market. In this case the internal exchange price of Pu is somewhat arbitrary and could be forced to zero.

H. Calculational Techniques

1. Economic Subroutine-FUN

The modeling of the previous Sections, IV.B-F, culminates with its implementation in the form of subroutine FUN. Many of the equations generated by the modeling process translate in a straightforward manner into computer coding. However, some equations require more than a simple algebraic solution. In these cases, the computational technique becomes interesting in itself. For this and other reasons a brief discussion of the subroutine FUN is presented below.

In this discussion the flow of the program as outlined by the flow charts of Figures 1-4 is followed, as the calculational sequence is very important. A quick survey of FUN's flowchart reveals many possible points at which a calculation can be terminated, denoted by a RETURN symbol. Only the very last RETURN in Figure 4 is the result of a completely finished calculation of the cost of electricity, P_e. All other occurences of RETURN signal an aborted calculation. The calculation is aborted only upon violation of the barrier type constraints of Section IV.F. Before any calculating is performed, the vector representation of the variables is checked to see if it is an element of the allowed 5-dimensional (W_o, T, n_a/n_e, a, h) domain. If the vector is not an element of the domain, the subroutine calculation is aborted. One step in the abort process is to print the reason for the abort. In this instance, a violation of the lower/upper bound constraint would be cited as the cause.

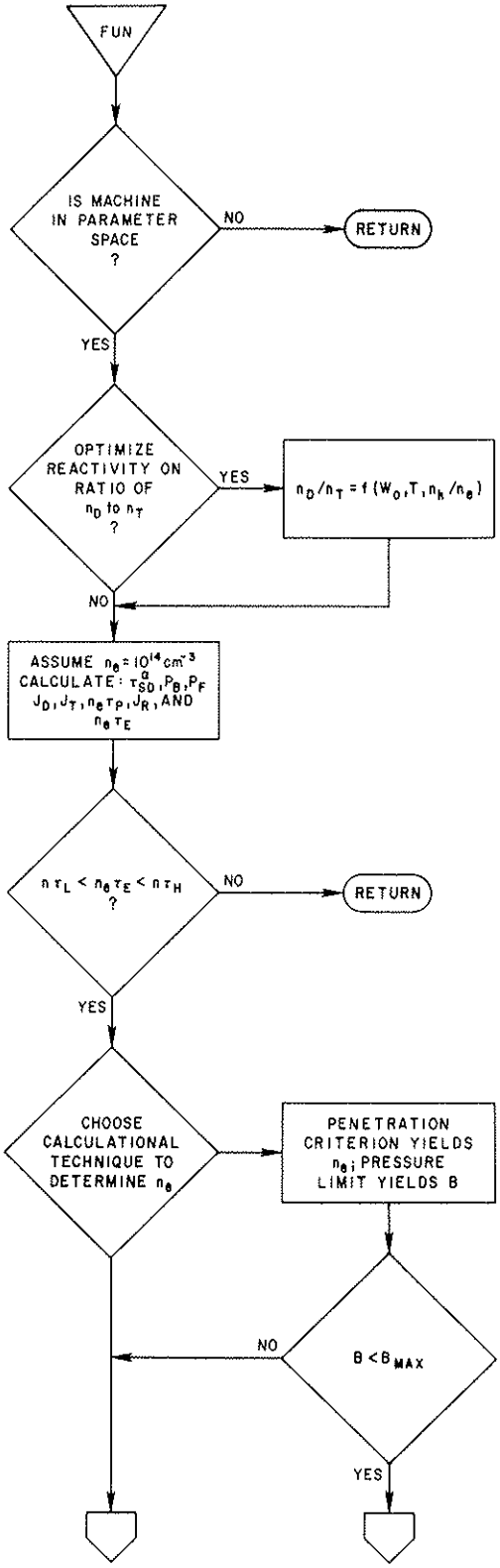

Fig. 1. Flow Chart of Subroutine FUN.

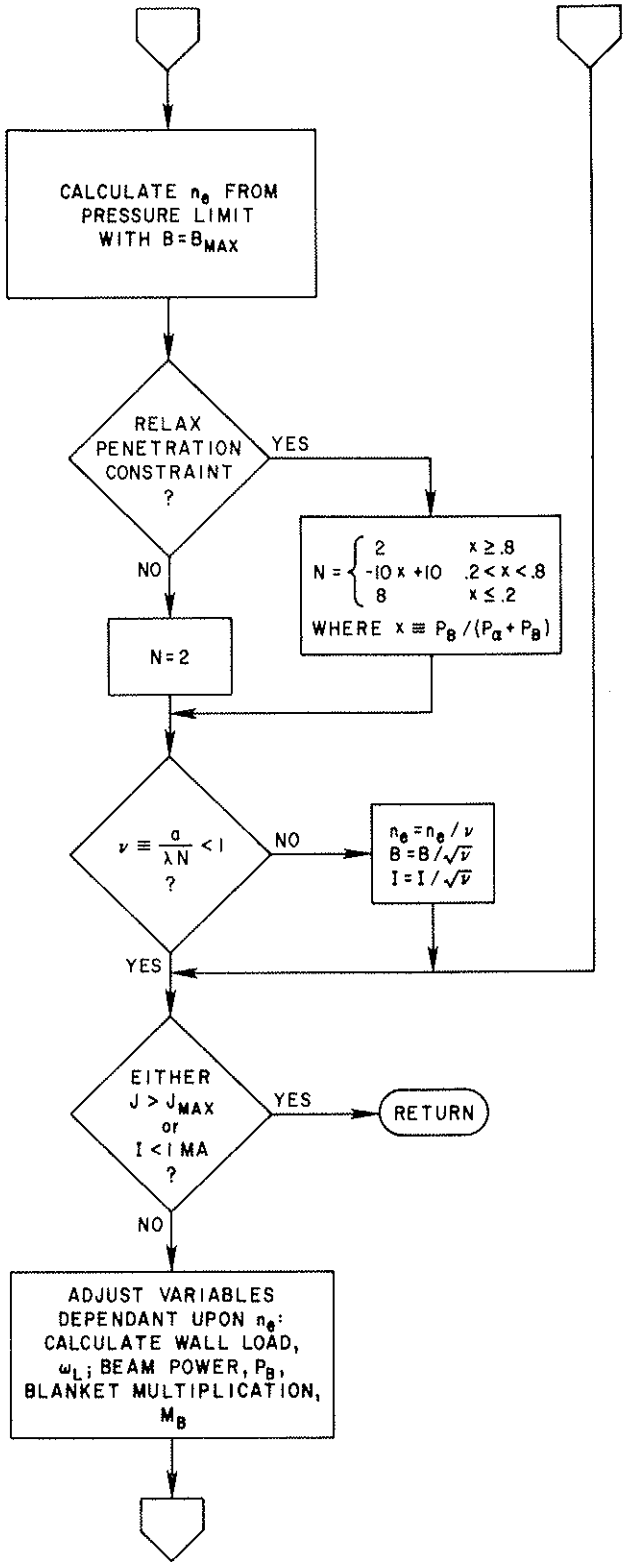

Fig. 2. Flow Chart (cont'd).

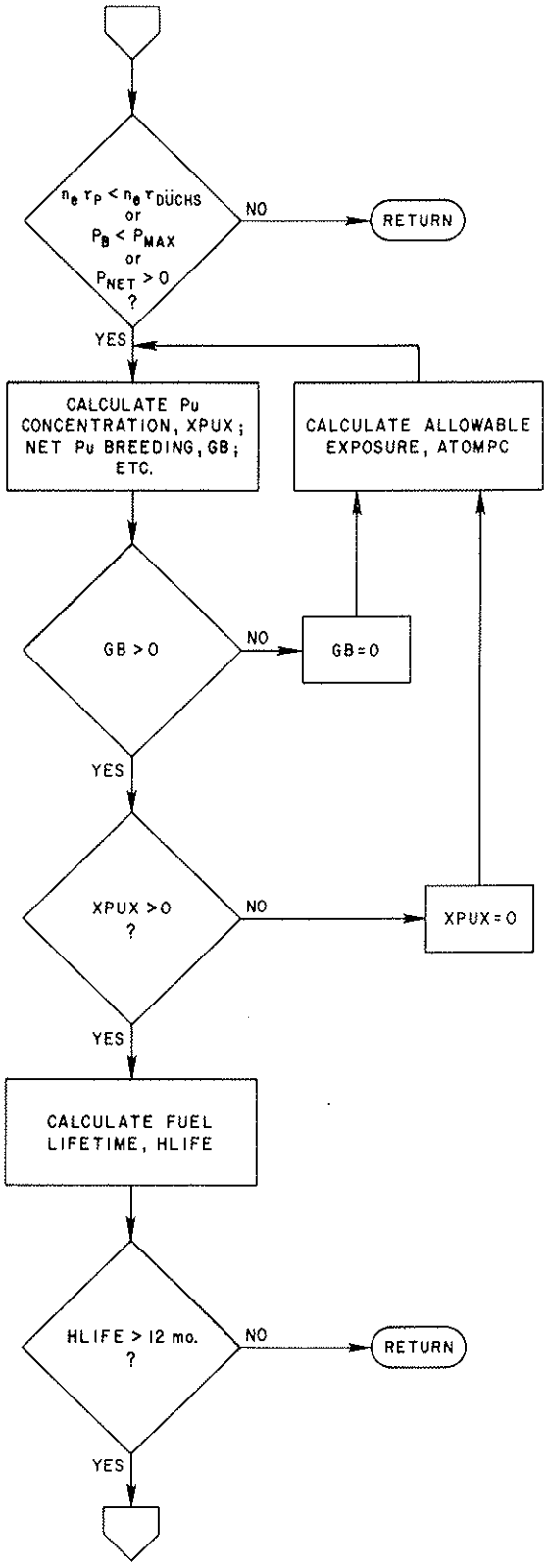

Fig. 3. Flow Chart (cont'd).

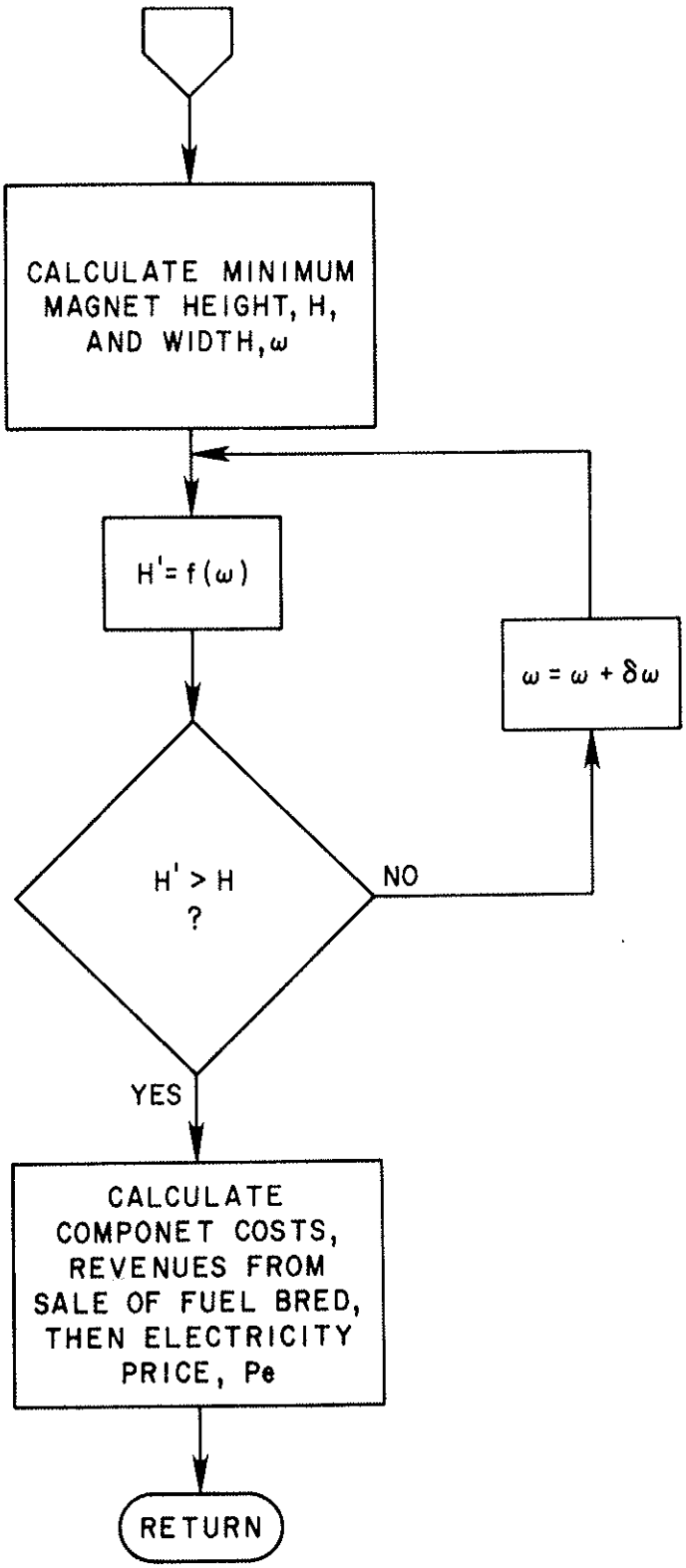

Fig. 4. Flow Chart (concluded).

The second imposition of a constraint subjects $n\tau$ to lower/upper bounds of constant value. It is important to realize that any vector that attains this point in the calculation had to survive the first constraint. If the first constraint is violated, the second constraint is never checked, let alone the remaining constraints. The possibility exists that one of the other constraints is simultaneously violated. However, only one constraint will be given as the reason for failure, the first constraint violation encountered. This point is very important when interpreting the various results presented in Section V. The constraint hierarchies employed in the various modes of calculation are summarized in Table I. The hierarchy of column A is the same as the one appearing in the flowchart of Figures 1-4. It is also used in the optimizer and mixed mode programs described later in this section. The hierarchy of column B is exclusively used in the survey programs, also described later. The two forms of the plasma confinement constraint refer to using a constant value as a standard of comparison for the allowed $n\tau$ (1st form) or using variable forms of $n\tau$ (2nd form) such as $n\tau$ DUCHS or $n\tau$ Alcator. The "interesting constraint" of column B eliminates uninteresting cases, e.g.,

$$P_e \leq 0 \qquad \text{mills/kWh}$$

$$P_B \geq 3000 \qquad \text{MW}$$

$$M_B > 27.2$$

$$P_e > 999 \qquad \text{mills/kWh} \quad .$$

Table I. The order in which the barrier type constraints are imposed.

Order Imposed	Constraint Hierarchy	
	A	B
1	Lower/Upper Bound Constraint	Lower/Upper Bound Constraint
2	The Plasma Confinement Constraint (1st form)	The Core Constraint
3	The Core Constraint	The Plasma Current Constraint
4	The Plasma Current Constraint	Neutral Beam Power Constraint
5	The Plasma Confinement Constraint (2nd form)	Net Power Constraint
6	Neutral Beam Power Constraint	Blanket Performance Constraint
7	Net Power Constraint	Interesting Constraint
8	Blanket Performance Constraint	The Plasma Confinement Constraint (all forms)

Returning to the point where the calculation begins, a decision is rendered as to what ratio of D and T densities is to be used. The two choices are to specify n_D/n_T through input or to let the code calculate the n_D/n_T ratio that maximizes the reactivity. All of the results reported in Section IV.I used the latter alternative for determining n_D/n_T.

The calculation of the reactivity necessitates the numerical evaluation of a 3-dimensional integral. Such a calculation can consume prohibitive amounts of computer time if it must be done frequently. During the design stages of subroutine FUN, several hundreds of calls to FUN, each requiring a reactivity calculation, were envisioned to occur within a typical program. Consequently, a table of reaction rates at $n_e = 10^{14}$ cm^{-3} was constructed to span the foreseen ranges of the variables, W_o, n_h/n_e, n_D/n_T, and T. The entries in the table were calculated at equally spaced intervals in these four variables. A function of the form given by Eq. (1) is used to interpolate between data points in the table.

$$\begin{aligned} f(w,x,y,z) = {} & f_o + a_1 w + a_2 x + a_3 y + a_4 z + b_1 wx + b_2 wy \\ & + b_3 wz + b_4 xy + b_5 xz + b_6 yz + C_1 wxy \\ & + C_2 wxz + C_3 wyz + C_4 xyz + Dwxyz \\ & + e_1 w^2 + e_2 x^2 + e_3 y^2 + e_4 z^2 \quad . \end{aligned} \tag{1}$$

The coefficients of Eq. 1 are determined by requiring the function to pass through the data at the 20 grid locations in Figure 5. The interpolation is performed only within the 4-D cell of Figure 5.

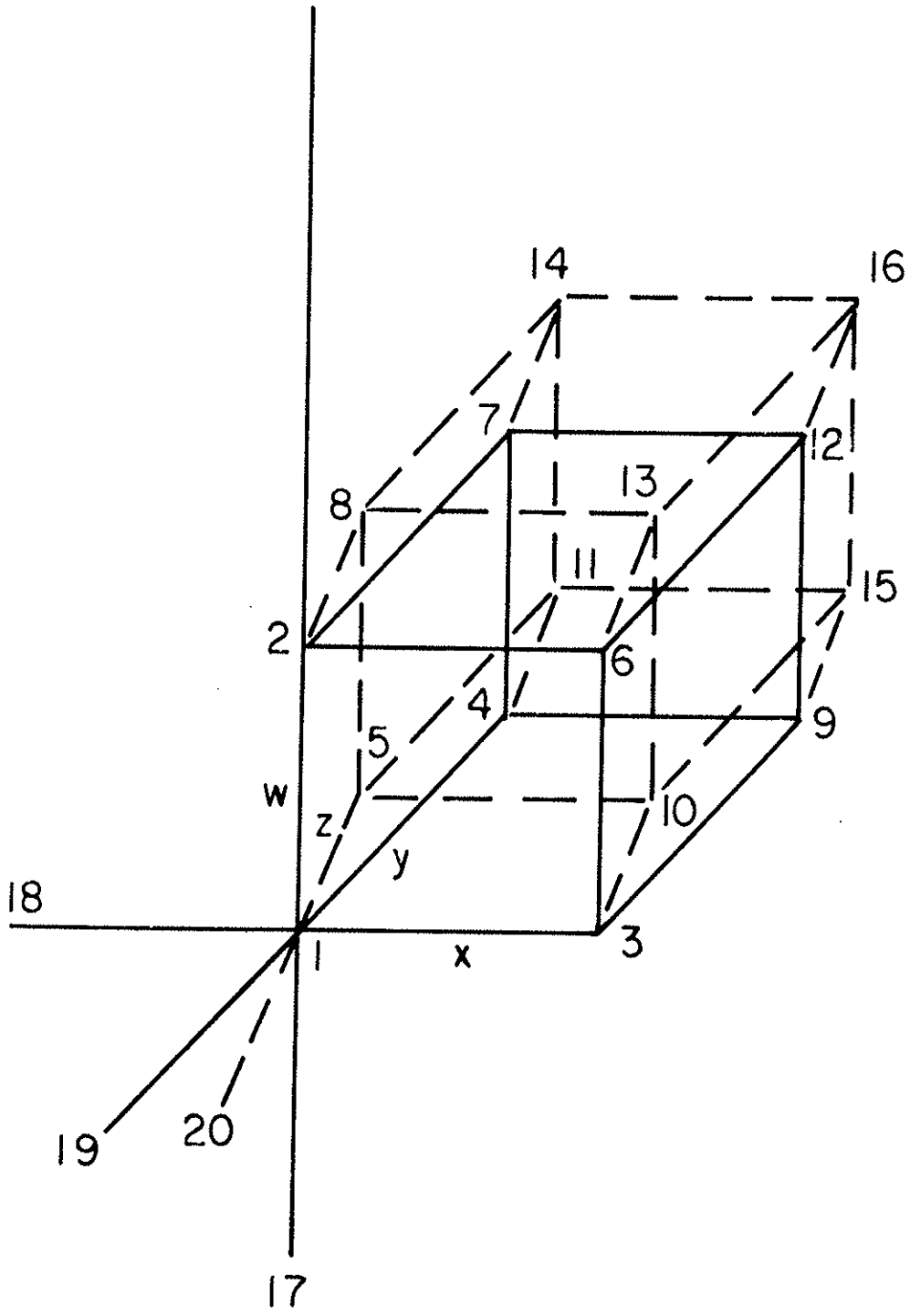

Fig. 5. Grid locations (numbered above) used in calculating coefficients for interpolation formula of Eq. (6). The 4-D cell in which the interpolation is performed is defined by all the points except points 17, 18, 19 and 20.

Furthermore, the points outside of this 4-D cell, e.g., point 18, must still be elements of the variable domain. Interpolation throughout the variable domain is accomplished through the construction of the additional 4-D cells necessary to span the entire domain.

This interpolation scheme minimizes the time spent in computation of the reactivity. An acceptable tolerance of $\leq$ 5% was observed between calculated and interpolated reaction rates at randomly chosen values of W_o, n_h/n_e, n_D/n_T, and T. One possible drawback of this interpolation scheme is that it is piecemeal, i.e., different regions in the variable domain use different coefficients in Eq. (1) and that continuity of the reactivity is not preserved at the junctures of the different interpolating regions. The repercussion of the loss of continuity will be discussed later in this section.

Once the reactivity is in the form of Eq. (1), it becomes a simple matter to determine the value of n_D/n_T for which the reactivity is a maximum. The program then proceeds to calculate the fusion power density, P'_F; the beam power density, P'_B, absorbed by a cubic centimeter of plasma; and the corresponding injection rates of D and T, J_D and J_T, respectively. The particle and energy confinement time, τ_p and τ_E, respectively, are then calculated according to Eq. (IV.F 23) and Eq. (IV.F 16), respectively. The recycle current, J_R, is also calculated at this time according to Eq. (IV.F 20). Since the calculation of the alpha particle slowing down time, τ^{α}_{sd} (see Eq. IV.B 11) requires the evaluation of an integral, a 3-dimensional interpolation

similar to that in the reactivity is performed for a table of τ_{sd}^{α}'s as a function of n_h/n_e, T, and n_D/n_T for a density $n_e = 10^{14}$ cm^{-3}.

With these calculations complete, the $n\tau$ is quickly checked to avoid dwelling on cases with grossly unreasonable or uninteresting $n\tau$'s.

The next task is to determine the electron density. Two methods are offered for this purpose, and the choice of method must be furnished as input to the subroutine FUN. One choice is to require the equality condition of Eq. (IV.F 29) to be met and then algebraically solve Eqs. (IV.F 29 and 30) for n_e. Upon substitution of n_e into Eq. (IV.B 8), the average plasma pressure is then determined. The magnetic field necessary to sustain the plasma pressure may in turn be determined depending on the pressure formulation used through Eqs. (IV.C 15, 17 or 18) after replacing h with the quantity $(\frac{Bh}{16})$ in Eqs. (IV.C 13 and 16). The resulting magnetic field is compared to a limiting value of the field usually taken to be 16 tesla. If the calculated magnetic field is lower than the limit, the code branches to a point just preceding the checks on the plasma current, I, and the current density, J, in the core. However, if the calculated magnetic field exceeds the limit, then the density is determined by the other method.

The second method for calculating the density is shown in more detail (see Figures 1 and 2) than the first method as it is the more commonly chosen. The method begins by assuming the magnetic field to be at the limiting value. The density is then determined by simultaneously solving Eq. (IV.B.8)

and one of the following Eqs. for the pressure, (IV.C 15, 17 or 18). The density is then checked to see that it satisfies the penetration criterion of choice.

The penetration criterion to be employed (see Figure 2) is one of two types: strict (i.e., N=2) and relaxed (i.e., $N \geq 2$). (Other forms of penetration criteria may readily be substituted for the two above due to the modular construction of the code.) For those cases of Section IV.I denoted as "ripple injection," which corresponds to setting $N = \infty$, the penetration criterion as coded in Figure 2 was simply removed.

For a penetration criterion of finite N, the violation of the criterion invokes a penalty type of constraint. The penalty conditions shown in Figure 2 (a reduction in electron density, n_e; magnetic field, B, in TF coils; and the plasma current, I) are the penalties adopted during the generation of the results of Section IV.I unless otherwise indicated. This particular set of penalty conditions was chosen for the cost benefit of reducing the B-field while preserving B and β_θ.

Upon finding satisfactory values of n_e and B, the plasma current, I, and the current density in the ohmic heating coils, J, are each checked for possible violations of their respective constraints. If either constraint is violated, the calculation halts with the associated n-vector of variables labeled as infeasible. If both constraints are met satisfactorily, the calculation progresses to its next stage.

Having established n_e, all those quantities that are a function of n_e and were necessarily calculated previously at $n_e = 10^{14}$ cm$^-$

are adjusted. These quantities include the fusion power density, P_F', and the beam power density, P_B'. From them the wall load, W_L, and the beam power, P_B, emanating from the injectors may be calculated according to:

$$W_L = \frac{14.06}{17.56} P_F' \frac{V}{A} \tag{2}$$

and

$$P_B = \frac{P'_B V}{1 - e^{-x}} \tag{3}$$

where

$$x = \lambda\sqrt{a(2R + a)} \tag{4}$$

$$V = 2\pi^2 R\, a^2 \tag{5}$$

$$A_1 = 4\pi^2 (a + \Delta)0.9R \tag{6}$$

$$A_2 = 4\pi^2 (a + \Delta)0.96R \quad , \tag{7}$$

and the various parameters are defined as

$V \equiv$ plasma volume

$A_1 \equiv$ wall area for single null configuration

$A_2 \equiv$ wall area for double null configuration

$\Delta \equiv$ the scrapeoff thickness

$\lambda \equiv$ mean free path for ionizing neutral beam (see Eq. (30) of Section IV.F.)

The factor of $1 - e^{-x}$ appearing in Eq. (3) is an estimate of the fraction of the neutral beam absorbed by the plasma along a trajectory tangent to the plasma center. The fraction,

14.06/17.56, appearing in Eq. (2) reflects the fact that the bulk of the fusion reactions are D-T reactions. The areas A_1 and A_2 are ideal areas and do not include missing areas for beam ports and divertor apertures. These factors are included in an effective wall coverage factor, Z:

$$Z_1 = \frac{1}{2}\,(1 + Z_2) \tag{8}$$

and

$$Z_2 = \frac{A_i - 0.02 \max\,(P_B, P_{ST}) - 2\pi \sqrt{a\Delta}\, D_i}{A_i} \tag{9}$$

where i = 1, 2, corresponding to single and double null configurations, respectively, and where

$$D_1 = 2\,(R - 1.95a) \tag{10}$$

and

$$D_2 = 4\,R - a \quad . \tag{11}$$

The quantity P_{ST} is the minimum beam power that is necessary to start up an ignited ($n_h/n_e = 0$) plasma. A value of 100 MW has been assumed for P_{ST} during all subsequent calculations. The effective wall coverage factor, Z, is related to Z_w of Eq. (IV.E 1) by

$$A_i Z = Z_w \quad . \tag{12}$$

Up to this point in the calculation no use has been made of the specified gross electric power of the hybrid reactor. Now, having found the power generated by the plasma, the required blanket power is determined and hence from Eq. (IV.E 1), the blanket multiplication, M_B, can be determined.

Before proceeding with the calculation, the plasma is subjected to one last round of constraints. The particle confinement time, $n_e\tau_p$, required by the plasma is checked against that which is envisioned as attainable, e.g., $n_e\tau_{\ddot{D}UCHS}$. The beam power, P_B, is compared to an estimate of the maximum beam power, P_{max}, that can be physically injected into the device. Also, the net electrical power generated, P_{net}, is checked for a positive value. If any of the above checks yield a constraint violation, then the case is labeled infeasible, and the calculation is abandoned. However, if all constraints are met, then the program proceeds, starting with a determination of further characteristics of the blanket.

The blanket and those calculations pertinent to its characterization are described in detail in Section IV.D. However it is appropriate at this point to discuss one facet, the calculation of the net plutonium breeding, G_B, and the plutonium concentration, XPUX. Their determination requires a double iteration (see Figure 3). One repercussion of such an iterative scheme is the introduction of numerical noise into the calculation. This will subsequently become important in the ensuing optimization calculations. The search for an optimum of a surface is complicated by the introduction of noise in the definition of that surface. This subject will be discussed later in this section.

Having determined the necessary blanket characteristics, the blanket is subjected to a constraint upon the irradiation

time, HLIFE, of the blanket. Should HLIFE be less than a year, the case is termed infeasible and the calculation abandoned as with all previous violations of the various constraints. Compliance with this last constraint will yield a feasible machine.

The remainder of the calculation is devoted to the economic analysis of the specified hybrid. The costing of most of the hybrid components is rendered by analytic expressions discussed in Section IV.E. However, one component of the reactor, namely the T-F coils, requires an iteration to yield its cost, since a snug fit of a D-shaped coil to the torus is desirable. The crucial dimensions in the fitting process are the coil height, H, and its width, w, given by

$$H = 5.5 \tag{13}$$

for the single null design and for the double null design,

$$H = 5.5 + 1.5a \tag{14}$$

and for both designs,

$$w = R + a + \Delta + L_B - h \tag{15}$$

where L_B is the width of the blanket. These formulae represent minimum values. The formulae for H are empirical relations, following from the plasma equilibrium study (Section IV.C), which are judged to provide sufficient room for the divertor arms. An analytic relation exists for calculating the height of a tension free D-coil given the location of the inner leg, h, and the outer leg, h + w, of the coil.[1] A snug fit is then obtained

by varying the coil width, w, as is portrayed in Figure 4 while holding h constant. The iterative scheme halts when a coil is fit to the torus within a specified tolerance. A snug fit is interpreted to mean the calculated values of w and H are very close to and yet exceed the required minimum values. In practice, one of the calculated quantities, either w or h, will be close to its corresponding required minimum value while the other calculated value will far exceed its minimum required value. The resulting "slack" may seem to be disadvantageous. However the alternative, a snugger fitting non-D-shaped coil requiring the necessary support structure, appears no more attractive.

Upon obtaining a T-F coil design, the cost of the magnets is calculated according to Eq. (IV.E 7). The subroutine then proceeds to the ultimate calculation of the cost of electricity, P_e, as set forth in Sections IV.E and G.

To briefly summarize the important features of subroutine FUN, the subroutine is designed as a quick, economical computer calculation of the quantities of interest of a hybrid design of specified gross electric power, especially P_e. This has been facilitated in part by: the functional fitting of time consuming calculations and an ordering of barrier constraints such that a minimum of time is spent on infeasible designs.

2. Applications

A number of problems can be investigated with subroutine FUN. The subroutine not only returns the price of electricity,

P_e, but also such secondary quantities as the plant capital cost, the amount of fuel bred, and neutron wall load to name a few. The latter quantities would be of interest in designing various experiments. In addition, that portion of the blanket calculation wherein the D-T neutrons are utilized for breeding fissile fuel and energy production may be bypassed. Thus, the fusion core of the hybrid configuration could be examined upon its own merits as a pure fusion reactor. However, resources permitted only the investigation of the cost of generating electricity from a hybrid reactor. To this end, several driver programs were written as the agent calling for the services of FUN. The driver programs fall into either of two categories: individual and optimization.

a. Individual Programs

The individual category of driver programs consists of two programs which investigate an individual hybrid design. One program permits the full output of the calculations of subroutine FUN. The quantities reported included those secondary quantities which are of interest in themselves but cannot be printed for every call to FUN in order to avoid voluminous output. These secondary quantities afford a detailed description of a hybrid design as well as a detailed economic analysis. The second program executes a sensitivity or perturbation analysis of various design parameters and model assumptions about a particular design point.

b. Optimization Programs

The optimization category of driver programs searches a predefined parameter space for an optimum hybrid design. The optimum is defined via a prescribed figure of merit. The programs are very general in design, rendering them independent of the choice of the figure of merit. Three separate figures of merit are reported in Section IV.I, namely, the cost of electricity, P_e; number of LWR's supported by the hybrid, N_{LWR}; and the capital cost, C.

Three programs constitute the optimization category. Each program therein employs a different combination of optimization techniques. Consequently, each program has a different range of applications and a different degree of accuracy associated with the calculated optimum. The three programs and their respective results are henceforth referred to as the survey, the optimizer, and the mixed mode.

i. Survey

The survey program performs, as its name suggests, a survey of an entire 5-dimensional domain, defined as:

$$6 \leq T \leq 18 \text{ keV}$$

$$150 \leq W_o \leq 300 \text{ keV}$$

$$0.0 \leq h_h/n_e \leq 0.3$$

$$1.0 \leq a \leq 4 \text{ m}$$

$$2.5 \leq h \leq 8.0 \text{ m} .$$

The figure of merit, usually the cost of electricity, P_e, is calculated for an assumed fissile fuel price, F_{FP}, at each

point in a grid whose locations are given in Table II. There are 21,504 distinct 5-vectors (grid points) in such a survey. The optimum (or grid point producing the minimum P_e) is then found by reviewing the values of P_e.

ii. Optimizer

The optimizer represents an algorithm for the application of a series of highly specialized optimization techniques. Both the techniques and the prescription for their application are of sufficient interest to warrant devoting a separate report to their detailed description.[2] For the purposes of this report, the optimizer is viewed only as a tool for minimizing P_e. However since the means for attaining the result has some bearing upon the result, a rudimentary description of the algorithm will be given here. For a more detailed discussion, the reader is referred to Ref. 2.

The optimization process is predominately performed by variations of the following three techniques: "random shrinkage," "steepest-descent," and "adaptive creeping," to employ the terminology of Ref. 3. The order in which the techniques were listed above is precisely the order in which they are applied. The "random shrinkage" technique is a global optimization technique whereas the "steepest-descent" and "adaptive creeping" techniques are local in nature. The "random shrinkage" technique involves a random sampling of a specified region. During various stages of the sampling process, the area of the region being sampled may be reduced so as to eliminate those regions least likely to contain the optimum. After many such reductions in

Table II. Grid Locations Employed in Survey Calculation.

T	6	7	8	9	10.5	12	15	18	keV
W_o	150	166	183	200	225	250	300		keV
n_{h/n_e}	0	.01	.03	.05	.075	0.1	0.2	0.3	
a	1.2	1.6	2.0	2.4	2.8	3.2	3.6	4.0	m
h	2.5	3.6	4.7	5.8	6.9	8.0		m	

area, a final region will be attained which ideally contains the optimum. Then the local techniques are invoked. First, the "steepest-descent" technique follows the gradient toward the optimum from the location of the "best" sample found during the "random shrinkage" technique. The steepest-descent technique is sufficient to reach the optimum unless constraints are encountered on one or more of the quantities that determine P_e. When a constraint boundary is encountered, the "adaptive creeping" technique is necessarily employed to continue the search for the optimum along the boundary.

iii. Mixed Mode

The third driver, the mixed mode program, is a mixture of the previous two driver programs. Over a subset of the five variables upon which the optimization is to be performed, a survey is performed. At each grid location of this survey, the optimizer program is employed to find the optimum in the remaining free variables. The optimum in all variables is then deduced from the optima in the free variables generated at the grid locations of the survey.

iv. Discussion

Each of the driver programs of the optimization category has its merits as well as its limitations. It is important to keep in mind that each driver program yields, as its result, an approximation to the optimum hybrid. Associated with each driver, then, is a degree of accuracy. Without knowing the optimum, the accuracy of the approximation must in turn also be approximated.

The accuracy of the survey relative to the optimizer may be gauged by performing the same task with each. Since the dependence of the price of electricity charged by the optimum hybrid, P_e, as a function of fissile fuel price, F_{FP}, is one of the more frequently reported results of Section V., it is used as a "benchmark" calculation. The "benchmark" consists of the calculation of the optimum P_e (in 5 variables) at seven values of F_{FP}, namely: 25, 50, 75, 100, 125, 150, 175 \$/kg. The results of the survey and the optimizer for such a "benchmark" calculation are displayed in Figure 6 for a hybrid reactor of 3 GW gross electric power. In order to further gauge the accuracy of the optimizer, it was rerun with twice as many functional evaluations of FUN employed in the sampling process. These results appear as x's in Figure 6. Additional information can be obtained by utilizing the linear relationship between P_e and F_{FP} for a given hybrid design. This information is plotted as the "best guess" curve in Figure 6. From the figure it can be concluded that the survey is accurate to within $\sim$ 30% from the known optimum, whereas the optimum is accurate to within less than 1%.

There is also an accuracy associated with the locations of the optimum hybrid in the parameter space of the five variables. The accuracy of the locations of these optima is difficult to assess because of the nature of the P_e function. The hypersurface defined by P_e possesses multiple local optima which may be of nearly equal value but be located far apart in the 5-vector space. However, the accuracy of the location may be inferred by comparing the 5-vector locations for the survey's optima

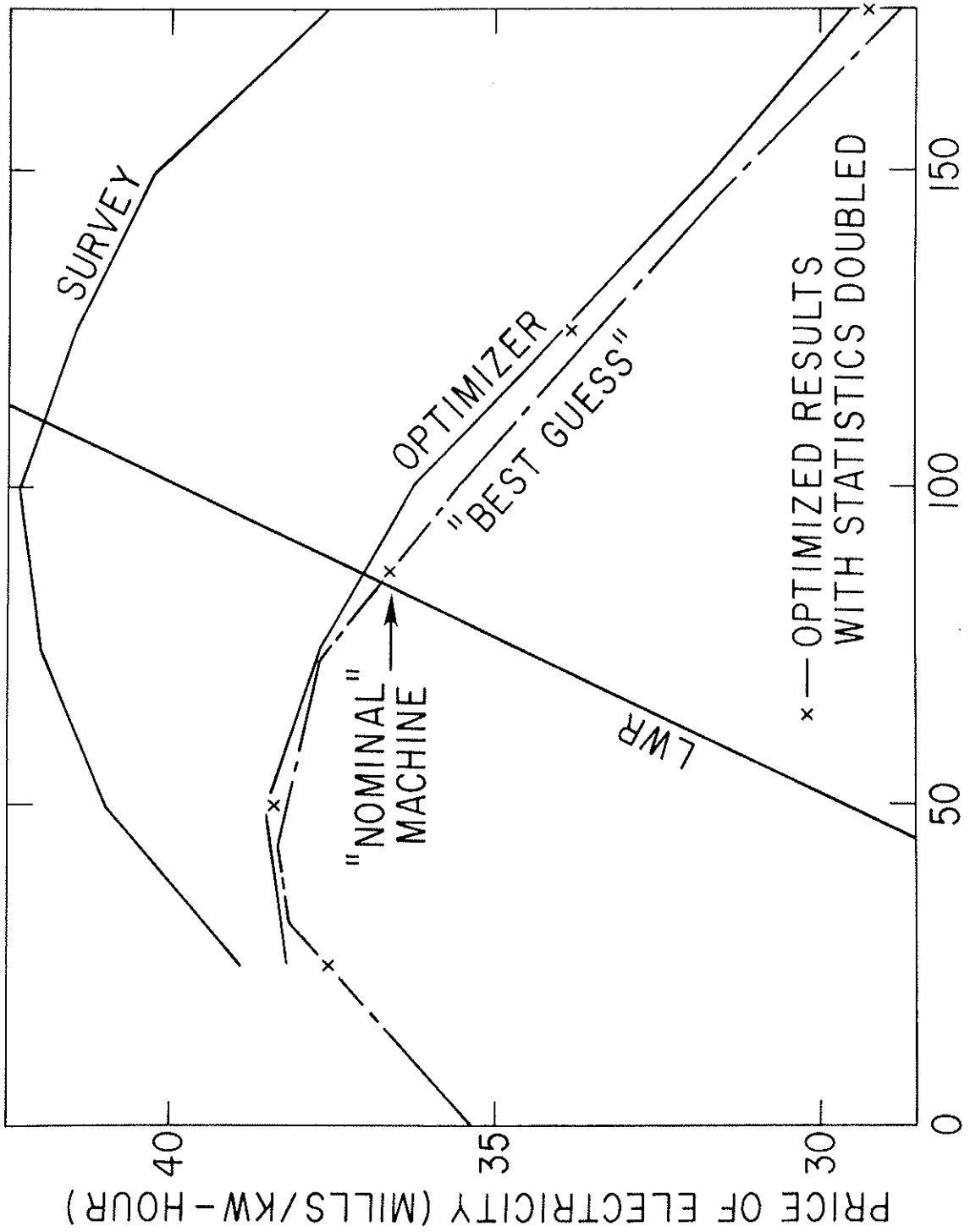

Fig. 6. Typical Survey and Optimizer Results.

(see Table III) with those from the optimizer (see Table IV). These tables reveal that the locations in n_h/n_e display the largest percent variation, as much as 2400%. However, the variance in the other variables is $\lesssim$ 26%.

The mixed mode calculation does not readily lend itself to the type of calculation necessary for the "benchmark". However, results at a particular value of $F_{FP} = 86.5$ are manageable and appear in Table V. The table is arranged to display P_e at each grid location in a and h. In addition the value of the optimum's free variables, T, W_o, and n_h/n_e, which are determined by the optimizer, are displayed about each P_e. These mixed mode results are to be compared to the following result from the optimizer:

Minimum	5-vector location of minimum				
P_e	T	W_o	n_h/n_e	a	h
36.67	6.0964	168.47	0.0018437	2.9395	7.4919

The agreement in P_e, T, W_o and n_h/n_e is quite good. In order to improve upon the accuracy in the variables, a and h, the "steepest-descent" and the "adaptive creeping"techniques of the optimizer can be applied with the results of Table V serving as starting locations. The results of such applications are presented in Table VI for four starting locations from Table V which bracket the optimizer result. The fourth entry of Table VI represents an improvement over the optimizer of 0.6% in P_e and variation in the 5-vector of $\lesssim$ 6%, except for an n_h/n_e which is ~ 18%. As the fourth entry of Table VI is the "best" result obtained, the above discrepancies are adopted as the accuracy

Table III. Survey Results of the Minimum Cost of Electricity Calculated at Various Values of F_{FP}

F_{FP}	5-vector location of minimum					Minimum P_e
	T	W	n_h/n_e	a	h	
25	8	150	.075	2.0	4.7	38.9
50	8	150	.075	2.0	4.7	41.0
75	7	183	.010	2.4	6.9	42.0
100	7	200	.010	2.8	5.8	42.3
125	7	200	.010	2.8	5.8	41.5
150	7	200	.010	2.8	6.9	40.2
175	9	166	.030	2.8	5.8	37.5

Table IV. Search Algorithm Results of the Minimum Price of Electricity Calculated at Various Values of F_{FP}.

F_{FP}	5-vector location of minimum					Minimum
	T	W	n_h/n_e	a	h	P_e
25	6.04	150	.0412	2.43	3.58	38.2
50	6.15	176	.0030	2.63	7.41	38.5
75	6.25	175	.0026	2.91	7.03	37.7
100	6.21	176	.0024	2.99	6.89	36.3
125	6.15	164	.0017	2.95	7.71	33.9
150	6.08	162	.0015	3.00	7.80	31.6
175	6.47	157	.0022	2.91	7.89	29.5

*	*	*	*	*	*	*	*	2.5
*	*	6.00 49.30 150 .126	7.26 44.08 150 .048	7.69 45.38 153 .043	8.40 46.75 151 .048	8.50 47.82 159 .040	7.78 48.15 178 .022	3.6
*	*	7.90 43.87 150 .065	8.26 44.41 152 .042	7.59 44.17 181 .020	6.99 42.56 194 .010	6.59 41.29 200 .005	6.18 40.78 207 .003	4.7
*	6.00 52.53 150 129	7.86 43.86 150 .040	6.56 42.83 196 .009	6.92 40.33 184 .007	6.23 38.32 193 .003	6.14 38.92 192 .002	6.04 40.01 195 .002	5.8
*	6.36 50.29 150 .114	6.49 43.67 182 .001	6.96 41.27 174 .008	6.47 37.92 175 .003	6.00 37.29 179 .001	6.01 38.76 183 .002	6.04 40.19 184 .002	6.0
*	6.70 50.72 150 .108	6.36 43.54 172 .008	7.12 40.35 159 .007	6.16 36.84 162 .002	6.15 37.57 167 .001	6.04 39.11 171 .002	6.00 40.32 173 .001	8.0
1.2	1.6	2.0	2.4	2.8	3.2	3.6	4.0	H A

Table V. A mixed mode calculation of the price of electricity, P_e, surveyed over a and h. Each entry is the result of the optimizer program working in T, W_o, and n_h/n_e. The location of the minimum in the three variables is displayed about P_e starting with T in the upper left-hand corner and proceeding counter-clockwise through W_o and n_h/n_e.

Table VI. The Results of an Application of the Ascent Phase of the Search Algorithm to Four Starting Locations Taken from Table V.

Start	Minimum P_e	5-vector location				
		T	W_o	n_h/n_e	a	h
(2.8,8.0)	36.81	6.1592	162.51	.0019592	2.8000	8.0000
(3.2,6.9)	36.75	6.0022	179.27	.0018814	3.9846	6.8129
(2.8,6.9)	37.15	6.4687	164.73	.0028804	2.8000	7.5900
(3.2,8.0)	36.45	6.0217	162.71	.0015549	2.8800	8.0000

of the optimizer. The only conclusion that can be drawn about the accuracy of the mixed mode program is that it is more accurate than the optimizer. So far, only the accuracy of the three optimization programs has been discussed. From these discussions the mixed mode driver program would be concluded as the program of choice for all calculations. However, other factors are involved in such a decision, such as calculational cost and amount of useful information to be gained. The calculational costs, in terms of the number of calls to subroutine FUN for the survey and optimizer curves of Figure 6, are 43,008 and 875,000, respectively. The survey makes so many fewer calls to FUN in part because the survey can take advantage of the fact that each hybrid need be evaluated at only two values of F_{FP} in order to determine its P_e at any F_{FP}. Basic differences in the optimization techniques used by the two programs contribute to the remaining disparity in calls to FUN. The survey's principal drawback is its inaccuracy in estimating the optimum. Its accuracy cannot be improved efficiently by increasing the number of grid points. However, for gauging the general nature of the effects of changing parameters, the survey is deemed adequate. For subtler effects the optimizer is preferable. One such large effect that can be investigated with the survey is the choice of the n_T constraint. Because of the constraint heirachy applied to the survey, different n_T constraints may be imposed upon the same design points, thereby sparing their unnecessarily repeated calculations. This proves

to be an additional advantage in using the survey.

As for the mixed mode program, the number of calls to FUN in order to generate Tables V and VI are 2,288,880 and 2,292,880, respectively. Such large numbers of functional evaluations make the mixed mode program unattractive for repeated applications. However, the mixed mode program returns the largest quantity of highly accurate information of all three optimization programs. The a-h carpet of P_e shown in Table V reveals much information about the effect of changing the size of a hybrid. In addition, the nature of the P_e function is partially revealed in this table. Two distinct valleys are present in the P_e carpet. One valley stretches from the (a,h) location of (4.0, 5.8) to (2.8, 8.0), while the other, shorter one goes from (2.4, 3.6) to (2.0, 4.7). Such behavior gives rise to multiple local optima, which can be very difficult to allow for from the optimization point of view. Further evidence of the existence of multiple local optima is revealed by following the value of W_o as a function of a for fixed h = 5.8 in Table V. The fact that application of the "steepest descent" and "adaptive creeping" techniques to four starting locations from Table V did not converge upon a unique optimum, but rather yields the four distinct optima of Table VI is also indicative of multiple local optima.

The constraints of Section IV.F are largely responsible for the multiple optima phenomena. Evidence of this can be seen by examining the sensitivity of an optimizer result

to variations in the 5-vector (see Table VII). The $n\tau$ constraint is observed to bound the optimum's location in all directions but one, a formation in five-parameter space analogous to a finger or peninsula.

In conclusion, the constraints and hence the multiple local optima phenomenon complicate the optimization calculations. The survey calculations are excellent for gauging broad trends while the optimizer is required for more detailed investigations. The mixed mode is an excellent means of measuring the accuracy of the previous two programs. Also, it provides much useful information about the functional dependence of P_e although it is of limited practicality because of the large amount of computer time required. Furthermore, when undertaking a systems study of hybrids (or any form of fusion device) some form of global optimization must be performed due to the presence of several optima, closely related in value yet located far afield from each other in parameter space.

Table VII. The sensitivity of the "Nominal" machine to perturbations in the six-vector.

	2% Decrease		2% Increase	
"NOMINAL" MACHINE* VARIABLES	P_{eH}	Constraint Violated	P_{eH}	Constraint Violated
P = 3 GW	37.1	-	36.1	-
T = 6.1 keV	37.1**	$n\tau$	36.2	$n\tau$
W_o = 168 keV	36.5	$n\tau$	36.6	$n\tau$
n_H/n_e = 0.00184	36.5	$n\tau$	36.6	$n\tau$
a = 294 cm	36.5	$n\tau$	36.7	$n\tau$
h = 749 cm	36.4	$n\tau$	36.7	-

**T was decreased to 6 keV.

* P_{eH} = 36.6 for "Nominal" Machine.

References

[1]S. L. Gralnick and F. H. Tenney, Analytical Solution of the Toroidal Constant Tension Solenoid, J. Appl. Phys. 47, 2710 (1976).

[2]C. G. Bathke, An Algorithm for Locating the Extremum of a Multi-Dimensional Constrained Function and its Application to the PPPL Hybrid Study, Princeton Plasma Laboratory Report PPPL-1424 (1978).

[3]S. L. S. Jacoby, J. S. Kowalik, and J. T. Pizzo, Iterative Methods for Nonlinear Optimization Problems (Prentice-Hall, Inc., Englewood Cliffs, New Jersey, 1972) pp. 90-91, 253-263.

V. Results of the Systems Analysis

A. Introduction

The results of this study derive from two styles of calculations, the "survey" style and the "optimization" style. These different styles of calculation have been described in Section IV.H. Most of the results are based on the survey calculations. The survey calculations scan over the six-dimensional parameter space by means of all the possible six vectors whose coordinates can be found in Table I.

The choice of values for the hybrid gross electric power, P_g, was based on early calculations which indicated that the cost of electricity for $P_g < 2$ GW would be too high to be of interest; the upper limit of 10 GW is probably excessive from the point of view of public utilities, but provides a large enough increase over 2 GW to reveal whatever advantages may lie in largeness of plant size. The choice of P_g itself as a parameter was also made as a result of early calculations that indicated that the cheapest electricity would be made by plants with the largest gross electric power rating. The gross electric power was selected as a parameter rather than the net electric power because the cost of the balance of plant is taken to be a function of only the gross electric power and, since the balance of plant cost dominates the capital cost of the plant, by fixing the gross electric power level one is roughly fixing the overall capital cost of the plant. It was felt that this correlation might be useful in evaluating the calculated data.

Table I. Survey Parameters

P_g (GW(e))	2	3	4	6	10			
T_e (keV)	6	7	8	9	10.5	12	15	18
W_o (kV)	150	166	183	200	225	250	300	
n_h/n_e	0.0	0.01	0.03	0.05	0.075	0.1	0.2	0.3
a (m)	1.2	1.6	2.0	2.4	2.8	3.2	3.6	4.0
h (m)	2.5	3.6	4.7	5.8	6.9	8.0		

[(R (m) ranges from (7.34) for a = 1.2 to (18.30) for a = 4.0 (single nul
(6.10) (14.40) (double nul

as determined from scaling shown in Figures IV.C-1 and 2.]

Total No. of 6-vectors = 107,520.

The "results" of this study are those hybrids that produce the cheapest electricity consistent with a selected set of constraints. Explorations have been made with different criteria for: energy or particle confinement by the plasma, beam penetration, blanket performance, pressure scaling, pressure profile, and for both single null and double null poloidal field divertor configurations. The "standard hybrids" are those for which: the particle confinement time was limited by the trapped electron mode of transport (Eq. (25) of Section IV.F), the beam penetration varied according to Eq. (29) of Section IV.F, the blanket performed as described in Section IV.D, and the pressure scaled according to Eq. (IV.C 15 or 17) with the profile factor, α, equal to 2.

Most of the results presented are for the single null configuration. The double null results will be specifically labeled.

B. Survey Results

Survey results for the "best standard hybrids" are shown in Figure 1. The "best hybrids" are described in Section IV.G.3 and represent those hybrid designs that produce the cheapest electricity for sale for a given fissile fuel price, f, and a given gross electric power production. The projected economics of a plutonium-fueled, 1 GW(e) net LWR is shown by the straight line. The intersections of the LWR line and the "best hybrid" curves define the "park solutions" and are labeled by the number of LWR's supported in each park. Present day economics place "the present time" at an f-value of about \$25/g of Pu.

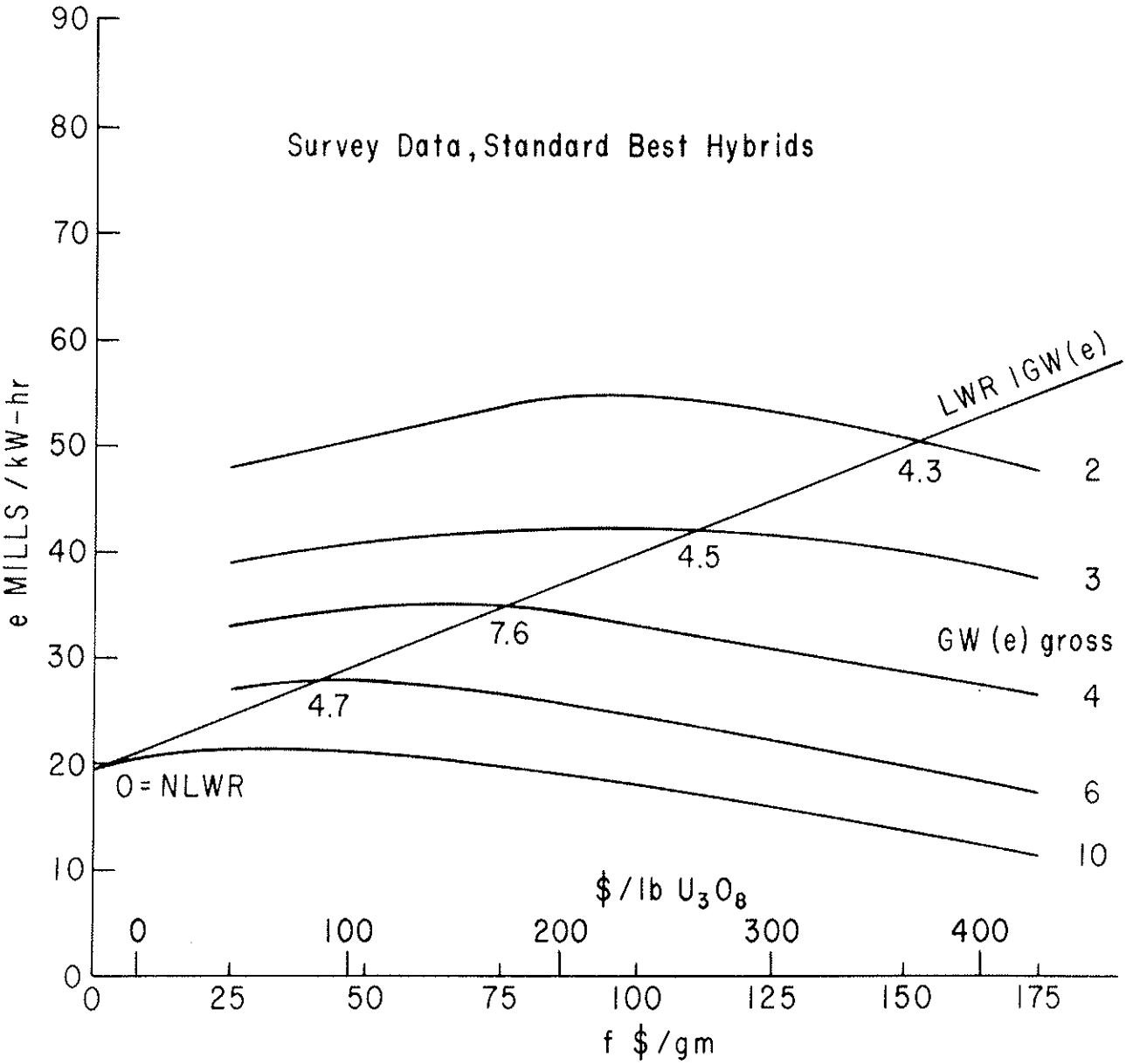

Fig. 1. Cost of electricity for Standard Best Hybrid Reactors. (Survey Data.)

The hybrid design varies as one proceeds along a "best hybrid" curve from low values of f to high values. Table II displays some features of the best hybrid of 3 GW(e) gross. Their variation as a function of f is typical of best hybrids of all gross power levels. We note in particular for low values of f, M is high, so very little net fissile fuel is produced as shown by the near zero value for NLWR. As fissile fuel becomes more valuable, the hybrid design shifts from high blanket multiplication to low blanket multiplication. This shift in M produces more fissile fuel for sale, as shown by the increase in NLWR, and requires less fissile fuel to be used in the blanket to facilitate energy production.

We also note from Table II that for increasing f, the quantities P_{net}, p_f, and A_T undergo only small changes, H/T increases, and a and R produce at first a "small" machine and then a "large" machine. We also note that β_θ = 0.82 R/a for all values of f. Thus the plasma pressure is being limited by the β_θ constraint (see Section IV.F.7).

The 3 GW(e) gross park solution (see Figure 1) has a value of f that falls between 100 and 125 \$/g and a blanket multiplication of M = 11.1. Although this "park hybrid" design calls for considerable net fissile fuel production, it does not call for either extreme, the maximum or minimum fuel production possible.

Table II. Some Characteristics of 3 GW (e) Gross Best Hybrids (Survey Data)

f	M	T_e	W_o	H/T	a	R	I	n_e	β_θ	B_c	Q	p_f	W_L	NLWR	P_{net}	A_T
25	23.1	8	150	0.075	2.0	11.1	3.2	0.47	4.55	6.7	1.12	0.460	0.34	0.042	2.12	1.00
50	23.1	8	150	0.075	2.0	11.1	3.2	0.47	4.55	6.7	1.12	0.460	0.34	0.042	2.12	1.00
75	13.6	7	183	0.01	2.4	14.0	4.2	0.86	4.81	7.8	2.33	0.428	0.39	2.84	2.17	0.97
100	11.1	7	200	0.01	2.8	13.7	5.2	0.82	4.03	6.7	2.35	0.390	0.43	4.46	2.04	0.98
125	11.1	7	200	0.01	2.8	13.7	5.2	0.83	4.03	6.7	2.35	0.390	0.43	4.46	2.04	0.98
150	9.9	7	200	0.01	2.8	14.8	5.1	0.83	4.35	7.1	2.35	0.401	0.44	5.50	1.96	1.06
175	9.1	9	166	0.03	2.8	13.7	5.2	0.58	4.03	6.7	1.86	0.462	0.51	6.24	1.81	0.96

f = fissile fuel price $/g

M = blanket energy multiplication

T_e = plasma temperature in keV

W_o = injection energy, kV

H/T = ratio of hot to thermal populations in plasma

a, R = plasma minor and major radius, respectively, in meters

I = discharge current in megamperes

n_e = average electron density in 10^{14} cm^{-3}

β_θ = plasma pressure/poloidal magnetic field pressure

B_c = magnetic field at major radius of tokamak in Tesla

Q = ratio of total fusion power produced to total beam power absorbed in the plasma

p_f = fusion power density in watts/cm^3

W_L = wall load in MW/m^2

NLWR = number of LWR's supported by net plutonium production

P_{net} = net electric power for sale in GW

A_T = penetration index = ratio of distance beams should penetrate to distance beams can penetrate without reduction in initially selected plasma density

For park hybrids we have the following correlation.

P_g:	2	3	4	6	10	GW(e) gross
M:	8.9	11.1	9.7	14.8	23.8	
(P_{net} + NLWR):	6.1	6.5	10.5	9.4	10.0	GW(e) net
T_e:	7.0	7.0	8.0	8.0	8.0	keV
W_o:	183.0	200.0	166.0	166.0	166.0	kV
a:	2.4	2.8	3.6	3.6	4.0	m
R:	14.1	13.8	15.3	15.3	16.1	m
H/T:	0.01	0.01	0.01	0.01	0.01	

Thus for hybrids of $\geq$ 6 GW(e) gross the design is that of a power producer. In contrast, the 2 GW(e) gross park hybrid produces about the maximum quantity of fissile fuel possible for its size plant and most of the power produced by the park is produced by the LWR's.

The general shape of the best hybrid curves in Figure 1 reflects variation in blanket performance. As described in Section IV.G.3 for a given hybrid design the cost of electricity, e, as a function of f will slope upward if the net fissile fuel production, G_B, is small enough. An upward slope reflects the inability of the revenue derived from the sale of fissile fuel to offset both the initial cost and the fuel cycle costs associated with the inventory of fissile fuel in the blanket. Hybrid designs with low values of M produce large values of G_B, require low inventories of fissile fuel and hence will have downward sloping costs of electricity as a function of f. The values of M for which the slope of the best hybrid curves vanishes lie between 12 and 16.

Two final remarks about Figure 1. First, the 6 GW park hybrid is almost competitive with today's market (the use of plutonium aside). Second, extensive quantities of U_3O_8 are deemed available at prices in excess of 180 \$/lb, and consequently park hybrids that require U_3O_8 prices in excess of this figure in order to be economically attractive may not become attractive for several centuries. In other words, in order for park hybrids to be of interest within, say, fifty years, the park value of f should fall below something like 80 \$/g. It appears from Figure 1 that the power rating of such "near term" park hybrids could not fall much below the 4 GW(e) gross level. Modifications of the "standard hybrid" design to be described below will ameliorate this last statement to some extent.

1. Size of Machine

In Figure 2 are shown the equivalent circular cross sections of some of the "best standard hybrids". For each gross power level there seem to be only two sizes of machines as mentioned above. The transition from the "small" size to the "large" size machine is correlated with the value of f for which de/df = 0 and, in turn, the bending of the best hybrid curves from positive to negative slope is correlated with the blanket multiplication falling from "high" values to "low" values. For example, compare the data in Table II for f = 50 and 100 \$/g.

To explain this shift in size, in fact to explain the size of the best hybrids at all, involves the economic

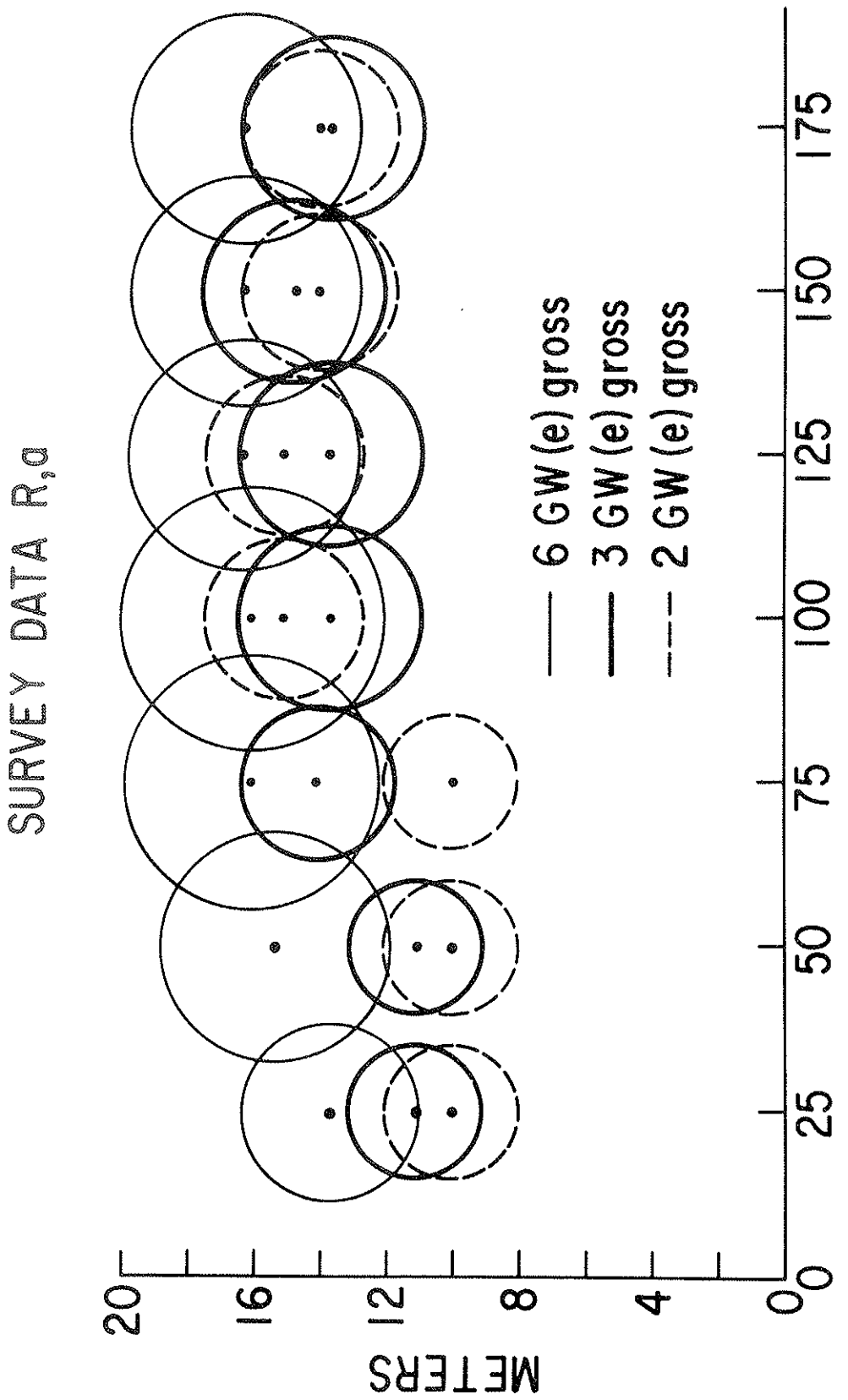

Fig. 2. Plasma Size for Standard Best Hybrid Reactors.

comparison of one hybrid design against another design. This comparison and selection is what the computer code does and to reproduce the comparison verbally would not shed light. However we can go part way in explanation.

The best hybrid curves are, by construction, curves of constant gross electric power, P_g. Now P_g is given by the following expression (that can be derived from the power flow shown in Figure IV.B.1).

$$P_g = \eta_t P_i \quad (1 + 0.2Q + 0.8QM) \quad . \tag{1}$$

Quite generally the last term in Eq. (1) dominates the other two so that to a good approximation we have for each best hybrid curve the relation,

$$P_g \sim P_i QM \approx \text{constant} \quad . \tag{2}$$

Furthermore the fusion power density in the plasma, p_f, is just $P_i Q/V$ where V is the plasma volume. Thus each best hybrid curve is well characterized by the relation,

$$V \cdot p_f \cdot M \approx \text{constant} \quad . \tag{3}$$

Noting that p_f is relatively insensitive to f, as shown in Table II, one would then expect from the relation (3) to find $V \cdot M \approx$ constant along a best hybrid curve, as is indeed the case.

The economics thus affects the physical size of the machine in basically two ways: selecting the value of M and setting the size of p_f.

The economic choices resulting in the best hybrids can only operate on the hybrids that survive the imposed "barrier type" constraints (see Section IV.F). The limitations on size due to the core constraint (Section IV.F.1) and the blanket performance (M) constraint (Section IV.F.4) are shown in Figure 3. In this figure the full line and dashed line circles display given values of R and a that cannot be used in the full calculation of reactor economics. All possible reactors surveyed for these values of R and a are in violation of one or the other of the above two constraints. For example, all possible (6 x 448 = 2688) 2 GW(e) gross machines in the survey with a = 1.2m are so denied. Of these machines with minimum R = 7.34 m (there are 448), 86% are denied by virtue of the M constraint and the rest by virtue of the core constraint. For a = 2.4 m and greater, all the 2 GW machines that have minimum survey values of R are denied by virtue of the core constraint. Since the core constraint is independent of the gross electric power level, P_g, rejection via the core constraint at the 2 GW level will be applicable to machines at all power levels. On the other hand, the blanket performance constraint is sensitive to P_g. For the small size 2 GW machines, the M constraint reflects the inability for the blanket to produce a large enough

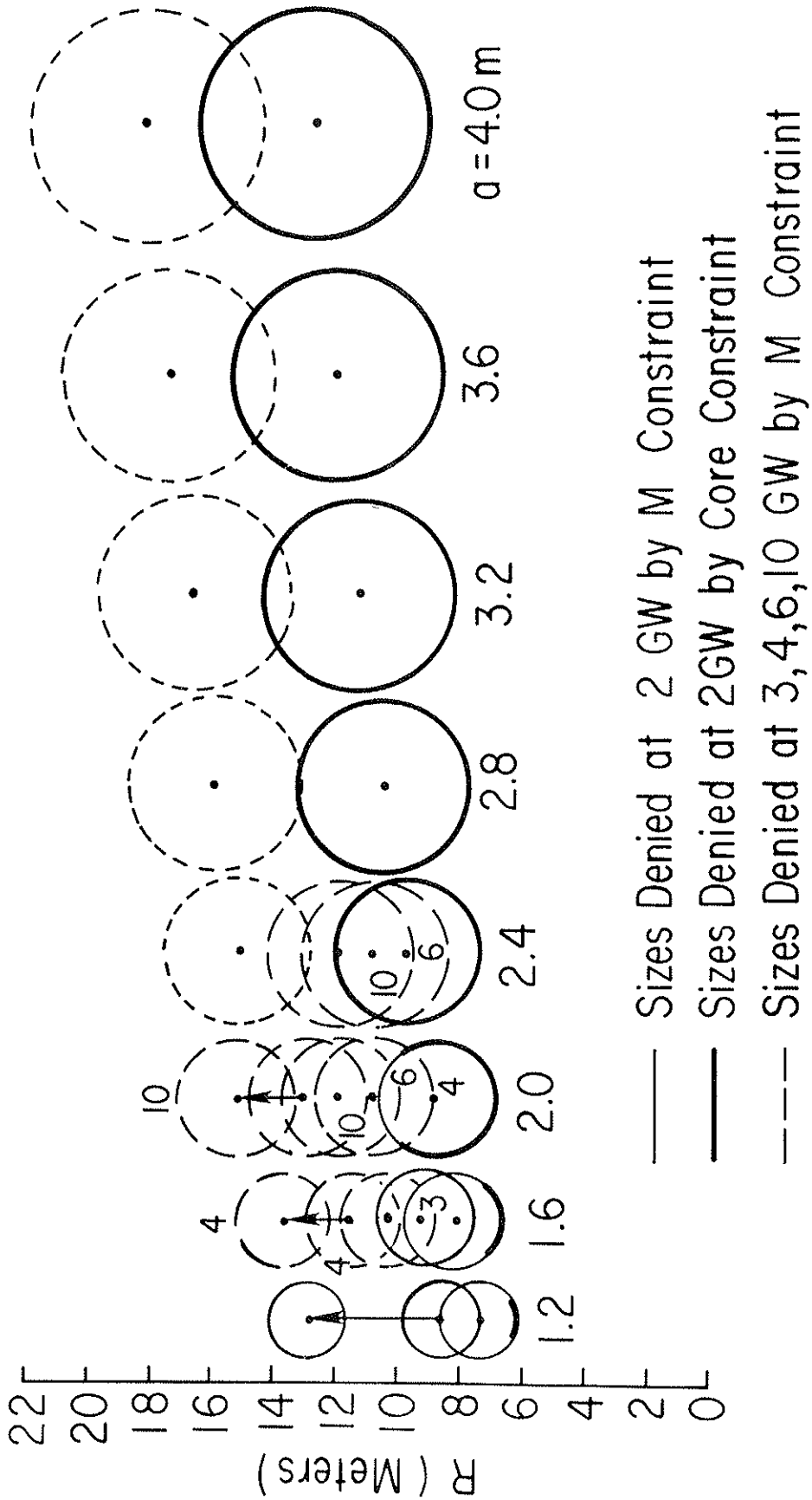

Fig. 3. Limitation on allowed plasma size due to the core constraint and the blanket performance constraint for single null configuration. (Survey data.)

value of M (consistent with the blanket $F \geq 0$) to meet the required value of P_g. Since P_g is an independent parameter, this limitation on blanket performance will be true for values of $P_g > 2$ GW(e) as well. Note, however, that for $P_g > 2$ GW(e) machines of larger size will fail to satisfy the M constraint for the same reason. The unusable sizes at the 3, 4, 6, and 10 GW(e) levels are shown by dashed circles. (The sizes shown by the dotted circles are not totally denied but simply show the maximum size machines available in the survey for the given values of a.)

For values of R and a not displayed by the full and dashed line circles in Figure 3 there is at least one machine in the survey that survives all the imposed barrier type constraints and is then subjected to economic evaluation. It is from among these machines that the "best hybrids" are selected.

The pressure "carpet" is shown in Figure 3a. The "unusable" regions for $P_g = 3$ and 4 GW(e) are given. Also depicted are the location of several best hybrids. We make several obervations. First, the pattern of pressures shows that p does not take on extremal values either in an absolute sense or for a fixed value of "h" or a fixed value of "a". Second, the pattern of pressure is different for both different values of P_g and different formulations of the $n_e\tau_{PHY}$ criteria. Furthermore, the penetration index is very nearly 1.0 for the 3 GW standard hybrids, as shown in Table II, but is a little above 1.0 for the 4 GW standard hybrids and in the range of

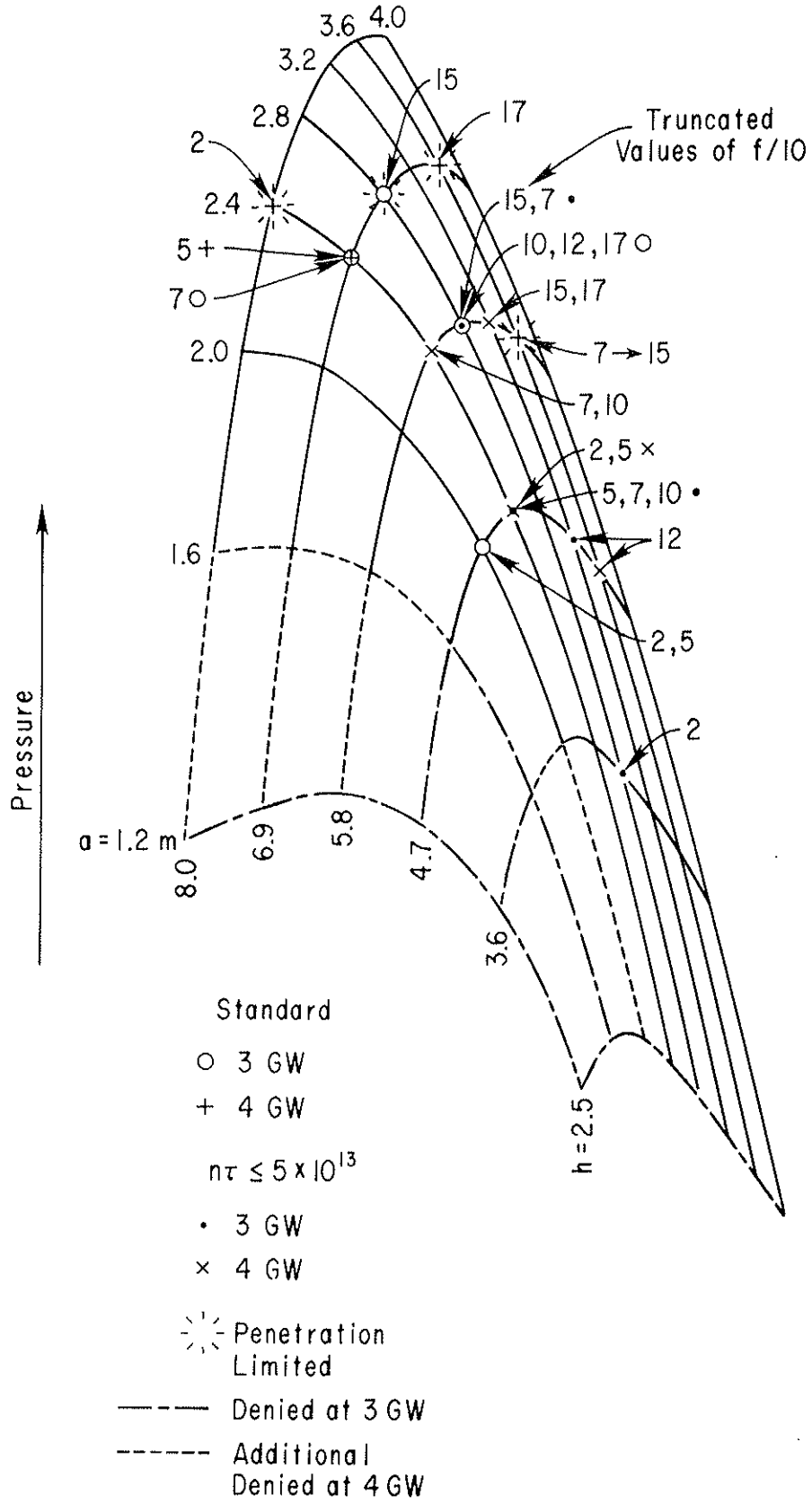

Fig. 3a. Pressure Carpet. This figure is the single null pressure carpet of Figure 7 in Section IV.C, but with an expanded ordinate. The appropriate values of the fissile fuel price, f, (truncated to fit on the figure) are indicated for each plotted point. The dashed portions of the pressure carpet grid show the limitation on available pressures due to the core and blanket performance constraints.

.5-.8 for the hybrids constrained to have $n\tau_p \leq 5 \times 10^{13}$ sec-cm^{-3}. Thus the best hybrids are economically determined not to operate at either an extreme pressure or always at a penetration limiting pressure.

The size of the best hybrid is not sharply defined. The meaning of this remark is revealed by examination of Tables IIIa and IIIb. Each of these tables is a matrix of entries, the row and column of each entry corresponding to a particular choice of h and a, respectively. The asterisks correspond to the denied values of R and a illustrated in Figure 3. These tables are called "e carpets". They display the cheapest price of electricity, e (mills/kWh), generated by hybrid reactors with a given value of a and h. These tables are calculated for P_g = 3 GW(e) and for an assumed price of fissile fuel, f, as indicated. The best hybrid for f = 50 \$/g is found in Table IIIa with e = 41.0 mills/kWh and at a value of a = 2.0 m and h = 4.7 m (R = 11.1 m). This result is also evident in Figures 1 and 2.

We shall designate a particular location in the "carpet" matrix in a conventional manner by specifying an ordered pair of integers, the first integer labeling the row and the second, the column. Thus the above best hybrid is located at (3,3). We note e equals 41.6 at (2,4) and 41.8 at (3,4). These two hybrids are somewhat different in size, but their value of e is less than 2% different from that of the "best hybrid". We also note at location (6,4) e = 41.4, a mere 1% higher than for the best hybrid, but having a = 2.4m and h = 8.0m (R = 15.18m) - a substantial difference in size from that of the best hybrid.

Table III. e Carpet (3 GW(e) gross)

h \ a	1.2	1.6	2.0	2.4	2.8	3.2	3.6	4.0	
2.5	*	*	*	*	*	*	*	*	
3.6	*	*	46.3	41.6	43.5	45.6	46.3	46.7	
4.7	*	*	41.0	41.8	43.3	45.0	46.0	48.3	(a)
5.8	*	50.7	42.3	42.6	44.0	45.6	43.9	45.4	
6.9	*	47.2	42.7	41.5	43.0	44.4	45.9	47.5	
8.0	*	47.6	43.0	41.4	44.4	45.8	47.2	48.6	

f = \$50/gm

h \ a	1.2	1.6	2.0	2.4	2.8	3.2	3.6	4.0	
2.5	*	*	*	*	*	*	*	*	
3.6	*	*	51.5	46.2	47.6	48.4	50.6	49.6	
4.7	*	*	45.2	46.3	46.0	44.9	43.6	45.0	(b)
5.8	*	55.9	45.7	45.5	42.3	43.7	44.5	45.4	
6.9	*	52.1	48.0	42.4	43.2	44.2	45.2	46.3	
8.0	*	52.9	46.0	43.4	44.2	45.2	46.3	47.5	

f = \$100/gm

e in mills/kWh

Turning to Table IIIb we see the same lack of sharp definition of the size of the best hybrid. The best hybrid is at (4,5) with e = 42.3 mills/kWh, a = 2.8m, and h = 5.8m (R = 13.76m). Around the best hybrid and extending somewhat diagonally through the matrix are hybrids with values of e not far from 42.3. Hybrids with values of e no more than 43.7 can be found between locations (3,7) (h = 4.7m, (R = 14.22m), and a = 3.6m) and (6,4) (h = 8.0m (R = 15.1m) and a = 2.4m). Although the values of R are similar, the values of a are quite different, and so is the volume of the plasma. On the other hand, the values of e at the "corners" of the carpet are indeed substantially higher than 42.3. Thus one can imagine a certain variation in size of the hybrid reactors without sustaining much of a penalty in increased cost of electricity, but such variation in size is not arbitrary. In this sense, then, we say the size of the best hybrid is not sharply defined.

The principal advantage of the carpet presentation is that it well displays the effect on the tabulated quantity of selecting different size machines. What is clear from the e carpet is that economics has not selected the smallest size machine available nor the largest.

To indicate the nature of the different hybrids that make up the e carpets of Table III, consider Tables IV, V, and VI displaying, respectively, carpets for the plasma temperature, T_e, the ratio of hot to thermal densities, H/T, and the deuteron injection energy, W_o. From these tables the complete 6-vector for each hybrid reactor is specified. To restate, these are "standard" hybrids (see introduction to this Section) operating at 3 GW(e) gross. Their economics are

Table IV. Temperature Carpet (3 GW(e) gross)

*	*	*	*	*	*	*	*
*	*	6.0	7.0	7.0	8.0	6.0	7.0
*	*	8.0	7.0	7.0	7.0	7.0	7.0
*	6.0	7.0	6.0	7.0	6.0	7.0	7.0
*	6.0	7.0	7.0	7.0	7.0	7.0	7.0
*	7.0	7.0	7.0	6.0	6.0	6.0	6.0

f = \$50/g

---

*	*	*	*	*	*	*	*
*	*	6.0	7.0	9.0	8.0	8.0	9.0
*	*	8.0	8.0	9.0	9.0	7.0	7.0
*	6.0	8.0	8.0	7.0	7.0	7.0	7.0
*	6.0	9.0	7.0	7.0	7.0	7.0	7.0
*	7.0	8.0	7.0	7.0	7.0	7.0	7.0

f = \$100/g

Temperature in keV

Table V. Hot/Thermal Carpet (3 GW(e) gross)

f = $50/g

*	*	*	*	*	*	*	*
*	*	.10	.05	.03	.05	.03	.03
*	*	.075	.03	.03	.03	.01	.01
*	.10	.03	.01	.01	.01	.01	.01
*	.075	.03	.01	.01	.01	.01	.01
*	.10	.03	.01	.01	.01	.01	.01

f = $100/g

*	*	*	*	*	*	*	*
*	*	.10	.05	.01	.05	.05	.05
*	*	.075	.05	.05	.03	.01	.01
*	.10	.05	.03	.01	.01	.01	.01
*	.10	.075	.01	.01	.01	.01	.01
*	.10	.03	.01	.01	.01	.01	.01

Table VI. Injection Energy Carpet (3 GW(e) gross)

f = $50/g

*	*	*	*	*	*	*	*
*	*	150.0	150.0	183.0	150.0	166.0	166.0
*	*	150.0	166.0	166.0	166.0	200.0	200.0
*	150.0	166.0	225.0	200.0	225.0	183.0	183.0
*	150.0	150.0	183.0	183.0	183.0	183.0	183.0
*	150.0	150.0	166.0	200.0	200.0	200.0	200.0

f = $100/g

*	*	*	*	*	*	*	*
*	*	150.0	150.0	150.0	150.0	150.0	150.0
*	*	150.0	150.0	150.0	166.0	200.0	200.0
*	150.0	150.0	166.0	200.0	200.0	183.0	183.0
*	150.0	150.0	183.0	183.0	183.0	183.0	183.0
*	150.0	150.0	183.0	183.0	183.0	183.0	183.0

Injection Energy in kV

evaluated for a chosen price of fissile fuel. These hybrids are selected by a process that first specified h and a and then calculates the value of e for all values of T_e, H/T, and W_o used in the survey. The parameters of these hybrids that produce the lowest value of e appear in the carpets. The hybrid producing the lowest value of e in an entire carpet is designated a "best hybrid".

From examination of Tables III through VI it is evident that the economic selection produces a variation in all the five components of the 6-vector that are allowed to vary. For example, the change in economics due to f changing from 50 $/g to 100 $/g moves the "location" of the best hybrid from (3,3) to (4,5) and in so doing the values of T_e, H/T, and W_o also undergo a change. Therefore if one restricts the variation in parameters, in effect reducing the dimensionality of the economic analysis, one can arrive at substantially different conclusions as to the specification of the most attractive hybrid reactor.

Turning to "park hybrids" we present in Table VII an e carpet for 3 GW(e) gross park hybrid reactors together with the carpet of associated park fissile fuel prices. We note the lowest value for e appears at (4,5) with an associated value for f of 110.3 $/g. This "point" appears in Figure 1 as well. In fact, the "points" for these two carpets all fall, by construction, on the straight line for the LWR in this figure.

Table VII. a) e Carpet b) f Carpet (3 GW(e) gross)

*	*	*	*	*	*	*	*
*	*	63.6	51.4	51.3	51.3	51.4	49.6
*	*	48.9	48.0	46.2	43.4	42.9	43.7
*	72.6	48.4	45.9	42.0	42.8	43.7	44.9
*	61.7	50.1	42.6	42.9	44.0	44.9	45.6
*	64.8	48.0	43.2	43.8	44.6	45.2	45.9

(a)

*	*	*	*	*	*	*	*
*	*	216.2	156.6	156.0	156.2	156.4	147.6
*	*	144.5	139.7	131.0	117.3	114.9	119.0
*	260.1	141.7	129.4	110.3	114.5	119.0	124.6
*	207.2	150.2	113.6	115.0	120.1	124.5	128.2
*	222.0	139.9	116.6	119.6	123.0	126.4	129.6

(b)

e in mills/kWh

f in $/g

The above "best park hybrid" coincides with the "best hybrid" one would expect to find for f = 110.3 \$/g. Since the park value of f is so close to 100 \$/g, it is not surprising to find that the 6-vector for the "best park hybrid" coincides, for the survey, with the 6-vector of the "best hybrid" for f = 100 \$/g as displayed in Table III.

We note that the pattern of e in Table VII is similar to the pattern in Table IIIb although there are differences in the values of e at the same locations on the carpets. These differences again point up the importance of allowing many parameters to vary at once.

It is clear from Table VII that the economics has not selected the smallest size park hybrid available.

2. Variation of Constraints

Survey calculations were made for variations in the physically achievable confinement, $n_e\tau_{PHY}$, and the pressure scaling. In addition, survey calculations were made for a "standard" (see Section III) double null configuration.

a. Variation of Confinement Parameter, $n_e\tau_{PHY}$

The product $n_e\tau_{PHY}$ was varied in three ways. The first method was to scale the "standard" value for τ_p, as given by Eq. IV.F.25, up and down by a factor of 10. The results on the cost of electricity, e, are shown in Figure 4 for several values of P_g. For the 1/10 scaling the data for the 3 GW(e) gross best hybrids are off scale, and there are no 2 GW(e) gross machines in the survey that survive this constraint. The results

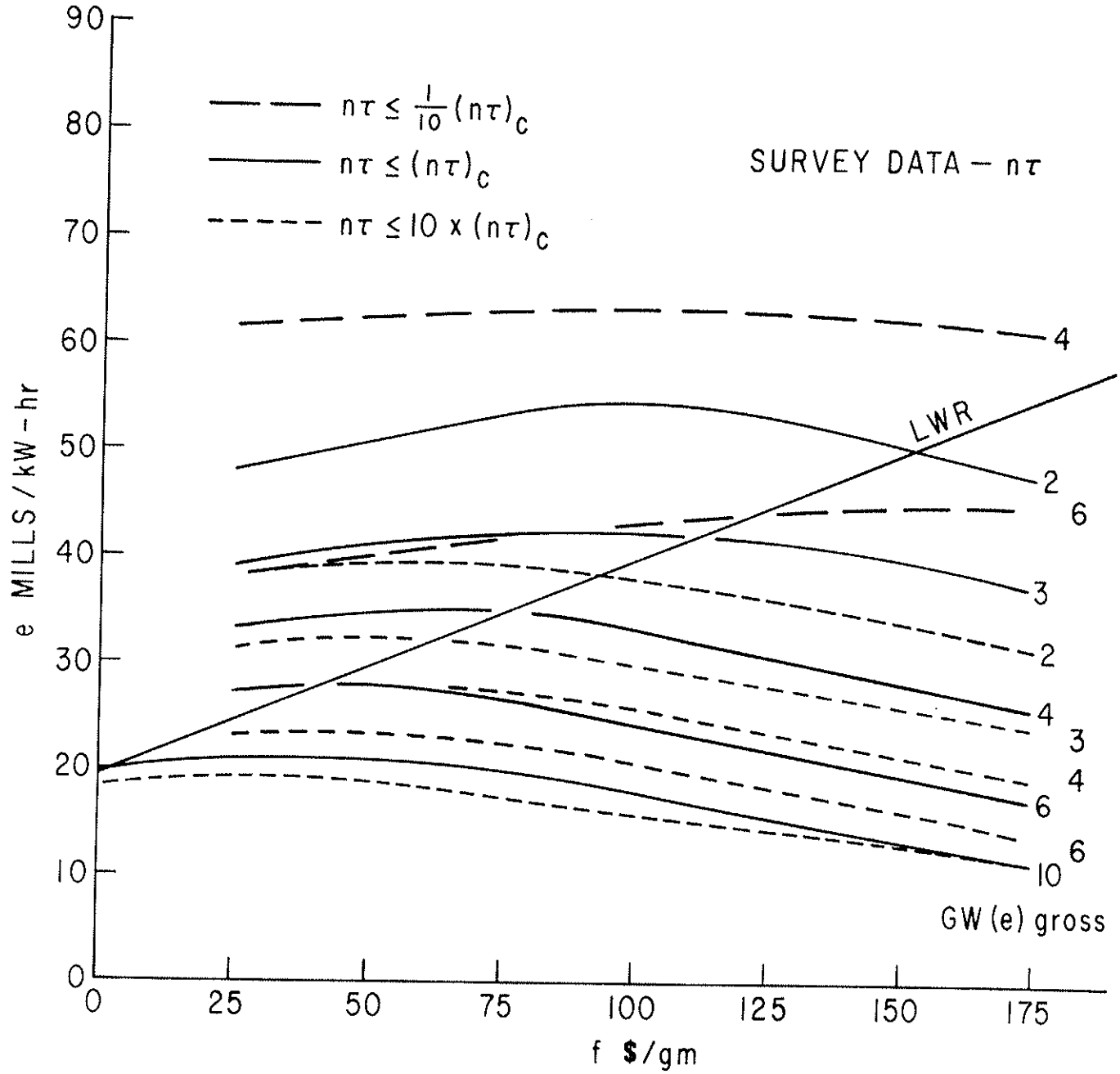

Fig. 4. The cost of electricity for different assumptions for the plasma confinement parameter nτ. The quantity $(n\tau)_c$ is the confinement parameter calculated using the trapped electron mode of particle transport described by Eq. (25) of Section IV.F.

for the 10 GW(e) gross hybrids for both the standard and 10x standard scaling should be treated with some reservation because in many cases both R and a for the "best hybrids" are at their maximum available values.

The second way $n_e\tau_{PHY}$ was varied was to take $n_e\tau_{PHY}$ as constant:

$$n_e\tau_{PHY} = n_e\tau_p = 5 \times 10^{13} \text{ sec cm}^{-3} \quad . \qquad (4)$$

The results on the cost of electricity are shown in Figure 5 together with the curves for the standard hybrids for comparison. Also in this figure are the results for the third way of varying $n_e\tau_{PHY}$, which was to adopt the so-called "Alcator scaling" as given by Eq. (IV.F.26). We note that this scaling places a requirement on τ_E rather than on τ_p. The sizes of the park hybrids for these variations in the $n_e\tau_{PHY}$ criterion are shown in Figure 5a.

These results reflect a profound sensitivity of the cost of electricity to the confinement constraint.

Consider the effect of scaling the standard value of τ_p shown in Figure 4. The cost of electricity is inversely correlated to the scaling factor, the lower the realizable confinement, the higher the cost of electricity. This result is understood in the following way. For a given level of P_g there is a strong correlation between the cost of electricity, e, and

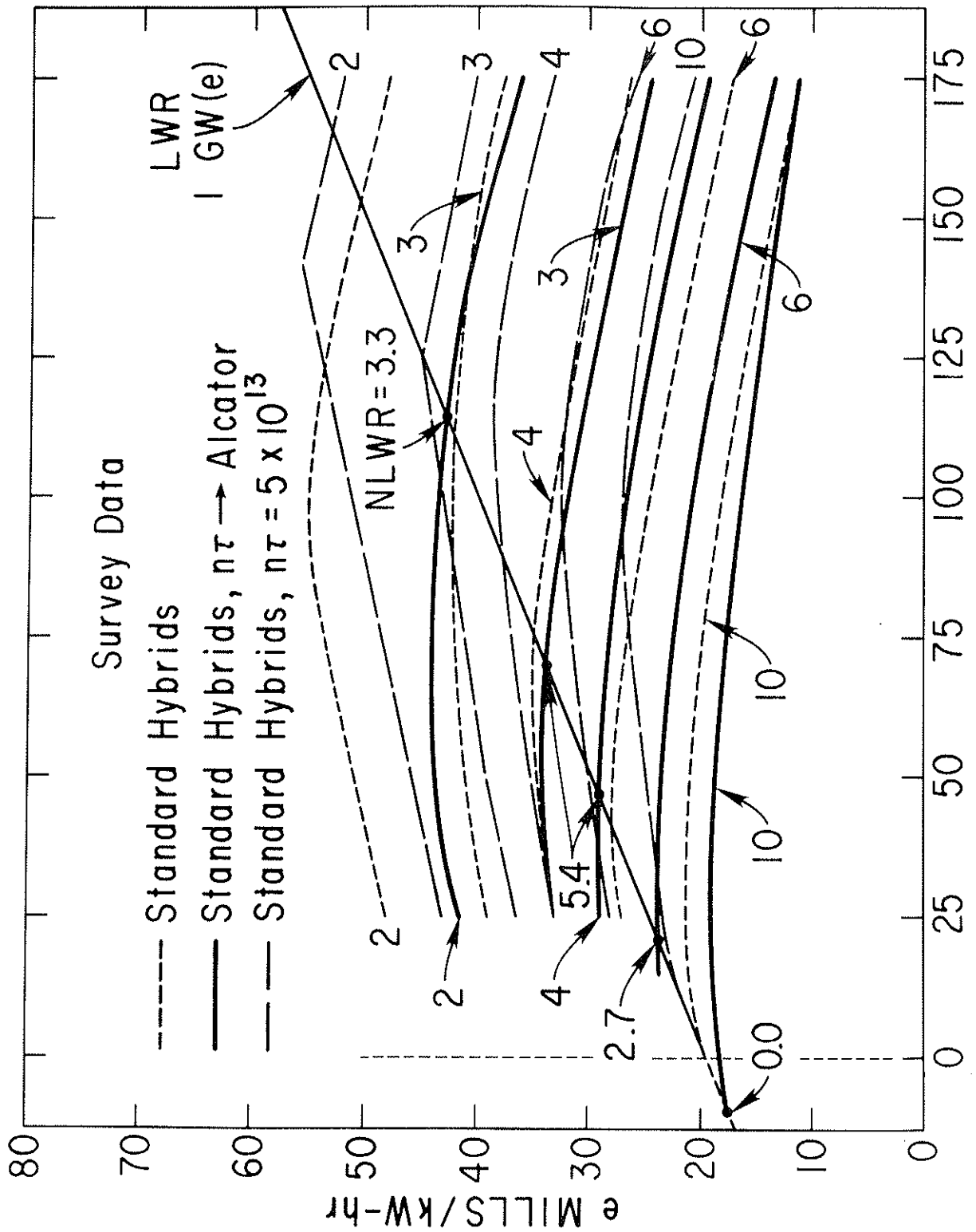

Fig. 5. The Cost of Electricity for some Different Criteria for Plasma Confinement.

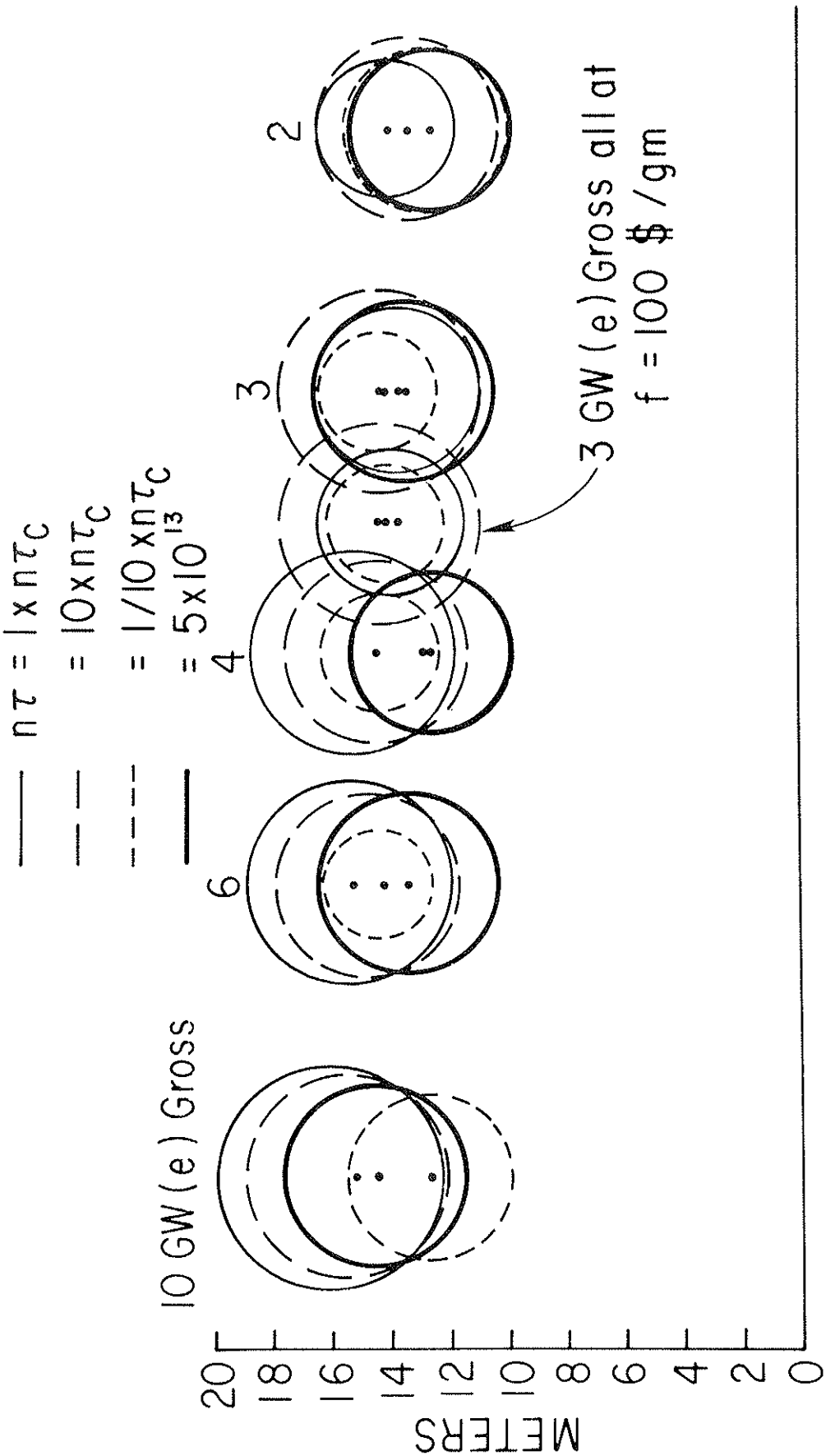

Fig. 5a. Plasma Sizes for "Park Hybrids" Under Various Assumptions for the Plasma Confinement. The Value of $n\tau_c$ is Calculated According to Eq. (25) of Section IV.F.

P_{net}: the higher P_{net}, the lower is e. Now P_{net} is given by the following expression (which can be derived from the power flow shown in Figure IV.B.1)

$$P_{net} = P_g \left(0.9 - \frac{P_i}{\eta_i P_g}\right) . \qquad (5)$$

In view of the correlation between P_{net} and e, we see by Eq. (5) that the lowest values of e will be associated with the lowest values of (P_i/η_i), which is the circulating power required to drive the injectors. Although this power depends on the injector efficiency, that in turn depends on W_o (see Section IV.E.1), the most sensitive quantity in determining P_{net} is P_i.

Now a decrease in the confinement capability of the plasma will require an increase in the power density per plasma particle delivered to the plasma by both the neutral beams and the alpha particles that result from fusion events. The increase in power density can be accomplished by increasing the beam power, P_i, to the detriment of P_{net} and e, or by decreasing the volume of plasma while keeping P_i and hence P_{net} essentially fixed. The experience of the survey calculations is that both effects occur. These effects are illustrated in Tables VIII, IX and X. The first three lines of these tables show the effects of scaling the standard $n_e\tau_{PHY}$ (trapped electron mode transport) by factors of 1/10, 1, and 10. We see that the better the confinement, the smaller the total beam power (Ignition of the tokamak plasma is reached for $P_i = 0.$), the larger the net

Table VIII. Survey Data at 3 GW(e) Gross f = \$50/g

f	M	W_o	R	a	H/T	T_e	n_e	$n\tau_{PHY}$	$n\tau$	P_i	Q	Vol.	p_f	P_{net}	e
\$/g		kV	m	m		KeV	$10^{14}cm^{-3}$	$10^{14}sec\ cm^{-3}$	$10^{14}sec\ cm^{-3}$	MW		10^3m^3	W/cm^3	GW	mills/kWh
50	11.0	183	14.4	2.0	0.20	6	0.41	0.95 × 1/10	0.09	998	0.8	1.13	0.673	0.92	107.7
50	23.1	150	11.1	2.0	0.075	8	0.47	0.38 × 1	0.36	360	1.11	0.876	0.460	2.12	41.0
50	12.8	150	13.7	2.8	0.0	10	0.56	0.81 × 10	6.03	0	∞	2.12	0.355	2.70	32.0
50	20.9	150	11.8	2.4	0.075	12	0.33	0.5*	0.5	276	1.63	1.35	0.333	2.25	39.2
50	10.4	150	15.3	3.6	0.0	6	1.02	5.51†	5.32	0	∞	3.91	0.236	2.70	34.1

*$n\tau$ = constant

†Alcator scaling

Note: For "Alcator" results the $n\tau$ refers to $n\tau_E$ rather than $n\tau_p$.

Table IX. Survey Data at 4 GW(e) Gross, f = \$50/g

f	M	W_o	R	a	H/T	T_e	n_e	$n\tau_{PHY}$	$n\tau$	P_i	Q	Vol.	p_f	P_{net}	c
\$/g		kV	m	m		keV	$10^{14}cm^{-3}$	$10^{14}sec\ cm^{-3}$	$10^{14}sec\ cm^{-3}$	MW		10^3m^3	W/cm^3	GW	mills/kWh
50	15.1	183	14.4	2.0	0.20	6	0.41	0.95 × 1/10	0.09	998	0.777	1.13	0.682	1.82	62.4
50	18.4	183	14.0	2.4	0.010	7	0.86	2.28 × 1	2.13	294	2.33	1.60	0.428	3.07	34.7
50	12.3	150	14.5	3.2	0.0	10	0.56	1.09 × 10	6.03	0	∞	2.93	0.356	3.60	27.8
50	24.5	150	11.8	2.4	0.075	10	0.38	0.5*	0.46	351	1.464	1.35	0.380	3.03	35.0
50	11.8	150	15.3	3.6	0.0	7	0.87	5.51†	5.32	0	∞	3.91	0.278	3.60	28.7

*$n\tau$ = constant

†Alcator scaling

Table X. Park Solutions at 3 GW(e) Gross, f ($/g) varies

f	M	W_o	R	a	H/T	T_e	n_e	$n\tau_{PHY}$	$n\tau$	P_i	Q	Vol.	p_f	P_{net}	e
$/g		kV	m	m		keV	10^{14} cm^{-3}	10^{14} sec cm^{-3}	10^{14} sec cm^{-3}	MW		10^3 m^3	W/cm^3	GW	mills/kWh
265.2	8.8	150	14.4	2.0	0.20	6	0.46	1.08 × 1/10	0.10	1190	0.8	1.13	0.814	0.78	73.6
110.3	11.1	200	13.7	2.8	0.010	7	0.82	2.47 × 1	2.15	352	2.5	2.12	0.390	2.04	42.0
62.0	10.7	166	14.2	3.6	0.0	10	0.46	0.88 × 10	6.03	0	∞	3.63	0.247	2.70	32.1
125.2	10.3	150	13.4	3.2	0.075	12	0.33	0.5*	∿ 0.5	536*	1.62	2.71	0.320	1.83	45.0
68.9	10.4	150	15.3	3.6	0.0	6	1.02	7.57†	7.46	0	∞	3.91	0.236	2.70	33.5

*$n\tau$ = constant

†Alcator scaling

power and the lower the cost of electricity. The fusion power density also falls monotonically as the confinement improves and, with the exception of the example of P_g = 3 GW and a scaling of 1/10 (line 1, Table VIII), the volume monotonically increases.

The cost of electricity is not correlated with the absolute value of $n_e\tau_{PHY}$ alone. As evidenced by lines 2 and 4 of Table IX, nearly identical values of e are produced at quite different values of $n\tau$. Comparing the corresponding curves in Figure 5 (4 GW), the shapes are different indicating that the choice of the best hybrid is affected by the functional dependence of $n_{e\ PHY}$ on various physical parameters as well as the actual value of $n_e\tau_{PHY}$.

Generally the Alcator scaling produces economic results similar to the x10 scaling of the standard $n_e\tau_{PHY}$, but produces somewhat larger machines.

A further observation in regard to the $n\tau$ constraint: The results of the scaling of the standard $n_e\tau_{PHY}$ by factors of 1/10, 1, and 10 support the general statement that for a given formulation of the $n\tau$ constraint in terms of a functional dependence on various parameters, a numerical scaling of the $n\tau$ constraint to increase its value will result in a lowering of the cost of electricity. This effect accounts for the observation that the $n\tau$ values required by the best hybrids of the survey always lie close to the allowed value of $n\tau$. (Compare $n\tau_{PHY}$ and $n\tau$ in Tables VIII, IX, and X.) For the optimized results discussed below in Section C the required values of $n\tau$

are nearly identical with the constraint values. The general conclusion, then, is that the best hybrids are characterized by the highest value of $n_e\tau_{PHY}$ attainable consistent with other constraints. In still other words, the best hybrids "try to ignite".

b. The $P_{net} < 0$ Constraint

All the survey examples (6-vectors) that led to $P_{net} < 0$ required an economic subsidy ($e < 0$) for values of $f < 200$ \$/g. The park solution for such hybrids occurred for values of f in the several hundred \$/g range. Thus the constraint $P_{net} > 0$ is judged to be a necessary condition for attractive hybrid economics.

c. Variation of Pressure Scaling

Survey calculations were made with the pressure limits, given by Eq. (IV.C - 15), multiplied by $\sqrt{10}$ and $1/\sqrt{10}$. These calculations were made only for gross power levels of 3 and 4 GW. The resulting best hybrid curves are presented in Figure 6. The increase in the cost of electricity was anticipated for a decrease in the pressure limit but not for the increase as well. This effect was investigated using the optimization style of calculation and will be further discussed below in Section 2.c and 2.e. We simply observe here that the reduction in pressure limit does not produce a park hybrid for $f < 200$ \$/gm. These results are therefore completely unattractive from an economic point of view.

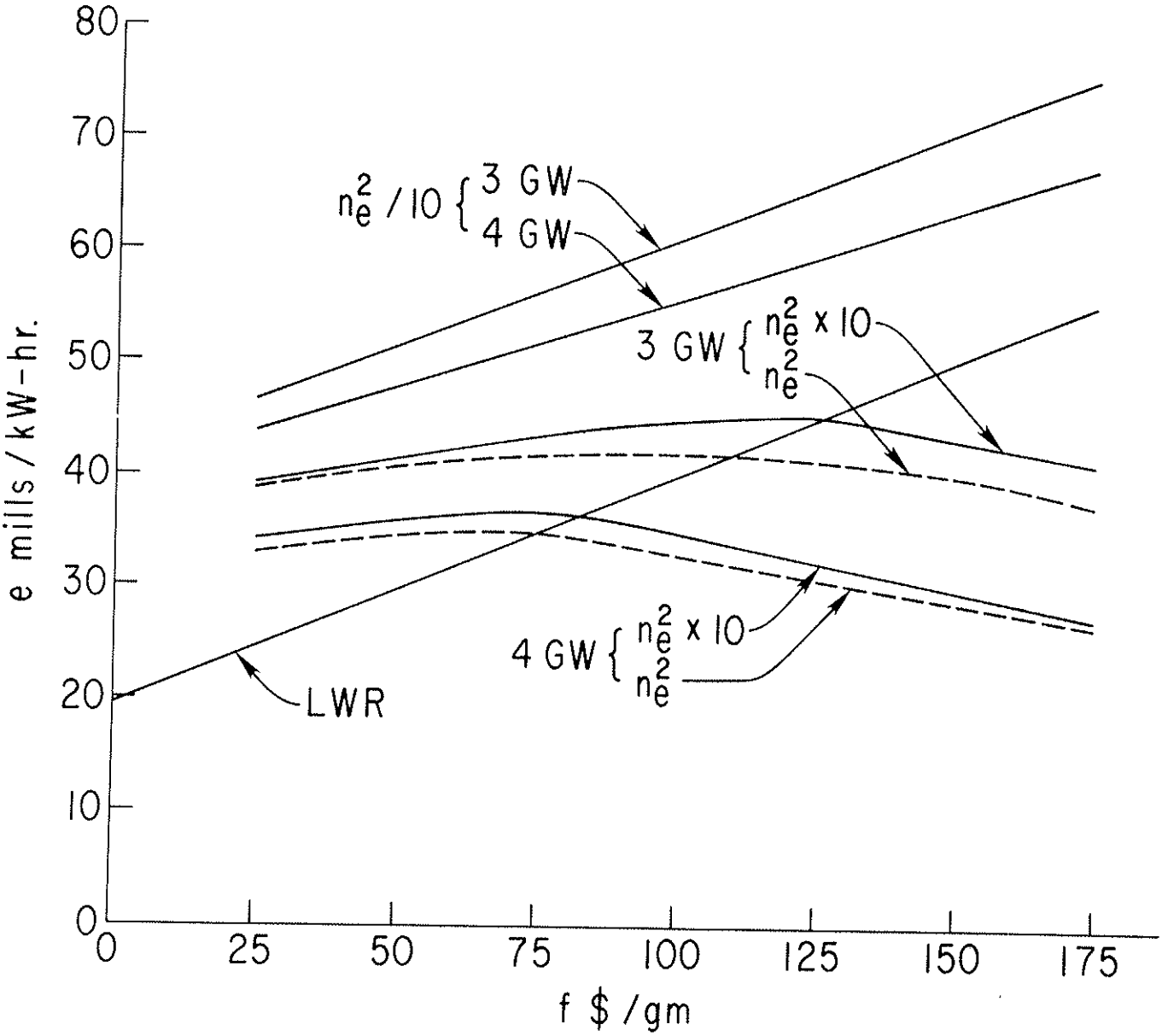

Fig. 6. Effect of Different Pressure Scalings on the Cost of Electricity for 3 and 4 GW(e) Gross "Best Hybrid" Reactors.

The physical size of the best hybrids is shown in Figure 7. The size of the best hybrid is quite sensitive to the pressure scaling. For the $1/\sqrt{10}$ scaling the size reaches the maximum value surveyed which suggests even larger sizes would produce cheaper electricity. Some features of the 3 GW(e) gross best hybrids for f = 100 \$/gm are shown in Table XI. We note that for the $\sqrt{10}$ scaling two different hybrids produce the same value of P_{eh} to three significant figures. These cases also illustrate the lack of "sharp definition" in hybrid size discussed in Section 1.

The range in size reflects the quite different fusion power densities developed in the plasma. (See Eq. (3).) Several features of the physical-economic model for the hybrid come into play to understand this result. Consider first the case for an increase in pressure scaling. We first note that the standard best hybrid (second line of Table XI) operates almost at the penetration limit (A_T = 0.98). Consequently for the increase in pressure scaling the 6-vector for this standard best hybrid would produce a violation of the penetration limit. The branch of the computer code FUN that is taken when the pentration limit is violated causes the density to be reduced to a level for which the penetration limit is just satisfied. (See discussion of code in Section IV.H and Figure IV.H-2.) In addition, I and B are both reduced in order to preserve the values of β_θ and β. The result of these reductions, for this 6-vector, is that the actual plasma density will not change very much, but the

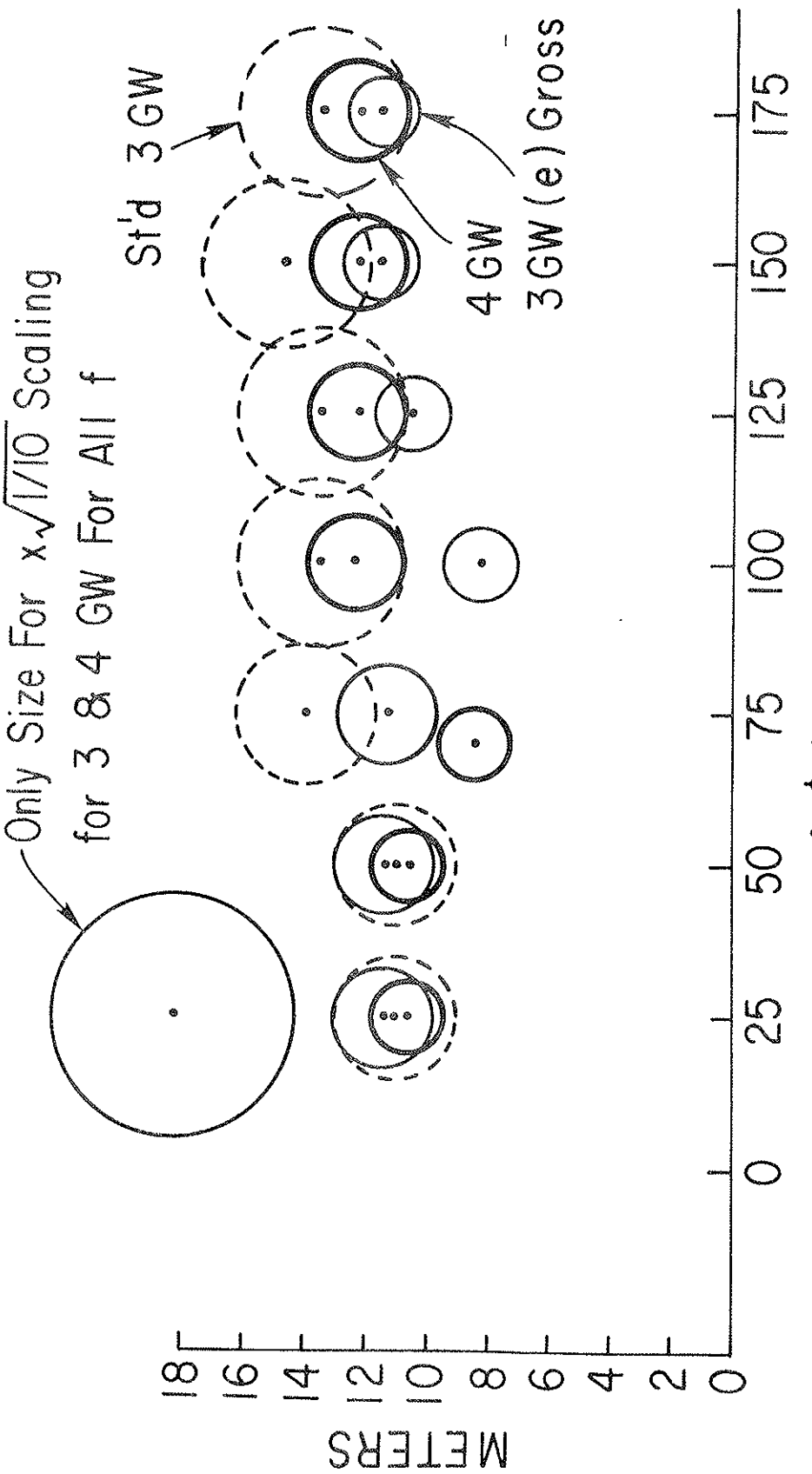

Fig. 7. Effect of Different Pressure Scalings on the Size of the Plasma of Several "Best Hybrid" Reactors.

Table XI. Survey Data at 3 GW(e) Gross, f = $100/g

B_c	I	Capital Cost	A_T	B_{max}	P-scale	P_{net}	a	$n\tau$	R	e	M	β	T_e	H/T	W_o	P_{Beam}	V	Q	P_f	n_e
T	MA	G$		T		GW	m	10^{14} sec cm^{-3}	m	mills/ kWh			keV		kV	MW	m^3		W/cm^3	10^{14} cm^{-3}
6.9	4.8	5.72	0.58	16.0	$1/\sqrt{10}$	2.37	4.0	0.95	18.29	61.0	24.1	0.39	9	0.030	150	207	5776	1.91	0.068	0.22
6.7	5.2	3.52	0.98	16.0	1	2.04	2.8	2.15	13.76	42.3	11.1	1.12	7	0.010	200	352	2129	2.36	0.390	0.82
6.0	2.3	2.92	1.28	14.1	$\sqrt{10}$	1.84	1.2	0.26	8.44	45.1	21.1	2.07	6	0.075	150	530	240	0.81	1.80	1.00
9.7	2.1	3.26	1.05	15.6	$\sqrt{10}$	1.98	1.2	1.89	12.84	45.1	18.6		6	0.010	250	317	364	1.58	1.37	1.82

value of $n_e \tau_{PHY}$ will be reduced (see Eq. (25) in Section IV.F). Since the $n_e\tau_p$ required by the standard best hybrid is close to the value of $n_e\tau_{PHY}$, this reduction in $n_e\tau_{PHY}$ will result in the code FUN rejecting this modified hybrid design. Thus, the set of 6-vectors in the survey that survive the calculation for e will depend on the magnitude of the pressure scaling as well as functional dependence of $n_e\tau_{PHY}$.

We also point out that the above reduction in B would result in a reduction in cost of the magnets so that the modified hybrid might have produced even cheaper electricity if it had not been rejected because of inadequate particle confinement. Such would have been the case if the confinement of the best hybrid had used Alcator scaling, which depends on (B/I) (see Eq. (26) of Section IV·F) and hence would be insensitive to the above reductions.

The 6-vectors that do survive the calculation for e will include those designs that could tolerate the increase in pressure and hence are calculated to operate at higher fusion power densities. In accordance with Eq. (3) we expect machines with smaller values of V × M to be generated. The smaller volumes can have less costly structures, but will produce less overall fusion events and hence require larger values of M to achieve their rated gross power level. Larger values of M imply more Pu in the blanket and hence larger blanket inventory charges. Furthermore, smaller sized machines may have poorer confinement and hence require larger beam power to the detriment of the net electric power and a subsequent increase in e. The

interplay between the above various factors is not transparent, but its complexity and subtlety are apparent.

The above discussion again points to the value of a multidimensional calculation for the evaluation of the performance of the hybrid reactor.

d. Other Variations of Constraints

Variations were made in the penetration criteria and the blanket neutronic performance. The effects of these variations on hybrids with a single null configuration were evaluated via the "optimization" type of calculation rather than the survey type and will be discussed in Section C below.

3. Double Null Divertor Configuration

The survey results of standard hybrids with a double null divertor configuration (see Figure IV.C-2) are shown in Figure 8. These "standard" hybrids use the same constraints as the standard single null hybrids, but use the double null scaling of pressure (Eq. IV.C-17) and discharge current (Eq. IV.C-16). The maximum allowed pressure for the double null is 2-3 times that for the single null designs as is evident from Figure IV.C-7 or Figure IV.F-4.

The standard double null design produces only a modest improvement in the cost of electricity, and the park hybrids support somewhat fewer LWR's than the corresponding single null park hybrids with the exception of the 10 GW(e) cases. (See Figure 1.) However the double null hybrids are considerably smaller in size than the single null hybrids as shown in

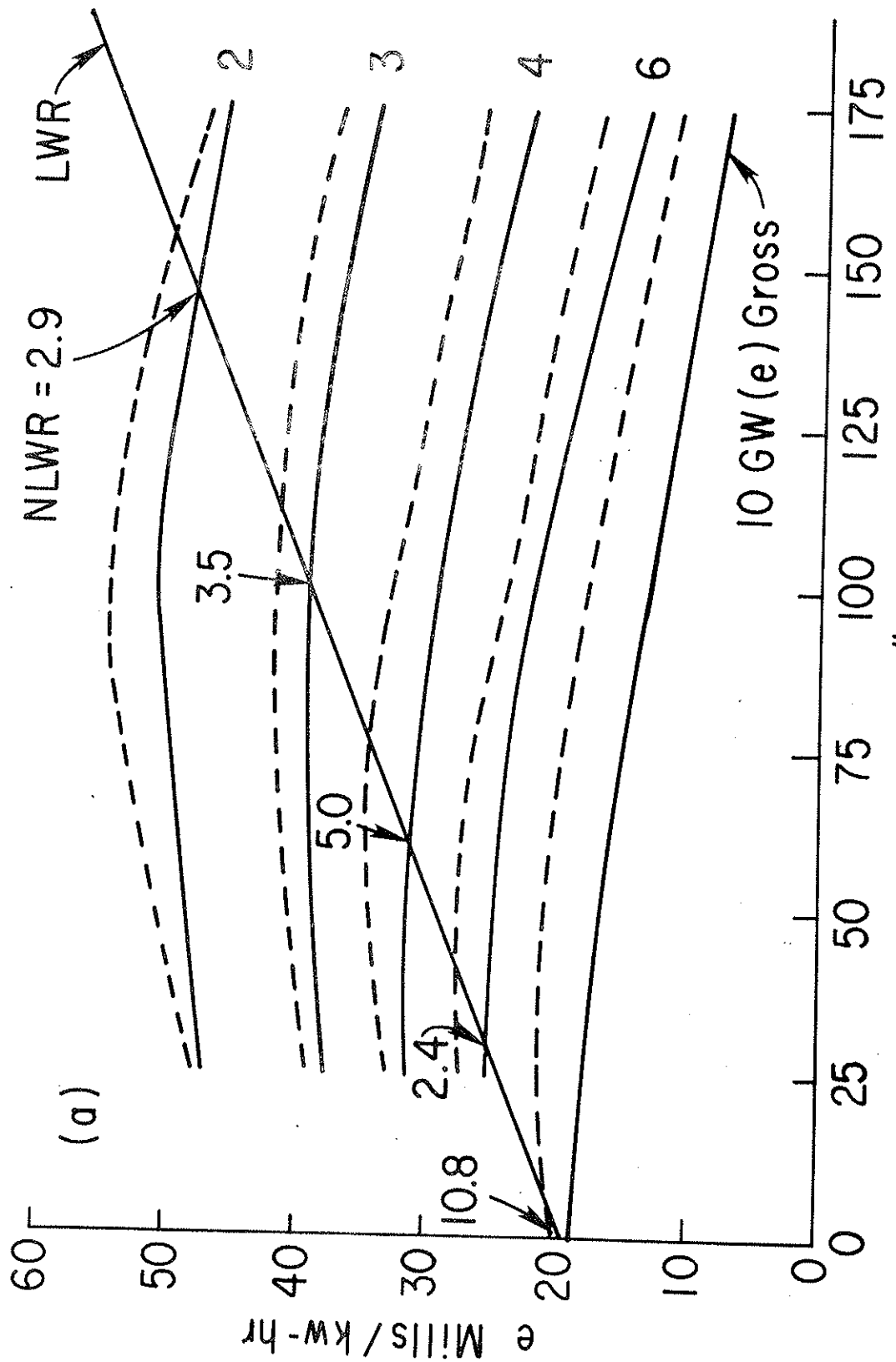

Fig. 8. Standard best double null hybrids, survey results (———). For comparison the standard single null data are shown as (– – – – –). The number of light water reactors (NLWR) supported by the "park hybrid" is also shown.

Figure 9. (In this figure the values of R and a for a given double null design are displayed as circles.) Table XII displays some features of the double null best hybrids of 3 GW(e) gross. Comparing this table with Table II for the single null best hybrids we note the double null machines have many similar features but are smaller, have somewhat higher densities, and generally operate at about twice the fusion power density as the single null hybrids. The higher fusion power densities available to the double null hybrids relieves the demand on blanket energy multiplication. Consequently small physical sizes are available to the double null hybrids (at a = 1.2 m) that were denied to the single null hybrids (see Figure 1 in Section III). However, the penetration constraint limits the double null density as evidenced by the large number of lines in Table XII that have $A_T > 1$. This limitation of the density compromises the advantages of higher allowed pressure to some extent, particularly for the larger values of "a" surveyed where the penetration constraint can require lower densities than at smaller "a".

The lower cost of electricity for the double null hybrids relative to the single null hybrids is related to the lower capital cost which in turn reflects the smaller physical sizes. The capital costs are enough lower to compensate for the somewhat lower values of P_{net} produced by the double null hybrids.

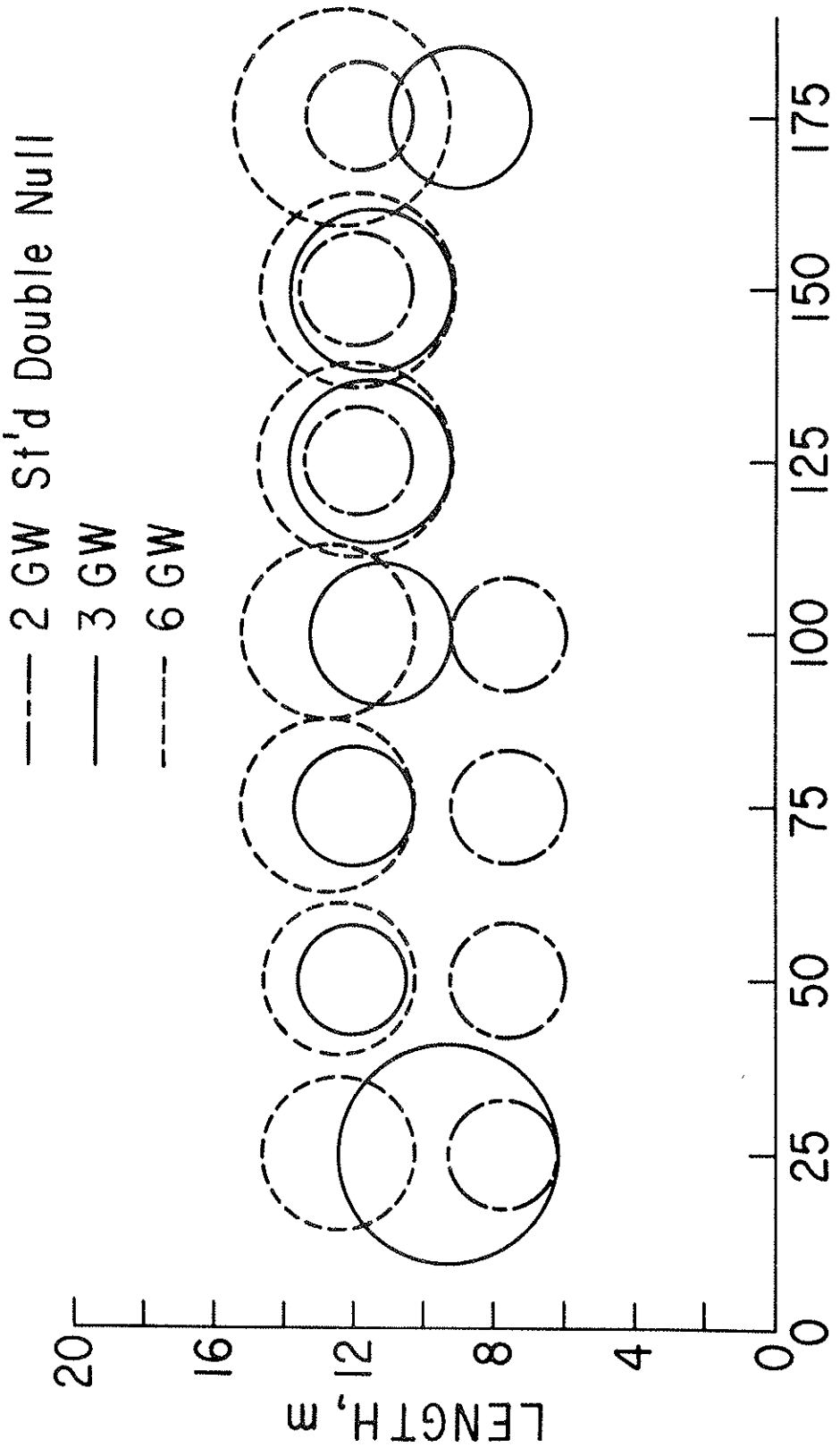

Fig. 9. Circularized Size of Plasma for Several Standard Best Hybrid Reactors of Double Null Configurations.

Table XII. Some Characteristics of 3 GW(e) gross, Double Null, Best Hybrids (Survey Data)

f	M	T_e	W_o	H/T	a	R	I	n_e	B_c	Q	p_f	W_L	NLWR	P_{net}	A_T
$/g		keV	kV		m	m	MA	$10^{14}cm^{-3}$	T		W/cm^3	MW/m^2		GW	
25	23.2	7	150	0.075	3.2	9.2	5.8	0.34	3.1	0.94	0.21	0.27	0	2.02	4.00
50	15.5	7	225	0.01	1.6	12.0	3.1	1.37	10.6	2.12	0.99	0.57	1.47	2.11	0.98
75	15.5	7	225	0.01	1.6	12.0	3.1	1.37	10.6	2.12	0.99	0.57	1.47	2.11	0.98
100	11.7	7	250	0.01	2.0	11.3	4.4	1.28	8.3	2.28	0.88	0.65	3.40	1.92	1.36
125	11.1	7	250	0.01	2.4	11.7	5.2	1.07	6.8	2.32	0.62	0.56	3.93	1.89	1.86
150	11.1	7	250	0.01	2.4	11.7	5.2	1.07	6.8	2.32	0.62	0.56	3.93	1.89	1.88
175	9.0	9	225	0.03	2.0	9.1	5.3	1.05	7.7	1.87	1.38	1.03	5.40	1.61	1.12

See Table II for definition of symbols.

a. Variation of Constraints

As for the single null configurations, the effect of varying the allowed $n\tau$ and the blanket neutronic performance was examined for the double null configuration. Survey type calculations were used. Only two different $n\tau$ constraints were considered: the 1 × T.E. scaling (Eq. IV.F-25) and the Alcator scaling (Eq. IV.F-26). For the variation of blanket performance the number of fissions in the converter region was increased to make a "super blanket". (See Section IV.D.) In addition, two different types of variation were also studied: the effects of a "new pressure" formulation given by Eq. 18 of Section IV.C and the effects of different "profiles" of plasma density and temperature. The manner in which the effect of the plasma profiles is introduced into the point model for the plasma is discussed in Appendix II. The plasma profiles affect the fusion reactivity assigned to the plasma.

The effect of changing the $n\tau$ constraint is shown in Figure 10. The use of Alcator scaling instead of 1 × T.E. scaling affects the single null and double null configurations in similar ways. The cost of electricity is reduced, the physical size of the plasma is increased, and the plasma state moves toward "ignition".

The effect on plasma size of the above variations of constraints is shown in Figure 11 for park hybrids.

Results using the standard blanket and the super blanket can be compared in Figures 12 and 13. From Figure 12 the relatively small impact on the park value of e is evident even though there are large differences in e for high values of the fissile fuel price.

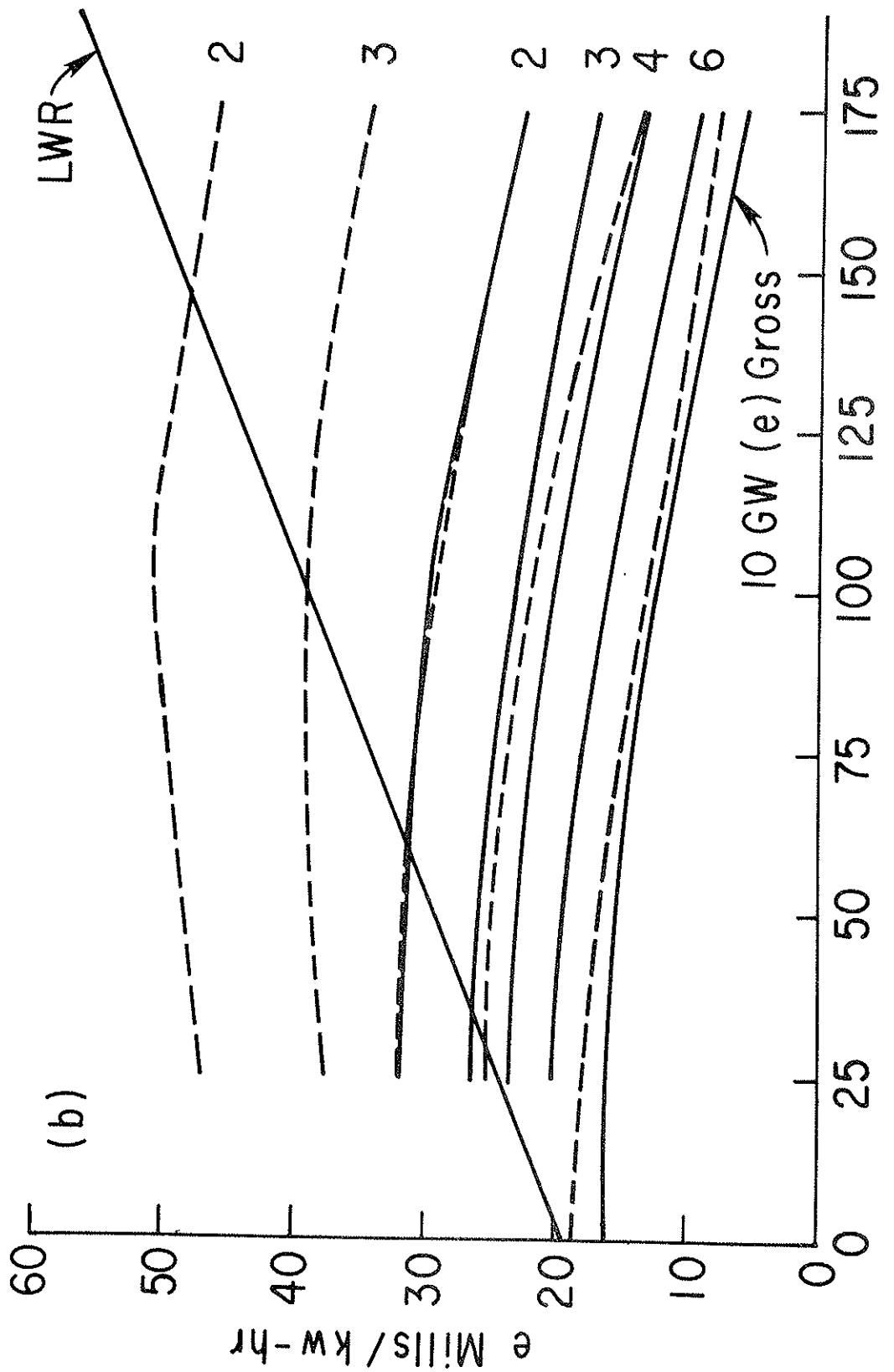

Fig. 10. Effect of varying nτ criterion.
----- nτ → 1 × T.E. Scaling.
——— nτ → Alcator Scaling.

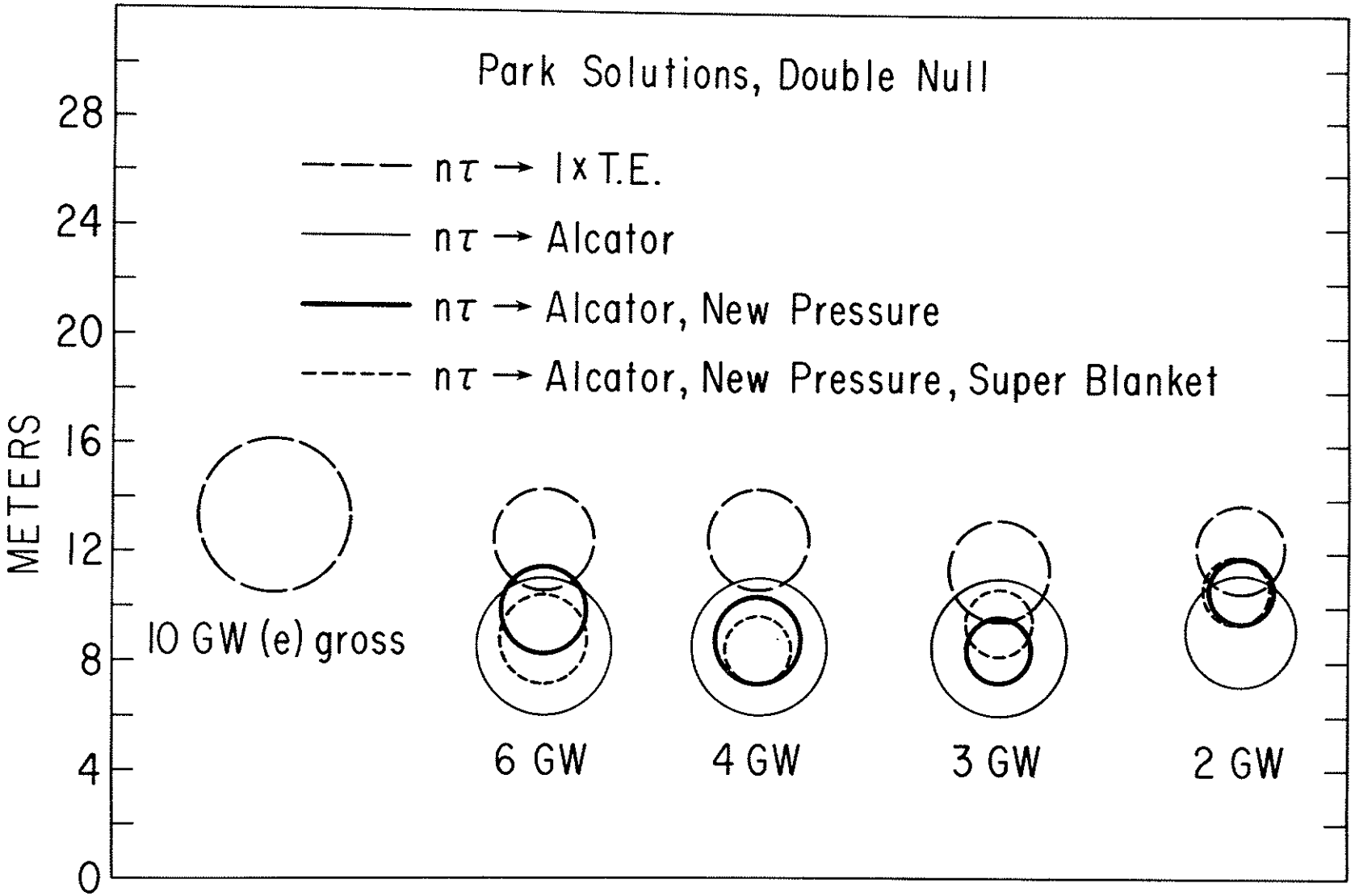

Fig. 11. Circularized Plasma Size for Double Wall "Park Hybrids" under Different Assumptions for Various Criteria.

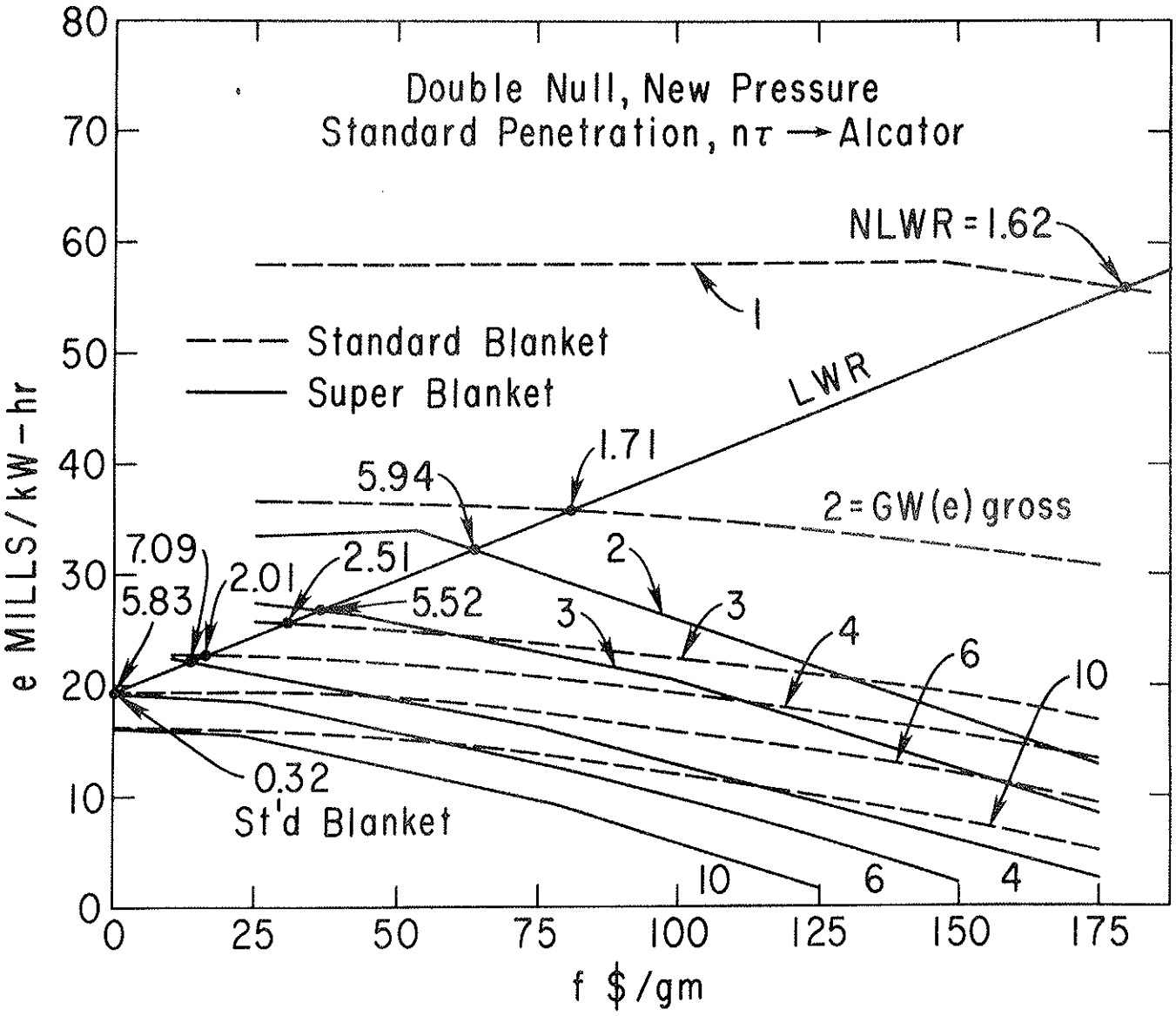

Fig. 12. The effect of two different blanket designs on the cost of electricity. NLWR is the number of light water reactors supported by the "park hybrids".

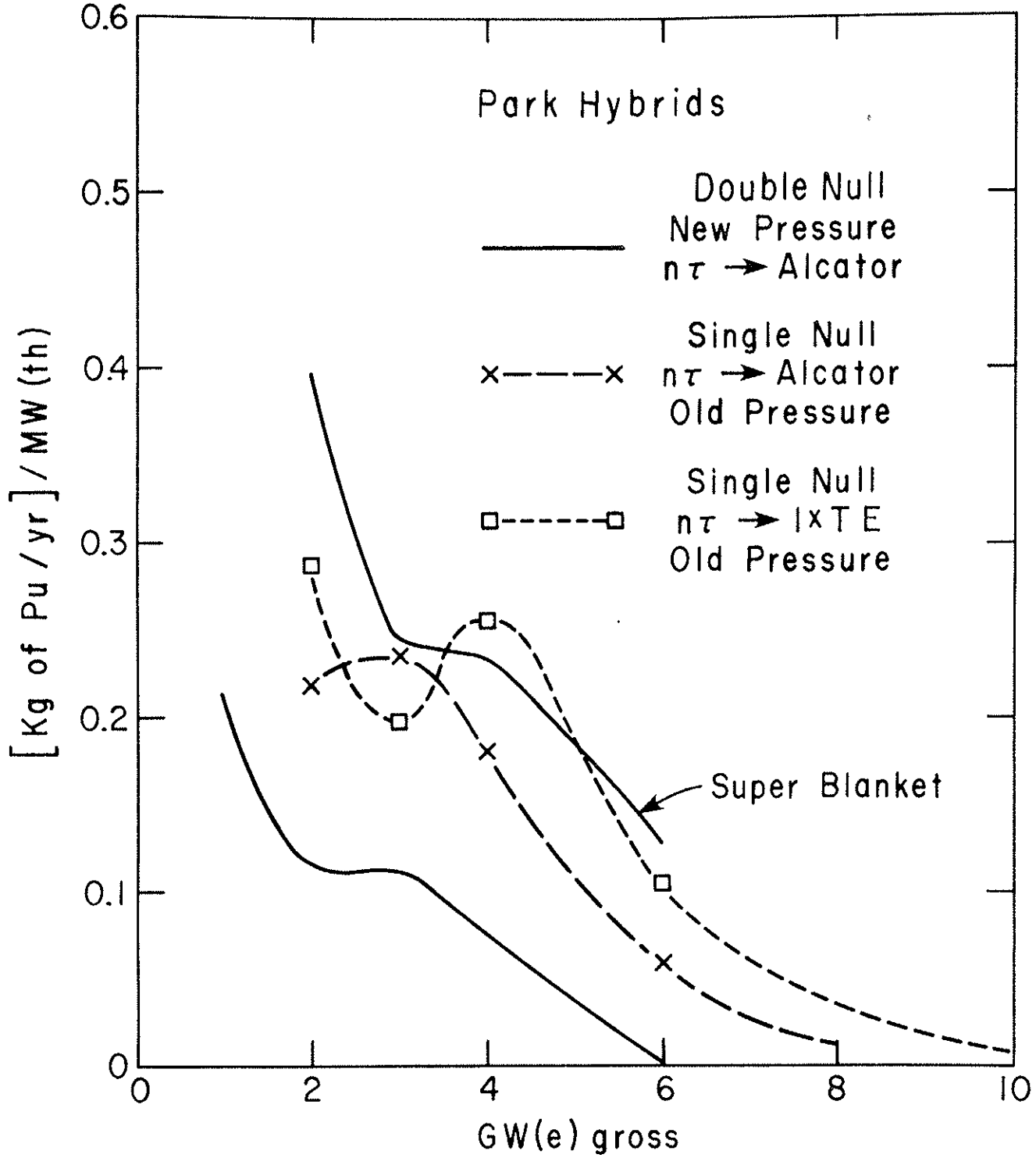

Fig. 13. Correlation Between Net Production of Fissile Fuel and Gross Electric Power Level for Various "Park Hybrids".

In Figure 13 the difference in Pu production for park hybrids is evident. Also evident, however, is that the two single null cases shown, using the standard blanket, do about as well as the double null hybrids with super blankets. There are several differences in these hybrid designs, of course. For instance, at the 3 GW(e) gross level, and comparing the two double null cases, the super blanket hybrid is a bit larger, is not ignited but driven with 199 MW of beams, has an M equal to 16.4 instead of 12.5, a lower plasma density, a higher temperature, and, in spite of its larger Pu production, produces electric power at very nearly the same bus bar cost as does the standard blanket case (see Figure 14). To rationalize this circumstance one must look at some of the economic details. The super blanket case has cheaper magnets and operating expenses, but more costly structural and beam injector costs. On balance the super blanket hybrid costs more to build and operate than the standard blanket case and produces less electric power for sale. However, its revenue from the sale of Pu essentially compensates for its higher costs. Hence the near equality in e for these two cases.

In Figure 14 we show the effect on e of the variations in pressure and the blanket performance. These variations do not produce appreciable change in e. The higher β (higher pressure) machines are physically smaller, but their allowed $n\tau$'s are also smaller and hence more beam power is required to drive them. The loss in net electric power for sale more or less offsets the reduction in capital costs for the smaller physical size.

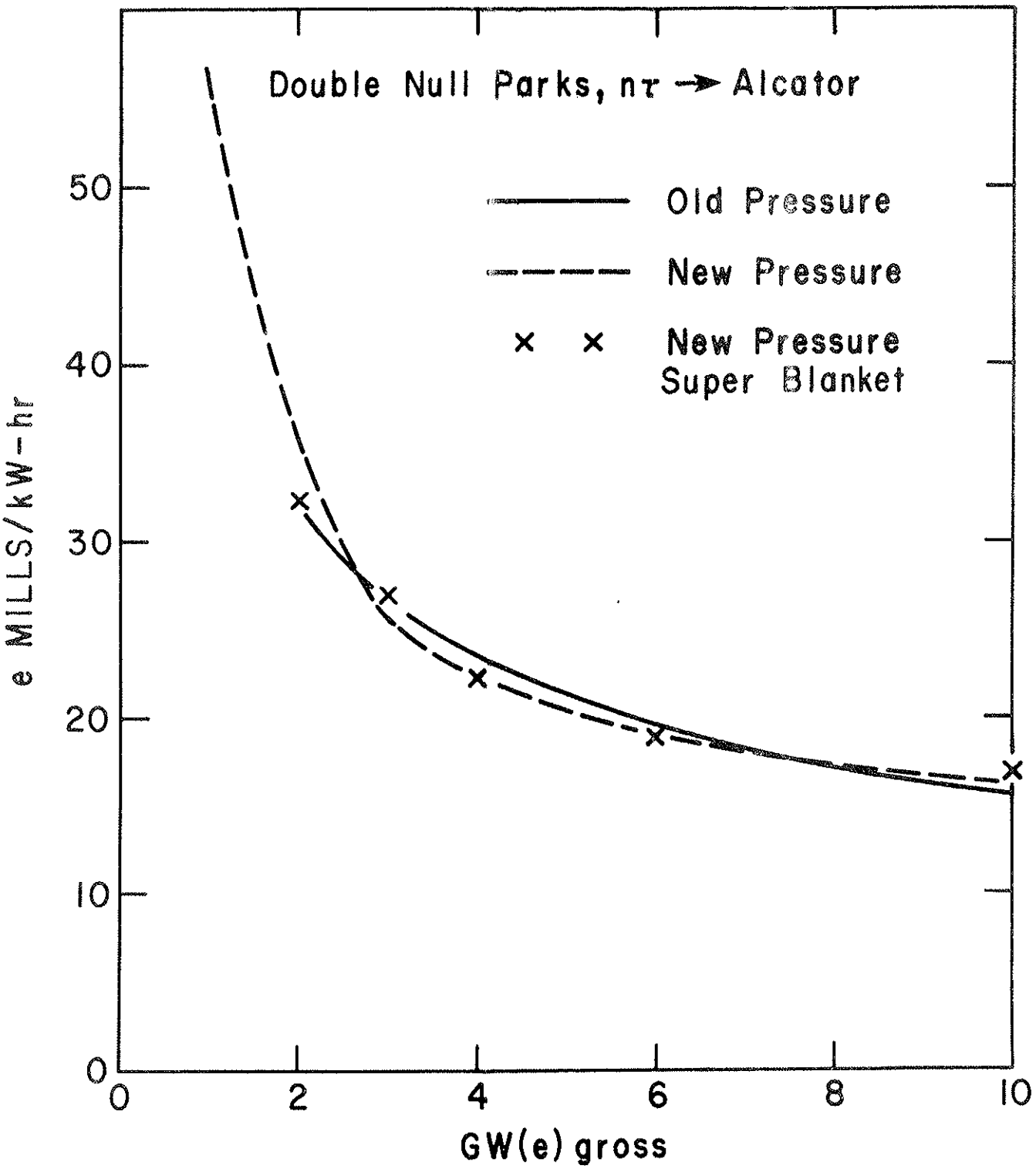

Fig. 14. The Cost of Electricity for Various "Park Hybrid" Reactors.

The effect of different plasma profiles on the bus bar cost of electricity, e, is shown in Figures 15 and 16. The magnitude of the effect when the trapped electron mode scaling is used for $n\tau$ is large and surprisingly small when the Alcator scaling is used. For the hybrids in Figure 15 an increase in plasma reactivity produces cheaper electricity primarily because the beam power is reduced and hence the net electric power is increased. In comparison, nearly all the hybrids of Figure 16 (Alcator scaling of $n\tau$) are ignited. Changes in reactivity produce a variety of small changes in reactor size, plasma density, wall load, blanket energy multiplication, etc., but the net economic effect is small.

Comparison of the data in Figures 15 and 16 shows the sensitivity of the effect of plasma profiles to the assumptions of the $n\tau$ criteria for plasma confinement.

A comparison of the effect of different $n\tau$ criteria on the cost of electricity for the park solutions of both single and double null configurations is shown in Figure 17. It is apparent that the confinement property of the plasma is one of the most influential factors in determining the cost of electricity for a hybrid plant. Note the near factor of three reduction in the cost of electricity for 3 GW(e) gross park hybrid reactors in going from a single null configuration with 1/10 × T.E. scaling for confinement to a double null configuration with Alcator scaling.

The above comparisons serve to underline the conclusion that to properly evaluate different hybrid designs and performances requires the simultaneous analysis of many factors.

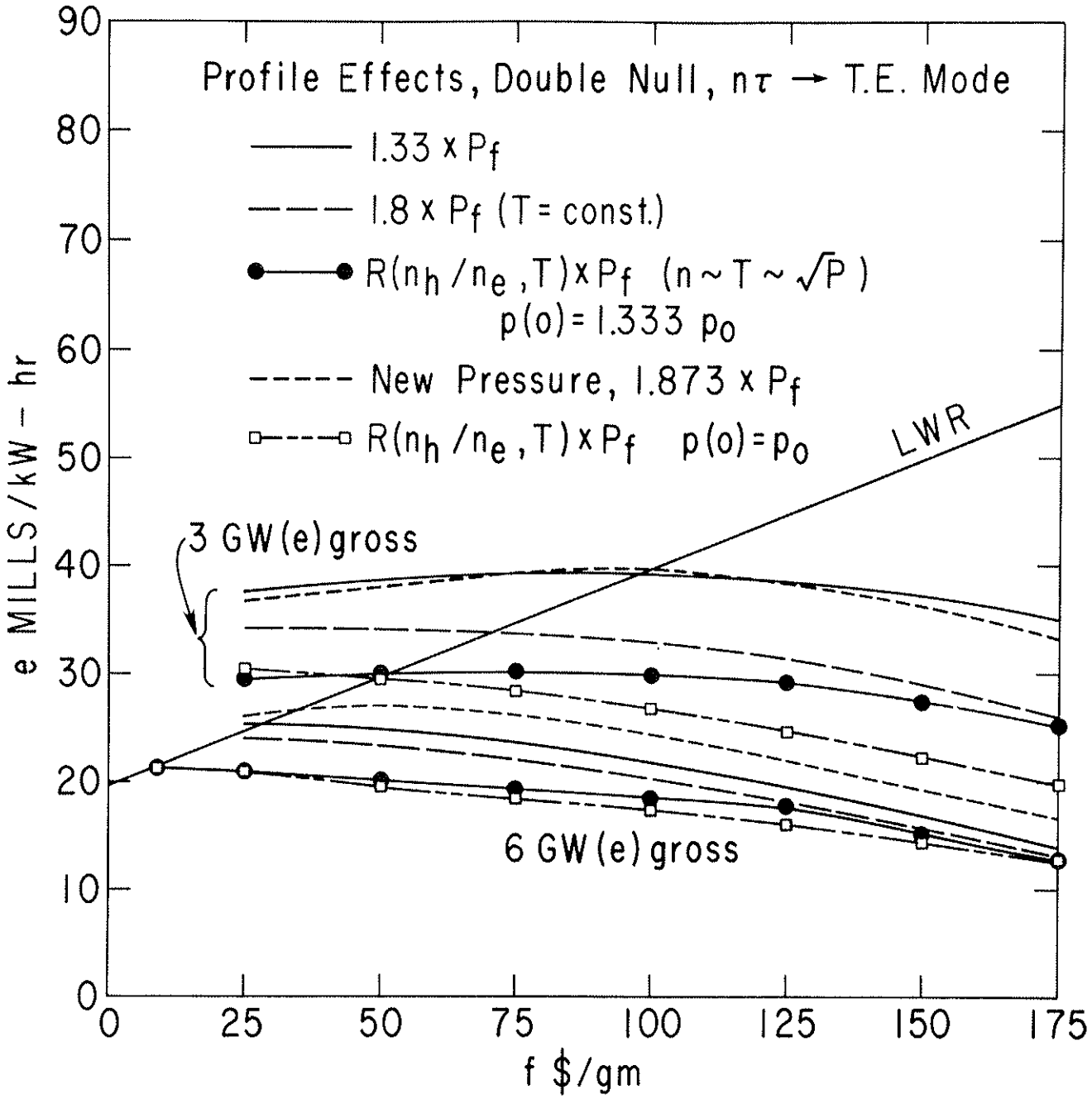

Fig. 15. The cost of electricity under various assumptions about the plasma profile (see Appendix II). The plasma confinement is assumed to scale according to the "trapped electron mode" of particle diffusion.

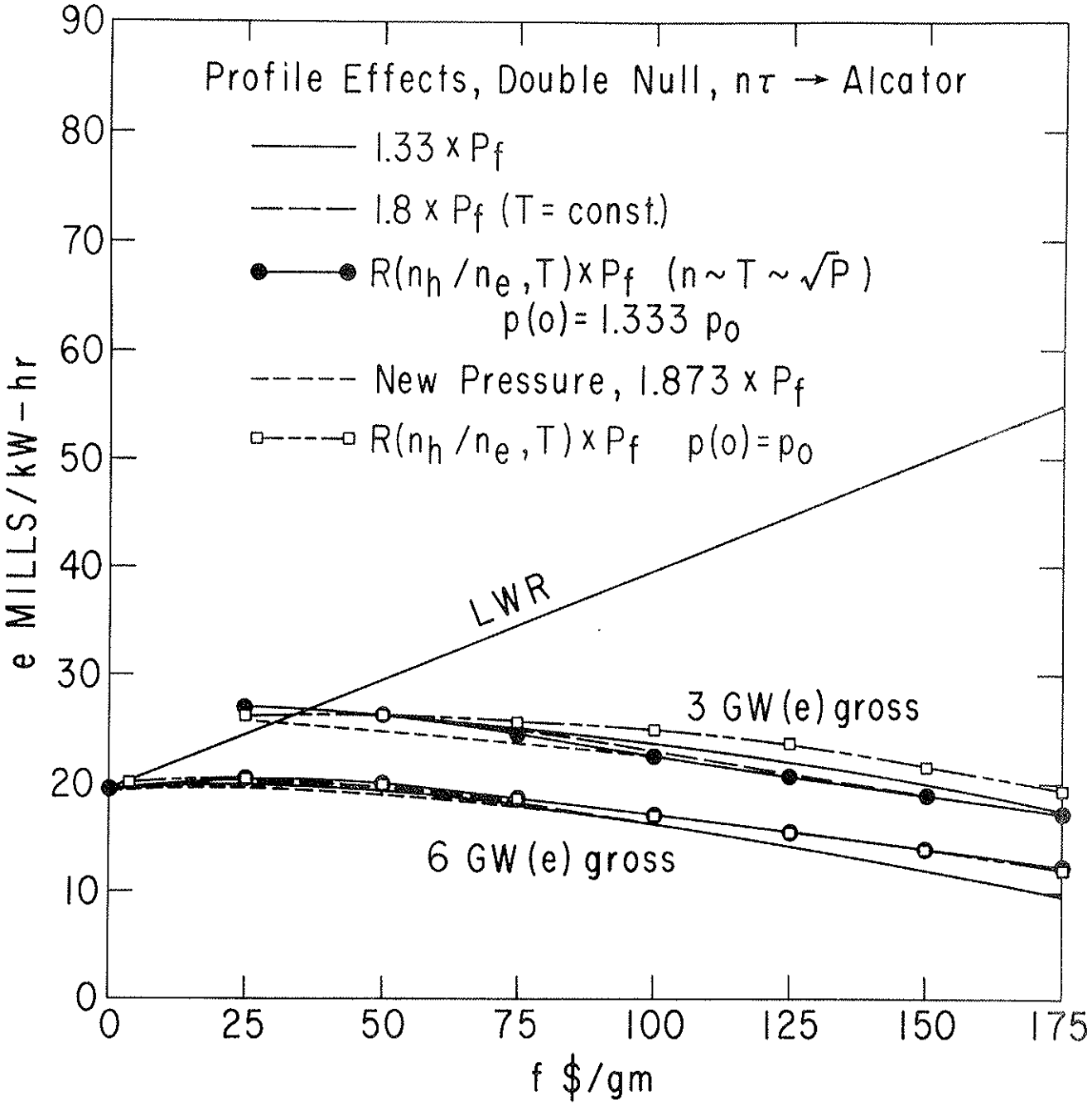

Fig. 16. The cost of electricity under various assumptions about the plasma profile (See Appendix II). The plasma confinement is assumed to scale according to the "Alcator scaling".

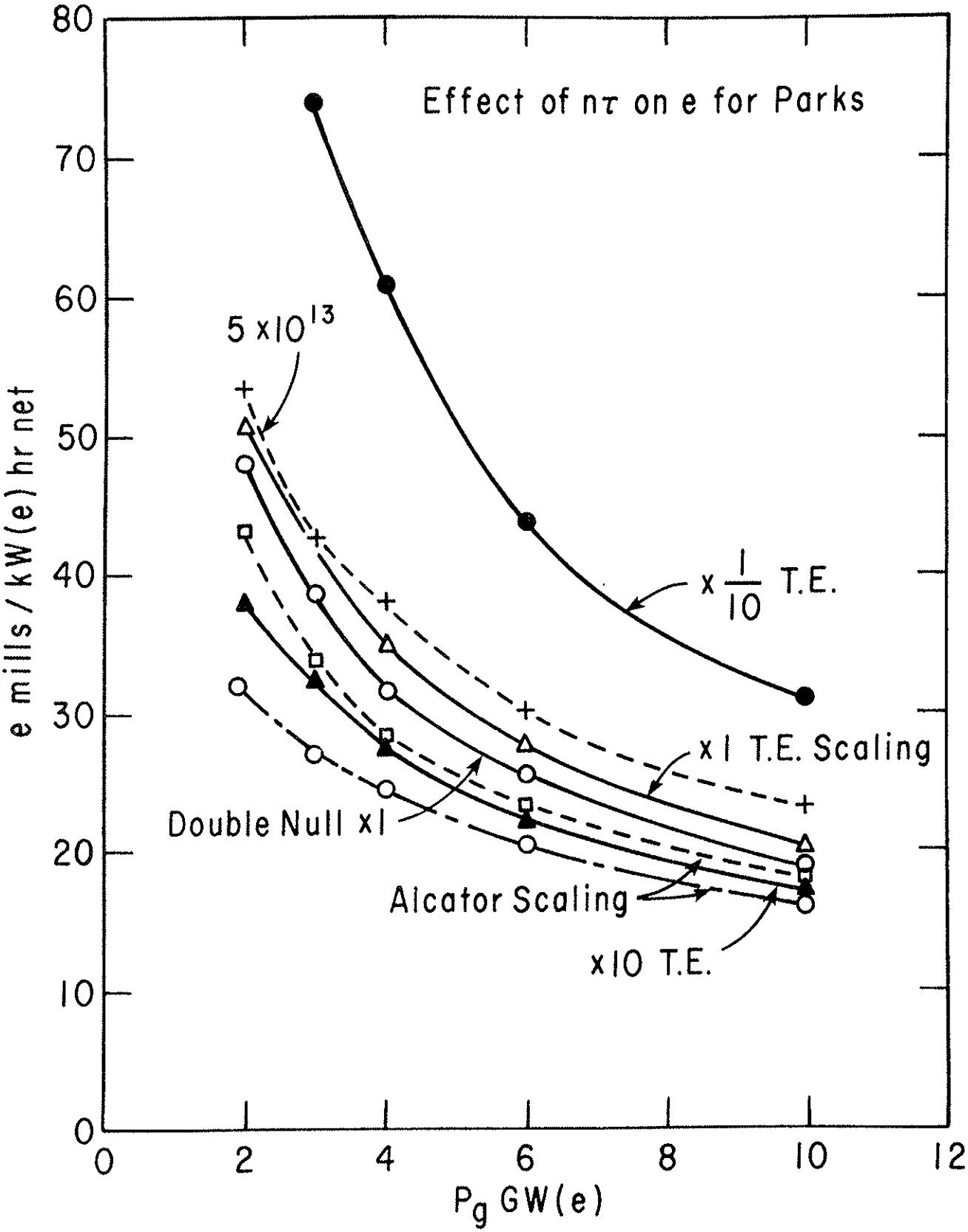

Fig. 17. The bus bar cost of electricity, e, versus the gross electric power, P_g, of the "park hybrid" reactor for different scaling laws for the plasma confinement parameter $n\tau$. The (o - . - o) data is for a double null configuration.

4. Capital Costs and Cost of Electricity

The correlation between capital costs and the gross electric power of various best hybrid designs is shown in Figure 18. The sensitivity of the capital costs to the price of fissile fuel is reflected in the separation of the 175 \$/gm and the 25 \$/gm lines. Except for the data relating to the $1/\sqrt{10}$ pressure scaling, this sensitivity is rather modest. The relatively lower values of capital cost for the double null design is apparent.

The correlation between the capital costs and the cost of electricity for the park hybrids under various constraints is shown in Figure 19. This figure is the investor's "bottom line". Apparently one can get cheaper electricity at the price of larger capital costs for the larger gross power level hybrids required. The profound effect of the assumed confinement constraint is also apparent. It is interesting to note the near identical results for the standard double null hybrid and the single null configuration when the later is using either the X 10 scaling of the standard $n_e \tau_{PHY}$ or the Alcator scaling for $n_e \tau_E$. Note the wide range of capital costs under various constraints.

The correlation between capital cost per net electric output and the cost of electricity is shown in Figure 20 for several hybrid designs. The straight line represents Eq. (1) of Section IV.G.1 but with the annual operating and maintenance costs and the fuel cycle costs neglected. The proximity of the plotted data to this straight line substantiates the claim, made above, that the cost of electricity, e, for the hybrid is strongly correlated with the net electric power produced, P_{net}. This substantiation is valid only to the extent that the capital cost, C,

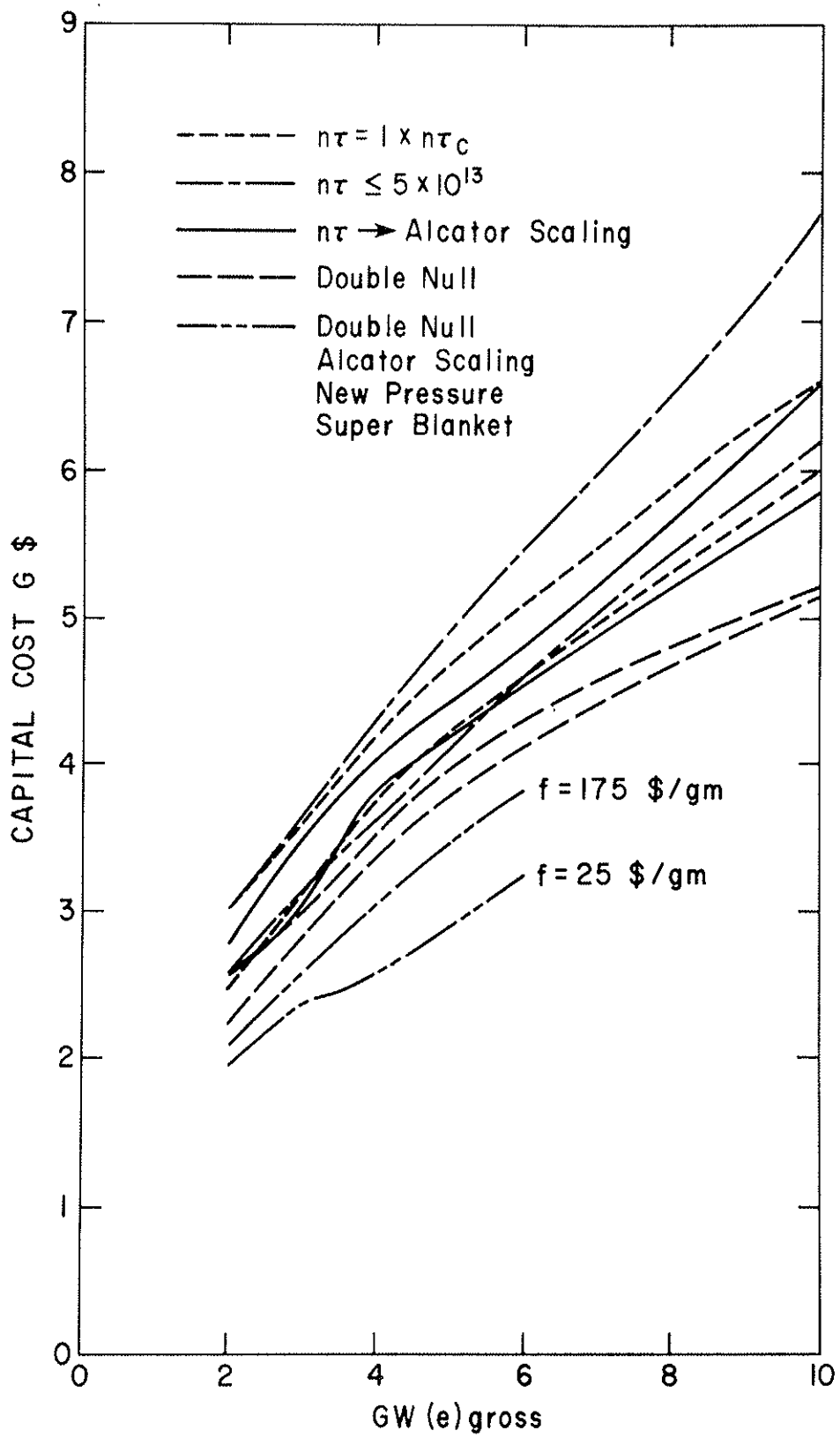

Fig. 18. Capital cost versus gross electric power for various hybrids. For a given gross electric power level the capital cost is given for two values of fissile fuel price.

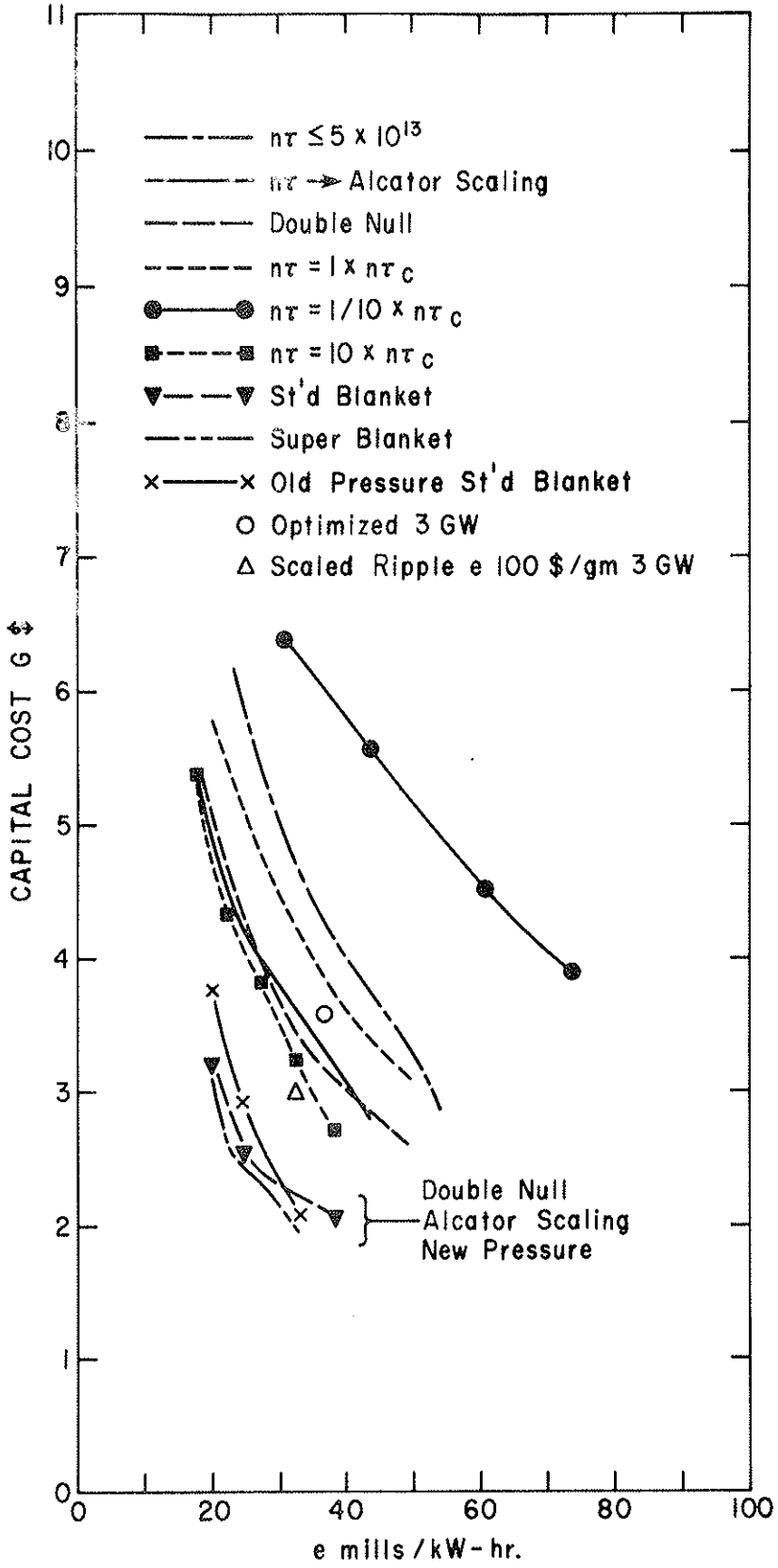

Fig. 19. Correlation of capital cost and cost of electricity for various "park hybrids". The gross electric power varies along each curve from 2 GW(e) at the lower end to 6 or 10 GW(e) at the upper end.

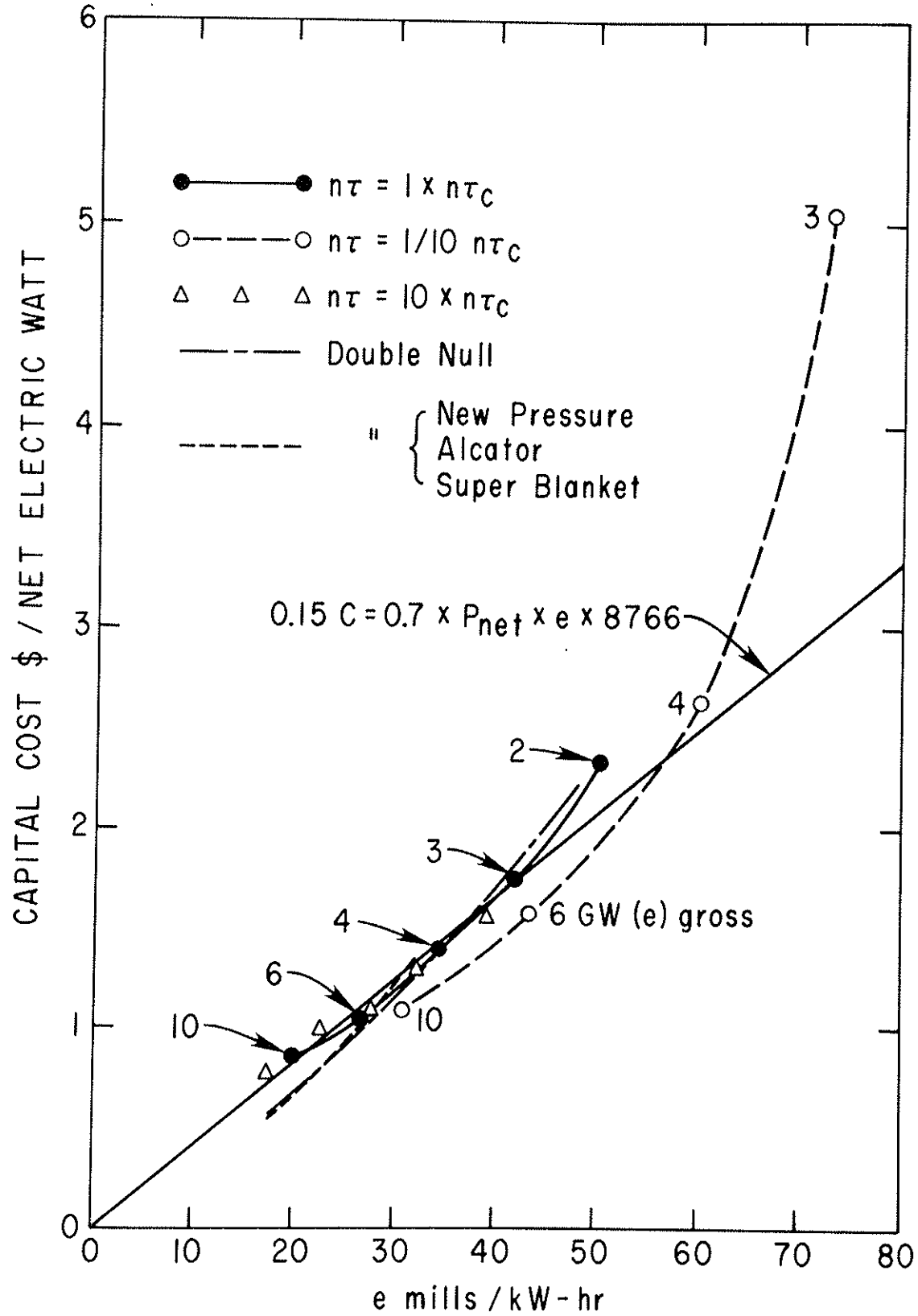

Fig. 20. Correlation between capital cost per net power output and the cost of electricity for various hybrids. The gross electric power varies along each curve.

at a given level of gross electric power output is independent of the price of fissile fuel, and this relation is shown in Figure 18. For the standard hybrids of P_g > 2 GW(e) the correlation between e and P_{net} is "strong".

In Figure 20 the displacement of a data point from the straight line measures the imbalance between the costs of operation, maintenance and fuel cycle charges and the revenue derived from the sale of fissile fuel. Points lying to the left of the line reflect designs where the fissile fuel revenue more than offsets the operation, maintenance and fuel cycle charges and therefore contributes to the defrayal of the capital cost charges.

b. Economic Penetration

A considerable analysis of the economic requirements for fission-fusion hybrids to penetrate the national market has been done by Deonigi, Engle and others at the Battelle Northwest Laboratory.[1] In another economic study, similar to the above study, Deonigi and Engel[2] consider a national energy system into which pure fusion reactors are chosen to enter in the year 2010 and to eventually dominate the electric power generation by the year 2040. The mix of power sources at any time is determined by the continuous minimization of the cost of the national electric power demand. Hybrids are introduced into this system about the year 2000 with different capital costs and different physical characteristics and produce different savings or benefits to the system. Hybrids are physically distinguished one from another through two characteristics: The annual yield of plutonium for sale per unit of thermal power generated and

the plant efficiency, here defined as the ratio of electric power for sale to the total thermal power generated.

To make a connection with this body of work we took the annual cost for selected hybrids and "capitalized" them over a 30-year plant life at 8.8% au Deonigi. The results are shown in Figure 21. Two curves from Ref. 2 are shown for a zero benefit scenario that has the hybrid entering the market in the year 2000, the LMFBR entering in 1992, and CTR in 2010. It appears that the tokamak hybrids of this study can become economically attractive if we choose double null geometry, assume Alcator scaling for the plasma confinement and produce at least 3 GW(e) gross.

C. Optimization Results

The optimization calculations are used in three ways: first, to find with the greatest precision the optimal behavior of the physical-economic model of the hybrid reactor; second, to evaluate the accuracy of the survey calculations; third, to investigate the effects of varying different constraints. Only single null designs were subject to the optimization style of calculations.

The use of optimization calculations was limited by available computer time. To determine one optimized hybrid design takes about 3 minutes on the central processing unit of a CDC 7600 computer and to generate one curve of optimized best hybrids takes about 21 minutes. By comparison an entire survey calculation could be done in about 14 minutes.

1. Best Hybrid Curves

Optimized best standard hybrid curves were generated for P_g equal to 3 GW(e) and 6 GW(e). These results are shown in Figure 22 where the corresponding best standard hybrid curves from the

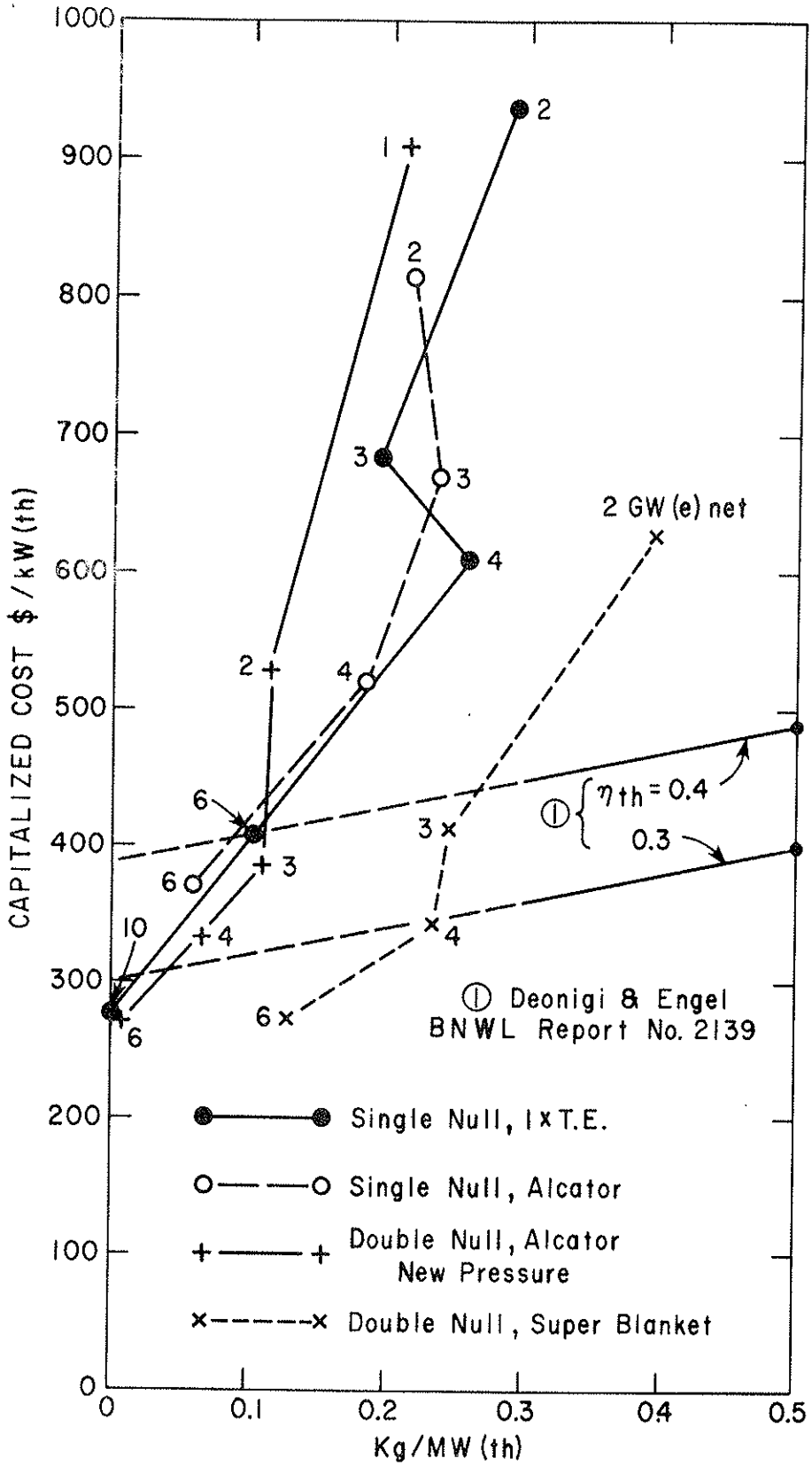

Fig. 21. Correlation between Normalized "Capitalized" Costs and Fissile Fuel Production for Various Hybrid Reactors.

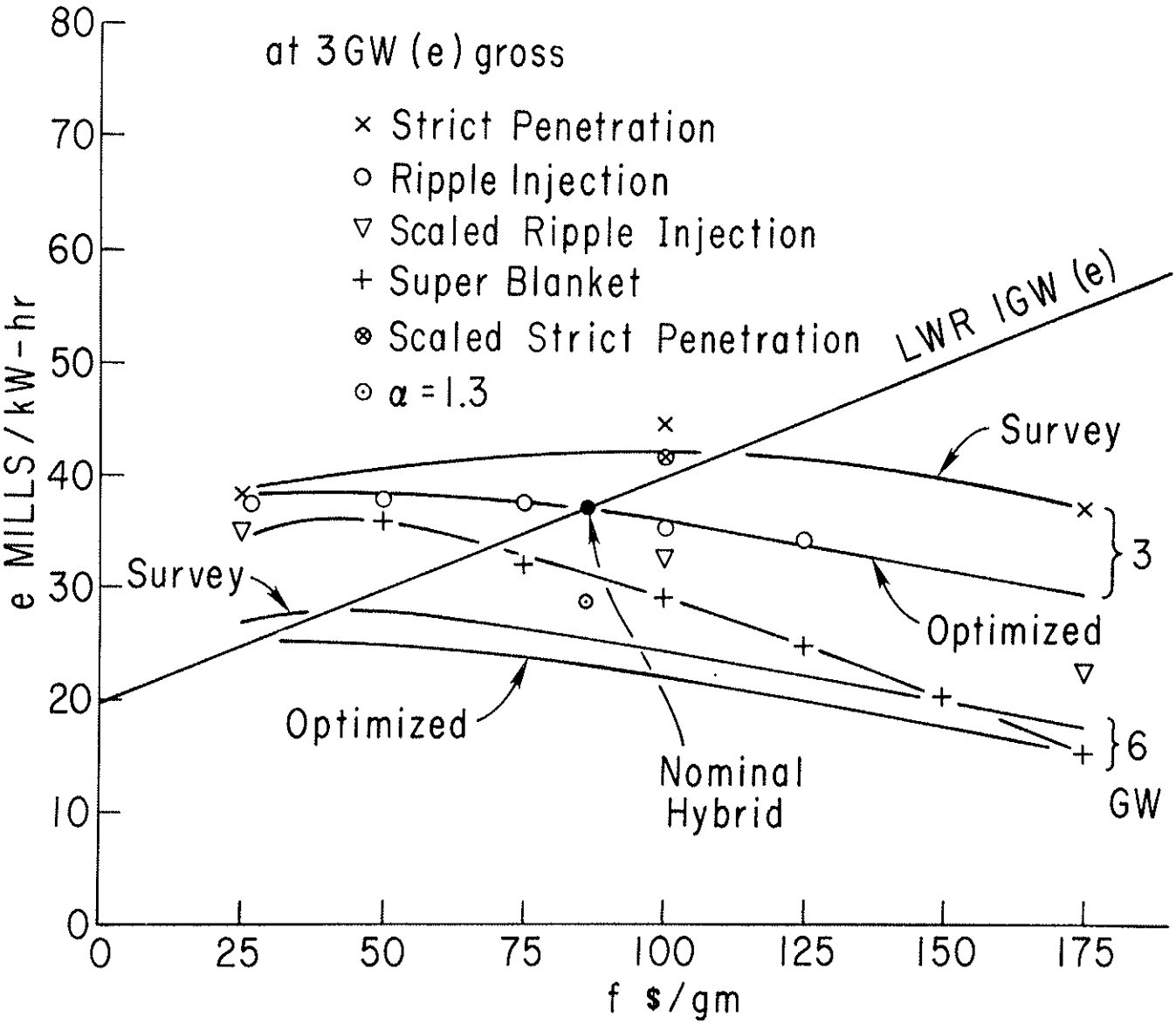

Fig. 22. Cost of electricity for various "best hybrids" using optimization style calculations. Two curves from Figure 1 are shown for comparison.

survey calculations are also shown for comparison. The physical sizes of these optimized hybrids are shown in Figure 23. The correlation between capital costs per watt and the cost of electricity is shown in Figure 24.

The optimized curves (in Figure 22) lie below the survey curves as expected. Their relative displacement measures the accuracy attributable to the survey results.

Some features of the optimized best hybrids of 3 GW(e) gross are displayed in Table XIII for comparison with the corresponding survey data in Table II. The optimized hybrids operate closer to ignition, as evidenced by higher values of Q, and with lower fusion power densities than do the survey hybrids. They are also somewhat larger, but otherwise there is little difference.

We conclude the survey calculations are close enough to the optimization results to provide a useful estimate of the properties of optimal hybrids.

A "nominal hybrid" has been chosen to be the optimized park hybrid operating at 3 GW(e) gross. The physical, operational and economic properties of the nominal hybrid are discussed in some detail in Section E below.

2. Variation of Criteria

The optimization style of calculation has been used to evaluate the effects of changing the magnitude of the pressure scaling, the shape of the pressure distribution, the penetration criteria, and the neutronic performance of the blanket.

a. The "Superblanket"

To see the effect of an enhanced blanket performance on the parameters of the best hybrids, the standard blanket

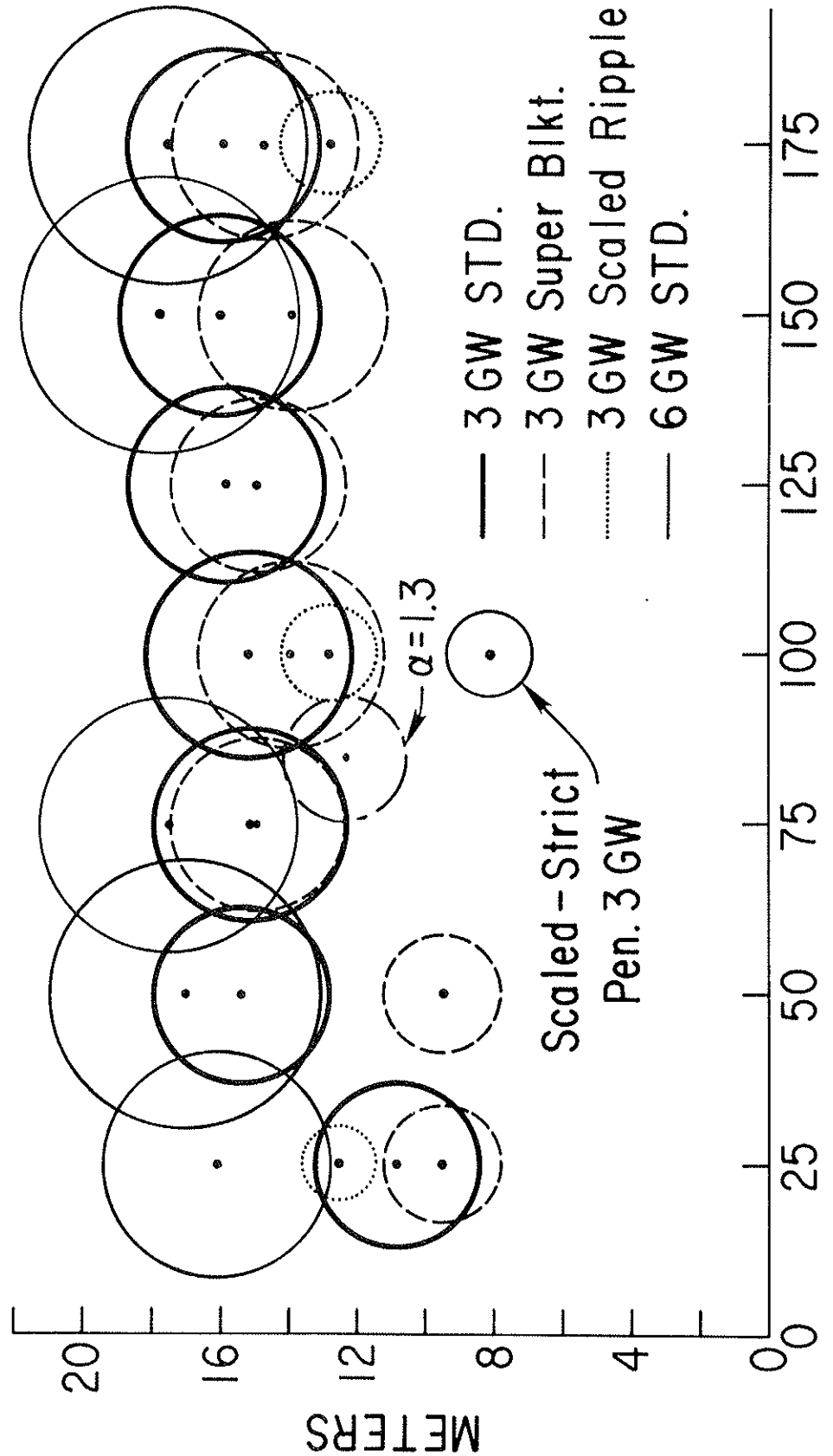

Fig. 23. Plasma Size for Various Hybrid Reactors. (Optimization Style Calculation.)

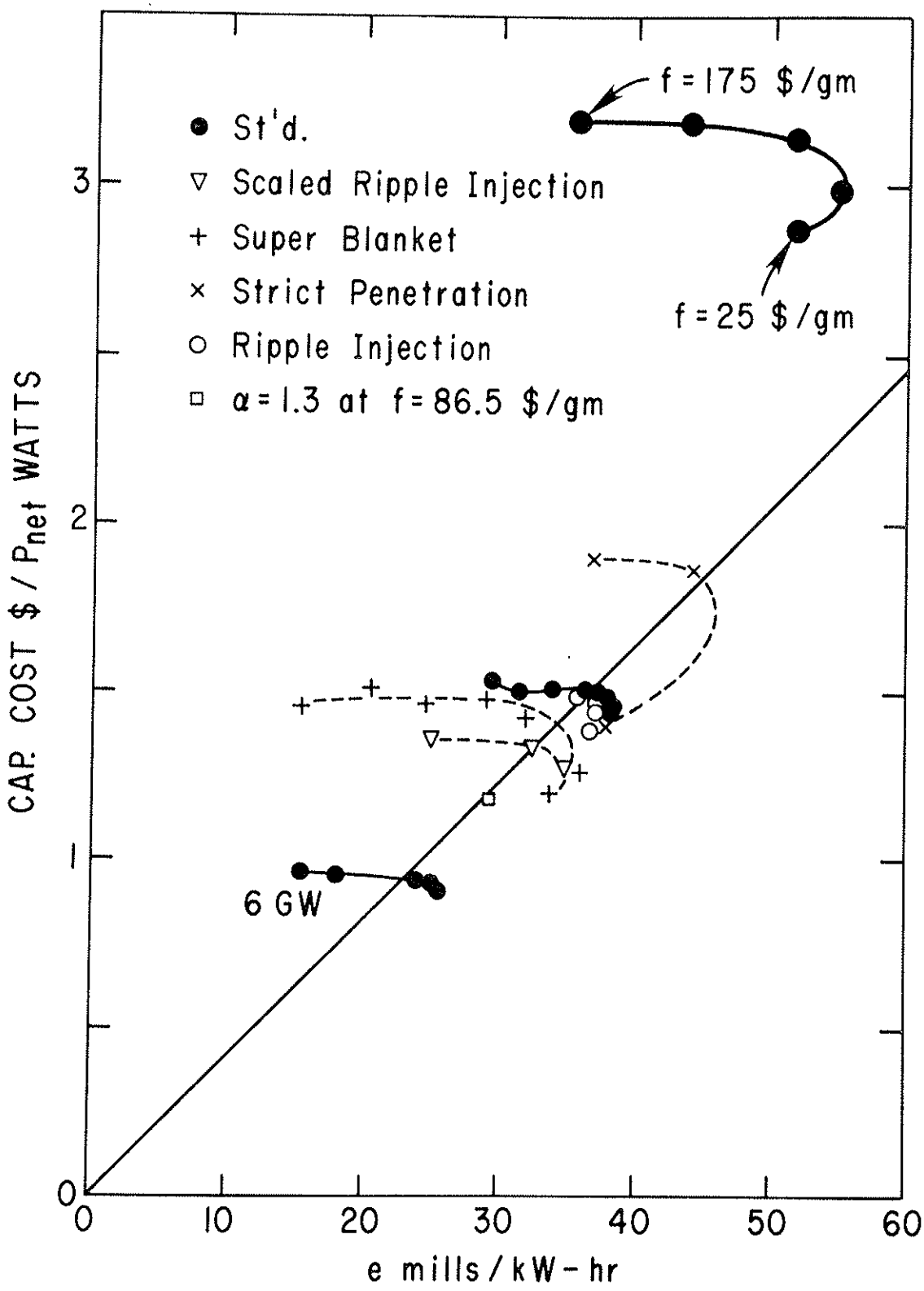

Fig. 24. Correlation between capital cost per net electric watt and the cost of electricity for the "optimized hybrids" shown in Figure 22. The price of fissile fuel, f, varies along each curve as indicated in the legend.

Table XIII. Some Characteristics of 3 GW(e) gross Optimized Best Standard Hybrids

f	M	T_e	W_o	H/T	a	R	I	n_e	B_c	Q	p_f	W_L	NLWR	P_{net}	A_T
\$/g		keV	kV		m	m	MA	$10^{14}cm^{-3}$	T		W/cm^3	MW/m^2		GW	
25	23.6	7	150	0.04	2.43	10.9	4.0	0.51	5.2	1.15	0.310	0.29	0.0	2.14	1.00
50	12.7	6	175	0.002	2.63	15.0	4.8	1.08	7.8	4.02	0.362	0.37	3.4	2.38	0.99
75	10.3	6	174	0.002	2.90	15.1	5.5	1.07	7.4	4.72	0.361	0.41	5.2	2.36	1.00
100	10.0	6	176	0.002	2.98	15.2	5.8	1.08	7.2	4.91	0.352	0.41	5.5	2.37	0.99
125	9.5	6	163	0.001	2.94	15.9	5.6	1.14	7.7	6.19	0.364	0.42	6.1	2.43	1.00
150	9.1	6	162	0.001	3.00	16.1	5.8	1.16	7.7	6.99	0.360	0.43	6.5	2.45	1.00
175	8.9	6	157	0.002	2.91	16.0	5.5	1.08	7.8	5.92	0.392	0.45	6.7	2.41	0.99

performance was changed by numerically increasing by a factor of 1.5 the number of fissions produced by the fusion neutrons in the converter region (See Section IV.D.3.). Optimization calculations were done only for P_g = 3 GW(e). The results are shown in Figures 22 and 23 and Table XIV.

The effect of the superblanket is to increase the maximum values for both the blanket energy multiplication, M, and the net fissile fuel atoms bred, F, as indicated in Figure IV.D.3. The larger values of M relative to the standard blanket make available smaller size machines at lower capital cost and for a given value of M, the larger value of F results in a larger revenue from fissile fuel. These effects result in the best superblanket hybrids producing cheaper electricity than the best standard hybrids. The correlation between capital cost per unit and e is shown in Figure 24.

b. Penetration Criteria

The plasma model in this study uses neutral beams as a means of injecting energy into the plasma and enhancing the fusion reactivity. The penetration criteria chosen require the beams to deposit their energy throughout the plasma according to a certain scheme. (See Section IV.F.7.a.) Future experience with neutral beams may lead to different penetration criteria. It is possible that RF heating may eventually be preferred over heating by neutral beams and require still different penetration criteria. We have therefore looked at two extreme limits: the strict penetration requirement given by setting N = 2 in Eq. (29) of Section IV.F.7.a and the removal of all penetration limitations. This latter situation, that we will call "ripple injection",

Table XIV. Some Characteristics of 3 GW(e) Gross Optimized Best Hybrid with Super Blanket

f	M	T_e	W_o	H/T	a	R	I	n_e	B_c	Q	p_f	W_L	NLWR	P_{net}	A_T
$/g		keV	kV		m	m	MA	$10^{14}cm^{-3}$	T		W/cm^3	MW/m^2		GW	
25	46.9	6	150	0.071	1.64	9.48	2.4	0.49	6.3	0.87	0.403	0.24	0.0	2.33	1.00
50	46.4	6	150	0.129	1.67	9.47	2.5	0.36	6.2	0.91	0.394	0.24	0.05	2.34	1.00
75	13.5	6	175	0.003	2.56	15.0	4.6	1.00	8.0	3.76	0.361	0.36	8.74	2.30	1.00
100	13.0	6	195	0.004	2.79	14.0	5.2	0.99	6.9	3.14	0.336	0.37	9.53	2.27	1.00
125	12.5	6	173	0.003	2.60	14.97	4.7	1.03	7.9	3.69	0.377	0.38	10.1	2.35	1.00
150	12.3	6	191	0.005	2.81	13.96	5.3	0.93	6.8	3.02	0.349	0.38	10.3	2.24	1.00
175	11.9	6	180	0.002	2.77	14.89	5.2	1.08	7.4	3.99	0.351	0.38	10.8	2.36	1.00

simulates the "ripple-trapping injection" of neutral beams as suggested by Jassby.[3]

Calculations have been done only for P_g = 3 GW(e). Best hybrids were calculated at five values of f for the case of "ripple injection" and at only three values of f under the strict penetration requirement. Some results are shown in Figure 22 and in Table XV.

The results of ripple injection are very close to the results using the standard penetration criteria except that the penetration index A_T exceeds 1.0. The strict penetration results show an increase in the cost of electricity, a reduction in both density and discharge current, a small reduction in R and a, and an increase in beam power.

The ripple injection results are surprising. It was anticipated that by removing all limitations on beam penetration, the optimization calculation would explore higher pressures (hence higher β's) than permitted by the standard penetration criteria. It was argued that an increase in pressure, and hence density, would increase the thermal contribution to the plasma reactivity and allow a decrease in beam power without reducing the overall reaction rate. The reduction in beam power would result in a higher Q, an increase in net electric power and thus a decrease in the cost of electricity. In fact, this is just what did happen, but to a lesser degree than anticipated.

Compare the "ripple" and "standard" cases in Table XVa. The change in parameters from the "standard" case to the "ripple" case entails a small increase in R and hardly any change in a. This particular change in R and a is rationalized in the following

Table XV. Some Results for Different Penetration Criteria at f = \$100/g; P_g = 3 GW(e)

Standard Pressure. (a)

Penetration Criteria	M	T_e	W_o	H/T	a	b	R	n_e	I	B_c	P_i	Q	ß	p_f	V	P_{net}	nτ	A_T	CapC	e
		keV	kV		m	m	m	$10^{14}cm^{-3}$	MA	T	MW			W/cm^3	10^3c^3	GW	$10^{14}\frac{sec}{cm^{-3}}$		G\$	mill/kWh
Ripple	9.7	6.21	150	0.0021	2.97	7.14	15.4	1.10	5.7	7.3	183	5.29	1.04	0.36	2.68	2.37	6.72	1.16	3.56	35.7
Strict	9.90	7.89	253	0.0123	2.69	6.93	14.5	0.76	5.0	7.4	332	2.80	0.97	0.44	2.08	1.93	2.02	1.00	3.59	44.4
Standard	10.0	6.21	176	0.0024	2.98	6.89	15.2	1.08	5.8	7.2	191	4.91	1.06	0.35	2.66	2.39	6.81	0.99	3.56	36.3
Scaled Pressure, $p \rightarrow \sqrt{10}\ p$. (b)																				
Ripple	10.2	6.29	150	0.0040	1.41	7.56	12.82	2.31	3.0	9.4	288	3.15	1.37	1.80	0.503	2.24	4.19	2.76	3.00	32.4
Strict	22.4	8.0	150	0.299	1.19	3.25	8.08	0.54	2.6	6.4	431	0.95	2.20	1.82	0.225	2.00	0.10	1.00	2.88	41.5
Standard	10.6	6.01	223	0.0027	1.43	7.70	12.99	2.46	3.1	9.4	233	3.78	1.38	1.68	0.524	2.22	5.63	0.99	3.03	33.1

CapC = capital costs in G\$

way. The standard case lies at point N on the "carpet" of pressure shown in Figure 25. This point is near the maximum pressure along an h = constant curve of the carpet.

Consider a decrease in "a", but an increase in h (and hence R) such that the pressure increases. A large enough decrease in "a" can lead to a decrease in the allowed $n\tau_p$. In this case the beam power must be increased in order to reduce the required $n\tau_p$ sufficiently to keep the required $n\tau_p$ less than the allowed $n\tau_p$. The effect of these changes on the cost of electricity depends in large part on the net balance between the reduction in cost due to the decrease in physical size of the reactor on the one hand and the increase in cost of injectors and the loss of net electric power, by virtue of the increase in beam power, on the other hand.

Alternatively, consider an increase in "a" alone. The volume of the machine and its cost will increase. The beam power would also increase unless the H/T is reduced and that, in turn, will require a larger value of $n\tau_p$. The increase in "a" may well provide a sufficient increase in the allowed $n\tau_p$ in order to keep the confinement constraint satisfied. However, the reduction in H/T must be sufficient to reduce the beam power in order to enhance the net electric power if the increase in cost due to the larger volume of machine is to be balanced and cheaper electricity produced.

The "ripple" results show that the optimization calculation actually found the cheapest electricity through an increase in h and a very small decrease in "a" (see point R in Figure 25). The result is higher density at only a small increase in

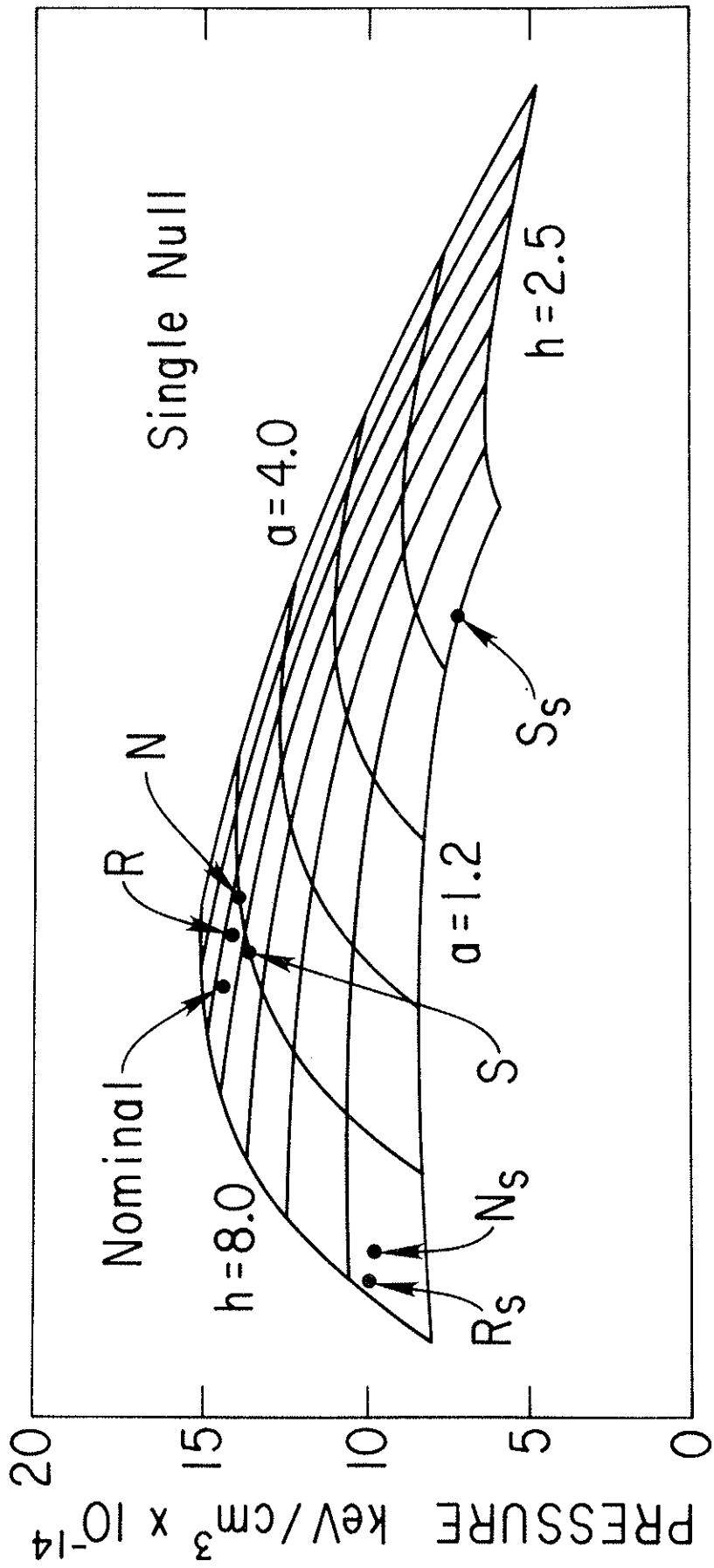

Fig. 25. Pressure Carpet.

volume keeping the cost of the physical machine nearly constant. The reduction in H/T was sufficient actually to decrease the beam power. The injection voltage was also decreased which results in a higher injector efficiency and hence a higher net electric power. The decrease in blanket energy multiplication, M, results in a decrease in the concentration of plutonium in the molten salt which would reduce blanket inventory costs if the increase in size is not too great. On balance the "ripple" case allowed e to drop from a value of 36.3 mills/kWh to 35.7 mills/kWh.

The strict penetration case shows a different response. We first note (see Table XVa) that for the standard case the Q of 4.91 indicates a somewhat relaxed penetration requirement. (See Eq. (29) in Section IV.F.7.a) Consequently imposing on the standard case the constraint of strict penetration requires a reduction in density that, in turn, produces a reduction in the value of the allowed $n\tau_p$. However, the required value of $n\tau_p$ is rather insensitive to the density (P_α and P_B, which dominate the denominator Eq. (IV.F-23) for the required τ_p, are proportional to n_e^2). Since the required and allowed values of $n\tau_p$ for the standard case are nearly identical, the confinement constraint can no longer be met when the density is reduced. Hence a new point in parameter space must be explored by the optimization calculation. The optimization calculation finally arrives at point S in Figure 25.

Some of these results of the optimization calculation can be rationalized in the following ways. In view of the argument for the advantage of increased density presented above for

the ripple case, we expect the optimization calculation to find the minimum required reduction in density to satisfy the penetration constraint. Therefore, since the application of the strict penetration criterion requires a reduction in the product $n_e a$, we expect a reduction in a and the production of cheaper electricity than for an increase in a. However, with the necessary reduction in $n_e a$ there is a reduction in the allowed $n_e \tau_p$. To reduce the required $n_e \tau_p$ to meet this lower value the beam power must be increased with the accompanying reduction in net electric power and consequent increase in cost of electricity. The increase in W_o (See Table XV.a) has the effect of allowing satisfaction of the strict penetration constraint at a higher value of $n_e a$ than otherwise, but at the price of a lower injector efficiency. The reduction in size of the physical machine produces a decrease in the cost of the reactor structure and magnets, but the increase in the cost of the neutral beam injectors results in the total capital cost actually increasing a small amount. Furthermore, the increase in beam power produces a reduction in net electric power. The overall result is that the cost of electricity for the strict penetration case is appreciably higher than for the standard case.

The above "explanation" of the results of changing the penetration criteria serves to show the interplay between the various factors that influence the exploration and final choice of the hybrid parameters.

c. Pressure Scaling

To explore the effects of a more optimistic pressure scaling than is taken for the standard hybrids, the plasma pressure

was increased in such a way as to preserve β_θ while allowing β to increase. This was accomplished by multiplying the discharge current, I, given by Eq. (IV.C.13) by a scale factor equal to $\sqrt[4]{10}$. This increase in I produces an increase in the average pressure by a factor of $\sqrt{10}$ according to Eq. (IV.C.15). No other changes are made in the model. In particular the geometry of the plasma cross section is not changed. Thus, for example, the effect on the beam penetration criterion of the shift in the spatial profile of the plasma expected by increasing β is not considered. Also ignored is the effect on q or the plasma profile of increasing I. The pressure scaling simply allows those quantities dependent on the density, such as the beam power density and the fusion reaction rate per unit volume, to be increased without changing the other parameters defining a hybrid design.

Calculations using the scaled up pressure were made using both the standard penetration criteria and the two variations of the penetration criteria discussed in the previous section, namely, the strict penetration and the "ripple injection" criteria. The case of ripple injection was calculated at three values of f. The results appear in Figures 22 and 23. The cases of standard and strict penetration criteria were calculated only for f = 100 \$/g. The results are shown in Table XVb, together with some features of the best hybrids for all three cases.

The results of the increased pressure scaling show a small decrease in the cost of electricity for each style of penetration criterion relative to the results using the standard pressure scaling. This relative decrease in e is at variance with the survey results shown in Figure 6 where a small increase

in e is recorded. We make three comments. First, the results presented so far suggest that the cost of electricity passes through a minimum as a function of the pressure scaling. The existence of such a minimum for fixed values of a and h is demonstrated and discussed below in Section 2.e. Second, the large "step size" in W_o, H/T and T_e of the survey calculation produces larger values of e than does the optimization calculation. Hence the small decrease in e produced by the optimization style calculation can be masked by the survey style calculation. Third, although gross trends are judged to be well displayed by the survey style calculations, a detailed study of the hybrid properties requires the optimization style calculation.

Examination of Table XV shows that the increase in pressure scaling produces an increase in β, but not by a factor of $\sqrt{10}$. For the standard penetration and ripple cases, the density increases, but for the case of strict penetration there is a decrease in density.

The increase in pressure scaling produces a large increase in fusion power density that allows, in accordance with Eq.(3), changes in a and R that reduce the plasma volume by about a factor of five. In Figure 25 the points labelled N_s, R_s and S_s locate on the pressure "carpet" the cases for standard, ripple and strict penetration, respectively. The pressure carpet is for the standard pressure scaling. It is these values of pressure that are scaled up by $\sqrt{10}$ in the optimization calculations reported here. We note that under the increase in pressure scaling the cases for standard and ripple penetration have moved together in "a,h space" across the pressure carpet, but the case for strict

penetration has moved to a quite different "location". In this connection it is interesting to note the two different hybrids from the survey calculations tabulated in lines 3 and 4 in Table XI. The hybrid of line 3 is located in (a-h) space at the point (1,2; 3,6), very close to the point S_s in Figure 25. The hybrid of line 4 is located at the point (1,2; 8,0) at the "corner" of the pressure carpet and in the vicinity of points N_s and R_s! Apparently at least two minima in e exist as a function of a and h according to the survey calculations using the standard penetration criteria and the $\sqrt{10}$ pressure scaling. Furthermore, the point N_s identifies the "exact" values of a and h for the lower of the two minima. The removal of limitations on the penetration (the ripple case) apparently causes the lowest minimum of e to shift to the nearby point R_s. However, application of the strict penetration removes the availability of the point N_s (see discussion of strict penetration in Section 2.b) and probably its vicinity as well. The changes in e are apparently such that the lowest minimum in e now lies at point S_s in the vicinity of the "other" minimum identified by the survey style calculations at a much smaller value of the major radius R.

To account for the fact that β has not increased by $\sqrt{10}$ we note from Figure 25 that the standard pressure of the points N_s, R_s and S_s is considerably lower than the pressure for the points N, R and S (See Section 2.b). This difference in standard pressure, together with the change in toroidal magnetic field, B_c, brought about by the changes in a and h, account for why the value of β does not increase as rapidly as the increase in pressure scaling.

We have noted that the response of the standard and ripple cases to the increase in pressure scaling is very nearly the same. It remains to observe that the decrease in the minor radius, a, results in a decrease in both the volume and the allowed value of $n_e\tau_p$. The increase in the cost of injectors is more than offset by the decrease in the combined costs of magnets, wall structure and blanket inventory. Hence e actually decreases a little, relative to the cases with standard pressure scaling, in spite of the increase in beam power and the decrease in net electric power.

The response of the strict penetration case is similar to that of the standard penetration case except that the minimum cost of electricity is found at a greater reduction in physical size and a greater increase in beam power. Furthermore to produce the 3 GW(e) gross power at the reduced physical size requires an increase in blanket energy multiplication, M, that prevents the blanket inventory from decreasing in proportion to the decrease in physical size. On balance the cost of electricity increases for the strict penetration case. It is smaller than it was using the standard pressure scaling, as is the situation for the standard and ripple penetration cases, but the cost of electricity is still the highest for the strict penetration case. Comparing in Table XV the cases for the largest (line 1) and smallest (line 5) size hybrids, there are large differences in volume, M, H/T, and fusion power density, in penetration criteria and pressure scaling but not more than a 16% difference in cost of electricity. This insensitivity of the cost of electricity argues for considerable latitude in hybrid design features

without severe economic penalty. This point has large practical value.

d. Variation of Profile Factor, α

The pressure profile used in this study is discussed in Section IV.C and is given by Eq. (IV.C-2). The standard value of the profile factor, α, is 2.0. We have made only a limited investigation of the effects of changing α and in the following manner. We have sought the optimum value of α by using it as one component of a 6-vector in the optimization calculation. The value of α was restricted to lie between 1.3 and 2.0. The lower limit for α was chosen because we had difficulty obtaining stable equilibria for $\alpha = 1.2$. The optimization calculation has been done only for the standard constraints and only for P_g = 3 GW(e) and f = 86.5 \$/g.

The principal result is that the least value of α produces the least cost of electricity. Features of the best hybrid with $\alpha = 1.3$ are presented in Figures 22 and 23 and in Table XVI. Features of the standard best hybrid ($\alpha = 2.0$) are also presented in Table XVI for comparison.

This result is not unexpected since a reduction in α broadens the pressure profile thereby making more efficient use of the plasma cross section. Furthermore, according to the pressure scaling given by Eqs. (IV.C-19 and 16), the average pressure supported by a given size plasma increases as α decreases, the peak average pressure being reached for $\alpha \gtrsim 1.2$. This increase in average pressure would be expected to produce an increase in fusion power density and a decrease in volume similar to the results of increasing the pressure scaling discussed above in

Table XVI. Features of Hybrids, P_g = 3 GW(e) , f = 86.5 $/g, α varied

α	M	T_e	W_o	H/T	a	R	CapC	Q	β	β_θ	n_e	$n_e\tau_p$	I	p_f	P_B	P_{net}	A_T	e
		keV	kV		m	m	G$				$10^{14}cm^{-3}$	$10^{14}sec\ cm^{-3}$	MA	W/cm^3	MW	GW		mills/kWh
1.3	10.6	6	167	0.001	1.86	12.2	2.95	7.52	3.06	1.59	2.02	9.24	5.7	1.06	119	2.50	1.00	29.4
2.0	9.9	6	174	0.001	2.93	15.7	3.57	5.80	4.39	0.99	1.14	7.61	5.6	0.35	164	2.42	0.99	36.7

Section 2.c. This expectation is borne out. The major difference in results is that the reduction in α is accompanied by an increase in Q and P_{net} (P_i decreases) rather than the reverse. This difference produces cheaper electricity than the simple pressure scaling alone.

We note two differences, however, between these two ways of increasing the average pressure. First, for $\alpha = 1.3$ the value of β_θ is limited (more severely) by the prohibition against there being a negative current density anywhere in the plasma (see Eq. (IV.C-11)) rather than being limited less severely by the aspect ratio as in the case for $\alpha = 2.0$. Second, for a given average density, the average of the square of the density increases as α decreases. The reactivity of the plasma ($\sim n_e^2$) is calculated to be about 12% higher for $\alpha = 1.3$ than for $\alpha = 2.0$. It is not clear if or how these two differences of contrary influence account for the rise in Q and drop in P_i observed as α goes from 2.0 to 1.3.

Finally, if the $\alpha = 1.3$ result plotted in Figure 22 is assumed to lie on a best hybrid curve similar to the optimized 3 GW(e) standard best hybrid curve, then one projects a park solution of e $\approx$ 31 mills/kWh and f $\approx$ 55 \$/g. These "park" numbers are similar to the results of the mirror hybrid study by Bender and Lee[4] who quote values of e = 24.7 mills/kWh and f = 55 \$/g.

e. Pressure Scaling at Fixed a and R

The data presented in Sections B.2.c and C.2.c indicated the existence of a minimum in the cost of electricity as a function

of the pressure scaling. To further investigate the nature of this minimum, and to do so with some economy in computer time, the physical size of the hybrid plasma and the gross electric power generated were fixed at the values pertaining to the nominal hybrid. Optimization calculations were then conducted over the remaining three-dimensional space of hybrid parameters (W_o, T_e, H/T) for a variety of pressure scale factors ranging from 0.5 to 1.25. The value of β_θ was held fixed for all pressures by appropriately scaling the discharge current as described in Section 2.c. The standard constraints were used.

The results for the best hybrids are given in Figure 26 and Table XVII. The minimum in e is evident and occurs for a pressure scaling factor of 1.06. It appears to be correlated with a peak in $n\tau_p$ and a minimum in beam power. This result is understood in the following way. The increase in e for scale factors progressively less than 1.06 is related to the progressive decrease in density. A decrease in density is associated with a decrease in both the fusion power density and the value of the allowed $n\tau_p$. A decrease in fusion power density requires, in order to maintain P_g, an increase in blanket multiplication, M, which increases the cost of the blanket and decreases the net production of fissile fuel. A decrease in allowed $n\tau_p$ requires a decrease in the required $n\tau_p$ that in turn results in an increase in beam power (accomplished in the face of decreasing density by increasing H/T) and injector costs and a drop in P_{net}. In the face of increased costs and decreased electric and fissile product, the cost of electricity must rise.

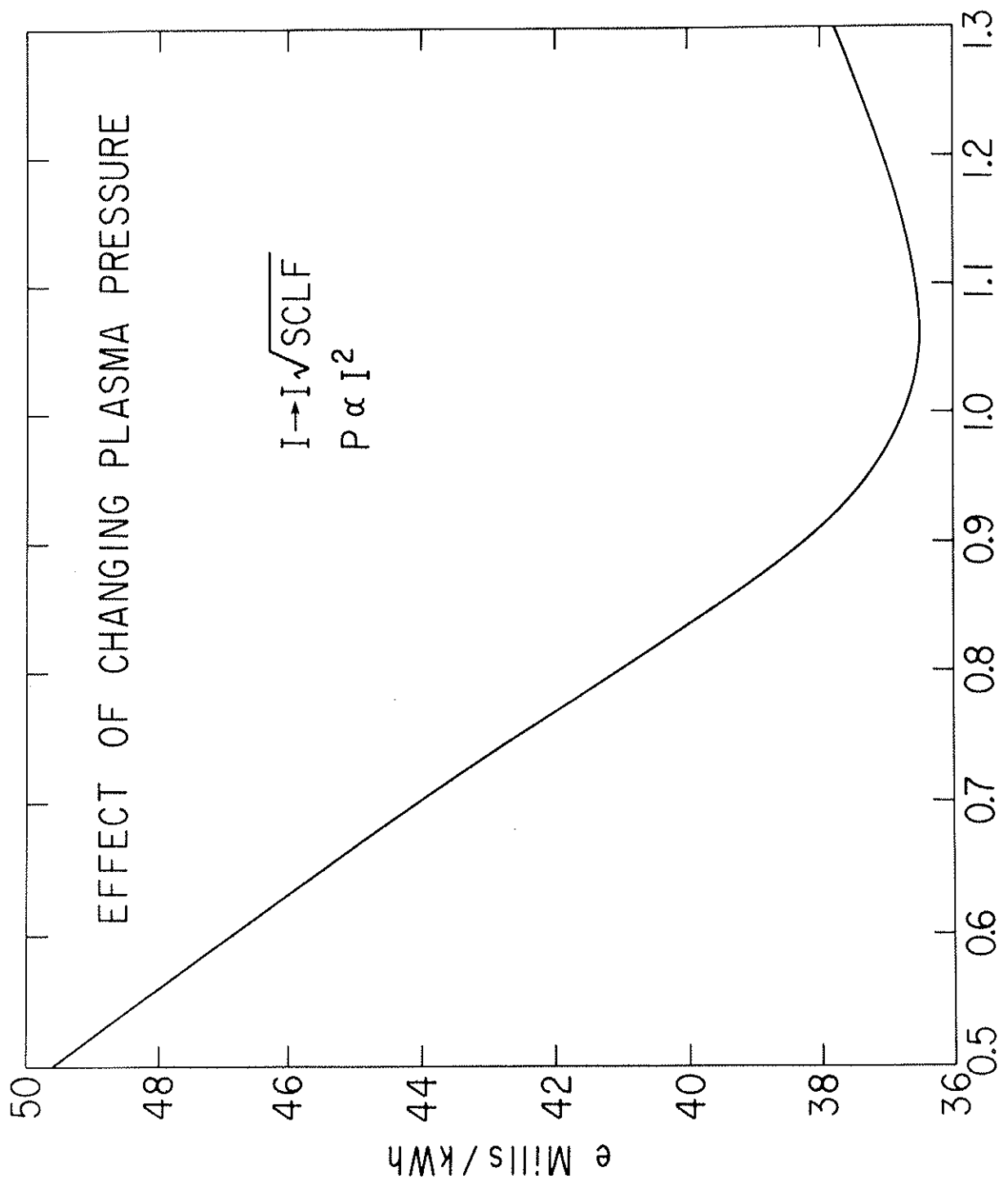

Fig. 26. Cost of Electricity Versus the Factor by which the Plasma Pressure is Scaled.

Table XVII. Pressure Scaling Data for fixed R, a, P_g = 3 GW(e), f = 86.5 \$/g

SCLF	M	T_e	W_o	H/T	n_e	CapC	$n\tau$	P_i	P_{net}	p_f	B	I	β	Q	A_T	NLWR/P_{net}
		keV	kV		$10^{14}cm^{-3}$	G\$	$10^{14}\frac{sec}{cm^{-3}}$	MW	GW	W/cm^3	T	MA				$(GW)^{-1}$
1.25	9.8	6.0	192	0.0024	1.13	3.48	6.38	212	2.31	0.3587	6.7	5.6	1.24	4.5	1.26	2.46
1.1	9.7	6.0	177	0.001837	1.17	3.53	7.70	174	2.39	0.3641	7.3	5.7	1.09	5.57	1.08	2.45
1.0	9.9	6.1	168	0.001843	1.14	3.57	7.61	164	2.42	0.3573	7.6	5.6	0.99	5.80	0.99	2.35
0.9	10.9	6.4	162	0.0031	0.95	3.64	5.24	192	2.38	0.3241	7.6	5.3	0.89	4.49	1.00	1.98
0.75	13.9	6.8	154	0.0057	0.34	3.83	3.28	213	2.35	0.2547	7.6	4.9	0.74	3.18	0.99	1.20
0.50	23.6	7.7	150	0.020	0.41	4.47	1.22	220	2.34	0.1509	7.6	4.0	0.50	1.82	0.82	0.0

SCLF ≡ (scaled pressure)/(standard pressure)

The increase in e for scale factors progressively larger than 1.06 is also related to the necessity for more beam power. However, the reason for the increase in beam power is more complex than for the case discussed just above. The increase in pressure scaling results in violation of the penetration limits, as evidenced by $A_T > 1.0$, with the consequence that the computer code FUN causes the density to be reduced by the factor $A_T > 1.0$. The reduction in density is accompanied by a reduction in both the discharge current, I, and the toroidal magnetic field, B, such that β and β_θ remain unchanged. (See discussion of code in Section IV.H.) The reduction in I and B produces a decrease in the allowed $n\tau_p$, and this, in turn, can require a sufficiently large increase in beam power to drive the cost of electricity, e, up. The increase in injection costs does not, however, offset the decrease in magnet costs associated with the reduction in B. The nearly constant value of M implies no change in blanket costs. Hence the capital cost of the plant will actually decrease, but the drop in electric power for sale is so large that e will be forced to rise.

Comparing the second and third lines of Table XVII, parts of the above argument do not seem to hold. The increase in beam power is accompanied by an increase rather than a decrease in $n\tau_p$. Furthermore, the decrease in P_{net} is not accompanied by an increase in e. However, the capital cost does decrease.

The closeness of both the parameters and the economics of these two cases reveals subtleties not so evident in comparing the first and third lines. The paradox is resolved by noting

the increase in both density and injection energy for the second compared to the third line. The increase in W_o enables the penetration criterion to be satisfied at a higher density than otherwise. The increase in density is sufficient to increase the allowed $n\tau_p$ in spite of the reduction in B. The small drop in Q, resulting primarily from the increase in W_o (Q depends on H/T, W_o, and T_e) is sufficient to produce an increase in the required $n\tau_p$ in spite of the increase in P_i. The decrease in M and consequent increase in net fissile fuel reduces the cost of the blanket, but more importantly increases the revenue from the sale of fissile fuel. However, the major reason for the reduction in capital cost is the reduction in magnet costs that far more than compensates for the increase in injection cost. On balance, then, the decrease in capital costs and the increase in fuel revenue does not require the cost of electricity to rise in spite of the drop in P_{net}.

The conclusion of this investigation of the minimum in e is that the minimum is the result of the constraints on and economic modeling of the entire hybrid reactor rather than a result of the plasma physics within the discharge itself. This minimum in e is thus a striking example of a systems effect that does not even exist in an isolated subsystem of the whole.

f. Variations of B, p, and Penetration Response For Fixed 6-Vector

The branch taken by the subroutine FUN when the penetration criterion is violated (see Figure 2 in Section IV.H) causes the plasma electron density to be reduced to conform with

the penetration requirement. Accompanying this reduction in electron density, the discharge current, I, and the toroidal magnetic field, B, are also reduced such that the values of β and β_θ existing when the program entered the branch are preserved. This "response" of the code to a violation of the penetration limit will be referred to as the "B,I" response. The original thought in designing the B,I response was to consider hybrids that had higher values of β than those produced by the standard pressure scaling. A favorable consequence of reducing B is a reduction in magnet costs and of reducing I is the relief of the core constraint. However, an unfavorable consequence of reducing B and I is the reduction of the standard value of $n\tau_{PHY}$ calculated on the basis of trapped-electron-mode diffusion coefficients.

For comparative purposes an alternative "response" to violation of the penetration criterion was constructed whereby the required reduction in electron density was accompanied by a reduction only in I such as to preserve β_θ. As a consequence the value of β is also reduced. This "response" will be referred to as the "β,I" response. The original thought in designing the β,I response was to avoid the reduction in the standard value of $n\tau_{PHY}$ associated with the reduction in B. The disadvantage of the β,I response is the reduction of β thereby obviating one of the effects sought in increasing the pressure.

Only a limited comparative study was made of the effects of using the B,I and the β,I responses. Best hybrids were determined for each style of response for both the standard and the strict penetration criteria (see Section 2.b above) and for the

standard and enhanced pressure scaling (see Section 2.c). Calculations were done only for P_g = 3 GW(e) and f = 100 \$/g.

The results using the B,I response were hardly distinguishable from the results using the β,I response. This result follows from the fact that the best hybrids for either style were characterized by a penetration index equal to 0.99 or 1.00, i.e., the electron density derived from the pressure scaling was at or very near to the maximum value compatible with satisfaction of the penetration criterion. Thus for the best hybrids the branch of the subroutine FUN containing either the B,I or the β,I response was not taken. Apparently the response of the hybrid model to either type of response is sufficiently deleterious to the cost of electricity that the best hybrids are found for 6-vectors that do not lead to violation of the penetration criterion at any point in the calculation.

The effect on the calculated cost of electricity for a fixed 6-vector using either the B,I or the β,I response was studied for variations of both the pressure scaling and the maximum magnetic field allowed at the toroidal field coils. Only one 6-vector, corresponding to the "nominal hybrid", was used in this small study. The calculations were done without the confinement constraint being applied. Violation of this constraint, however, was noted. The results of these calculations are shown in Figure 27.

For a reduction in B_{max} or the pressure scaling the $n\tau$ constraint is violated, and the cost of electricity increases. Violation of the $n\tau$ constraint occurs because the allowed value of $n\tau_p$ decreases with either density or magnetic field strength (see Eq. (25.a) of Section IV.F), whereas the

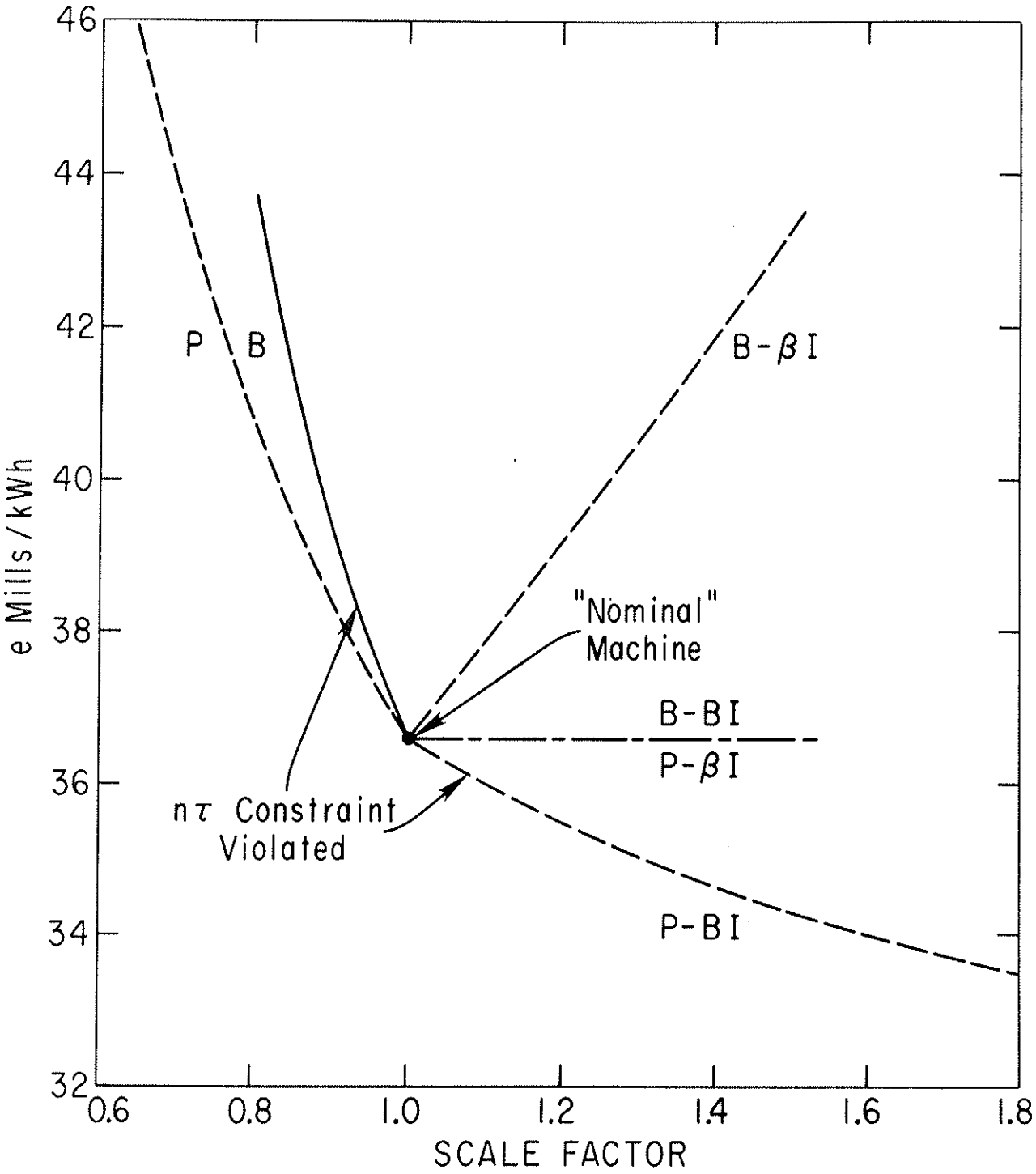

Fig. 27. Correlation between the cost of electricity for the "nominal hybrid" and the factor by which the magnetic field, B, or the normalized pressure, β, is scaled. The "six vector" is held fixed.

required $n\tau_p$ is insensitive to the density and independent of B_{max}. The rise in the cost of electricity represents the interplay of several factors as follows. For a decrease in pressure the density falls, hence the beam power decreases and hence the cost of injectors is reduced, and the net power is increased. Such changes would produce a decrease in the cost of electricity. However, because the gross electric power must be held fixed in this calculation, the decrease in beam power produces an increase in the required blanket multiplication and hence an increase in both the blanket inventory of plutonium and the concomitant blanket costs. The result is a net increase in capital costs with decreasing pressure. Furthermore the increase in blanket multiplication reduces the net fissile fuel production and the revenue therefrom. On balance the cost of electricity is increased. The reduction in B_{max} produces a similar chain of effects. This is so because the pressure scaling (see Eq. (15) of Section IV.C) is changed by a factor of k^2 when B_{max} is changed by a factor k. However, the reduction in B_{max} reduces the cost of the magnets which diminishes the increase in the cost of electricity over what would be expected on the basis of change in pressure alone.

For an increase in B_{max} or the pressure scaling above the nominal values the effect on the cost of electricity is quite different depending on what is being scaled and which response, the B,I or the β,I, is being used. In any case, an increase in the pressure results in a violation of the penetration criterion since the penetration index stands at 0.99 for the nominal hybrid. The response branch of the subroutine FUN maintains the density and hence the beam power at the values

pertaining to the nominal hybrid. Consequently the blanket multiplication remains unchanged as well as the blanket and injector costs.

In the case of scaling the pressure and the β,I response the toroidal magnetic field remains fixed, hence magnet costs are fixed; there is no change in capital costs, and therefore the cost of electricity remains fixed. Scaling B_{max} with the B,I response also leaves the magnetic field unchanged, and hence the cost of electricity will remain fixed. However, using the β,I response to the scaling of B_{max} allows the magnetic field and hence the magnet costs to increase. Therefore this case leads to an increase in the cost of electricity since the capital cost has been increased with no change in either the net electric power or the fissile fuel production. Finally, using the B,I response with the scale-up of pressure results in a decrease in magnetic fields and hence magnet costs. There is a reduction in capital cost with no change in product, and hence the cost of electricity drops. However, the drop in B reduces the value of the allowed $n\tau_p$ whereas the required $n\tau_p$ has remained unchanged. Therefore this case leads to a violation of the $n\tau$ constraint.

These effects display the working of the physical-economic model used in this study. Both the survey and the optimization calculations reported outside of this section have used the B,I response.

g. Optimized Carpets

As described in Section IV.G.3, the "best" hybrids are determined for given values of fissile fuel prices, f, and gross

electric power, P_g, by finding the 5-vector (a, h, T_e, W_o, H/T) that produces the lowest cost of electricity. The nominal hybrid is the "best" hybrid for f = 86.5 \$/g and P_g = 3000 MW(e). To display the characteristics of hybrids in the neighborhood of the nominal hybrid we display several "carpets", Tables XVIII - XXXII, defined for the above values of f and P_g. The carpets are a matrix of numbers in which the row and column location specifies the values of h and a, respectively. The discrete values of h and a are those used in the survey calculations displayed in Table I. For each choice of h and a the optimization calculation was used to find the 3-vector (T_e, W_o, H/T) that produced the lowest value of e. These lowest values of e constitute the "e carpet" shown in Table XVIII. The temperatures associated with each of these optimized results constitute the "T_e carpet" shown in Table XIX. Tables XX - XXXII constitute carpets of other quantities associated with these optimized hybrids.

The e carpet of Table XVIII reflects the same "broad flat valley" in e seen for the survey results shown in Table III. The minimum e of the e carpet is located at the sixth row, fifth column (6,5) and is 36.8 mills/kWh. The nominal hybrid lies between the 5th and 6th rows and between the 5th and 6th columns. The value of e for the nominal hybrid was found with an optimization over the 5-vector (a, h,T_e, W_o, H/T); its location on the optimized e carpet is entirely credible since it lies within the lowest region of the e carpet. This circumstance validates the ability of the 5-vector optimization calculation to find the correct neighborhood of the minimum value of e even though it

Table XVIII. e (mills/kWh) Carpet

h \ a	1.2	1.6	2.0	2.4	2.8	3.2	3.6	4.0
2.5	*	*	*	*	*	*	*	*
3.6	*	*	49.3	44.1	45.4	46.8	47.8	48.2
4.7	*	*	43.9	44.4	44.2	42.6	41.3	30.8
5.8	*	52.5	43.9	42.8	40.3	38.3	38.9	40.0
6.9	*	50.3	43.7	41.3	37.9	37.3	38.8	40.2
8.0	*	50.7	43.5	40.3	36.8	37.6	39.1	40.3

Note: Tables XVIII through XXXII are for P_g = 3000 MW(e), f = 86.5 $/g.

Table XIX. Temperature (keV) Carpet

*	*	*	*	*	*	*	*
*	*	6.00	7.26	7.69	8.40	8.50	7.78
*	*	7.90	8.26	7.59	6.99	6.59	6.18
*	6.00	7.86	6.56	6.92	6.23	6.14	6.04
*	6.36	6.49	6.96	6.47	6.00	6.01	6.04
*	6.70	6.36	7.12	6.16	6.15	6.04	6.00

Table XX. Hot/Thermal Carpet

*	*	*	*	*	*	*	*
*	*	0.126	0.048	0.043	0.048	0.040	0.022
*	*	0.065	0.042	0.020	0.010	0.005	0.003
*	0.129	0.040	0.009	0.007	0.003	0.002	0.002
*	0.114	0.011	0.008	0.003	0.001	0.002	0.002
*	0.108	0.008	0.007	0.001	0.001	0.002	0.001

Table XXI. Injection Energy (kV) Carpet

*	*	*	*	*	*	*	*
*	*	150.0	150.0	153.0	151.0	159.0	178.0
*	*	150.0	152.0	181.0	194.0	200.0	207.0
*	150.0	150.0	196.0	184.0	193.0	192.0	195.0
*	150.0	182.0	174.0	175.0	179.0	183.0	184.0
*	150.0	172.0	159.0	162.0	167.0	171.0	173.0

Table XXII. Q Carpet

*	*	*	*	*	*	*	*
*	*	0.812	1.13	1.27	1.37	1.51	1.73
*	*	1.14	1.35	1.79	2.34	2.93	3.59
*	0.803	1.34	2.06	2.70	3.92	4.37	4.33
*	0.846	1.73	2.47	3.94	5.36	4.85	4.51
*	0.889	2.03	3.92	5.67	5.95	5.20	5.22

Table XXIII. Capital Cost (G$) Carpet

*	*	*	*	*	*	*	*
*	*	3.42	3.48	3.50	3.50	3.53	3.60
*	*	3.42	3.44	3.45	3.49	3.53	3.59
*	3.54	3.48	3.54	3.45	3.51	3.57	3.63
*	3.60	3.69	3.52	3.52	3.57	3.62	3.69
*	3.70	3.80	3.58	3.59	3.65	3.71	3.75

Table XXIV. Capital Cost per Net Electric Power ($/W) Carpet

*	*	*	*	*	*	*	*
*	*	1.73	1.63	1.71	1.79	1.85	1.87
*	*	1.60	1.67	1.71	1.68	1.66	1.64
*	1.79	1.63	1.61	1.59	1.54	1.56	1.60
*	1.83	1.62	1.58	1.52	1.50	1.55	1.60
*	1.86	1.62	1.57	1.48	1.51	1.56	1.59

Table XXV. Plasma Electron Density ($10^{14}cm^{-3}$) Carpet

*	*	*	*	*	*	*	*
*	*	0.41	0.48	0.45	0.39	0.38	0.42
*	*	0.49	0.53	0.63	0.71	0.75	0.78
*	0.48	0.60	0.86	0.84	0.97	0.91	0.83
*	0.49	0.85	0.88	1.01	1.07	0.92	0.80
*	0.48	0.90	0.89	1.13	1.05	0.89	0.81

Table XXVI. Wall Load (MW/m^2) Carpet

*	*	*	*	*	*	*	*
*	*	0.34	0.30	0.28	0.32	0.31	0.29
*	*	0.34	0.36	0.38	0.37	0.35	0.32
*	0.36	0.32	0.34	0.41	0.38	0.36	0.32
*	0.35	0.29	0.34	0.41	0.39	0.33	0.29
*	0.33	0.27	0.40	0.40	0.36	0.32	0.28

Table XXVII. "Required" $n\tau$ (10^{14}sec cm^{-3}) Carpet

*	*	*	*	*	*	*	*
*	*	0.15	0.49	0.58	0.58	0.69	1.08
*	*	0.40	0.62	1.21	2.12	3.20	4.72
*	0.15	0.65	2.09	2.61	5.07	5.84	6.06
*	0.18	1.70	2.35	4.64	7.43	6.82	6.25
*	0.20	2.29	2.74	7.26	8.07	7.12	7.29

Table XXVIII. "Allowed" $n\tau$ (10^{14} sec cm^{-3}) Carpet

*	*	*	*	*	*	*	*
*	*	0.38	0.49	0.58	0.58	0.69	1.08
*	*	0.41	0.62	1.21	2.12	3.20	4.72
*	0.47	0.65	2.09	2.61	5.07	5.84	6.06
*	0.53	1.70	2.35	4.64	7.43	6.82	6.25
*	0.54	2.29	2.74	7.26	8.08	7.12	7.29

Table XXIX. Blanket Multiplication Carpet

*	*	*	*	*	*	*	*
*	*	25.4	23.5	18.2	14.5	12.5	11.9
*	*	23.5	17.4	13.5	11.7	10.5	9.8
*	25.7	20.1	17.0	11.7	10.4	9.5	9.4
*	23.9	23.3	14.0	10.9	9.8	9.7	9.5
*	23.7	23.0	12.6	10.4	9.7	9.6	9.2

Table XXX. Beam Power (MW) Carpet

*	*	*	*	*	*	*	*
*	*	447	350	381	448	479	460
*	*	347	393	381	347	301	264
*	447	316	268	302	224	225	229
*	455	248	219	218	179	199	217
*	438	203	254	160	163	188	200

Table XXXI. Fusion Power Density (W/cm^3)

*	*	*	*	*	*	*	*
*	*	0.46	0.32	0.28	0.25	0.21	0.17
*	*	0.45	0.39	0.34	0.29	0.24	0.20
*	0.62	0.48	0.37	0.37	0.30	0.25	0.19
*	0.60	0.39	0.42	0.37	0.30	0.23	0.18
*	0.56	0.36	0.43	0.36	0.28	0.21	0.17

Table XXXII. NLWR Carpet

*	*	*	*	*	*	*	*
*	*	0.00	0.00	0.58	1.27	1.83	2.05
*	*	0.00	0.67	1.45	1.94	2.39	2.64
*	0.00	0.29	0.69	1.85	2.28	2.68	2.75
*	0.00	0.00	1.20	2.03	2.43	2.54	2.64
*	0.00	0.02	1.48	2.12	2.42	2.53	2.76

does not produce a unique value for e.

The e carpet confirms the survey results of Table III that less than a 10% increase in e above its minimum value embraces a wide range of sizes of hybrid plasma.

The capital cost carpet of Table XXIII is quite flat, varying by less than 6% from its average value over the entire carpet. However the capital cost per net electric power (displayed in Table XXIV) does not reach its minimum value at the minimum value of e. However, the beam power, P_i, is a minimum at the minimum value of e (see Table XXX). The plasma Q, the wall load, the required $n\tau_p$ and the plasma density are near their maximum values (see Tables XXII, XXV-XXVII) at the minimum value of e.

Looking at the smaller machines in the upper left region of the carpets we see that both the blanket multiplication, M, and P_i take on relatively high values (see Tables XXIX and XXX). This result is to be expected since the gross power is held fixed and therefore as the plasma volume decreases, the fusion power density (see Table XXXI) and/or M must increase. Consequently H/T will be relatively high (see Table XX), and hence Q will be low. A relatively large amount of beam power is therefore required to produce the fusion power which the blanket amplifies. The smaller heavily beam-driven plasmas also require values of $n\tau_p$ that are lower than the allowed values of $n\tau_p$ (compare Tables XXVII and XXVIII).

The larger machines, in the lower right region of the carpets, have low values of both M and P_i. These devices have

large plasma volumes, and hence the fixed gross power level can be met with more modest values of fusion power density and M. The lower levels of fusion power density are accomplished with smaller values of H/T and hence higher values of Q.

The capital costs reflect competing trends that tend to balance each other. In small machines the large injection costs are offset by the smaller structure and magnet costs. The reverse is true for the large machines.

The small machines, with their large values of M, produce relatively little fissile fuel whereas the large machines with their low values of M produce relatively large amounts of fissile fuel (see Table XXXII).

D. Variation of the Six-Vector

The change in the cost of electricity (the sensitivity) of the nominal hybrid was determined for a 2% change in each component of the nominal 6-vector taken singly. The results are displayed in Table XXXIII.

For most of the components a 2% change in either sense produced a violation of the confinement constraint. The cost of electricity is most sensitive to the gross electric power, P_g, and equally least sensitive to the injection energy, W_o, and the hot to thermal ratio, H/T. The changes in the cost of electricity are understood in the following ways.

1. Variation in P_g

An increase in the gross electric power level, P_g, will increase the balance of plant cost. Since the fusion power and beam power are determined by the other components of the 6-vector that are held fixed, to meet an increase in P_g the blanket

Table XXXIII. Sensitivity of Nominal Hybrid to 2% Variation of the 6-Vector

Variable	M	n_e	W_L	Q	e	CapC	$n\tau$	$n\tau_{PHY}$	P_i	P_{net}	A_T
		$10^{14}cm^{-3}$	MW/m^2		mills/kWh	G$	$10^{14}\frac{sec}{cm^{-3}}$	$10^{14}\frac{sec}{cm^{-3}}$	MW	GW	
P_g ↑	10.1	1.14	0.41		36.09	3.60	7.61	7.61	164	2.47	0.99
P_g ↓	9.7	1.14	0.41		37.10	3.54	7.61	7.61	164	2.37	0.99
T_e ↑	9.7	1.11	0.42	6.393	36.2	3.56	7.56	7.09	156	2.43	0.94
T_e ↓	11.0	1.10	0.37		37.1	3.59	7.65	7.26	156	2.43	1.04
W_Q ↑	9.858	1.1356	0.41	6.009	36.60	3.570	7.624	7.608	163.96	2.418	0.97
W_Q ↓	10.356	1.1094	0.39	5.961	36.51	3.572	7.597	7.199	157.59	2.43	1.02
H/T ↑	10.00	1.126	0.41	5.884	36.61	3.57	7.51	7.46	165.08	2.42	1.00
H/T ↓	9.884	1.136	0.41	6.092	36.47	3.57	7.71	7.61	161.35	2.43	0.99
a ↑	9.776	1.1136	0.40	5.986	36.68	3.576	7.61	7.57	165.8	2.417	1.02
a ↓	10.45	1.1312	0.40	5.986	36.46	3.565	7.61	7.24	155.6	2.44	0.97
h ↑	9.76	1.1359	0.41	5.986	36.7	3.58	7.61	7.77	166	2.417	1.00
h ↓	10.1	1.1275	0.40	5.986	36.4	3.558	7.61	7.33	160	2.43	0.99
Nominal Hybrid	9.857	1.1358	0.41	5.986	36.56	3.569	7.611	7.611	164.60	2.419	0.99

multiplication, M, also must be increased. An increase in M will increase the cost of the blanket and decrease the production of net fissile fuel and the revenue therefrom. These effects would lead to an increased cost of electricity, e, were it not for the increase in the net electric power, P_{net}, that is a consequence of increasing P_g while keeping the beam power fixed (see Eq. (5)). The increase in P_{net} is sufficient to reduce e.

A decrease in P_g reverses all the above argument and produces an increase in e.

2. Variation of T_e

The increase in plasma temperature, T_e, produces an increase in Q and an increase in the partial pressure of the background plasma. Since the total plasma pressure is determined solely by a, h, and B_{max}, all of which are fixed for this calculation, the increase in T_e produces a decrease in electron density. The drop in density reduces the beam power, P_i. In order to preserve P_g the product, QM, must therefore be increased (see Eq. (1)). In the case at hand, the increase in Q is such that M actually undergoes a small decrease. Thus on balance the fusion power developed, QP_i, has actually increased. The increase in wall loading is further evidence of this result. Thus the cost of electricity is reduced. However, the increase in T_e and the decrease in n_e both act to reduce the allowed $n\tau_p$ more rapidly than the required $n\tau_p$ is reduced so that the confinement constraint is violated.

The decrease in T_e increases the density causing a violation of the penetration criterion and invoking a B,I response (see Section C.2.f) that reduces the density and decreases both

B and I. Consequently the allowed $n\tau_p$ decreases producting a violation of the confinement constraint. Furthermore the reduction in T_e results in an increase in the effective cross section for the ionization of the neutral beams by electron impact (see Section IV.F, Eq. (30)). Consequently to satisfy the penetration criterion the density must be reduced below the original nominal value. Hence the beam power is reduced, and QM must be increased to preserve the value of P_g. However, the reduction in T_e leads to a reduction in Q. Hence M must be increased and concomitantly so are the blanket costs. The increase in blanket costs is larger than the savings in injection costs so, on balance, the capital cost of the hybrid is increased. Furthermore the increase in M reduces the net production of fissile fuel thereby reducing the revenue from the sale of fuel. On balance the cost of electricity is increased in spite of the small increase in P_{net} due to the decrease in P_i.

3. Variation in W_o

The increase in the injection voltage, W_o, produces a very small increase in Q and an increase in the partial pressure of the beam particles. However the nominal value of H/T is so small that the change in the beam partial pressure has a negligible effect on the electron density, n_e. The increase in Q is sufficient to compensate for the small decrease in beam power so that the fusion power does not change essentially and hence the partial pressure of the alpha particles is unchanged. Thus the increase in W_o results in no appreciable change in n_e. The small decrease in beam power results from the circumstance that the fractional reduction in beam current, J, exceeds the fractional increase in W_o.

The reduction in beam current follows from the increase in the slowing down time, τ_s, of the beam particles injected with greater energy. For if n_e and H/T are both fixed, then the density of beam particles is fixed; and if the "lifetime" of the beam particles, τ_s, is extended, then the injection rate of the beam particles must be decreased. (For a fixed density if $d(JW_o)/dW_o < 0$, then $(W_o/\tau_s)(d\tau_s/dW_o) > 1$. This condition is satisfied when W_o is less than approximately $1.4W_c$ where W_c is the "critical energy" at which the beam particle delivers energy at equal rates to the background electrons and to the ions.) A constant density implies no change in the values of $n\tau_p$, allowed or required (see Eqs. (23) and (25a) in Section IV.F.). However, the reduction in beam power with the density fixed does require an increase in the required $n\tau_p$ that, in turn, creates the recorded violation of the confinement criterion. The largest factor in raising the capital cost is the increase in injector cost; an increase that occurs, in spite of the decrease in beam power, because of the decrease in injector efficiency with increasing W_o. Thus the power required to produce the beams has increased while the beam power absorbed by the plasma has decreased. Therefore the net power decreases slightly, and in view of the increase in capital costs, the cost of electricity rises.

The decrease in W_o produces a violation of the penetration criterion with the consequent reduction in n_e, B, and I. The reduction of these quantities reduces the allowed $n\tau_p$. The reduction in n_e reduces the beam power so much that M must be increased in order to maintain P_g fixed. The injection and magnet costs decrease, and the blanket costs increase in nearly equal amounts

leaving the capital cost essentially unchanged. The increase in net electric power is sufficient to allow a small decrease in the cost of electricity.

It is interesting to note that either raising or lowering W_o by 2% produces a decrease in beam power absorbed by the plasma, but for different reasons, and produces opposite effects on the cost of electricity. Furthermore, throughout most of the analysis in this hybrid study a decrease in beam power has been accompanied by an increase in net electric power and a decrease in the cost of electricity. That the response of the hybrid model to the 2% increase in W_o produces opposite effects to a decrease in beam power speaks to the subtle and complex interplay of different parts of the model.

4. Variations in H/T

The increase in H/T reduces Q and increases the beam power. These two effects produce, through the pressure balance, a decrease in electron density. The increase in P_i reduces the required $n\tau_p$ whereas the decrease in density reduces the allowed $n\tau_p$ to a greater extent thereby producing a violation of the confinement constraint. The increase in P_i also requires deeper penetration of the beams so that A_T increases to 1.00 even though n_e decreases. Only a small increase in M is required to compensate for the small decrease in the product P_iQ. Although the increase in P_i and M increases capital costs and reduces net electric power (and hence acts to increase the cost of electricity), the magnitude of the changes produces less than a 0.2% change in the cost of electricity.

The decrease in H/T increases Q and reduces the beam power. These two effects produce only a very small increase in density. The reduction in P_i increases the required $n\tau_p$ more than the increase in density can increase the allowed $n\tau_p$, thereby producing a violation of the confinement constraint. The decrease in beam power and the increase in Q result in only a very small decrease in fusion power so that only a small increase in blanket multiplication is required. The increase in blanket costs is more than offset by the reduction in injector costs which together with the increase in net electric power (associated with the drop in beam power) results in a decrease in the cost of electricity.

5. Variations in a

An increase in the plasma minor radius, a, produces an increase in the plasma volume and an increase in the overall physical size of the hybrid reactor. The allowed pressure is also slightly increased (see Figure 25), and the beams have a little further to penetrate. To meet the penetration constraint the electron density is reduced along with B. The reduction in electron density reduces the beam power density but does not produce a reduction in beam power because of the increase in plasma volume. In fact both the beam power and fusion power increase, resulting in a reduction in both M and the net electric power.

Furthermore the increase in size results in an increase in magnet and blanket inventory costs even though B and M are reduced. On balance the cost of electricity increases. In addition the changes in a, B and I produce a reduction in allowed $n\tau_p$ while leaving the required $n\tau_p$ unchanged. Thus a violation of the confinement constraint is produced.

A decrease in a reduces all sizes, the allowed pressure and the value of the allowed $n\tau_p$. The reduction in beam power and fusion power results in an increase in M together with the cost of the blanket inventory. However, the reduction in the costs of the magnets, injectors, and structure produces a net reduction in capital cost which, together with the increase in net electric power, reduces the cost of electricity. The required $n\tau_p$ remains unchanged, being insensitive to the density change, but the drop in the allowed $n\tau_p$ creates a violation of the confinement constraint.

6. Variations in h

The increase in h, the radius of the point of maximum toroidal field strength (see Section IV.C. Figure 1), increases the allowed pressure and the plasma major radius and hence both the plasma volume and the value of the allowed $n\tau_p$. The increase in pressure is sufficient to create a violation of the penetration constraint. The beam power and fusion power increase, primarily because of the increase in plasma volume, and lead to a reduction in M. The consequent drop in blanket inventory is more than offset by the increase in magnets and structure costs due to the size increases as well as by the increase in injection costs. The rise in capital cost together with a drop in the net electric power due to the increased beam power results in the increase in the cost of electricity. The required $n\tau_p$ is not affected by the above changes, and in view of the increase in allowed $n\tau_p$ there is no violation of the confinement constraint for this increase in h.

The decrease in h reverses all the above effects, and the cost of electricity is reduced below the nominal value. However, the reduction in the value of the allowed $n\tau_p$ produces a violation of the confinement constraint.

7. Remarks

The only variations of the components of the 6-vector that did not produce a violation of the confinement constraint were the variations of P_g and the + 2% variations of h. It would appear that the 6-vector for the nominal hybrid is in a severely restricted region of parameter space and the the optimization calculation had to "walk" along a narrow "path" to find it. These results also suggest that the "best" hybrids in general are characterized by operating "up against" the $n\tau$ and penetration constraints. The details of the hybrid operation are model dependent, but the tendency to raise the "required" $n\tau_p$ to the limit "allowed" reflects the advantage of reducing circulating power within the power plant, and the tendency to keep the penetration index from falling below 1.0 reflects the advantage of the higher reactivity of the plasma at higher densities.

E. Characteristics Along a Best-Hybrid Curve

The hybrid systems code will search for the optimum reactor (the one producing the cheapest electricity) constrained to a given gross electric power and a given price of plutonium. A curve of lowest-achievable price of electricity versus price of plutonium can be constructed, holding the power level fixed; this is the basic method of presenting the code results. In general, each point on the curve represents a different reactor, whose various sub-categories of economics combine at that price of plutonium to yield the cheapest electricity.

In order to discuss the shift of reactor characteristics three specific examples have been selected from the curve at 3000 MW gross electric. Reactor A produces the cheapest electricity when the price of plutonium is 25 $/g, while reactor C produces the cheapest power at 175 $/g. Reactor B is the Nominal Hybrid: the optimum reactor at 87.50 $/g, where the hybrid and LWR cost curves intersect.

Selected physical parameters of these reactors are given in Table XXXIV, while Table XXXV presents the corresponding major economic parameters. Of immediate interest in these data are the comparisons between A and B and between B and C. In the former case, hybrids A and B are physically very different, but have nearly the same price of electricity. In the latter case, the reverse is true: hybrids B and C are very similar, but C produces much cheaper power.

The revenues of a hybrid are from the sale of electricity and plutonium. The "price of electricity" is calculated such that the annual revenues just equal the annual charges. For the hybrid

Table XXXIV. Physical Parameters of Three Optimum Hybrids Rated at 3000 MWe.

Reactor	A	B	C	
Size Parameters				
Major radius	10.83	15.72	16.07	m
Minor radius	2.435	2.940	2.912	m
Aspect ratio	4.45	5.35	5.52	
Plasma volume	1267.00	2682.00	2690.00	m^3
Wall area	1129.00	1922.00	1948.00	m^2
Plasma Parameters				
Density	50.06	113.6	108.3	μm^{-3}
Temperature	7.0	6.1	6.5	keV
$n\tau$	56.0	761.0	657.0	$s/\mu m^{-3}$
Hot/thermal ratio	0.041	0.001	0.002	
β pressure ratio	1.29	0.99	0.95	%
Beam voltage	150.0	168.0	157.0	keV
Beam power	344.1	164.6	178.4	MW
Fusion power	409.8	985.3	1087.0	MW
Blanket Parameters				
Wall load	0.2905	0.4106	0.4467	MW/m^2
Burnup	0.480	0.242	0.157	%
Batch lifetime	7.68	3.53	2.17	yr
Energy multiplication	23.64	9.86	8.91	
Average Pu inventory	7494.00	2800.00	2422.00	kg
Gross Pu bred	1941.00	2681.00	2855.00	kg/yr
Net Pu sold	0.0	1988.00	2336.00	kg/yr
U inventory	978.0	1666.00	1668.00	Mg
Power Production				
Net power	2144.00	2419.00	2406.00	MW
Capacity factor	69.7	69.1	68.9	%
Annual output	13.10	14.65	14.53	TWhr

Table XXXV. Economic Parameters of Three Optimum Hybrids Rated at 3000 MWe.

Reactor	A	B	C	
Annual Revenue	500.83	709.08	837.16	M$
Price of electricity	38.22	36.67	29.48	$/MW-hr
Electric power	2144.00	2419.00	2406.00	MWe
Electricity revenue	500.53	537.14	428.31	M$
Capacity factor	69.73	69.12	68.94	%
Price of plutonium	25.00	86.50	175.00	$/g
Plutonium production	0.0	1987.70	2336.30	kg
Plutonium revenue	0.0	171.94	408.85	M$
Annual Charges	500.72	709.31	836.05	M$
Fixed charges	420.79	494.87	501.57	M$
Wall replacement	0.43	1.04	1.14	M$
Maintenance	19.65	21.98	21.80	M$
Salt processing	1.00	1.00	1.00	M$
Fuel cycle	58.84	190.42	311.68	M$
Capital Items	3316.54	3299.10	3343.81	M$
Magnets	244.14	493.90	509.35	M$
Wall and Structure	140.63	209.21	213.80	M$
Injectors	126.60	64.09	67.23	M$
Invariant	50.00	50.00	50.00	M$
Balance of plant	891.95	891.95	891.95	M$
Indirect charges	653.99	769.12	779.55	M$
Interest during construction	481.34	566.07	573.75	M$
Cost of Capacity (including inventory)				
Electricity	1428.00	1477.00	1525.00	$/kWe
Plutonium	-	1242.00	1083.00	$/(kg/yr)

sytems code the charges are figured in five categories, of which only two -- fixed charges and fuel cycle -- are significant and variable. The fixed charges are figured on five categories of capitalization (including indirect expenses); the balance-of-plant dominates but depends only on the gross power, while the magnet cost is the major variable. The fuel cycle cost is based on an annualized equilibrium batch model following standard nuclear accounting practices; roughly half the cost is for blanket fabrication, interest, and processing, while the other half is a plutonium inventory charge.

Comparing reactor C to reactor B, the annual cost has increased substantially, but the plutonium revenue has risen more; therefore the required price of electricity is lower. Three-quarters of the increase in the Pu revenue is directly due to the higher assumed price of plutonium. Unfortunately the price increase also would boost up the Pu carrying charge portion of the fuel cost; the net effect, if applied to reactor B, would be to lower the required price of electricity to 31.2 $/MWhr.

Reactor C beats this because it has a greater net production of Pu. Small changes in the beam and plasma specifications lead to an increase of about 10% in the fusion power; this in itself will increase the Pu production by 10%. In addition, since the gross power is fixed, the blanket energy multiplication must be reduced. This is accomplished by lowering the burnup of the uranium in the multiplier region because the Pu salt in the burner region is already being ramped down to zero at refueling time. Reducing the burnup has several ramifications: the Pu production ratio increases slightly, the average Pu inventory decreases

slightly, while the batch lifetime decreases substantially. The fuel cycle cost component due to blanket fabrication and reprocessing rises since it is inversely proportional to the lifetime, but this extra cost is just balanced by the revenue from the extra Pu for sale. Carrying charge savings on the reduced Pu inventory, only partially cancelled by increased fixed charges, provide the final decrement in the required price of electricity.

Overall then, in the vicinity of the B and C hybrids two factors explain the declining cost of hybrid power as the Pu price is raised. First, there is the simple fact that in these reactors the Pu production is large enough that the sale revenue increases faster than the inventory charges. Second, the trade-offs among blanket throughput charges, Pu inventory charges, and net Pu production earning are reoptimized. As the Pu price rises, the extra revenues will balance off the incremental throughput charges at lower burnups, leaving a net gain due to the lowered carrying charge.

In contrast to B versus C, the differences between the A and B hybrids illustrate substantially different approaches to minimizing the price of electricity. Reactor A, which is the optimum when the market price of plutonium is only 25 $/g, has a large Pu inventory, high blanket energy multiplication, and no net production of Pu for sale.

Reactor A is much smaller than reactor B: the major radius is only two-thirds, the volume one-half, and the wall area about 60%; this results in a 45% decrease in the capital cost of the magnets, wall and structure. On the other hand, the beam power is more than doubled, with corresponding effect on the beam

cost. Since the plasma density of A is half that of B and the $n\tau$ only 7.4%, the fusion power of reactor A is less than half that of B, and only 20% greater than the beam power.

To compensate for the low fusion power the blanket multiplication is raised nearly to its limit by increasing the Pu content of the burner salt. Keeping the gross power high minimizes the impact of the low plasma Q; the large Pu inventory is tolerable because of its (comparatively) low price. The multiplier region burnup is nearly at the target of 0.5%, so that the batch lifetime is quite long; this factor, along with the lower uranium inventory in the smaller machine, keeps the blanket processing portion of the fuel cycle cost low.

Relative to reactor B, the reductions in the fixed charges and fuel cycle costs of reactor A slightly more than compensate for the lack of Pu sale revenue. Unfortunately the extra power required for the beams comes out of the net electrical output, requiring a slightly higher price for that electricity to achieve breakeven.

However, this is the best hybrid in the given circumstances, i.e., 3000 MWe gross power and 25 $/g for plutonium. If the fusion power were increased, there would be a net production of Pu for sale and a reduced Pu inventory charge; against these factors would be increased blanket processing charges because the batch lifetime would be shorter. (It is interesting to note that the Pu inventory charge and the blanket U processing charge each constitute about one-half the fuel cycle cost in all three cases considered here.) Furthermore, increasing the fusion power by increasing the device size would raise the capital cost, while

increasing the beam power would lower the net electrical output still more. The sale of Pu at only 25 $/g is simply not worthwhile.

These cases illustrate an observation drawn from examination of many hybrid cases: for a given power level there is a critical price of plutonium which separates two opposing reactor regimes. When the Pu price is high, the sale of plutonium is a lucrative business, and so fuel producers are favored. The blanket energy multiplication in these reactors is kept to the bare minimum; increased physical size is the cheapest way (overall) to raise the fusion power to make up the difference. When the price of Pu is low, better economics result from a small reactor with low fusion power and a high blanket multiplication. This provides in situ conversion of the bred fissile material to energy, which is comparatively more valuable. The transition betweeen these two regimes generally occurs over a narrow range of Pu prices, and sometimes occurs as a sharp "snapthrough" at a critical price.

F. General Conclusions

We close this section of the study with some brief general conclusions supported by the above results.

1. There are economically interesting hybrids. They must produce electricity for sale. They are large ($\geq$ 2 GW(e) gross), but not too large (< 4 GW(e) gross), and expensive (capital costs $\leq$ 1 G$/GW(e) gross).

2. The bus bar cost of electricity is sensitive to gross electric power, decreasing as the power increases.

3. There are different combinations of physical size, plasma temperature, ratios of "hot" to "thermal" plasma ion

populations and beam injection voltages that can lead to nearly equal bus bar costs of electricity. Therefore there is some latitude in physical design of hybrid reactors without major economic penalty.

4. The bus bar cost of electricity is sensitive to the confinement property of the plasma ($n\tau$) and to the distribution of plasma density and temperature in minor radius.

5. Multidimensional analysis of both the physical and economic elements that make up a hybrid reactor is necessary to evaluate a hybrid design.

6. In view of the sensitivity of the economic performance of the hybrid to plasma physics quantities, a more precise modeling should await more experimental knowledge of plasma behavior.

References

[1]D. E. Deonigi and R. L. Engel, The Economics of Fusion-Fission Systems, Proceedings of the US-USSR Symposium on Fusion-Fission Hybrid Reactors (National Technical Information Service, Springfield, Virginia, 1976) Conf. 760733, pp. 231 - 238; also Battelle Northwest Laboratories Report BNWL-SA-5976 (1976).

[2]D. E. Deonigi and R. L. Engel, Performance Targets for Fusion-Fission (Hybrid) Reactors, Battelle Northwest Laboratories Report BNWL-2139 (1977).

[3]D. L. Jassby, Neutral-Beam-Driven Tokamak Fusion Reactors, Nuclear Fusion 17, 309 (1977) p. 324.

[4]D. J. Bender and J. D. Lee, The Potential for Fissile Breeding with the Fusion-Fission Hybrid Reactor, Trans Am. Nuclear Soc. 23, 24 (1976); also Lawrance Livermore Laboratory Report UCRL-77887 (1976).

VI. Some Characteristics of a Particular Tokamak Hybrid

A. Hybrid Design Point

In this section we describe the equilibrium and ideal MHD stability of the nominal hybrid plasma which were calculated using the Princeton Equilibrium[1] and Stability Codes (PEST).[2]

The poloidal field code system that supports the equilibrium is calculated following the procedure described in Section IV.C, and consists of a series of coils surrounding the plasma at a distance of 2 m from the plasma surface (0.5 m scrape-off + 1.5 m blanket and shield). The resultant field is uniform and slightly convex in the vicinity of the nominal magnetic axis R_o = 15.37 m but is strongly curved near the 'x' point. The poloidal flux contours of the equilibrium field are shown in Figure 1 with the corresponding coil positions and currents listed in Table I.

The plasma equilibrium configuration with parameters listed in Table II that is supported by this equilibrium field is shown in Figure 2. This equilibrium is stable to axisymmetric N = 0 modes, where N is the toroidal mode number, because of the shape of the equilibrium field, and is also stable to ideal and resistive local interchange modes.[3] However, it is marginally unstable to high N ballooning modes[4,5] and unstable to low N surface kink modes[6] according to ideal MHD theory. The projections of the displacements on a poloidal plane of an N = 1 kink mode and an N = 3 ballooning mode are shown in Figures 3 and 4 respectivel In practice the low pressure plasma outside the separatrix can be expected to provide significant passive stabilization of

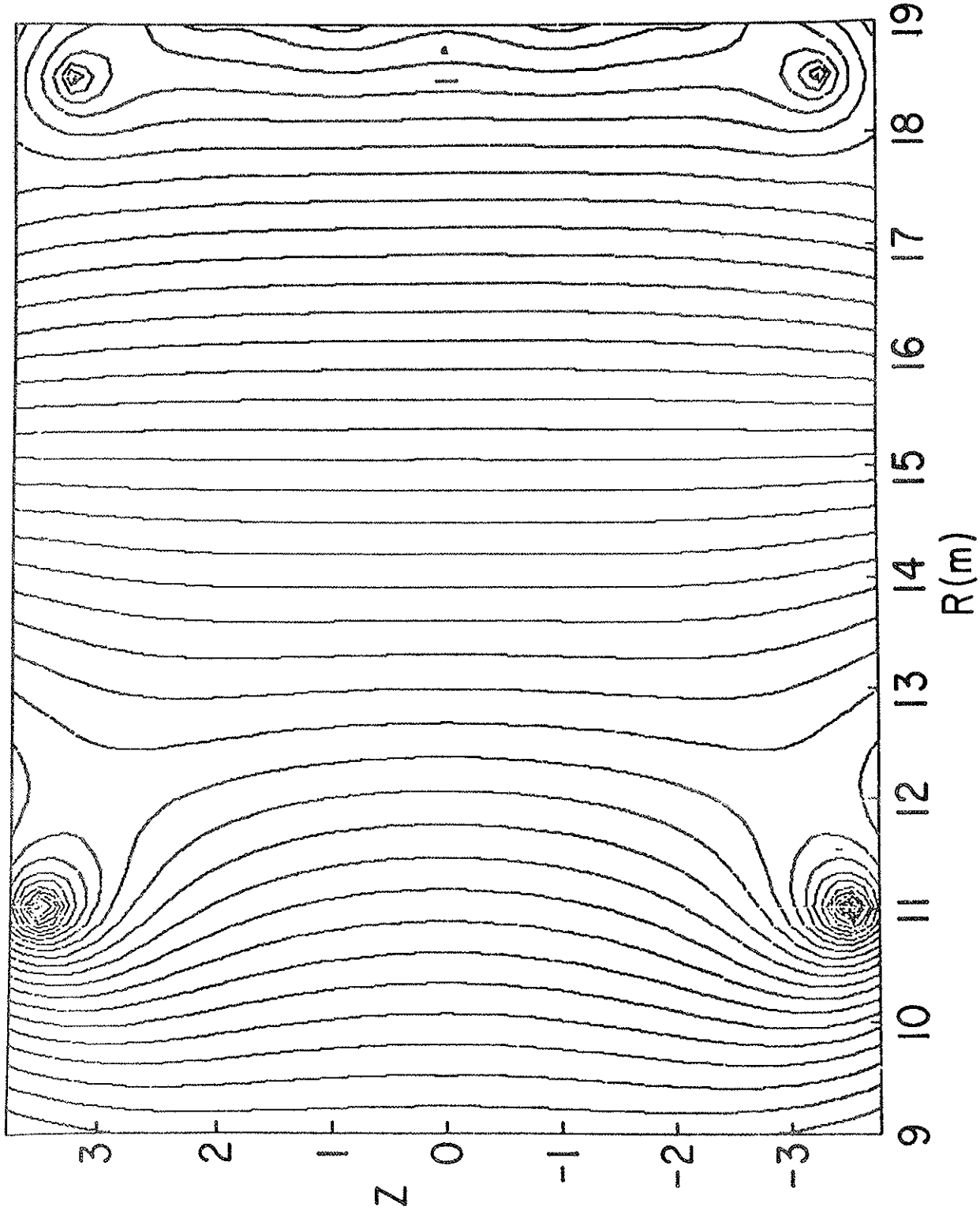

Fig. 1. Equilibrium Vacuum Magnetic Field

Table I.

Coil Pair	R(m)	Z(m)	I(MA)
1	11.00	± 3.50	-2.395
2	11.00	± 6.50	+2.395
3	13.50	± 5.00	-0.102
4	14.50	± 5.25	-0.289
5	15.50	± 5.25	-0.472
6	16.50	± 5.00	-0.627
7	17.50	± 4.50	-0.698
8	18.50	± 3.25	-0.542
9	19.25	± 2.25	-0.357
10	19.50	± 1.00	-0.801

Table II.

R_o	15.37 m
a	2.9 m
A	5.3
B_o	7.5 T
I	6.3 MA
P_o	1.05×10^6 Nm^{-2}
q_o	1.05
q_ℓ	5.77 (∞) (q) instead
$<\beta>$	1.11%
$<\beta^*>$	1.69%
$<\beta^\theta>$	3.39

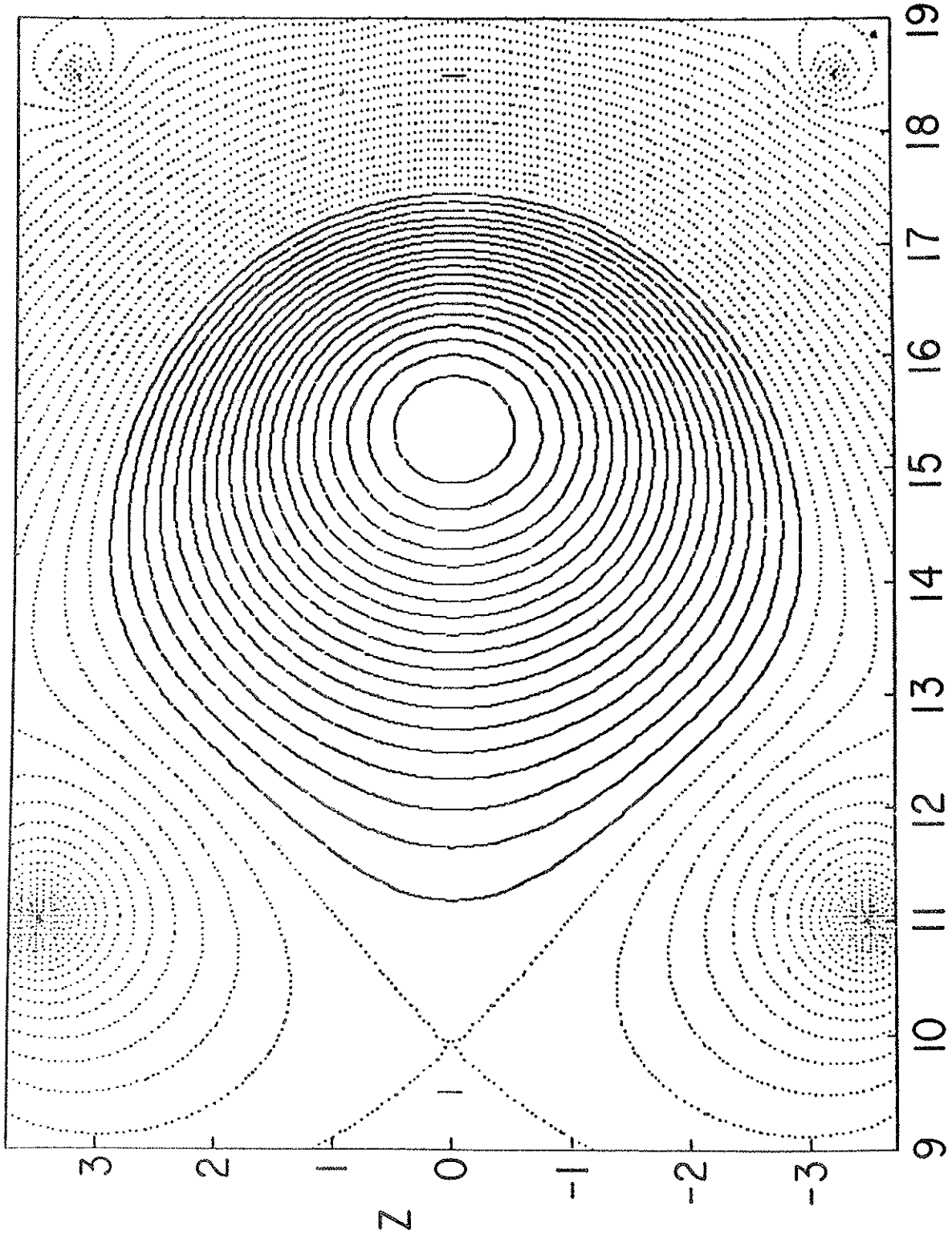

Fig. 2. Plasma Equilibrium Poloidal Magnetic Field, Vacuum Field plus Field Due to Plasma Currents.

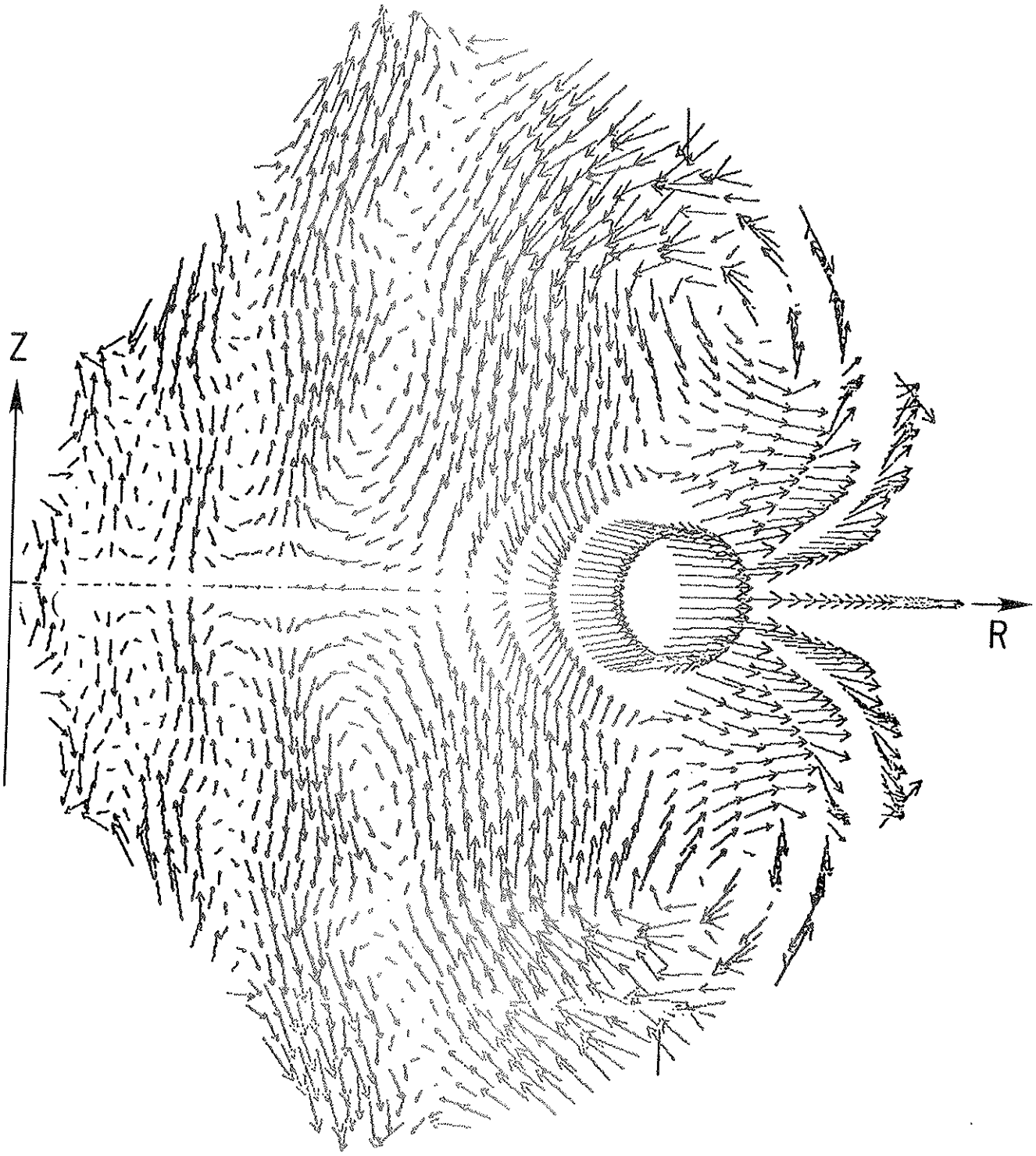

Fig. 3. Displacement Vector Field for N = 1 Kink Mode.

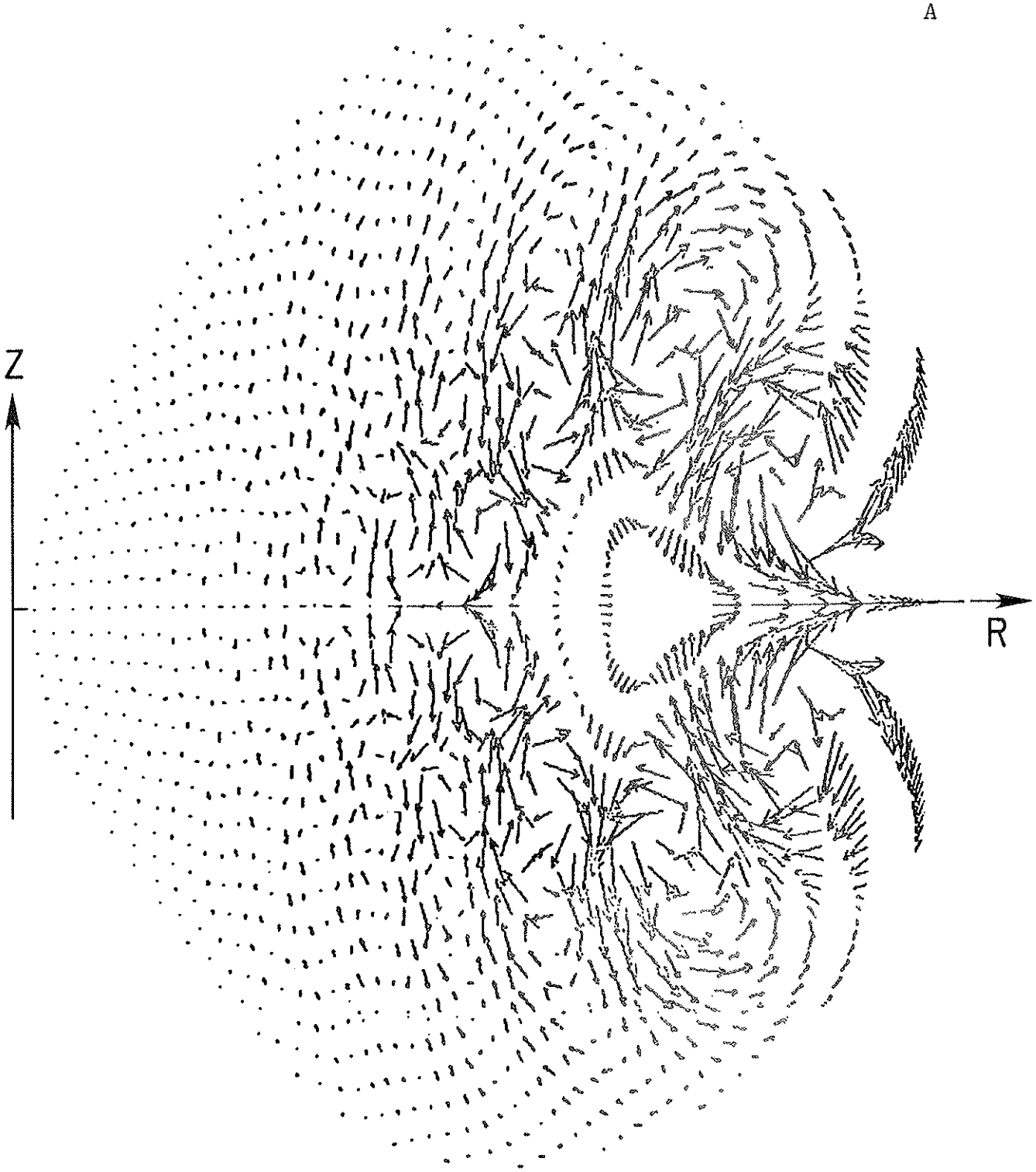

Fig. 4. Displacement Vector Field for N = 3 Ballooning Mode.

external kink modes.[7] Further, nonlinear effects and optimization of the pressure profile by anomalous transport driven by the instability can be expected to raise the critical beta for the onset of destructive ballooning instabilities. The destabilizing effect of resistivity on these modes has been shown to be slight,[8] and thus our choice for the parameters of the nominal hybrid are considered reasonable. Should a reduction in the average beta be necessary, we have also designed a $< \beta > \sim 0.5\%$ equilibrium configuration that is stable to all ideal MHD modes. The effect of this reduction in $< \beta >$ on the hybrid economics is discussed in Section V.

The overall poloidal plane cross section of the nominal hybrid equilibrium configuration is shown in Figure 1 of Section IV.C with the separatrix surface passing behind the blanket to the pumping region.

References

[1]J. L. Johnson, H. E. Dalhed, J. M. Greene, R. C. Grimm, Y. Y. Hsieh, S. C. Jardin, J. Manickam, M. Okabayashi, R. G. Storer, A. M. M. Todd, D. E. Voss and K. E. Weimer, Numerical Determination of Axisymmetric Toroidal Magnetohydrodynamic Equilibria, Princeton Plasma Physics Laboratory Report PPPL-1463 (1978); accepted for publication in J. Comp. Phys.

[2]R. C. Grimm, J. M. Greene, and J. L. Johnson, Computation of the Magnetohydrodynamic Spectrum in Axisymmetric Toroidal Confinement Systems, Methods in Computational Physics, J. Killeen, ed. (Academic Press, New York, 1976) Vol. 16, pp. 253-280.

[3]A. H. Glasser, J. M. Greene, and J. L. Johnson, Resistive Instabilities in General Toroidal Plasma Configurations, Phys. Fluids 18, 875 (1975).

[4]H. P. Furth, J. Killeen, M. N. Rosenbluth and B. Coppi, Stabilization by Shear and Negative V'', Proceedings of a Conference on Plasma Physics and Controlled Nuclear Fusion Research (International Atomic Energy Agency, Vienna, 1966) Vol. 1, pp. 103-126.

[5]A. M. M. Todd, M. S. Chance, J. M. Greene, R. C. Grimm, J. L. Johnson, and J. Manickam, Stability Limitations on High-Beta Tokamaks, Phys. Rev. Letters 38, 826 (1977).

[6]M. D. Kruskal, J. L. Johnson, M. B. Gottlieb, and L. M. Goldman, Hydromagnetic Instability in a Stellarator, Phys. Fluids 1, 421 (1958).

[7]A. M. M. Todd, J. Manickam, M. Okabayashi, M. S. Chance, R. C. Grimm, J. M. Greene, and J. L. Johnson, Dependence of Ideal MHD Kink and Ballooning Modes on Plasma Shape and Profiles in Tokamaks, Princeton Plasma Physics Laboratory Report PPPL-1470 (1978); submitted to Nuclear Fusion.

[8]A. H. Glasser, M. S. Chance, A. M. M. Todd, and J. M. Greene, Resistive Ballooning Modes in Tokamaks, Bull. Am. Phys. Soc. 23, 778 (1978).

B: Major Components

1. Fuel Handling Systems

a. Introduction

This chapter deals with the processing problems associated with the fuel flows in the Princeton Hybrid Power Plant. There are four principal fuel loops in this plant. As indicated in Figure 1 they are the primary fusion fuel loop, the uranium converter loop, the fission burner loop, and the neutron scavenger loop. In addition to these fuel loops there is a tritium recovery loop on the coolant helium system and an emergency tritium containment system for the nuclear island. Radioactive waste disposal facilities are included in the burner loop.

2. Primary Fusion Fuel Loop

Figure 2 shows the primary fusion fuel loop, comprising the neutral beam injectors, pellet injectors, reactor, divertors, vacuum pumps, fuel processing system, and fuel storage system. With the single exception of the neutral beam injectors these fuel handling elements are in many respects quite similar to the corresponding elements of the Princeton Reference Design (PRD).[1] The recycle fuel purification system, for example, is a small scale cryogenic fractional distillation system, somewhat larger but simpler than the PRD system because of the absence of argon in the exhaust from the reactor.

The beam injectors pose no special problems in fuel purification, but they present serious difficulties in gas handling because of the large flows that must be accommodated around the beams.

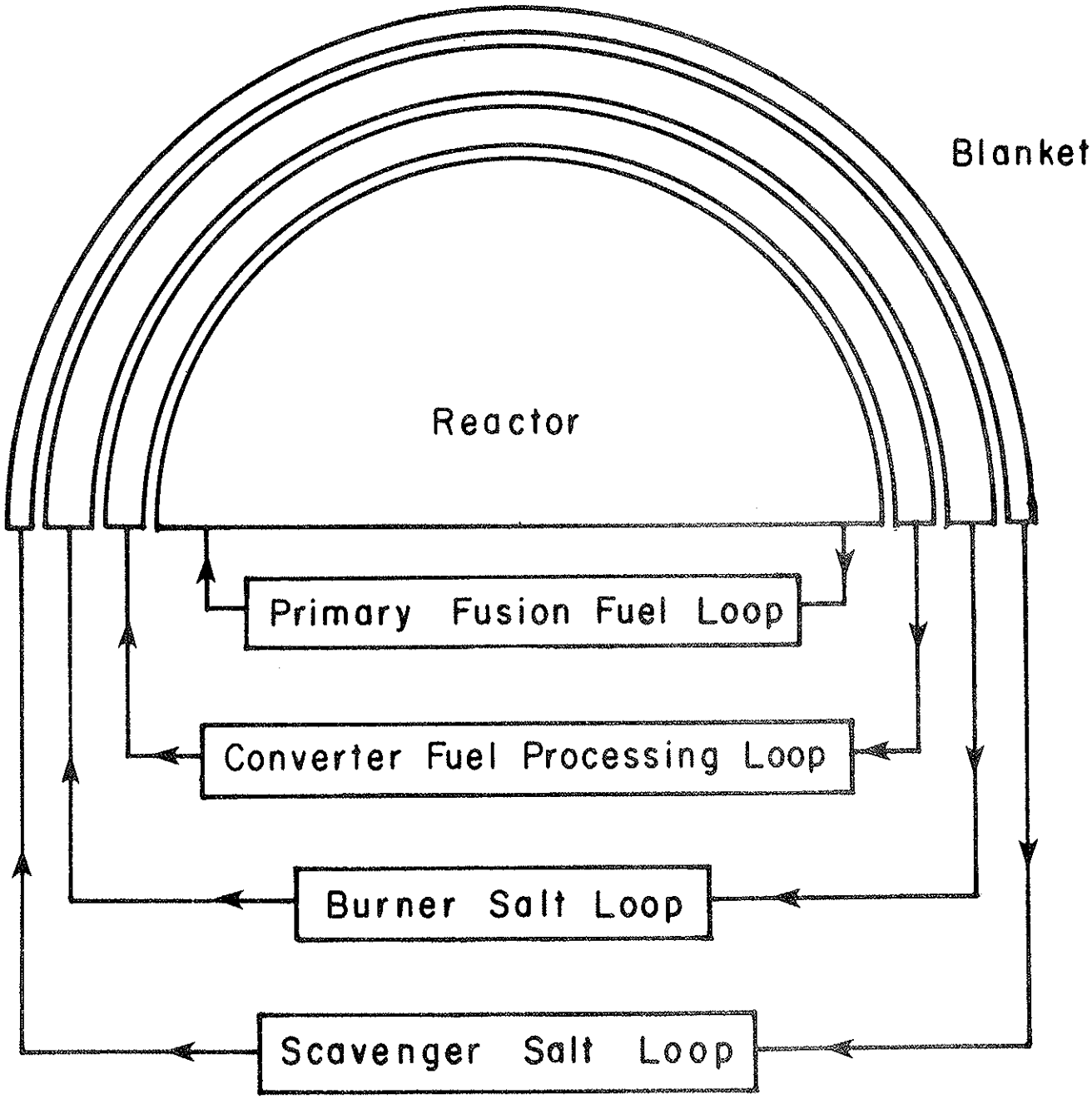

Fig. 1. Principal Fuel Loops.

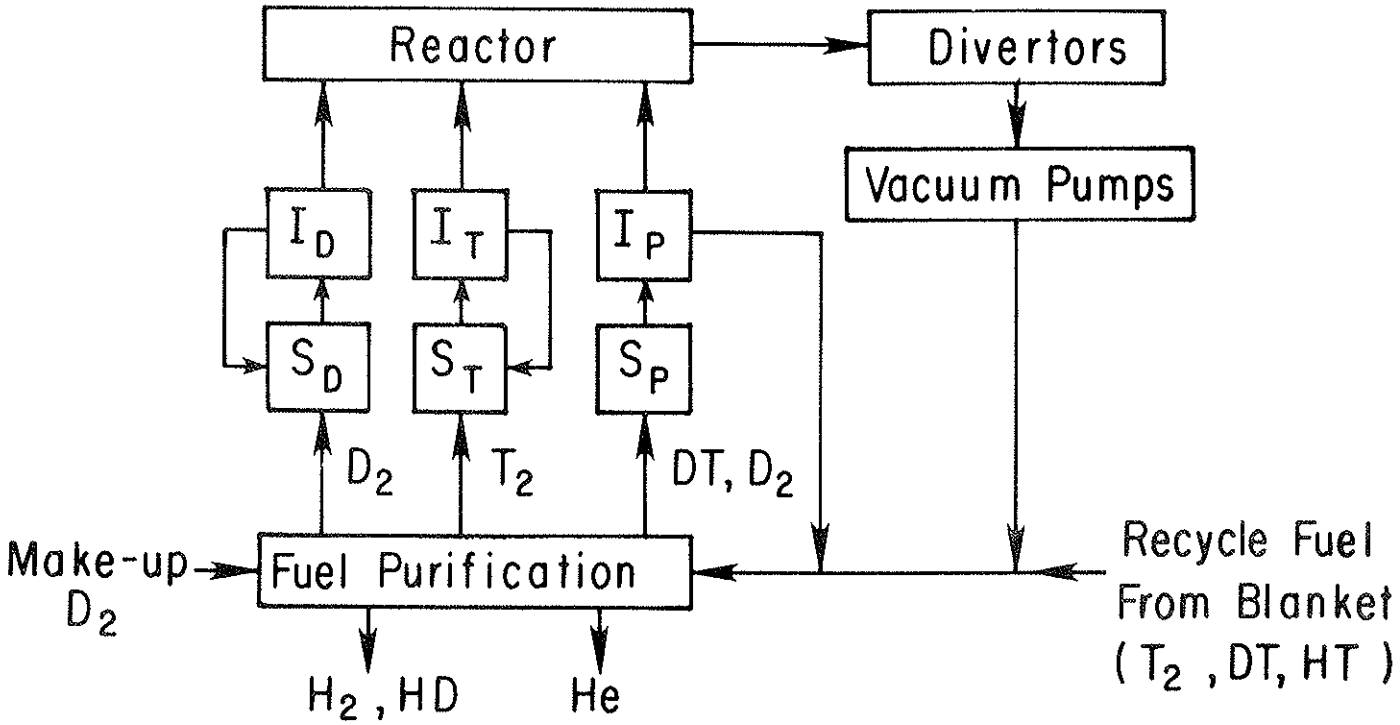

I = Injection

S = Storage

D = Deuterium

T = Tritium

P = Pellet

Fig. 2. Primary Fusion Fuel Loop.

As a conservative basis for analyzing the design we assume that ten atoms of fuel species will have to be circulated around the beam injections for every atom injected into the reactor torus.[2]

Since the neutral beam injectors provide only 12% of the total fuel flow to the reactor, pellet injectors must make up the balance. It is possible that the fuel flux in the reactor can be sustained in large measure through internal recycle of the plasma off the reactor walls, but it is likely that the maintenance of this recycle would still require a considerable external recycle through the divertors. We shall make the conservative assumption that the requisite plasma density and residence time must be supported by external recycle of the fuel. Table I summarizes the typical mass rates.

The reactor exhaust will also contain some protium and small amounts of high-Z elements. Approximately 0.6 g protium is produced for every kilogram of helium formed from fusion reactions. Some modest amounts of protium might be allowed to accumulate in the primary fusion fuel loop, thereby simplifying the fuel purification steps and related tritium control in the ultimate reaction ash (protium plus helium). The economic tradeoff with this simplification would be the increased cost of running inert materials through the reactor and the primary cycle.

a. Neutral Beam Injectors

Equal numbers of deuterium and tritium ions are injected to the reactor in separate neutral beam injectors comprising two beam lines for each species with perhaps five ion guns per line.

Table I. Typical Flows in Primary Fuel Loop (kg/d)

	Deuterium	Tritium	Helium	Total
Neutral Beams				
Net injection to reactor	0.71	1.06	-	1.77
Recycle around lines	7.07	10.60	-	17.67
Pellet Injection	5.86	8.78	-	14.64
Reactor Exhaust	6.50	9.75	0.13	16.38
Reactor Burn-up	0.07	0.10	-	0.17

The separate injection is necessary to ensure equal penetration of the two species into the plasma.

Backstreaming of ions from the plasma in the reactor into the injectors occurs at a rate equal to about 0.5% of the injection rate.[2] As a result the average composition of the injection beams will be 0.9976 atom fraction D and T in the tritium and deuterium beams respectively. Thus the deuterium beams are appreciably contaminated with tritium, but a large holdup in their recycle systems would involve a relatively small tritium inventory. For example, if the pumps on the deuterium beam lines were regenerated only once per day, the tritium holdup would be 7.07 (1.0 - 0.9976) 3.019/2.014 = 0.0254 kg.

On the other hand, large holdups in the recycle systems on the tritium beam lines could not be tolerated. The cryosorption panels necessary for pumping the large gas flows to sustain the beams must be regenerated on a frequency not less than several times per day. Even at 12 cycles per day the tritium inventory on the panels would approximate 10.6/12 = 0.88 kg, and, if we maintain a feed reserve equivalent to four hours operation, the total inventory requirement would be 10.6 (4)/24 + 0.88 = 2.65 kg.

This large tritium inventory could be avoided by injecting only deuterium via the neutral beams. However, this saving would come at the expense of a correspondingly higher tritium recycle in the pellet injectors to maintain a sufficiently high tritium concentration in the reactor for adequate fusion. If we assume the tritium rate via pellet injection must be increased by 50%, the incremental increase in tritium inventory for the same regeneration rate and same fuel reserve would be 0.5 (9.75) (1/12 +

4/24) = 1.22 kg compared with 3.65 kg when tritium is injected by neutral beams and by pellet.

b. Pellet Injectors

The pellet injectors are presumed to be similar to those proposed for the PRD with the simplification that argon need not be incorporated in the pellets. Recent experiments[3] suggest that pellet injection is not an unreasonable fueling mode.

c. Reactor Exhaust

We assume that the divertors will be pumped either by mercury diffusion pumps as in the PRD or by cryosorption pumps.[4] The latter have the advantage of simplicity and a sealed configuration assuring tight control of tritium, but their cyclic regeneration results in a relatively high average tritium inventory retained on the cryopanels during normal operation. The final choice of pump will depend on a detailed economic analysis.

Since the hybrid machine does not employ argon in its plasma, the cooling of the plasma in the divertors and beyond is more difficult than in the PRD. Furthermore the gas flows are more than fourfold greater than those in the PRD. We assume these flows and their cooling, with appropriate ducting to control neutron streaming, can be accommodated without undue compromise of structures and pump loads, but these problems have not been addressed formally.

d. Tritium Inventory

The tritium inventories in regions of the hybrid plant outside of the primary fusion fuel loop are quite small. Table II summarizes the likely inventories for the entire plant. Cryosorption pumps are assumed to be used for the neutral beams and the reactor exhaust with 12 regenerations per day in the tritium beam

Table II. Overall Tritium Inventories in Hybrid Plant

Primary Fusion Fuel Loop				5.94 kg
Cryopumps			1.72 kg	
Neutral Beams		0.91 kg		
D Beam	0.03 kg			
T Beam	0.88			
Reactor Exhaust		0.81		
Fuel Reserves (4 hr.)			3.40	
Neutral Beams		1.76		
Pellet Injectors		1.64		
Purification System (2 hour cycle)			0.82	
Dissolved in Structure				0.03
Blankets				0.04
Tritium Recovery Sytem (8 hour cycle)			0.03	
Dissolved in Salts			0.01	
Total				6.01 kg

pumps and the vacuum pumps on the divertors.

3. Uranium Converter Loop

We assume that the uranium cannisters in the converter region of the reactor blanket will be recycled at an average residence time in the blanket of one year and that the hot cannisters will be reprocessed off site at relatively large scale, fully automated facilities. While it is difficult to estimate reliably the likely cost for this reprocessing, Hammond[5] has observed that the cost, which was as low as $30/kg material processed in the early 1970's, might be expected to run as high as $200-300 in the early 1980's.

If we assume that the typical cost in 1978 dollars is $100/kg including the cost of handling the cannisters at the plant and shipping them, the total annual cost for recovering plutonium from a uranium inventory of 1.66×10^6 kg in the converter would be $166M. The corresponding unit reprocessing cost per gram of plutonium recovered based on an annual make of 1000 kg would be $166.

This cost scales inversely with the average residence time of a cannister in the blanket. For two years residence the cost would be $83/g plutonium, provided the more heavily converted uranium did not result in more difficult reprocessing. As noted by Metz,[6] highly converted fuels, as would obtain in breeder reactors, are harder to dissolve initially in nitric acid and because of their higher radioactivity cause more rapid degradation of the Purex process solvent tributyl phosphate. Thus the unit reprocessing cost for longer residence times probably would be somewhat higher, but well within the range of values considered in this study (Section IV.E.4.d).

4. Burner Loop

Because of fission reactions the burner loop poses difficult fuel handling problems.

In the burner loop plutonium in the form of the trifluoride dissolved in molten lithium beryllium fluoride undergoes fission. At the same time tritium is bred from the transmutation of lithium-6 and lithium-7. Fission wastes and corrosion products must be removed before they can have adverse effects on fission rates, and the tritium must be recovered essentially in toto and efficiently. A simplified flow diagram for the burner loop is shown in Figure 3.

a. Tritium Recovery

For the bulk of the tritium recovery we propose to take advantage of the tendency for tritium to permeate the walls of the heat exchange tubes in the reactor blanket. In the presence of plutonium trifluoride it should be possible to maintain tritium principally in the form of T_2 with relatively little TF. By allowing the tritium pressure to rise above 10^{-4} atm the normal permeation rate of tritium through the cooling tube walls and into the coolant helium should equal the production rate of tritium in the breeder salt.

Once the tritium enters the coolant helium it is oxidized to water by low pressure oxygen in the helium, probably aided by catalyst beds to ensure complete oxidation. As indicated in Figure 4 the tritiated water is removed continuously from the helium by mole sieve adsorbers operated cyclically. Periodic regeneration of the adsorber beds by heating them to 260°C under vacuum permits complete recovery of the tritium. The evolved

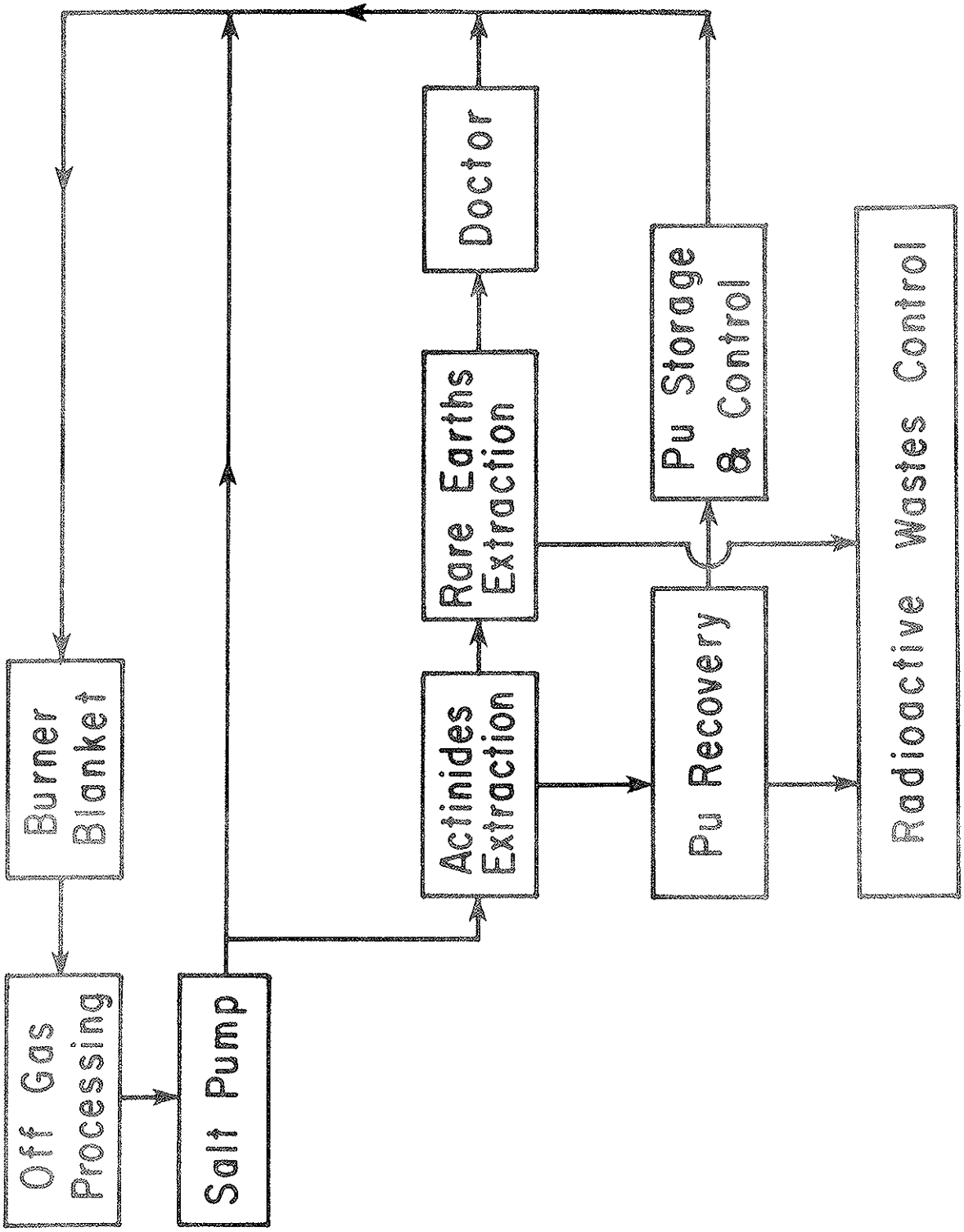

Fig. 3. Burner Salt Loop.

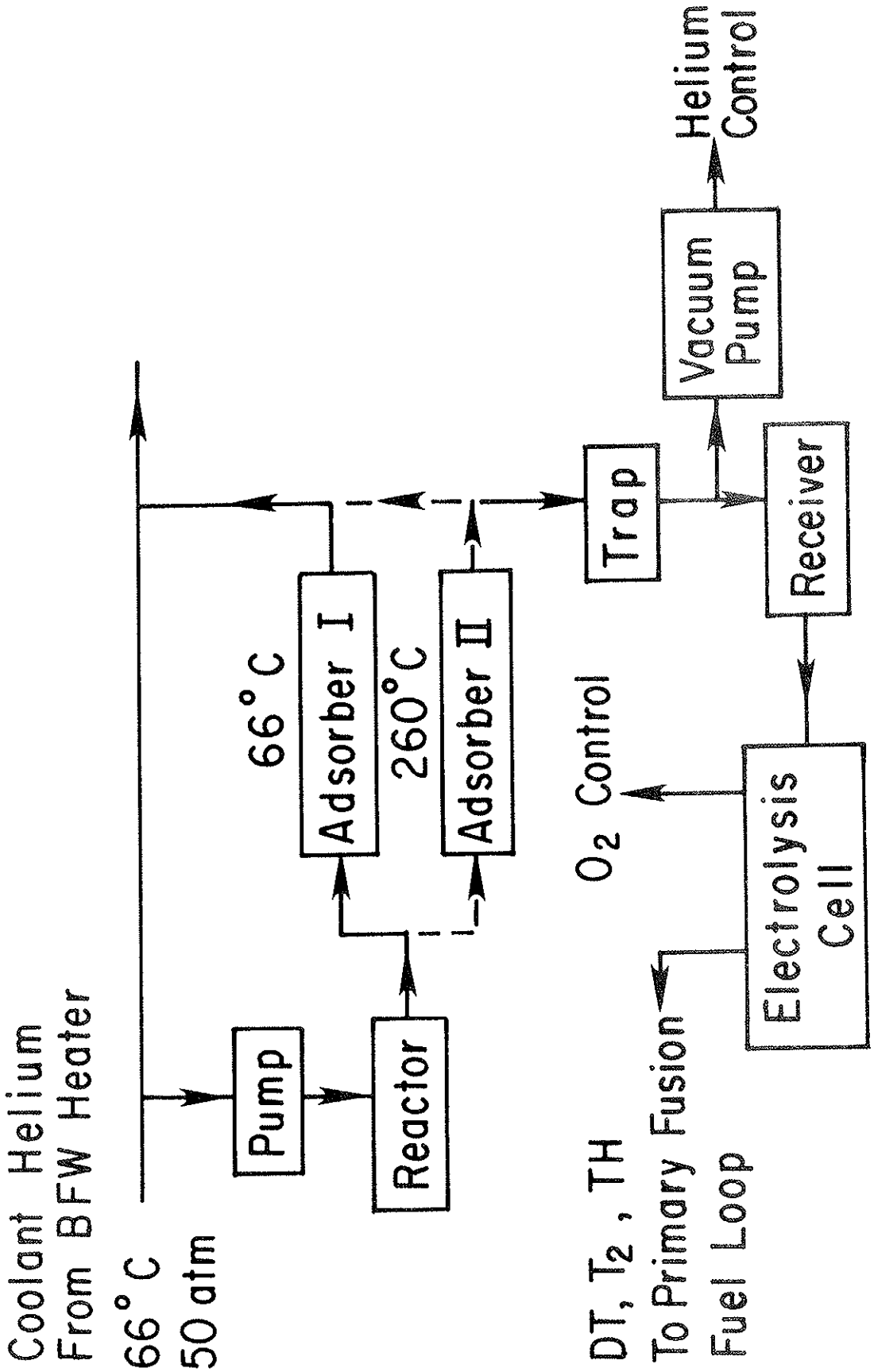

Fig. 4. Coolant Helium Loop.

water is frozen out in cold traps and subsequently passed to cells for electrolysis to molecular tritium and oxygen. This operation is similar to that proposed for the PRD.

Under steady operating conditions the equilibrium vapor pressure of molecular tritium above the blanket salt will rise to a level such that the losses of tritium from the salt, either through permeation into the coolant helium or through escape in the off gases routinely removed from the blanket, will just equal the tritium production in the salt. Given the uncertainties in estimating permeation rates, the steady state tritium pressure would probably lie in the range 10^{-2} to 10^{-4} atm. At these pressures some tritium, possibly as much as ten percent of the tritium make, will go out with the off gas and have to be recovered.

b. Off Gas Processing

In addition to helium, T_2, and TF from the tritium breeding, the blanket salt will contain gaseous fission products and gaseous corrosion products including xenon, krypton, TI and possibly TBr. Although the production rates for these latter species are very low, totaling less than 0.02 kg mole per day based on estimates for the Molten Salt Breeder Reactor (MSBR),[7] they must be maintained at very low concentrations, especially the xenon, to avoid adverse parasitic effect on the blanket neutron economy. In the MSBR these gases are sparged from the salt with a small helium stream.

For the hybrid plant we propose that the salt be saturated with helium at slightly less than one atmosphere in a packed column scrubber. Molten salt flows through the scrubber at rates consonant with the rates required for heat transfer in the blanket.

Helium is drawn from the top of the scrubber at rates sufficient to remove the net helium production in the blanket and carry off xenon and other contaminants. As indicated in Figure 5 this low helium flow is treated with fluorine gas before cooling to burn any molecular tritium to tritium fluoride and convert all other tritium halides to tritium fluoride. The gas is then cooled to knock out any salt vapor, then subcooled to liquid nitrogen temperatures to crystallize out the TF, and finally passed through adsorbers to remove the gaseous fission wastes. The relatively clean helium is recycled to the scrubber.

Much of the process and equipment for treating the off gas from the salt is similar in size and nature to that proposed for the MSBR. The principal difference arises from the need to recover the tritium in the gas. In the MSBR the tritium, produced in very small amount, is removed but not recovered.

c. Fission Wastes in Salt

Although the production of fission wastes in the burner loop is at a very low rate, approximately 6.6 kg/day, they should not accumulate in the salt to concentrations much higher than a few percent of the plutonium concentration. These wastes will include some heavy isotopes arising from neutron capture by the plutonium together with the fission products comprising some eighty species with mass numbers ranging from 72 to 160.

The separation of these different species from the blanket salt requires a number of process steps, probably including selective reductions to metals followed by liquid-liquid solvent extractions with both liquid metal (bismuth) and molten salts (lithium chloride) as solvents. For the purpose of this study we

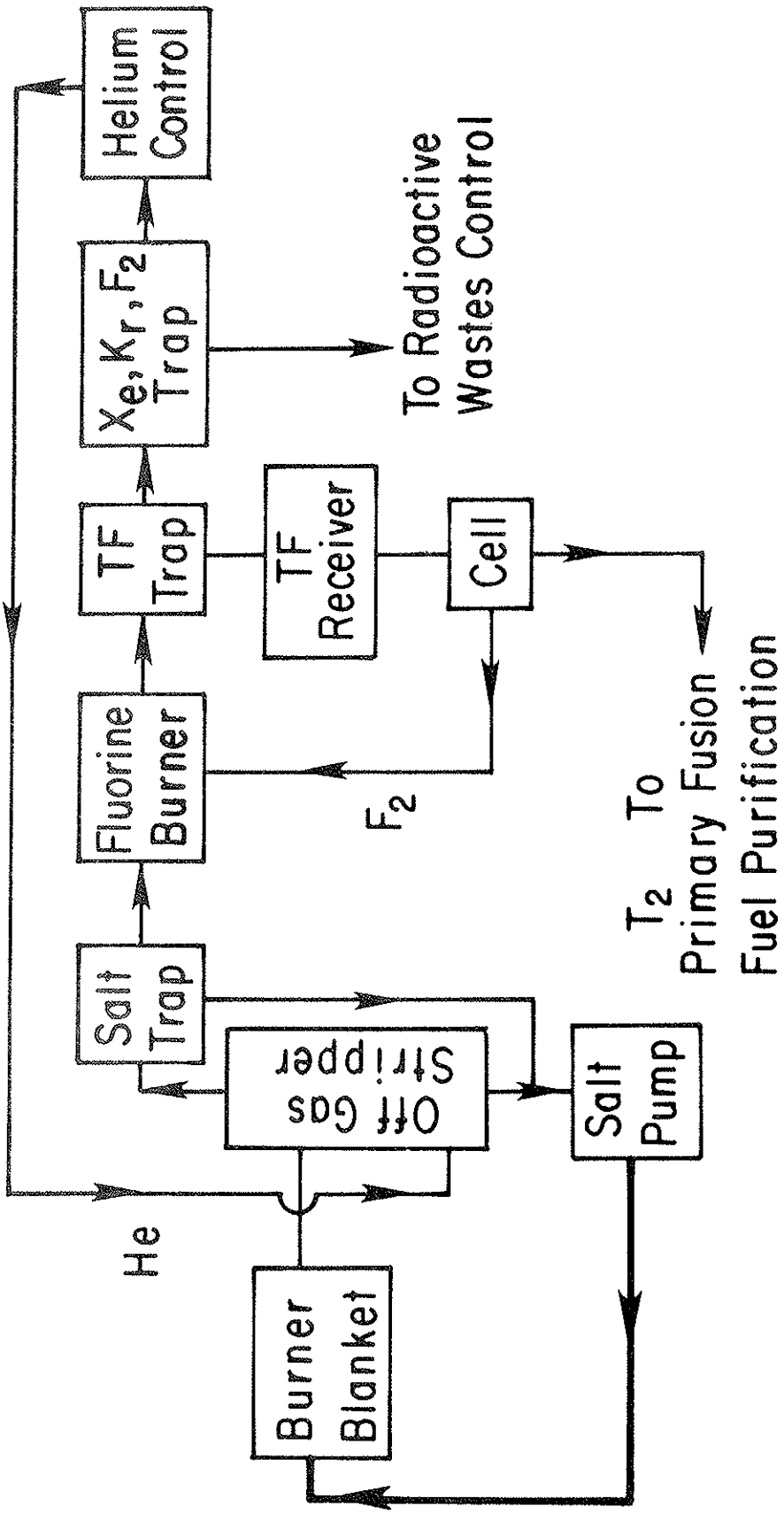

Fig. 5. Burner Salt Loop Offgas Processing System.

shall assume that the processing sequences developed for the MSBR are of the same order of complexity as those required for the hybrid machine, and hence the costs for the MSBR, properly adjusted for scale and time, are reasonably applicable. This assumption is probably conservative because the hybrid system does not have the problem of rapid removal of protactinium as is required for the thorium cycle of the MSBR.

Carter, Nicholson and McNeese[8] estimated the total plant investment for the salt processing system for a 1000 ME(e) MSBR at $35.6M in 1961 dollars assuming that molybdenum is used to contain the bismuth solvent system. They also estimated that the investment would scale as the 0.28 power of the processing rate. McNeese[9] estimated that the plant investment could be reduced to $25M if stainless steel were used in place of the molybdenum.

The electric energy production attributable to fission in the hybrid machine is approximately 3.0 GW(e) gross (9.85)/(1 + 9.85) = 2.72 GW. Taking the inflation rate at 6% and using the above scaling law, the corresponding plant investment for the hybrid salt processing system in 1978 dollars would be $\$25M\ (2.72/2)^{0.28}\ e^{0.06\ (7)} = \$50.4M$.

If this processing plant is depreciated over a period of ten years and the fixed charges comprise the principal cost component, the total operating costs might run $6M per year.

The above costs are believed to be moderately conservative and would include tritium recovery and radioactive wastes disposal. As pointed out in Section IV.E.4.e they contribute negligibly to the unit power cost.

5. Scavenger Loop

As shown in Figure 6 the only processing elements in the scavenger loop are a degasser to take out helium and tritium, probably continuously, and a salt doctor operating intermittently to control the buildup of impurities in the salt.

By maintaining small surfaces of metallic beryllium in contact with the salt in the blanket, the ratio of molecular tritium to tritium fluoride in the salt can be kept high enough to ensure that most of the tritium production in the scavenger permeates into the coolant helium in the blanket. Small amounts of molecular tritium and tritium fluoride will come off the stripping tower along with all the helium production. As in the burner loop the offgas will be burned with fluorine to convert the tritium to tritium fluoride so that it can be recovered readily by condensation for subsequent regeneration.

The likely investment in processing facilities and the related operating costs for this loop should be quite modest. We assume they are reasonably accommodated in the above costs for the burner loop processing system.

6. Tritium Containment and Control

The hybrid power plant, like all fusion power plants based on the deuterium-tritium fuel cycle, has a considerable investment in features for routine and emergency containment of tritium. These features include appropriate jacketing of lines and vessels, shrouds on valves, and the like, all with helium purges. For emergencies the nuclear island must be fully isolated from the atmosphere and equipped with catalytic oxidizers and mole

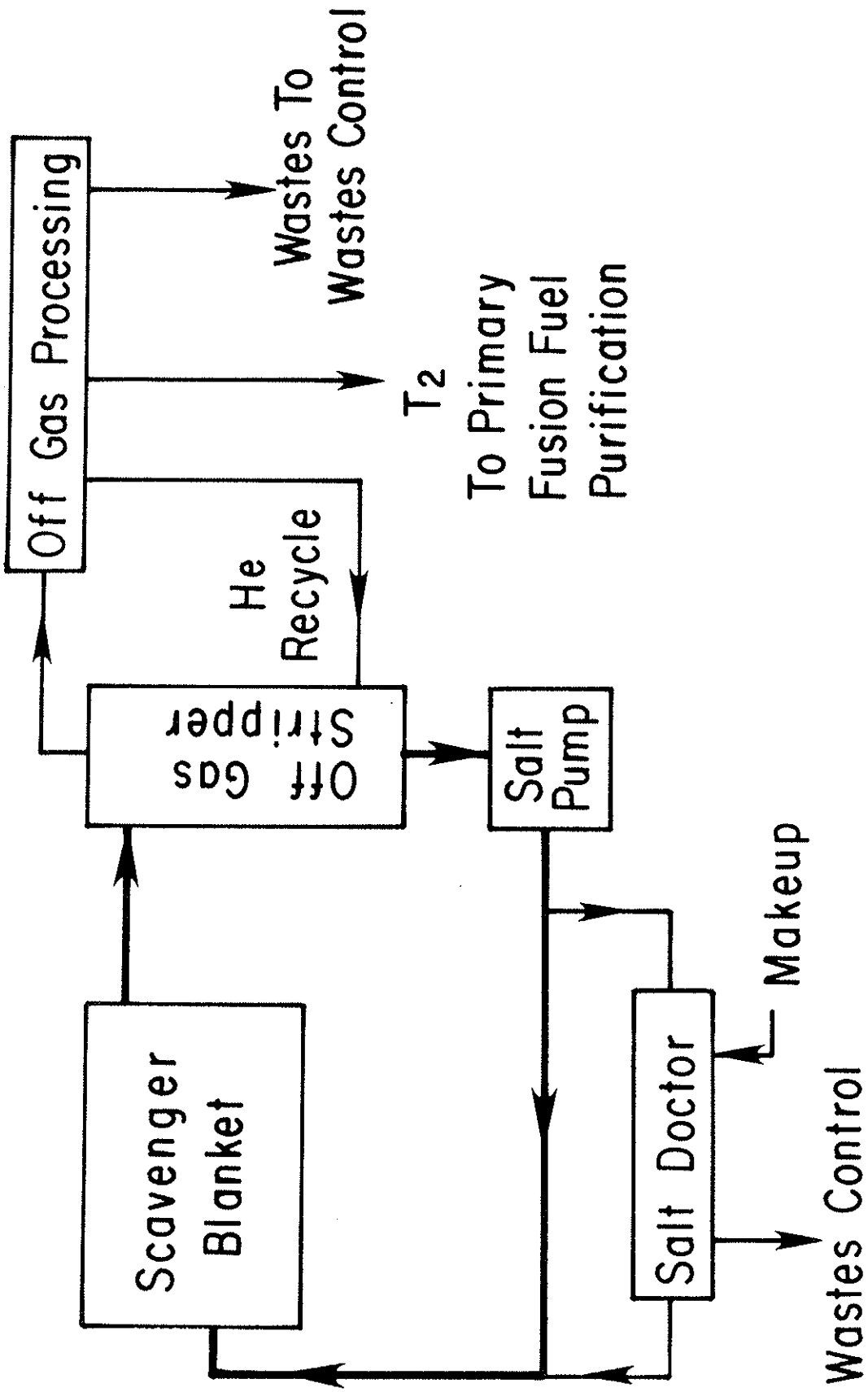

Fig. 6. Scavenger Loop.

sieve adsorbers to convert any tritium releases to water and trap it entirely.

Hickman[10] reports that cost studies for a proposed fusion engineering research facility employing a driven tokamak machine without tritium breeding would require something like $20M capital expenditure for tritium containment safety. We may assume the corresponding costs for the hybrid machine could be no less.

7. Radioactive Wastes Disposal

Because of the fission processes occurring in the blanket of the hybrid there is a serious problem of wastes disposal. We have not dealt with this problem in this study beyond assuming that the likely costs are included in our estimates of the costs of processing the salt in the burner loop.

References

[1]A Fusion Power Plant, R. G. Mills, ed., Princeton Plasma Physics Laboratory Report MATT-1050 (1974).

[2]TFTR Neutral Beam Systems Conceptual Design, TFTR Final Conceptual Design Report, Vol. 5, Oak Ridge National Laboratory Report ORNL-CF-75-9-15 (1975).

[3]C. A. Foster, Production of Uniform Micropellets of Hydrogen and Hydrogen Pellet Injection on ORMAK, Ph.D. Thesis, University of Illinois (1977); as described in Fusion Forefront 10, 6 (1977).

[4]P. W. Fisher and J. S. Watson, Cryosorption Vacuum Pumping of Deuterium, Helium and Hydrogen at 4.2 K for CTR Applications, Transactions of the American Nuclear Society 1976 Winter Meeting (American Nuclear Society, Hinsdale, Illinois, 1976) Vol. 24, pp. 501-502.

[5]A. L. Hammond, Nuclear Proliferation I, Science 193, 126 (1976).

[6]W. D. Metz, Reprocessing: How Necessary Is It for the Near Term?, Science 196, 32 (1977).

[7]Ebasco Services, Inc., 1000 MW(e) Molten Salt Breeder Reactor Conceptual Design Study, Final Report Task 1, Ebasco Services, Inc., New York, New York, February 1972.

[8]W. L. Carter, E. L. Nicholson, L. E. McNeese, Cost Estimate for an MSBR Processing Plant, Molten Salt Reactor Program, Semi-Annual Progress Report for Period Ending 31 August 1972, Oak Ridge National Laboratory Report ORNL-4782 (1972) pp. 189-183.

[9]L. E. McNeese, private communication 1976.

[10]R. G. Hickman, Tritium in Nuclear Fusion Power, Lawrence Livermore Laboratory Report UCRL-75546 (1974).

2. Reference Blanket

a. Physical Description

As a result of the initial scoping studies of the hybrid conceptual blanket, a particular combination of dimensions and compositions was chosen for analysis as the "Reference Blanket". Please note that this is not the "Nominal Hybrid" selected from the output of the systems optimization; in order to carry out all the desired calculations the model had to be frozen before the systems code was fully operational. Furthermore, this is not a blanket that is exactly representable by the nominal blanket model in the systems code; that model was based on the reference blanket (and variations), but using the simplified parameterization requires a certain license in representation of the more exact results.

The dimensions and composition of the reference blanket are illustrated in Figure 1. Facing the plasma is a radiation shield wall occupying (but not fully) a region 5 cm thick. Behind this is the 15 cm thick multiplier region. The burner region is 50 cm thick overall, with graphite for moderation in the middle 30 cm. Behind this is the scavenger region, 15 cm thick. The shield begins with a 15 cm layer of steel, and continues with alternating 10 cm layers of boron carbide and steel. Most of the analyses of this blanket were performed with the one-dimensional cylindrical approximation usually applied to tokamaks. Only region-averaged homogenized material compositions are required for this type of analysis.

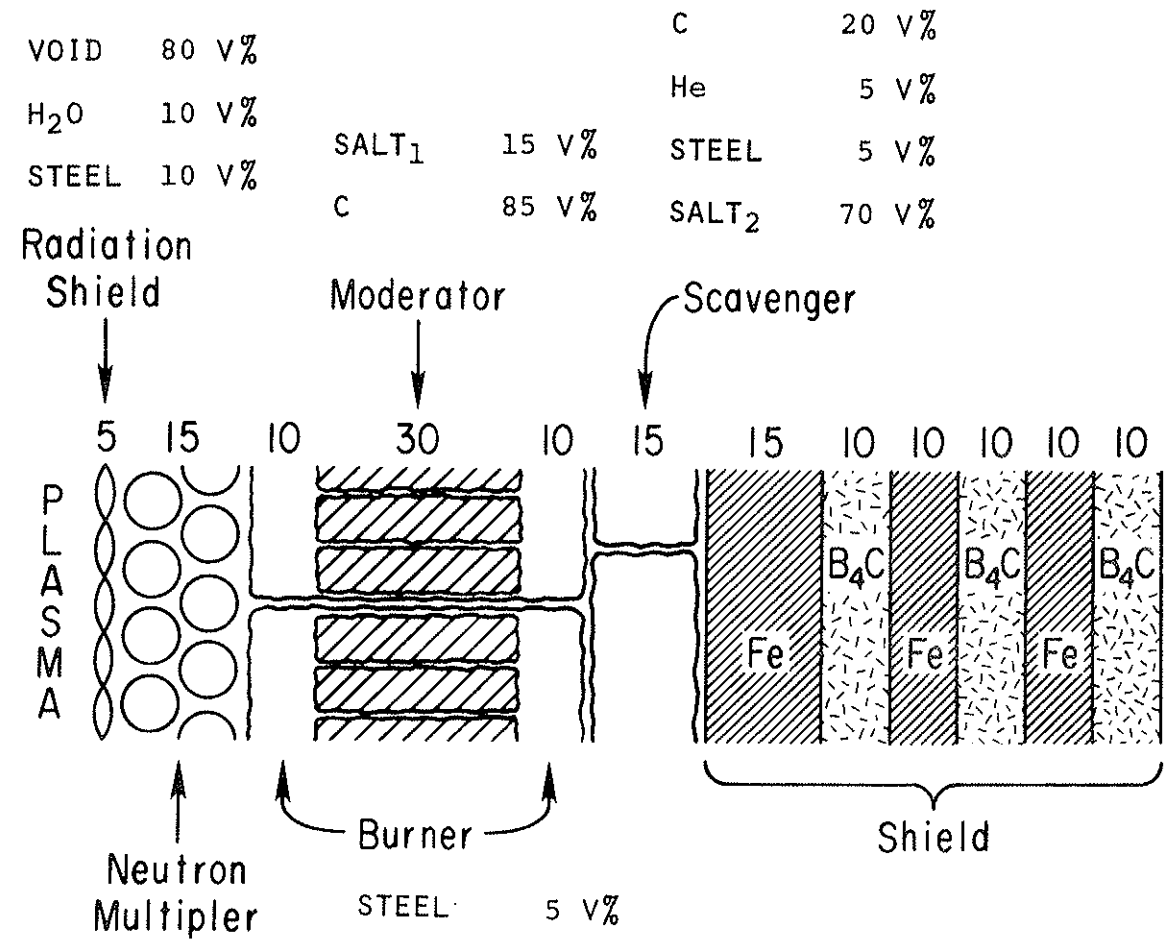

VOID 16 V%
STEEL 8 V%
He 32 V%
U-MO 44 V%
7 W%
93 W%
(0.3 a% U-235)

STEEL 5 V%
He 15 V%
$SALT_1$ 80 V%

$SALT_1$: BeF_2 52 m%;
LiF 47.75 m%; 0.10 a% Li-6
PuF_3 0.25 m%;

$SALT_2$: BeF_2 52 m%;
LiF 48. m%; 15.0 a% Li-6

Fig. 1. Schematic Diagram of Reference Blanket.

The radiation shield region is assumed to be 80% void (by volume, of course), 10% steel, and 10% water. The choice of water as a coolant is discussed below in the section on thermal-mechanical design, as is the double shell wall which justifies these volume fractions.

In the multiplier region the U-7 Mo fuel is assumed to occupy 44% of the volume. (Uranium depleted to 0.3% in U-235 is specified.) In addition, the steel of the pressure tubes takes 8% and the helium coolant 32%. (However the helium is lumped with the 16% void and ignored.) These values are based upon the use of 80 mm OD pressure tubes with 2 mm walls, and fuel in the form of hollow cylinders with 62 mm OD and 22 mm ID.

The burner consists of three sub-regions. The middle one is 85% graphite (in blocks with channels) and 15% salt. The outer regions are 80% salt, with allowances of 15% for the helium coolant and 5% for structural steel. The salt in this region is flibe near the eutectic: 52 mole % BeF_e and 47.75% LiF, with a fissile loading of 0.25% PuF_3. According to Ref. 1, the solubility of plutonium trifluoride in $(LiF)_2$-BeF_2 is given in mole percent by log S = 3.2305 - 3096 K/T. At 550°C, this would allow a loading of 0.294%. In order to suppress the competition for thermal neutrons, which would require an increase in the plutonium density, the lithium is assumed to be depleted to only 0.1% in lithium-6.

The scavenger region is designed as a kind of pre-shield, to absorb most of the neutrons leaking out of the multiplier. It is composed of 70% salt, 20% graphite, 5% helium, and 5% steel. Here the salt is 52% BeF_2 and 48% LiF, enriched to 15% in lithium-6. The lithium from the scavenger and that from the burner would, if

mixed, have approximately the natural ratio of isotopes. Thus a dedicated separation plant could prepare a head enrichment for the scavenger and tails for the burner, with no net reject stream.

The steel used in all blanket regions is taken to be SS-316 at 7.75 Mg/m^3, with the following nominal composition: 64 Fe, 18 Cr, 14 Ni, 2 Mn, and 2 Mo (weight percent). The water in the first wall is assumed to have a density of 0.9584 Mg/m^3 (i.e. a temperature of 100°C); the density of graphite is assumed to be 2. Mg/m^3. The multiplier fuel is specified as 7% Mo - 93% U (by weight) at 18. Mg/m^3. The densities of the two salts were calculated by addition of fractional molar volumes from the following data: BeF_2 - 24.20; LiF - 13.77; PuF_3 - 32.08 (cm^3/mole). Implied densities are 1.9589 Mg/m^3 for the burner salt and 1.9297 Mg/m^3 for the scavenger.

b. Neutronic Performance

As mentioned above, the reference blanket has been analyzed in an infinite one-dimensional approximation. Thus the following results are nominal values, comparable to those quoted in other tokamak conceptual design studies. It was not felt to be worthwhile to perform more exact (more expensive) calculations for an as-yet ill-defined hybrid.

Calculations were performed with the PPL-ANISN code,[2] version of the widely used ANISN one-dimensional discrete-ordinated transport code[3] modified principally in the input and output stages. Table I gives the spatial mesh of 75 intervals used to describe the blanket. A P-3 Legendre scattering expansion and the symmetric S-8 angular quadrature were used to complete the discretization. The fusion neutron source was uniformly distributed in the cylinder of radius less than 200 cm.

Table I. Spatial mesh used for the reference blanket

Zone	Material	Left Radius	Interval widths
1	Plasma	0.0 cm	200, 50
2	Wall	250.	2, 2, 1
3	Multiplier	255.	15 @ 1
4	Burner	270.	10 @ 1
5	Moderator	280.	15 @ 2
6	Burner	310.	10 @ 1
7	Scavenger	320.	10 @ 1.5
8	Shield	335.	10 @ 2
	Void	355.	

Transport cross section were taken from the DLC-2F data set distributed by the Radiation Shielding Information Center (RSIC). The data in this library were derived from the national evaluated nuclear data file ENDF/B-III. (The data for U-238 were amended to include cross sections for the n-3n reaction.) To reduce the cost of computation to the available resources, the 100-group DLC-2 cross sections were further collapsed to the 30-group structure described in Table II. The boundaries of this structure were chosen with an eye to the principal modes of transport expected and the reactions (and thresholds) of major interest. The spectrum from a preliminary blanket similar to the reference was used as the weighting function for the group collapsing code.[4]

Figure 2 shows a perspective plot of the scalar flux as a function of energy and position in the blanket. Note the steady attenuation of the top group, compared to the flux below 2 MeV. The former is due to removal of the fusion neutrons, while the latter results from the large number of fissions in the burner salt regions. The dips in groups 23 (23-61 eV) and 25 (3-8 eV) at the multiplier-burner interface are due to the strong resonance absorption of the U-238. In anticipation of this effect, the effective capture cross sections for U-238 used in these calculations were scaled down from the infinite-dilution values given in DLC-2, using self-shielding factors derived from a preliminary version of the DLC-41/VITAMIN-C library. (The whole uranium file from DLC-41 was not used because: a) it was derived from ENDF/B-IV, and therefore inconsistent with the DLC-2 data; and b) the library was only released in preliminary form for review,

Table II. Energy Structure of the 30-Group Neutron Cross Section Library.

Group #	Upper Energy	Lethargy Width	Group #	Upper Energy	Lethargy Width
1	14.918 MeV	.1	16	302.0 keV	1.0
2	13.499	.1	17	111.1	1.5
3	12.214	.1	18	24.79	1.5
4	11.052	.1	19	5.53	1.5
5	10.	.1	20	1.234	1.
6	9.048	.2	21	.454	1.
7	7.408	.2	22	.167	1.
8	6.065	.4	23	61.4 eV	1.
9	4.066	.4	24	22.6	1.
10	2.725	.4	25	8.32	1.
11	1.827	.2	26	3.06	.5
12	1.496	.2	27	1.855	.5
13	1.225	.4	28	1.125	.5
14	.821	.5	29	.683	.5
15	.498	.5	30	.414	

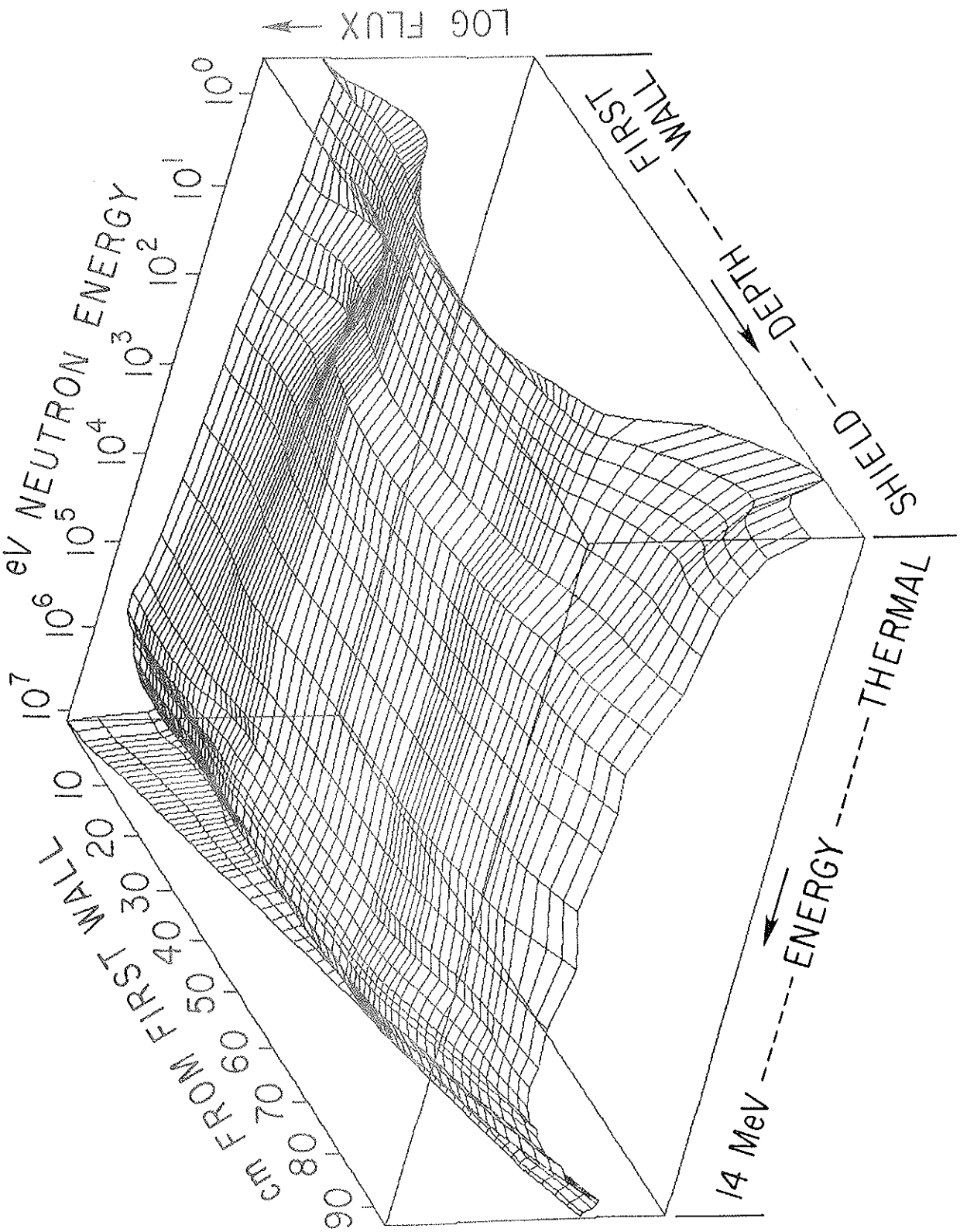

Fig. 2. Scalar Neutron Flux in Blanket.

and not all questions of reliability had been resolved.

Figure 3 shows spectra at the center of the first wall region and the center of the multiplier. Major features are the fusion neutron peak, a secondary peak due to secondaries from source neutron collisions, and a strong energy attenuation. Figure 4 shows spectra at the center of the moderator region, and at the centers of the adjacent burner salt regions. Because of the strong source of fission neutrons the fusion neutron peak is comparatively unimportant. Below the fission peak the flux exhibits typical "1/E" slowing down spectrum, with a thermal peak in the graphite region. Figure 5 shows spectra at the center of the scavenger and at 10 cm into the steel shield. The effectiveness of the lithium-6 in suppressing the low-energy flux is evident.

Profiles of the flux through the blanket are shown in Figure 6. The top group, which receives 85.61% of the source, is strongly attenuated. (The other 14.39% of the source is allocated to group 2, because of the surprisingly large width of the DT neutron spectrum in beam-driven reactors.) Group 10 (1.8 - 2.7 MeV) straddles the fission spectrum peak and illustrates the flatness of this secondary source. Group 19 (1.2 - 5.5 keV) typifies the slowing-down region. Group 25 (3 - 8 eV) is subject both to the resonances of both U-238 and to the lithium-6 thermal absorption.

Of course, the flux is only an intermediate result; useful design parameters must be obtained by convoluting it with specific reaction probabilities. Cross sections for various reactions discussed below were taken principally from DLC-24/SINEX and DLC-29/MACKLIB, data sets distributed by RSIC and derived from ENDF/B-III in a manner compatible with DLC-2. Since these libraries

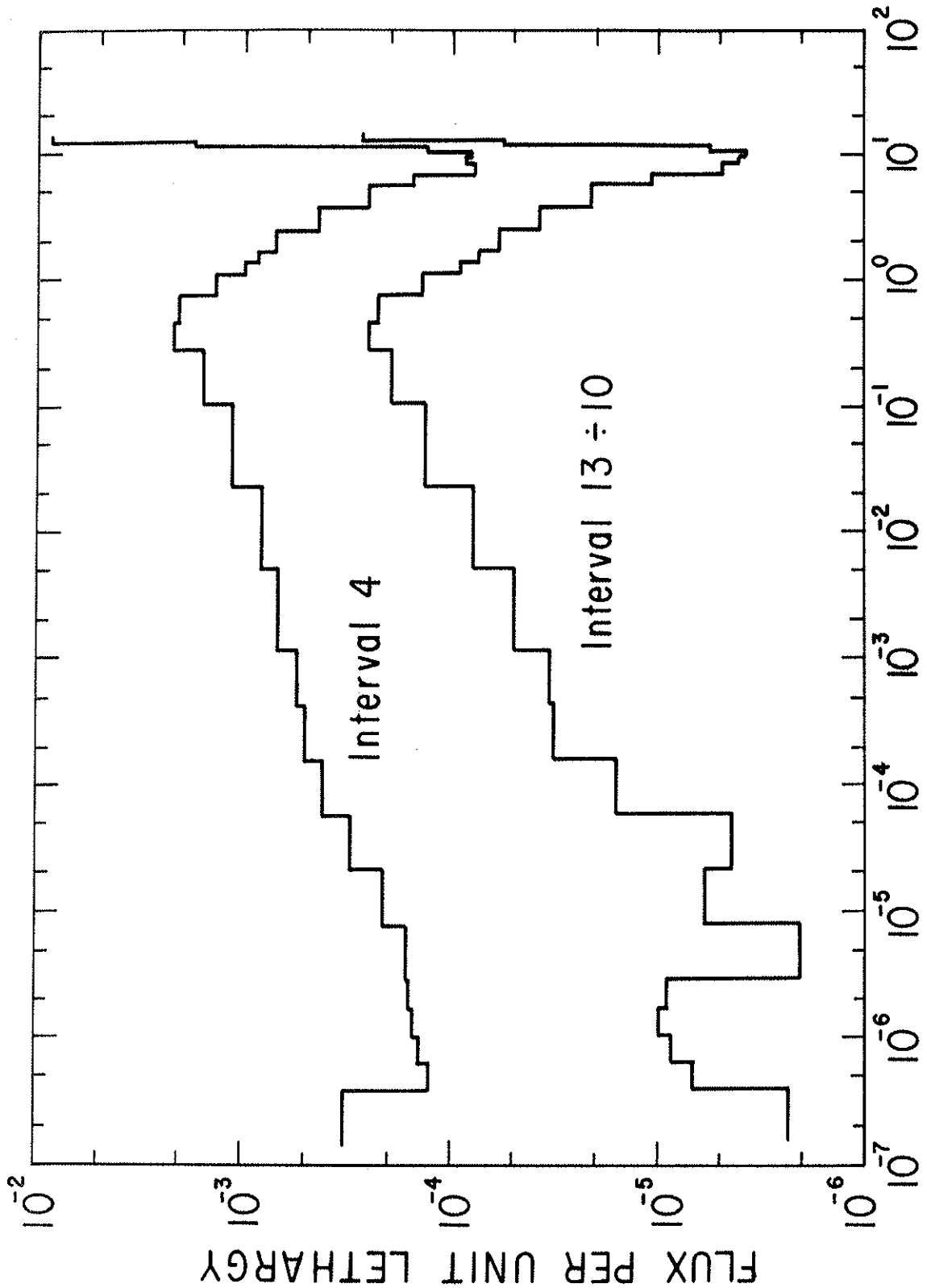

Fig. 3. Spectra at First Wall and in Multiplier.

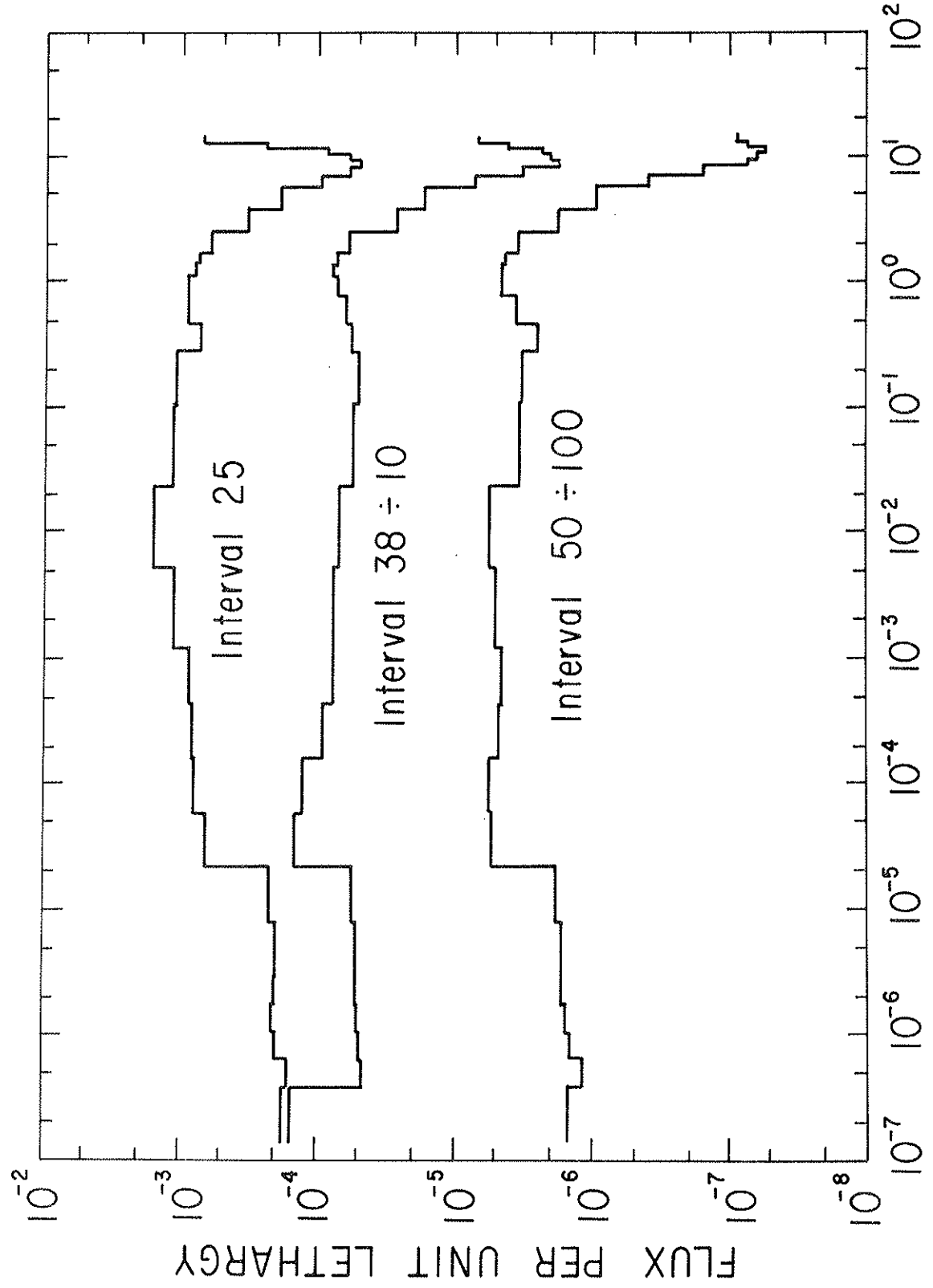

Fig. 4. Spectra in Moderator and Adjacent Burner Regions.

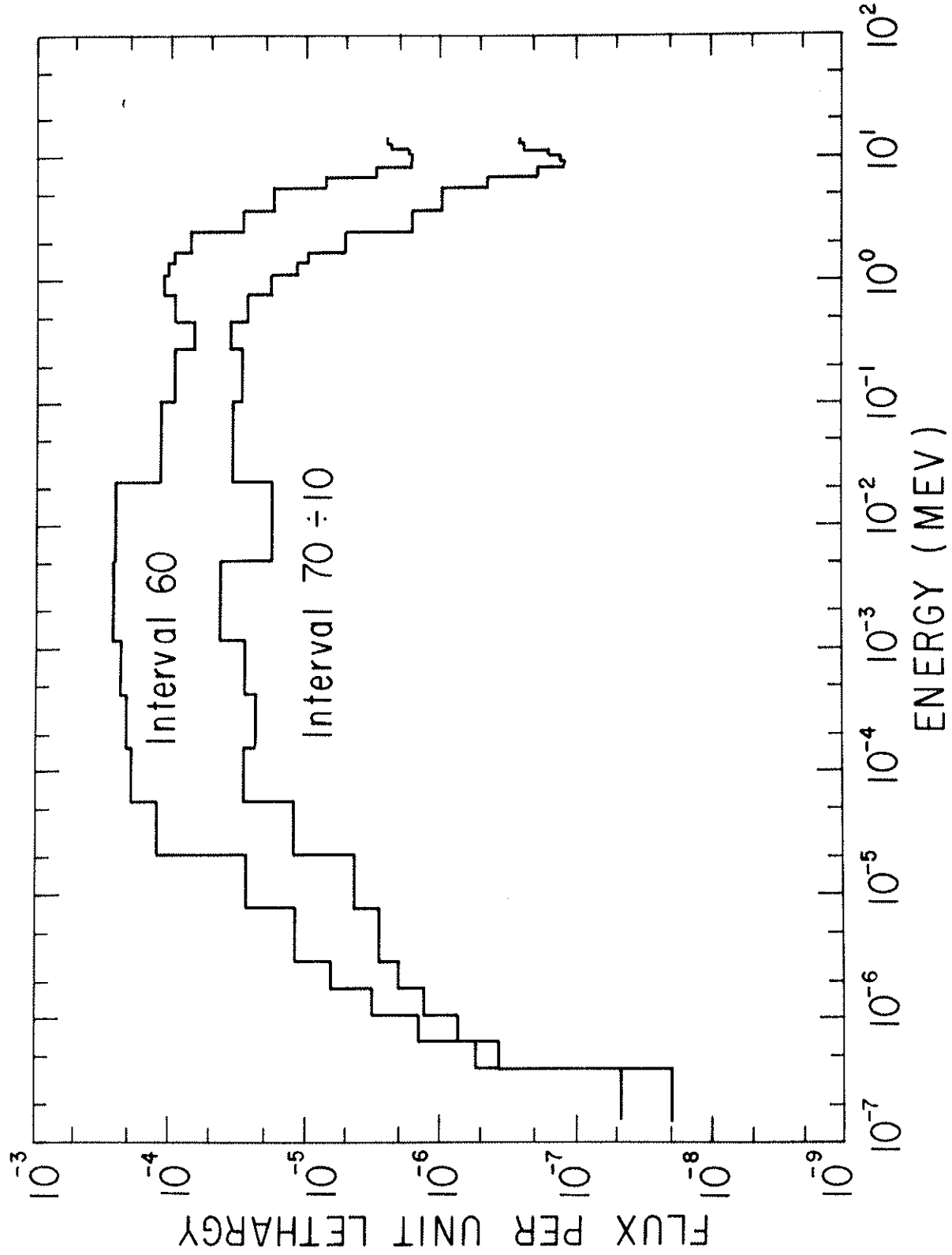

Fig. 5. Spectra in Scavenger and Steel Shield.

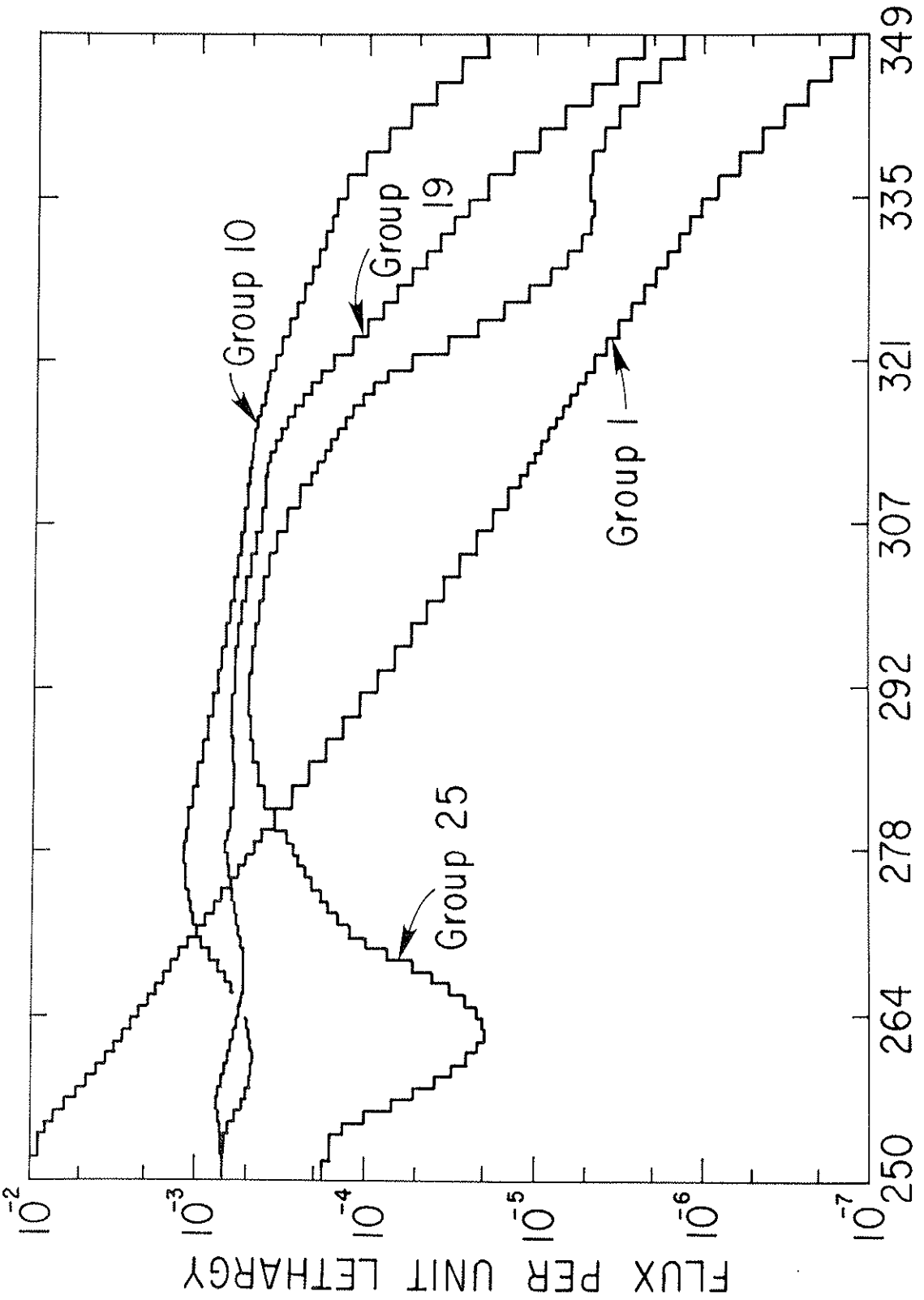

Fig. 6. Flux Profiles.

both give 100-group data, the weighted collapse to 30 groups applied to the transport library was applied here also.

Tritium is produced in a fusion reactor blanket by the neutron-stimulated breakup of lithium-7 and lithium-6. (The former has a high-energy threshold and releases a secondary neutron; the latter is a predominately thermal capture reaction.) In the reference blanket there are 1.094 tritons produced per incident DT neutron.

Of this, only 0.022 comes from lithium-7 reactions, and 2/3 of that is in the first burner zone. The thick multiplier attenuates the fusion neutrons too much for significant lithium-7 interactions, while the copious production of fission neutrons is unfortunately below the reaction threshold.

Actually, most of the tritium (0.788) is produced in the scavenger region, as neutrons leaking out of the burner are soaked up by the enriched lithium. Figure 7 shows a profile of the tritium production density through the blanket. The burnup in the moderator zone reflects the thermalization of fission neutrons and subsequent diffusion. The jump at the boundaries of the graphite region results from the fact that the burner region is 80% salt while the moderator is only 15% salt. The leakage from the scavenger region into the primary shield is 0.152 neutrons per DT neutron; actually this is only a 2.1% leakage, since blanket fissions, n-2n, n-3n, etc. constitute a secondary source of 6.067 neutrons per DT fusion.

In this reference blanket, fission breeding is accomplished by neutron capture in uranium-238 to produce plutonium-239. The calculated gross production in the multiplier region is 2.007 atoms

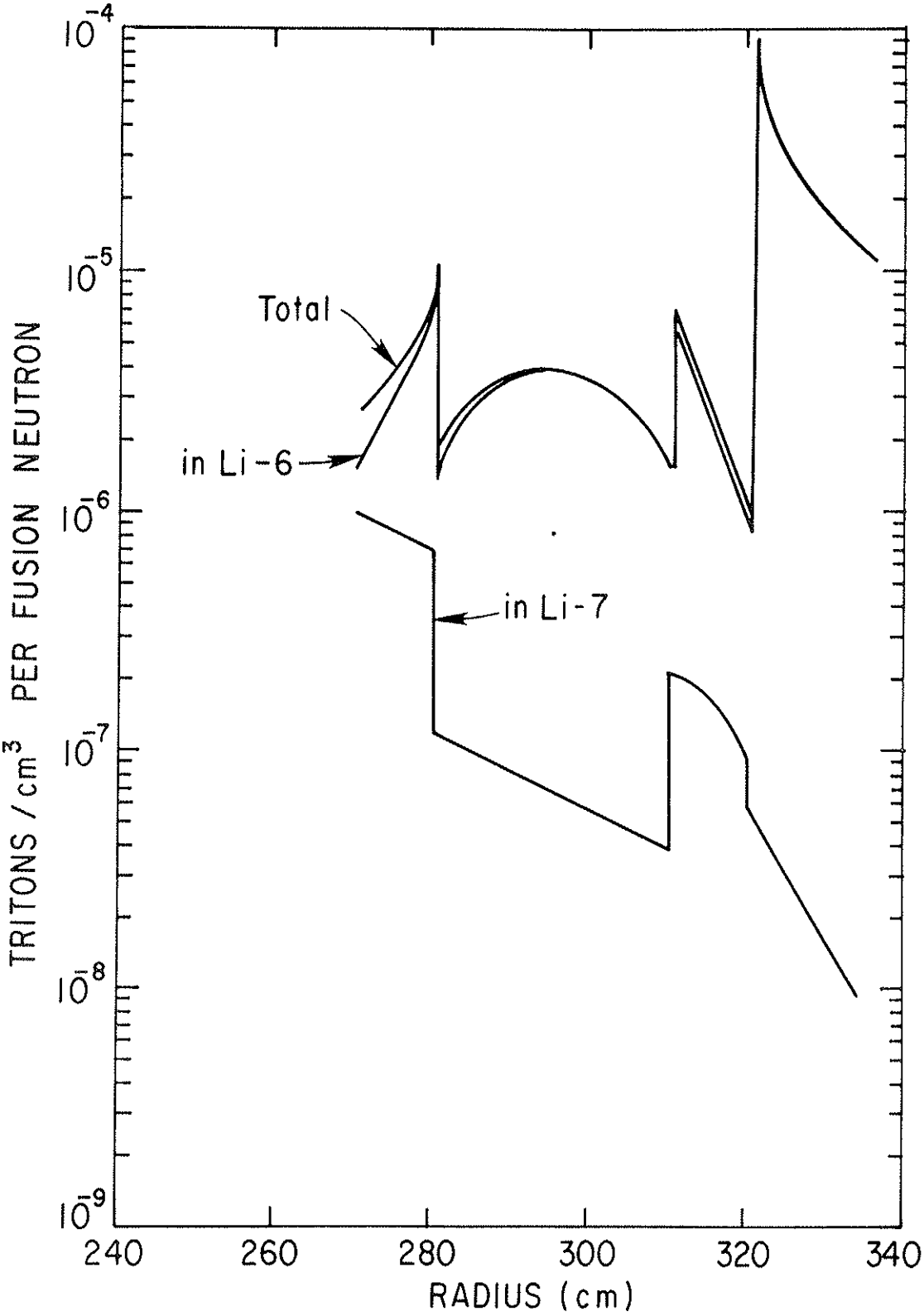

Fig. 7. Normalized Tritium Production Density.

of Pu per incident DT neutron. A large part of this must be due to absorption of fission neutrons leaking out of the burner region, in the same way that the scavenger produces tritium. There is also a substantial amount of fission in the uranium - this is called the multiplier region precisely because of this. The rate of fast fission of U-238 is 0.399 fissions per DT, releasing 1.460 secondary neutrons. (An additional 0.361 extra neutrons are produced by n-2n and n-3n reactions.) Furthermore, although the uranium is depleted to 0.3% U-235, the thermal flux is high enough to induce 0.111 fissions (and 0.146 absorptions) per DT neutron.

The production of plutonium in the multiplier is balanced by consumption in the burner regions where the flibe has been loaded to 0.25 mole % PuF_3. The fission rates in the inner burner, moderator, and outer burner are 0.306, 0.751, and 0.249 respectively, per incident DT neutron. Corresponding neutron absorption rates are 0.480, 1.100, and 0.391, for an overall capture-to-fission ratio of α - 0.510 in the burner regions. Figure 8 shows profiles of the fission rate density in the blanket for both uranium and plutonium, while Figure 9 compares the U-238 capture rate density to the Pu-239 absorption rate density.

Net breeding ratios can be figured from the values given above. Subtracting loss from gain, the net Pu breeding amounts to 0.036 atoms of Pu-239 per DT neutron. Since there is a great deal of fission going on, the traditional fission reactor breeding ratio may also be meaningful: 1.018 Pu atoms bred per Pu atom destroyed. However, if the U-235 is included, the breeding picture changes from slightly positive to slightly negative: -0.110 net

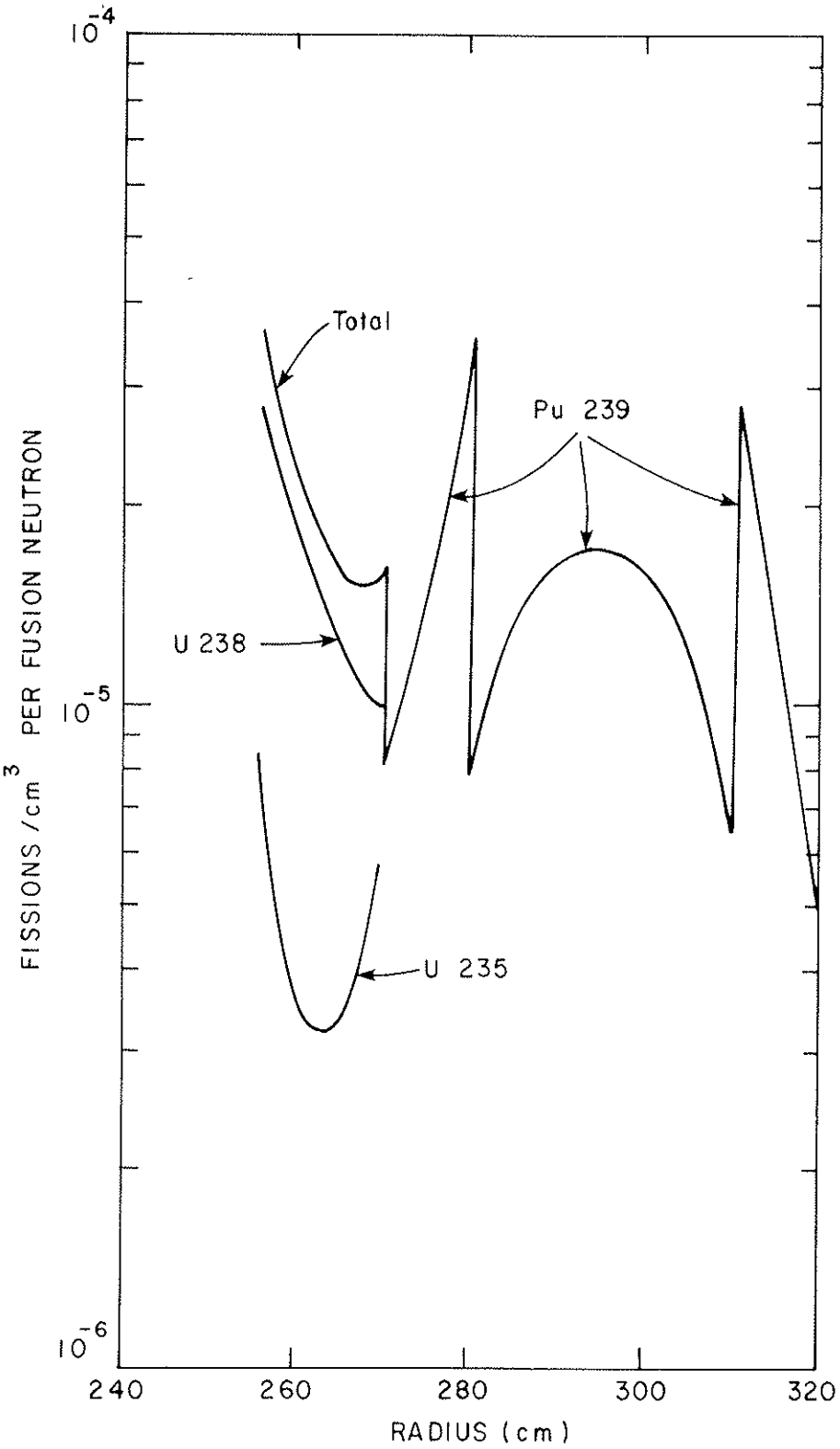

Fig. 8. Normalized Fission Rate Density.

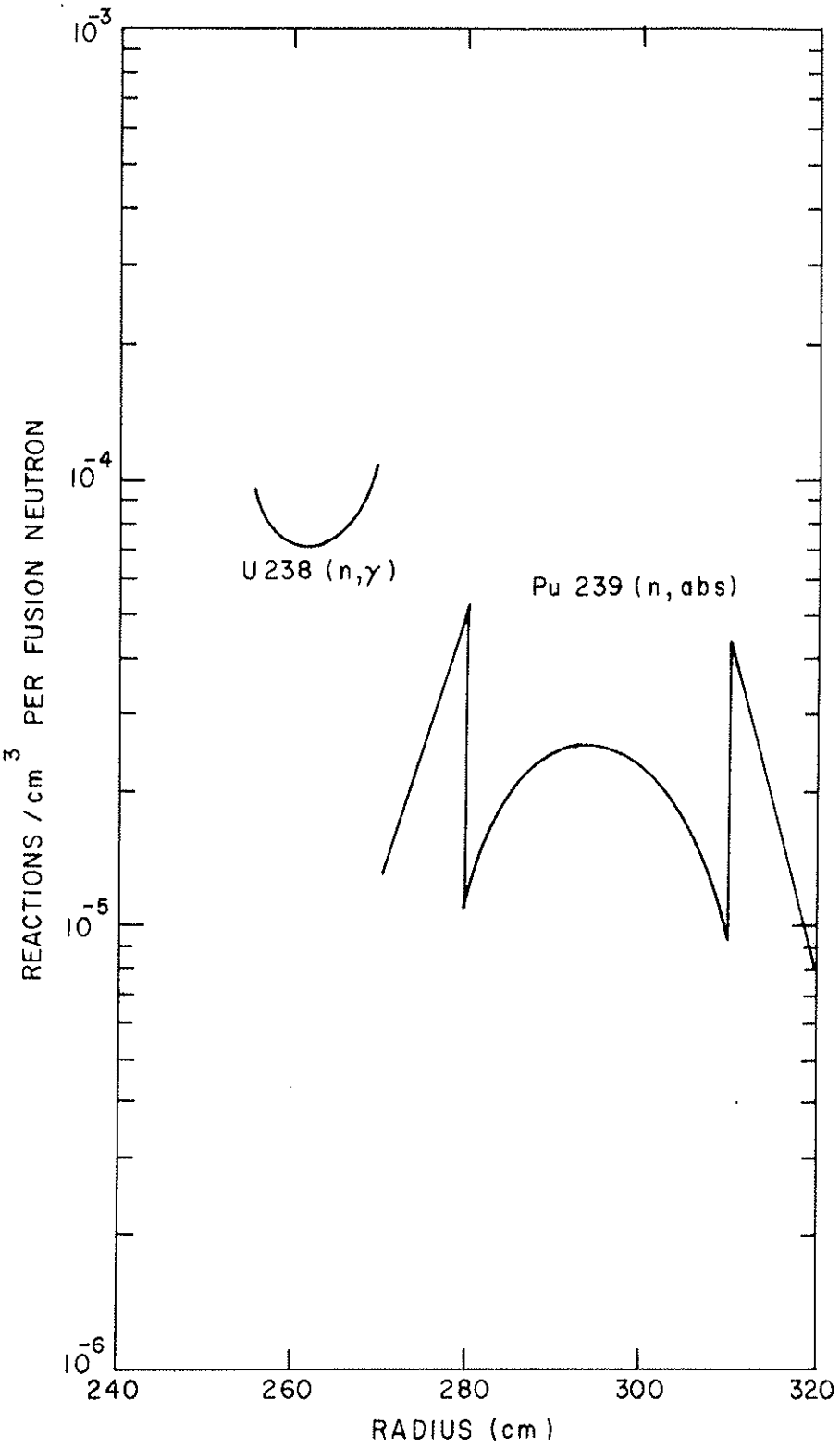

Fig. 9. Comparison of U-238 Relative Capture Density to Pu^{239} Relative Absorption Rate Density.

fissile atoms per DT neutron; or 0.948 fissile atoms bred per fissile atom destroyed.

c. Energy Production

The actual energy production in the reference blanket cannot be calculated, since this is proportional to the strength of the driving fusion source. However, various normalized energy output parameters can be evaluated.

As reported above, per incident fusion neutron there are 1.306 fissions of plutonium in the burner regions and 0.509 fissions of uranium in the multiplier. Assuming a recoverable energy release 198 MeV per fission, and adding 20 MeV for the kinetic and capture energy of the original DT neutron, the implied blanket energy multiplication is 27.0. Where this energy is deposited is not so easy a question to answer.

Much of the kinetic energy of the DT neutron is converted to high energy gamma radiation by inelastic scattering. In addition, about 13 MeV of gammas are released from each fission. Therefore, a significant fraction of the energy produced will be transported away from the neutron interaction site, so that the power density profile will not match the neutron flux profiles.

Consequently an auxiliary calculation of both neutron and gamma transport was performed specifically to produce a power density distribution. This calculation was performed with ANISN using the same model as previously, but with an expanded cross section data set. This 36-group library contained 30-group neutron transport cross sections and 6-group gamma transport cross sections, with coupling coefficients for neutron-induced gamma production disguised as down-scattering cross sections.

This library was produced by collapsing, as before, a 121-group (100 neutron groups plus 21 gamma groups) library distributed by RSIC as DLC/37C-EPR. Unfortunately, this library was derived from ENDF/B-IV and hence is not strictly compatible with the 30-group library, although large differences are not expected. In addition to transport cross sections, this library also contains kerma (i.e., energy deposition) factors. When multiplied by the atomic density and the flux of neutrons and gammas, these factors give the energy deposition density.

The DLC/37C library was assembled for use in pure fusion reactor design studies, and does not contain all the data required for this hybrid heating study. Transport cross sections for Pu-239 had to be assembled as follows: neutron transport cross sections were taken from DLC/2 (augmented by the n-3n reaction); gamma transport cross sections were assumed to be the same as for U-238; and gamma production coefficients were generated from a fission gamma spectrum normalized to 13 MeV and scaled by the sum of the fission and capture cross sections.

In addition several kerma sets were lacking. For both uranium and plutonium the gamma kermas were generated by applying energy conservation to the gamma transport cross sections. Neutron kermas were generated from the fission cross section times the residual fission energy: 198 MeV minus 13 MeV for the fission gammas, minus the kinetic energy of the fission neutrons. (An estimate of energy deposited per collision times the total cross section was used at energies below the U-238 fission threshold.) The kerma library was completed with the fluorine neutron kerma used in previous PPL studies.

Because of the difference in transport cross section data between DLC/37 and DLC/2, the results of the coupled neutron-gamma transport calculation do not match those of the reference neutron-only calculation. Since the purpose of this exercise was to generate illustrative power density profiles, the mole fraction of plutonium in the burner salt was adjusted until, at 0.18%, an indicated blanket multiplication of 26.7 was obtained, with 0.415 U-238 and 1.321 Pu-239 fission versus 0.399 and 1.306 in the original.

The power density profiles from this calculation are shown in Figure 10 while Table III gives the neutron, gamma, and total power densities averaged over each region. These and all values reported below are normalized to a DT neutron wall load of 1 MW/m^2. Material densities averaged over each whole region were used in computing these values.

In the multiplier and burner regions the neutron-deposited energy dominates, because of the fission rate, while in the shield the gamma energy is much larger. In the wall and the scavenger the gamma energies are comparable to, but still smaller than, the neutron energies, probably because of the leaking fission gammas.

In the first wall proper (considering only the steel and water) the average power density is 13.8 W/cm^3; this should not pose a cooling problem. In the multiplier the average power density discounting the void and helium is 96.5 W/cm^3; in the U-Mo fuel itself the peak is 191 W/cm^3. Again, this should not be too difficult to cool.

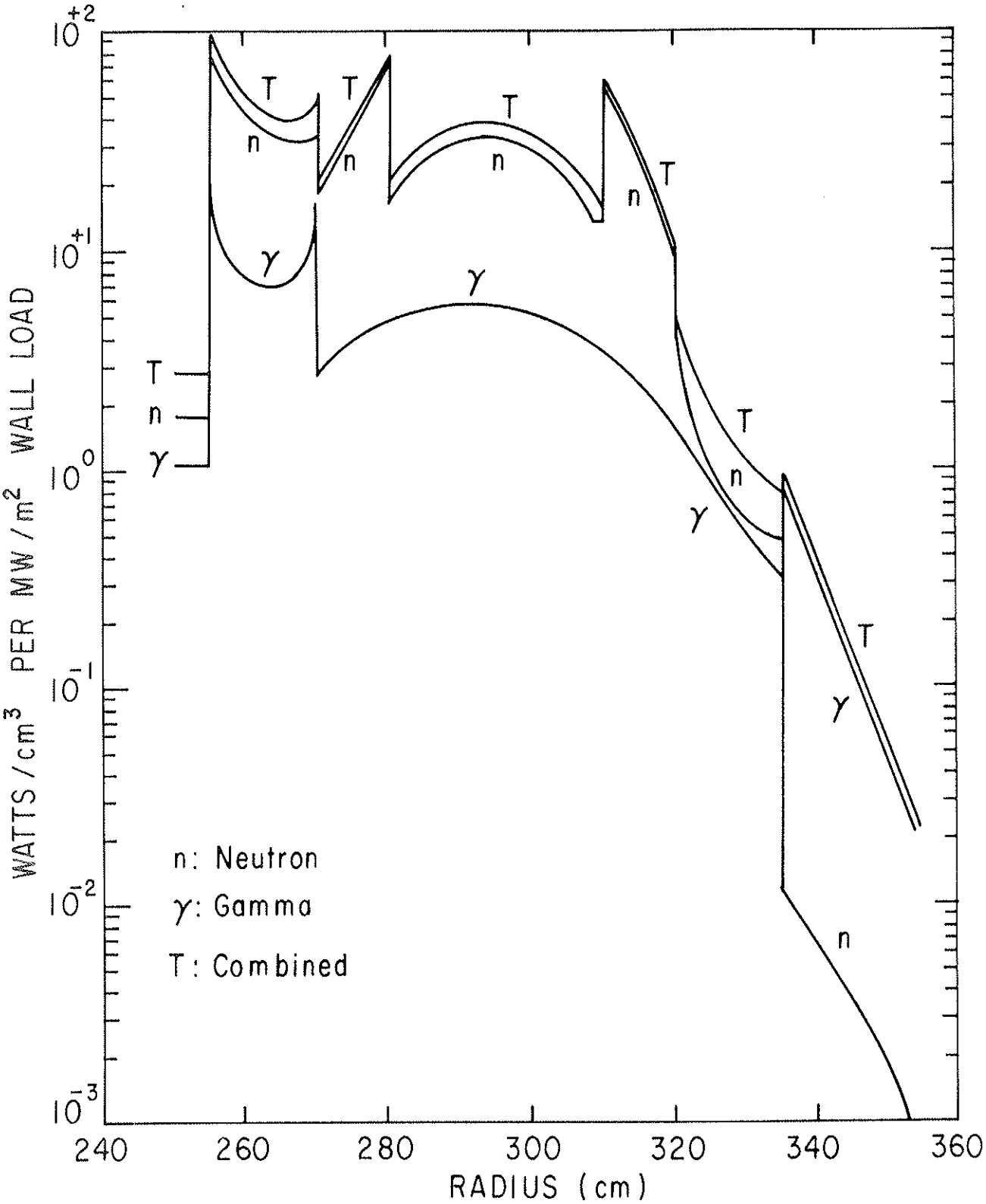

Fig. 10. Normalized Power Density.

Table III. Power densities in each region of the blanket (normalized to 1 MW/m^2 wall load).

Region	Total	Neutron	Gamma
First Wall	2.76 W/cm^3	1.73 W/cm^3	1.03 W/cm^3
Multiplier	50.19	41.28	8.91
First Burner	43.26	39.41	3.85
Moderator	30.86	25.99	4.87
Second Burner	29.92	27.44	2.48
Scavenger	1.84	1.12	0.72

The first and second burner regions show peaks of 73 and 56 W/cm^3, respectively, adjacent to the moderator. Within the moderator the peak powers are 220 W/cm^3 in the salt and 6.1 MW/cm^3 in the graphite, for a weighted total of 38 MW/cm^3. As discussed in the section of this report on thermal-hydraulics, the removal of this amount of power may require some changes in the assumed layout (and hence compositions) of the blanket regions. It should be noted, however, that the wall loads of interest identified by the hybrid systems code are typically only about 1/3 MW/m^2; scaling the power densities down by this factor could well obviate any redesign.

d. Relevance to Systems Code Parameterization

The blanket performance parameterization incorporated in the hybrid systems code purports to describe a range of blankets which includes the Reference described above. Therefore, it is expected that an evaluation of the parametric equations at the reference point should give nearly the same results as those obtained by direct calculation.

Insofar as the parameterization is concerned, the reference blanket is defined by: the energy multiplication, 26.98; the tritium breeding ratio, 1.0938; and the multiplier burnup, 0.0 (i.e., beginning of life). For these conditions the parameterization predicts: plutonium salt concentration of 0.2535 compared to 0.25; gross plutonium breeding of 1.978 compared to 2.007 calculated; and net plutonium breeding of 0.030, compared to 0.036. (The burnout of the U-235 in the depleted uranium multiplier is not explicitly reported by the parameterization, since this further depletion is not a factor in the economics;

it is, however, figured into the energy multiplication.)

The good match observed supports the use of the parameterization in the systems code. Indeed, for high-power reactors and/or low prices of plutonium, the systems code often calls for blanket parameters similar to those of the reference blanket. Presumably blankets realizing these performance goals could be found as small variations of the reference.

It has been observed, however, that the economically optimal blankets generally lie at the extremes of the allowable range of blanket multiplication. When high power is desired, the plutonium salt concentration is raised until the net fissile production is nearly zero, i.e., blankets like the Reference are chosen. When maximum fissile output is desirable, the plutonium is used in the salt only to levelize the output, and low blanket multiplications are selected. The resulting performance parameters are rather different from the Reference.

The question naturally arises, whether the Reference blanket, or even the basic conceptual blanket, is relevant in such low-M situations. Obviously the Reference blanket, per se, is not applicable to a reactor requiring low blanket multiplication, but it represents only one end of the continuum of blankets constituting the basic concept. In fact, with the plutonium fluoride taken out of the salt, the conceptual blanket shows a rather conventional approach to the design of a low-M system. The usual treatment of the basic requirements exhibits a vacuum wall-radiation shield, a neutron multiplier consisting largely of uranium, and a tritium-producing lithium region.

For the conceptual blanket the active ingredient of the last region is the molten salt flibe, chosen (as in the Princeton Reference Design[5]) because of its compatibility with steel and its good tritium recovery characteristics. For a low-M blanket one might dispense with the graphite and with the distribution between burner and scavenger zones, but the basic configuration should be suitable.

This should not be construed to be a claim that the conceptual blanket is necessarily the best blanket. The determination of an optimal design would require the detailed comparison of the performance of alternative blankets as it affects the final economics of the hybrid. Such an explicit comparison of alternatives has not been attempted; if it were, an economic model of the whole hybrid more precise than is available would probably be required for valid conclusions to be drawn. The conceptual blanket provides a reasonable approach to the low-M requirements, and offers a rather good solution to the high-M problem; this was the justification for its use in a systems study which was expected to survey the entire range of possibilities.

Indeed, for the systems study the physical model used to derive the blanket parameterization is not entirely relevant. The blanket factors affecting the evaluation of a postulated hybrid are principally the energy multiplication, the fissile inventory, and the net fissile output. As long as the parameterization produces reasonable values, its derivation is unimportant. Since the blanket parameterization is keyed to several full neutronic analyses, it is felt that it spans and describes a full range of realizable blankets. If a reactor designer were to choose to

achieve a particular performance point with some different approach (say U_3Si backed with molten lithium), this would not invalidate the parametric formulation.

To the extent that blanket concepts other than the design basis might offer performance beyond the range of the basic parameterization, blanket surveys could be biased. (But only if the extra range actually offered superior economics.) This effect can be explored easily, however, by varying the constants in the parametric equations. In fact, just such an approach was used for a few hybrid surveys using a "super" blanket. For these cases the parameterization was modified, without justification, to indicate significantly greater net production of plutonium. It was found that the qualitative descriptions of optimal solutions were not greatly affected.

References

[1]J. C. Mailen, F. J. Smith, and L. M. Ferris, J. Chem. and Eng. Data 12 (January 1971) as abstracted in ORNL-TM-3595 (1971) p. 66.

[2]W. G. Price, Jr., A Revised Version of the ANISN Code, Princeton Plasma Physics Laboratory Report MATT-1035 (1974).

[3]W. W. Engle, Jr., A User's Manual for ANISN, A One-Dimensional Discrete Ordinates Transport Code with Anisotropic Scattering, Oak Ridge Gasseous Diffusion Plant Report K-1693 (1967).

[4]W. G. Price, Jr., XCNVRT - A Cross Section Group Collapsing or Expanding Code, Princeton Plasma Physics Laboratory Internal Report (1977).

[5]A Fusion Power Plant, R. G. Mills, ed., Princeton Plasma Physics Laboratory Report MATT-1050 (1974).

3. Mechanical Design and Thermal Analysis of Blanket

a. Introduction

The principal effort in this hybrid study was the development and exercising of a parametric economic model of the reactor. Plasma physics and blanket neutronic performance parameters for the model were developed from scoping studies based on a nominal design concept; the suitability of the concepts was explored with a set of detailed design studies.

The responsibility for these detailed studies was shared between PPPL and Battelle-Pacific Northwest Laboratories as part of the cooperative hybrid study program. Plasma equilibrium and stability and blanket neutronics were examined at Princeton, while the plausibility of the blanket mechanical design was assessed by PNL.

From the initial round of scoping studies one particular blanket was selected and analyzed to determine its structural, thermal, and hydraulic performance characteristics. (Of course, this blanket turned out not to be the chosen reference design, but since it has a higher power, it constitutes a more stringent test of the concept.) Separate consideration was given to the radiation shield or "first wall", the neutron multiplier or converter region, and the moderator-burner salt region. A summary of these studies and the conclusions are given in the following sections, which are extracted from a more complete report issued by PNL.[1]

b. Summary Conclusions and Recommendations

Preconceptual scoping studies were performed on the major components of the TCT Hybrid blanket. To do this, a case

was taken from the parametric neutronic studies, which identified the configurations of general interest and the desired volume fractions of materials and approximate thermal loadings. The overall blanket and shield configuration considered is shown schematically in Figure 1. The three components of the overall blanket that needed preconceptual scoping studies were the radiation shield (first wall), the neutron multiplier region (converter) and the burner-moderator region (blanket). The studies and resultant recommendations that will help in selecting a mechanically viable TCT Hybrid blanket design are summarized in Figure 1.

c. First Wall

One question necessary to consider in a preconceptual study was whether or not the first wall should be the primary vacuum barrier or more simply a radiation shield to protect the converter pressure tubes from direct thermal loading by the plasma. Considerable incentive exists to make it the primary vacuum vessel since its location (compared to alternatives) eliminates many coolant line penetrations. If a stable structure with adequate life requires more coolant and stainless steel than the volume fractions shown in Figure 1, it would seriously affect the hybrid's neutronic performance. Alternative vacuum barrier locations would then have to be considered.

The BOSOR4 computer code[2] was used to perform stability analyses on a toroidal chamber with approximate major and minor radii of interest, i.e., R = 8.15 m, r = 1.6 m. A wall thickness of about 0.525 in. was required to keep the vacuum chamber from collapsing under two atmospheres pressure. Two first wall concepts were then designed (Figure 2). The single wall concept of Figure 2(b)

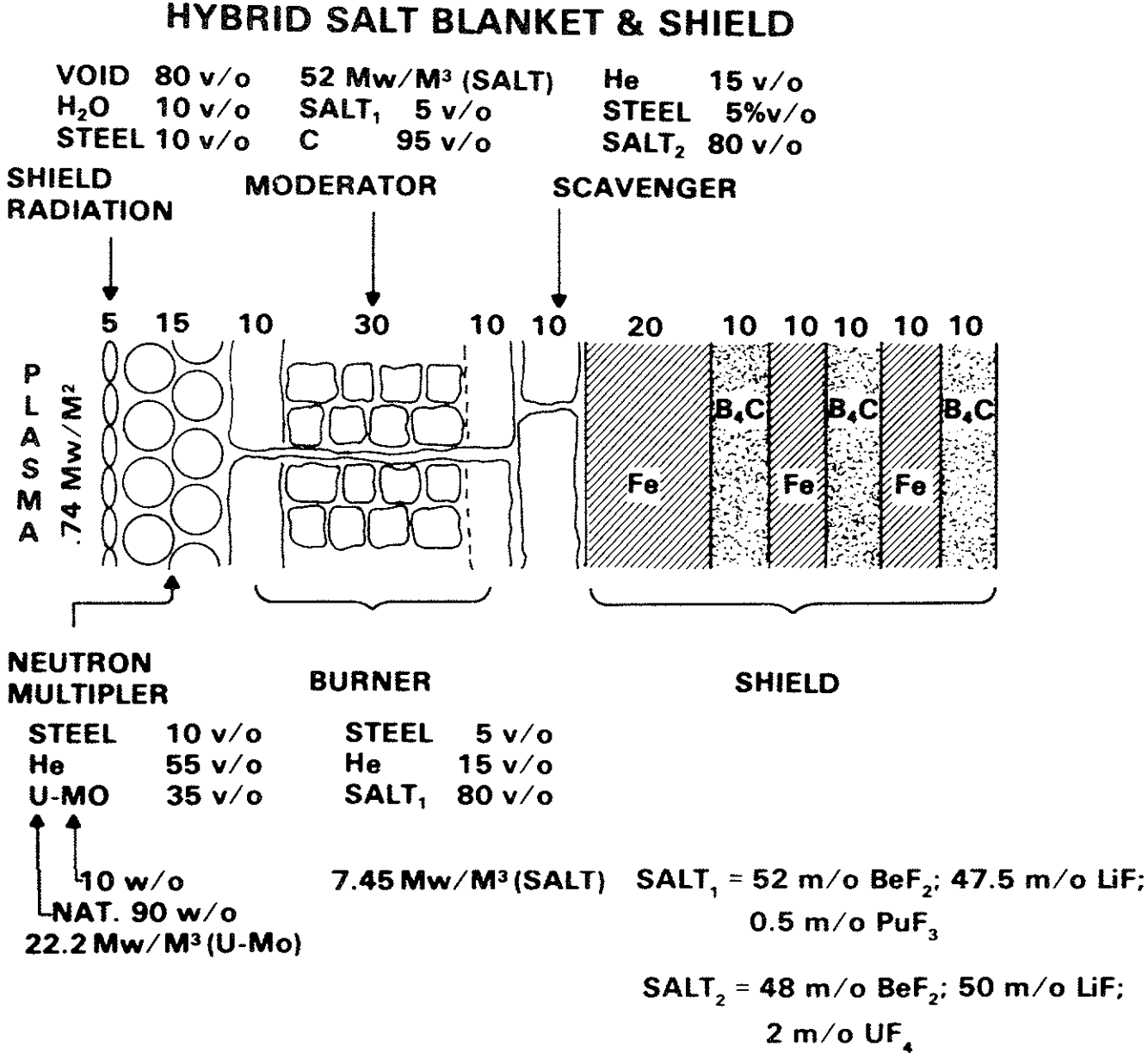

Fig. 1. Hybrid Salt Blanket and Shield.

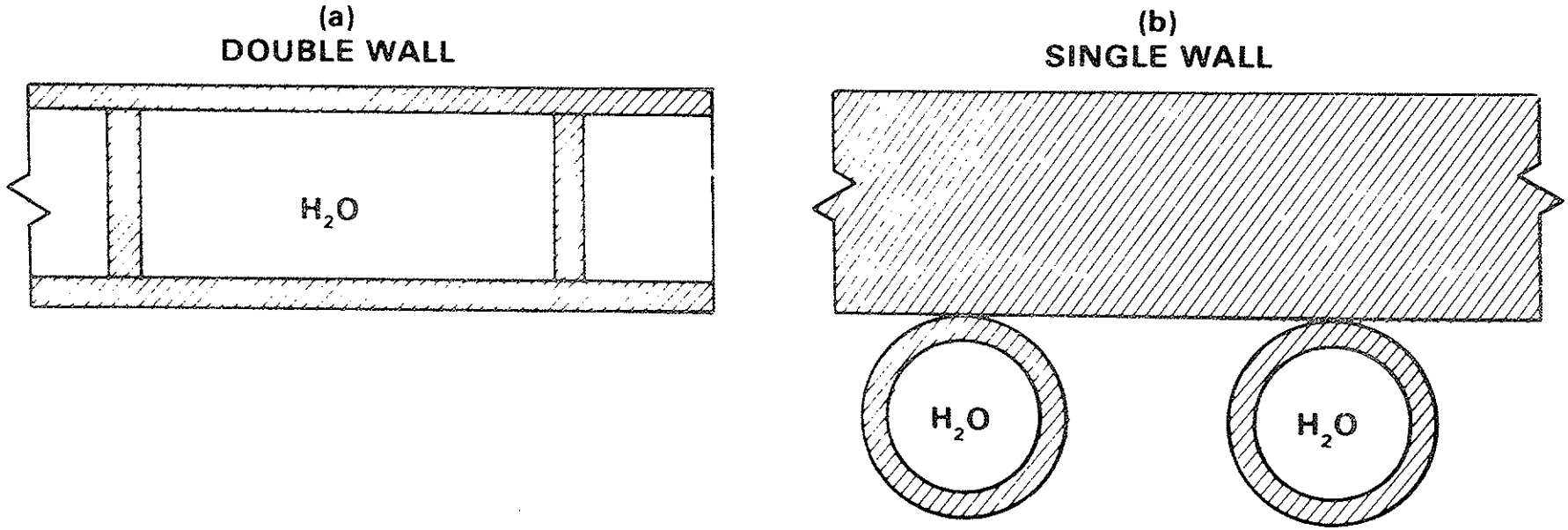

Fig. 2. First Wall Concepts.

is relatively easy to fabricate but cannot meet the desired 10 vol% of structural material. The wall itself would be 27 vol% of the 5 cm region. The double wall concept of Figure 2(a) was then evaluated; it has the same stability characteristics as a solid wall but requires much less structural material.

The maximum spacing of the ribs in the double wall concept primarily depends on the coolant pressure. In selecting a coolant and coolant pressure, low temperature, low pressure water can be used, which will minimize the structural material required and extend wall life considerably. This is due to the fact that thermal loading on the first wall does not affect overall plant energy balance (less than 1% of the plant output). For this evaluation, 30 psia water was used.

The flow channel was designed to follow the minor circumference of the toroidal chamber as shown in Figure 3(a). A neutron wall loading of 0.74 MW/m^2 (0.1258 MW/m^2 thermal) was used with a relative power distribution along the flow channel as shown in Figure 3(b). The resulting temperatures (referenced to the coolant inlet) are shown in Figure 4. Stability analyses using the BOSOR4 code confirmed the ability of the local channel to handle the 30 psia coolant pressure. The maximum spacing of the ribs coupling the inner and outer walls was set at 4 in.

Critical first wall stresses at different times in the operating cycle were established using AXISOL, an axisymmetric finite element code.[3] Figure 5 shows the maximum stresses for a full operating load of 14.7 psi vacuum load, and 30 psi in the coolant channel and temperature gradients corresponding to a

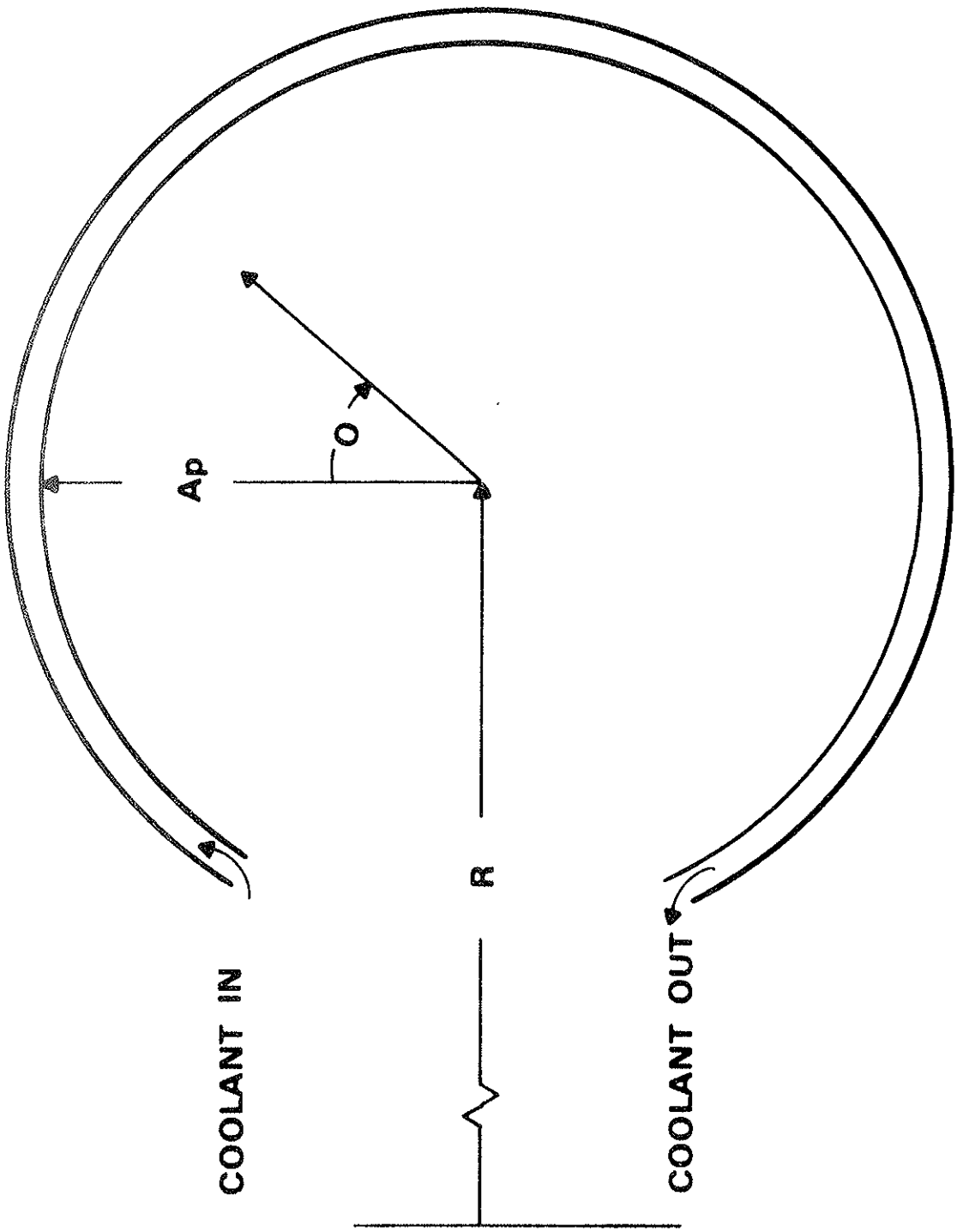

Fig. 3(a). Characterizations of First Wall Coolant Flow Path.

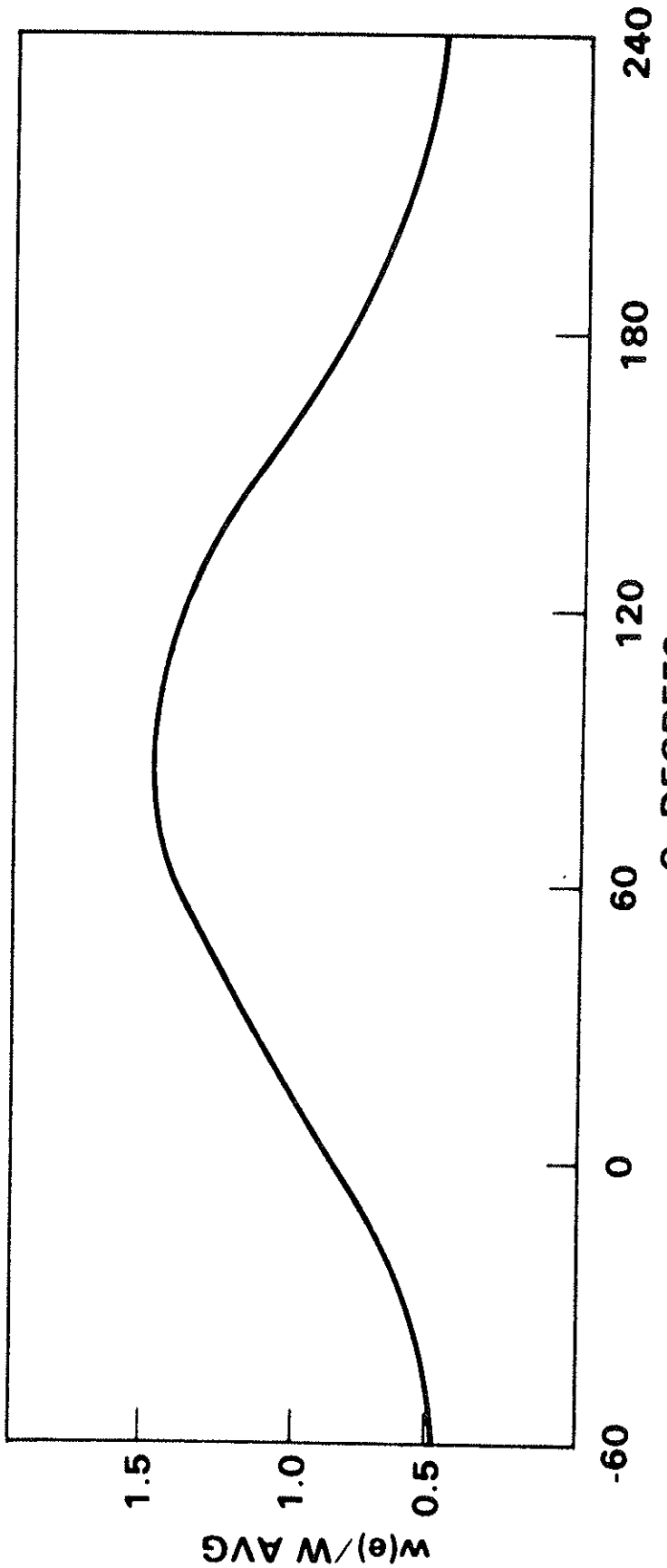

Fig. 3(b). Normalized Wall Load around Minor Circumference.

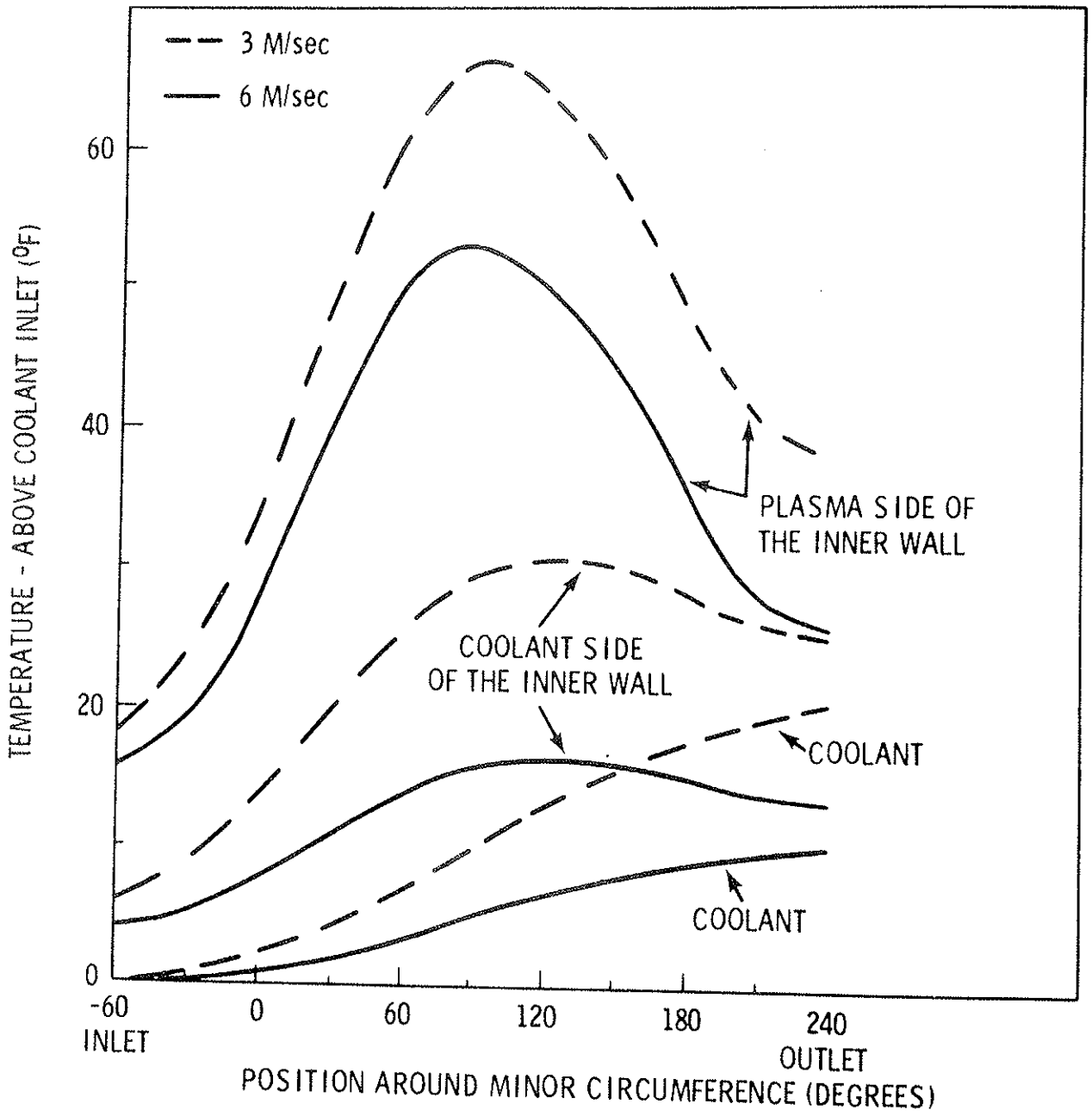

Fig. 4. TCT Hybrid First Wall Operating Temperature (Double Wall Concept).

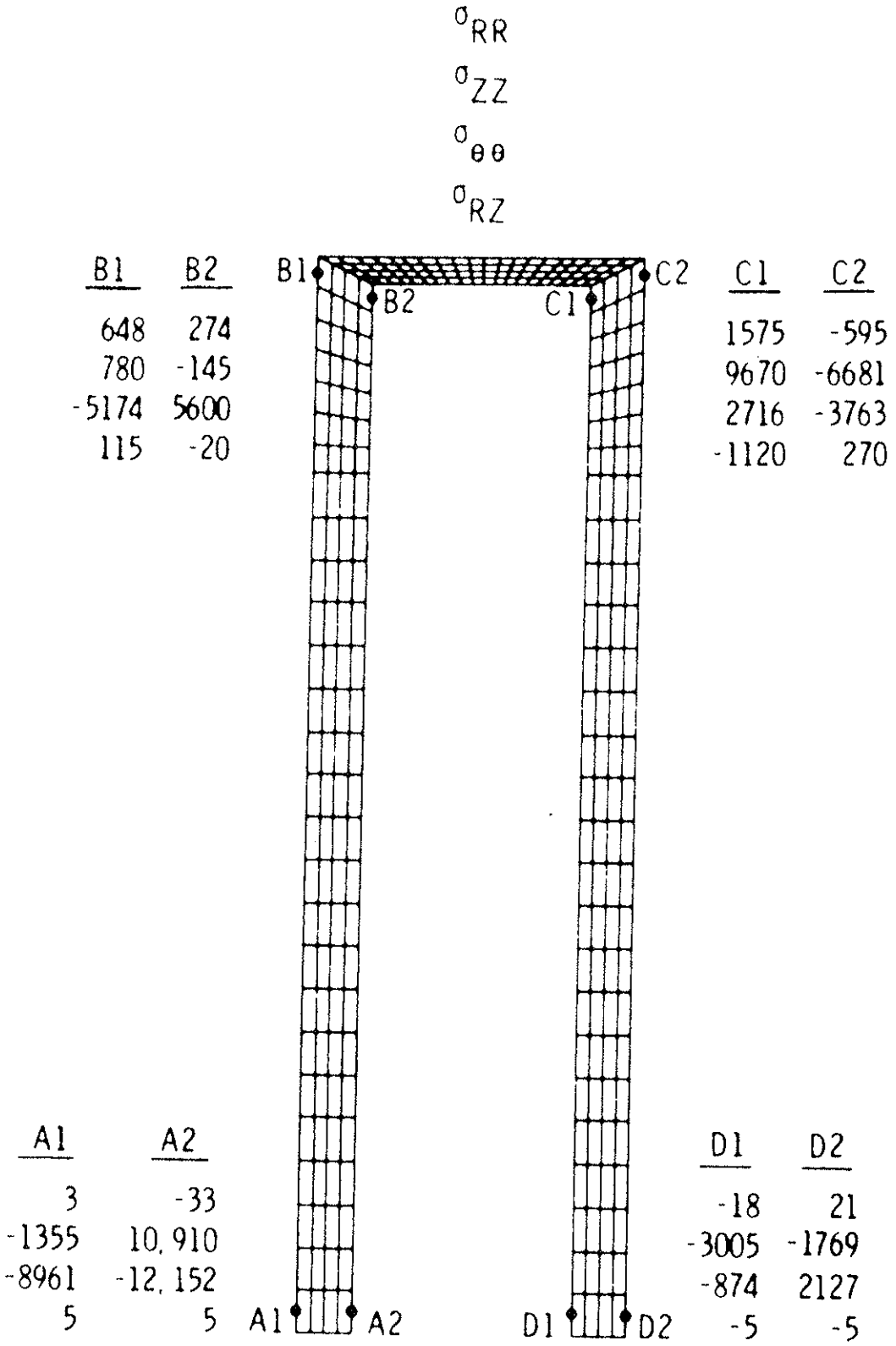

Fig. 5. Maximum Stress Component Operating Conditions.

neutron wall loading of 0.74 MW/m^2. Several potential failure modes were examined using the stress results to estimate the potential life of the double wall. The following conclusions resulted:

- Irradiation Swelling

  Since the 316 stainless steel (SS) operating temperature will be well below 350° C, no irradiation-induced swelling is expected to occur in the life of the plant.

- Tensile Strength

  The structure experiences the maximum stress intensity on the outer surface of the outer wall at the junction with the stiffener:

  $$S_{MAX} = 9956 \text{ psi}$$

  From the ASME Boiler and Pressure Vessel Code, Section VIII, Division 2, the allowable stress intensity for 316 SS (reference 17, Table AMA-1) for 100°F - 200°F is given as:

  $$SM = 20 \text{ ksi}$$

  For secondary loading, a factor of 3 is permissible for the allowable stress intensity. Negligible degradation of tensile properties for 316 SS at typical TCT hybrid fluences is expected. Thus, tensile strength does not limit the structure life.

- Plastic Cycling (Ratcheting)

  If stresses exceed the yield during the operational cycles, it is possible that incremental plastic growth could occur with each cycle. Since stresses are well

below the yield at all times in this structure, it is not possible for plastic cycling to occur.

- Creep

  The creep rupture characteristics of 316 SS indicate that creep is not a problem below 500°C. Thus, creep rupture does not limit the structure life.

- Crack Growth

  It was assumed that a crack of semicircular shape existed in the 0.1 inch thick shell. The crack radius initially was 0.01 inches. A simple stress intensity factor was used:

$$S.I.F. = \sigma\sqrt{\pi c}$$

  where σ = maximum stress
  = 20,000 psi (with a factor = 2.0)
  c = semicrack length
  = 0.01 inch.

  Using an extrapolation of data for 20% cold-worked 316 SS at a much higher temperature than the operating temperature, computations indicate that it would take several decades for this crack length (and depth) to increase by 10%. Thus, crack growth does not threaten the structure's integrity, nor is it likely to induce leaks.

- Fatigue

  The maximum stress intensity due to thermal cycling is:

$$S_{MAX} = 6590 \text{ psi.}$$

  With a concentration factor of 5, this amounts to a cyclic strain of less than 0.1%. Comparison of this

strain with data of irradiated SS indicates the structure has infinite fatigue life.

The feasibility of fabricating a toroidal vacuum chamber using the double wall concept was briefly examined. A method of fabricating a 30^{o} segment of the toroidal chamber has been determined, involving stretch forming the components (i.e., innermost wall and integral rib and outermost wall plates) and then TIG or E-beam welding them together. Figure 6 shows the resulting wall cross section. The assembly method allows adequate weld quality control inspections. Although the fabrication would be relatively expensive for thin section stainless steel, the long life should compensate for the expense.

From this brief study, it was concluded that a double wall structure cooled with low pressure water should be used as a basis for the conceptual design of the TCT Hybrid first wall. The first wall could also serve as a vacuum barrier with adequate life. Although this study was based on a toroidal chamber, the basic concept would be adaptable to either a double or single wall divertor design. A different fabrication method would be considered for these designs, however.

d. Converter Region

The ^{238}U in the converter region provides neutron and energy multiplication, due to fast fission, (n,2n) and (n,3n) reactions of the 14 MeV fusion neutrons, and ^{239}Pu production due to neutron capture in the ^{238}U. In contrast, the burner-moderator portion of the blanket in Figure 1 breeds tritium from neutron reactions with lithium and produces power due to ^{239}Pu fissions. It thus appears desirable, from a neutronics viewpoint, to separate

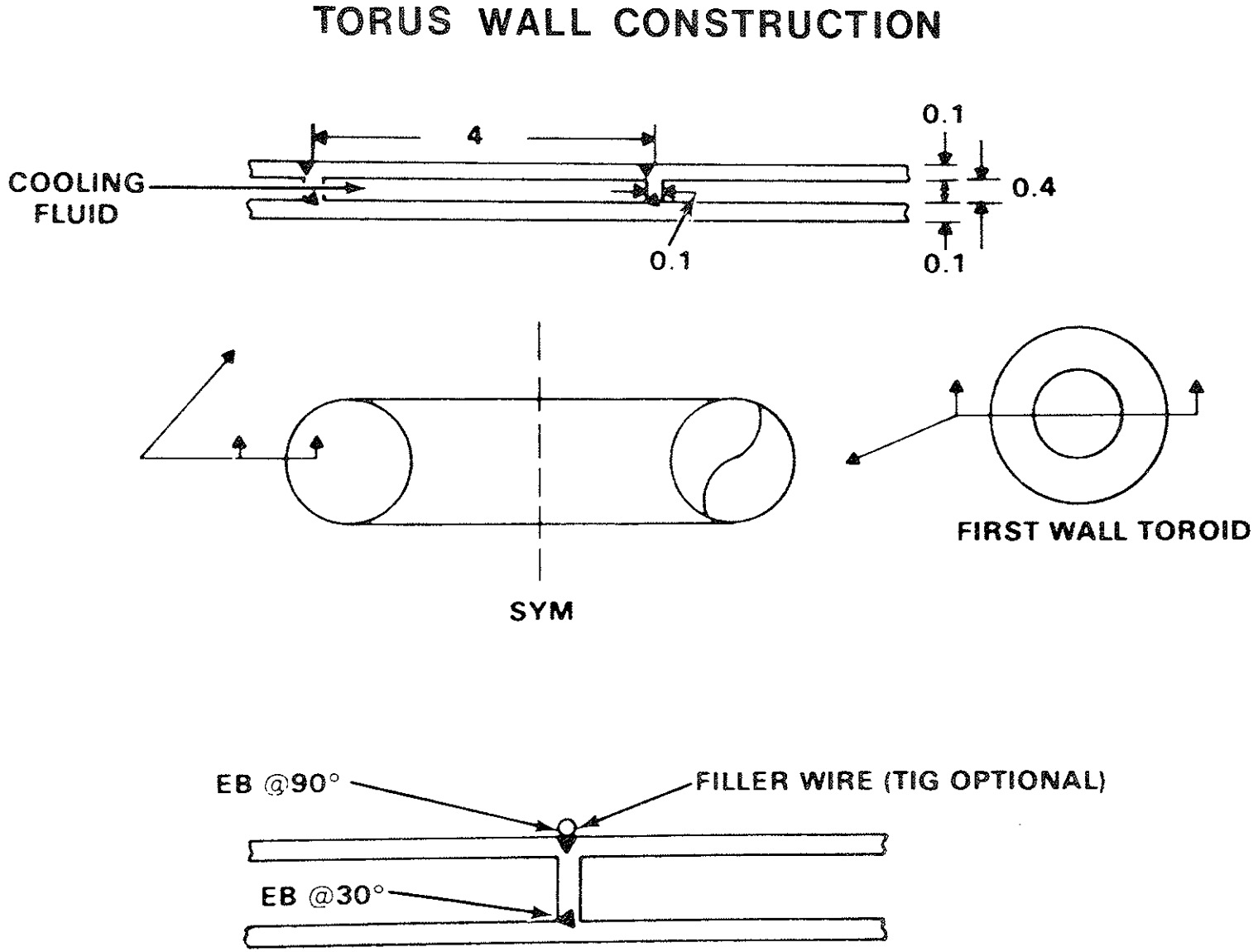

Fig. 6. TCT Hybrid First Wall Fabrication (Double Wall Concept).

the fuel cycle of these two regions. The pressure tube converter fueled with U-Mo slugs or spheres would provide the fuel cycle flexibility desired in the plutonium producing converter. The objectives of this study were to adjust the initial U-Mo slug dimensions and the length of the pressure tube to maintain peak U-Mo temperatures below 900°C, where an undesirable phase transition takes place.

Uniform coverage of the plasma chamber by the pressure tubes is critical. Since a poloidal divertor will probably be used in the TCT Hybrid, most of the preconceptual effort was directed at evaluating a horizontal pressure tube layout. This type of lay-out provides better coverage of the poloidal divertor geometry but does sacrifice flexibility in fueling the converter region.

The converter region used in the thermal hydraulic analyses is described schematically in Figure 7. In sizing the fuel slug, the inner and outer radii were simultaneously changed to maintain a constant fuel cross section. Inlet conditions of helium at 50 atm and 579°F were used for the coolant. Sensitivity studies were performed on slug size, pressure tube length and coolant conditions. The following parameters are recommended as a con-ceptual design basis:

U-Mo dimensions

Inner diameter	1.15 in. (2.92 cm)
Outer diameter	2.47 in. (6.27 cm)

Helium

Pressure	700 psi (47.6 atm)
Inlet temperature	579°F (304°C)
Outlet temperature	870°F (466°C)
ΔP	10 psi (0.68 atm)
Pumping power	2% of converter thermal power

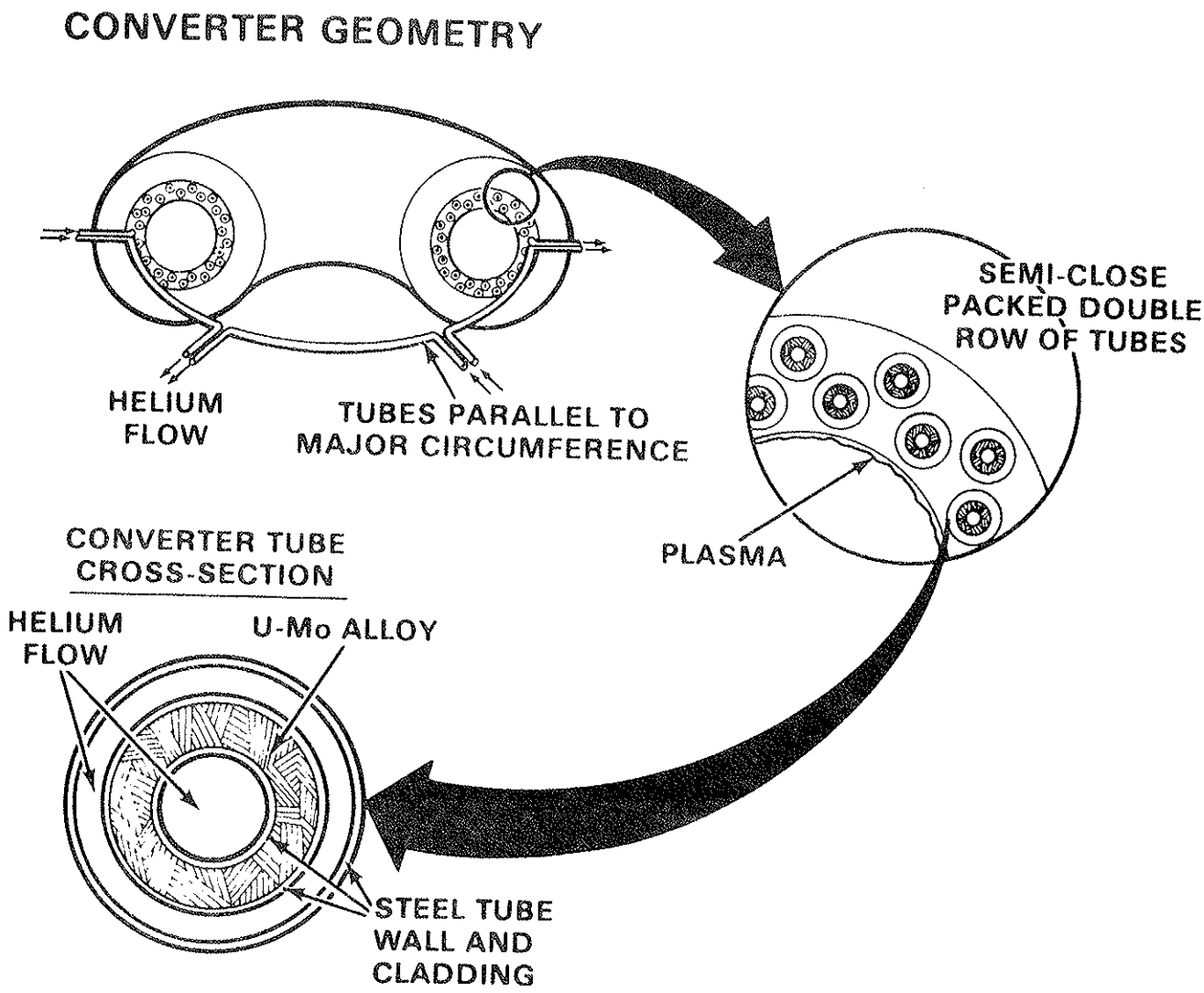

Fig. 7. Converter Geometry.

Pressure tube dimensions

Inner diameter	2.84	in. (7.21 cm)
Outer diameter	3.05	in. (7.75 cm)
Length (maximum)	24	ft. (7.32 m)

The thermal hydraulic evaluation was made on a reactor operating at 0.74 MW/m^2 average neutron wall loading and circumferential power peaking factor of 1.5. The assumed operating cycle was 1000 sec on, 100 sec off. The thermal response of the converter slugs in a 16 ft. channel during the operating cycle is shown in Figure 8.

The structural response of the U-Mo slugs to the operating cycle and startup cycle was determined using AXISOL. The following results were obtained:

Load Case 1 - Startup Cycle

Maximum Fuel Stress Intensity = 6060 psi

Major components of this stress intensity were hoop and longitudinal tensile stresses near the inner cladding. A major source of stress was the radial temperature gradient causing the outer, hotter fuel to pull the cooler, inner fuel outward and longitudinally. This stress is approximately one-third of the yield stress of the fuel at operating temperature.

Maximum Clad Stress Intensity = 22,290 psi

Major components of this stress intensity are plastic compressive strains in the cladding due to the bulk temperature rise and the difference in clad and fuel coefficients of thermal expansion. Maximum effective strain is approximately 0.00323, which is nearly four and one-half times the yield strain at operating temperature. This value is within the elongation bounds of the material, but a detailed cyclic strain history analysis

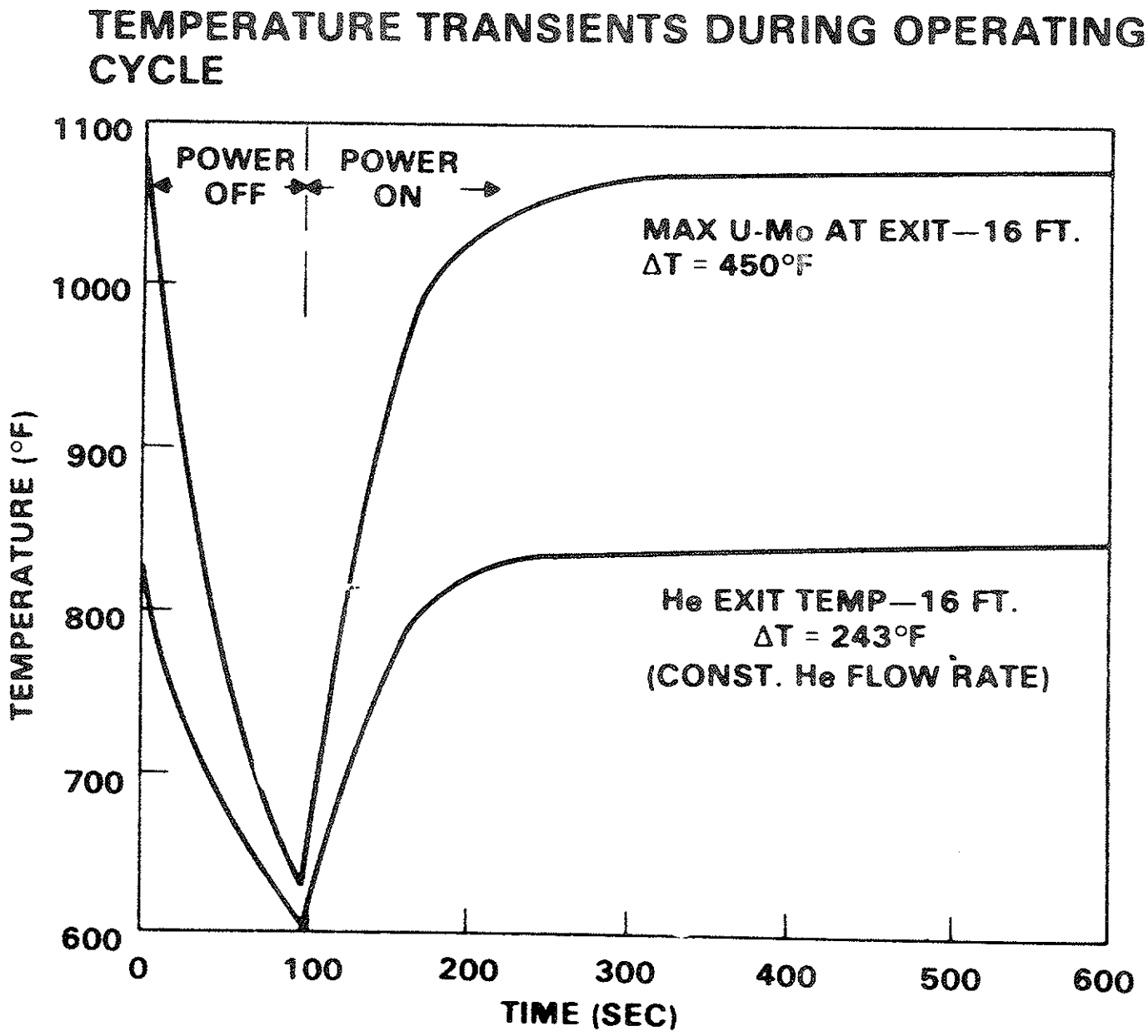

Fig. 8. Temperature Transients during Operating Cycle.

would be necessary to determine if the cladding would ultimately undergo elastic action for this loading cycle.

A simplified strain history tracing from the single cycle analysis performed indicates significant plastic action into the second cycle due to the radial temperature gradient. The bulk temperature rise from room temperature to around 1100°F can be shown to cycle elastically, resulting in cladding tensile stresses of approximately 27 ksi (RT yield = 30 ksi) on cool down.

The cyclic life of the cladding can be roughly approximated by using the ASME Boiler and Pressure Vessel Code (BPVC) fatigue curves with a stress based on the effective strain and the modulus at temperature. This "elastic" stress level indicates a fatigue life near 1000 cycles, adequate for the short life of a fuel slug. Incremental plastic deformation, or ratcheting, has not been examined at this analysis level.

Load Case 2 - Operating Cycle

Maximum Fuel Stress Intensity = 4062 psi

This completely elastic stress intensity primarily results from the radial temperature gradient and is in the same location as the startup cycle peak fuel stress.

Maximum Cladding Stress Intensity = 18,490 psi

This stress intensity indicates slight inelasticity, but effective strain is much less than twice yield strain at temperature, indicating elastic cycling starts immediately for the operating cycle. Effective strain is 0.00094, which, with the modulus at temperature, can be used to approximate fatigue life for the operating cycle strain traverse. This elastic stress indicates a fatigue life of 10^6 cycles, adequate for a short-term pellet cladding.

A potential concept of a horizontal converter tube layout for a R = 8.15M, r = 1.6M plasma, using a single null divertor is shown on Figures 9 and 10. The pressure tubes run a full 60^{o} arc; however, the bayonet joints every 30^{o} allow disassembly of the vacuum vessel and converter into 30^{o} segments To refuel the converter region, the horizontal layout would probably require blanket disassembly; however, more knowledge about magnet design, divertor openings and neutral beam ports would be required for developing a specific disassembly procedure.

Adequate plant availability would result only if the converter fuel has a long residence time. The burnup effects due to fission product buildup and retention in the fuel appear to physically limit the U-Mo slug life; U-Mo alloys have proved dimensionally stable to 10,000 MWD/MT. In the TCT Hybrid converter region, this would give approximately a 3-4 year life. If, however, fuel cycle economics dictate a shorter converter fuel residence time, a vertical tube layout is recommended. Perhaps the U-Mo should be in spherical form for easier fuel handling, although fabrication of clad U-Mo spheres would require development.

e. Burner and Moderator Region

The blanket burner and moderator were analyzed as a single unit (Figure 11). The burner consisted of 5 vol% 316 SS, 15 vol% He, and 80 vol% salt. The moderator consisted of 5 vol% salt and 95 vol% graphite. The composition of the salt is 52 mole % BeF_2, 47.5 mole % LiF (0.83 a/o Li^6), 0.5 mole %PuF_3. This composition resembles the molten salt, flibe. The power generated in the salt in the burner region is 7.4 MW/m^3 and 52 MW/m^3 in the salt in the moderator region (negligible power is generated in the graphite).

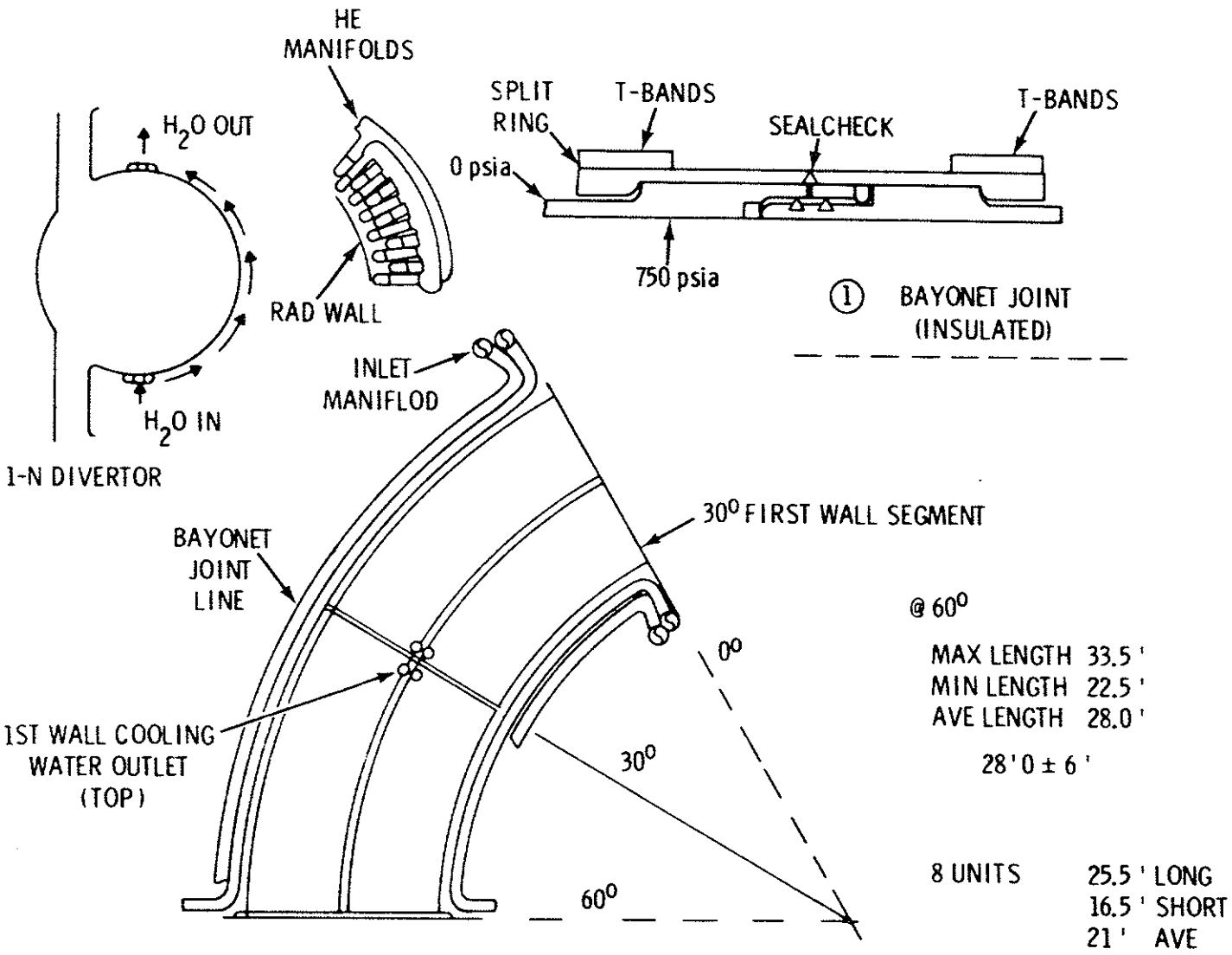

Fig. 9. Converter 60° Segment.

RADIAL SUPPORT PLATE CONCEPT

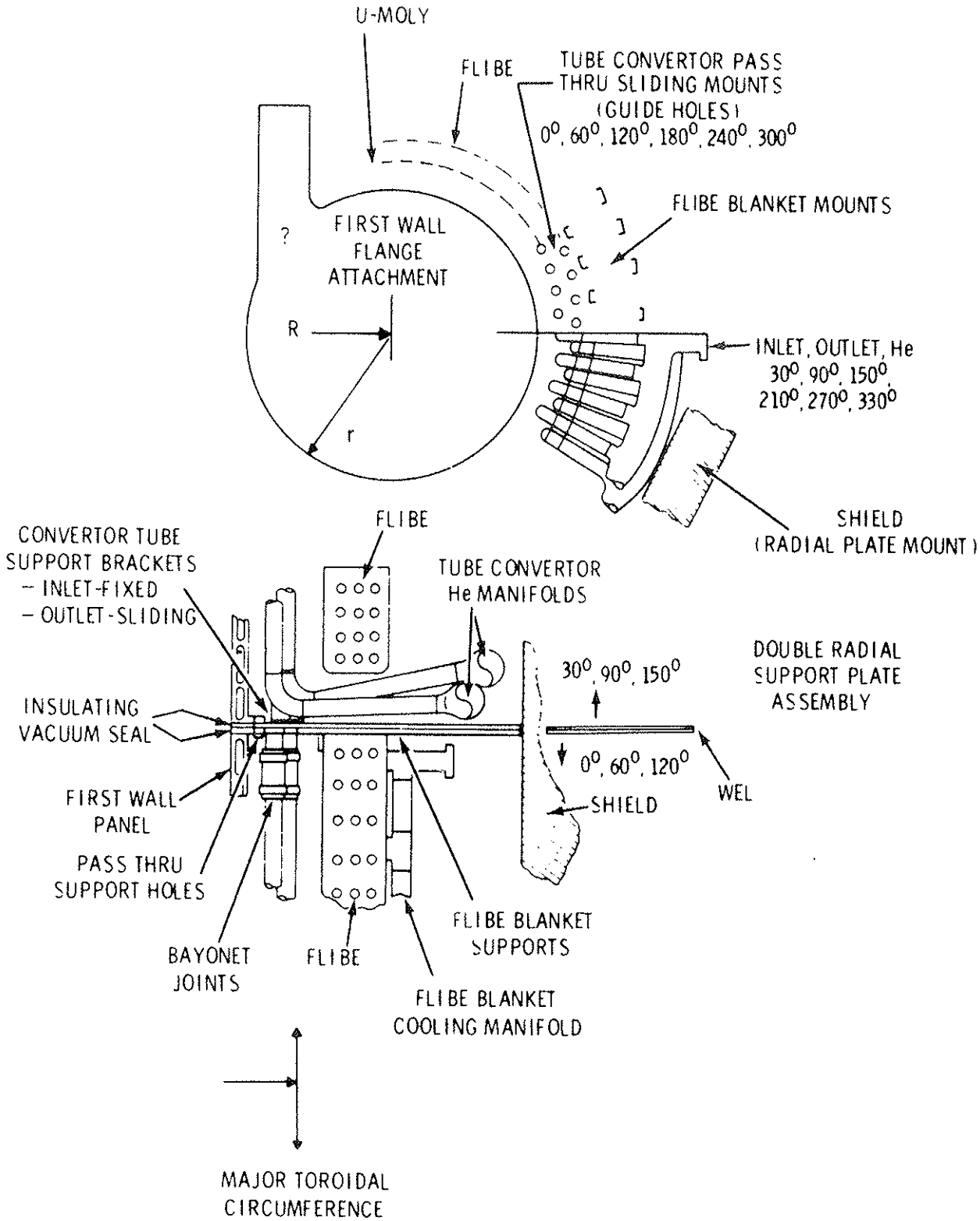

Fig. 10. Radial Support Plate Concept.

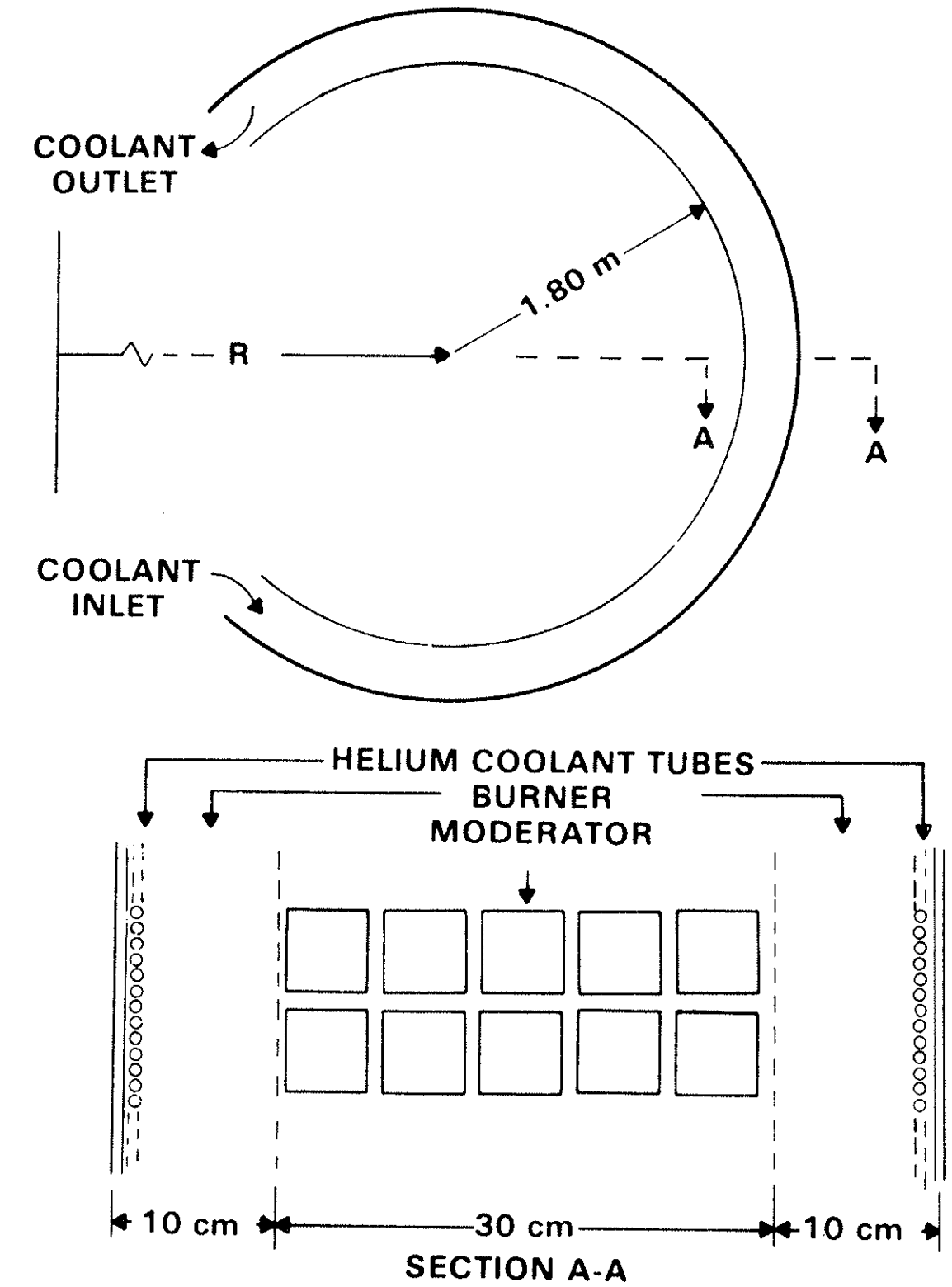

Fig. 11. Schematic of Burner and Moderator.

In designing the heat removal system for the burner-moderator region, transfer of the heat to the helium system in the blanket appeared desirable, as this has two beneficial effects. First, if the salt remains in the blanket during the power-off portion of the cycle, it acts as a thermal storage medium. This minimizes the thermal shock to the structural materials, piping, etc. Secondly, not removing the energy with the salt would eliminate the development of large molten salt pumps. Only a processing stream flow to remove the tritium would be required; this can be accomplished with MSRE pumps.

The question then becomes whether the heat can be removed from the moderator region and still maintain acceptably low (600^{o}C) graphite-salt interface temperatures. The concept shown in Figure 11 would be the most acceptable from the neutronics standpoint and perhaps from a fabrication standpoint.

A two-dimensional code was written to analyze the heat transfers in the blanket. It included the appropriate power generation in each region, conduction in the moderator, conduction and natural convection in the burner, and heat transfer to the bank of helium coolant tubes. The code was also equipped to handle phase changes in the salt since the heat of fusion is substantial and a region of permanently solid salt is undesirable. Thermophysical properties were permitted to be temperature dependent. Average thermophysical properties and power generation rate were applied in the moderator region based on volume percentages and structure; however, a lack of complete agreement seems to exist in the literature on the thermophysical properties of this particular salt (notably liquidus temperature and viscosity).

Thermal profiles in the helium coolant, SS tube wall, burner and moderator are shown in Figure 12(a). These profiles represent conditions at the reactor midplane (Section A-A in Figure 11) at the end of a power-on period (1000 sec) and at the end of a power-off period (100 sec). The helium coolant inlet temperature is 350°C and outlet temperature is 490°C with a nominal pressure of 50 atm, 1 atm pressure drop, and velocity of 100m/sec.

The salt and graphite will be in contact in the moderator at temperatures near 1800°C. Compatibility problems begin to appear above a temperature of approximately 600°C. This temperature difference cannot be reduced significantly by any reasonable changes in helium velocity or inlet temperature. Note: Natural convection in the salt effectively promotes a nearly isothermal profile except at the SS interface. At this interface, the relatively low thermal conductivity of the salt leads to a very steep thermal gradient.

In view of the excessively high temperatures, another situation was examined where one bank of helium coolant tubes was placed at the burner-moderator interface and an additional bank was placed in the center of the moderator. The thermal profile for this case satisfied compatibility requirements for both graphite and SS as shown in Figure 12(b). Unfortunately, introducing additional SS results in excessive neutron absorption, thus yielding inadequate tritium and plutonium production. Using this configuration would require using a tubing material with much lower absorption cross section than SS or higher fissile plutonium enrichment in the burner salt.

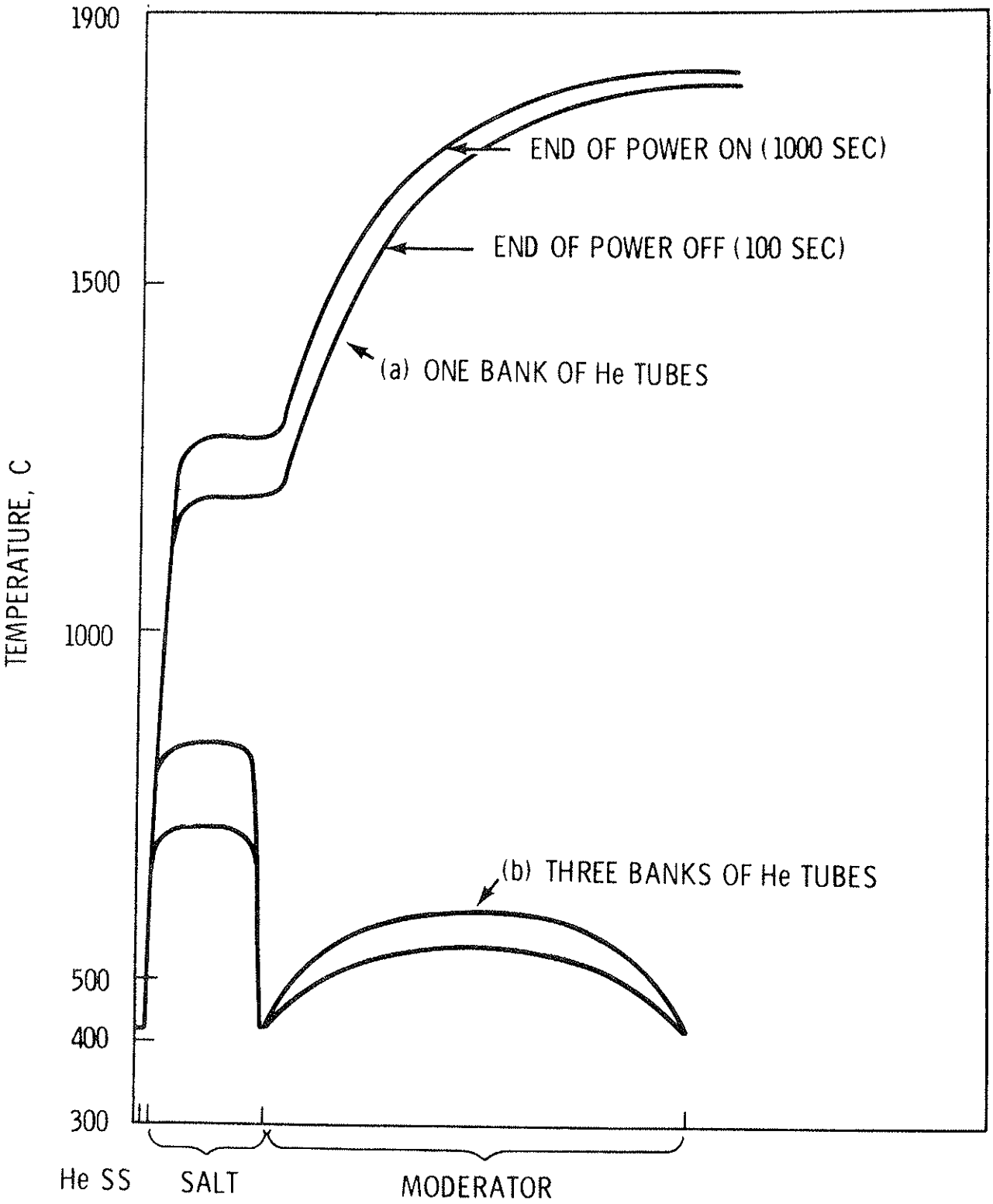

Fig. 12. Thermal Profile in Burner and Moderator at Mid/Plane.

Neither case considers circulation of the burner salt in the graphite moderator. With the large temperature gradients calculated in Case 1, significant natural circulation would probably occur. To make any meaningful calculations, however, would require spending some time designing discrete channels in the graphite moderator. The channels would have to vary, depending on the orientation of the blanket as it wraps around the plasma chamber. (This effort was beyond the scope of this study).

It may also be possible to induce forced circulation of the burner salt in the graphite moderator. The process stream for extracting tritium could be brought back into the blanket so that it caused some circulation in that region. More work must be done on laying out the blanket tanks before any meaningful analysis of this concept can be made.

A final situation was briefly examined. The original helium coolant configuration (two rows, one each at the outer face of each burner) was maintained, but the molten salt was pumped through the burner and moderator regions. An average velocity of approximately 10 cm/sec is estimated to be sufficient to keep temperatures within bounds. A heat exchanger along with the tritium recovery cycle loop would then be used external to the blanket and shield. This situation could be considered as a last resort since it grossly changes the dynamic characteristics of the blanket heat removal and requires the development of large molten salt pumps.

The analysis did not include magnetohydrodynamic (MHD) effects. MHD effects are expected to be especially noticeable on natural convection currents in the molten salt and, hence, the

temperature profile. Transient natural convection velocities of the order of 1 m/sec were noted in the absence of MHD forces. Other MHD effects of potential concern are increased pumping losses and corrosion. It is recommended that MHD effects be included in future detailed thermal hydraulic studies.

References

[1]D. T. Aase, M. C. C. Bampton, T. J. Doherty, B. R. Leonard, R. A. McCann, D. F. Newman, R. T. Perry, C. W. Stewart, TCT Hybrid Preconceptual Blanket Design Studies, Battelle Pacific Northwest Laboratories Report PNL-2304 (1978).

[2]D. Bushnell, Stress, Stability and Vibration of Complex Branched Shells of Revolution: Analysis and Users Manual for BOSOR4, Lockheed Missile and Space Company Report No. D243605 (1972).

[3]A. J. Lovell, Effect of Fast Reactor Fluence on Post-Irradiation Rupture of Type 316 Stainless Steel, Nuclear Technology 26, July 1975.

4. Electrical Systems

a. General

The electrical systems for the hybrid reactor accept (supply) energy from (to) the commercial high voltage transmission system and transform, condition, store, transfer, and distribute it in accordance with the needs of the hybrid reactor and the commercial power system.

i. Commercial Power System

The interface between the hybrid reactor and the commercial power system is established at a high voltage, high power location in the commercial system. The stiffness of the commercial system is typically such that a 1000 MW power plant can be instantaneously disconnected from the system (equivalent of 1000 MW load imposition) without producing unacceptable voltage or frequency transients. Hence the load duty cycles imposed on the system by the hybrid reactor operational requirements need not be cushioned but can be imposed directly on the system.

ii. Hybrid Reactor Electric Power Generation

The conversion of heat energy to electric energy (3000 MW) in the hybrid reactor complex is accomplished by relatively conventional steam turbine generation units which derive their steam from helium heated steam generators. The steam turbine units are rated 1000 MW.

iii. Operational Energy Storage and Transfer

The energy storage and transfer functions required for proper reactor operation include energization and deenergization of the toroidal, ohmic heating, vertical and divertor field coils as well as the neutral beam injectors. The choice of devices to

achieve the requisite storage and transfer is dependent, for each purpose, upon the amount of energy involved, the rate of transfer and the cost effectiveness of the approach. Establishment of the requisite coil fluxes inevitably results in energy being stored in those fields. Changing the flux levels, therefore, involves transfer of energy between the coil system of interest and some alternate energy storage repository. In the case of the hybrid reactor, the energy storage repository is the power grid.

b. Constraints/Ground Rules

The constraints, assumptions and ground rules upon which the candidate system is based are as follows:

a) The commercial power system stiffness at its interface with the hybrid reactor is more than adequate to accept the reactor pulsed loads. No pulsed load cushioning is required.

b) Maximum utilization of commercial equipment is made in consideration of cost, schedule and proven performance considerations.

c) Personnel safety and equipment protection features are factored into the designs, considering both normal and abnormal operating modes.

d) The toroidal field will remain energized.

e) Energize time for ohmic heating, vertical and divertor coil systems is 10 seconds. Deenergize time is also 10 seconds.

f) Electrical output of the power generation equipment must be maintained constant at 3000 MW.

c. Electrical Systems

The hybrid reactor electrical system is presented with minimal justification for its candidacy. Advantage is taken of prior tradeoff studies and conclusions to establish this viable candidate system.

The block diagram of Figure 1 shows the overall electrical systems configuration. Each of the hybrid reactor coil systems (TF, OH, VF, DF) as well as the NBI system is energized from the power system via appropriate voltage transformation and controlled rectification/inversion power supplies to permit energy transfer from power system to coil and vice versa.

i. General

The electrical systems treatment primarily is oriented to the reactor coil and neutral beam injector systems. Interfaces with the power grid and the power plant are established.

The superconducting parallel circuits in the various coil systems present a potential problem because their essentially zero resistance introduces the possibility of large disparity in parallel path currents. Each path in a superconducting circuit should be energized by its own power supply, the power supplies controlled for appropriate coil current coordination.

The ac input harmonic current demand of the rectifier/inverter power supplies has negligible effect on the commercial power grid voltage by reason of the stiffness of the power system. No interference is anticipated among the several rectifier/inverter equipments supplying dc to the various reactor coils.

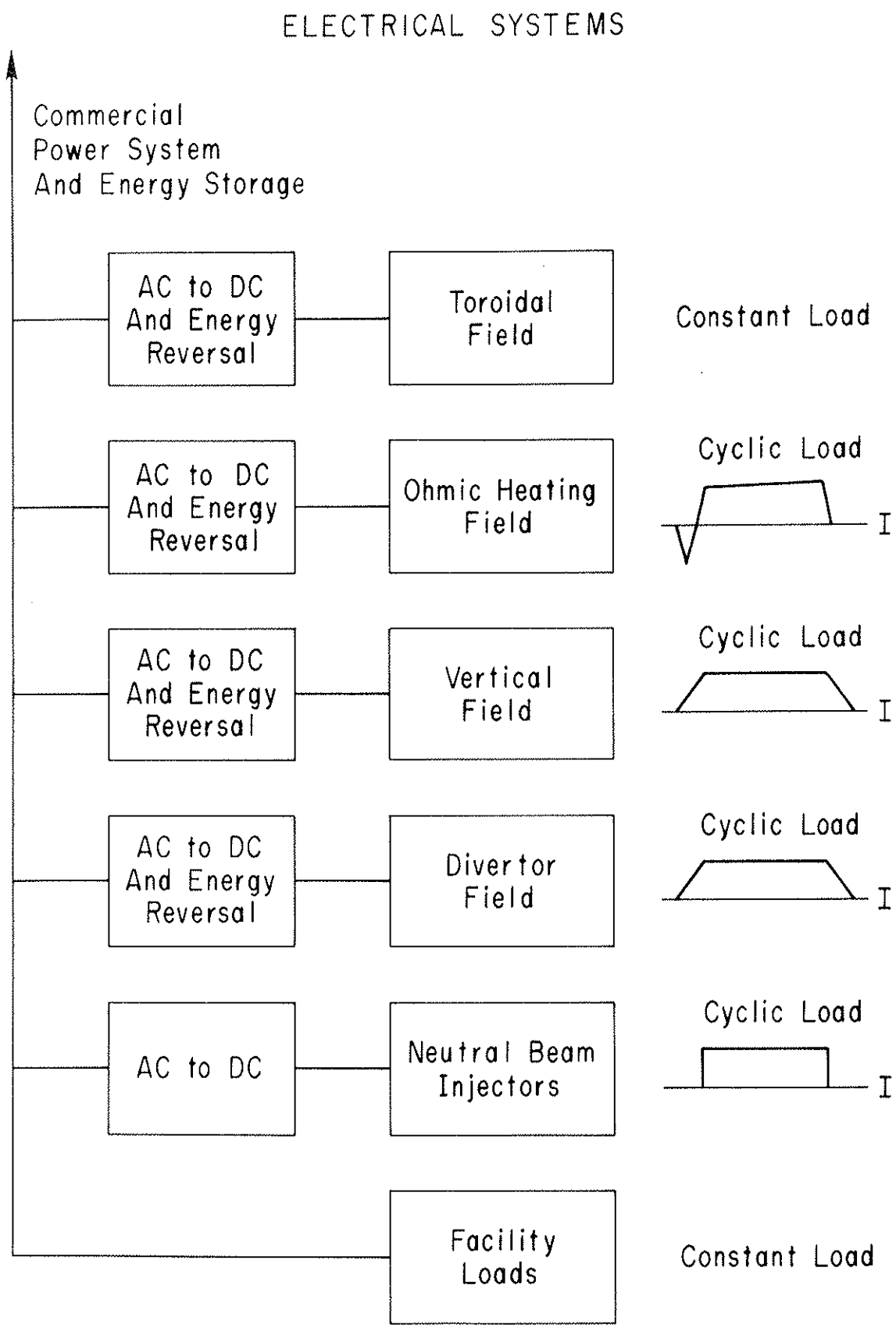

Fig. 1. Electrical Systems of Hybrid Reactor.

Equipment and personnel protection is designed into the electrical systems in the form of overvoltage protection and fast energy dump capability for the coils.

aa. Commercial Power System Interface

The interface between the hybrid reactor and the commercial power system is represented by the summarization of the plant auxiliary and energy storage and transfer system loads. The plant auxiliary load is approximated at 300 MW and includes such loads as compressors, pumps, fans, blowers, heaters, and lighting and utility systems. The interface load characteristic is shown in Figure 2a. The steady state and cyclic loads are indicated in Figure 2b.

bb. Power Plant Interface

The heat energy developed by the hybrid reactor is recovered by helium heated steam generators whose steam output drives steam turbine generator units.

cc. Energy Storage and Transfer

The energy storage and transfer system requirements are determined by the needs of the plasma and the relationships between the plasma and the pressure vessel.

The toroidal field, whose function is to contain the plasma, remains energized throughout the cyclic operation of the hybrid reactor. The inductance of the toroidal field circuit is so high (9.2×10^3 H for 748 turns/coil, 68 coils) that the resulting long energizing time prevents timely cyclic decay and buildup to the required field strength without excessively high applied voltage.

Energization to the toroidal field strength of 75,000 gauss at plasma center requires 8400 volts for 3 hours. Superconducting

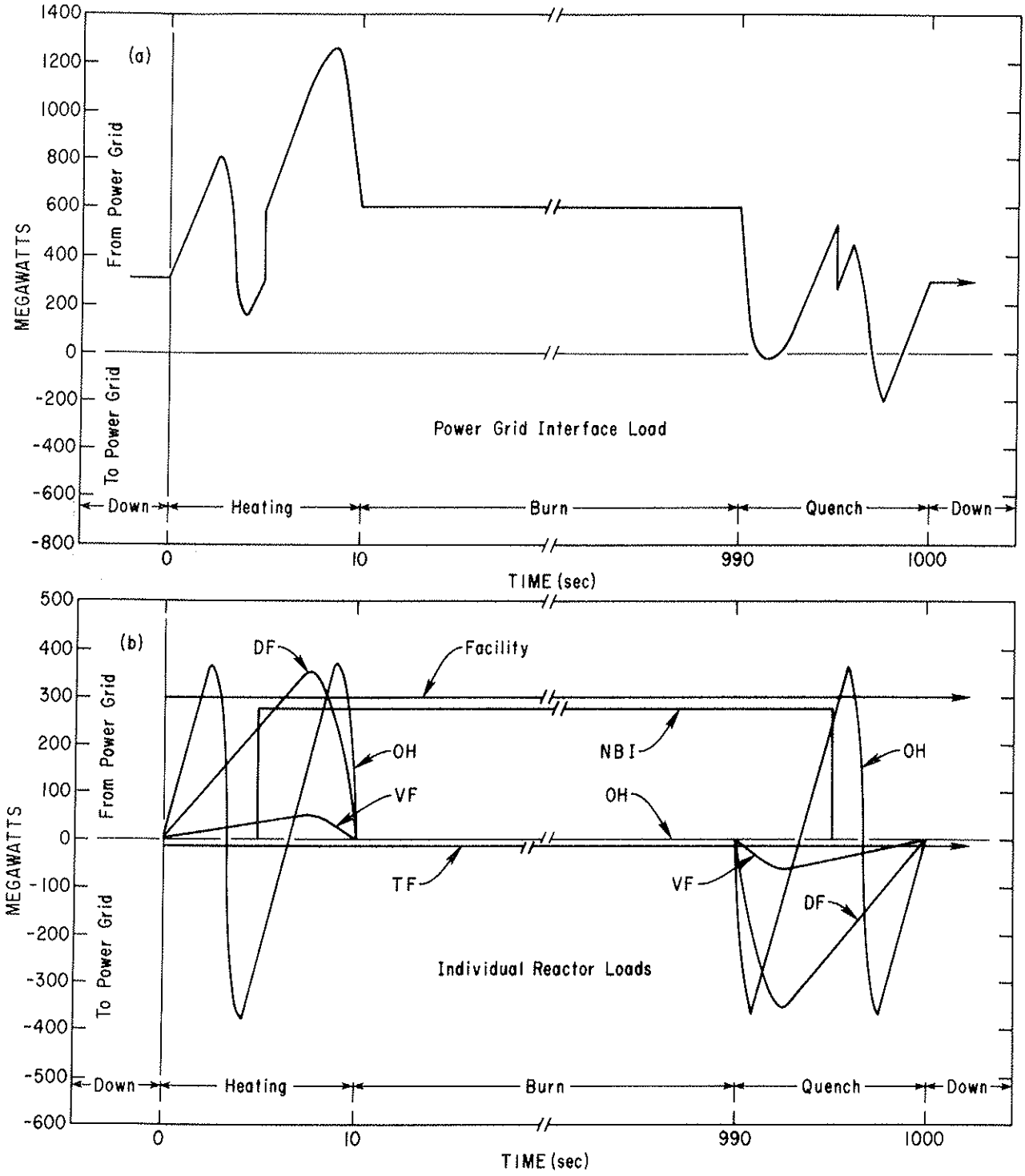

Fig. 2. Electrical Load Characteristics for Hybrid Reactor.

coils require some profiling of voltage and current so the last hours of energization incorporates voltage reduction to limit the rate of change of current. The energy stored in the TF magnetic field is 460 GJ.

The toroidal field energy conversion system (TFCS) consists of controlled thyristor rectifier/inverter devices appropriately interconnected with the TF coils for optimum voltage and current performance to be equivalent to an all-turns-in-series rating of 8400 volts, 10,000 amperes.

The ohmic heating field, whose functions are to initiate and heat the plasma and to adjust plasma current during burn, acts as the primary of a transformer whose secondary is the plasma. The required voltage (of the order of 100 volts) is induced in the plasma by forcing a high value of di/dt in the ohmic heating coils, thus causing a high value of $d\phi/dt$ in the plasma loop. Incidentally, a high value of voltage (37 kV) is also induced in the ohmic heating coils, assuming all turns in series.

The OH, VF and DF coils are inductively coupled with each other and with the plasma. Consequently there is considerable current loop interaction that must be taken into account in the analysis of current responses and design of the poloidal field coils and control circuits.

The current in the ohmic heating coils is forced to a peak value (10kA) in one direction, then reversed rapidly (6.7 sec) to a similar peak in the opposite direction and maintained with a constantly increasing small variation until the end of the burn period when the reverse operation takes place. The energy stored

in the OH magnetic field is 0.62 GJ.

The ohmic heating field energy conversion system (OHCS) consists of controlled thyristor rectifier/inverter devices appropriately interconnected with the OH coils for optimum voltage and current performance. Each circuit path is powered by its own thyristor device, the equipment complex exhibiting equivalence to an all-turns-in-series rating of 37 kV, 10,000 amperes. The field reversal requirement dictates the high voltage as well as greater sophistication in the OHCS design.

The vertical field determines the radial position of the plasma within the torus. For a fixed plasma position, this field must be generally proportional to the plasma current. The rapid initial rise of plasma current, and consequently of vertical field and current, is the compelling factor in equilibrium field system design.

The divertor field, whose function is to establish a field contoured to divert spent plasma to a removal point, must similarly be controlled to be generally proportional to the plasma current.

The current in the vertical/divertor field coils reflects the plasma current variations and, at burn cycle initiation, is forced rapidly (10 sec) to a high value (10,000 amperes). During the remainder of the burn the current is held constant. At the end of the burn the current decrease is essentially the reverse of the initial current buildup.

The vertical/divertor field energy conversion system (VFCS/DFCS) consists of controlled thyrister rectifier/inverter devices interconnected with the VF/DF coils for optimum voltage

and current performance. Each circuit path is powered by its own thyristor device, the equipment complex exhibiting equivalence to an all-turns-in-series rating of 5700/36,000 volts, 10,000 amperes.

The neutral beam injection function serves to raise the plasma temperature and to maintain it at the required level. The duration of injection depends upon plasma density, plasma temperature, burn time and whether the plasma is ignited.

The neutral beam injector (NBI) requirements differ from those of the functions (TF, OH, VF, and DF) already discussed. The functions discussed earlier incorporated the energy storage characteristics of the fields as prime factors to be considered, whereas the neutral beam injector system utilizes the input power (energy) to provide, and pass on, the required output power. No inherent energy storage exists although recoverable energy losses unavoidably occur as dictated by the NBI system design.

The input power requirements of the NBI power supply function are 100 MW or more. The sudden load imposition can easily be tolerated by the power grid.

The neutral beam injector energy conversion system includes ac to dc power supplies, each feeding an ion source, neutralizer and ion dump mechanism. The NBICS design further incorporates recovery of the ion dump energy.

5. Energy Storage for Hybrid Reactor Cycles

a. Introduction

It is likely that tokamak reactors will have an inherent characteristic requiring periodic plasma reignition. This introduces the problem of energy storage to permit continuous electrical output to the power grid. The cycle under consideration in this section is a 1000-second burn followed by a 100-second rest time.

The physical size of the toroidal plasma reaction chamber for the hybrid reactor is comparable to that of the fusion power plant reactor described in Ref. 1, and the thermal energy storage requirements are almost identical. For these reasons, Ref. 1 will serve as a basis for much of the ensuing discussion.

b. Energy Transfer Mechanism

The heat transfer mechanism from the blanket to the electric power grid involves four energy transfer "loops" as shown in Figure 1. The plasma reaction vessel is surrounded with a molten blanket of plutonium-bearing flibe for the purpose of energy multiplication and tritium breeding. Distributed throughout the flibe is a flibe/helium heat transfer pipe grid for cooling the flibe. The hot helium, in turn, is circulated through helium/steam generators to produce steam. The steam powers steam turbine generator units which deliver electric power to the power grid.

Inherent in the heat transfer mechanism is some significant energy storage capability. The blanket has heat storage capability (assuming a $100^{\circ}F$ temperature drop) corresponding to approximately 35% of the total thermal storage requirement of 920 gigajoules. There is some nuclear afterheat which amounts to approximately 5% of the total requirement. There is additionally

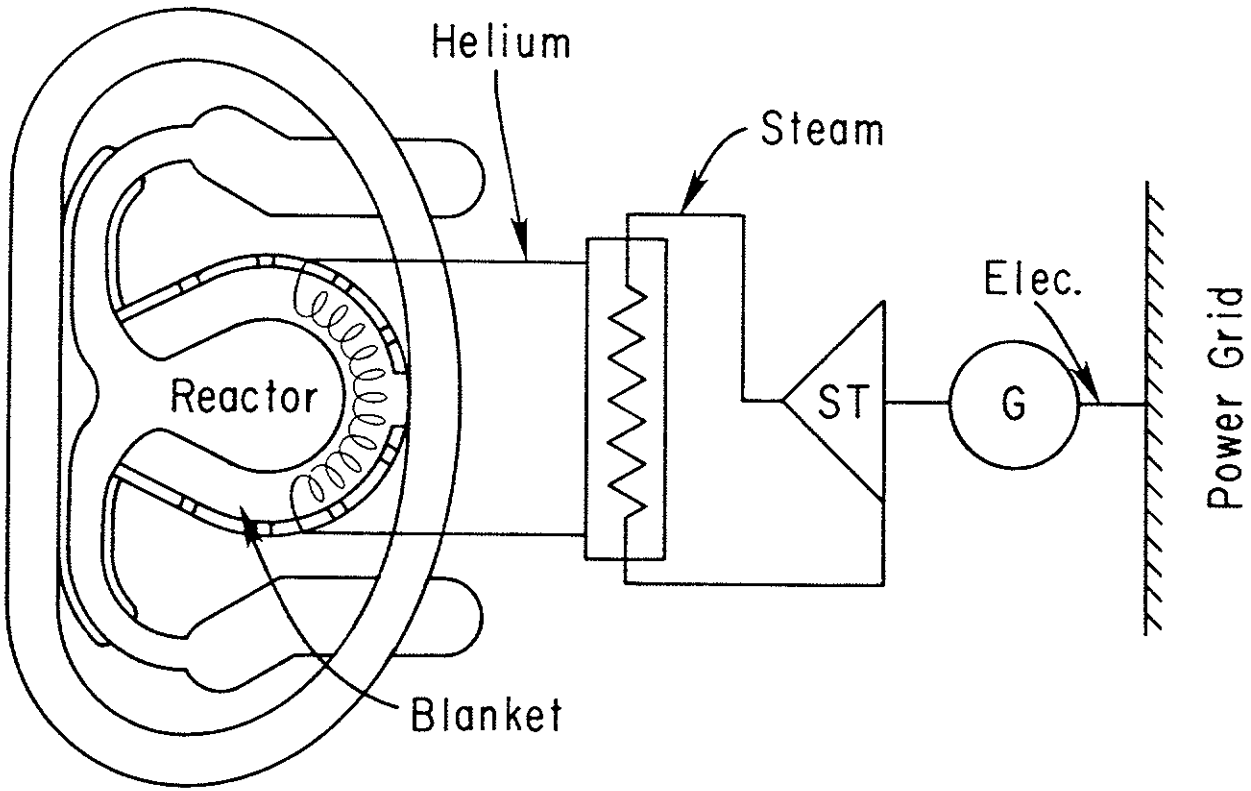

Hybrid Reactor Energy Transfer

- Reactor operation is cyclic - 1000 sec burn, 100 sec rest
- Electrical output is constant - 3000 MW (or 9000 MW thermal)
- Energy storage requirement is 920 GJ thermal (or 870×10^6 Btu)
- Steam turbines require steam at 1000 lb., $600^{\circ}F$
- Allowable temperature variation - steam $50^{\circ}F$, helium $100^{\circ}F$

Figure 1

some storage in the helium and steam volumes whose contributions are assumed to be negligible.

i. Flibe Loop

The four energy transfer loops of the hybrid reactor present a variety of possibilities for energy storage. The flibe loop offers the possibilities of storage in an extra volume of flibe or in a volume of a less expensive salt via an additional heat exchanger.

ii. Helium Loop

The helium loop offers the potential for incorporation of a variety of heat storage devices such as ceramic refractory blocks, fluidized beds or steel tubes, referred to generally in this discussion as "hot rocks".

iii. Helium/Steam Interface

The interface between the helium and steam loops offers the possibilities of integrated heat transfer and energy storage, utilizing either the fluidized bed or the flash steam approach.

iv. Steam Loop

The steam loop offers the possibility of storage of steam itself.

v. Electrical Loop

The electrical loop offers the potential for utilization of mechanical/electrical energy storage in the form of rotating machines incorporating flywheels, hydraulic storage in the form of pumped storage, magnetic field storage in the form of superconducting coils or electric field storage in the form of capacitors. A further possibility is modification of power grid operating procedures (and possibly configuration) to permit inherent compatibility with the reactor cycles.

c. Assumptions/Constraints

The constraints and assumptions guiding this energy storage study are:

a) Electrical output to the power grid must be maintained constant at approximately 2500 MW.

b) Steam temperature change at the turbine inlet cannot exceed 50°F. This constraint derives from data applicable to the 1000 MW steam turbine generator units used presently in nuclear power plants. Utilization of 250 MW units might permit a relaxation of this requirement. Designs of these smaller machines have been developed to permit temperature and load cycling.

c) For metallurgical reasons the helium temperature at the hottest helium loop point in the reactor should be limited to 600°C (1113°F). To allow a reasonable margin, a helium hot spot temperature of 550°C (1022°F) is postulated.

d) Allowable helium and flibe temperature change during the reactor downtime is judged to be 100°F. This judgment is based on the probability that flibe and helium mass flow rates can be controlled to limit the steam change to the 50°F required by the steam turbines. The helium loop cool side temperature must be maintained no cooler than 710°F to prevent flibe solidification.

e) Implementation of the energy storage concept will be achieved by methods closely approached by state-of-the-art to the extent that no breakthroughs are required.

d. Energy Storage

Various energy storage methods incorporated into the flibe, helium, steam and electrical loops were investigated. Several of these methods are shown, and their advantages and disadvantages summarized in self-explanatory figures 2, 3, 4, 5, 6, 7, 8 and 9.

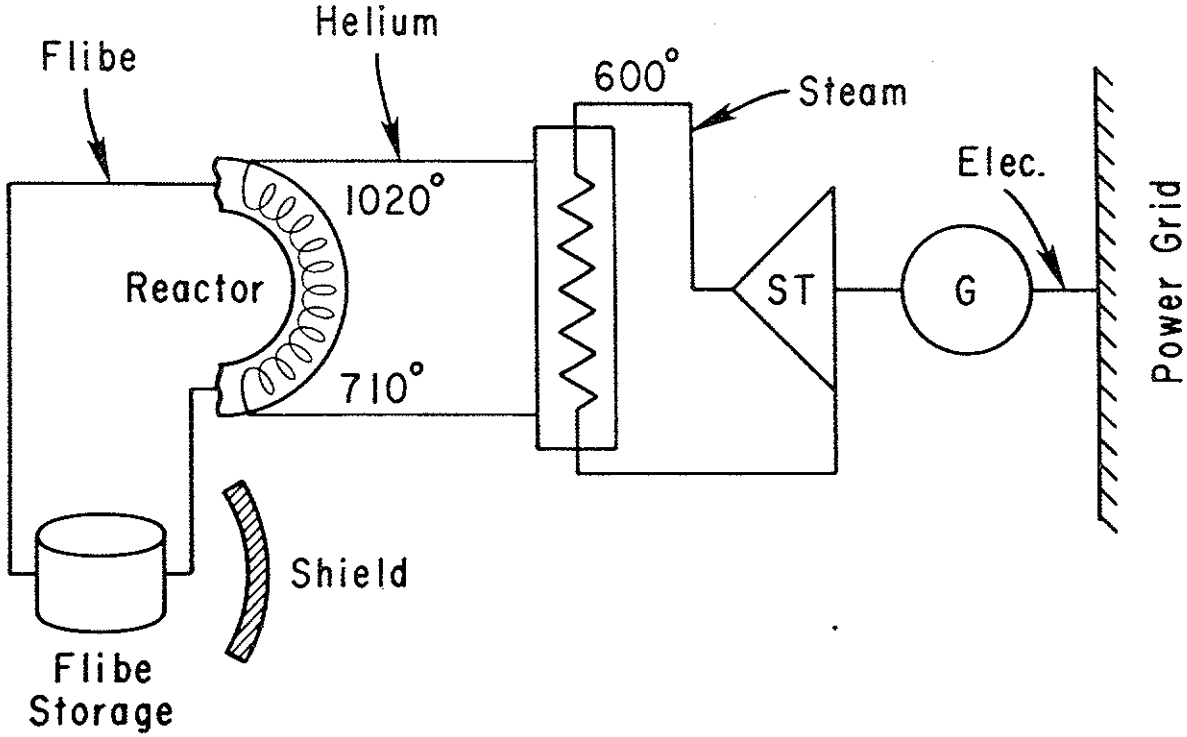

Hybrid Reactor Energy Storage Systems

Flibe Loop

Reactor operation is cyclic
1000 sec burn, 100 sec rest

Advantages

1. No additional heat exchanger.

Disadvantages

1. Flibe is costly > $0.64 billion
2. Flibe is radioactive - shielding of extra flibe storage is required.
3. Energy retrieval is difficult -- large quantity flow required.

Figure 2

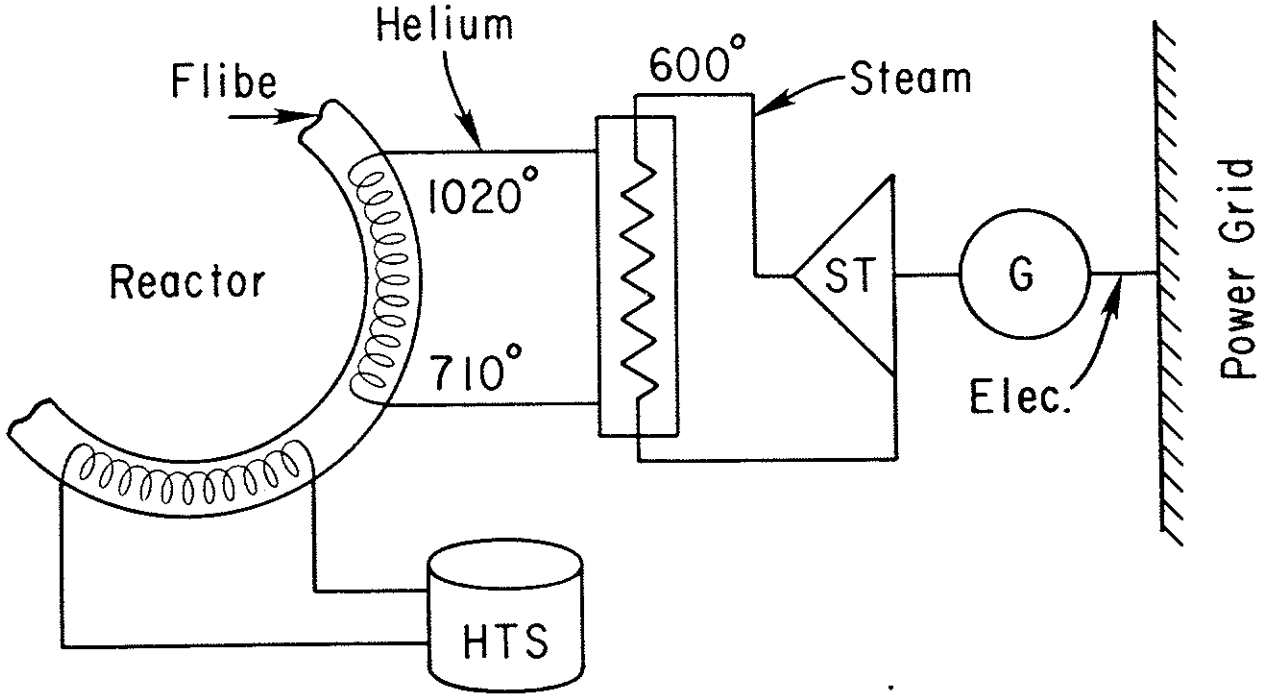

Hybrid Reactor Energy Storage Systems

Flibe Loop

Reactor operation is cyclic
1000 sec burn, 100 sec rest

Advantages

1. Heat storage in Dupont HTS commercial high temperature salt is relatively inexpensive.

Disadvantages

1. Extra heat exchanger required.
2. Energy retrieval is difficult - large quantity flow required.
3. Insufficient temperature difference.

Figure 3

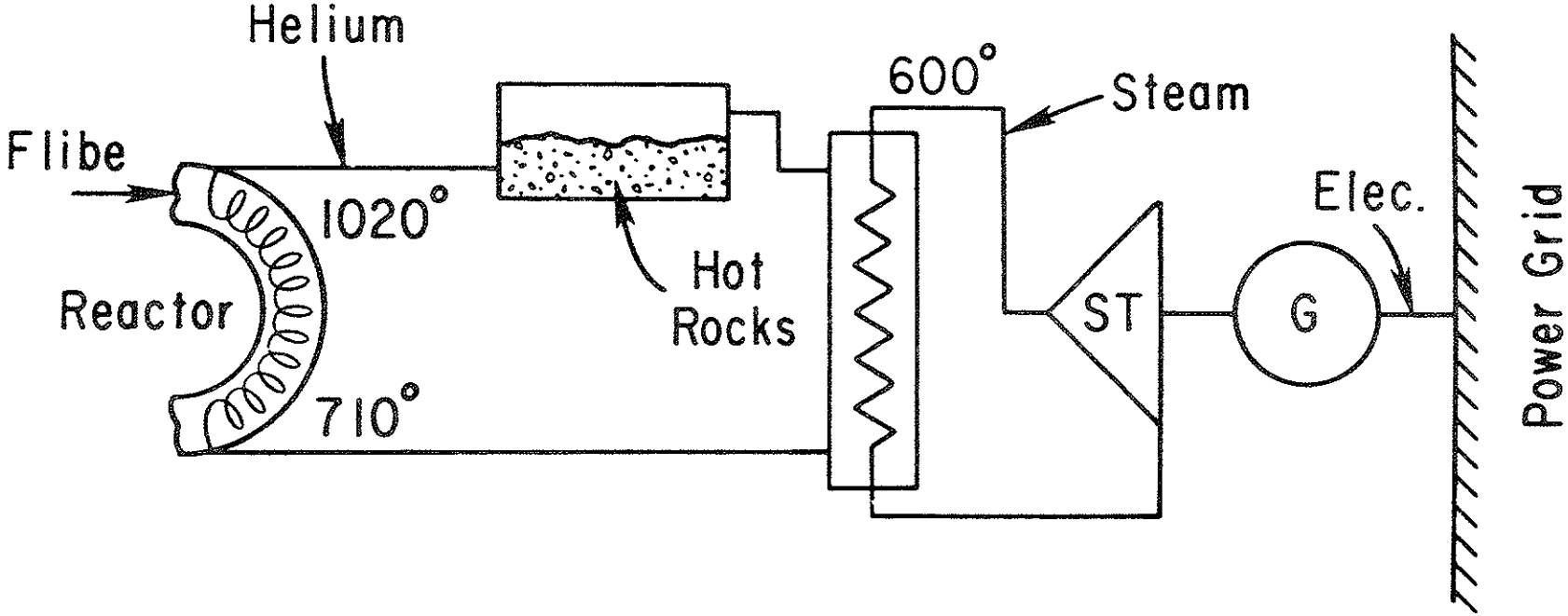

Hybrid Reactor Energy Storage Systems

Helium Loop Series

Reactor operation is cyclic
1000 sec burn, 100 sec rest

Advantages

1. Heat storage material can be inexpensive.

Disadvantages

1. Insufficient temperature difference, storage probably very large.
2. Impurity separation at bed exit required for rocks or fluidized bed.
3. Estimated cost > $50 million.

Figure 4

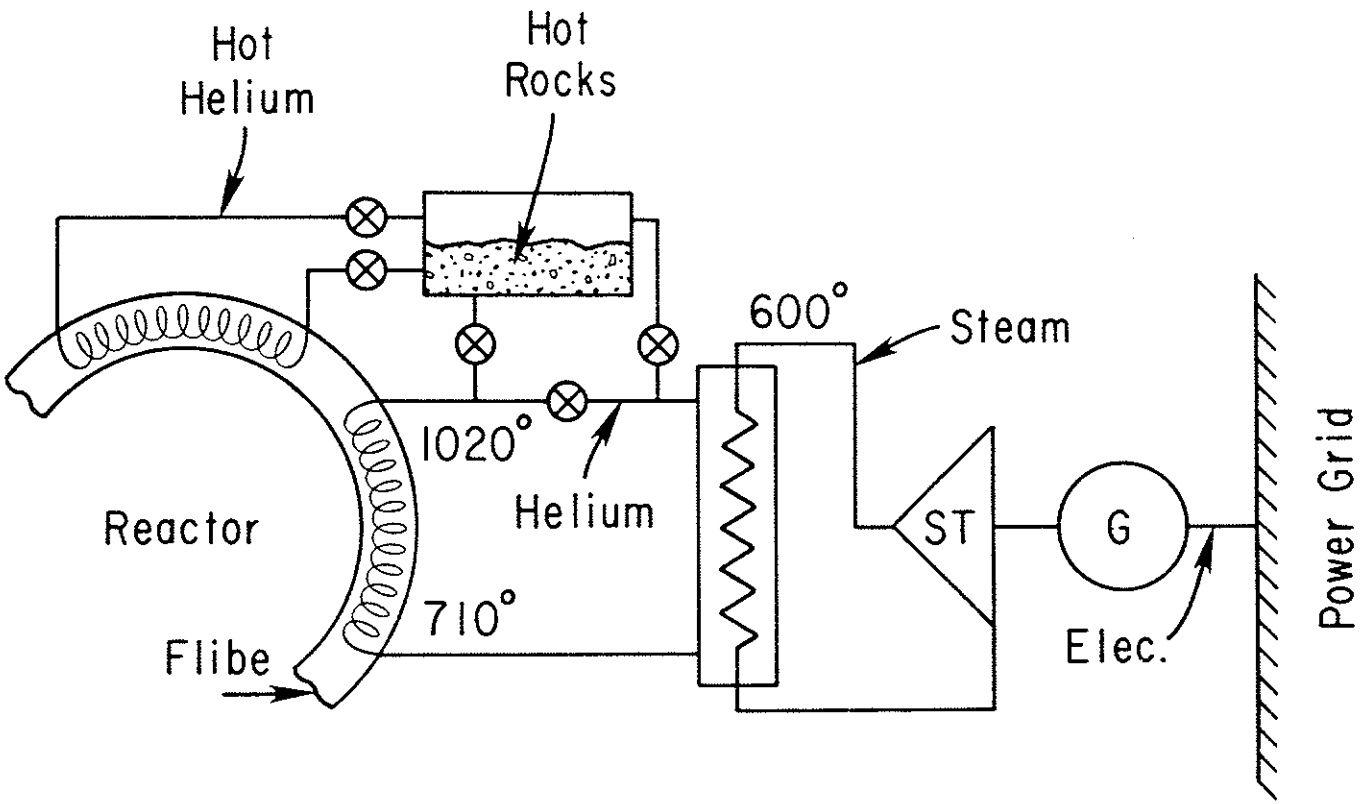

Hybrid Reactor Energy Storage Systems

Helium Loop Parallel

Reactor operation is cyclic
1000 sec burn, 100 sec rest

Advantages

1. Heat storage material can be inexpensive.
2. Improved temperature difference.

Disadvantages

1. Extra heat exchanger required.
2. Extra valving required.
3. Impurity separation at bed exit required for rocks or fluidized bed.

Figure 5

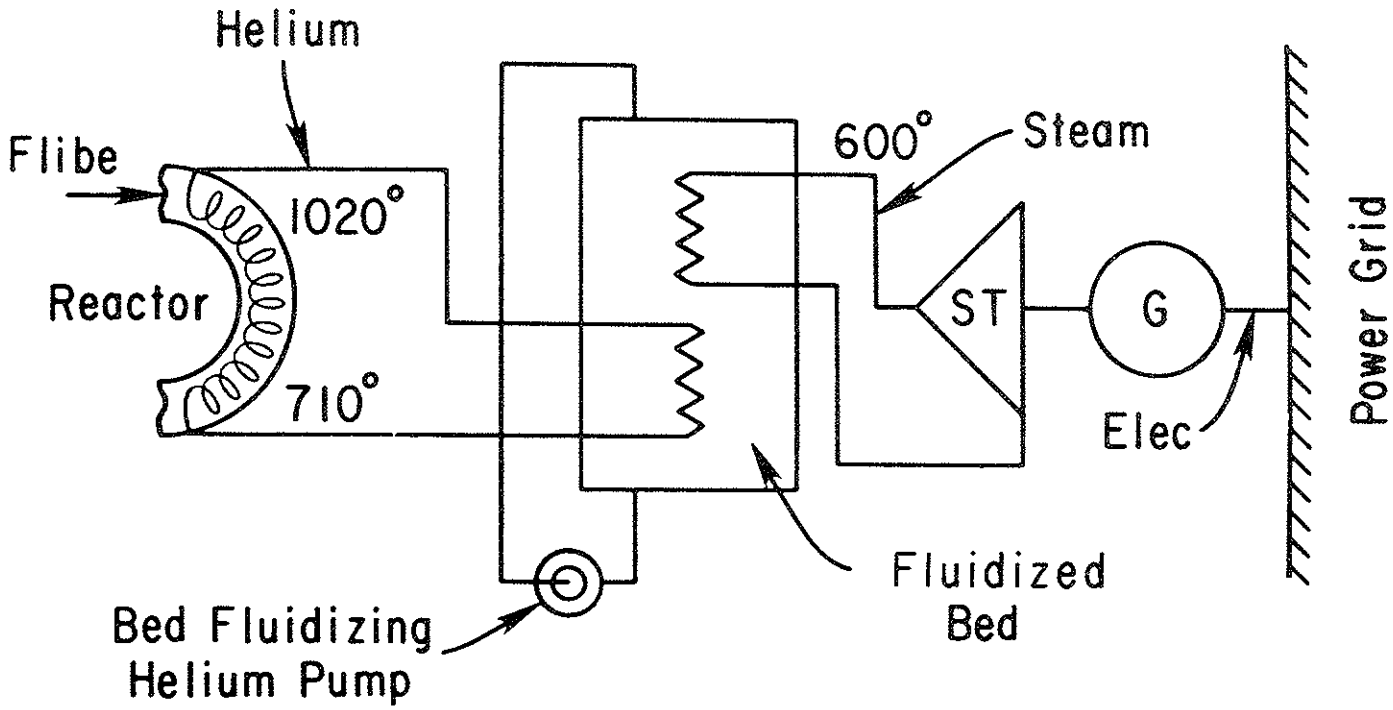

Hybrid Reactor Energy Storage Systems

Helium/Steam Interface

Reactor operation is cyclic
1000 sec burn, 100 sec rest

Advantages

1. Heat storage capability incidental to heat transfer -- Δ cost for storage is negligible.

Disadvantages

1. Fluidized bed performance and reliability are controversial.

Figure 6

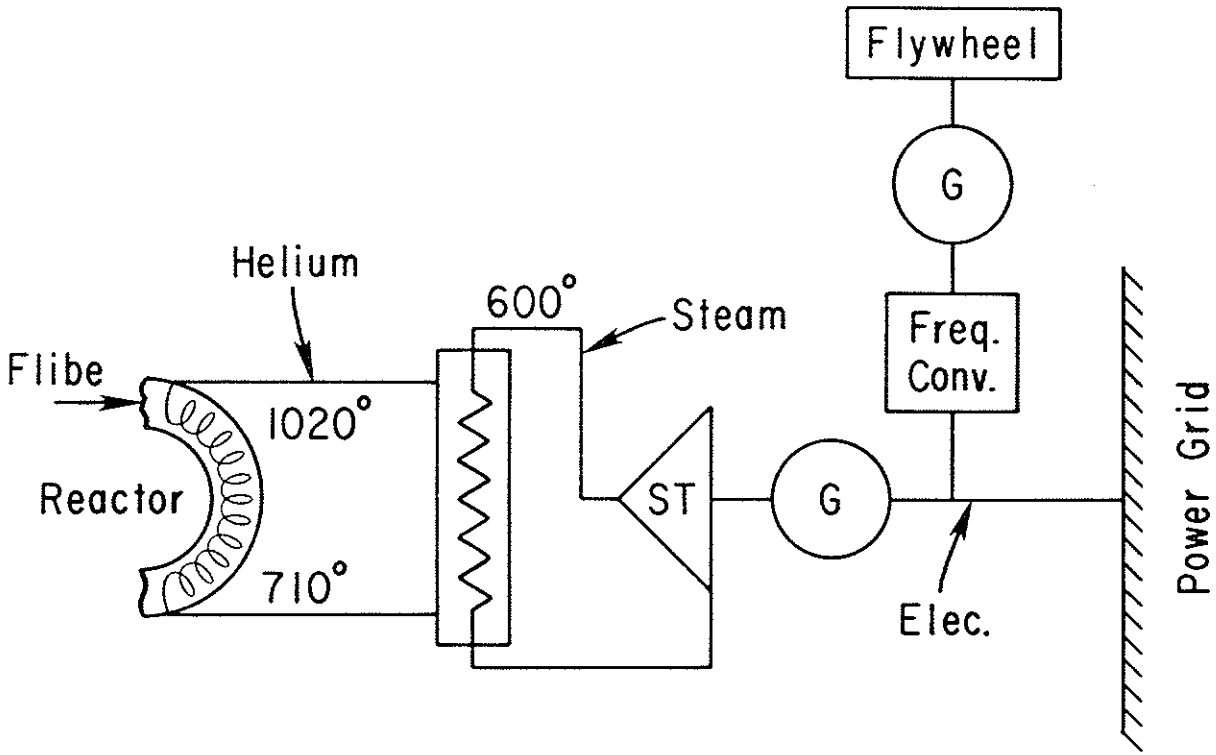

Hybrid Reactor Energy Storage Systems

Electric Loop

Reactor operation is cyclic
1000 sec burn, 100 sec rest

Advantages

1. Storage requirement is 33% of thermal storage.
2. Proven technique -- state of the art.

Disadvantages

1. Throttlable steam turbines required -- smaller than 250 MW rating.
2. Costly > $0.8 billion.

Figure 7

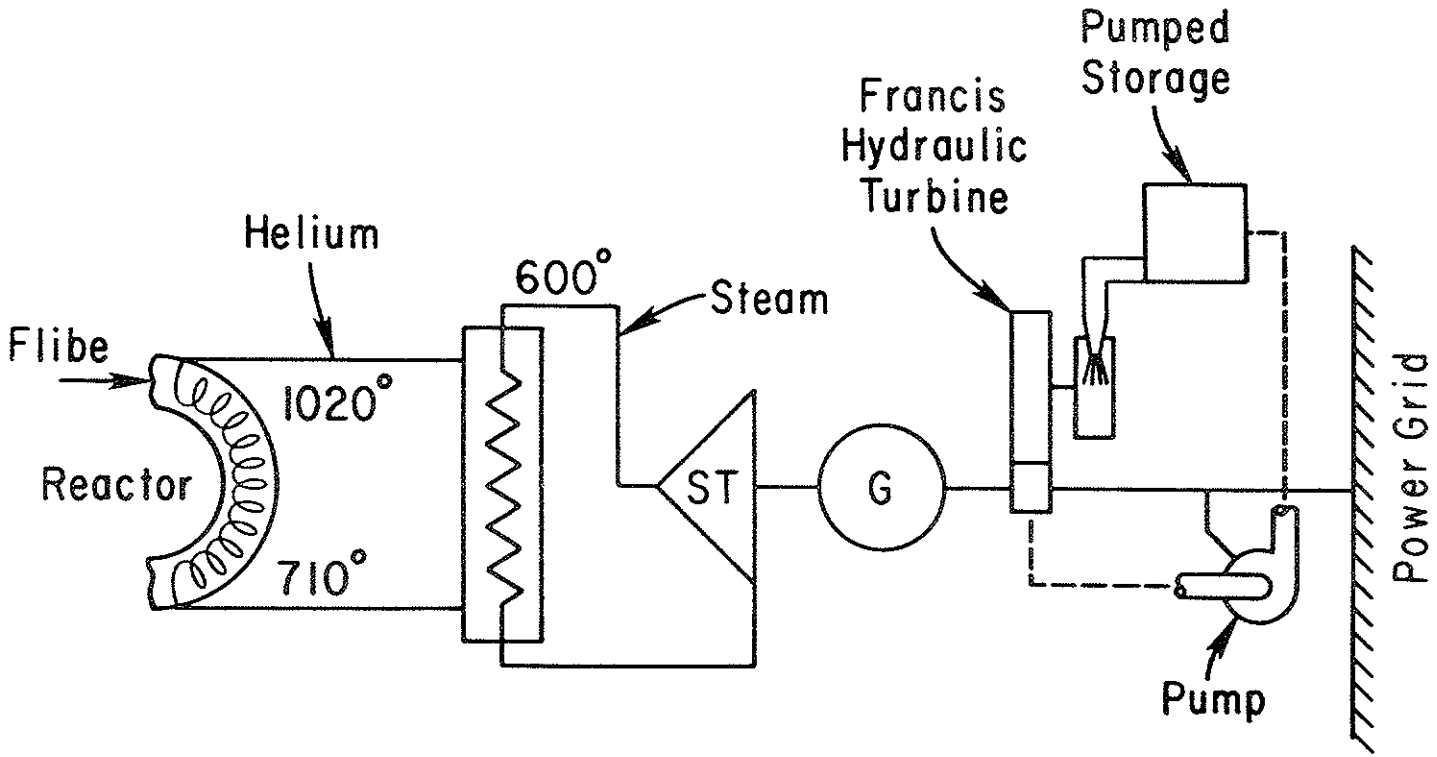

Hybrid Reactor Energy Storage Systems

Electric Loop

Reactor operation is cyclic
1000 sec burn, 100 sec rest

Advantages

1. Storage requirement is much less than thermal storage.

Disadvantages

1. Throttlable steam turbines required -- 250 MW rating or smaller.
2. Δ cost > $100 million.

445
B5

Figure 8

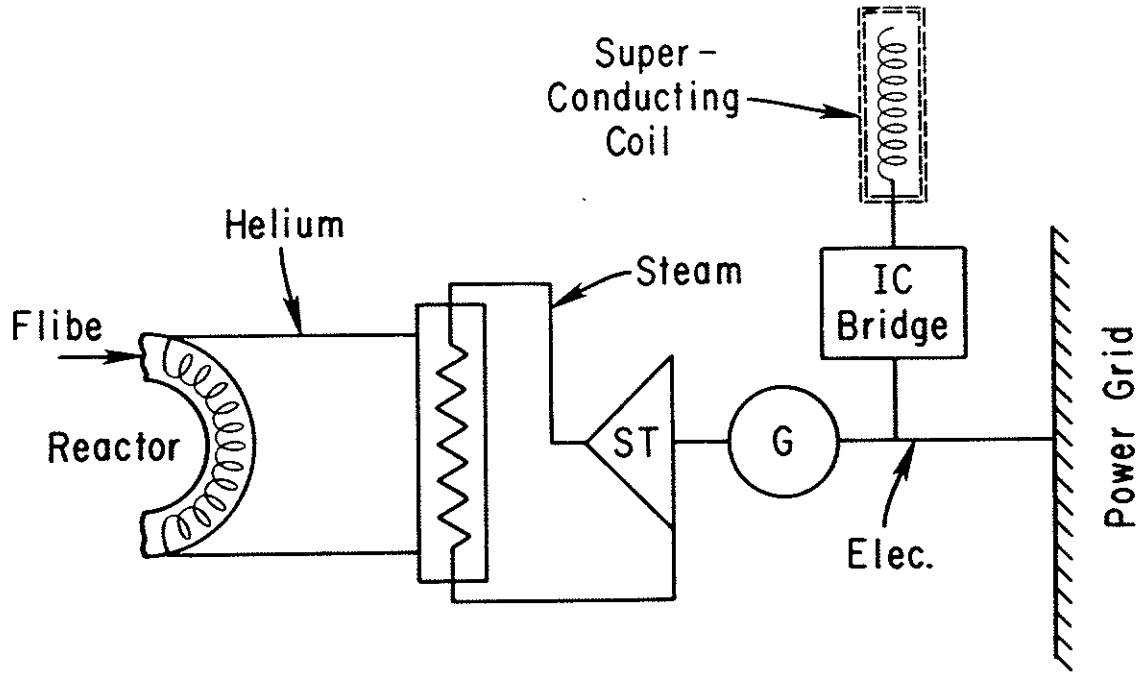

Hybrid Reactor Energy Storage Systems

Electric Loop

Reactor operation is cyclic
1000 sec burn, 100 sec rest

Advantages

1. Storage requirement is 33% of thermal storage.

Disadvantages

1. Throttlable steam turbines required -- smaller than 250 MW rating.
2. Costly > $1 billion.

Figure 9

One disadvantage is common to several of the approaches. It is identified in the figures as "insufficient temperature difference", and it is based on the fourth assumption/constraint which assumes a 100°F temperature excursion for the flibe and the hot side helium and a 50°F excursion for the steam. When energy is transferred across a heat exchanger alternately in both direction (i.e., hot rocks are heated by, and then heat, the helium) and when the temperature differential is small (cannot be more than 100°F, probably closer to 50°F), the heat exchanger must necessarily have a very large heat transfer area. Size and cost are consequently large.

The preferred method, the flash steam approach, is one which constitutes the helium/steam interface and which incorporates the energy storage function as well as the basic energy transfer (steam generation) function.

i. Flash Steam Concept

The flash steam concept given in Figure 10 stores energy in containers which are filled with a water/steam combination at at temperature determined by regulation of the pressure. The containers are essentially fire tube boilers with the boiler and tube axes oriented vertically. The hot helium passes through the tube and transfers its heat through the tube walls to the water/steam combination which occupies the spaces between the tubes and the boiler shell.

The boiler complement constitutes a series element in the heat transfer system, all of the helium/steam energy being transferred via the flash steam medium. Further, the boiler complement integrates the two functions of helium/steam heat transfer

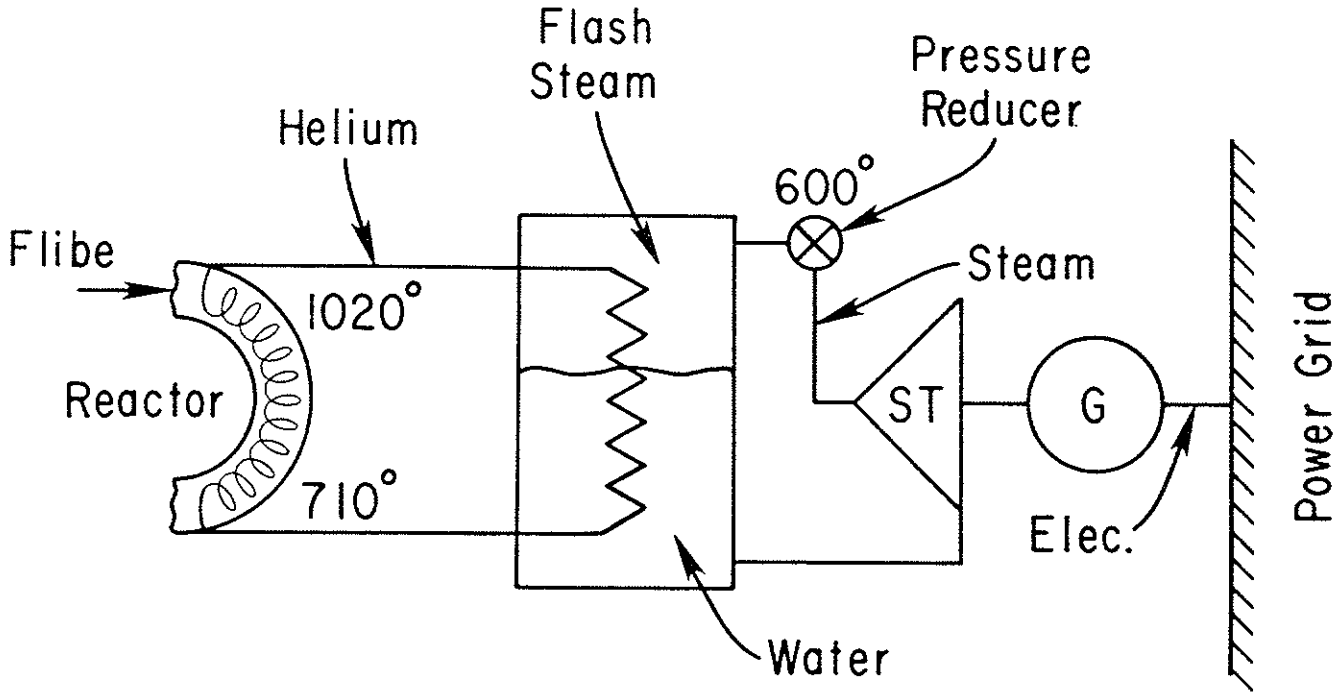

Hybrid Reactor Energy Storage Systems

Steam Loop

Reactor operation is cyclic
1000 sec burn, 100 sec rest

Advantages	Disadvantages
1. Heat storage capability incidental to heat transfer -- Δ cost for storage is negligible.	None apparent.
2. Well understood technique.	

Figure 10

and the required rest time energy storage and recovery. During the 1000-second reactor burn the helium transfers more energy to the water/steam combination than is demanded by the steam turbine generator units. Therefore, there is an increase in the pressure, and hence the temperature, of the boiler contents. A pressure regulator function governs the steam delivery to the steam turbine units. During the 100-second reactor downtime the pressure regulator demands constant steam, thereby depleting the steam in the boilers and reducing boiler pressure. The reduced pressure lowers the boiling point of the boiler water, some of which immediately flashes into steam and lowers the boiler contents temperature. The pressure and temperature reduction continues until the next reactor burn occurs. The flashed steam drives the steam turbine generator units for constant electrical output.

aa. Flash Steam System Preliminary Design

Twelve boilers are required, each being 105 feet high and 17 feet in diameter and incorporating 4000, 1 1/4 inch tubes for an active surface area of 125,000 square feet. Each boiler is rated 250 MW electric.

Water partially fills the boiler immersing the tubes to the 54 foot level, the remaining height being occupied by steam. Although the boilers are 105 feet high, only 95 feet of height is tubes. The remaining 10 feet of boiler is manifolding at top and bottom. Hence, 41 feet of the tube height is immersed in steam. Approximately 39 feet of tube at the bottom heats solid water while the next 15 feet constitute the area where the steam is formed. The top 41 feet act as a superheater, perhaps making a moisture separator unnecessary.

bb. Flash Steam System Cost Investment

The basic uninstalled cost of the helium/steam energy transfer system is estimated by Foster-Wheeler (boiler) and Leslie Company (pressure regulators) to be $145,000,000.

The increase in costs to provide the energy storage function is very low, perhaps non-existent, in view of the fact that the compelling factors determining the boiler design are the steam generation factors rather than the energy storage factors.

References

[1]A Fusion Power Plant, R. G. Mills, ed., Princeton Plasma Physics Laboratory Report MATT-1050 (1974).

C. Balance of Plant

1. Power Conversion Systems

The power conversion system selected for the reference plant uses three 1,000 MWe turbine generators in parallel to achieve a gross output capability of 3,000 MWe. These machines are considered current technology suitable for operation in the late 1980's. The steam cycle for each 1,000 MWe turbine generator is typical of present practice.

Each turbine consists of one high pressure, one intermediate pressure, and three low pressure sections arranged on a single shaft. Two moisture separator/reheaters condition exhaust steam from the intermediate pressure section. Low pressure section last stage blades are 31 in.; rotation speed is 3,600 rpm.

Main steam conditions are 2,200 psig at 850°F, with flow of 8,600,000 lb/hr at rated power output. To supply steam at these conditions, three steam generators are provided per turbine. Each steam generator consists of an evaporator and superheater, each in separate vessels with a moisture separator/dryer between the vessels. Assuming bulk helium inlet temperatures between 932°F (500°C) and 968°F (520°C), this arrangement allows for a pinch point of 82-118°F at the steam exit from the superheater. Each set of three steam generators will produce approximately 2,600 MWt at design conditions.

Five feedwater heaters, plus a deaerator, are required. A topping heater, which reclaims heat from the moisture separator/dryer supplements the feedwater heaters to give a final feedwater temperature of 380°F. All drains are cascaded, allowing for full-flow condensate polishing. Feedwater pumps are turbine driven

with reheat steam extracted downstream of the moisture separator/ reheater.

This cycle produces electric power at a gross thermal conversion efficiency of 38 percent. An alternate cycle consisting of two cross compound turbine generators, each of 1,500 MWe gross capacity, is also possible. This cycle efficiency is also near 38 percent. However, turbine generators of this size for the prescribed inlet steam conditions are currently planned. Consistent with the study guidelines utilizing current or near steam technology, the three-turbine generator scheme was selected.

The circulating water system must reject 4,900 MWth at 100 percent power. Assuming a circulating water temperature use of $27^{\circ}F$ through the condenser necessitates a circulating water flow rate of 2.0×10^{8} lb/hr or 445,000 gpm for each turbine and a total flow of 1,335,000 lb/hr for the unit. This heat load can be accommodated by two natural draft (hyberbolic) cooling towers or multiple cell mechanical draft towers.

2. Auxiliary Systems

With the exception of helium purification and tritium extraction system, balance-of-plant auxiliary systems would closely resemble those conventional fossil (in the turbine plant) or LWR (in the reactor plant) systems.

3. Structures and Plant Arrangement

The plant arrangement is expected to consist of the following structures:

a. Reactor Building including Primary Containment

Contains fusion reactor with blanket, magnets, neutral beam injectors, tritium extraction and

recycle equipment, and liquid helium refrigeration system.

b. Steam Generator Building

Contains evaporator, superheater, and moisture separator/dryer vessels, helium circulators, thermal energy storage system, helium purification and makeup system, and (unspecified) blanket standby cooling system equipment.

c. Fuel Building

Houses irradiated fuel storage facility, fuel transport equipment, molten salt processing and conditioning equipment, and remainder of blanket standby cooling system equipment.

d. Turbine Building

Contains turbine generators and auxiliaries, condensers, feedwater and condensate system equipment, compressed air equipment, plant chilled water system equipment, and condensate polishing equipment.

e. Control Building

Contains plant control room, standby electrical equipment, and control building atmosphere conditioning equipment.

f. Diesel Generator Building

g. Radwaste and Health Physics Building

Contains health physics laboratory and office, plant chemistry laboratory, liquid and solid radwaste storage and processing equipment, and hot machine shop.

h. Magnet Power Supply Building

Contains energy storage and transfer equipment for poloidal field coils, normal switchgear, and relay equipment.

i. Cooling Towers, Screenwell, and Makeup Treatment Equipment

j. Office Building and Warehouse

Contains offices, warehouse, normal machine shop, and instrument calibration facility.

Appendix I. Blanket Nucleonics

A. Blanket Design Options

Designing a hybrid blanket requires that choices be made among reasonable alternative approaches to many design features. Such choices obviously must be made based on prior experience and preliminary evaluations; only the process of actual design can validate their suitability. Even the final analysis cannot establish optimality: this requires the comparison of results from designs where alternative choices actually were made.

Since this study was initiated as an exploration of the potential of the TCT concept as a neutron source, even the fundamental goal of the blanket had to be chosen: to produce energy or fissile fuel. Beyond that were choices of fertile material, fissile material, tritium breeder, coolant, structural material, configuration, spectrum, residence time, etc. The conceptual blanket of Section III.B and the reference design of Section VI.B.2 were the final results.

Because of the current low price of plutonium, preliminary studies[1] were done on the economics of trading net Pu breeding for in-situ burnup. Since the conclusion was that the latter could well be preferable, depending on the relative market prices of fissile fuel and electricity, it was felt that the option of producing power as the major output should be preserved.

This dictated the choice of a blanket which could be loaded with fissile fuel.

The next major decision was the choice between the uranium cycle and the thorium cycle. Tentatively thorium was chosen because of an anticipated higher market price for U-233 than for Pu-239. This was based on the superior performance of U-233 in thermal reactors; poorer performance in fast reactors was deemed irrelevant, since if fast reactors were in wide use, the hybrid would not be needed as a source of fuel. However, a fuel cycle study[2] predicted parity values (relative to 90% enriched uranium) in the 1990's of 0.85 and 0.76 for U-233 used in LWR's and HTGR's, respectively, compared to 0.67 and 0.75 for Pu-239. Hybrid fabrication costs penalized the U-233 in this analysis.

The choice of the Th-U cycle was reversed following a few preliminary blanket neutronic calculations. A hybrid blanket may consist of a sub-critical lattice driven by the fusion neutrons to produce power, or it may have a neutron multiplier region and optionally produce power or breed fissile fuel. The latter configuration is more flexible in output, and also better exploits the high energy DT neutrons. For blankets of this kind, and in terms of neutron multiplication, thorium is inferior.

At about 14 MeV, the number of neutrons per fission for U-238 is N = 4.4; while N = 4.0 for Th-232. However, the fission cross sections for these nuclides are 4.4 barns vs 1.4

barns, so that thorium is substantially poorer as a fast fission multiplier. This is not the whole story, though, as Figure 1 shows. When scattering and the n-2n and n-3n reactions are taken into account, the overall number of secondaries per collision for U-238 is about 1.9, and about 1.8 for Th-232. Unfortunately most of these secondaries will have energies below the n-2n threshold at about 7 MeV, where the U-238 fission cross section is about four times that of thorium. The net effect, through several generations, is that the neutron multiplication in a uranium zone will be two or three times greater than in a thorium zone, a factor which substantially benefits the performance of a uranium blanket.

Since there is no way to prevent neutron capture by the multiplier, a blanket using uranium in that region will, by necessity, produce plutonium. Although it would probably be possible to load an additional U-233-breeding thorium region in such a blanket, the idea of running both fuel cycles simultaneously is not attractive. Therefore the thorium cycle was dropped, since it did not appear that the unit value of U-233 would be sufficiently high to offset a greater production of Pu-239.

The lack of even a tentative commitment by the U.S. nuclear industry to the use of the thorium cycle, compared to the firm plans for recycling plutonium, seemed an additional justification for this decision. However, recent pronouncements

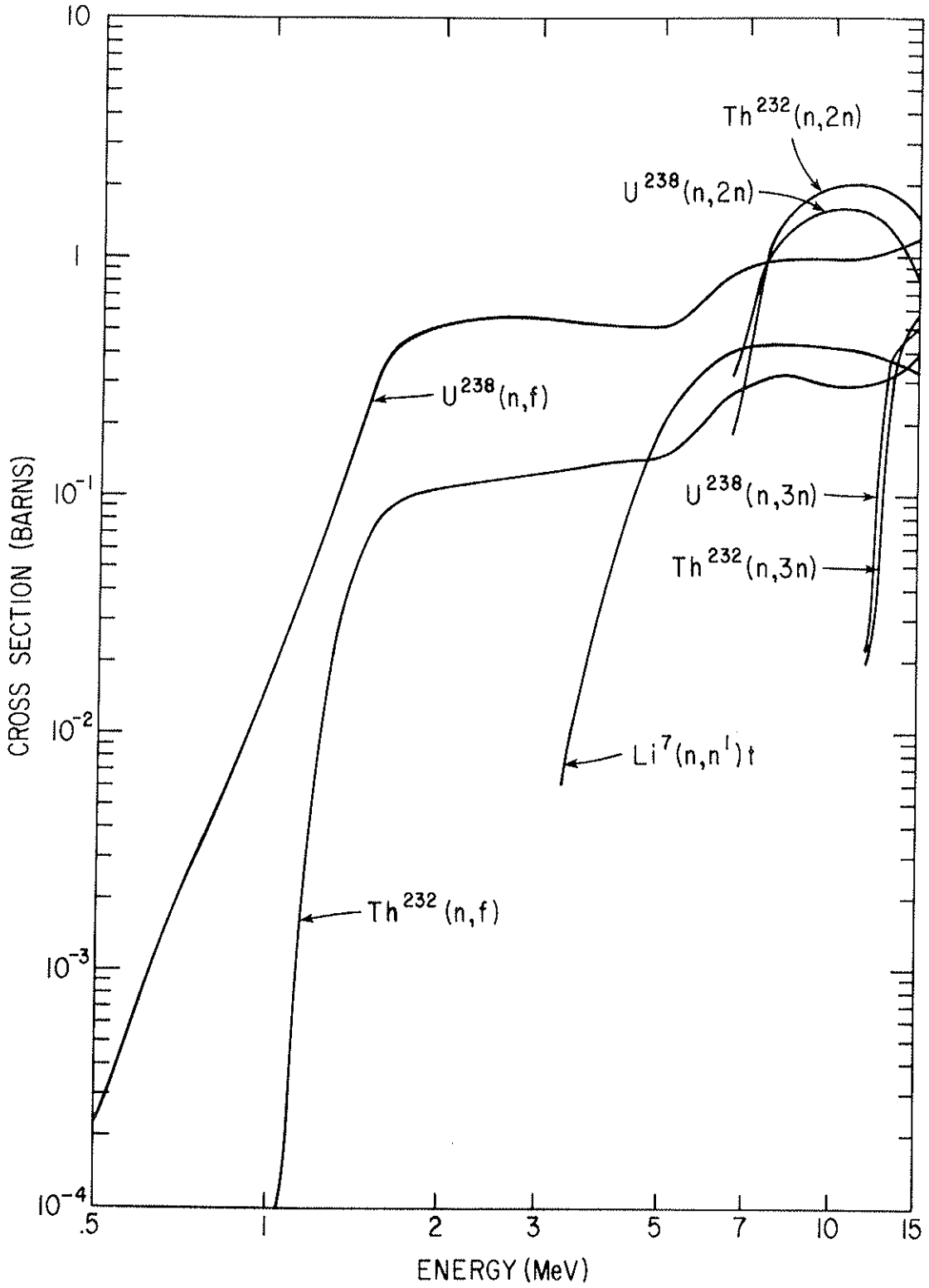

Fig. 1. High Energy Cross Sections of Interest in a Hybrid Reactor.

on the use of plutonium in the future cast doubt on its wisdom.

In order for the multiplier material chosen to be effective, the source flux of DT neutrons must be as little attenuated as possible. Therefore the material, configuration, and coolant of the multiplier are very important. It is readily apparent that helium cooling will provide the best neutronic performance, because of the very low density of atoms which would compete with the uranium. A scoping calculation of the heat load in the multiplier indicated that helium at 5 MPa (50 atm) could provide sufficient cooling with a ΔT of 150 K at a flow of about 200 m/s. These conditions seemed acceptable (the speed of sound would be about 1000 m/s) so helium cooling was adopted.

The use of pure metallic uranium would obviously provide the best neutronic performance, but physical requirements rule this out. The next best possibility is metallic fuel of uranium alloyed with some other strengthening element. Early work in the fission reactor program identified alloys with low weight percents of molybdenum as candidate reactor fuels. The molybdenum stabilizes the swelling which otherwise occurs at catastrophic rates during even moderate burnup. With 7% Mo, exposure to at least 0.5% burnup seems feasible, with 1% burnup not out of the question. The economics of LWR's makes burnup in this range impractical, but it was felt that buildup of Pu in the multiplier might actually require frequent reprocessing

(and hence low burnup) in order to avoid large power excursions.

Although there has been a great deal of experience in the fabrication and reprocessing of metallic fuel, the commercial nuclear industry is more oriented to uranium oxide. Therefore a series of scoping blanket neutronic calculations were performed to see if a UO_2 rod-type multiplier could be developed. As summarized in Ref. 3, these studies indicate that the initial multiplication is simply too low. This is probably due to the low atom fraction of uranium, which in the U-7 Mo is about 84%. On this basis, U- Mo was chosen as the fuel material for the multiplier. The material U_3Si, recently suggested for hybrid use,[4] is qualitatively similar and perhaps quantitatively superior to U-7 Mo. Future studies should include it among the multiplier options.

The configuration of the multiplier region was chosen by analogy with calandria-type reactors. Pressure tubes confine the helium coolant and contain long cylindrical slugs of metallic fuel, centered by spring clips. Stresses in the tubes are suitably low when the diameter is about 8 cm. A double layer of close-packed tubes provides reasonably good interception of the streaming paths of the fusion neutrons. Using hollow fuel rods decreases the thermal thickness and increases the surface area, thereby reducing the peak temperatures in the uranium.

Other configurations were considered, with greatest attention given to rod-type fuel contained in large canisters.

Actual comparisons of manufacturing steps were not performed, but it was felt that the simplicity of the basic pressure tube would compensate for the complications of the helium inlet and outlet plena. A further consideration was the potential for "on-line" or "continuous" refueling.

Despite a desire to minimize the amount of material between the plasma and the multiplier, it was felt necessary to incorporate a genuine "first wall" in this reactor design. This wall serves both as the radiation shield to absorb plasma x-ray losses and also as the primary vacuum vessel. The structural material chosen for the wall and for the multiplier region is type 316 stainless steel. Less conventional materials were ruled out because of lack of experience with fabrication and because of uncertainties in the lifetime under irradiation. Predicted lifetimes for steel have been disappointingly short, but at least there are experimental programs underway which give some confidence to the predictions. Furthermore, as more data are accumulated the recommended design lifetimes are being increased. Recent reviews[5] suggest that if the temperature can be kept below about 550-650^{o}C, a design life of about 6 MW - yr/m^{2} may be achieved. This would allow operation for half the plant life (15 years at 3/4 load factor) at 0.5 MW-yr/m^{2}.

Cooling of the first wall is achieved with water (non boiling, perhaps pressurized). Because of the high energy multiplication of a hybrid blanket, the surface radiation and

volume heating of the wall can be removed at a low temperature and dumped without greatly affecting the overall net efficiency. Although the water has a rather strong negative impact on the performance of the multiplier, it should greatly simplify the design of the wall. The low temperature should ameliorate the radiation damage problem, while reduced thermal cycling should increase the reliability of the wall or the main vacuum barrier. (Putting the vacuum wall here, rather than outside the blanket, allows refueling and repair of the blanket without disturbing the vacuum seals.)

Behind the wall and the multiplier there must be regions where tritium is bred and extra power may be produced. The active material in these regions is the molten salt flibe: lithium-beryllium-fluoride. As discussed in the Princeton Reference Design Fusion Power Reactor report,[6] flibe is a satisfactory material for tritium recovery. Furthermore, as explored in the Molten Salt Reactor project,[7] it is an excellent medium for fueling a fission reactor: fissile and fertile nuclides may be dissolved and circulated as fluoride salts, while fission products are continuously removed from drag streams.

The use of molten lithium was considered, but rejected. Pure lithium is an excellent material for breeding tritium, but no sure method of recovering that tritium from reasonably low blanket concentrations has been proposed. Furthermore, the incorporation of a fissile lattice in a lithium region would

complicate the design. Finally, molten lithium is a rather corrosive material, leading to concerns about failure of the fuel cladding as well as the basic blanket structure.

Solid lithium compounds were also considered. In this case some mixed arrays of lithium pins or cans and fissile rods could be envisioned, with lithium as the coolant. Disadvantages of this design are the marginal trituim breeding characteristics (poor neutron economy) of the solid breeders, the buildup of fission-product neutron poisons in the fuel, and the problem of designing large blanket modules to withstand the helium pressure.

Having selected flibe as the active material, the choice of coolant arises. In the molten salt fission reactor concept flibe serves as both the fuel and the coolant. In tokamaks a flowing conductor will interact with the magnetic field, leading to suppression of the turbulent regime and to EMF's across the flow channel. The former effect decreases the cooling capability, while the latter effect increases the corrosiveness.

Since the magnitude of these effects is still a subject of some dispute, it was felt necessary to design for cooling with high pressure helium flowing through tubing embedded in the blanket salt tanks (as in the PRD). This has the advantage of allowing a combined cycle with the cooling of the multiplier region; the disadvantage is the introduction of a significant amount of steel, a neutron parasite, into the blanket. The option of circulating and partially cooling with the flibe itself

has not been entirely ruled out.

Although the molten salt is the active ingredient, a large portion of the burner region actually consists of graphite. Again, this follows the lead of the molten salt fission reactors, where graphite moderates the neutron spectrum. For tritium production in a low power blanket this would probably not be an important consideration, since the decreased amount of lithium required in a more thermal spectrum would be offset by the volume required for the graphite. However, for power production the moderation is very important.

The fissile inventory of the reactor will depend on the relative magnitude of the fission cross section compared to all other cross sections in the region. For plutonium, the fission cross section increases as 1/v as the neutron energy is decreased; therefore moderation toward a thermal spectrum will reduce the required plutonium concentration. Thermalization will also increase the effective cross section of lithium-6, which is good for tritium breeding but very bad for fissile inventory. This leads to the conclusion that the fissile-bearing flibe must be made with depleted lithium, i.e., lithium with a very small fraction of lithium-6.

In order to accommodate these various factors, a subdivision of the burner region into four individual zones was adopted. The first and third zones consist of the burner salt with helium coolant. The zone between them is mostly graphite,

with a small volume fraction of salt for heat transfer to the cooled regions. The fourth zone, facing the shield, is loaded with a fissile-free flibe made with enriched lithium. The first three zones form a composite burner with a strong central moderator and adjacent all-salt regions for absorption of the resulting thermal flux. The last zone serves as a scavenger of neutrons leaking out of the burner, producing substantial amounts of tritium from neutrons which would otherwise overload the shield.

The choice among alternative shielding materials has not been explored in this study. Instead the iron-boron carbide layered shield discussed by Abdou[8] has been adopted as a nominal reference. For superconducting magnets shielded by this combination of materials roughly one order-of-magnitude reduction in radiation damage is provided by each 17cm increment of thickness. This has not been shown to be an optimal shield, but it is a cost-effective material where thinness is not the prime requirement.

In a review of radiation damage to superconducting coils, Ullmaier[9] has suggested that the fast neutron fluence should be limited to 3×10^{17} n/cm^2 for reliable operation. This criterion, together with the attenuating power of Fe-B_4C, provides a basis for estimating shield thicknesses. As an example, for the Reference Blanket of this study the leakage from the scavenger region into the shield is calculated to be 0.15 neutron per DT

fusion neutron. At a wall load of 1 MW/m^2, this would result in an unshielded total flux of 4.5×10^{13} n/cm^2-sec, of which 32% is for energies above 0.1 MeV. For an exposure of 30 years at 3/4 load factor, an Fe-B_4C shield thickness of 80 cm would be required to meet Ullmaier's criterion (giving a total blanket-plus-shield thickness of 165 cm). Changes in the wall load or reductions in the scavenger leakage would affect this thickness only logarithmicly, but the use of special shielding materials where space is critical would reduce the thickness in direct proportion to the attenuation length.

References

[1]D. L. Chapin and R. G. Mills, Optimization of Fusion-Driven Fissioning Systems, Proceedings of the US-USSR Symposium on Fusion-Fission Reactors (National Technical Information Service, Springfield, Virginia, 1976) Conf - 760733, pp. 63-70.

[2]Economic Study of Potential Fissile Fuels Bred in Fusion/Fission Hybrids, Combustion Engineering, Inc., Nuclear Power Systems Report CEND-373 (1976).

[3]D. T. Aase, M. C. C. Bampton, T. J. Doherty, B. R. Leonard, R. A. McCann, D. F. Newman, R. T. Perry, C. W. Stewart, TCT Hybrid Conceptual Blanket Design Studies, Battelle Pacific Northwest Laboratories Report PNL-2304 (1978).

[4]J. D. Lee, D. J. Bender, R. W. Moir, K. R. Schultz, Mirror Hybrids - A Status Report, Proceedings of the Second Topical Meeting on the Technology of Controlled Nuclear Fusion, G. L. Kulcinski, ed. (National Technical Information Service, Springfield, Virginia, 1976) Conf - 760935, Vol. II, pp. 689-710; also Lawrence Livermore Laboratory Report UCRL - 78079 (1962).

[5]E. E. Bloom, F. W. Wiffen, and P. J. Maziasz, Temperature and Fluence Limitations for a Type 316 Stainless-Steel CTR First Wall, Transactions of the American Nuclear Society 1975 Winter Meeting (American Nuclear Society, Hinsdale, Illinois, 1975) Vol. 22, p. 178.

[6]A Fusion Power Plant, R. G. Mills, ed., Princeton Plasma Physics Laboratory Report MATT-1050 (1974).

[7]M. W. Rosenthal, P. N. Haubenreich, R. B. Briggs, The Development Status of Molten-Salt Breeder Reactors, Oak Ridge National Laboratory Report ORNL-4812 (1972).

[8]M. A. Abdou, Nuclear Design of the Blanket/Shield System for a Tokamak Experimental Power Reactor, Nucl. Tech. 29, 7 (1976).

[9]H. Ullmaier, Radiation Damage in CTR Magnet Components, Proceedings of the Conference on Radiation Effects and Tritium Technology for Fusion Reactors (National Technical Information Service, Springfield, Virginia, 1976) Conf-750989, Vol. II, pp. 403-421.

B. Development of Parameterization

Within the hybrid reactor systems optimization code the blanket is represented by a "black box" routine which supplies values of the basic performance parameters. The inputs to this routine are the desired energy multiplication, M, the required tritium breeding ratio, T, and the target fuel region burnup, B. The principal outputs are: J, the integrated wall load corresponding to B; F, the net fissile production per fusion reaction; P, the gross fissile production; and p, the density of plutonium in the burner salt.

The blanket performance is calculated from a set of simple equations in which M, T, and B are the independent variables. This parametric formulation is essential in keeping the code execution time within acceptable limits, and parallels the treatment of the plasma physics of the fusion core. Variation of the constants in the parameterization allows the performance of any type of blanket; the derivation of specific values corresponding to the chosen U-Mo, Flibe-PuF_3 blanket is the subject of this section.

The forms of the various equations were chosen after consideration of the basic neutronic effects associated with each physical variation. The constants were then fixed by using either performance parameters or average cross sections from

several blankets derived from the basic conceptual design. These include the reference design (case No. 8163), a blanket with no plutonium in the salt (No. 8624), a blanket with high lithium-6 loading (No. 1929), and a blanket containing Pu-240 (No. 4976) (the one used to illustrate actinide buildup in another section of this Appendix).

1. Fissile Production

The derivation of the equation for F will be described first since it is the most involved. The net fissile production is the difference between gross production in the multiplier and self-consumption in both the multiplier and burner regions. It is dependent on J because a longer exposure increases the probability of burnout in the multiplier. It also depends on M because more energy multiplication requires a greater fission rate in the burner.

The equation for F (M,J) was developed in stages, the first one being for $F(M,O) = F_o(M)$. Actually, it is $F_o(f)$ that is derived, where f is the total number of fissions per fusion. M is replaced by f using the assumption that $14.06\ M = 198f + 20$. Initially a straightforward neutron balance was used to find F. The total source, S, of neutrons is taken to be the sum of: one DT neutron; f_o DT-induced fast fissions in uranium times ν_o neutrons per fission; $f-f_o$ other fissions times ν; and e extra neutrons produced by n-2n, n-3n, etc., reactions of DT neutrons. The total loss of neutrons L(=S) is taken to be the sum of: the absorptions

in lithium, taken to be T; f_oDT-induced fast fissions in uranium; g, other fissions in uranium (e.g., in U-235); F_o^+ captures in uranium; F_o^- absorptions in plutonium; and A, neutrons lost by parametric absorption. Now $F_o^+ = F + F_o^-$, while $F_o^- = (f - f_o - g) * (1 + \alpha)$, where α is the capture-to-fission ratio; thus the loss equation can be rewritten

$$L = T + F + g + 2\ (1 + \alpha) * (f - f_o - g) + A \quad ,$$

while

$$L = S = 1 + \nu_o f_o + \nu(f - f_o) + e \quad .$$

From case 8624 (no Pu) f_o is about 0.352, and $f = f_o + g = 0.426$, while from case 8163 $(f = 1.815)f_o + g$ is about 0.509; from this a linear equation in f can be derived for g. In both cases e is about 0.45, and ν_o is about 3.75. In case 8163, S = 7.040, and A takes 19.9%; in case 8624, S = 2.977 and A takes 22.67. Because of this agreement in greatly different circumstances, the parasitic absorption is put in the form A = a * s, using 0.20 for a. In case 8163, $\alpha = 0.5098$, and $\nu = 2.92$, with similar values observed in other cases; 0.51 and 2.90 are used for the equations.

Using these values, L = S can be solved for $F_o + T = 2.207 - 0.580f$. Checking this against the reference cases, it predicts T + F = 1.960 for No. 8624, compared to 1.856, and it predicts 1.155 for No. 8163, compared to 1.130. The agreement across the full expected range of f is not bad. However, since

the derivation is only approximate and the functional form so simple, an alternative approach to T + F was adopted.

An ad hoc linear form was simply forced to fit the two cases, giving $T + F_o = 2.078 - 0.521f$ (which is not greatly different). Making the back substitution for M finally yields a nominal equation for F_o:

$$F_o(M) = 2.1308 - 0.037025\ M - T \quad .$$

2. Effects of Exposure

Because plutonium bred in the multiplier will have some probability of fission or capture before it is removed from the blanket, the cycle-average net production will also be a function of J, the integrated wall load. Whereas F_o can be calculated from the production and loss rates at zero exposure, an integral balance approach is required to find F (J). J is proportional to the total DT neutron source per unit area of blanket, and hence is an index of the total fluence; the total DT neutron production corresponding to J is equal to J/eA, where A is the wall area, and e is the neutron energy per fusion.

Letting P and U stand for the densities of Pu-239 and U-238 and V for the volume of the multiplier, the amount of plutonium built up after an exposure J is

$$P(J) = V\left(1 - e^{-\sigma_a^P \phi}\right) U\sigma_\gamma^U/\sigma_a^P \ ,$$

where ϕ is the fluence corresponding to J, and the σ's are microscopic cross sections (averaged over energy and space). For low exposure the exponential can be expanded in a series; truncation

after the squared term leaves

$$P(J) \approx VU\sigma_\gamma^U\phi \left(1 - \sigma_a^P\phi/2\right) \quad .$$

Dividing by J/eA gives F^+, the average production per fusion neutron:

$$F^+ = (V/A)U\sigma_\gamma^U(\phi/J)e \left(1 - \sigma_a^P(\phi/J)J/2\right) \quad .$$

The first part of this expression is just F_o^+, as calculated previously. The last term gives a deduction for the loss of plutonium before reprocessing, equal to the loss probability $\left(\sigma_a^P\phi\right)$ times the first-order approximation to the average Pu present, $F_o^+/2$. Thus F^+ is in the form F_o^+ (1-hJ).

Now an expression for F(M, J) can be devised, since $F^- = F_o^-$ accounts for depletion in the burner and is assumed not to depend on J:

$$\begin{aligned} F(M, J) &= F^+ - F^- = F_o^+(1 - hJ) - F^- \\ &= \left(F_o^+ - F_o^-\right) - JF_o^+h \\ &= F_o(M) - JF_o^+(M)\ h\ (M) \quad . \end{aligned}$$

Rather than attempt to derive equations for F_o^+ and h directly, the procedure used previously for F_o was applied again: linear equations in M were fitted to data from cases 8163 (the Reference) and 1929 (plutonium bearing but with low multiplication). The linear approximation is justified by the dependence on (ϕ/J), since a higher multiplication due to more burner fissions would increase the fluence for a given wall load.

Inserting the relations, $F_o^+ = (1.5013 + 0.05925\ M - T)$ and $h = (0.05453 + 0.003883M)$, gives an expression for F which is

linear in J, quadratic in M, and includes a JT cross term. The latter is eliminated by approximating T = 1.1 in the F_o^+ equation, leading to the final results for the net fissile breeding ratio:

$$(FM,J) = (2.131 - T - 0.037M) - J(0.0219 + 0.00479M + 0.0002301M^2) .$$

3. Relationship to Burnup

The natural form for the equation for F is in terms of J, the integrated wall load; however it is B, the burnup, that is the externally specified measure of blanket exposure. Therefore an equation relating B and J must be developed. Letting S be the density of U-235, with P and U for Pu-239 and U-238 as before:

$$U = U_o e^{-\sigma_a^U \phi} \qquad S = S_o e^{-\sigma_a^S \phi},$$

$$P = U_o \left(1 - e^{-\sigma_a^P \phi}\right) \sigma_\gamma^U / \sigma_a^P,$$

$$B\left(U_o + S_o\right) = U_o \left(1 - e^{-\sigma_a^U \phi}\right) \sigma_f^U / \sigma_a^U + S_o \left(1 - e^{-\sigma_a^S \phi}\right) \sigma_f^S / \sigma_a^S + U_o \left(\sigma_\gamma^U / \sigma_a^P\right) \left(\sigma_a^P \phi - \left(1 - e^{-\sigma_a^P \phi}\right)\right) \left(\sigma_f^p / \sigma_f^p\right) .$$

For small exposures, the exponential can be expanded:

$$B\left(U_o + S_o\right) \approx U_o \sigma_f^U \phi + S_o \sigma_f^S \phi + U_o \sigma_\gamma^U \sigma_f^P \phi^2 / 2 .$$

Once again, linear equations in M are fitted to $\sigma_f^U\phi$, $\sigma_f^S\phi$, $\sigma_f^P\phi$, and $\alpha_\gamma^U\phi$ (which is related by a scale factor to F_o^+), using the results of cases 8163 and 1929. The result is an equation for B which is quadratic in both J and M, due to the ϕ^2 term:

$$B(M,J) = J * 10^{-6} * (2140. + 6.93M) + J^2 * 10^{-6} * (75.35 + 16.218M + 0.7519M^2) .$$

For later convenience this was factored into the final form

$$B(M,J) = J \times 10^{-6} \times (2140. + 6.93M) \times \left[1 + J \times (0.0343 + 0.00758M + 0.000351M^2)\right]$$

where a 6.93×10^{-6} M term has been ignored in the denominator.

4. Plutonium Inventory

An important factor in the reactor economics is the inventory of plutonium in the burner salt. To provide this number, the blanket parameterizations calculate p(M), the mole fraction of PuF_3 required to achieve a given level of energy multiplication.

As noted before, M = (198f + 20)/14.06, where f is the number of fissions per DT neutron. Furthermore, simple chain reaction theory shows that in a subcritical assembly with multiplication constant k, the total number of fissions due to S initial fissions will be f = S/(1 - k). In case 8163 (the Reference Blanket) there were a total of 1.815 fissions per fusion neutron, and a special eigenvalue calculation (reported in another section) gave the value 0.7778 for k. Using the formula S = f (1 - k) gives 0.4033, in good agreement with the actual number of U-238 fast fissions, in this case, 0.3986. The nominal value S = 0.40 was adopted.

Given S, a relationship for k(p) would allow the derivation of M(p), and thus p(M) by inversion. In fact, the "four

factor formula" states that k is proportional to the thermal utilization and to three other factors which are (more or less) independent of p. Since the thermal utilization is the ratio of fuel (here Pu) absorption to total absorption, and the Pu absorption is proportional to its density, k can be written in the form:

$$k(p) = cp/(d + p) .$$

Rather than try to derive values for c and d, they are calculated to fit two points: f = 1.815 for case 8163 with p = 0.25; and p = 0.30 for case 6221 where f = 2.200 implies k = 0.8182. The result is

$$k(p) = 1.1016p/(0.10401 + p) .$$

This can be substituted into the equation for f, which then is inserted into the equation for M. Solving for p(M) with S = 0.4 gives

$$p(M) = (1.4624M - 10.318)/(1.4285M + 77.168) .$$

This equation predicts p = 0 at M = 7.05, whereas a rounded nominal M of 7.0 for no-fissile blankets had been adopted earlier. To meet this nominal value a revised final formula for p was adopted:

$$p(M) = (1.468M - 10.276)/(1.429M + 77.17) .$$

This predicts p = 0.25 at M = 26.6, a good match to the performance of the Reference case.

5. Gross Pu production

A formula for the gross plutonium production is

required by the systems code, since losses in the reprocessing cycle are specified as fractions of the process stream. A suitable formula for P seemed to be at hand from the middle of the previous derivation: $P = F_o^+(M)$. One slight revision was made, however. P should equal F at the value of M corresponding to no plutonium in the burner. This has been assumed nominally to be 7.0, based on about 0.4 uranium fissions in the multiplier. The previous equation for the plutonium production rate was

$$F_o^+ = 1.5013 + 0.05926\ M - T\ ;$$

to ensure that P(7) = F(7), the slope was preserved but the intercept modified so that

$$P(M) = 1.457 + 0.0593M - T\ .$$

Actually, this equation is not entirely appropriate for the intended use. The gross plutonium processed is really the gross produced minus the amount burned in situ. Thus

$$P(M,\ J) = F^+ = F_o^+(M)(1 - Jh(M))$$

would be more accurate. As indicated, this was not the formula used; however, the economic impact of the reprocessing losses is very small.

a. Average Power Level

In all of the formulae above, the variable M implicitly represents the energy multiplication at zero exposure. Since it is assumed that some bred plutonium will fission, a corrected formula for the average M as a function of exposure, M(J), is required.

In the derivation of F(J), it was assumed that the depletion of bred plutonium amounted to $JF_o^+(M)h(M)$. This is due to all absorption; the corresponding number of fissions is $1/(1 + \alpha)$ times this value, where α is the capture-to-fission ratio. For the Reference case, the average α in the multiplier was 0.5098. Other cases were not greatly different, so a nominal value of $\alpha = 0.51$ was adopted. Using the equations for h(M) and $F_o^+(M)$ derived above gives a quadratic formula for the increment in the average number of fissions per fusion. Applying the energy scale factor finally yields

$$\bar{M}(J) = M + (0.7409 + 0.08289M + 0.002146M^2)J \ .$$

6. Initial Enrichment

One last correction to M might be required. In all the blanket calculations the multiplier was assumed to contain depleted uranium with 0.3% U-235. If in fact some other isotopic composition, u, were specified, there would be a small effect on the number of fissions. To account for this it was assumed that the actual number of U-235 fissions would be proportional to: the number in the Reference Blanket, 0.1108; the enrichment ratio, u/0.3; and the relative thermal fission level, (M - 7)/(27 - 7), since this is the predominant factor in scaling the thermal flux. Altogether this gives a correction term, $M^{tails} + 0.26007 (u - 0.3) = M^u$.

7. Super Blanket Option

The discussion above summarizes the derivation of the

set of equations which define the performance of the Nominal Blanket as used in the hybrid systems code. So that the code could be used to explore the impact of more optimistic assumptions about the blanket performance, an alternative set of equations for a "Super Blanket" was developed.

An example of a more optimistic blanket is that reported in Ref. 1. This blanket features a multiplier zone loaded with U-Mo fuel but has no fissile loading to produce extra fission. However, the calculated performance parameters are M = 10, T = 1.14, and F = 1.8.

To achieve M = 10 would require about 0.6 fast fissions, yielding 2.25 secondary neutrons (at 3.75 per fission). Adding in about 0.45 more from n-2n and n-3n reactions, plus the initial DT neutron, implies a total neutron source of about 3.70 neutrons per fission. Setting this equal to T + F plus the number of fissions plus the parasitic absorption implies that the latter is only 0.16 neutrons per fusion, or 4.3% of the total source. The high number of initial fissions and low rate of non-productive absorption are very favorable figures of merit. The reason why they differ from the neutronic results of this study (using standard, but different, codes and data) has not been determined. An exploration of this question is reported in Ref. 2.

8. Super Blanket Derivation

The Super Blanket equations were developed by propagating assumed values of 0.6 fast fissions and 10% parasitic absorption

through the derivations reported above, retaining the other factors which presumably depend on the molten salt blanket. No attempt to justify this boosted performance was made.

For the Nominal Blanket, the minimum M is M' = 7, corresponding to zero fissile loading. Thus $T + F_o = 2.131 - 0.0370M = 1.856 - 0.0370(M - 7)$, and $T + F_o = 1.856$ is the maximum no-exposure composite breeding ratio. For the Super Blanket the corresponding figure is found by the neutron balance procedure outlined above: $2.730 = F_o + T$. For the variation with M the same slope is preserved, since this depends on the burner salt region, but the zero point is set to M' = 10 (corresponding to the 0.6 fast fissions):

$$T + F_o = 2.730 - 0.0370(M - 10) .$$

To derive the variation with J, formulas for F_o^+ and h are required, but the latter can be carried over from before. For any blanket, $T + F_o = T + F_o^+$ when M = M'. Since the variation with M should not depend on the fast fission calculation, the previous slope is used again, but now zeroed at M':

$$F_o^+ = 2.730 + 0.0593(M - 10) .$$

Combining all these factors, for the Super Blanket

$$F(M,J) = (3.100 - T - 0.0370M) - J(0.0566 + 0.00726M + 0.0230M^2).$$

Using the same factors in a consistent derivation yields for the gross fissile production

$$P(M) = 2.137 + 0.0593\ M - T .$$

To adjust the burnup equation a similar procedure is applied: the plutonium fission factor is unchanged; the uranium capture factor

is F_o^+ derived above; and the uranium fission factor keeps its same slope with intercept of 0.6 at M = 10 = M'. The result is

$$B(M, J) = J * (2958. + 6.93M) * 10^{-6} * 1 + J * (0.0658 + 0.00821M + 0.000254M^2) .$$

The inventory formula is easily rederived using the same equation for k(p) but setting S = 0.6, to give (after slight adjustment to force p(10) = 0):

$$p(M) = (1.468M - 14.68)/(1.429M + 116.77) .$$

Finally, the relation between the average and initial values of M is revised to be

$$\bar{M} = M + (1.0871 + 0.10754M + 0.002146M^2)J .$$

This completes the parameterization for the Super Blanket.

9. Options in the Systems Code

As discussed in the chapter on the systems code there are six blanket options available, three each for the Nominal Blanket and the Super Blanket. The first short-circuits the burnup calculation and sets J to zero. The second uses the performance equations as described above to calculate F, p, P, and J when given B and $\bar{M}$. The energy multiplication is assumed to ramp up while p is held constant, and $2 - M/\bar{M}$ is returned as a power peaking factor to be imposed on the balance-of-plant costs. For the third blanket type it is assumed that the energy multiplication is held constant at M_o. This is achieved by allowing p to decline from its initial level to the value consistent with $M = \bar{M} - (M_o - \bar{M})$. The value of p for inventory charge purposes is the average of this final p and the initial $p(M_o)$. The

equations for F and P are evaluated at $\bar{M}$ to allow for the ramping of the burner fission rate.

Certain combinations of energy multiplication, tritium breeding, and multiplier burnup specified by the systems code would require blankets with negative fissile loading (M very low) or negative fissile output (M very large). Since the one case is unphysical and the other "illegal", the parameterization attempts to solve for a reduced level of burnup at which the offending parameter (p or F) is just zero. (Actually F is required to be just enough positive to cover normal reprocessing losses.) Since a smaller value of B implies a smaller integrated wall load an additional ultimate constraint is imposed: the value of J/(wall load times capacity factor), i.e., the installed lifetime of the multiplier fuel, is required to be greater than one year.

10. Graphs of the Parameterizations

To end this section, a series of figures is presented in which the blanket parameterization equations are plotted. Figures 1, 2, and 3 for three values of the target burnup show the performance of the ramping-power Nominal Blanket as a function of the average multiplication. Figures 4, 5, and 6 show the performance of the ramping-power Super Blanket. Figures 7, 8, and 9 show the performance of the constant-power Nominal Blanket as a function of the constant value of blanket multiplication. Figures 10, 11, and 12 show the performance of the constant-power Super Blanket. Table I gives the key for all 12 figures.

Table I. Parameter Key for all Performance Plots.

□	Integrated Wall Load	J
Δ	Initial Multiplication	M
O	Gross Pu Bred	P
×	Net Pu Bred	F
◇	Limit Pu Density	P(M) (× 10)
●	Average Pu Density	$\left[p(M) + p(M') \right] /2$ (× 10)
*	Power Peaking Factor	

Abscissa = $\overline{M}$ or M'

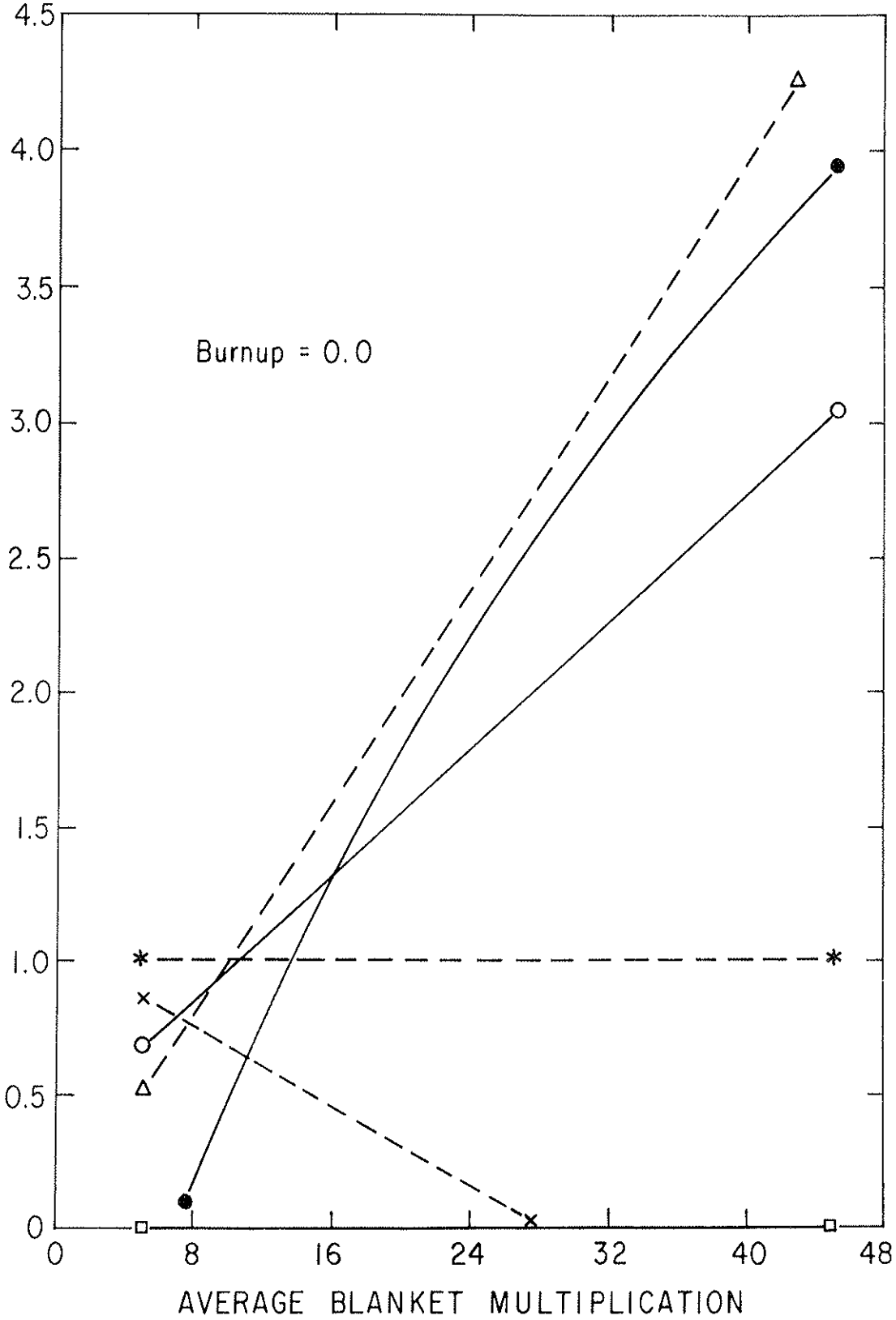

Fig. 1. Performance Parameters for the Ramping-Power Nominal Blanket, for B = 0.0.

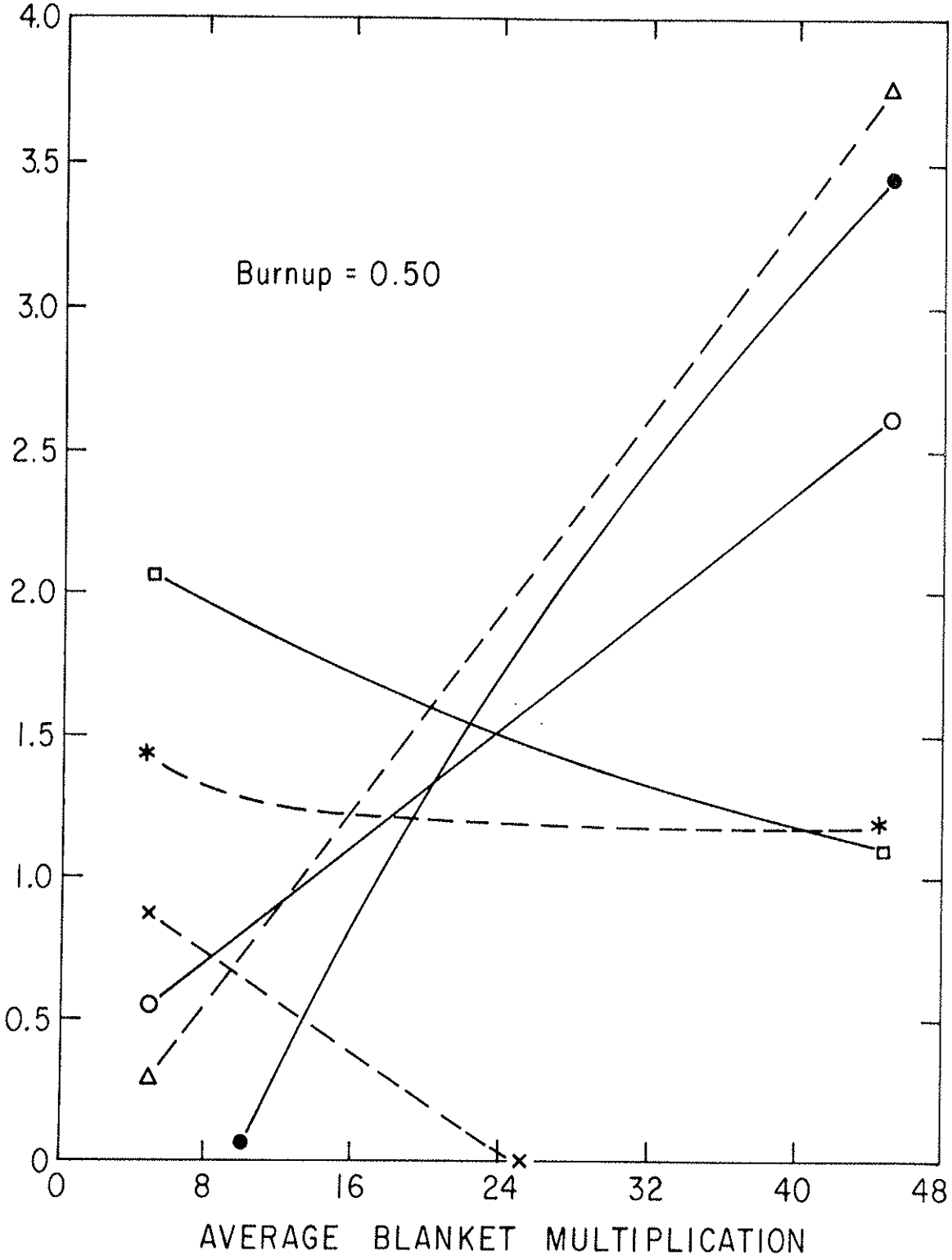

Fig. 2. Performance Parameters for the Ramping-Power Nominal Blanket, for B = 0.5.

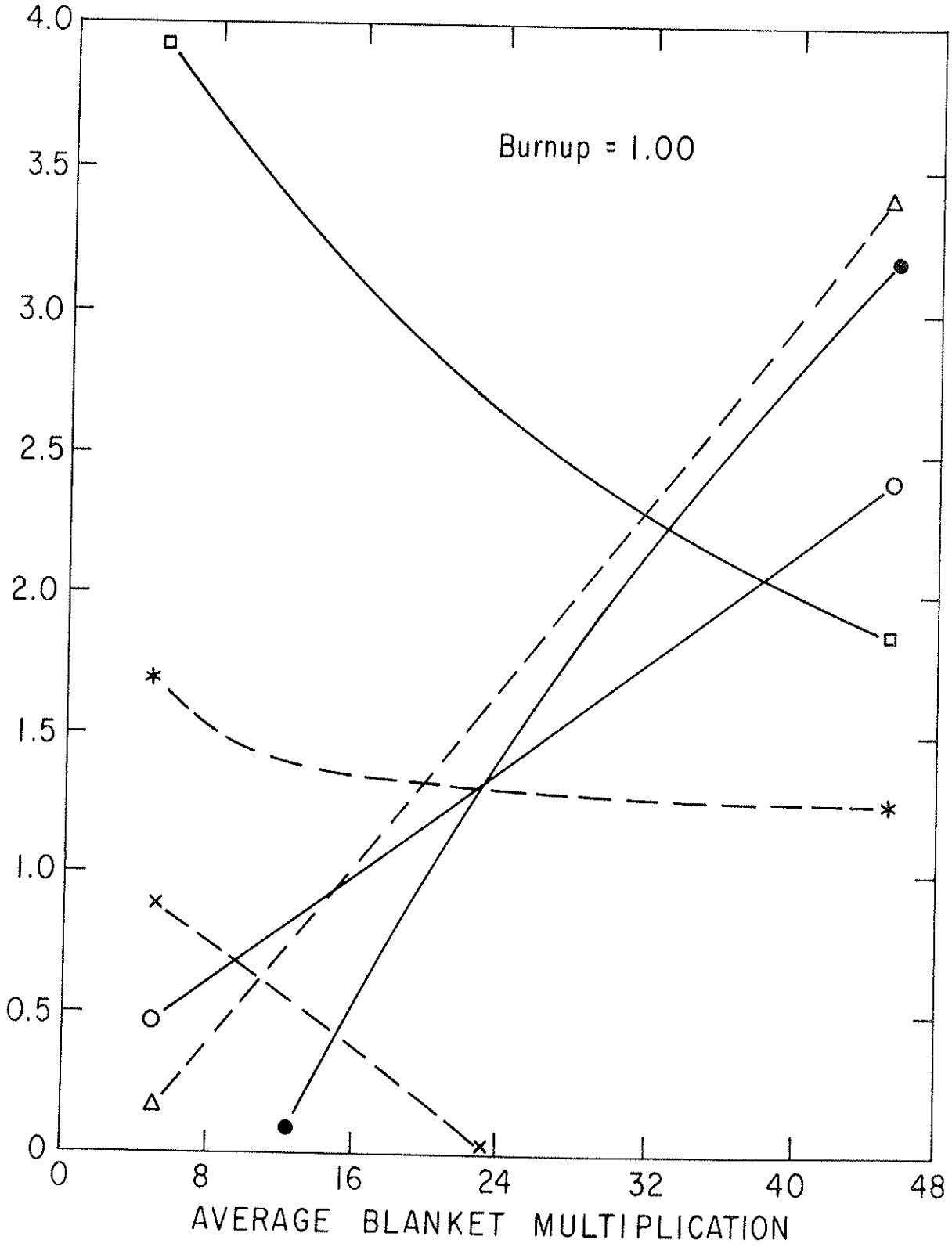

Fig. 3. Performance Parameters for the Ramping-Power Nominal Blanket, for B = 1.0.

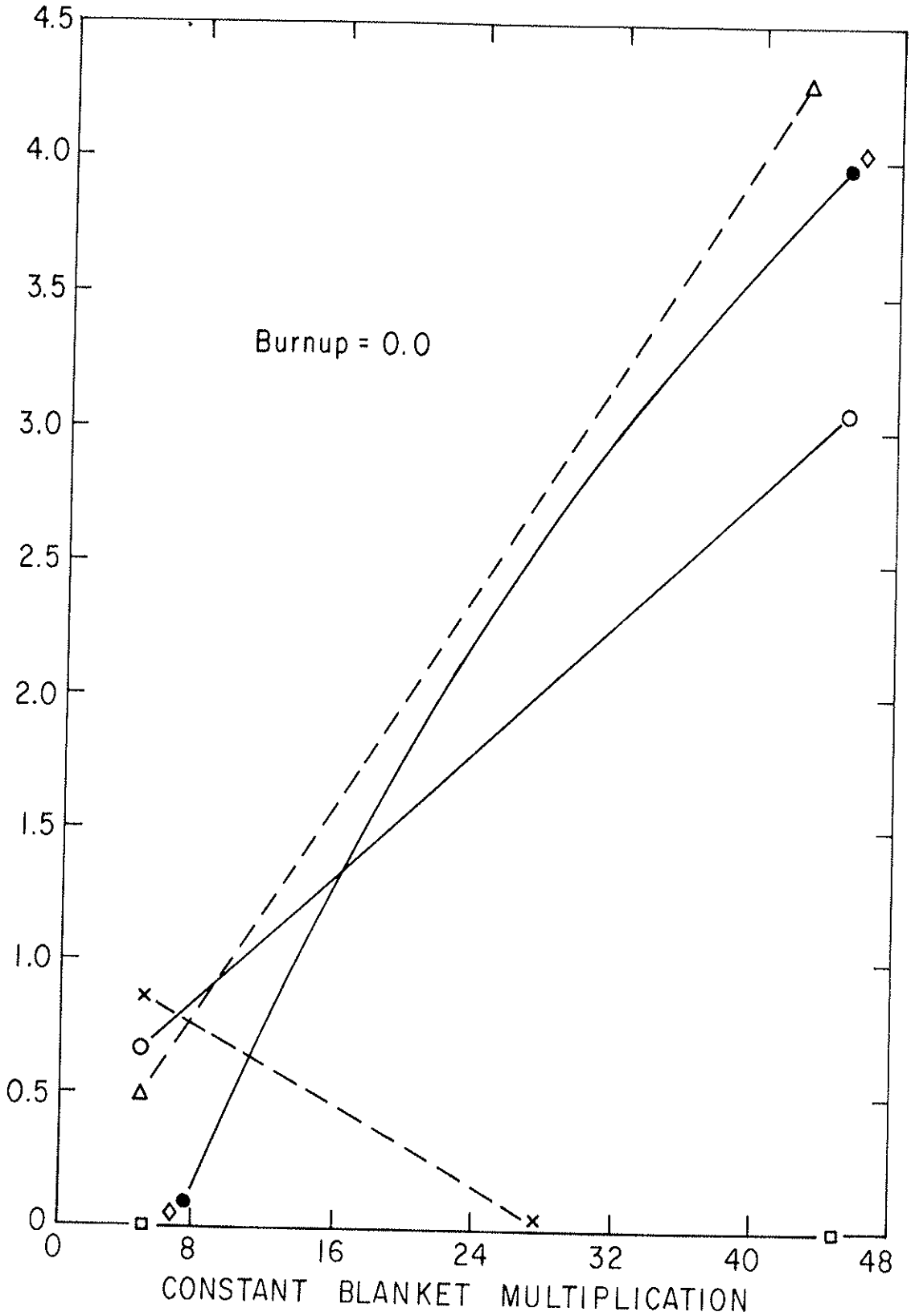

Fig. 4. Performance Parameters for the Ramping-Power Super Blanket, for B = 0.0.

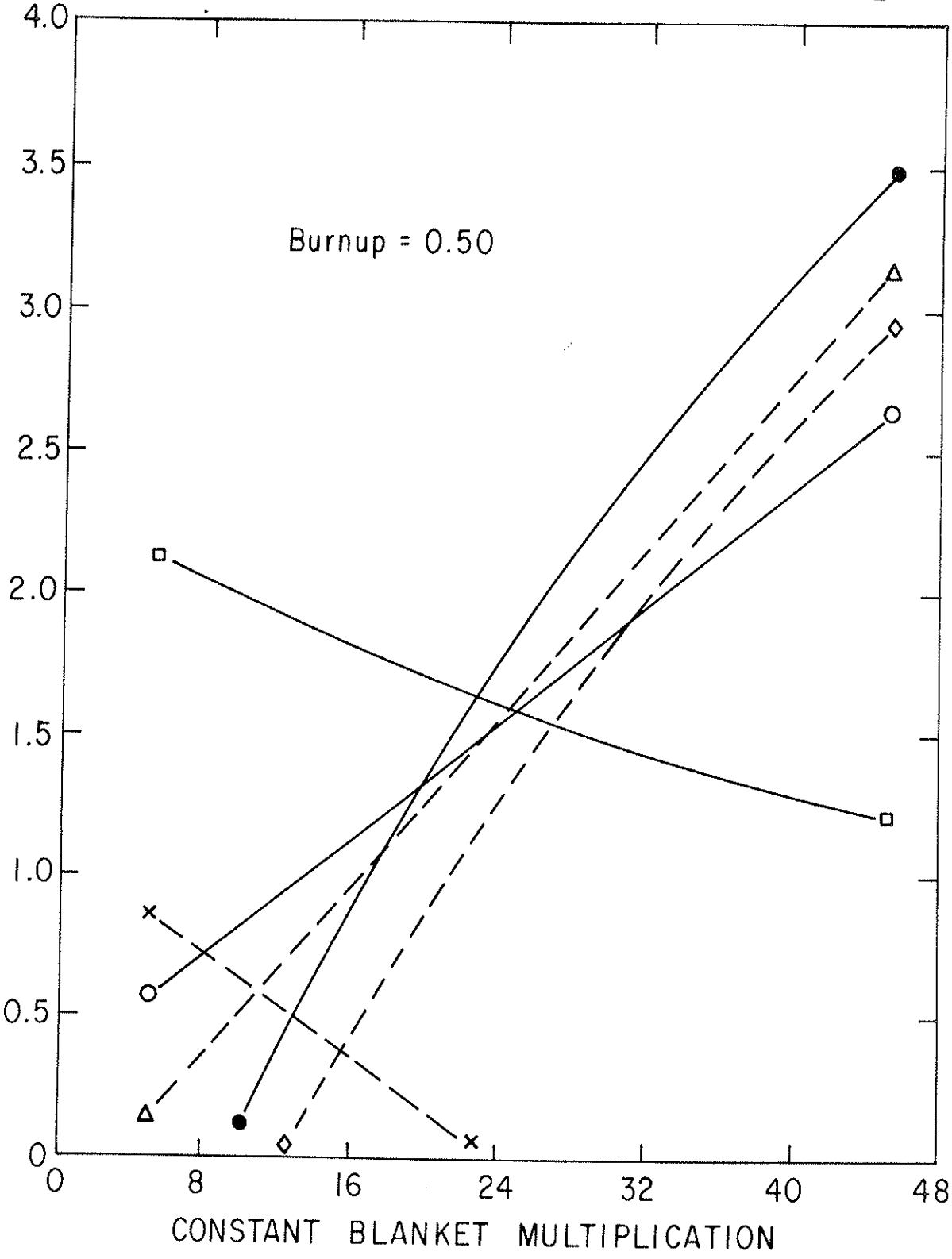

Fig. 5. Performance Parameters for the Ramping-Power Super Blanket, for B = 0.5.

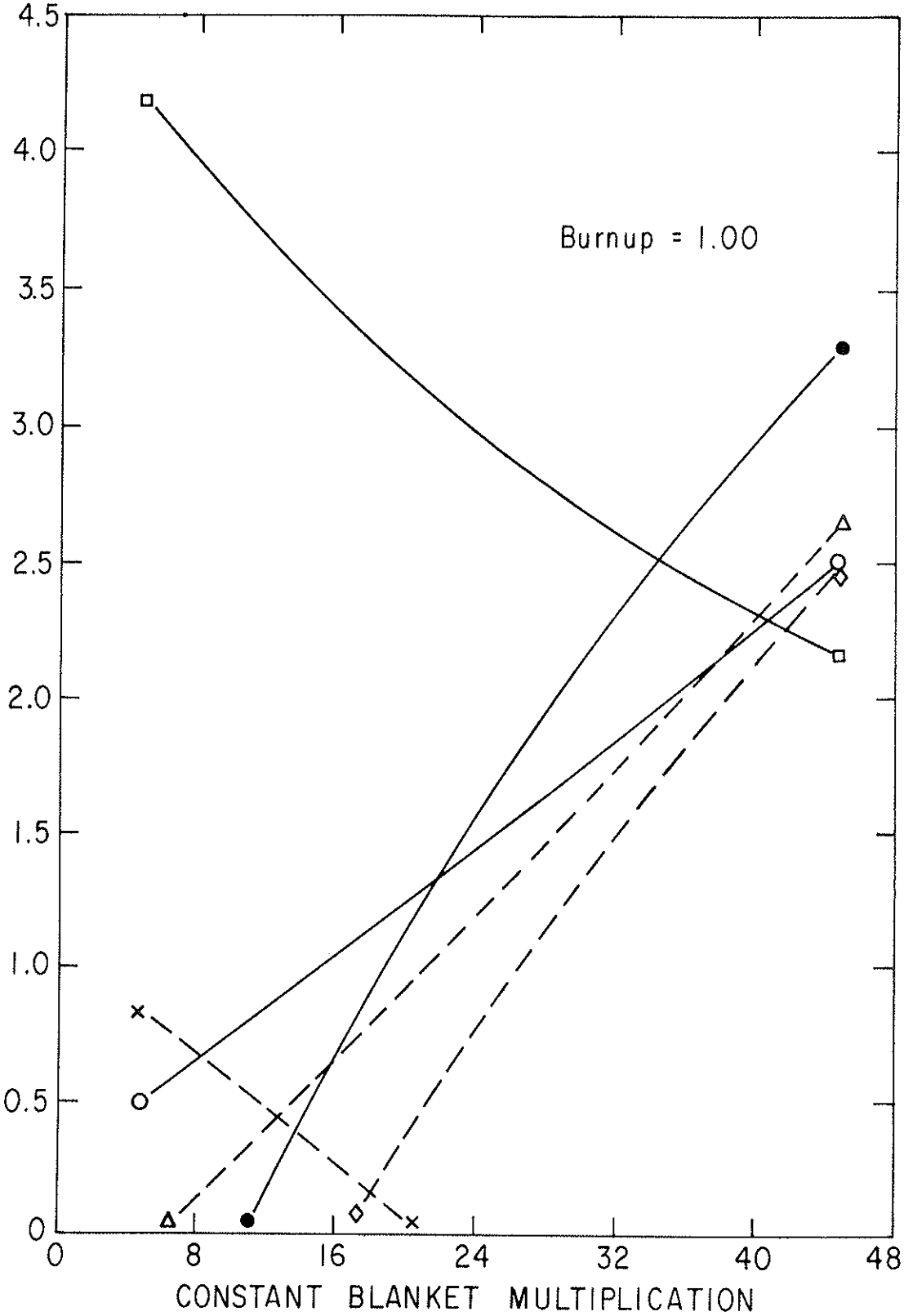

Fig. 6. Performance Parameters for the Ramping-Power Super Blanket, for B = 1.0.

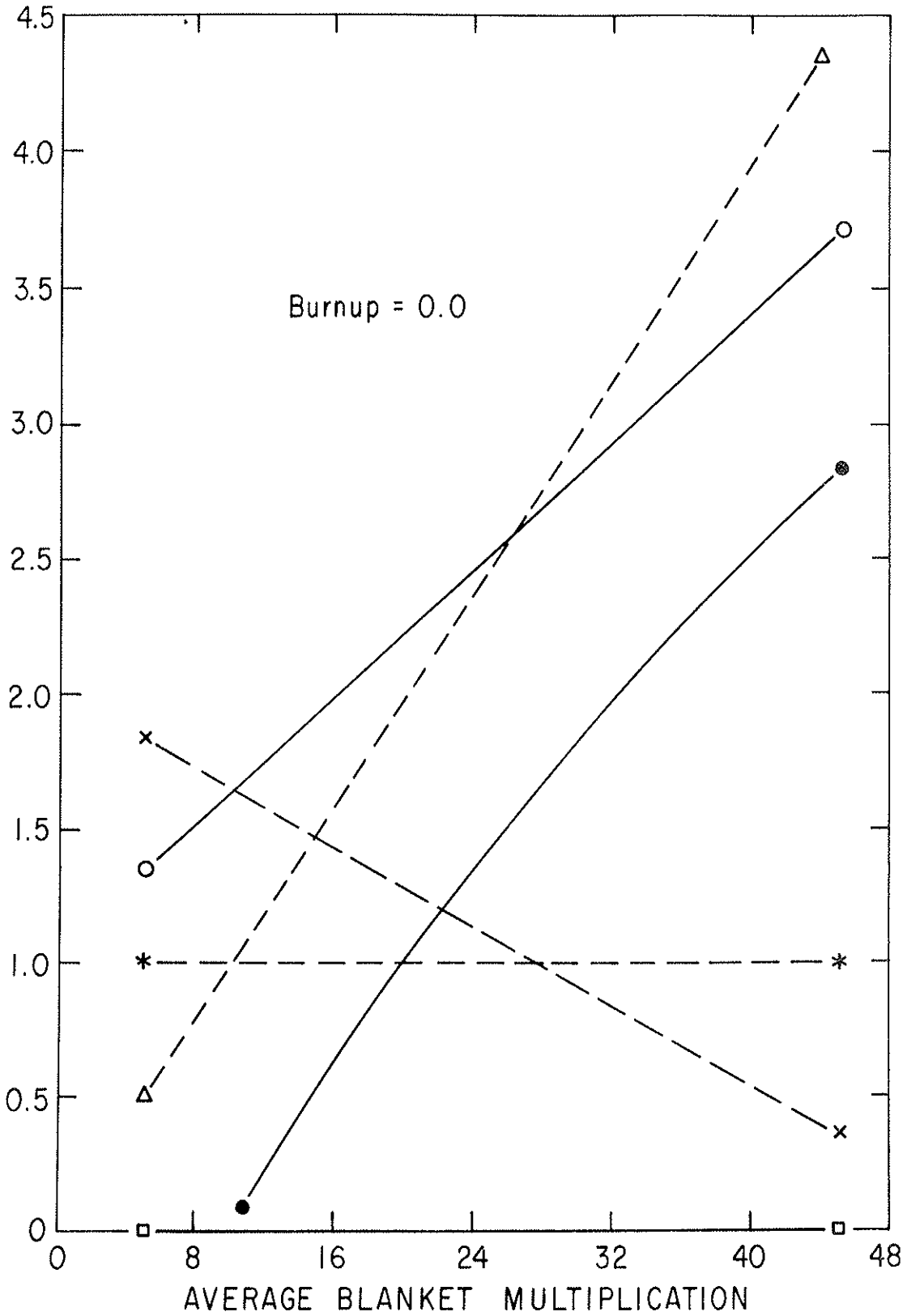

Fig. 7. Performance Parameters for the Constant-Power Nominal Blanket, for B = 0.0.

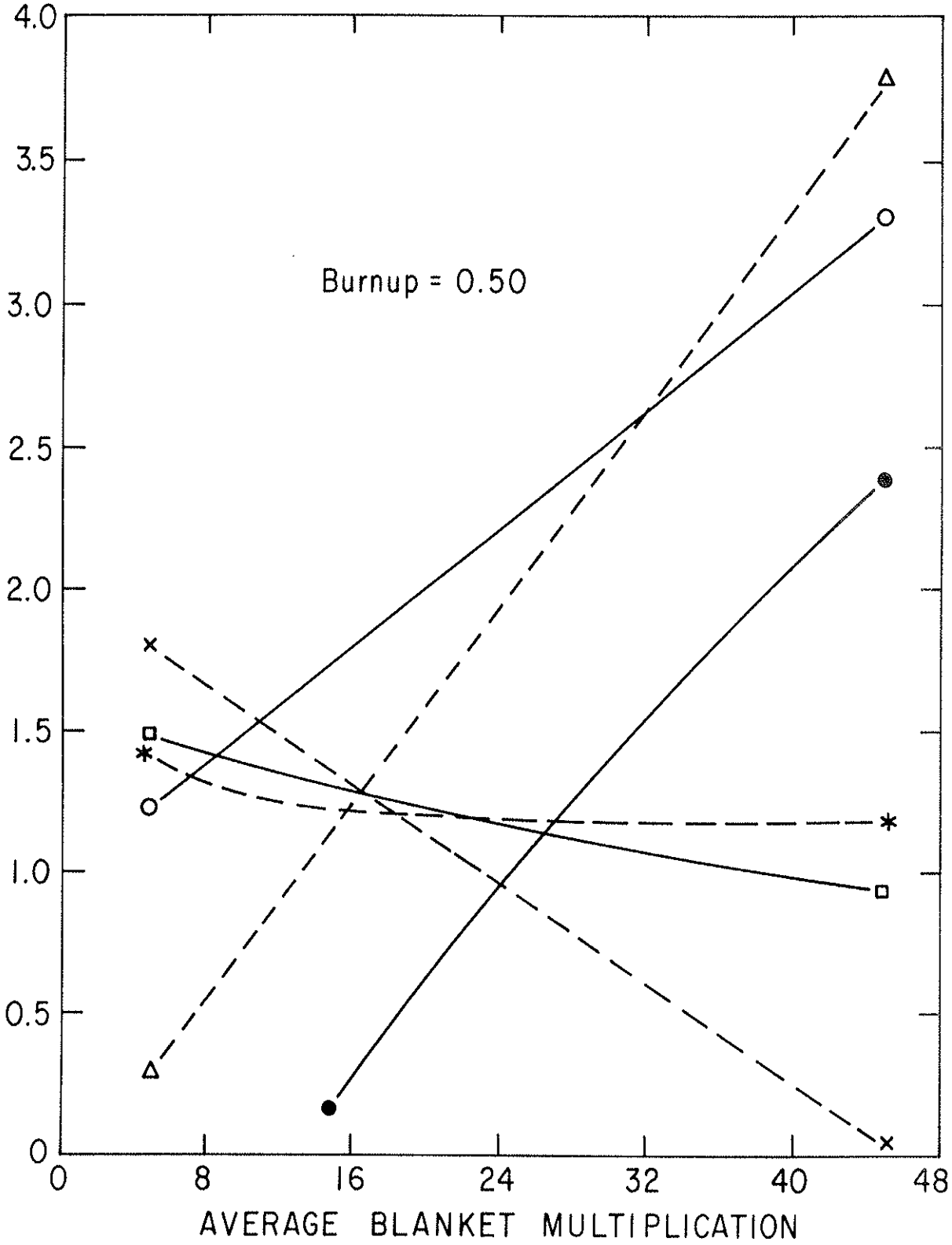

Fig. 8. Performance Parameters for the Constant-Power Nominal Blanket, for B = 0.5.

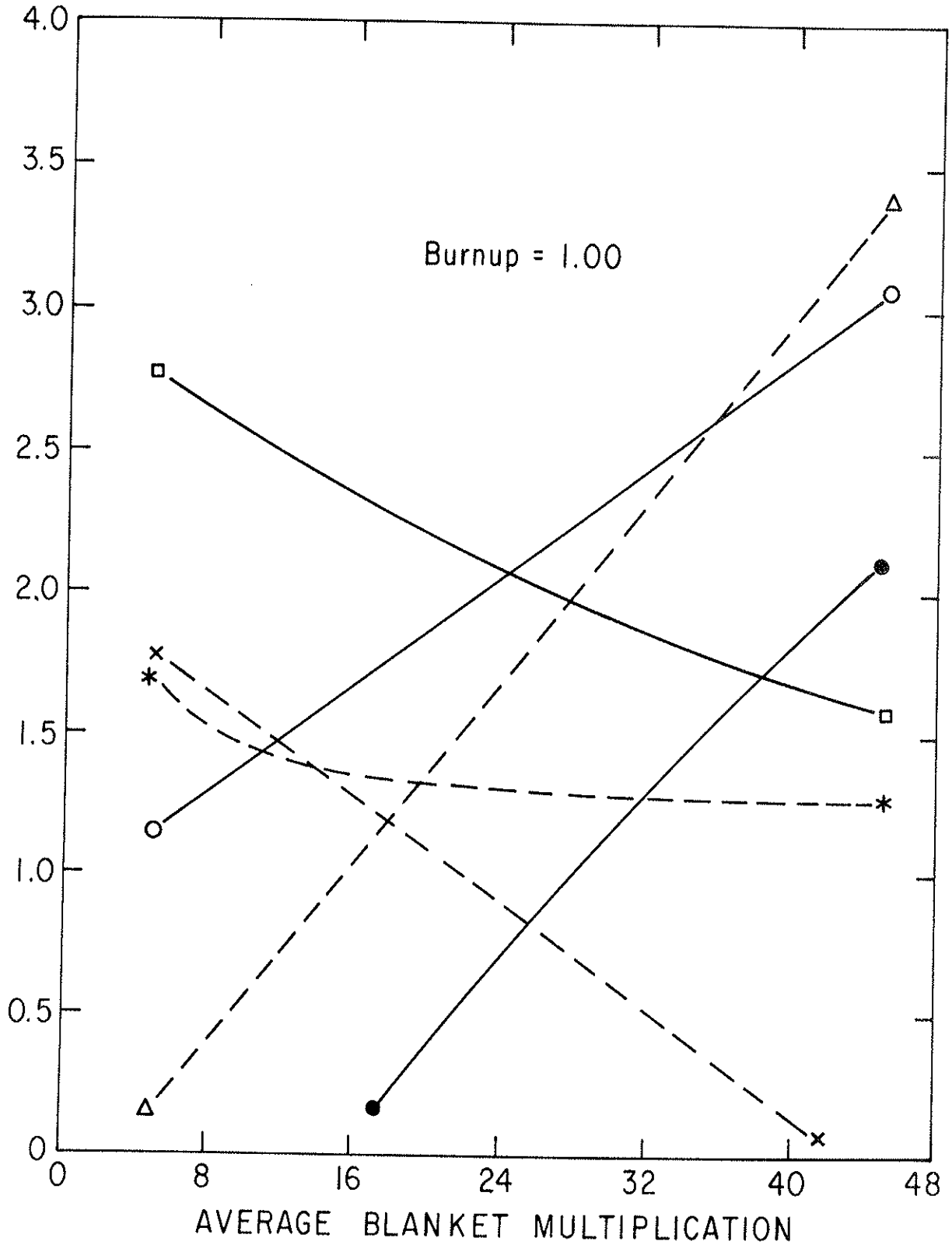

Fig. 9. Performance Parameters for the Constant-Power Nominal Blanket, for B = 1.0.

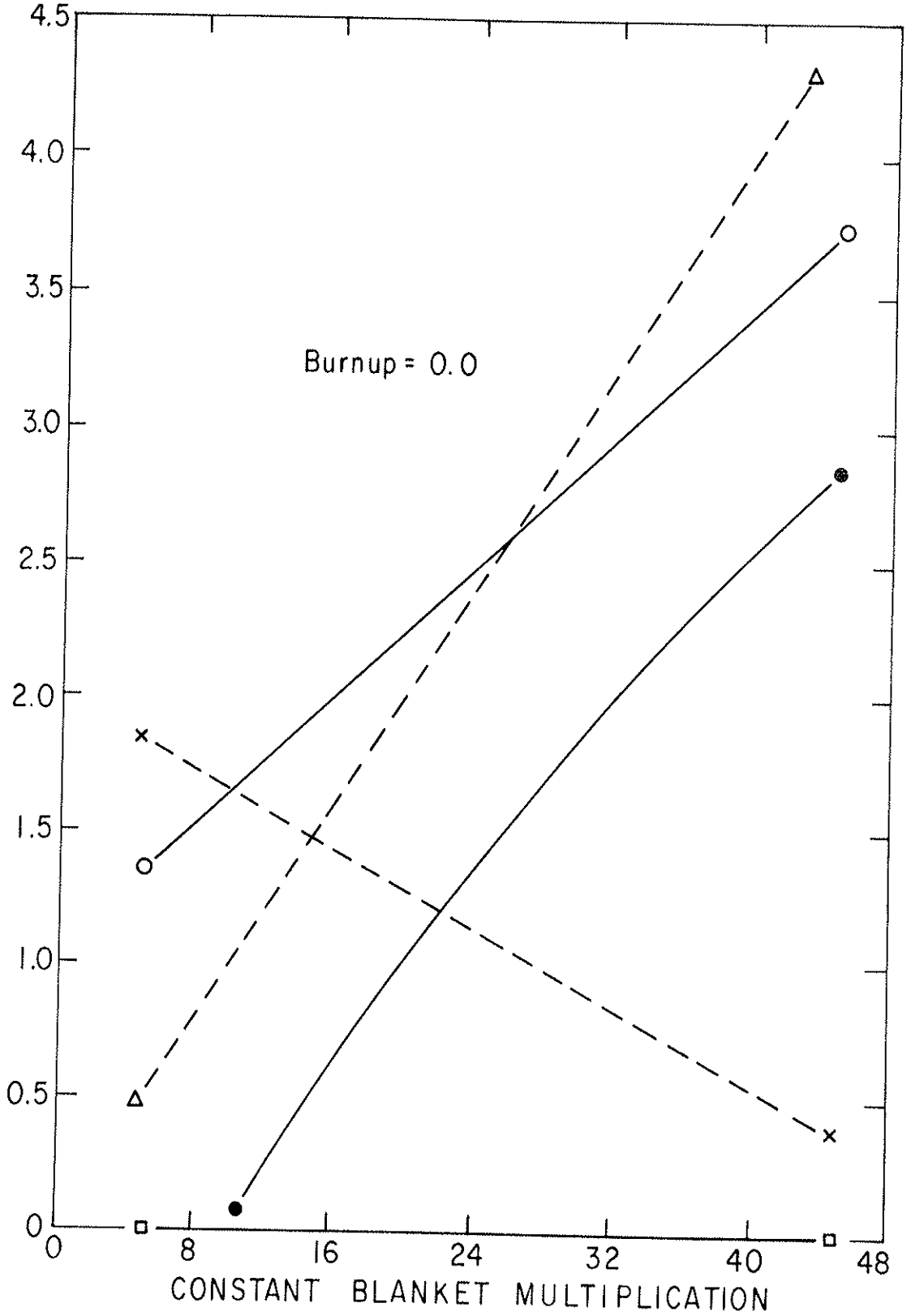

Fig. 10. Performance Parameters for the Constant-Power Super Blanket, for B = 0.0.

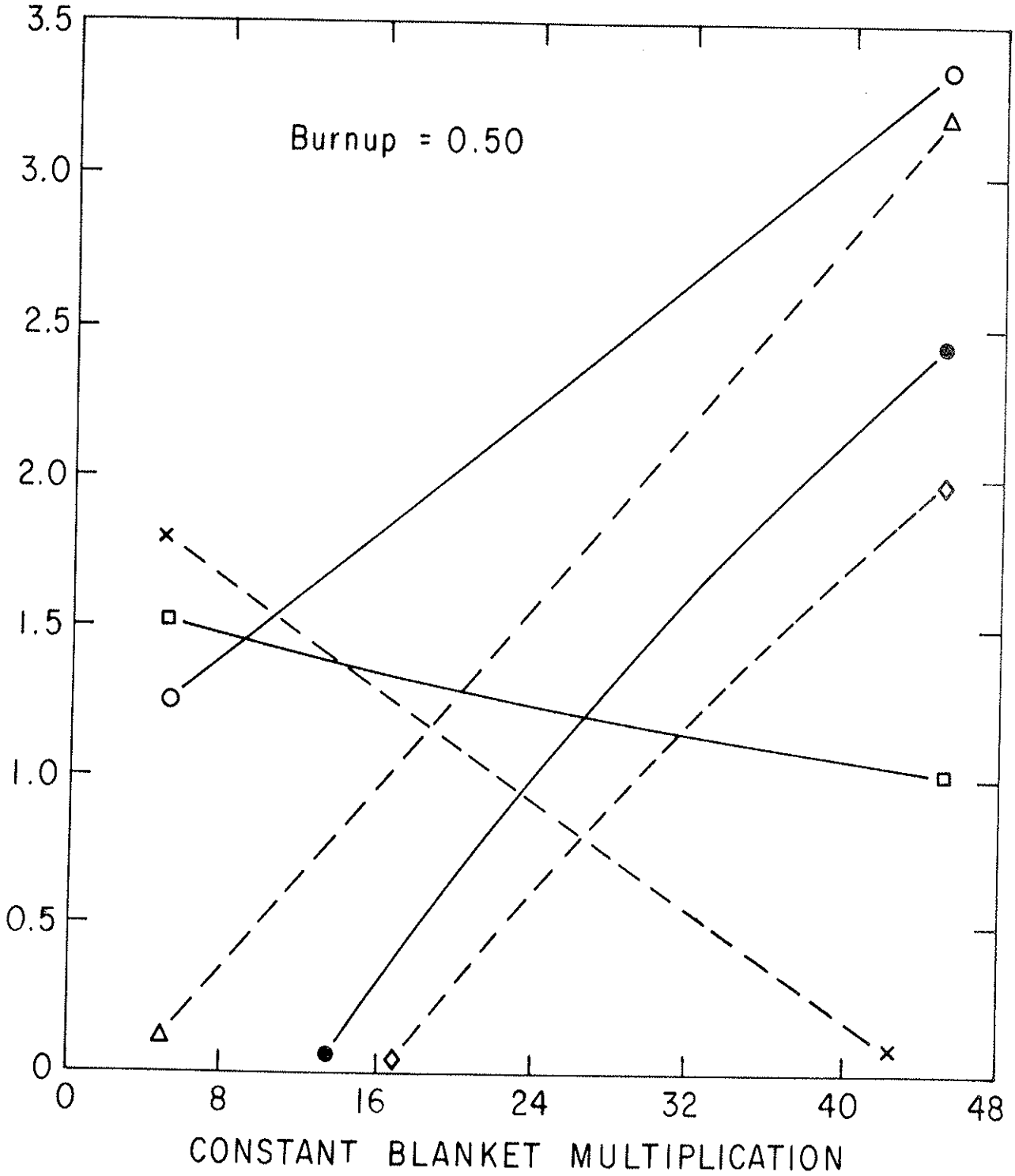

Fig. 11. Performance Parameters for the Constant-Power Super Blanket, for B = 0.5.

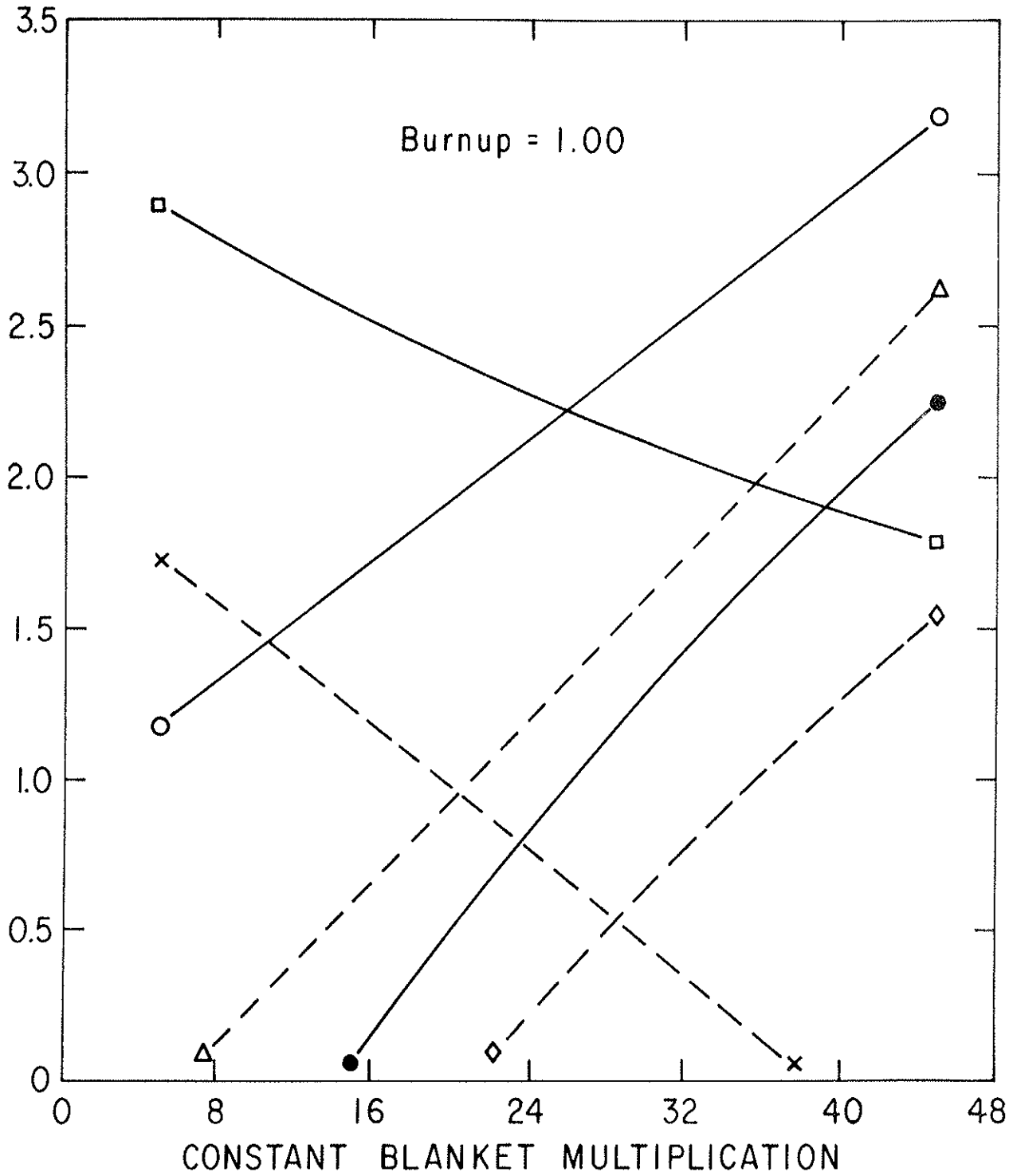

Fig. 12. Performance Parameters for the Constant-Power Super Blanket, for B = 1.0.

References

[1]D. J. Bender and J. D. Lee, The Potential for Fissile Breeding with the Fusion-Fission Hybrid Reactor, Transactions of the American Nuclear Society Annual Meeting (American Nuclear Society, Hinsdale, Illinois, 1976) Vol. 23, pp. 24-25; also Lawrence Livermore Laboratory Report UCRL-77887 (1976).

[2]L. Ku and W. G. Price, Jr., Neutronic Calculation and Cross Section Sensitivity Analysis of the Livermore Fusion/Fission Hybrid Reactor Blanket, Princeton Plasma Physics Laboratory Report PPPL-1370 (1977).

C. Special Calculations

In addition to the basic neutron transport and reaction rate analysis for the Reference Blanket, several sets of special calculations were performed. The most important of these was aimed at providing estimates of the power density in the blanket; this work is reported in a separate section on heating. Three additional categories will be discussed below: blanket criticality; actinide buildup; and design sensitivities.

1. Criticality

One of the advantages frequently claimed for hybrid reactors is freedom from the criticality accident. Fission reactors by necessity must be made of materials which will sustain a critical chain reaction; possible perturbations into a super-critical state constitute one severe (but well constrained) class of accidents. For fissile fuel producing hybrids it is probably true that no reconfiguration of the materials would lead to a critical state; therefore such reactors could be considered safer in some degree than fission reactors.

Unfortunately this is not a valid conclusion in general for hybrids which are optimized to produce power. Loading the blanket with fissile material to promote extra fission provides the potential for an accident. Specific analyses of possible rearrangements of the fuel must then be checked to determine the

need for engineered safeguards.

A brief exploration of this aspect of the Reference Blanket was undertaken. Criticality is determined by the eigenvalue of the transport equation, commonly known as the multiplication constant, k. The ANISN code, which was used to calculate the flux distribution in the Reference Blanket performance studies, can also solve for the multiplication constant in one-dimensional, cylindrical systems and for infinite media. The former condition is the same geometrical approximation applied in the original blanket analysis, i.e., ignoring the toroidal curvature and assuming symmetry around the poloidal axis. The infinite medium calculation ignores the effect of leakage from a finite body and hence overestimates (usually) the effective k.

The eigenvalue calculation for the Reference Blanket, using the same cross sections and discretization as for the flux calculations, gives k = 0.7778. By fission reactor standards this is substantially less than 1, the critical value.

This result can be used as the fixed point to derive a simple formula to estimate k. Let S be the number of fast fissions induced by the external source DT fusion neutrons, and let f be the total number of fissions in the blanket. The original fissions, releasing typical fission-spectrum neutrons, will initiate a damped chain reaction with a ratio of k fissions in each later generation: thus $f = S + kS + K^2S + \ldots$, which reduces to $f = S/(1 - k)$. For the Reference Blanket, f = 1.815,

implying that S = 0.403; indeed, for this blanket a fast fission rate of S = 0.39 was calculated. Therefore a nominal value of S = 0.4 was adopted for the remaining analysis.

For the Reference Blanket, the concentration of PuF_3 in the burner salt was 0.25 mole %. The performance of a blanket which differed only in having a 0.30% loading of Pu was calculated, giving f = 2.200. Using the nominal formula, this implies k = 0.8182. These two values of k can be used to form a simple formula for k in terms of P, the mole percent of plutonium.

An elementary expression for k is the so-called four-factor formula: $k = \eta\varepsilon pf$. Here η describes the fission source, ε and p describe interactions of fast and intermediate energy neutrons, while f (the thermal utilization factor) is the ratio of fissile to total absorption at thermal energies. Variations in P should only affect f, and in a simple manner: the numerator is proportional to P, while the denominator is a sum of terms, one of which is proportional to P. Therefore the four-factor formula can be rewritten as K = cp/(d + p) where c and d are parameters which can be calculated from a two-point fit. The result is k = (1.1016P)/(0.10401 + P). By substitution, an equivalent formula, f = S*(0.10401 + P)/(0.10401 - 0.1016P), is found. These equations actually fit 3 points which span the range of interest in P: the point P = 0, k = 0, f = S is included by construction.

The preceding discussion was addressed to the normal operating state of the hybrid, i.e., with the salt properly confined to the blanket. It should be recognized that this blanket has, by fission reactor standards, a rather peculiar configuration: a thin fissile fuel layer bounded by a strong uranium absorber on one side and a strong lithium absorber on the other. To attain a satisfactory effective multiplication in this highly poisoned system, the infinite medium, k, of the fissile region must be rather high. This is confirmed by a calculation for the moderator zone, 85% graphite and 15% salt, with P = 0.25%: $k_\infty = 1.706$. However, it is difficult to conceive of an accident which could assemble a rather large volume of this mixture without the addition of other materials.

A more plausible accident would be leakage of molten salt from the blanket, with the possibility that it might accumulate in some compact configuration. Thus the k_∞ for just the burner salt is of interest. Two calculations were performed, giving $k_\infty = 1.182$ for P = 0.25 and $k_\infty = 1.034$ for P = 0.15. Fitting a formula of the form previously explained gives an equation for k_∞ as a function of P: $k_\infty = (1.5052P)/(0.06835 + P)$. From this, a critical value of P can be derived: $k_\infty = 1$ when P = 0.135.

The conclusion to be drawn from these analyses is that this hybrid concept is not free of concern about criticality accidents or accidents aggravated by criticality. However, the

seriousness of this is open to question. Obvious engineered safeguards can be applied to reduce the accident potential. Indeed, this approach has taken criticality off the list of most important concerns for fission reactors.

2. Actinide Buildup

In considering the uranium-plutonium cycle for the conceptual hybrid blanket, only the buildup of plutonium was specifically assessed. The justification for this was that the production of other actinides occurs at a lower rate, so that the low burnup expected would mean that only low concentrations would accumulate. A very simple actinide chain model was developed to investigate the actual situation.

The following definitions are required:

S = density of uranium-235

U = density of uranium-238

P = density of plutonium-239

Q = density of plutonium-240

R = density of plutonium-238

T = density of neptunium-237

B = burnup as fraction of original uranium

t = time

ϕ = total flux

σ_x = cross section for reaction x

x = absorption, fission, n-γ or n-2n

D = time derivative.

With these definitions, a set of simple equations for the nuclide concentrations can be written:

$$DU = -\sigma_a^U U\phi \ , \quad U = U_o e^{-\sigma_a^U \phi t} \ ;$$

$$DS = -\sigma_a^S S\phi \ , \quad S = S_o e^{-\sigma_a^S \phi t} \ ;$$

$$DP = \sigma_\gamma^U U\phi - \sigma_a^P \phi \ , \quad \text{with } U \approx U_o$$

$$P \approx \left(U_o \sigma_a^U / \sigma_a^P\right)\left(1 - e^{-\sigma_a^P \phi t}\right) ;$$

$$DQ = \sigma_\gamma^P P\phi - \sigma_a^Q Q\phi \ , \text{ with } U \approx U_o$$

$$Q \approx \left(U_o \sigma_\gamma^U / \sigma_a^P\right)\left(\sigma_\gamma^P / \sigma_a^Q\right)\left(1 - e^{-\sigma_a^Q \phi t}\right)$$

$$+ \left(U_o \sigma_\gamma^U / \sigma_a^P\right)\left(\sigma_\gamma^P / \left(\sigma_a^P - \sigma_a^Q\right)\right)\left(e^{-\sigma_a^P \phi t} - e^{-\sigma_a^Q \phi t}\right) \ ;$$

$$DT = \sigma_n^U U\phi - \sigma_a^T T\phi \ , \quad T \approx \left(U_o \sigma_n^U / \sigma_a^T\right)\left(1 - e^{-\sigma_a^T \phi t}\right) ,$$

$$\text{with } \sigma_a^T \approx 0 \ , \quad T \approx U_o \sigma_n^U \phi t \ ;$$

$$DR = \sigma_n^P P\phi + \sigma_\gamma^T T\phi - \sigma_a^R R\phi \ , \quad \text{with } \sigma_a^R \approx 0 \ ,$$

$$DR \approx \sigma_n^P P\phi + \sigma_\gamma^T U_o \sigma_n^U \phi^2 t \ ,$$

$$R \approx \left(U_o \sigma_\gamma^U / \sigma_a^P\right)\left[\sigma_n^P \phi t - \left(\sigma_n^P / \sigma_a^P\right)\left(1 - e^{-\sigma_a^P \phi t}\right)\right]$$

$$+ \sigma_{\gamma}^{T} U_o \sigma_n^U \phi^2 t^2/2 \quad ;$$

$$B * \left(S_o + U_o\right) = \left(S_o \sigma_f^S/\sigma_a^S\right)\left(1 - e^{-\sigma_a^S \phi t}\right)$$

$$+ \left(U_o \sigma_f^U/\sigma_a^U\right)\left(1 - e^{-\sigma_a^U \phi t}\right)$$

$$+ U_o\left(\sigma_{\gamma}^U/\sigma_a^P\right)\left(\sigma_f^P/\sigma_a^P\right)\left[\sigma_a^P \phi t - \left(1 - e^{-\sigma_a^P \phi t}\right)\right].$$

A special transport calculation was performed so that spectrum-averaged cross sections could be obtained for these equations. (Obviously the validity of their solution depends on the suitability of the parameters supplied.) The blanket for this calculation is a variant of the Reference Blanket, with some judicious anticipation of the buildup of the actinides. In the multiplier, the uranium density was reduced by a factor of 0.992 (i.e., 0.8% total loss), and the U-235 enrichment was dropped to 0.25%. In addition, Pu-239 was added at a density of 0.5% of the initial uranium concentration, and Pu-240 was added at 3% of the Pu-239 density. In the burner salt, the PuF_3 mole fraction was raised to 0.3% to counteract the added poisons, and 7% of this plutonium was assumed to be Pu-240. The resulting blanket performance parameters were: energy multiplication M = 24.5; net fissile production F = 0.165; and tritium breeding ratio T = 0.79. (It is assumed that the T value could be boosted at the expense of F and M, but this was not explored.)

Solutions of the actinide equations for this blanket are shown in Figure 1, and selected values are listed in Table I. The independent variable is the integrated wall load, i.e., the period of exposure to the driving fusion source. Notice that the burnup rate accelerates as the bred Pu-239 is fissioned; the burnout of bred plutonium causes a decrease in the net production rate. The cumulative time-average net fissile production per fusion neutron is reported as F. It is calculated by subtracting a constant Pu-239 burnup rate in the burner region (where the salt processor keeps the composition fixed) from the declining net multiplier production rate. Reprocessing of the multiplier at relatively low burnup is desirable to keep F near its initial value. The burnout of U-235 increases also with exposure, but since the initial loading is with tails, the enrichment of the spent uranium is presumably of little concern.

The density of Pu-240 builds up from zero at a declining rate because the burnout increases with the density. The saturation ratio of Pu-240 to Pu-239 would be 9.49%; the ratio reaches half this value at a burnup of 0.63%. This ratio is substantially lower than that for plutonium bred in LWR's, where values around 22% are more typical. This has both good and bad aspects. As a fuel for thermal fission reactors, the cleaner material will give better neutronic performance. However, clean plutonium is also more suitable for the production of fission weapons, leading to a more difficult safeguards problem.

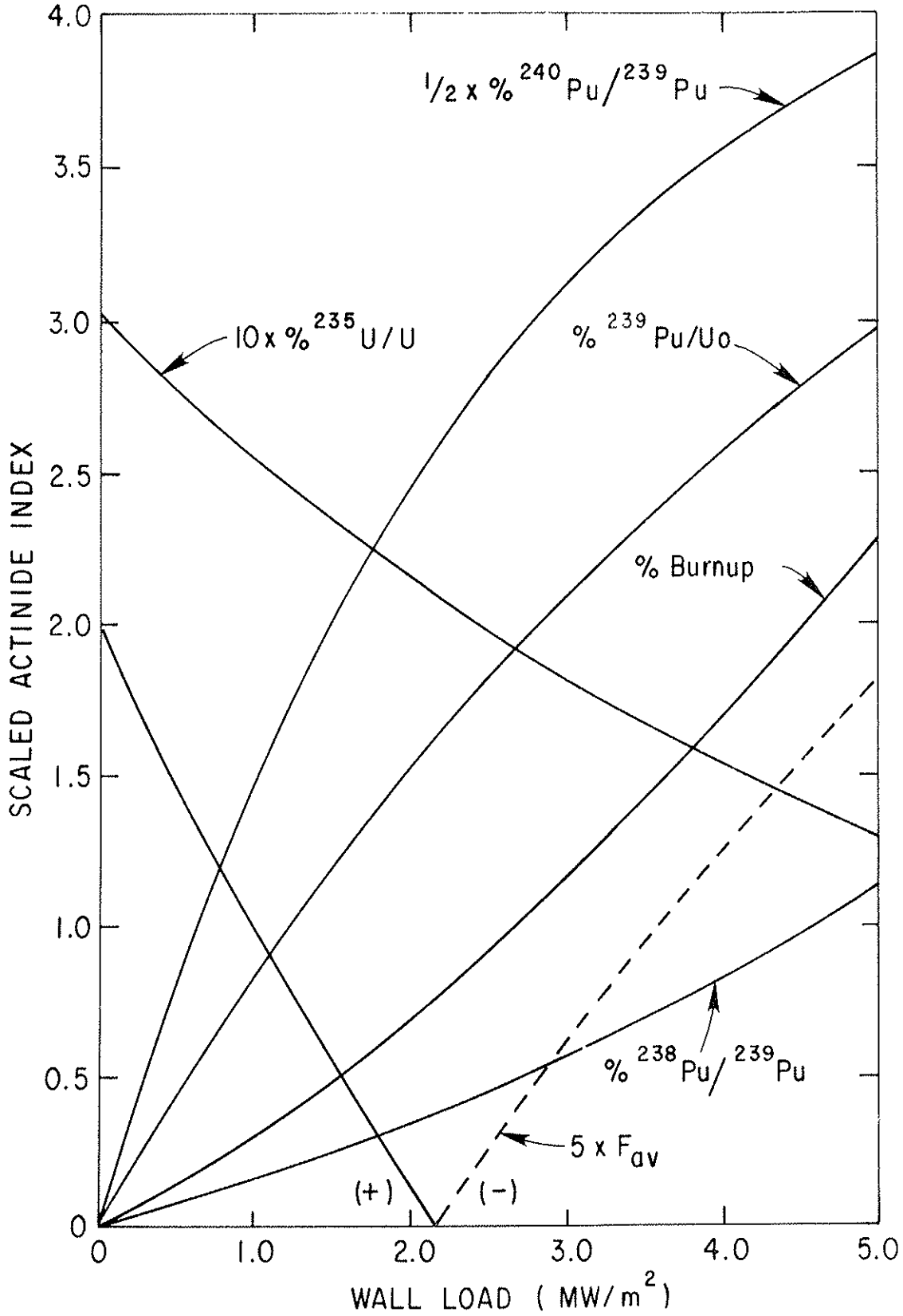

Fig. 1. Plots versus Integrated Wall Load of Results of the Simple Actinide Production Model.

Table I. Results of a Simple Actinide Production Model.

Integrated Wall Load	0.00	0.85	1.55	2.10	2.65	$MW\text{-}yr/m^2$
Multiplier Burnup	0.00	0.25	0.50	0.75	1.00	%
U/U_o	100.00	99.00	98.20	97.57	96.94	%
U-245/U-all	0.3	0.260	0.231	0.211	0.192	%
Pu-239/U-all	0.0	0.726	1.241	1.599	1.922	%
Pu-240/Pu-239	0.0	2.65	4.207	5.141	5.887	%
Pu-238/Pu-239	0.0	0.130	0.255	0.365	0.486	%
Average F	0.393	0.233	0.098	0.009	-0.074	

Since the blankets considered in this hybrid study are consumers as well as producers of fissile material, the production of actinides in the burner sale is also of concern. A simple model again based on the use of time-independent spectrum and volume averaged cross sections has been applied to the same model blanket discussed above.

Using the previous notation, equilibrium balance equations for Pu-239 and Pu-240 can be written:

$$P\sigma_a^P\phi = \delta^P \quad ,$$

$$Q\sigma_a^Q\phi = \delta^Q + P\sigma_\gamma^P\phi \quad .$$

Here δ stands for the equivalent external source density, i.e., the total external source divided by the total volume of salt to which it is added. However, the feed rates are related by the isotopic composition of the external source material, $\delta^Q/\delta^P = Q'/P'$. This allows solution for the equilibrium composition of the burner region plutonium.

$$\left(Q/P\right) = \left(\sigma_\gamma^P/\sigma_a^Q\right) + \left(Q'/P'\right)\left(\sigma_a^P/\sigma_a^Q\right) \quad .$$

Using effective cross sections from the model blanket described above,

$$Q/P = 0.1212 + 0.3483\left(Q'/P'\right) \quad .$$

This shows that the composition is principally determined by the local balance between production and burnout, with a per-

turbing effect due to the extra Pu-240 feed brought along with the Pu-239 makeup fuel. Using (Q'/P') = 0.042, the isotopic ratio in the multiplier plutonium at 0.5% burnup, the overall ratio for the burner is 0.1195, i.e., 12%.

This is still substantially better than the LWR ratio, but would definitely hurt the neutron balance of the hybrid blanket. Comparison of the performance of two blankets covered in a series of scoping studies illustrates this. For a blanket like the Reference Blanket except that the PuF_3 concentration in the burner was 0.3%, the basic performance was: T = 1.306, M = 32.4, and F = -0.393. Adding 7% Pu-240/Pu-239 to the burner salt drastically decreases the fission rate, giving M = 20.6 and F = +0.404; while T drops to 0.698 due to the reduced neutron population. (Of course, optimization of the blanket for the presence of Pu-240 should greatly improve these figures.)

One possibility for minimizing this effect would be to feed all the freshly produced multiplier plutonium into the burner salt, while extracting older plutonium with a higher Pu-240/Pu-239 ratio from the salt for sale. Of course, this drag-stream approach to isotope control will only be possible if the hybrid does indeed produce a net excess of plutonium for use in fission reactors.

3. Design Sensitivities

The design of the Reference Blanket began as a process of trial-and-error examination of possible configurations and compositions[1] and developed into a more rational search technique as the basic conceptual design was identified.[2] As the parameters of the Reference were tentatively determined, a series of calculations was performed to study the variations in performance due to changes in the blanket specification. An important consideration was a desire to minimize the inventory of plutonium in the burner salt while keeping the energy multiplication high, tritium breeding ratio greater than one, and net fissile breeding non-negative.

The results of a number of variations are listed in Table II. The same results are displayed in Figure 2 as points on a plot of F versus T. As the plot makes obvious, the values of F and T are strongly correlated, even when perturbed by rather different blanket changes. These results are also displayed in Figure 3 as points on a plot of M versus T + F. Again, strong correlation is shown, with the points generally lying in a band.

The Reference Blanket consists of seven regions:

First Wall (5 cm) - 10% SS, 10% Water

Multiplier (15 cm) - 8% SS, 44% U-7 Mo

Burner (10 cm) - 5% SS, 80% Flibe with PuF_3

Moderator (30 cm) - 85% Graphite, 15% Flibe-Pu

Table II. Results of Some Parameter Variations on the Reference Blanket.

Case No.	$^{6}Li\%$	$PuF_3\%$	M	F	T	Comments
8163	0.10	0.25	26.2	+0.036	1.094	Reference Blanket
8094	0.10	0.25	26.2	+0.246	1.030	50% U-Mo in Multiplier
8161	0.10	0.25	22.2	+0.443	0.851	95% Graphite in Moderator
6221	0.10	0.30	32.4	-0.549	1.306	Scan in Lithium-6
3600	0.10	0.30	31.0	-0.341	1.220	15% Water in Wall
3565	0.10	0.30	39.7	-0.770	1.689	No Water in Wall
6233	0.10	0.30	20.6	+0.404	0.698	7% Pu-240/Pu-239
3879	0.15	0.30	27.5	-0.047	1.155	Scan in Lithium-6
4301	0.25	0.30	23.4	+0.260	1.008	Scan in Lithium-6
1929	1.00	0.30	12.4	+0.929	0.766	Scan in Lithium-6

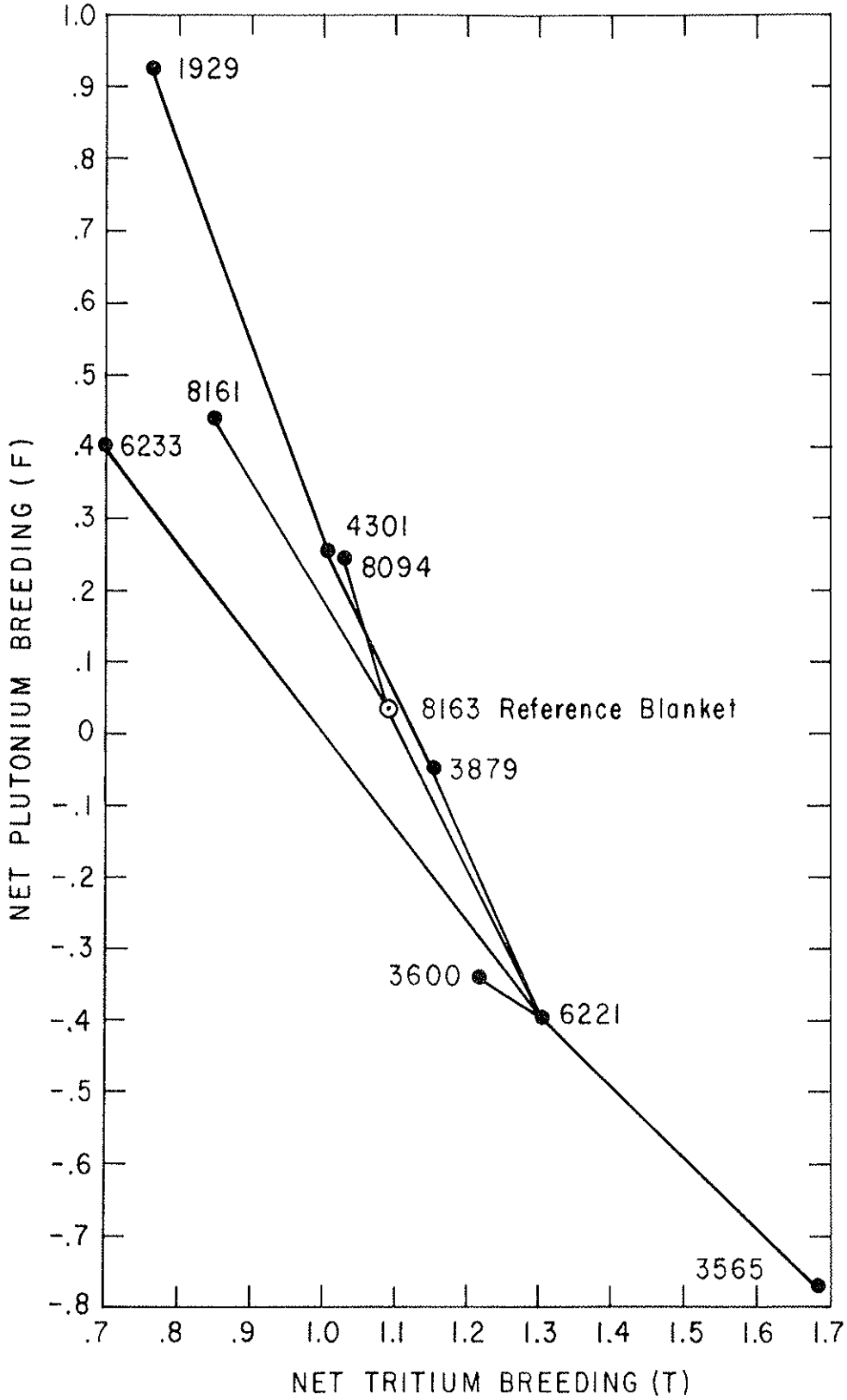

Fig. 2. Performance of a Number of Variations on the Reference Blanket, Plotted as F versus T.

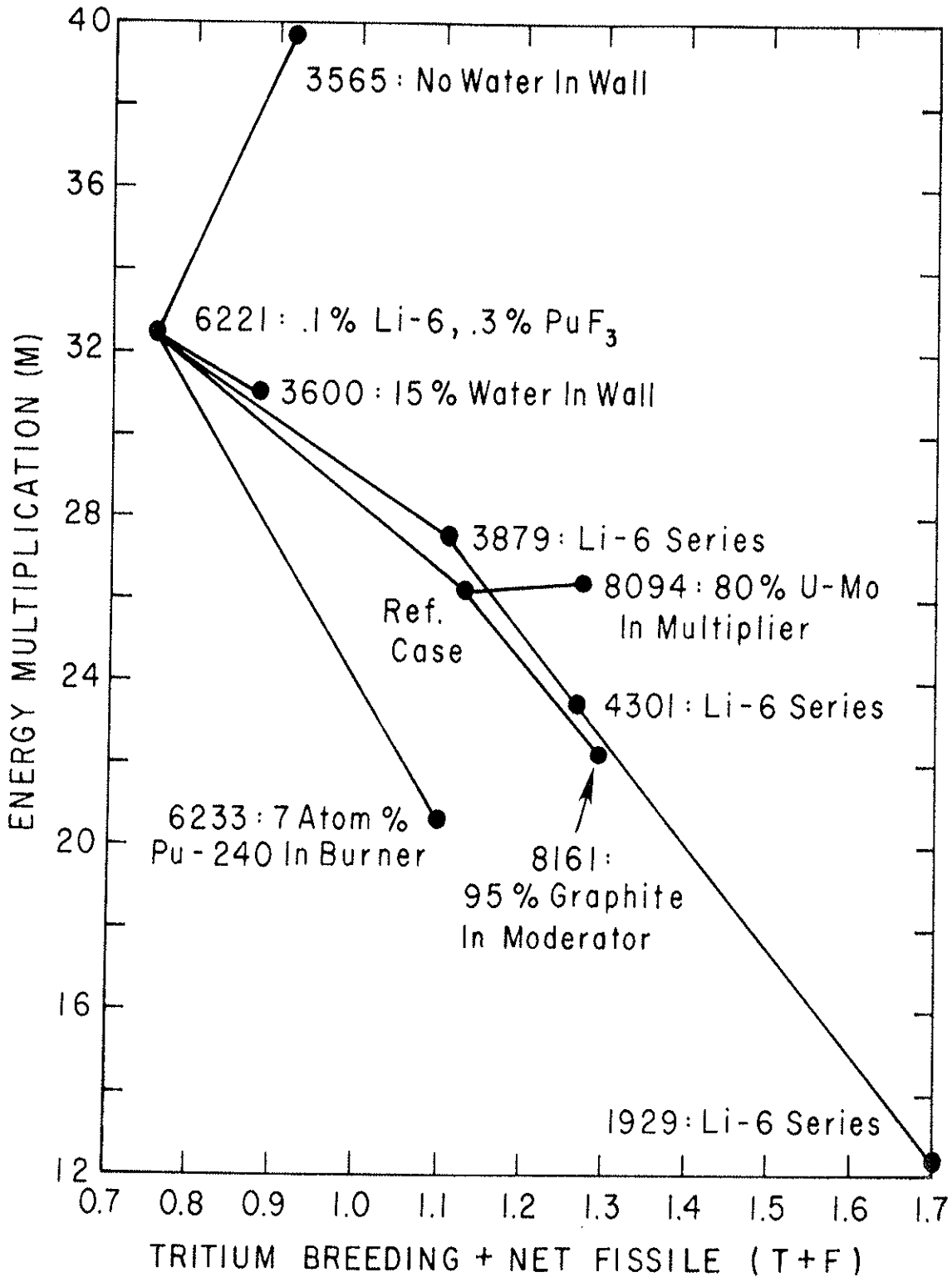

Fig. 3. Performance of a Number of Variations on the Reference Blanket, Plotted as M versus T + F.

Burner (10 cm) - 5% SS, 80% Flibe-Pu

Scavenger (15 cm) - 5% SS, 20% Graphite, 70% Flibe

Shield (~ 80 cm) - SS and Boron Carbide.

Three of the variations involve single changes to this specification. In the first, the volume fraction of the U-Mo fuel in the multiplier is increased to 50% (reducing the void fraction). This increases F substantially (compared to its near-zero reference value) but drops T very close to one. However, since the F increase is partially due to increased fast fission, the $\Delta T/\Delta F$ ratio is the smallest among all the variations. The second change is to increase the volume fraction of the graphite in the moderator to 95%, at the expense of the burner salt. This increases F due to a reduced fission rate, with a resulting large impact on T. The third variation is an increase in the PuF_3 mole fraction in the burner salt to 0.30%. This boosts the fission rate, reducing F, and thereby raises T because of the increased neutron flux.

The remaining cases can be considered to be double changes to the Reference, or single parameter variations to this last, higher inventory blanket. Two complementary variations examine the effect of the water coolant assumed for the first wall. Raising the volume fraction to 15% has a relatively small impact, increasing F and decreasing T comparatively sharply. On the other hand, removing all the water allows a harder spectrum and more fast fission. This substantially raises T and

decreases F because the burner region is driven to a greater fission rate by the higher source. Adding plutonium-240 to the burner salt so that the Pu-240/Pu-239 ratio is 7% decreases the fission rate (M falls to 20.6), which raises F and decreases T. Time did not permit a proper study of the impact of the higher actinides on net breeding and tritium production; clearly a reoptimization of the blanket would be required.

The last series of variations examines the effect of changing the lithium isotopic ratio. As the lithium-6 is raised from 0.1% to 0.15, 0.25, and finally 1%, the increased competition with the plutonium for thermal neutrons causes the fission rate to fall. This raises F, but the reduced supply of fission neutrons more than compensates for the increased density of Li-6, lowering T. It can be seen from the plot that performance nearly the same as the Reference Blanket could be achieved with about 0.2% Li-6 and 0.3% PuF_3. While this might result in some savings due to the reduced lithium isotopic separation requirement, it would entail a 20% increase in the blanket inventory of plutonium. This was presumed to be the more important effect and justifies the specification of depleted lithium.

A more elegant approach to the problem of design sensitivities is that incorporated in the computer code SWAN.[3] This program is a numerical embodiment of the first-order perturbation theory for variations in a response function with respect to variations in material densities. It uses the trans-

port code ANISN to calculate the direct flux and the adjoint flux for the target reaction, multiplies these by the cross sections of materials of concern, and then integrates to obtain sensitivity coefficients. SWAN was originally written for shielding and pure-fusion reactor application;[4] for this hybrid study it has been extended to treat fissionable materials properly.

The principal performance parameters for a hybrid blanket are: T, the tritium breeding ratio; F, the net fissile breeding ratio; and M, the energy multiplication. Four SWAN calculations were performed to find the sensitivity of these parameters for the Reference Blanket to changes in the composition of the blanket. (Two calculations, one for breeding and one for burnup, are needed for F sensitivities.)

The primary output of SWAN is a table of "effectiveness functions". These give the variation in response due to a unit change in density of each material in each interval of the blanket model. From these numbers a sensitivity profile can be plotted; the volume integral of the sensitivity times a hypothetical density change profile gives the predicted variation in the response functions. Figures 4, 5, and 6 show several such sensitivity profiles, together with superimposed zone-averaged sensitivities. (Note that proper evaluation of a density increase usually involves subtraction of the variation due to removal of some displaced material; SWAN can calculate "substitution effectiveness functions" for this purpose.)

Figure 4 shows the effectiveness function for carbon multiplied by the smeared density equivalent to 1 volume % graphite, i.e., sensitivity profiles for 1% graphite additions. In the burner salt regions all four sensitivities are positive and quite flat. This reflects the importance of moderation in increasing the fission rate and hence the flux. All the profiles ramp negative in the multiplier, where extra slowing down of the fast neutrons decreases the production of secondaries from the fusion neutrons. It should be noted, however, that since the Pu burnup's sensitivity is greater than the breeding sensitivity, the effect on net plutonium breeding from adding graphite would be positive in the multiplier and negative in the burner.

Figure 5 shows the effectiveness functions for type-316 stainless steel multiplied by the smeared density equivalent to 1 volume %, i.e., sensitivity profiles for 1% addition of steel. These are mostly negative. In the multiplier region extra steel would increase the slowing down rate of the high energy neutrons, thus decreasing the driving source. In the burner region steel is a parasitic absorber which poisons the blanket. The comparatively large magnitude of the sensitivities demonstrates that the placement of steel in the blanket should be given considerable study. The strong spatial dependence of the profiles shows that judicious placement of the required structural material can minimize the impact on performance.

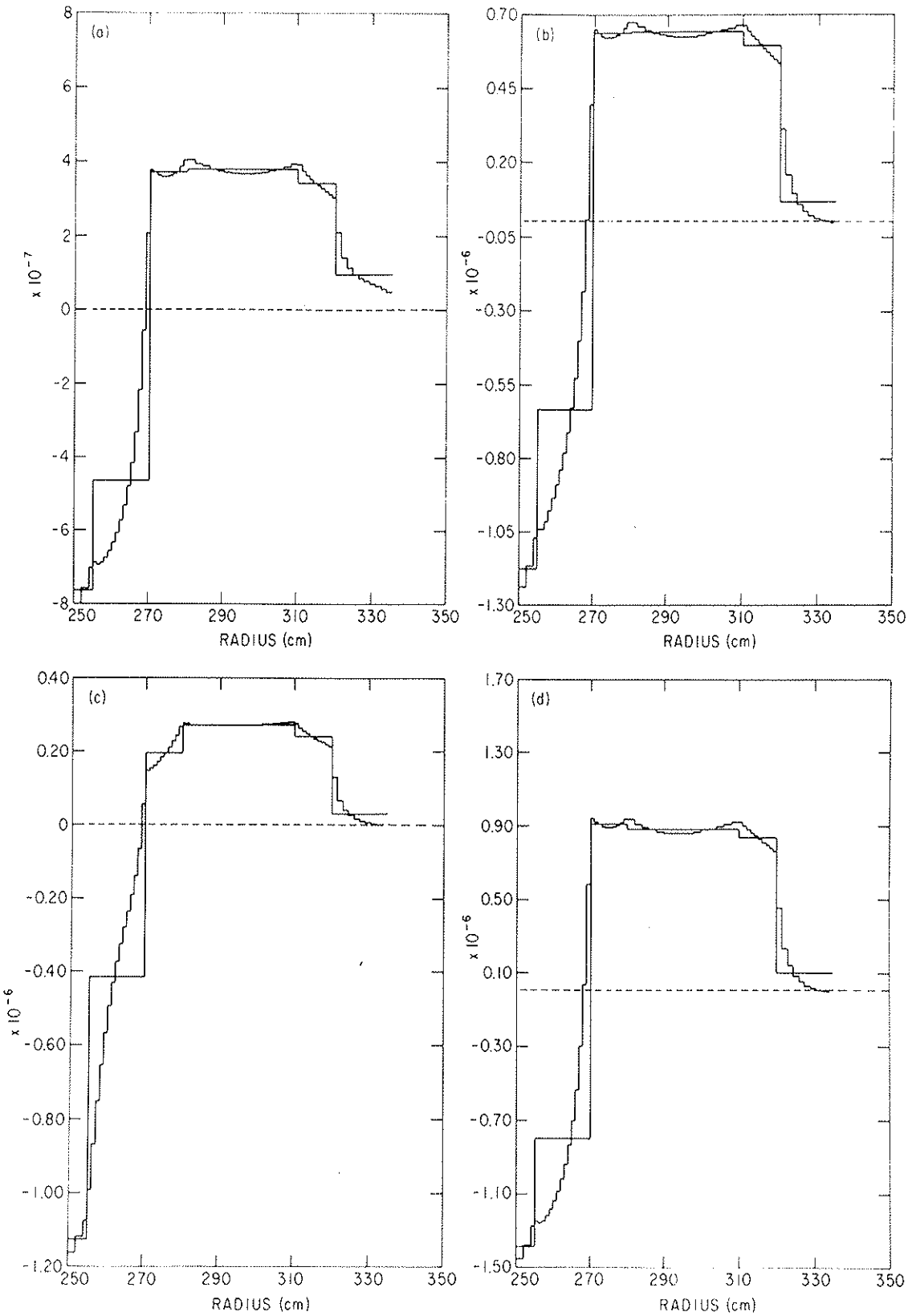

Fig. 4. Profiles of Sensitivity of the Reference Blanket to Graphite.

a) Tritium Breeding
b) Pu Production
c) Fission Rate
d) Pu Depletion

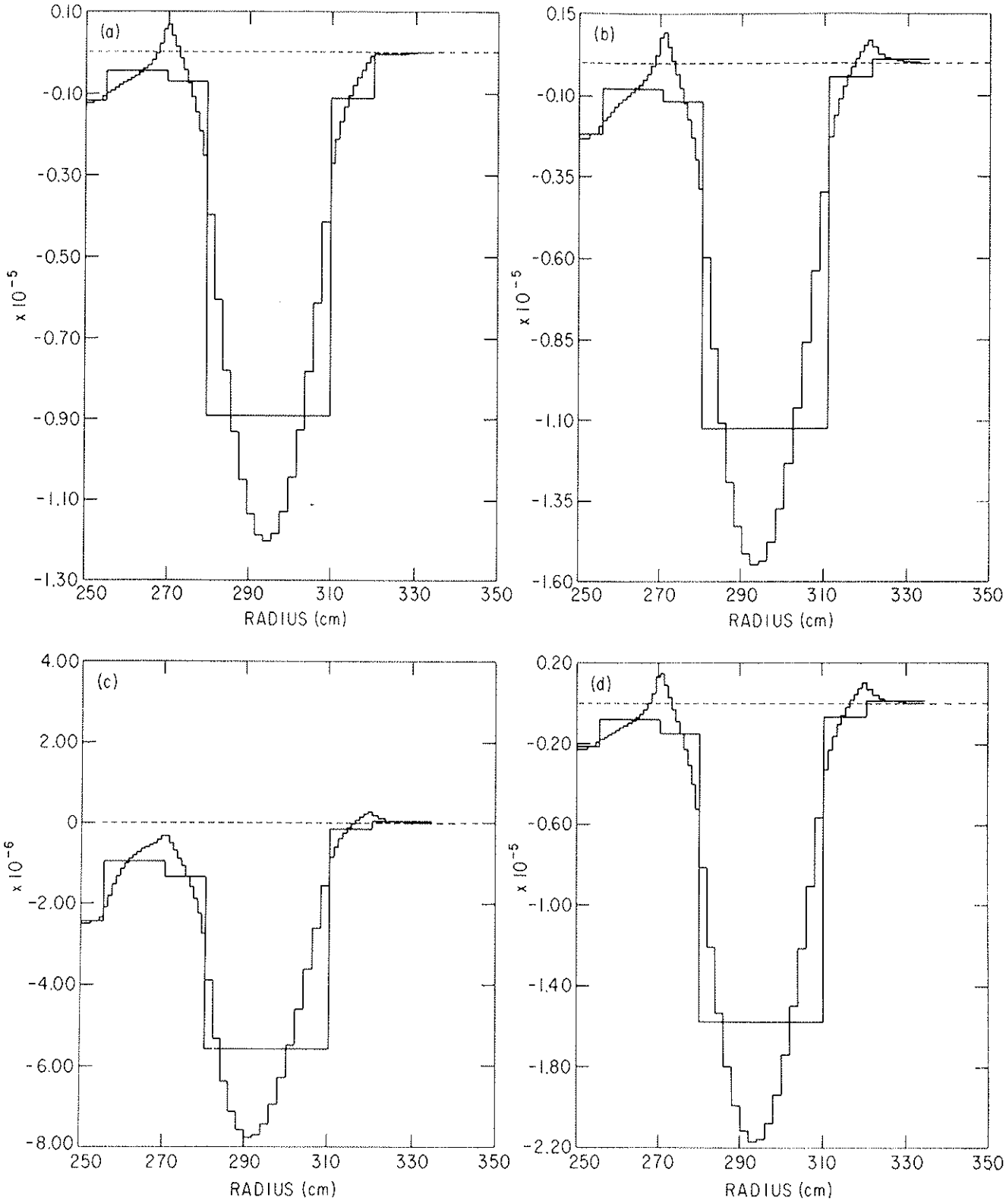

Fig. 5. Profiles of Sensitivity of the Reference Blanket to Type 316 Stainless Steel.

a) Tritium Breeding
b) Pu Production
c) Fission Rate
d) Pu Depletion

Figure 6 shows effectiveness functions for two material variations involving uranium. The profiles in the multiplier give the sensitivity to the depleted uranium in a 1% volume increase of U-7 Mo (the effect of the molybdenum is not shown here). The profile in the scavenger region gives the sensitivity to a 1 mole % addition of 238-UF_4 (the effect of the fluorine has been added).

The shifting sensitivities in the multiplier reflect the changing spectra through this zone. Uranium added adjacent to the burner region would be in a soft spectrum and hence very effective at absorbing neutrons and producing plutonium; it would also decrease the fission and tritium rates by their absorption. In the hard spectrum at the other face extra uranium would mean extra fast fissions. Unfortunately, material added to a homogeneous medium effectively increases the density uniformly, so that only the zone averages are important for the uranium in the multiplier. On this basis extra fuel would lower T and M, but raise F.

In the scavenger region all the profiles are similar, as the thermal flux leaking from the burner region is rapidly attenuated. The sensitivity was calculated for UF_4 to investigate the possibility of breeding plutonium in the scavenger salt as well as the multiplier. (The idea of using ThF_4 to produce fissile U-233 might also be considered.) However, this is seen to be a bad idea. The plutonium production rate is small because of the strong competition of the lithium-6, but enough

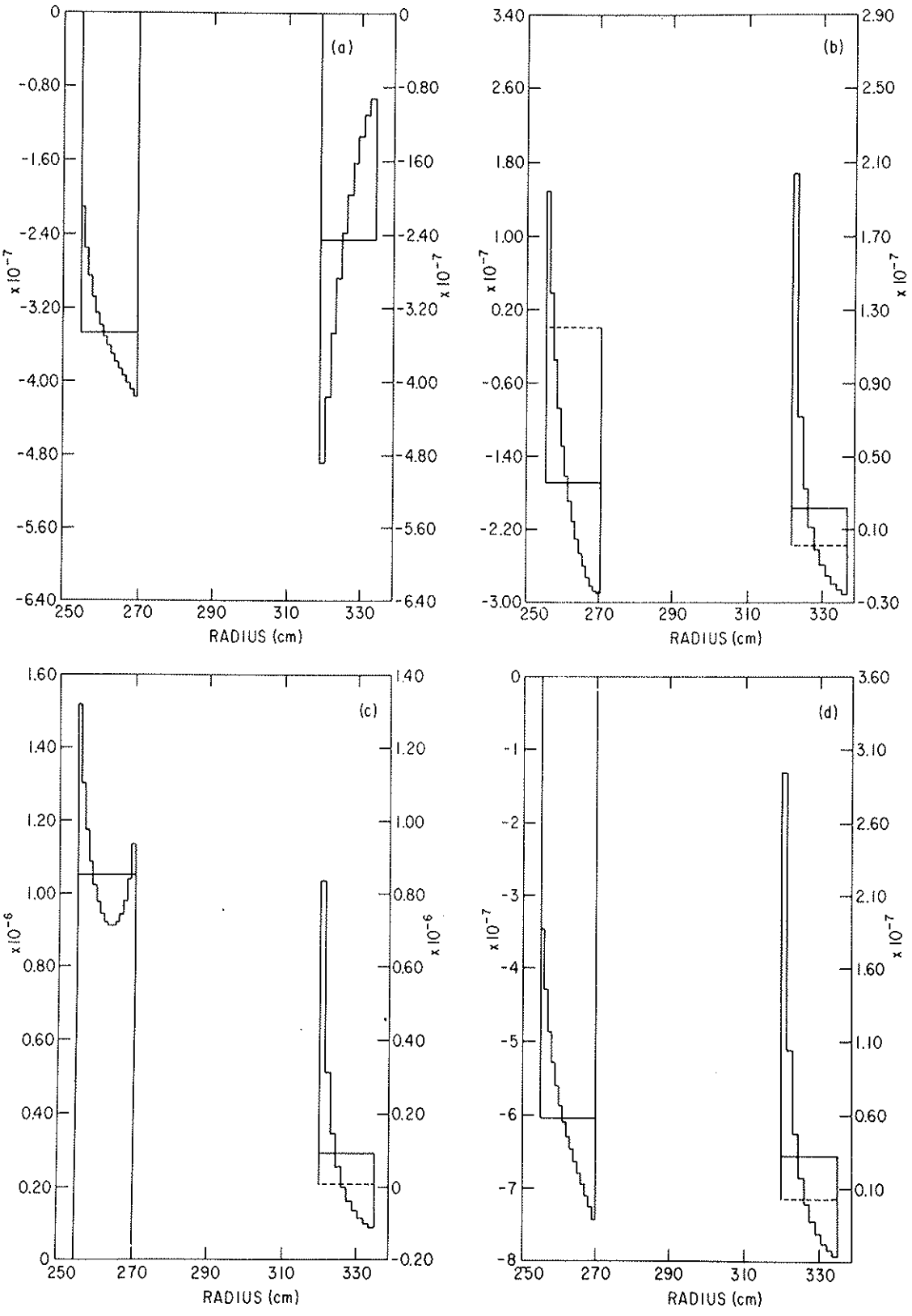

Fig. 6. Profiles of Sensitivity of the Reference Blanket to Depleted Uranium in the Multiplier and 238 UF_4 in the Scavenger.

a) Tritium Breeding
b) Pu Production
c) Fission Rate
d) Pu Depletion

neutrons could be absorbed to depress the tritium breeding ratio. Worse yet, uranium added near the burner would enhance the fission rate, probably by faster slowing down and greater reflection of fission neutrons which otherwise would have been lost from the burner. This causes the sensitivity of the net fissile breeding to be negative, too. An increase in F and a minimal decrease in T could be arranged, however, if the uranium were added only to the back half of the scavenger.

4. Predicted Performance Variations

The effectiveness functions are functional first partial derivatives. Integration of these times a shape function for perturbing the independent variable gives a first order partial derivative of the response function (reaction rate) with respect to the magnitude of the perturbation. The algebraic sum of a set of these derivatives constitutes a first order derivative of the response function and may be used to predict the joint effect of simultaneous changes. Ignored in such a prediction are the cross terms (synergistic effects) and, of course, second order factors. This limits the range of usefulness to a region which must be experimentally determined.

From the SWAN results for the Reference Blanket a number of these partial derivatives or "sensitivity coefficients" have been extracted; the values are listed in Table III. The independent variations considered are: dL, an increase of the lithium-6 enrichment of the burner salt (in atom %); dP, an increase of the plutonium content of the burner salt (in mole % of 239-PuF_3); dU, an increase in the amount of uranium fuel in the multiplier region

(in volume % of U-Mo); dW, an increase in the amount of water in the first wall (in volume %); dS, the addition of steel (SS-316) to the moderator region, displacing an equal volume of graphite (in volume %); and dC, an increase in the amount of graphite in the moderator, displacing an equal volume of the burner salt (in volume %).

The sensitivity coefficients are displayed for tritium breeding, net fissile production (production minus depletion), and energy multiplication. Typically the dM values are much larger than the others because of the 198/14.06 factor which scales up the reaction rate changes. For all six cases the dM and dT coefficients have the same sign, and dF the opposite.

The success of these coefficients in predicting actual performance change has been explored for a few of the cases in Table III. The results are displayed in Figure 7, an F versus T plot similar to Figure 2. Changes to dP, dU, and dW are well predicted, and the change due to dL is reasonably close. The altered performance resulting from changing the moderator for 85% graphite and 15% salt to 95% graphite and 5% salt is not well predicted, but this is a rather large change. No case is available to check the coefficient for the steel, but the accuracy is probably not very good: the effect is very strong and would quickly outstrip the first-order formulation. Surprisingly good results were obtained for the simultaneous increase of both the lithium-6 and the plutonium salt; the coefficients are of opposite sign and so the effects nearly cancel, with small error.

Table III. Sensitivity Coefficients for Variations to the Reference Blanket

Variation		dT	dF	dM
dL:	1 atom % increase of the Li-6 enrichment of the burner salt.	-2.3244	+5.7463	-92.068
dP:	1 mole % increase of the PuF_3 content of the burner salt	+3.7292	-7.5379	+100.427
dU:	1 volume % increase of the U-Mo content of the multiplier	-0.012106	+0.038942	-0.13979
dW:	1 volume % increase of the H_2O content of the first wall	-0.016698	+0.008105	-0.25329
dS:	1 volume % increase of the steel content of the moderator (replacing graphite)	-0.51726	+0.60187	-9.3140
dC:	1 volume % increase of the C content of the moderator (replacing burner salt)	-0.013426	+0.026444	-0.26398

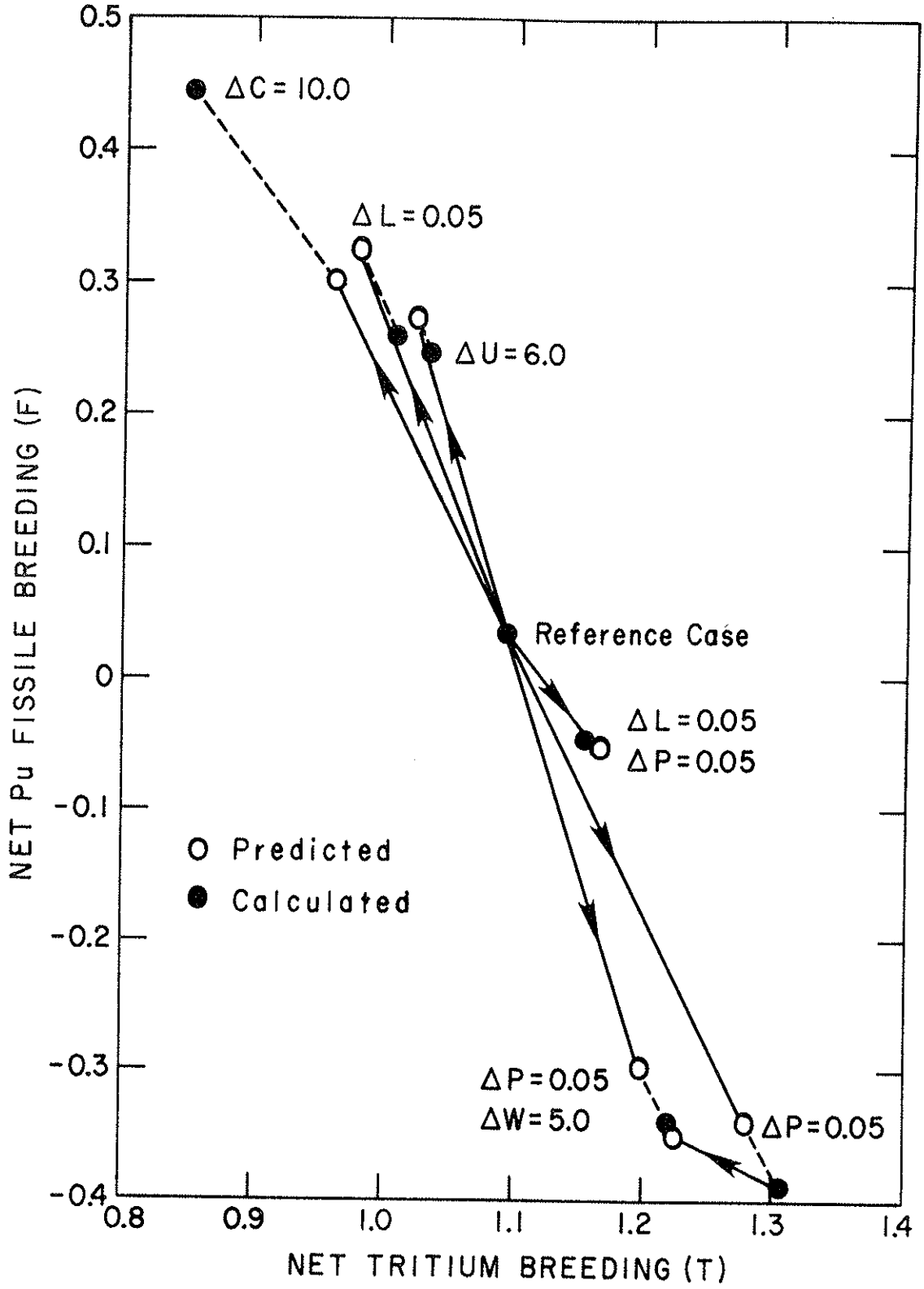

Fig. 7. Comparison of the Actual Performance of Several Blankets to Predictions Based on the SWAN Analysis of the Reference Blanket. Each Prediction is Connected to its Base Case by a Solid Line and to its Real Result by a Dotted Line.

Sensitivity coefficients can be used to write an equation for the change in each of k major blanket parameters in terms of the I independent variations (good to first order), e.g.,

$$\Delta T = t^{L}\Delta L + t^{P}\Delta P + t^{U}\Delta U + t^{W}\Delta W + t^{S}\Delta S + t^{C}\Delta C \quad ,$$

$$\Delta F = f^{L}\Delta L + f^{P}\Delta P + f^{U}\Delta U + f^{W}\Delta W + f^{S}\Delta S + f^{C}\Delta C \quad ,$$

$$\Delta M = m^{L}\Delta L + m^{P}\Delta P + m^{U}\Delta U + m^{W}\Delta W + m^{S}\Delta S + m^{C}\Delta C \quad .$$

If specific changes in N of the performance parameters are derived ($N \leq k$, and $N \leq I$), these equations can be solved to determine the values of N of the independent variations in terms of specified values for the other I - N variations.

For example (and using matrix notation):

$$\begin{bmatrix} \Delta T' \\ \Delta F' \\ \Delta M' \end{bmatrix} = \begin{bmatrix} \Delta T \\ \Delta F \\ \Delta M \end{bmatrix} - \begin{bmatrix} t^{W}t^{S}t^{C} \\ f^{W}f^{S}f^{C} \\ m^{W}m^{S}m^{C} \end{bmatrix} * \begin{bmatrix} \Delta W \\ \Delta S \\ \Delta C \end{bmatrix} = \begin{bmatrix} t^{L}t^{P}t^{U} \\ f^{L}f^{P}f^{U} \\ m^{L}m^{P}m^{U} \end{bmatrix} * \begin{bmatrix} \Delta L \\ \Delta P \\ \Delta U \end{bmatrix} .$$

This will give the changes in lithium-6 enrichment, plutonium concentration, and uranium thickness (the three major blanket parameters) required to produce a desired set of changes in T, F, and M, as corrected for variations in the other parameters.

In fact, the matrix to be solved can be inverted, using the values of the sensitivity coefficients from Table III.

$$\Delta L = + 1.2324\ \Delta T' + 0.2996\ \Delta F' - 0.02328\ \Delta M'$$

$$\Delta P = + 1.2000\ \Delta T' + 0.3406\ \Delta F' - 0.00904\ \Delta M'$$

$$\Delta U = + 50.429\ \Delta T' + 47.408\ \Delta F' + 1.6857\ \Delta M' \quad .$$

This predicts, for example, that F could be raised by 0.1 with T and M held constant if the Reference Blanket were changed to 0.13% lithium-6, 0.284% PuF_3, and 48.74% U-Mo.

Forcing ΔU to be zero yields reduced equations for the two remaining parameters:

$$\Delta L = 1.9288\ \Delta T' + 0.9542\ \Delta F'$$

$$\Delta P = 1.4703\ \Delta T' + 0.5948\ \Delta F'.$$

Now the 0.1 increase in ΔF would require L = 0.195% and P = 0.309%, and this would cause a 2.8 decrease in M.

It should be apparent that when sensitivity coefficients can be obtained, they are quite useful in two ways. First, they provide quick estimates of the effects of hypothetical design variations (perhaps required by non-neutronic considerations). Second, they can be used to estimate the magnitude of design changes required to meet performance objectives imposed on the neutronics. Since the sensitivity coefficients are only first-order, successive refinement will still be necessary, but predictions of the direction and distance are of great help in this process.

References

[1]D. T. Aase, M. C. C. Bampton, T. J. Doherty, B. R. Leonard, R. A. McCann, D. F. Newman, R. T. Perry, C. W. Stewart, TCT Hybrid Preconceptual Design Studies, Battelle Pacific Northwest Laboratories Report PNL-2304 (1978).

[2]D. L. Chapin, Molten Salt Blanket Calculations for a Tokamak Fusion-Fission Hybrid Reactor, Princeton Plasma Physics Laboratory Report MATT-1236 (1976).

[3]E. Greenspan, W. G. Price, Jr., H. Fishman, SWAN: A Code for the Analysis and Optimization of Fusion Reactor Nucleonic Characteristics, Princeton Plasma Physics Laboratory Report MATT-1008 (1973).

[4]E. Greenspan and W. G. Price, Jr., Tritium Breeding Potential of the Princeton Reference Fusion Power Plant, Princeton Plasma Physics Laboratory Report MATT-1043 (1974).

Appendix II. Profile Effects

The model of the plasma used in this study is a zero-dimensional or point model. In this model several reactor paramaters, such as the total fusion power, the injected beam power, radiative power, etc., are found by first calculating the quantity of interest of a "typical unit of plasma volume" and then multiplying this result by the total volume of plasma. Certain values for the plasma temperature, T_e, and density, n_e, etc., enter into these calculations and are assigned in the mind's eye to the "typical unit of plasma volume". The relationship between T_e, for example, and the spatial average of the plasma temperature, $\langle T \rangle$, is not well defined since it will depend upon both the temperature profile and the reactor quantity being calculated with the help of the number, T_e. It is not clear how one should interpret the point model calculation of reactor quantities for various assumptions about the plasma temperature and density profiles. In this appendix we make a few remarks on these questions. We concern ourselves with the fusion power density, P_F, and the injected beam power density, P_B.

For a uniform plasma it is a good approximation that $P_F \sim n_e^2$, and $P_B \sim n_e^2$ (see section IV.B). Hence the ratio, P_F/P_B, will be essentially independent of the density. Therefore, under the assumptions that P_F and P_B are determined only by local properties of the plasma and that the temperature is uniform, the ratio, P_F/P_B, will be independent of any density profile. The temperature dependence of both P_F and P_B is more complex and will render P_F/P_B dependent on the temperature profile. Thus P_F/P_B will be sensitive to the total pressure profile.

If one assumes P_B is not determined by only local quantities, but depends on the spatial averages of the plasma temperature and density, then it would seem reasonable to take $P_B \sim \langle n_e \rangle^2$. (Motivation for such an assumption is the possibility that the slowing down orbit of an injected particle can undergo a radial excursion of 50 cm in a typical hybrid plasma. The distribution function of the "hot ions" is sensitive to how the injected particles slow down.) Under this assumption, then, P_F would be compounded of thermonuclear terms proportional to the local n_e^2 and terms reflecting beam interactions that would be proportional to $\langle n_e \rangle$ or $\langle n_e \rangle^2$. We are thus led to consider that the ratio, P_F/P_B, can be sensitive to density profiles even for a uniform temperature plasma.

For most of the calculations in this study we have used the relation, $P_F/P_B \sim \langle n_e^2 \rangle / \langle n_e \rangle^2$. In these calculations the value of n_e produced by the point model (see Section IV.B, Eq.(9)) is used for $\langle n_e \rangle$. To evaluate this ratio of averages we have used a density profile of the form $(1 - r^2/a^2)^x$ which reflects the choice of pressure profile adopted for most of this study (see Section IV.C). This density profile leads to $\langle n_e^2 \rangle / \langle n_e \rangle^2 = (x + 1)^2/(2x + 1)$. This ratio equals 1.33 for $x = 1$ and 1.80 for $x = 2$. The "new pressure" profiles correspond to a different spatial density profile and numerically produce $\langle p^2 \rangle / \langle p \rangle^2 = 1.873$.

To explore the effect of temperature profiles we have considered a particular plasma in which both the density and temperature profiles have the above form with $x = 1$. We assume all power densities are determined by only local parameters. Curves for the temperature, T, T^2, P_B, P_F and the thermal fusion power density, P_F',

are shown in Figure 1. These curves were calculated for the following paramaters:

$$\langle n \rangle = 10^{14}\ cm^{-3}$$

$$\langle T \rangle = 6.2\ keV$$

$$W_o = 180\ keV \quad \text{(injection energy)}$$

$$n_h/n_e = 0.16 \quad \text{(hot to thermal ratio)}$$

$$\%D = 52$$

The last two parameters are assumed to be independent of the radius. The calculated quantities have been scaled so that the spatial average of each quantity has the same geometric ordinate.

Results from six such calculations as described above are shown in Table I. The quantities in column A are calculated using only the average plasma parameters. The value of P_F has not been enhanced by the factor $\langle n_e^2 \rangle / \langle n_e \rangle^2$. The quantities in column B are spatial averages reflecting the effects of the density and temperature profiles. The effect of the profiles is to enhance both P_F and P_B, somewhat differently, by modest amounts except for a condition of low temperature "ignition" where P_F is enhanced by almost a factor of five.

Producing Table I took a large amount of computer time (>100 minutes on a CDC 7600 computer). Due to limitations in time and effort this type of calculation was not extended over a wider range of parameter space. To provide a technique for testing the sensitivity of many hybrid reactors to profile effects, the enhancement of P_F displayed in column C of Table I was used. Let this enhancement be called R. R was taken to be independent of both the injection energy, W_o, and the percent of D in the plasma on the grounds that the probability of beam induced fusion has a

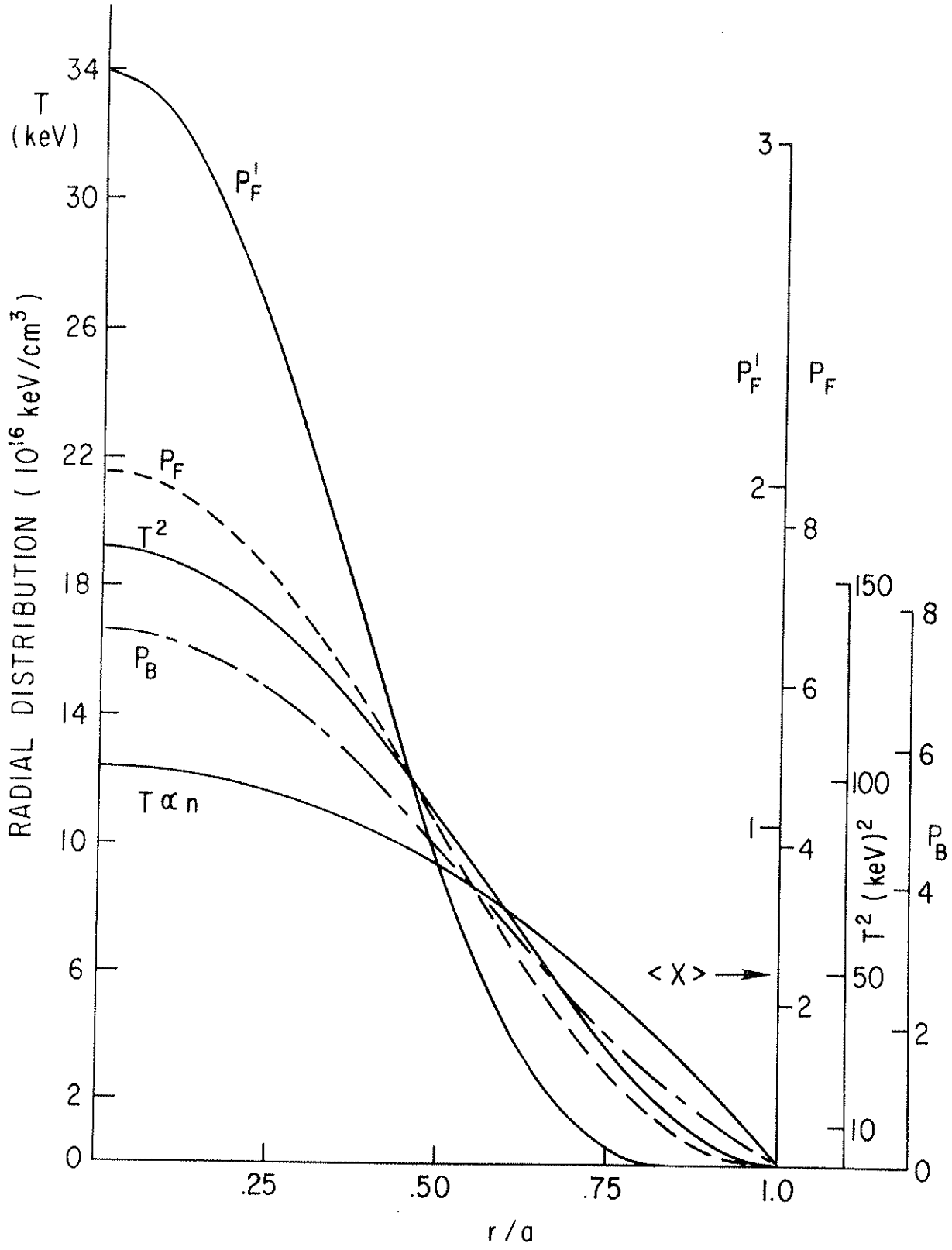

Fig. 1. Temperature and Power Profiles in Plasma. P_F, P_F', and P_B Are in Units of 10^{16} keV/cm^3 sec.

Table I.

%D	W_o keV	T keV	n_h/n_e	Quantity	Without Profile Effect A	With Profile Effect B	With Profile Effect C (= B/A)
50	200	14	0.16	P_F	2.255	3.683	1.63
				P_B	1.844	3.095	1.67
			0.0	P_F	1.028	2.614	2.54
				P_B	0.0	0.0	0.0
50	180	6.2	0.16	P_F	1.572	2.475	1.57
				P_B	2.361	2.854	1.20
			0.0	P_F	0.119	0.583	4.90
				P_B	0.0	0.0	0.0
45	225	13	0.04	P_F	1.204	2.648	2.19
				P_B	0.478	0.684	1.43
			0.0	P_F	0.875	2.351	2.68
				P_B	0.0	0.0	0.0

broad maximum for $150 < W_o < 250$ keV, and that the optimum D-T mixture is never far from 50-50. The tabulated values of R were fit with the following function:

$$R = \exp \{2.400 - 12.59\ (n_h/n_e) - 0.1584\ T + 0.5401\ (n_h/n_e)\ (T) + 14.16\ (n_h/n_e)^2 + 0.003830\ T^2\}\ .$$

This function for R was introduced into the survey type calculation of hybrids reported in Section V.B.3.a.

Acknowledgments

Unknown to the senior author of this report, other authors wish to acknowledge the contribution of F.H.T. by including a special remark here. He should receive credit for making the largest portion of the effort by far to produce this report. Without this contribution, the work would not have been completed.

This work was supported by the U.S. Department of Energy Contract No. EY-76-C-02-3073.

III. Symbol Table

A

a	distance
a	inventory of fissile fuel
a	minor radius
A	aspect ratio
A	distance to magnetic center
A	neutrons lost by parametric absorption
A	plasma area
A	power plant availability
A	wall area
A_T	penetration index
A_W	theoretical wall area
α	capture-to-fission ratio
α	profile factor

B

B	burnup discharge value
B	magnetic field
B_c	magnetic field at major radius of tokamak
B_c	toroidal magnetic field
B_p	average magnitude of poloidal magnetic field
B_s	field at TF coil $\sim$ 160 kG
B_v	vertical magnetic field
β	plasma pressure/poloidal magnetic field pressure

C

c	semicrack length
c	stability constant
C	plant capital cost, $
CR	conversion ratio

D

D	theoretical diffusion coefficient
DF	divertor field
D_{TE}	trapped electron mode diffusion coefficient
δ	duty factor
Δ	scrapeoff layer thickness

E

e	cost of hybrid generated electricity, $/MWehr = mills/kWehr
e	neutron energy per fusion
e_c	combined cost of total annual production of electricity
e_p	"park cost" of electricity
e_1	minimum price of electricity
E	annual energy production, MWehr
E	proton energy measured in eV
η	plasma resistivity
η_D	divertor thermal collection efficiency
η_I	injector efficiency

F

f	final value
f	fraction
f	price of fissile fuel
f	total number of fissions per fusion
f_α	fraction of total fusion power density in alpha particles
f_o	DT induced fast fissions in uranium
f_p	"park value" of fissile fuel
F	fissile breeding ratio
F	fuel cycle costs, $/yr
F	net fissile production
F_{FP}	fissile fuel price
F_o^+	captures in uranium
F_o^-	absorptions in plutonium

G

g	other than fast fissions in uranium
g	plant capacity factor
G_B	net fissile fuel production
G_{Bf}	revenue from sale of fissile fuel

H

h	distance
h	radius of the point of maximum toroidal field strength
h	toroidal field coil location
H	height of coils
H	net recoverable production of fissile material
H/T	ratio of hot to thermal population in plasma

I

i	initial values
I	plasma current

J

J	current density
J	integrated wall load
J_D	injection current of D
J_R	recycle current
J_T	injection current of T

K

k	multiplication constant
k_∞	multiplication constant of infinite medium of fissile region

L

L	load factor
L	total loss of neutrons
L_B	width of blanket
λ	mean free path for ionizing neutral beam
$\ell n\ \Lambda$	coulomb logarithm

M

m_i	mass species
M	blanket energy multiplication
M_B	blanket multiplication

N

n	density
n_e	electron density
n_D/n_T	deuterium to tritium ratio
n_h/n_e	hot-to-thermal ratio
n_{hot}	hot population density
n_{hot}/n_e	hot-to-thermal ratio; fraction suprathermal
n_i	density of plasma species (arbitrary)
$n\tau$	confinement property of the plasma
N	average number of neutrons per fission
N	toroidal mode number
NBI	neutral beam injector
N_{LWR}	number of LWR's supported by the hybrid
N_{ps}	standard penetration
ν	fraction of the incident beam power actually absorbed by the plasma
ν	number of fission neutrons released per neutron absorbed
$<n>$	spatial average of the plasma density

O

O	annual operating and maintenance costs, $/yr
OH	ohmic heating field

P

p	density of plutonium in burner salt
p	fractional parasitic loss
p	pressure
p_f	fusion power density

p_o	maximum pressure
P	density of Pu-239
P	gross fissile breeding ratio
P	gross fissile production
P	plasma pressure
P_α	alpha particle power
P_B	beam power density
P_{BL}	blanket power, MW
P_{cond}	power lost by plasma due to thermal conduction
P_{cx}	power lost by plasma due to charge exchange
P_D	power deposited in divertor
P_{diff}	power lost by plasma due to diffusion
P_e	price of electricity
P_{eh}	price of electricity from hybrid
P_F	fusion power density
P'_F	thermal fusion power density
P_g	gross electric power
P_i	beam power
P_I	power to injectors, MW
P_{ion}	power lost by plasma due to ionization
P_{MAX}	maximum beam power
P_{net}	net electric power for sale
P_{rad}	power lost by plasma due to radiation
ϕ	annual fixed charge rate, yr^{-1}
ϕ_{BURN}	flux swing required for maintenance of the plasma current over burn time

ϕ_{CORE}	flux swing produced by OH windings in core
ϕ_{PLASMA}	flux swing required to induce the plasma current
ϕ_{VERT}	flux swing due to vertical field rise
Ψ (X,Z)	poloidal magnetic flux

Q

q	safety factor
Q	ratio of total fusion power produced to total beam power absorbed in the plasma

R

r	plasma resistance
R	distance
R	major radius
R_α	general reaction rate
R_p	ripple penetration

S

S	density (or other index) of the fissile loading
S	injection rate
S	stress
S	total source of neutrons
SM	stress intensity
S_s	strict penetration
σ	fusion cross section
σ	maximum stress

T

t	length of time associated with burn
T	absorptions in lithium
T	plasma temperature
T	tritium breeding ratio
T_e	plasma temperature
T_F	equivalent annual time at full power
TF	toroidal field
T_i	temperature of a plasma species (arbitrary)
T_M	maintenance time (hour/year)
T_p	time at power (hour/year)
T_R	refueling time (hour/year)
T_W	total wall replacement time
τ_E	energy confinement time
τ_{EB}	energy balance derived confinement time
τ_o	wall capability ($MWyr/m^2$)
τ_p	particle confinement time
τ_{PHY}	physics derived confinement time
τ_s	"slowing down" time for injected particles
τ_{SD}^{α}	slowing down time for alphas
<T>	spatial average of plasma temperature

U

U	density of U-238

V

v_i	velocity of an arbitrary plasma species
v_o	injection speed

V	plasma volume
V	volume of the multiplier
VF	vertical field
V_p	plasma volume

W

w	coil width
W	wall load
W_c	"critical energy" at which beam particle delivers energy at equal rates to background electrons and to ions
W_L	wall load
W_o	injection energy

Z

Z	fraction of neutrons to hit blanket
Z_w	effective wall area backed by blanket, m^2
Z_1, Z_2, Z_3	effective wall coverages

EXTERNAL DISTRIBUTION IN ADDITION TO TIC UC-20

ALL CATEGORIES

. Askew, Auburn University, Alabama
. T. Wu, Univ. of Alabama
eophysical Institute, Univ. of Alaska
.L. Johnston, Sonoma State Univ, California
. H. Kuehl,Univ. of S. California
nstitute for Energy Studies, Stanford University
. D. Campbell, University of Florida
. L. Oleson, University of South Florida
. M. Stacey, Georgia Institute of Technology
enjamin Ma, Iowa State University
lagne Kristiansen, Texas Tech. University
. L. Wiese, Nat'l Bureau of Standards, Wash., D.C.
ustralian National University, Canberra
.N. Watson-Munro, Univ. of Sydney, Australia
. Cap, Inst. for Theo. Physics, Austria
cole Royale Militaire, Bruxelles, Belgium
. Paulumbo, Comm. of Eur. Comm., Belgium
.H. Sakanaka, Instituto de Fisica, Campinas, Brazil
. R. James, University of Alberta, Canada
.W. Johnston, INRS-Energie, Vareenes, Quebec
. M. Skarsgard, Univ. of Saskatchewan, Canada
ibrarian, Culham Laboratory, Abingdon, England
.M. Dupas Library, C.E.N.-G, Grenoble, France
entral Res. Inst. for Physics, Hungary
. Shingal, Meerut College, India
. Naraghi, Atomic Energy Org. of Iran
iblioteca, Frascati, Italy
iblioteca, Milano, Italy
. Rostagni, Univ. Di Padova, Padova, Italy
reprint Library, Inst. de Fisica, Pisa, Italy
ibrary, Plasma Physics Lab., Gokasho, Uji, Japan
. Mori, Japan Atomic Energy Res. Inst.,Tokai-Mura
esearch Information Center, Nagoya Univ., Japan
. Shioda, Tokyo Inst. of Tech.,Japan
st. of Space & Aero. Sci., Univ. of Tokyo
. Uchida, Univ. of Tokyo, Japan
. Yamato, Toshiba R. & D. Center, Japan
. Yajima, Kyushu Univ., Japan
. England, Univ. Nacional Auto-noma de Mexico
. S. Liley, Univ. of Waikato, New Zealand
. A. Moss, Saab Univas Norge, Norway
A.C. Cabral, Univ. de Lisboa, Portugal
. Petrus, AL.I. CUZA Univ., Romania
de Villiers, Atomic Energy Bd., South Africa
. Maurech, Comisaria De La Energy y Recoursos Minerales, Spain
ibrary, Royal Institute of Technology, Sweden
en. de Res. En Phys.Des Plasmas,Switzerland
ibrarian, Fom-Instituut Voor Plasma-Fysica, The Netherlands
. E. Golant, A.F. Ioffe Physical-Tech. Inst.,USSR
B. Kadomtsev, Kurchatov Inst. of Atomic Energy, USSR
ne Kharkov Physical-Tech. Inst., USSR
. S. Rabinovich, Academy of Sci, USSR
bliothek, Stuttgart, West Germany
D. Buhler, Univ. of Stuttgart, West Germany
ax-Planck-Inst. fur Plasmaphysik, W. Germany
ucl. Res. Estab., Julich, West Germany
. Schindler, Inst. Fur Theo. Physik, W. Germany

EXPERIMENTAL
THEORETICAL

M. H. Brennan, Flinders Univ. Australia
H. Barnard, Univ. of British Columbia, Canada
S. Screenivasan, Univ. of Calgary, Canada
J. Radet, C.E.N.-B.P., Fontenay-aux-Roses, France
Prof. Schatzman, Observatoire de Nice, France
S. C. Sharma, Univ. of Cape Coast, Ghana
R. N. Aiyer, Laser Section, India
B. Buti, Physical Res. Lab., India
L. K. Chavda, S. Gujarat Univ., India
I.M. Las Das, Banaras Hindu Univ., India
S. Cuperman, Tel Aviv Univ., Israel
E. Greenspan, Nuc. Res. Center, Israel
P. Rosenau, Israel Inst. of Tech., Israel
Int'l. Center for Theo. Physics, Trieste, Italy
I. Kawakami, Nihon University, Japan
T. Nakayama, Ritsumeikan Univ., Japan
S. Nagao, Tohoku Univ., Japan
J.I. Sakai, Toyama Univ., Japan
S. Tjotta, Univ. I Bergen, Norway
M.A. Hellberg, Univ. of Natal, South Africa
H. Wilhelmson, Chalmers Univ. of Tech., Sweden
Astro. Inst., Sonnenborgh Obs.,The Netherlands
N.G. Tsintsadze, Academy of Sci GSSR, USSR
T. J. Boyd, Univ. College of North Wales
K. Hubner, Univ. Heidelberg, W.Germany
H. J. Kaeppeler, Univ. of Stuttgart, West Germany
K. H. Spatschek, Univ. Essen, West Germany

EXPERIMENTAL
ENGINEERING

B. Grik, Univ. de Quebec, Canada
P. Lukac, Komenskeho Univ., Czechoslovakia
G. Horikoshi, Nat'l Lab for High Energy Physics, Tsukuba-Gun, Japan
V. A. Glukhikh, D.V. Efremov Sci. Res. Instit.of Elect. App., USSR

EXPERIMENTAL

F. J. Paoloni, Univ. of Wollongong, Australia
J. Kistemaker, Fom Inst. for Atomic & Molec. Physics, The Netherlands

THEORETICAL

F. Verheest, Inst. Vor Theo. Mech., Belgium
J. Teichmann, Univ. of Montreal, Canada
T. Kahan, Univ. Paris VII, France
R. K. Chhajlani, India
S. K. Trehan, Panjab Univ., India
T. Namikawa, Osaka City Univ., Japan
H. Narumi, Univ. of Hiroshima, Japan
Korea Atomic Energy Res. Inst., Korea
E. T. Karlson, Uppsala Univ., Sweden
L. Stenflo, Univ. of UMEA, Sweden
J. R. Saraf, New Univ., United Kingdom